

Aarhus School of Architecture // Design School Kolding // Royal Danish Academy

Parametric Workflow to Conceive Facades as Indoor and Outdoor Climate Givers

Naboni, Emanuele; Ofria, Luca; Danzo, Eric

Published in:

2019 Proceedings of the Symposium on Simulation for Architecture and Urban Design

Publication date:

2019

Document Version:

Publisher's PDF, also known as Version of record

Document License:

Other

[Link to publication](#)

Citation for pulished version (APA):

Naboni, E., Ofria, L., & Danzo, E. (2019). Parametric Workflow to Conceive Facades as Indoor and Outdoor Climate Givers. In S. Rockcastle, T. Rakha, C. Cerezo Davila, D. Papanikolaou, & T. Zakula (Eds.), *2019 Proceedings of the Symposium on Simulation for Architecture and Urban Design* (pp. 11-18). Society for Modeling & Simulation International (SCS).

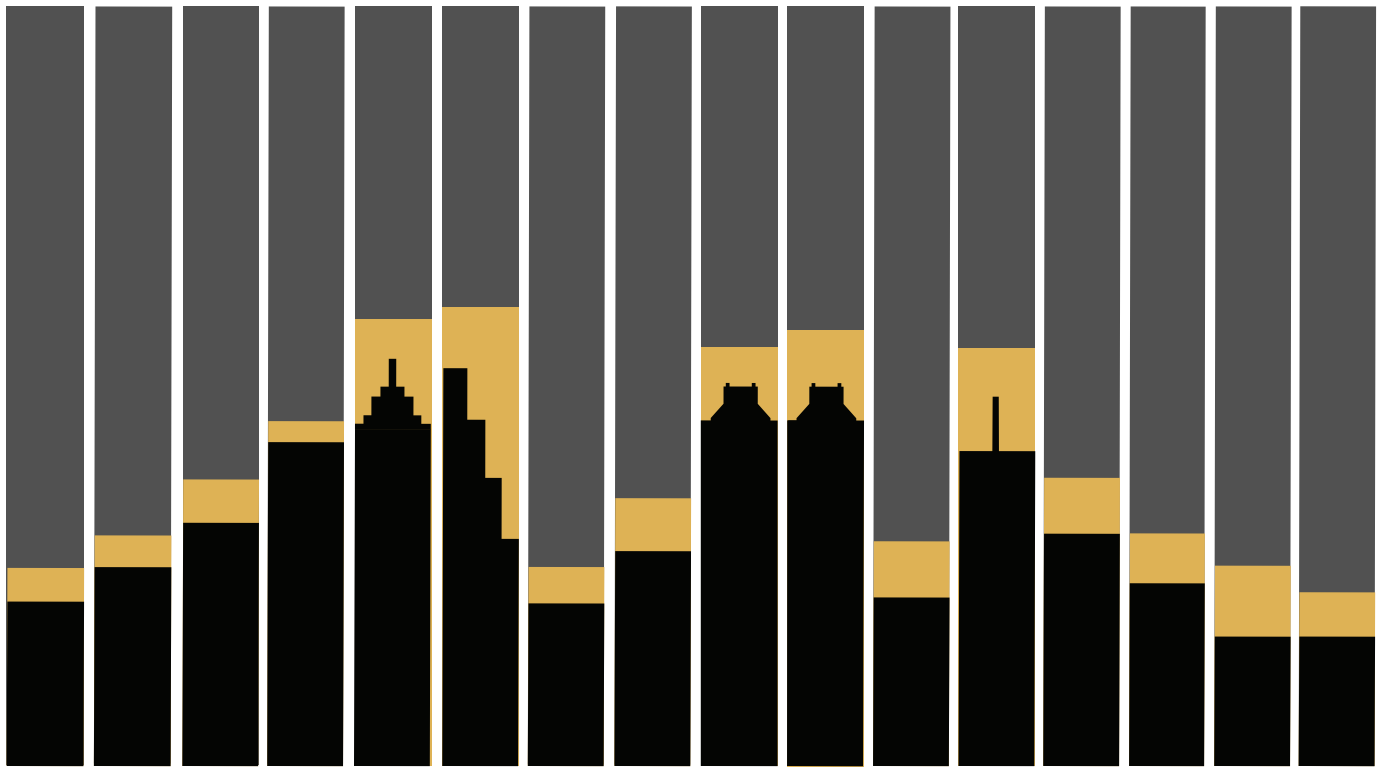
General rights

Copyright and moral rights for the publications made accessible in the public portal are retained by the authors and/or other copyright owners and it is a condition of accessing publications that users recognise and abide by the legal requirements associated with these rights.

- Users may download and print one copy of any publication from the public portal for the purpose of private study or research.
- You may not further distribute the material or use it for any profit-making activity or commercial gain
- You may freely distribute the URL identifying the publication in the public portal ?

Take down policy

If you believe that this document breaches copyright please contact us providing details, and we will remove access to the work immediately and investigate your claim.



SimAUD 2019

10th ANNIVERSARY EDITION

Edited by:

2019 Proceedings of the

Siobhan Rockcastle
Tarek Rakha
Carlos Cerezo Davila
Dimitris Papanikolaou
Tea Zakula

**Symposium on Simulation for
Architecture & Urban Design**



Georgia Tech, College of Design, School of Architecture, Atlanta, GA, USA
April 07-09, 2019



SimAUD 2019

10th ANNIVERSARY EDITION

Edited by:

2019 Proceedings of the

Siobhan Rockcastle
Tarek Rakha
Carlos Cerezo Davila
Dimitris Papanikolaou
Tea Zakula

**Symposium on Simulation for
Architecture & Urban Design**



Georgia Tech, College of Design, School of Architecture, Atlanta, GA, USA
April 07-09, 2019

2019 Proceedings of the Symposium for Architecture and Urban Design
Siobhan Rockcastle, Tarek Rakha, Carlos Cerezo Davila, Dimitris Papanikolaou, Tea Zakula, editors

© 2019 SIMULATION COUNCILS, INC.

Responsibility for the accuracy of all statements in each paper rests entirely with the author(s). Statements are not necessarily representative of nor endorsed by The Society for Modeling and Simulation International.

Permission is granted to photocopy portions of this publication for personal use and for the use of students provided credit is given to the conference and publication. Permission does not extend to other types of reproduction nor to copying for incorporation into commercial advertising nor for any other profit-making purpose. Other publications are encouraged to include 300-500-word abstracts or excerpts from any paper contained in this book, provided credits are given to the author and the conference. For permission to publish a complete paper, write: The Society for Modeling and Simulation International (SCS), 11315 Rancho Bernardo Road, Suite 139, San Diego, CA 92127, USA.

Preface

Over the last decade, simulation and design computation have become synonymous with the pursuit of building performance and integrated environmental design. The rapid acceleration of computing power, through the continued development of hardware, software, and web-based applications, allows architects and urban designers broad access to tools that can aid the design process in new ways. With this expanded capacity comes a blurring of disciplinary boundaries, as simulation-based decision support unites stakeholders from various fields. In many ways, this increased collaboration between disciplines has made the building industry more amenable to reiteration, optimization, and integration across a range of performance considerations - from energy to form generation, fabrication, human comfort, and behavior. Like any significant change in an applied field, this transformation in computational capacity has resulted in a disruption to the status quo and has opened the doors to a broad array of new performance considerations and generative design methods.

The 10th annual Symposium on Simulation for Architecture and Urban Design (SimAUD) unites researchers and practitioners in the fields of architecture, urban design, urban planning, building science, software development, and data science. With a special emphasis on methods that bridge disciplinary gaps, SimAUD 2019 crosses human, building, and urban scales to offer an exciting lineup of research - both theoretical and applied. In addition to our original research contributions, this year's program includes four keynote speakers from academic and mixed professional backgrounds: Dennis Shelden from Georgia Tech, Billie Faircloth from Kieren Timberlake, Stefano Schiavon from UC Berkley, and Dana Cupkova from Carnegie Mellon and Epiphyte Lab.

In 2019, we are delighted to celebrate the 10th Anniversary of SimAUD at Georgia Tech in Atlanta. As organizer for this year's edition, we are humbled by the opportunity to unite prominent academic and industry professionals with students and emerging researchers in what we hope will be a truly memorable event. This year's symposium presents novel research contributions in topics ranging from experiential climates to retrofitting analysis, data in mixed realities, designing urban futures, mediums of indoor comfort, simulating people, performative structures, robots that make, design decision models and geometric explorations.

To complement our program with a more hands-on opportunity for learning and sharing, SimAUD 2019 continues the 2017 trend of offering pre-conference workshops. This year's program includes 8 workshops that cover topics ranging from fabrication to optimization and virtual assembly information modelling. We are proud to support our growing community and provide structured opportunities for dissemination between academic, industry, and design professionals.

SimAUD 2019 is made possible by a large team of committed volunteers, who have worked diligently over the last 10 months to organize and manage this year's event. We would like to recognize and thank our Scientific Chairs: Carlos Cerezo Davila, Dimitris Papanikolaou and Tea Zakula for structuring and managing our rigorous peer-review process and committing many hours to the planning of this event. We would also like to thank the 2019 Scientific Committee for their time and thoughtful review of more than 90 submissions. Their commitment to this community ensures that we maintain the high standards we have all come to associate with SimAUD proceedings. We are also tremendously grateful for the record support and guidance of our

sponsors: Autodesk, the U.S. Department of Energy through NREL and IBPSA US, KPF, the University of Oregon College of Design, EDSL, cove.tool, and IES. SimAUD is run in partnership with the Society for Modeling & Simulation International (SCS). We would like to thank Oletha Darensburg and Carmen Ramirez for helping us to organize and manage the conference. We would also like to extend our gratitude to Kristi Connelly and Holly Meyers from Omnipress for developing the 2019 proceedings. Furthermore, we are indebted to the faculty, staff, and students of Georgia Tech's College of Design for offering their space, enthusiasm, and support for this year's event. We offer a special thanks to Scott Marble for his treasured support from the School of Architecture, as well as Carmen Wagster and Isra Hassan for their valuable contributions to the conference logistics and planning

Finally, we would like to extend our sincere gratitude to all the authors who submitted a paper or workshop proposal to SimAUD 2019. As our symposium grows more and more competitive each year, we are grateful for the breadth and depth of scholarly contributions to this conference. We value your trust in our community with the review, dissemination, and publication of your research. As we look forward to 2020 and beyond, we are confident in the continued growth and impact of SimAUD. Thanks to all of you who continue to push us forward into exciting new frontiers for research and application in the built environment.

Siobhan Rockcastle

General Chair, SimAUD 2019

Assistant Professor, University of Oregon

Tarek Rakha

Program Chair, SimAUD 2019

Assistant Professor, Georgia Tech

All accepted papers will be published in the ACM Digital Library at the SpringSim Archive.
Sponsored by The Society for Modeling and Simulation International.

Contents

Experiential Climates	1
Sun and Wind: Integrated Environmental Performance Analysis for Building and Pedestrian Comfort	3
<i>Francesco De Luca</i>	
A Parametric Workflow to Conceive Facades as Indoor and Outdoor Climate Givers.	11
<i>Emanuele Naboni, Eric Danzo and Luca Ofria</i>	
Streets, Parks & Plazas: Analyzing Daylight in the Public Realm	19
<i>Elizabeth de Regt and Tomothy Deak</i>	
Retrofitting Analysis	27
Unleashing the Diversity of Conceptual Building Renovation Design: Integrating High-Fidelity Simulation with Rapid Constraint-Based Scenario Generation	29
<i>Aliakbar Kamari, Carl Peter Leslie Schultz and Poul Henning Kirkegaard</i>	
Application of Surrogate Modeling to Multi-Objective Optimization for Residential Retrofit Design.	37
<i>Arfa N. Aijazi and Leon Glicksman</i>	
Aerial Thermography as a Tool to Inform Building Envelope Simulation Models	45
<i>Norhan Bayomi, Shreshth Nagpal, Tarek Rakha, Christoph Reinhart and John Fernandez</i>	
Data in Mixed Realities	49
Towards Assembly Information Modeling (AIM).	51
<i>Ayoub Lharchi, Mette Ramsgaard Thomsen and Martin Tamke</i>	
Subjective Impressions of a Space Influencing Brightness Satisfaction: an Experimental Study in Virtual Reality	57
<i>Azadeh Sawyer and Kynthia Chamilothoni</i>	
Immersive Representation of Urban Data	65
<i>Amber Bartosh and Rongzhu Gu</i>	

Modeling Urban Energies69

A Data-driven Framework For Urban Building Operational Energy Use Modeling71
Narjes Abbasabadi and Rahman Azari

An Integrated Urban Planning and Simulation Method To Enforce Spatial Resilience
Towards Flooding Hazards 79
Julius Morschek, Reinhard Konig and Sven Schneider

A Method for Integrating an Udem with Gis for Spatiotemporal Visualization and Analysis. . 87
Bess Krietemeyer and Rawad El Kontar

A Technique for Developing High-Resolution Residential Occupancy Schedules for
Urban Energy Models 95
Diba Malekpour, Farzad Hashem, Vinciane Tabard-Fortecoeuf and Ulrike Passe

Designing Urban Futures103

Environmental Data and Land Use: Integration of
Site-Specific Ecology and Urban Design 105
Claudio Campanile and Shih Hsin Wu

How to Generate a Thousand Master Plans: A Framework for Computational
Urban Design. 113
Luc Wilson, Jason Danforth, Carlos Cerezo Davila and Dee Harvey

CityFiction – Scenarios for Densification. 121
Henrik Malm and Petra Jennings

Exploring Urban Walkability Models and Pedestrian Movement Trends in a
Vancouver Neighbourhood 129
Nicholas Martino, Cynthia Girling and Edja Trigueiro

Mediums of Indoor Comfort133

A Simulation-Based Design Analysis for the Assessment of Indoor Comfort Under the
Effect of Solar Radiation 135
Andrea Zani, Henry David Richardson, Alberto Tono, Stefano Schiavon and Edward Arens

Black Globe Free Convection Measurement Error Potentials. 143
Eric Teitelbaum, Jovan Pantelic, Adam Rysanek, Kian Wee Chen and Forrest Meggers

Assessing the Performance of UFAD System in an Office Building Located In
Various Climate Zones 147
*Roshanak Ashrafi, Mona Azarbayjani, Robert Cox, Benjamin Futrell, Joseph Glass, Amir Zarrabi and
Armin Amirazar*

Evaluating the Influence of Three Simplifications on Natural Ventilation Rate Simulation . . 155
Yuchen Shi and Xiaofeg Li

Simulating People 159

Adaptive Occupancy Scheduling: Exploiting Microclimate Variations in Buildings 161
Max Marschall and Jane Burry

Toward a Multi-Level and Multi-Paradigm Platform for Building Occupant Simulation 169
*Davide Schaumann, Seonghyeon Moon, Muhammad Usman, Rhys Goldstein, Simon Breslav, Azam
Khan and Mubbasir Kapadia*

Multi-Constrained Authoring of Occupant Behavior
Narratives in Architectural Design 177
Xun Zhang, Davide Schaumann, Brandon Haworth, Petros Faloutsos and Mubbasir Kapadia

Including Occupant Behavior in Building Simulation: Comparison of a Deterministic vs.
a Stochastic Approach 185
Max Marschall, Farhang Tahmasebi and Jane Burry

Robots that Make 189

Rotoform - Realization Of Hollow Construction Elements Through Roto-Forming With
Hyper-Elastic Membrane Formwork 191
Oliver Tessman and Samim Mehdizadeh

Environmentally Informed Robotic-Aided Fabrication 199
Carmen Cristiana Matiz, Heather “Brick” McMenomy and Elif Erdine

Curved-Crease Folding and Robotic Incremental Sheet Forming in Design and
Fabrication. 207
*Elif Erdine, Antiopi Koranaki, Alican Sungur, Angel Fernando Lara Moreira, Alvaro Lopez Rodriguez,
George Jeronimidis, Michael Weinstock*

Performative Structures 215

Structural Performance of Semi-Regular Topological Interlocking Assemblies 217
Michael Weizmann, Oded Amir and Yasha Jacob Grobman

Data-driven Material System of Graded Concrete Structures 225
Elisabeth Riederer and Anuradha Suryavanshi

Modularizing Tensegrity Systems: An Approach to Controllable Independent Modules. 231
Arian Seedfar and Paniz Farrokhsiar

A Framework for Cost-Optimal Zero-Energy Lightweight Construction 239
Mohamed Amer and Shady Attia

Design Decision Models 243

An Automated Framework Creating Parametric BIM from GIS Data to Support
Design Decisions. 245
Chengde Wu, Saied Zarrinmehr, Mohammad Rahmani Asl and Mark J. Clayton

Digital Energy Performance Signature Extensible Markup Language (DEPSxml):
Towards a New Characterization Framework for Sharing Simulation and Measured
Data on Building Design and Energy Performance 253
Justin McCarty and Adam Rysanek

From Optimization to Performance-Informed Design 261
Thomas Wortmann and Thomas Schroepfer

Linear and Classification Learner Models for Building Energy Predictions and
Predicting Saving Estimations 269
Kevin Eaton, Nabil Nassif, Pyria Rai and Alexander Rodrigues

Geometric Explorations 277

From Drawing Shapes to Scripting Shapes:
Architectural Theory Mediated by Shape Machine 279
Heather Ligler and Athanassios Economou

Interpreting Non-Flat Surfaces for Walkability Analysis 287
Mathew Schwartz and Subhajt Das

Generating Acoustic Diffuser Arrays with Shape Grammars 295
Jonathan Dessi-Olive and Timothy Hsu

A Unified Framework for Optimizing the Performance of a Kinetic Façade 303
Ok-Kyun Im, Kyoung-Hee Kim, Armin Amirazar and Churlu Lim

Author Index 311

Presenting Authors 313

Organizing Committee 327

Sponsors 331

Keynote Speakers

Dana Cupkova

Lecture Title: **Shape Matters**



Dana Cupkova is a Co-founder and a Design Director of *EPIPHYTE Lab*, an interdisciplinary architectural design and research collaborative. She currently holds Assistant Professorship at Carnegie Mellon University's School of Architecture and serves as a graduate program Track Chair for the Master of Science in Sustainable Design (MSSD). She has been a member of the ACADIA Board of Directors since 2014-2018, and currently serves on the Editorial Board of *The International Journal of Architectural Computing (IJAC)*.

EPIPHYTE Lab is a design practice immersed in interdisciplinary research, testing material behaviors and design processes that directly engage the inevitable computerization of our environment, and provoke a series of critical questions about the overlaps between technology, environment and perception. Dana's designs explore the built environment at the intersection of ecology, computational processes, and systems analysis. In her research, she interrogates the relationship between design-space and ecology as it engages computational methods, thermodynamic processes, and experimentation with geometrically-driven performance logics. Her design work has been published internationally and presented at many academic conferences. In May 2018 Epiphyte Lab received the *Next Progressives* design practice award by *ARCHITECT Magazine*, *The Journal of The American Institute of Architects*.

Abstract:

Energy has both empirical and perceptual qualities. Dana's talk focuses on role of form in architecture to propose design strategies related to energy usage. Operating under the premise that complex geometries can be used to improve both the aesthetic and thermodynamic performance of passive heating and cooling systems, this line of inquiry tests the figuration of surfaces as primary actuators of heat transfer in thermal mass. The intention is to instrumentalize principles that offer a wider range of design tactics in the choreography of thermal gradients between buildings and their environment, while mitigating overuse of mechanical systems in buildings by offering insights into shape-making.

Billie Faircloth

Lecture Title: “Wait, What?”



Billie Faircloth is a practicing architect, educator, and Partner at KieranTimberlake, where she leads transdisciplinary research, design, and problem-solving processes across fields including environmental management, urban ecology, chemical physics, materials science, and architecture. She fosters collaboration between trades, academies, and industries in order to define a relevant problem-solving boundary for the built environment. Billie has published and lectured internationally on themes including research methods for a trans-disciplinary and trans-scalar design practices; the production of new knowledge on materials, climate, and thermodynamic phenomena through the design of novel methods, tools and workflows; and the history of plastics in architecture to demonstrate how architecture’s ‘posture’ towards trans-disciplinary practices and new knowledge has changed over time.

Abstract:

For more than a decade, KieranTimberlake has leveraged computation and simulation as a means to bridge gaps in architectural knowledge. As a transdisciplinary practice with individuals from fields as diverse as urban ecology, chemical physics, architecture, and sculpture, the firm’s models have become the means to explore design opportunities at the interface of disciplines and socialize knowledge normally bound to a single discipline. The firm’s modeling process is as much technical as it is social: It requires firm members to productively grapple with questions surrounding acceptable data sources, data coarseness and granularity, and levels of knowledge abstraction—simultaneously through the lens of multiple disciplines. KieranTimberlake Partner and Research Director Billie Faircloth will dissect examples of her firm’s models and share insights from ten years of pursuing a transdisciplinary modeling practice.



Stefano Schiavon

Lecture Title: **The Future of Thermal Comfort
in a Warming Climate**

Stefano Schiavon, PhD, is Associate Professor of Architecture at UC Berkeley and Associate Director of CEDR. Stefano's research is focused on finding ways to reduce energy consumption in buildings and, at the same time, increase occupant health, well-being and productivity. Stefano works on thermal comfort, radiant systems, occupant satisfaction, underfloor air distribution (UFAD), air movement, personal comfort systems and models, LEED, energy simulation and statistical modeling. At the University of Padova he received a PhD in Energy Engineering, and a MS in Mechanical Engineering. He has been a visiting scholar at Tsinghua University and DTU. He received the 2010 REHVA Young Scientist Award and 2013 ASHRAE Ralph Nevins Award

Abstract:

We spend most of our time in built spaces that substantially affect our health and well-being and the built environment has a large influence on climate change, mainly due to the energy we use to keep acceptable levels of indoor comfort. In this presentation, I will show that we are still systematically measuring high thermal dissatisfaction, even in green and high performance buildings, and that the thermal comfort models that we use for designing buildings have low prediction accuracy. How can we enhance occupant satisfaction without increasing our environmental impact? Personal comfort systems are individually controlled micro-environmental systems that improve thermal comfort to suit the needs of occupant. Personal comfort model is a new approach to thermal comfort modeling that predicts individuals' thermal comfort responses, instead of the average response of a large population and it can be applied to any HVAC system. Personal comfort systems and models have the potential to increase comfort and reduce energy use.

Dennis Shelden

Lecture Title: **Cyber-Physical Systems
and Open Data Platforms**



Dennis Shelden is an Associate Professor of Architecture and Director of the Digital Building Laboratory at Georgia Tech. He is an expert in applications of digital technology to building design, construction, and operations, with experience spanning education and research, technology development, and professional practice across architecture, engineering, and computing disciplines. He directs Georgia Tech's Ph.D. in Architecture and M.S. in Architecture: Building Information and Systems Concentration programs.

Prior to joining Georgia Tech, he led the development of architect Frank Gehry's digital practice, first as Director of R&D and Director of Computing, and subsequently as Co-founder and Chief Technology Officer of the technology spin off Gehry Technologies.

He was an Associate Professor of Practice in Computation and Design at MIT from 2005-2015 and has taught at UCLA and SCIARC. He holds a B.S. in Architecture, an M.S. in Civil and Environmental Engineering, and a Ph.D. in Architecture: Computation and Design from MIT, and he is a licensed Architect in California.

Abstract:

The past two decades have marked a proliferation of modeling and simulation capabilities in architecture, engineering and construction (AEC), enabling radical advances in efficiencies of production, expanded geometries, improved simulation capabilities, and cross process data exchange and collaboration. These advances provide the base capabilities for an emerging set of next generation advances, driven by the development of large scale, integrated digital-physical ("Cyber-Physical") systems, connecting the built environment to simulation and analytics in real time over cloud and IoT technologies. New research agendas that integrate information sciences, systems and sensing with traditional built systems design and engineering to support the development of scalable intelligent Cyber-Physical systems will be among the central drivers of next generation of the building industry. This presentation will focus on specific technical, organizational and cultural advances supporting the expansion of the AEC agenda into the design, delivery and operation of intelligent building systems and environments.

Experiential Climates

Sun and Wind: Integrated Environmental Performance Analysis for Building and
Pedestrian Comfort 3

Francesco De Luca

A Parametric Workflow to Conceive Facades as Indoor and Outdoor Climate Givers 11

Emanuele Naboni, Eric Danzo and Luca Ofria

“Streets, Parks & Plazas:
Analyzing Daylight in the Public Realm” 19

Elizabeth de Regt and Tomothy Deak



Sun and Wind: Integrated Environmental Performance Analysis for Building and Pedestrian Comfort

Francesco De Luca

Tallinn University of Technology

Tallinn, Estonia

francesco.deluca@taltech.ee

ABSTRACT

Solar access and pedestrian wind are important factors for the design of comfortable dwellings and livable urban areas. At the same time they influence the shape and image of cities. Daylight is the most appreciated source of building interiors illumination. Urban wind can significantly increase the discomfort of pedestrians for its mechanical action around buildings. In Estonia the daylight standard regulates access to sun light. Different pedestrian wind comfort criteria exist. This paper presents a research work which analyzes the performance of direct solar access according the Estonian daylight standard and pedestrian wind comfort according the Lawson criteria of 27 building cluster variations in the city of Tallinn. A method which integrates different building and urban performance analysis is developed. Results show different optimal patterns for each environmental performance, though significant trade-offs are found, and critical periods of the year for pedestrian wind comfort.

Author Keywords

Urban Design; Daylight; Solar Access; Wind Comfort; Environmental Analysis; Performance-driven Design.

ACM Classification Keywords

I.6 SIMULATION AND MODELING - Applications; J.5 ARTS AND HUMANITIES – Architecture; J.6

1 INTRODUCTION

Building interiors access to sun light constitutes an important factor for the shape of the urban environment. The renowned urban grid of the city of Barcelona, made of squared blocks to be occupied only on two opposite sides with orientations NE-SW or NW-SE, has been designed to favor solar access and ventilation in the dwellings [3]. Also the image of New York has been strongly influenced by the requirement of the New York Zoning Resolution of 1916 that made designers chose the characteristic terraced shape for the skyscrapers to permit sun light access to lower floors [22].

In the same way as sun light also wind influenced the urban layout of cities in history. The shape and streets pattern of the fortified center of Korčula in Croatia protects from

northerly cold winter winds and let the summer winds from east and west pass through and cool the buildings [10]. The plan of the city of Washington designed by Pierre L'Enfant in 1791 presents wide street axis that convey cooler air to city center from green belts and from the Potomac River through prevailing southerly breezes [2].

After having been undervalued for many decades, in recent years natural light has become increasingly important for energy saving and comfort concerns. Daylight is the most appreciated source of illumination of interiors of buildings for its capacity to penetrate the floor plan, render the objects with their true colors and create contrast between interior surfaces improving architectural quality [17]. Access to sun light improves not only the comfort of building occupants but also their physiological well-being through normally entrained circadian rhythms [15].

Contemporary cities alter climate at mesoscale and microscale. Even groups of few buildings can modify the physical environment related to solar radiation, temperature and wind flow, influencing urban comfort and quality of life. Urban wind alteration can be uncomfortable when it increases speed and generates eddies and gusts due to effects such as downwash and channeling [8]. Urban winds can cause high discomfort in the cold season due to lower perceived temperatures and in extreme cases the mechanical effect of increased wind speed can cause casualties [12].

Daylight regulations exist to guarantee the healthiness and comfort of dwellings and working environments. Solar access is regulated in Estonia by the standard “Daylight in Dwellings and Offices” [6]. It requires that in new dwellings at least one room receives 2.5 hours of direct sun light every day between 22nd of April to 22nd of August.

Different wind comfort criteria exist [9]. Some consider a single wind speed threshold and different frequencies of occurrence, others are mainly based on different wind velocity thresholds. The Lawson comfort criteria is based on pedestrian activities, wind threshold values for each activity and probabilities of exceedance [13].

Different studies investigate the relation of urban morphology, wind profiles and solar access. Straight streets and parallel buildings facilitate air flows whereas narrow street and staggered buildings reduce wind velocity [20]. Studies conducted for latitude 48° show that linear buildings with different orientations receive larger direct solar radiation than block buildings. Open blocks favor ventilation of internal areas and L-shaped buildings protect pedestrian from strong winds [16]. Solar radiation, surface temperature and wind simulations conducted on different building patterns in the city of Zürich during warm season show that aligned blocks morphology cause smaller air temperature than line and court building morphologies [1]. Nevertheless are still scarce the research works about the integration of building and urban performance in northern Europe.

Architects and planners are urged to improve the performance of buildings and urban environments for comfort of dwellers. The present study investigates residential building patterns in the urban environment for direct solar access according the Estonian daylight standard and for pedestrian wind comfort in the city of Tallinn. Since in Estonia is not present a wind comfort regulation, for this study is used the LDDC variant of the Lawson comfort criteria that is the industry standard for mechanical wind comfort assessments for new developments [14].

2 METHODS

The study is conducted through the parametric model of a cluster of buildings located in the city of Tallinn, Estonia (Lat. $59^\circ 26' N$ Lon. $24^\circ 45' E$). Different variations are generated and for each one sun light hours analysis and wind velocity analysis through Computational Fluid Dynamics (CFD) are performed. The results of the first analysis are used to assess compliance of the different building cluster variations with the direct solar access requirement of the Estonian daylight standard. The results of the second analysis are used to assess pedestrian wind comfort of the areas around and between the buildings of each cluster.

For the study the software Grasshopper for Rhinoceros [18] is used to build the parametric model of the building clusters and the surrounding urban environment, to automate sun light hours analysis and wind comfort assessment using the plug-in Ladybug Tools [11] and to build the parametric model to perform CFD simulations with the validated software OpenFOAM [19] using the plug-in Swift [21].



Figure 1. The area and the lot (in red) used for the study.

2.1 Urban Area

The empty lot used for the study is located in the city of Tallinn, in the Soviet era quarter of Lasnamäe (Figure 1). The area is populated mostly by panel housing buildings about 29m in height, malls and warehouses about 12m in height. On the northern edge of the area a quarter of family houses of 2 floors begins. The reason to choose this location is that in recent years different in-fill developments are in progress.

2.2 Building Clusters

For the study 3 types of building cluster pattern are used: grid, staggered and irregular (Figure 2). All of the 9 buildings of the cluster are 18m in height and have the same footprint size of 36m x 12m except the staggered pattern that presents 2 smaller buildings with footprint size 12m x 12m for a total of 10. For the staggered pattern one building is split in two parts to keep the building density consistent with the others. The building size and patterns selected are common typologies for new developments in Tallinn.

The lot is 180m x 126m in size. For the 3 cluster buildings 3 incremental distances and 3 orientations are used for a total of 27 variations used in the study. The distances used for the grid pattern are 12m, 18m and 24m (small, medium, large). For the staggered pattern the same distances are used except for the two smaller buildings that are located at 9m, 12m and 12m from the closer one for the three variations. The distances between the buildings of the irregular pattern vary from 9m to 27m, increasing for the 3 variations. The distances from the lot limit vary inversely from 24m to 12m for all the pattern types. Building density FAR value is 1.03, ratio between building footprints and plot area is 0.17.

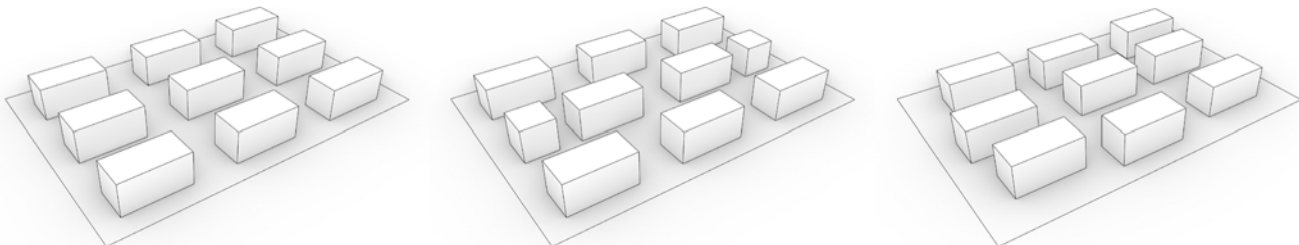


Figure 2. The three building cluster patterns used in the study: grid (left); staggered (center); irregular (right). Plan diagrams of building cluster patterns are presented in the wind flows and velocity plots of Figure 5 and in the wind comfort maps of Figure 7.

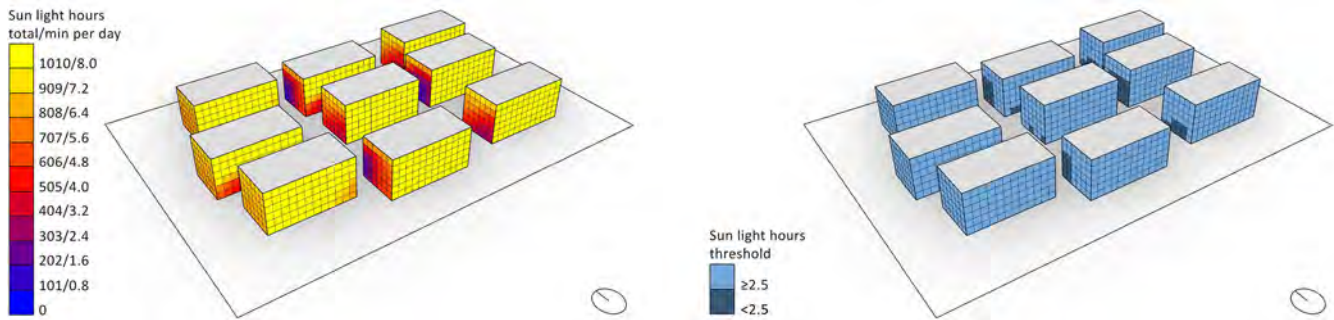


Figure 3. Sun light hours analysis (left) and computation of façade portions fulfilling the Estonian daylight standard (right) for the building cluster type irregular, distance small and orientation 0°.

The 3 orientation variations of the building clusters are 0°, 45° and 90° clockwise using the long side of the lot aligned east-west for the 0°. All the 27 variations are used to evaluate building and urban performance of direct solar access and pedestrian wind comfort of the pattern types, distances between buildings and orientations.

2.3 Direct Solar Access Analysis

For the assessment of direct solar access performance of the different building cluster variations in relation to the Estonian daylight standard requirement an algorithm composed of four main parts is realized. It is based on computational methods for the assessment of façade solar access performance developed by recent research [4, 5].

The first part of the algorithm generates the analysis grid on the building facades. The building models are polysurfaces or meshes. The algorithm extracts the vertical faces and subdivides them in grid of cells 3m x 3m in size, the standard floor to floor distance for residential buildings. The algorithm generates as well wall thickness to take into account a dead angle of 10° as required by the standard.

The second part of the algorithm uses an off-the-shelf component of the plug-in Ladybug Tools to generate the sun path for the city of Tallinn and the sun positions for the required period from 22nd of April to 22nd of August. For the analysis a time step of 2 is used, determining in this way the sun positions every 30 minutes and the relative sun vectors.

A second off-the-shelf component calculates the quantity of sun light hours, and portion of hours, that each façade grid cell receives during the analysis period, using the sun vectors (Figure 3). The shading context used in the calculations are the cluster and existing buildings. The output of the sun light hours analysis is a list of 4172 0s and 1s for each cell indicating when the sun is not or is visible during daytime.

The fourth part of the algorithm subdivides the list of 4172 results in 123 day durations, computes if each cell receives every day at least 2.5 sun light hours and calculates the total façade ratio fulfilling the requirement (Figure 3). Finally the algorithm automates the solar access analysis of all the 27 cluster variations selecting automatically all the possible combinations of pattern type, buildings distance and orientations.

2.4 Wind Analysis

For the assessment of pedestrian wind comfort of the areas around and between the cluster buildings, wind velocities are obtained through CFD simulations using the validated software OpenFOAM for each of the cluster variations. The simulations are performed following recommendations of best practices [7] and the methods used by the plug-in Swift to build the computational domain and the parametric model for CFD simulations in Grasshopper.

The computational domain mesh, built almost entirely by hexahedral cells, has dimensions 1328m x 1328m x 288m (Figure 4). Buildings in the range of 500m are modeled. The height of the domain is 10h (being h the height of the tallest modeled building) to allow considerable distance between the roofs and the top of the computational domain in order to avoid air acceleration above the buildings. The squared domain has the same extensions in the flow direction of about 20h. The considerable upstream length (northerly) permits flow establishment and the downstream length (southward), that best practices recommend of a minimum of 15h, permits redevelopment of flows in the wake region.



Figure 4. The domain used for CFD simulations. In the center the area of interest characterized by a highly refined mesh surrounded by context buildings for which a larger refinement mesh is used.

The mesh of the computational domain is built using cells of 16m and is refined in areas where higher accuracy is needed to guarantee adequate quality of results. The context buildings refinement level is 2, which reduces the cells size around the existing buildings to 4m, the area of interest refinement level is 3, which reduces the cells size around the cluster buildings to 2m and the refinement level of the cluster plot is 4, which generates cells of 1m in size for the cluster ground, where the highest accuracy is needed.

After the construction of the computational domain mesh 16 CFD simulations are run through the Virtual Wind Tunnel (VWT), a cylindrical domain mesh extension that the plug-

in Swift builds around the main domain. This way the domain meshing process is performed only one time for all the wind directions. The 16 CFD simulation directions, one every 22.5° clockwise starting from north (0°), guarantee an adequate level of accuracy to account for the diversity of wind patterns in an urban environment during long period of analysis such as a month or the entire year.

For all the CFD simulations is used a fixed velocity of 5m/s. The value of roughness length of the terrain used is the one for urban areas $Z_0=1$. The obtained wind velocities from the 16 directions are finally probed on a grid of 1872 cells 3m x 3m in size placed at 1.5m from the ground (Figure 5).

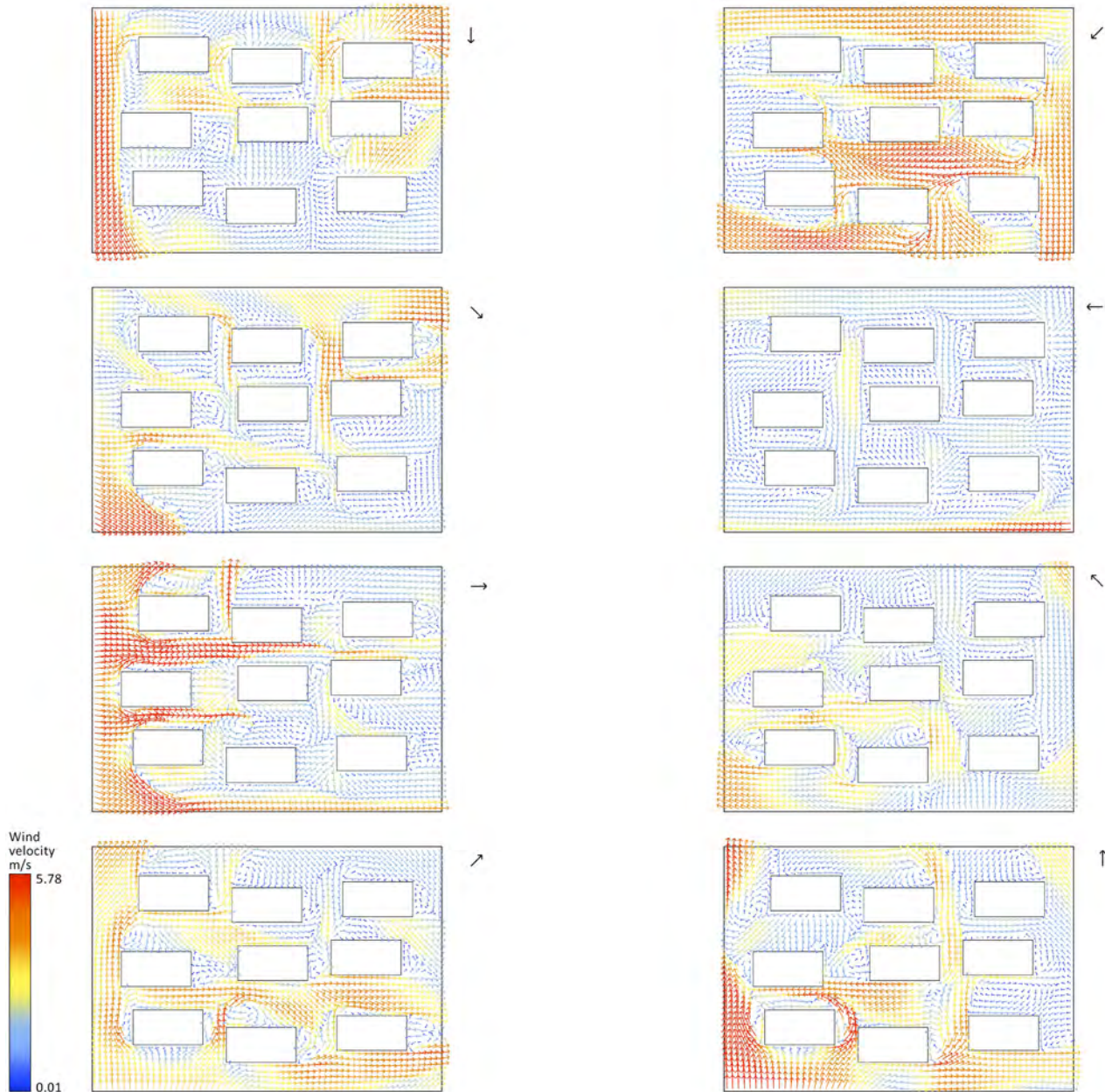


Figure 5. Plots of the wind flows and velocities for the cluster buildings of the pattern type irregular, distance medium and orientation 0° of 8 out of 16 CFD simulation directions obtained with fixed velocity 5 m/s at the inflow boundary of the domain.

2.5 Wind Comfort Assessment

The LDDC variant of the Lawson comfort criteria used for this study through a specific component of the environmental design plug-in Ladybug Tools presents 5 categories of wind comfort (Table 1). Each category presents a different wind velocity threshold and all the categories consider the same probability of exceedance.

Each category is indicated by the criteria for a specific type of pedestrian activity. The probability of exceedance used by the criteria for all the comfort activities is 5% to account for infrequent occurrences of wind velocities. The LDDC Lawson pedestrian comfort criteria presents as well wind danger criteria characterized by different categories. For the present study only the wind comfort criteria is used.

Category	Comfort activity	Threshold Wind Velocity (m/s)
1	Sitting	4
2	Standing	6
3	Walking	8
4	Business walking/Cycling	10
5	Uncomfortable for all activities	>10

Table 1. Categories and wind thresholds of the LDDC Lawson pedestrian comfort criteria.

Category 1 is suitable for areas such as parks with benches, restaurants and cafes terraces. Category 2 is indicated for building entrances, playgrounds and bus stops. Areas belonging to category 3 can be used for street sidewalks, window shops and paths. Category 4 areas are not suitable for quiet and leisure pedestrian activities such as those already mentioned but can be used only for fast walking or cycling. Category 5 is uncomfortable for all types of pedestrian activities.

Wind factors are generated by dividing the 16 wind velocities obtained for each of the 1872 points of the grid of the area of interest for each building cluster variation through CFD simulation with the meteorological wind speed at reference height of the Tallinn weather data. Consequently the component uses the wind factors and the hourly values of wind velocity and direction from the weather data to determine one wind velocity for each point of the grid and the relative comfort category.

The comfort category value of each grid cell is used to generate pedestrian comfort maps color coded on the basis of the 5 categories of the LDDC variant of the Lawson comfort criteria (Figure 7). Finally a script developed by the author is used to compute the ratio of the quantity of cells for each category and to determine a single comfort performance value for each building cluster variation.

3 RESULTS

Results of the study are presented for direct solar access and pedestrian wind comfort for all the 27 building cluster variations and performance are analyzed. The solar access performance is the total buildings façade ratio fulfilling the Estonian daylight standard requirement of 2.5 hours of daily direct sun light between 22nd of April and 22nd of August.

The pedestrian wind comfort assessments are performed for the entire year and for two months with opposite conditions, March and July. In Tallinn March is the windiest month and one of the coldest of the year (Figure 6). The discomfort due to wind mechanical action is significantly increased by the thermal discomfort due to wind chill effect. July is one of the months with the least wind velocity and the warmest of the year. Though in July temperatures do not constitute harm it is of interest include this analysis period in the study.

The acronyms of the 27 variations use the cluster type names grid (G), staggered (S) and irregular (I), the building distances small (S), medium (M) and large (L) and the orientations 0° (0), 45° (45) and 90° (90).

3.1 Direct Solar Access

The performance of direct solar access range from 54.7% for variation GS0 to 85.7% for variation GL45 (Figure 8). The cluster type with the highest solar access is G with 5 more performative variations out of 9 comparing 3 for I and 1 for S. The largest difference between same variation of different cluster types is that between GL90 and IL90 having the first 9% more of total façade area fulfilling the requirement.

As expected variations with building distance L have better performance, second M and last S. The difference of performance is larger between variations of type G, being the largest 31.4% between variations GL90 (more performative) and GS90. For the cluster type S the largest difference is 27.1% between variations SL90 and SS90. For cluster type I differences are smaller being 14.3% between variations IL0 and IS0 the largest. The orientation of buildings has a significant effect on solar access. For 8 out of 9 variations the orientation 45 has the best performance (as there is no façade exposed toward north) comparing 1 for 90 and none for 0. The largest increment per cluster type are 28.5% between GL45 and GL0, 26.9% between SL45 and SL0 and 22.7% between IL45 and IL0.

A small flaw of the presented comparisons is due to the slightly larger total façade area of the staggered type. Nevertheless this do not influence significantly the results.

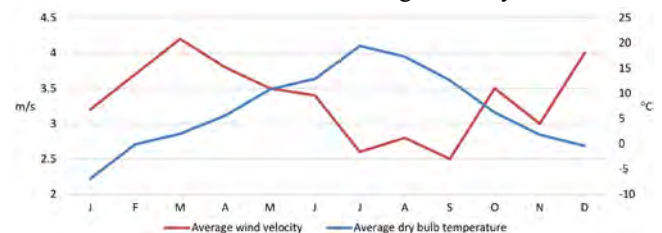


Figure 6. Monthly averages of wind velocity and temperature for the city of Tallinn.

3.2 Pedestrian Wind Comfort

Wind comfort assessment is done using grids of 1872 squared cells 3m in size for the 27 building cluster variations. As already discussed, assessments are performed for the entire year and for the months of March and July.

For each variation a comfort map is generated using the 5 categories of the LDDC Lawson criteria and the grid area ratio of each category is calculated (Figure 7). For the entire year all the 27 variations have significantly larger area ratios of LDDC Lawson categories 1 and 2, and smaller areas of category 3 (Figure 7). For the month of March due to higher wind velocities, comparing the entire year all the 27 variations have smaller areas of LDDC Lawson category 1 and 2, significantly larger areas of category 3, present small areas of category 4 and in few variations also very small areas of category 5. The only two LDDC Lawson categories for the month of July are 1 and 2 due to very low wind velocities during this period (Figure 7).

For the entire year patterns performance are assessed through a wind comfort level (WCL) bare number obtained multiplying the area ratio of each category by a factor (Table 2), to decrease the comfort level of variations with stronger wind odds. The highest possible WCL is 100 (all area cat. 1).

Category	1	2	3	4	5
Multip. factor	1	0.5	0.33	0.25	-1

Table 2. Factors for pedestrian wind comfort comparisons.

For the month of March cluster patterns performance are assessed through the ratio of plot areas of LDDC Lawson criteria category 1, to guarantee maximum comfort against strong and cold winds. For the month of July category 2 is used because being the warmest of the year faster breezes decrease potential thermal discomfort. For the assessments higher area ratio indicates better performance.

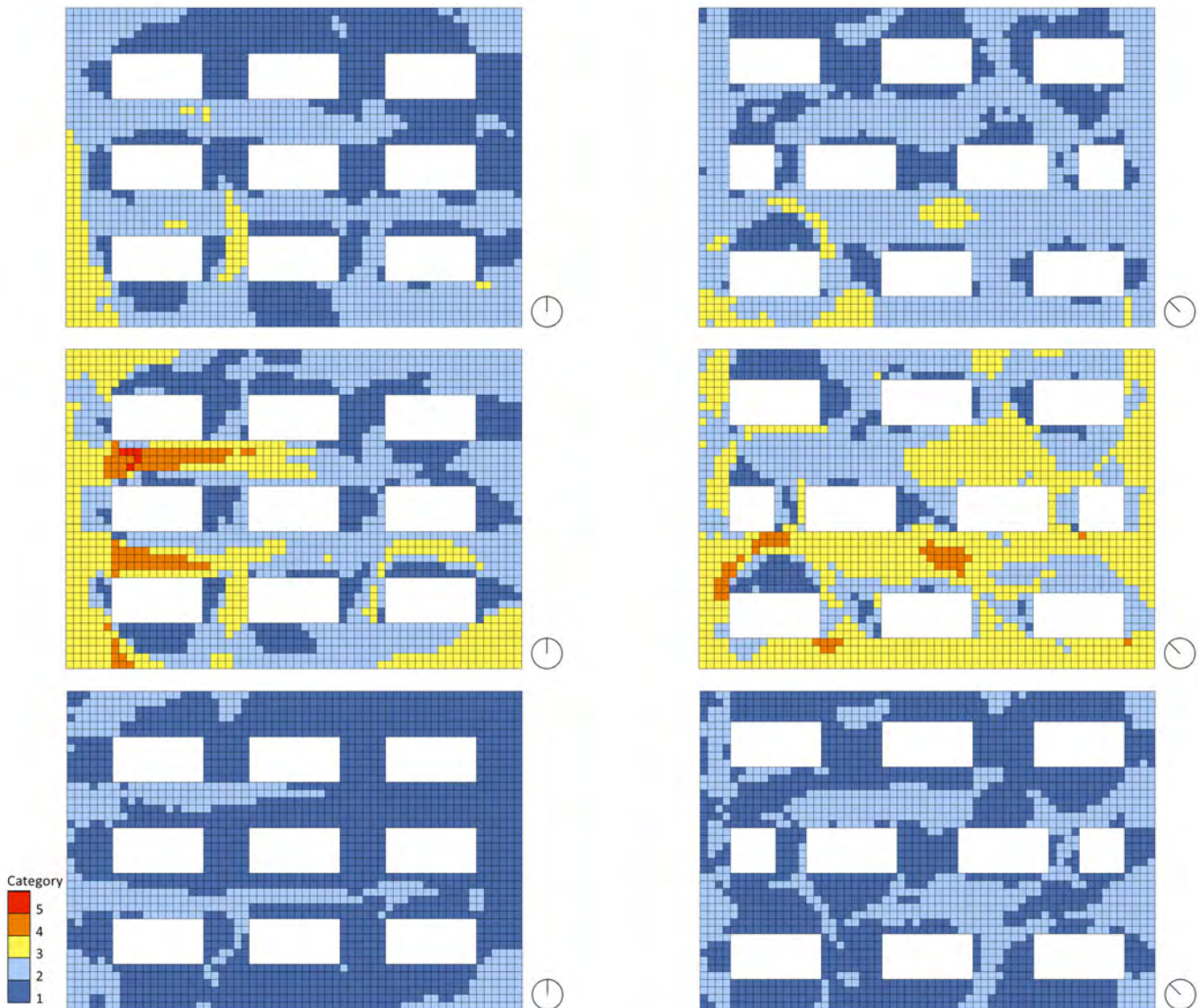


Figure 7. Wind comfort maps for variations LGM0 (left) and LSL45 (right) for the entire year (top), March (middle) and July (bottom).

For the entire year wind comfort levels (WCL) range from 63 to 76.3 for variations GL45 and IL90 respectively (Figure 8). The most performative patterns are S and I. Evidence show no significant difference among building distances. Most performative orientation is 0 (Table 3).

For the analysis period of March plot area ratios of LDDC Lawson criteria category 1 range from 9.6% to 31% of variations SM45 and IS90 respectively (Figure 8). The most performative pattern is I and building distance is S. Most performative orientations are 0 and 90 (Table 3).

For the analysis period of July the plot area ratios of category 2 range from 16.7% to 36.6% of variations IL90 and SL45 respectively (Figure 8). Evidence show no significant difference among patterns. The most performative distances are M and L and orientation is 45 (Table 3).

	Pattern			Build. Dist.			Orientation		
	G	S	I	S	M	L	0	45	90
All year	-	4	5	3	4	2	6	-	3
March	1	3	5	6	2	1	5	-	4
July	2	4	3	1	4	4	3	5	1

Table 3. Number of more performative variations (max. 9).

3.3 Integrated Performance Results

For the entire year integrated results show no optimal solution for both performance of direct solar access and pedestrian wind comfort. Nevertheless evidence show that best trade-offs exist (Figure 8). These are relative to building clusters of all the three patterns, size L and orientation 90°. Patterns SM0 and IM0 are significant trade-offs as well.

Also for the analysis period of March integrated performance results show there is no optimal pattern for both the analyzed environmental performance, though trade-offs exist. Evidence show that best trade-offs for the analysis periods of entire year and month of March are consistent, inasmuch for the latter all the patterns size M and L, and orientation 90 present the best balance of performance (Figure 8).

For the month of July, though an optimal solution is not present, evidence clearly identify best trade-offs with orientation 45 and size L for all the cluster patterns and for variation SM45 (Figure 8). The difference of best trade-off orientations between all year and March, and July is due to similar prevailing wind directions for the first two periods.

Considering the analysis periods entire year, being the most inclusive, and March, being the most critical for urban comfort in Tallinn, integrated performance results indicate the building cluster distance Large, orientation 90° and all the patterns Grid, Staggered and Irregular as those with the best trade-off performance. Significant trade-offs are also those of the same patterns and orientation with distance Medium. These finding suggest that for the analyzed location and building cluster, distance and orientations are more important characteristics than pattern layout.

4 CONCLUSIONS

The presented study analyzes direct solar access and pedestrian wind comfort performance of building clusters located in an urban environment in the city of Tallinn, Estonia. The aim is twofold. On one side develop a method for the integration of different building and urban performance analysis. On the other investigate optimal cluster configurations or best trade-offs. The performance benchmarks used in the study are the direct solar access

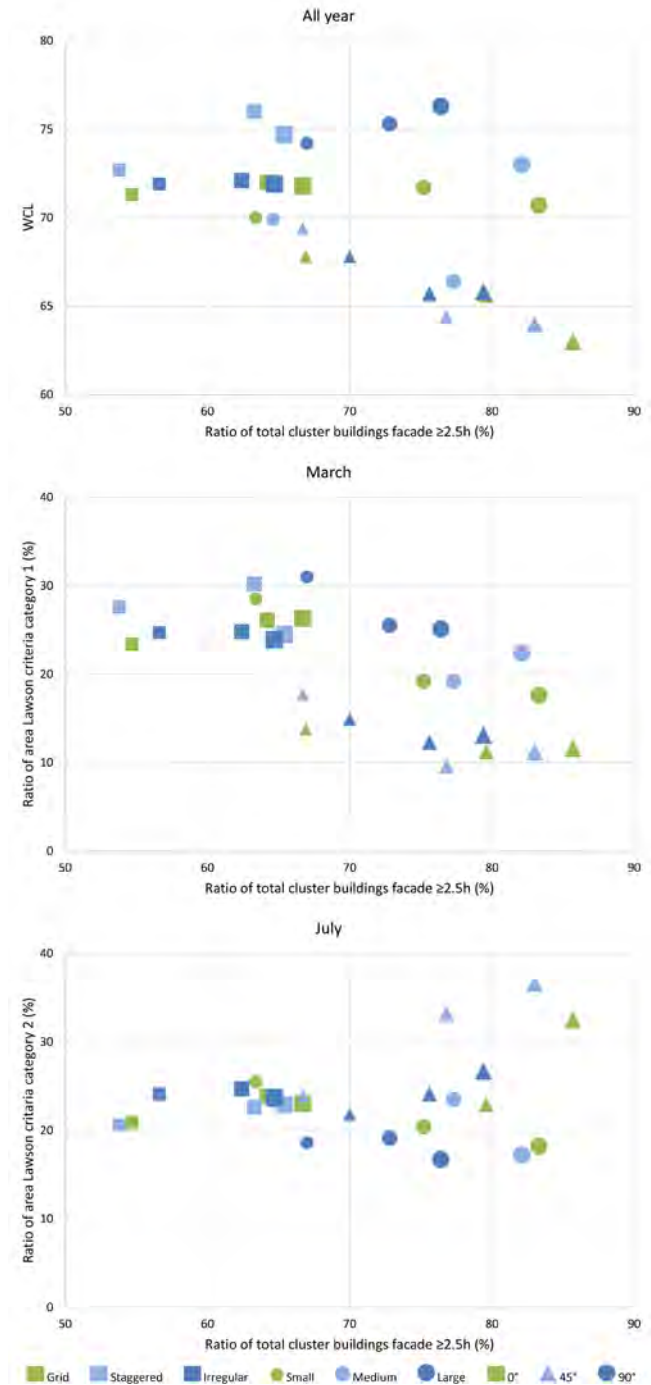


Figure 8. Integrated direct solar access and pedestrian wind comfort results for the 27 building cluster variations.

requirement of the Estonian daylight standard and the LDDC variant of the Lawson pedestrian wind comfort criteria.

A parametric model is realized to generate 27 building cluster variations different for pattern, distances and orientation, to perform sun light hours analysis and compute façade performance, to run CFD simulations and compute pedestrian wind comfort. The realization of a single parametric model has proven an efficient method to integrate building and urban performance investigations. The method will be developed in a tool to be used by designers to improve the comfort of buildings and livability of urban open spaces.

Results show that for solar access the building cluster type Grid with largest distance between buildings and orientation 45° is the most performative. For pedestrian wind comfort during the entire year and the month of March patterns Staggered and Irregular with orientations 0° and 90° are the most performative, whereas for July patterns Grid and Staggered with orientation 45° perform better. Evidence show that though optimal solutions are not present, best trade-offs are found for all three cluster patterns with distance Medium and Large and orientation 90°. These findings are actionable insights to be used by designers to increase the comfort of new residential areas in Tallinn.

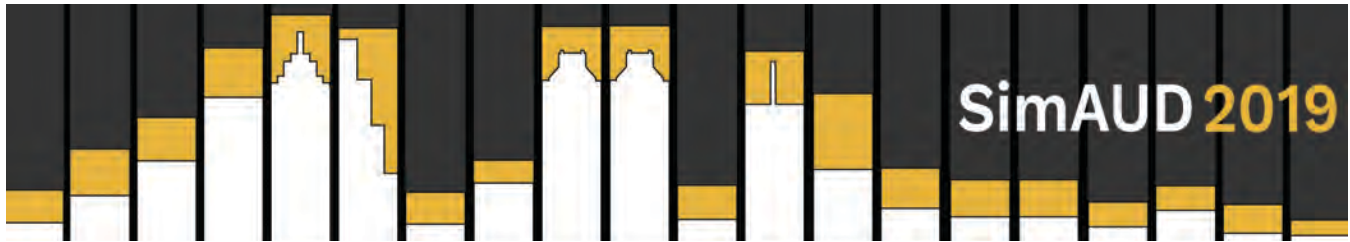
Results show also critical discomfort during March, during which plot areas are suitable only for fast walking or uncomfortable for all activity types, underlining the importance of wind comfort analysis to conveniently locate building entrances, paths and playgrounds. The study will be used to raise Estonian government's awareness of the adoption of wind comfort regulations for new developments. Future work is to perform the investigations using a larger number of building patterns located in different areas of the city and integrating urban thermal comfort analysis.

ACKNOWLEDGEMENTS

The research has been supported by the European Regional Development Fund grant ZEBE 2014-2020.4.01.15-0016.

REFERENCES

1. Allegrini, J., Dorer, V. and Carmeliet, J. Influence of morphologies on the microclimate in urban neighbourhoods. *Journal of Wind Engineering & Industrial Aerodynamics* 144, (2015), 108–117.
2. Brown, G.Z. and DeKay, M. *Sun, Wind and Light. Architectural Design Strategies*. 2nd edition, John Wiley & Sons, New York, USA, 2001.
3. Coch, H.R. and Curreli, A. Solar access in the compact city: a study case in Barcelona. *Proc. PALENC 2010*.
4. De Luca, F. and Voll, H. Computational method for variable objectives and context aware solar envelopes generation. *Proc. SIMAUD 2017*, 335-342.
5. De Luca, F. Solar Form-finding. Subtractive Solar Envelope and Integrated Solar Collection Computational Method for High-rise Buildings in Urban Environments. *Proc. ACADIA 2017*, 212-221.
6. Estonian Centre for Standardization. *Daylight in Dwellings and Offices. 894:2008/A2:2015*, EVS, Tallinn, 2015.
7. Franke, J., Hellsten, A., Schlünzen, H. and Carissimo, B. *Best Practice Guideline for the CFD Simulation of Flows in the Urban Environment*. COST Office, Brussels, Belgium, 2007.
8. Gendemer, J. *Discomfort Due to Wind Near Buildings: Aerodynamic Concepts*. U.S. Department of Commerce, National Bureau of Standards, Washington, US, 1978.
9. Janssen, W.D., Blocken, B. and vanHoff, T. Pedestrian Wind Comfort Around Buildings: Comparison of Wind Comfort Criteria Based on Whole-flow Field Data for a Complex Case Study. *B. and Env.* 59, (2013), 547-562.
10. Krauthelm, M., Pasel, R., Pfeiffer, S. and Schultz-Granberg, J. *City and Wind. Climate as an Architectural Instrument*. DOM publishers, Berlin, Germany, 2014.
11. Ladybug Tools. <https://www.ladybug.tools>. As of 6 February 2019.
12. Lawson, T.V. and Penwarden, A.D. The Effects of Wind on People in the Vicinity of Buildings. *Proc. Int. Conf. on Wind Effects on Build. and Str.* 1975, 605-622.
13. Lawson, T.V. The Wind Content of the Built Environment. *J. Ind. Aerodynamics* 3, (1978), 93-105.
14. Lawson, T.V. *The Determination of the Wind Environment of a Building Complex Before Construction*. Department of Aerospace Engineering, University of Bristol, TVL/9025, Bristol, UK, 1990.
15. Lockley, S.W. Circadian Rhythms: Influence of Light in Humans. In: *Encyclopedia of Neuroscience*, Academic Press, Cambridge, USA, 2009, 971-988.
16. Okeil, A. A holistic approach to energy efficient building forms. *Energy and Buildings* 42, (2010), 1437-1444.
17. Reinhart, C.F. *Daylighting Handbook I. Fundamentals. Designing with the Sun*. MIT Press, Cambridge, USA, 2014.
18. Rhinoceros and Grasshopper. <https://www.rhino3d.com>. As of 6 February 2019.
19. Robertson, E., Choudhury, V., Bhushan, S. and Walters, D.K. Validation of OpenFOAM Numerical Methods and Turbulence Models for Incompressible Bluff Body Flows. *Computer and Fluids* 123, (2015), 122-145.
20. Shishegar, N. Street Design and Urban Microclimate: Analyzing the Effects of Street Geometry and Orientation on Airflow and Solar Access in Urban Canyons. *J. of Clean Energy Tech.* 1, 1 (2013), 52-56.
21. Swift. <https://www.ods-engineering.com/>. As of 6 February 2019.
22. Willis, C. *Form Follows Finance. Skyscrapers and Skylines in New York and Chicago*. Princeton Architectural Press, New York, USA, 1995.



A Parametric Workflow to Conceive Facades as Indoor and Outdoor Climate Givers

Emanuele Naboni, Luca Ofria and Eric Danzo

Institute of Architecture and Technology,
The Royal Danish Academy (KADK)
Copenhagen, Denmark
Emanuele.naboni@kadm.dk

ABSTRACT

Within the bounds of climate change, it is legitimate to expect that buildings will be developed to mitigate and adapt to environmental transitions. In this context, façades are essential as they are not the only determinants in reducing energy demand, but could increase the livability of indoor and outdoor spaces. Being that there are several simulation tools which allow indoor comfort simulation, and a few that enable outdoor comfort simulation, it is rare to find tools that allow simulation of both. Filling this particular gap, the present research develops a Ladybug Tools based digital workflow, which simultaneously accounts for the indoor and outdoor thermal and visual effects of façade designs. Once created, the workflow is tested and calibrated against indoor and outdoor Mean Radiant Temperature and Illuminance measurements, via the use of a test room equipped with sensors. It is concluded that the workflow is a reliable tool for the design of façades intended as a dual climate giver, for both the indoor and the outdoor.

Author Keywords

Climate change, urban design, façade, test room, indoor comfort, outdoor comfort, mean radiant temperature, illuminance, Ladybug Tools

1 INTRODUCTION

Cities are being densified with a rate that is proportioned with population growth. It is estimated that since 2016, 54,5% of the world's population lives in urban areas. For 2050 it is estimated this percentage will increase up to 60%. Climate change is happening because of higher levels of emissions, increasing CO₂ levels and greenhouse gases in the atmosphere [1]. This makes it imperative to focus on microclimate design in order to raise people's health and wellbeing [2].

Because of this fast-paced climate change, the architectural guild is gradually shifting its interest into the impact of architectural design on outdoor thermal comfort. Enhancing the health and well-being of citizens, reducing heat and cold

stress, and prolonging periods of comfort in outdoor spaces, are among the new focuses on design. This is sustained by a few investigations have shown the potential of design towards altering the local microclimate [3]. More specifically, previous literature has shown that façades characteristics can influence the way heat and light are absorbed and reflected or re-emitted towards the outdoor [4]. Other researches discuss the influence of façades on the outdoor daylighting environment [5].

The façade is thus a primary element that thermally and visually connects or establishes bounding flows between the outdoor and in the indoor environment. Designing to optimize the thermal comfort in both the indoor and the outdoor could be a crucial role, and the façade could be intended as a dual climate giver. However, following the several studies affirming that people spend more than 90% of their time indoors [6], most of the research in the field has primarily focused on the internal comfort as the only issue to address via design (the control of interior thermal comfort gained a certain attention from the 1930s) [7] and it keeps its central role [8, 9].

There is certainly a lack of research regarding the impact of facades toward the outdoor climatic and visual conditions [10]. It is thus a rare finding to encounter in literature the concept of a façade as a climate giver for both indoor and outdoor [11, 12]. The current research focuses on facilitating the design of temperate outdoor climates ensuring that people will spend more time outside their offices and houses [13]. The focus is thus on create a digital workflow that allows for the design of façades that are intelligently supporting the orchestration of indoor and outdoor thermal and visual qualities. More in detail, the present research assembles a series of Ladybug Tools scripts in a comprehensive digital workflow that allows testing façade solutions effects on the indoor and the outdoor and compare it against real-life measurements.

2 BACKGROUND

In recent years, interest in outdoor thermal comfort continued to rise, and the demand for passive, comfortable urban microclimates increased alongside global city growth [14]. The need for simulating and mapping these microclimates has also increased [15]. While the building simulation field possesses several tools and methods for evaluating indoor comfort to high spatial and temporal resolutions, there is a need for comprehensive methods for evaluating outdoor comfort to the same degree of accuracy [16]. As outdoor thermal fluxes are considerably diverse spatially and temporally, determine outdoor comfort in urban environments with various surface conformations is still a challenge.

The definition of the surrounding surfaces properties, solid angle proportions, and the measurement of short and longwave radiation fluxes reaching the human body are the main calculation issues. Some modelling tools try to solve such complexity. Previous research [17,18, 19] has discussed those that could be used by designers: CitySim-Pro, ENVI-met, Autodesk Thermal CFD, Grasshopper plug-ins Ladybug Tools. When referring to the modelling of façade implication toward the outdoor and the indoor, most of these tools are disconnected and could not be coupled. Recently Ladybug Tools [20] has introduced workflows that allows the simulation of outdoor physical conditions, thus becoming a set of designer-friendly tools that potentially allows for a comprehensive analysis of both indoor and outdoor qualities [21]. Ladybug Tools allows the use of different simulation engines and their dynamic coupling.

At the time of writing two gaps are found that could be addressed by the current research. The first is that a complete script that iteratively and dynamically allows the modelling of the thermal and visual comfort implications of the design of façades, for both indoor and outdoor, has not been assembled yet. There are separate scripts for indoor and outdoor Mean Radiant Temperature, but these are not coupled when targeting the design of facades. As well, indoor and outdoor illuminance studies are conducted separately. The research thus aims at filling such gaps by creating a user-friendly parametric workflow that aids the design of façade intended as an external and internal climate giver.

The second gap is that the Ladybug Tools workflow for outdoor comfort has not yet been validated against a set of outdoor thermal and light measurements. Being that the workflow developed in the paper is novel by coupling indoor and outdoor, it is essential to validate it. Whereas the indoor calculation is made with validated engines invoked by Ladybug Tools, the customised and complex combination of several engines and scripts used by Ladybug Tools for the outdoor comfort calculation is not validated yet. It is thus critical to verify simulated data against measured ones. Working with test rooms and physical sensors allows the calibration and preliminary validation of the workflow.

3 METHODOLOGY

A three-phase approach is established. The first phase consists of measuring indoor and outdoor thermal and daylight parameters on a dedicated test room. The second phase is the creation of the “Façade thermal and visual, indoor and outdoor” Ladybug Tools based simulation workflow. This is achieved by assembling and customising existing scripts. The third phase consists of comparing the scripts against the measured data and perform a preliminary validation. In the discussion the outcomes of the three phases are reviewed showcasing the capabilities of the script when applied to the design of façades intended as outdoor and indoor climate givers.

3.1 Setting up the Test Room

The test room used for this research is located within the campus of the Royal Danish Academy of Fine Arts (KADK) (Figure 1). Data were recorded between the 20th and the 23rd of September 2018. The dimensions of the test room are 5,5x2,7x7,9 meters, and the façade faces south-east (Figures 2, 3). The measuring tools are placed as if follows: one inside at point A, and one outside at point B (Table 1). The location of points resembles the position of a person in the room operating close to the façade and of someone being on the outside in the proximity of the façade.



Figure 1. Campus and test room location in red.

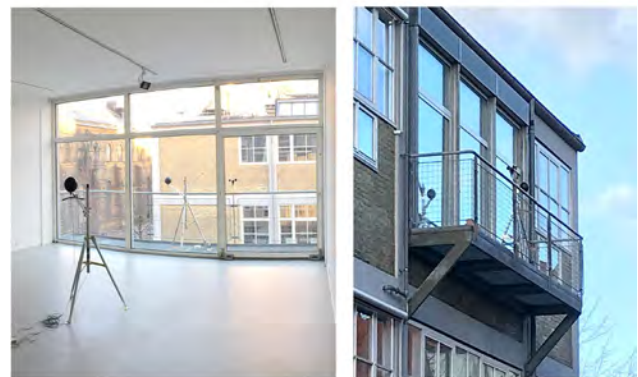


Figure 2. A view from the test room (on the left) and a view of the balcony (on the right).

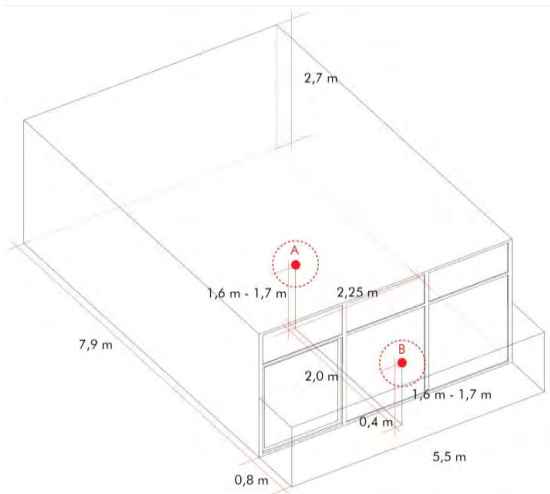


Figure 3. Test room and testing points.

	Tool	Type	A	B	Unit
1	Kimo Black Ball Thermometer	Sensor	x	x	Mean radiant temperature
2	HOBO U12-U21	Data Logger	x	x	Dry Bulb Temperature, Relative humidity, Light intensity
3	HOBO SLIB-M003	Silicon pyranometer 3m cable	x	x	Solar radiation
4	HOBO S-WSB-M003	Sensor		x	Wind Speed

Table 1. Tools used for measurements.

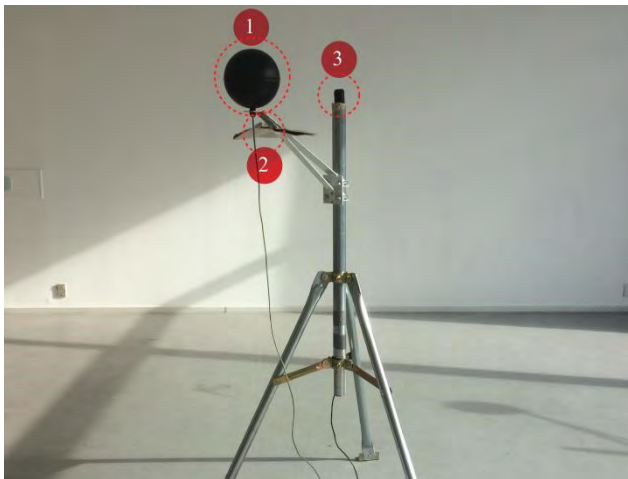


Figure 4. Point A, indoor measuring tools. For explanations refer to Table 1.

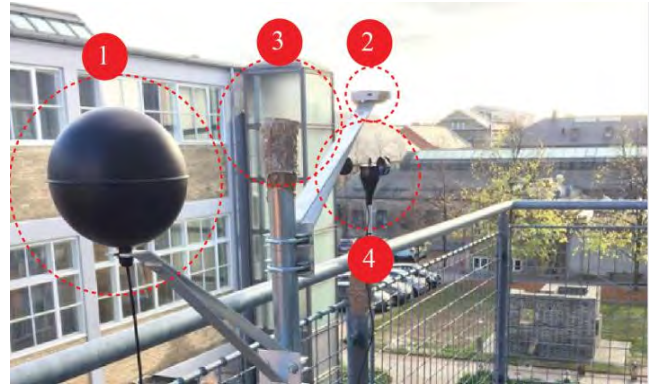


Figure 5. Point B, outdoor measuring tools. For explanations refer to Table 1.

3.2 Simulation Workflow

The simulation process comprises daylighting and thermal scripts for indoor and outdoor. These are associated with two types of input geometry: one that is geometrically accurate for daylighting modelling, and one simplified in thermal zones for thermal modelling. Both models are comprehensive of the campus context. The campus is modelled in order to account for light reflections and shading (Figure 6). The campus is also included in the thermal model so that outdoor short and longwave radiation could be accounted for. All the surrounding buildings, free-standing surfaces and the ground temperature are thus calculated. Both simulations are performed based on a customised weather file created with the use of local data collected by a weather station located on the KADK campus.

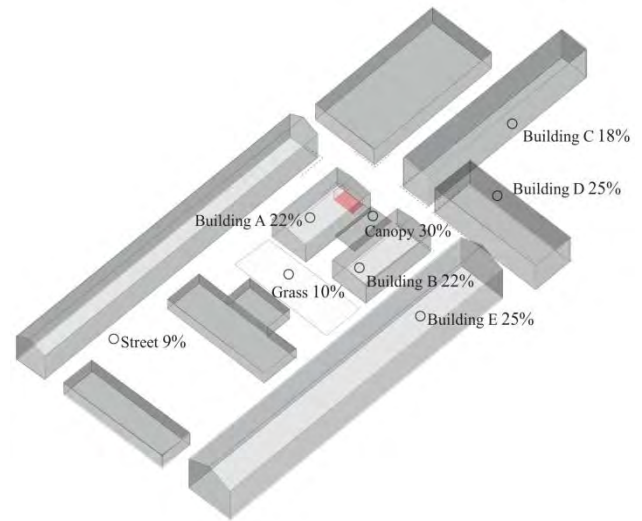


Figure 6. Building and surrounding model including reflectance values of surfaces.

3.3 Indoor Thermal Model Characterization

The script described in Figure 6 runs a daylighting simulation which used to calculate hourly illuminance values in point A and point B. It was developed customising Honeybee to account for both outdoor and indoor illuminance values (lux). Honeybee supports detailed daylighting modelling based on Radiance. The script starts with the modelling of geometry (1), and its characterisation using “Radiance Opaque Material” or “Radiance Glass Material” (figure 8). Honeybee readable objects are created by using “Create HBSurfaces” component. Following Simulation Grid and Parameters are set (2), and the simulation is performed by connecting all geometries, grid surface and the analysis recipe into the component “Honeybee_Run Daylight Simulation” (3).

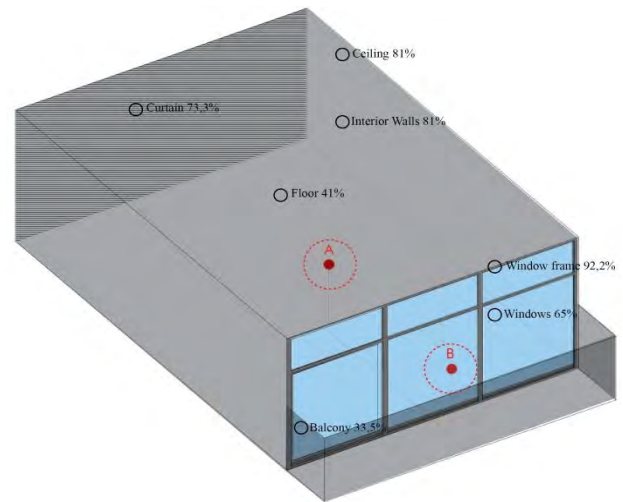


Figure 8. Reflectance values for each material.

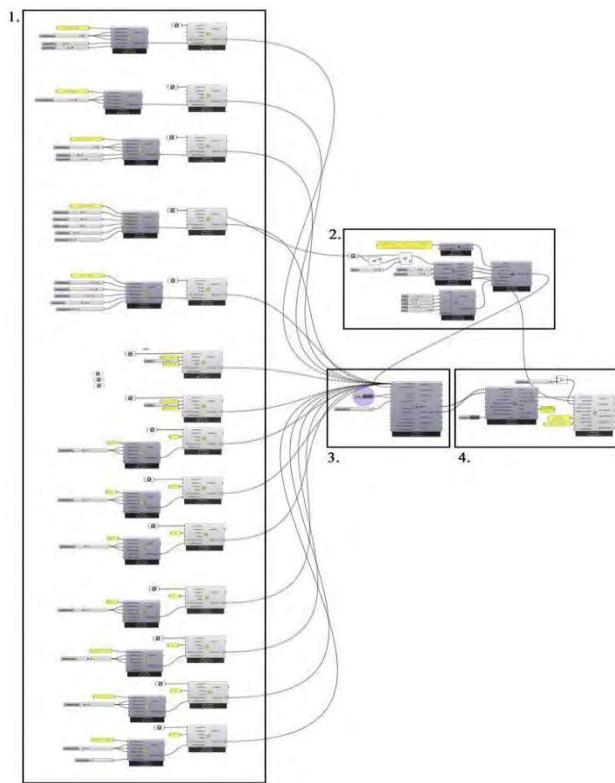


Figure 7. Daylighting Script; 1. Building Geometry and create Honeybee surfaces; 2. Import EPW file and set the Analysis Period, 3. Run the Simulation, 4. Visualise the Results

3.4 Indoor Thermal Model Characterization

The thermal script outlined in Figure 10 runs an EnergyPlus multizone energy modelling commanded by Honeybee in order to calculate MRT value at point A. The building is subdivided into thermal zones (Figure 9) by using the “Mass2Zone” component (1). The creates weather file is imported by using the “Open EPW+Stat Ladybug” component (3). Specific period is analysed with the Analysis Period component (4) and connecting inputs. The solving of adjacent geometries and material characterization is possible with the “solveAdjc” and “setEPZoneConstruct” components (5). The context is processed through “HB_EPContextSrf”, with Rhino imported geometries (6). The simulations results are commanded with “Generate EP Output” (7) and the “Honeybee Run Energy Simulation” components. The simulation report “readEPResult” (9) is visualized with the “Quick Graph” component.

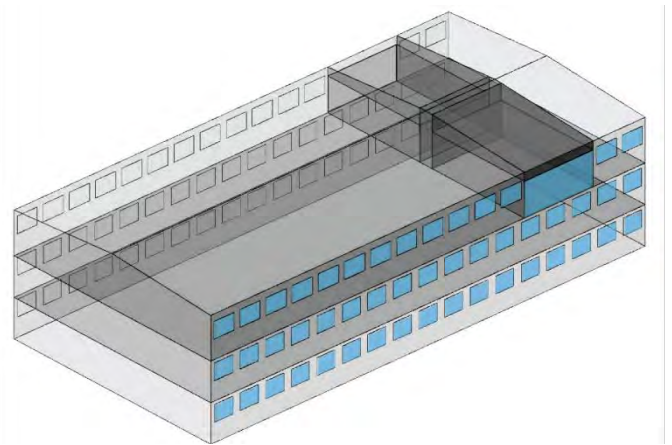


Figure 9. The thermal model of the building and the test room used for the thermal analysis.

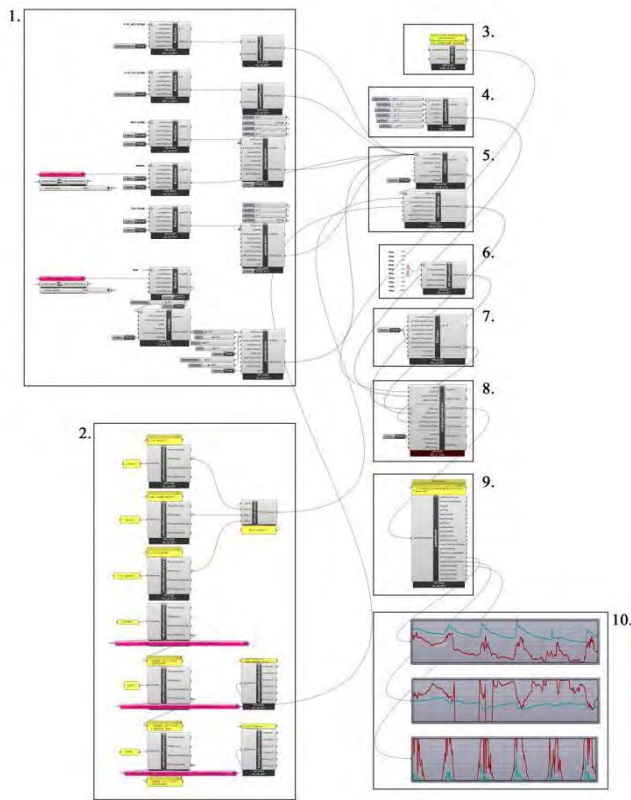


Figure 10. Thermal Script: 1. Building geometry, 2. Custom material, 3. Import EPW file, 4. Analysis period, 5. Set EP zone construction, 6. Context geometry, 7. Set the simulation output, 8. Run simulation, 9. Analysis report, 10. Visualise result

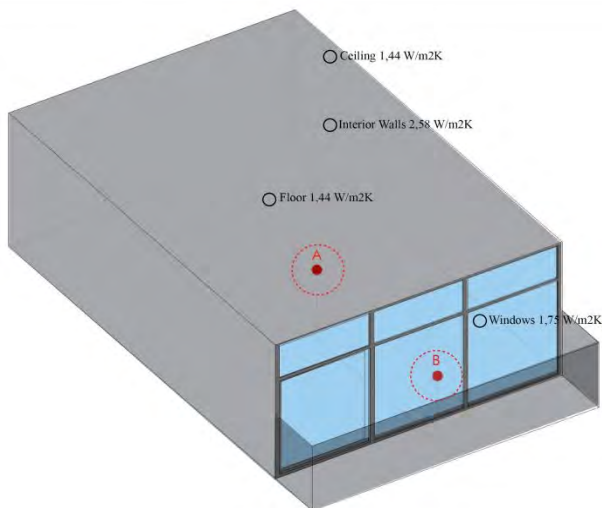


Figure 11. Mockup room geometry with U values of the walls and the window g-value.

3.5 Outdoor Mean Radiant Temperature

The purpose of this script is to estimate the Mean Radiant Temperature of point B corresponding to the outdoor globe thermometer [21]. The Ladybug and Honeybee calculation of outdoor MRT is based on a specific component defined by Mackey as “hybrid”. MRT is simulated by first computing a first longwave MRT based on surface temperatures calculated with the EnergyPlus simulation engine. The view factors of every surface are calculated with the ray-tracing capabilities of the Rhino 3D modelling engine. The temperature of each building surface viewed from the face of the target point B is calculated as a weighted temperature, where the weight is defined by how much surrounding surfaces are viewed by the face of a given point. The outdoor calculation takes into account the sky temperature and the consequent longwave loss to the sky. The calculated longwave MRT is then adjusted to account for shortwave solar radiation that falls on people using the SolarCal model, which is a part of ASHRAE-55 thermal comfort standard.

The script (Figure 13) runs a multi-zone energy modelling with Honeybee, using EnergyPlus as a software engine. Only the geometries which have a significant view factor calculated from point B are included in the MRT calculation (figure 12). Each of the surrounding buildings that “view” point B are thermally modelled in order to obtain the hourly variation of their temperature which influences the longwave radiation exchanges with point B. The ground also exchanges long radiation with point B, and it is thus subdivided into four different surfaces according to material and solar exposure. Adjacency of the zones is adjusted using the relational “HB component” (1). After that, windows are added using “HB_Glazing” based on ratio component assigning different WWR on every façade (2). Finally, free-standing objects such as a canopy and a terrace are included in the model as thin thermal zones without internal gain by using EPPlenum component. Figure 13 shows the average temperature of the surfaces for a single time step.

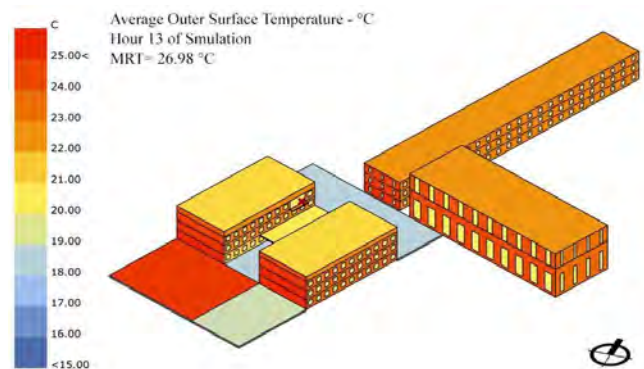


Figure 12. The thermal model of the building and surrounding the outdoor MRT simulation. The colour scale indicates surfaces temperature for a point-time: from the blue (colder) to the red (hotter).

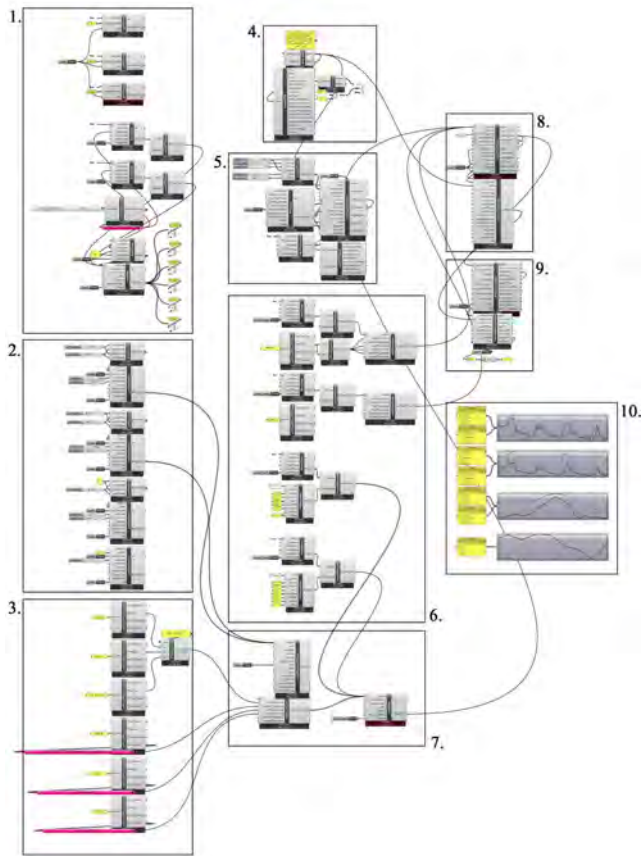


Figure 13. MRT Outdoor Script: 1. Geometry, 2. Create Windows, 3. Add material, 4. Import EPW file, 5. Run Energy simulation, 6. Create thermal zones; 7. Set adiabatic surfaces, 8. Indoor view factor, 9. Microclimate map, 10. Visualise the results.

4 RESULTS

After the simulations are run, and measurement values recorded on-site at point A and B are imported into the Grasshopper environment with the use of the TT Toolbox plugin [22]. Figure 14 shows the interactive display that allows for the comparison of simulated and recorded data, and it shows the initial results before the calibration process began.

To understand the accuracy of the simulation model outputs against the onsite data, the root-mean-square error (RMSE) method is applied. RMSE is used to measure the differences between the values predicted by the simulation and the values observed. The comparison results with an RMSE of 1.3 °C, whereas the minimum RMSE for ASHRAE is 4,425 °C for this specific case, thus showing that the simulation leads to results. Following this verification, data collected from the on-site measurements undertaken between the 20th and the 23rd of September 2018, and the simulations are compared. (Figures 15, 16, 17 and 18).

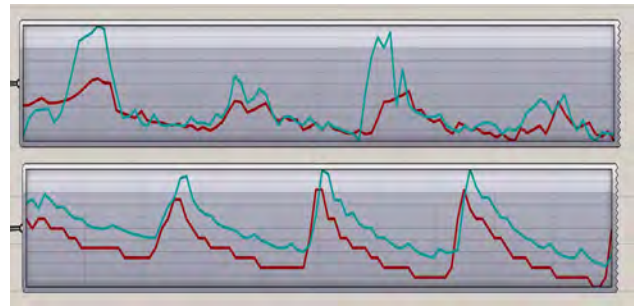


Figure 14. The tool used in Grasshopper environment for the interactive comparison of simulation results (red) and on-site measurements (grey), graphs refer to (starting from the top): Dry Bulb Temperature (°C), and Mean Radiant Temperature(°C). Both refer to the indoor.

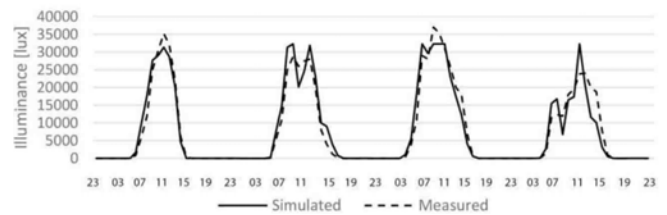


Figure 15. Outdoor Illuminance at Point B

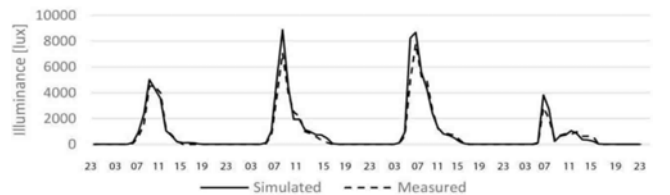


Figure 16. Indoor Illuminance at Point A

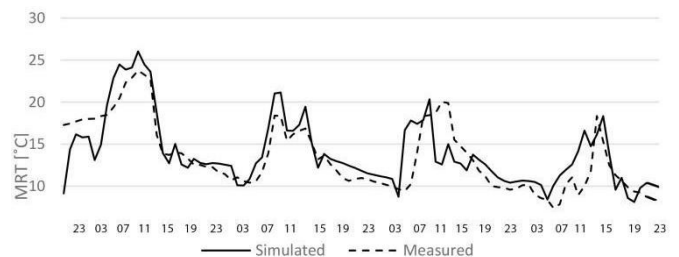


Figure 17. Outdoor MRT at point B

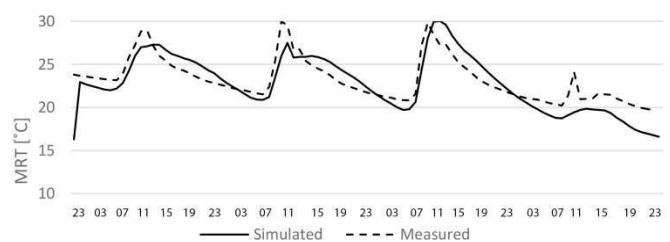


Figure 18. Indoor MRT at point A

5 DISCUSSION

Following measurement scripting, simulation, and data comparison, the discussion branches into four main areas: the script, the quality of the results, the implication of these towards future developments, and the relevance of the research for the design of façades as climate givers.

Several “out of the shelves” scripts were assembled in a novel fashion for real-time indoor and outdoor thermal and visual simulation thus establishing a workflow where each façade design variation (e.g. geometry, material types, and dynamic behaviours) would affect the thermal and visual related results. The scripts are linked to a specific test room located at KADK campus, but these could easily be adapted to any façade studies with a little degree of customization.

The research attempts at verifying this Ladybug Tools assembly of scripts for indoor and outdoor thermal and visual parameters against measurements results. The comparative graphs show that the simulated are matching the measured ones. According to root-mean-square-error (RMSE) verification, the simulation results acceptably match the measured ones.

Designers and researchers using parametric strategies could use this workflow. Furthermore, the workflow could be paired with genetic and optimisation techniques to generate façade that is responsive to both outdoor and indoor thermal and visual parameters. It should be highlighted that the computational and time requirements for the outdoor MRT of complex site studies may limit the applicability of the workflow in large parametric studies, especially in the short time frames of concept design stage in real life projects. In this case, the modeller should operate a series of simplification of the context.

Users with some degree of familiarity with Ladybug Tools could use the scripts to perform a design that negotiates the thermodynamic and optical phenomena in a way that both indoor and outdoor comfort are accounted for. In future developments, the workflow is going be used to create static and dynamic solutions that mitigate and adapt to climate change, in order to reduce energy consumption and carbon emission, while providing indoor comfort and outdoor comfort.

6 CONCLUSION

The research focuses on the assembly and the verification of a designer-friendly workflow that allows the prediction of outdoor and indoor mean Radiant Temperature and illuminance that is determined by façade design.

The present works bring together two means of optimising climate behaviour: digital simulations physical and measurements. The obtained result is a comparison between indoor and outdoor settings, between measured and simulated MRT and Illuminance levels.

The workflow is currently being used and tested in the study that relates different sets of façade design solutions to outdoor and indoor climates in canyons in Copenhagen, Madrid and Catania. The results will be shared in upcoming publications.

The workflow thus constitutes a precise process that could be incorporated into other practice-related and research projects investigating façades as climate givers within the context of providing solutions that cope with mitigation and adaptation to climate change within urban contexts.

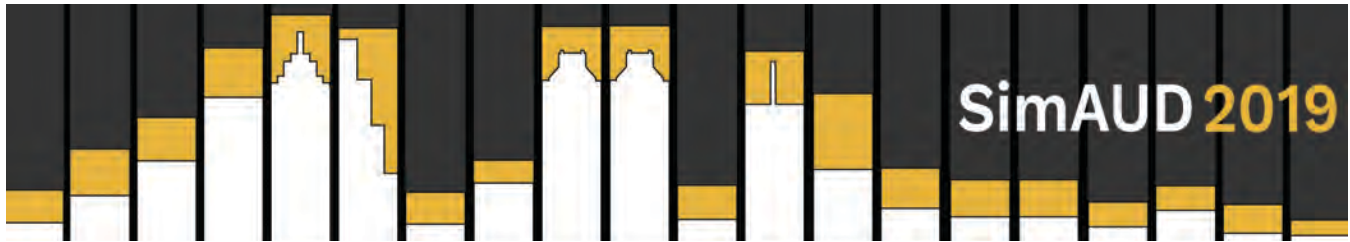
Acknowledgements

Thanks to Katja Bulow for the support with the daylighting room, Olesja Lami Jacopo Cataruzzi, Lidia Ratoi, Vincenzo Rossi, Angel Asis for the contributions offered at different times in the progressive developments of the scripts. We would like to thanks Chris Mackey for the pieces of advice provided along the developments. The article was developed with the support of the COST Action CA16114 ‘RESTORE: Rethinking Sustainability towards a Regenerative Economy’.

REFERENCES

1. The Paris Agreement. <https://unfccc.int/processand-meetings/the-paris-agreement/the-paris-agreement>
2. Naboni, E.; Meloni, M., Coccolo, S., Kaempf, J.; Scartezzini, J.L.; An overview of simulation tools for predicting the mean radiant temperature in an outdoor space, (2017)
3. Shahmohamadi, P., Che-Ani, A. I.; Maulud, K. N.; Tawil, N. M.; Abdullah, N. A. . The impact of anthropogenic heat on formation of urban heat island and energy consumption balance. *Urban Studies Research*, (2011)
4. Matusiak, B.; Daylighting in linear atrium buildings at high latitudes. *Norwegian University of Science and Technology*, (1998)
5. Nelson, W. C; Ott, W R., Robinson, J. P.; Tsang, A. M.; Behar, J. V.; Engelmann, W. H.; *The National Human Activity Pattern Survey* (2001)
6. L.Taleghani, M. Tenpierik, M.; Kurvers, S.; den Dobbelsteen, A. A review into thermal comfort in buildings, *RSER*, 2013
7. Alonso, C.; Martin-Consuegra, F.; Otezia, I.; Pérez, E.A.; Martínez, I.; Frutos, Borja; *Effect of façade surface finish on building energy rehabilitation. Solar Energy*, 2014
8. Gaspari J, Naboni E, Ricci A, Ponzio C,. “A Study on the Impact of Climate Adaptive Building Shells on Indoor Comfort.” *Journal of Facade Design and Engineering* 7, no. 1 (2018)
9. Ponzio C, Ricci A, Naboni E, Fabbri K, Gaspari J, “Development of an Adaptive Passive Façade: A

- replicable approach for managing multiple design solutions” in PLEA 2018, Vol.2
10. Zinzi, M.; Carinielo, E.; Mattoni, B.; On the relation between urban climate and energy performance of buildings. AE (2018)
 11. Foxx, J; De Pooter, N.; Effect of building facades on outdoor microclimate–dependence model development using thermography and multivariate analysis, SBE, (2016)
 12. Kondo, MM.; Jacoby, S.; South, E.; Does spending time outdoors reduce stress? A review of real-time stress response to outdoor environments. Health & Place, 2018
 13. Wan, K.K.W.; Li, D.H.W.; Pan, W.; Lam, J.C.; Impact of climate change on building energy use in different climate zones and mitigation and adaptation implications, Applied Energy, 2012
 14. Naboni, E.; Integration of outdoor thermal and visual comfort in parametric design, (2014)
 15. Santamouris, M.; Ding, L.; Fiorito, F.; Oldfield, P.; Osmond, P.; Paolini, R.; Prasad, D.; Synnefa, A. Passive and active cooling for the outdoor built environment – Analysis and assessment of the cooling potential of mitigation technologies using performance data from 220 large scale projects. Solar Energy, 2017
 16. Dunichkin, I.; Naboni, E.; Hamad, M.H.; Features of assessment of bioclimatic comfort for modern residential buildings in hot-dry climates. IOP, 2017
 17. Naboni, E.; Sustainable design teams, methods and tools in international practice, Detail Magazine, Green 01/14, (2014)
 18. Naboni, E., Meloni, M., Coccolo, S., Cucchi, F., Macrelli, G., Kaempf, J., & Scartezzini, J-L. (2017). The Integration of Outdoor Thermal Simulation Tools in Architectural Design. In *Design to Thrive* (Vol. 2, pp. 2100-2107)
 19. Dasaraden M, Coccolo S, Tharindu DP, Nik V, Scartezzini JL, and Naboni E. 2018. “A New Framework to Evaluate Urban Design Using Urban Microclimatic Modeling in Future Climatic Conditions.” Sustainability 10 (4)
 20. Roudsari, M. S.; Pak, M.; Smith, A.; Gill, G.; Ladybug: A Parametric Environmental Plugin for Grasshopper. Chicago, USA, (2013)
 21. Mackey, C.; Galanos T.; Norford, L.; Roudsari, M.S. Wind, Sun, Surface Temperature, and Heat Island: Critical Variables for High-Resolution Outdoor Thermal Comfort. 15th International conference of Building Performance Simulation Association. San Francisco, USA, (2017)
 22. <https://www.food4rhino.com/app/tt-toolbox>



Streets, Parks & Plazas: Analyzing Daylight in the Public Realm

Elizabeth de Regt and Timothy Deak

ZGF Architects LLP

Seattle, WA USA

{elizabeth.deregt, timothy.deak }@zgf.com

ABSTRACT

Research has shown how integral daylight access is to both physical and mental health. While this has gained traction within building interiors, very little research has delved into the daylight that hits streets, parks, courtyards, and other exterior spaces that impact the urban experience. This paper provides a better understanding of how daylight affects these spaces and suggests a framework for the design of livable cities.

276 unique respondents answered a questionnaire. The results were utilized to qualitatively analyze the impact of daylighting within 25 well-known exterior urban spaces on city-users. Computer modeling, daylight simulation, and both correlation and regression analyses tied these respondents' answers to quantitative data. New metrics, both data-driven and graphic, were used to summarize the daylighting qualities of these spaces, allowing designers to use these spaces and metrics for future comparison analyses.

Given further exploration into the use of these metrics, they may also be applied to future zoning code alterations by providing the framework for a performance-based compliance path for achieving necessary daylighting at grade. Public and private sectors, from individual buildings to large-scale master plans, may utilize these metrics to create benchmarks for improving the urban experience.

ACM Classification Keywords

G.3 Probability and Statistics; I.6.5 Model Development; I.6.6 Simulation Output Analysis

1 INTRODUCTION

1.1 Daylight Importance

Access to daylight inherently affects humans, but our societal views have shifted over time. At one point, daylight exposure was reduced due to concerns of cancer,

but more recently the benefits of daylight access have been emphasized and promoted. Architectural studies have especially focused on daylight's impact within buildings, such as studies that show increased productivity and better sleep quality to workers with daylight access over those in windowless areas [3]. Such studies have emphasized the clear link between individuals' daylight access and their happiness, physical health, productivity, and even perception of safety.

1.2 Existing Metrics

This shift in understanding has led to new metrics for interior spaces, especially those in office environments. Spatial Daylight Autonomy (sDA) has become a commonly assumed metric for these areas. While the common metric for sDA uses 300 lux for 50% of the time as the benchmark, exterior Daylight Autonomy (DA) may be used as well. Most trees need a DA of at least 85% at 2000 lux in order to thrive [1]. IESNA also lists more detailed lighting requirements for various plant species. This list that may be utilized to further the use of exterior daylighting analysis and better inform plant selection in courtyards, street corridors, and similar spaces [8]. These requirements vary but most commonly require 750-2000 lux for 14 hours a day, or a larger quantity for slightly fewer hours a day.

Human beings also have a physical requirement for daylight. Between keeping our circadian rhythms in check and staving off proven weather-based mood swings, we require sunlight. While most light therapy boxes suggest 10,000 lux for 30 minutes a day, most argue that 2500 lux is all that is required to minimize Seasonal Affective Disorder; much less is required to reset our internal clock [9]. This amount of sunlight is almost never achieved in indoor environments and therefore must be gained through outdoor exposure. Many urban environments, particularly in narrow streets or those lined by very tall buildings, rarely reach this illuminance level. City-

dwellers currently must seek out brighter areas in order to stay mentally and physically healthy.

1.3 Previous Research

While many metrics have been developed regarding interior access to daylight, very little has been done to link outdoor urban experiences with sunlight in a quantitative manner. Most discussions on this topic have one of three goals in mind:

- Inform *Interior Daylight* analysis
- Maximize *Solar Access* for energy generation
- Better the *Pedestrian Experience* of the public realm

They most commonly use exterior daylight analysis as a quick way to gain knowledge about how much light hits a building façade. This information is then used to extrapolate interior daylighting statistics or to calculate the potential for energy generation within a site. A great example of this approach is found in Emmanouil Saratsis's research on daylight analysis's potential impact on zoning rules [12, 13]. While this is one of the first attempts at large urban daylight analysis, it still focuses on building interiors' access to daylighting rather than the public spaces within the urban fabric between them.

The final goal found in existing research relates to the comfort felt by those experiencing the city from the outside. Urban designers have long discussed the impacts of tall buildings on street experience in qualitative terms. Wary of the "urban canyon" effect, they have tried to put numbers to a height-to-width ratio based only on their experiences. Ewing and Bartholomew summarize these claims handily, varying from Allan Jacobs's 1:2 ratio to others going up to 3:2 [7]. These assumptions have rarely been tied to either user experience or quantitative daylight analysis in any scientific way. They instead focus on a general impression of what "too tall" may mean.

Rare studies, such as Mark DeKay's work into height-to-width ratios, look at this figure in a more quantitative way. Following his 1993 research on height-to-width ratios' impact on buildings' daylight factor, he looked in more depth at building setbacks [5, 6]. DeKay overlaid a "daylight envelope" setback based on the feeling of enclosure at grade with a "solar envelope" that addressed building interiors' access to the sun. This approach begins to get at the urban scale, but it fails to address exterior daylighting or tie these relationships to human experience directly.

1.4 Existing Zoning

For decades, traditional zoning codes have utilized similar approaches to building massing along streets. While many describe a need for stepping down to street level to allow for daylight access at the street as well as address urban canyon concerns, they rarely give quantitative

explanations for these requirements or take a façade's solar orientation into account.

Some cities also address access to daylight in specific zoning requirements based on use rather than in form-based manipulation of buildings. For instance, Vancouver BC incorporates three hours of direct daylight at the winter solstice into its requirements for childcare outdoor play areas [4].

One recent exception to these simplified requirements can be found in the zoning rules for Central SoMa in San Francisco [11]. This document attempts to address these variations in solar conditions. The planners take a "skyplane" approach, applying various setback rules depending on street orientation as well as allowing a percentage of the façade to break this rule, thereby allowing for design variation and flexibility. Unfortunately, this approach is both complicated and lacks a performance-based alternative, showing no analytical explanation for these prescriptive setbacks. This leaves designers without flexibility in addressing the concerns this ruleset attempts to counteract.

1.5 Research Intent

This existing wealth of daylight research presents holes in exterior daylighting analysis methodologies, particularly in tying urban experiences to quantitative daylighting metrics. As evidence mounts regarding how building forms affect experiences at street level, zoning rules should become more informed, including both prescriptive and performance options for designers to follow. The research contained within this paper responds to the need for a more scientific understanding of exterior daylighting. It attempts to chip away at the complexities of human urban experience and its relationship to building massing and daylighting. This brings a deeper understanding of why some urban spaces may be more successful than others, thereby allowing designers to make more informed design decisions.

2 EQUIPMENT + METHODOLOGY

2.1 Survey

In order to link human experience to data, a qualitative survey was performed. 25 publicly accessible world-wide urban locations were identified as shown in figure 1. With the researchers based out of Seattle, WA and respondents spread throughout the United States, these cities were chosen in order to maximize survey respondents' familiarity with the cities while also providing a variety of size, scale, style, weather patterns, and urban solar orientation. Variation in latitude was minimized in order to limit the variables. This allowed the research to focus on the ways in which building massing impacts solar exposure and human experience.



Figure 1. Simulation locations across six cities (map [10]).

276 individuals participated in the survey, each familiar with only some locations. Therefore, respondents answered only questions regarding areas they identified as being familiar, using their memory of these spaces when answering. Requiring familiarity with the site allowed for a greater understanding of each space rather than reliance on a single point in time or photo. The response rate per location ranged from a minimum of 37 responses to a maximum of 157. Each location included between one and four spot locations that were additionally tested. The spots, shown in figure 3 as red dots in the direct daylight graphic, were indicated in plan and perspective within the survey. They vary in type of space: along a “path” such as a street, sidewalk or alley, or within a “place” such as a park, dining area, or plaza. These spots vary greatly in daylight access even within each location and were compared to one another and linked back to survey responses in order to begin to understand daylight’s impact on human experience.

The survey asked respondents to “Please ignore other impacting elements such as landscaping, shop entrances, ‘sketchy areas’ effects, or other common urban design features that affect the ways in which we perceive the safety and pleasantness of an urban area.” It then asked them to avoid labelling entire spaces or even spot locations as good or bad but instead to specify their expectations of experience within those areas. Respondents were requested to “Please rate the feasibility of this location with regard to daylighting” and were given 6 options for each spot with which they were familiar:

1. “Great for Active Use (frisbee, gatherings)”
2. “Great for Long Use (picnic, reading)”
3. “Good for Short Use (coffee, pleasant walk)”
4. “Acceptable for Walking (from A to B)”
5. “Uncomfortable for Walking (from A to B)”
6. “Dangerous for Walking (from A to B)”

In order to normalize responses, the 6-point Likert Scale was used to rate the spaces based on type of experience. While not perfectly linear due to the qualitative descriptions, this allowed the research team to associate responses with experiences in a consistent manner. While respondents would not be able to accurately remove all impacts on their perceptions beyond daylighting, the intent behind the survey was to reduce outside influences as much as possible. As these non-daylight-related factors cannot ever be wholly removed from influence, outlying data points present opportunities to identify the impact of these characteristics, such as active tourist locations, well-designed street frontages, or the presence of large street trees.

2.2 Model Setup

The 25 locations were built in Rhinoceros 3D and analyzed in Grasshopper using Diva’s daylight simulation plugin. Due to the drastic variation in exterior conditions, only simple massing and material assignment was required in order to produce results accurate enough to be tied back to survey results. Building materials, for instance, vary in reflectance values between roughly 30 and 40, with most hovering closer to 30. An example location model only produced a shift in average illuminance values of 17% when every building surface in the model was shifted from 30 to 40. Since most urban areas include a mix of these reflectance values, a much smaller error is expected in assuming a single value for reflectance. For similar reasons of efficiency, Diva’s “low” raytrace setting was used after performing a test that showed only a 4-13% variation in the four metrics used when comparing “low” to “high” results. This test was performed on an area receiving primarily reflected rather than direct light, thus exaggerating the differences. Since the “low” method consistently yields slightly lower light levels, the 25 locations may therefore be compared to one another with confidence. With illuminance levels and metrics between locations varying by more than 1000% in many cases, these tested variations of 17% and 4-13% would become trivial when comparing spaces.

Similarly, trees were also simplified, modeled as conically spherical shapes with transparency applied. Transparency was based on an average of street trees’ transmission values in summer (15%) and winter (65%) as described by Wilkinson, Yates, and McKennan in 1991 (referenced in [2]).

Each location was therefore simply modeled, including any buildings that would likely cast a direct shadow on the area under consideration. Taller areas such as Manhattan were therefore modeled more extensively than shorter areas such as Brooklyn. Separately, each city was also analyzed using weather files as applied to simple flat-plane settings to create a weather baseline for each city.

The following analysis constraints were then assigned in performing each analysis.

2.3 Material Values and Analysis Settings

- Walls: 30% reflectance (representing a mix of solid materials and reflective metals and glazing)
- Ground: 20% reflectance (reflecting the most common paving and grass combinations)
- Canopy Glazing: 70% transmission
- Trees: 40% transmission (average of 15% summer and 65% winter, using two 63% transmission surfaces)
- Daylight Plane: Simplified based on Sketchup-generated topography; raised 5ft (1.524m) above grade (representing average eye height); 1m x 1m grid for daylight plane on each location
- Spot locations: Modeled separately from plane; also raised 5ft (1.524m) above grade
- Raytrace quality: “Low” (-aa .15 -ab 2 -ad 512 -ar 256 -as 128 -dr 2 -ds .2 -lr 6 -lw .004 -dj 0 -lr 6 -sj 1 -st 0.15)

2.4 Data Gathering

Survey data was simplified into a single number representing the average and the standard deviation for that spot location. Each location was also noted by city, use (alley, boulevard, park, plaza, or street), type (path or place), and the major presence of trees (yes or no). Simulation data for each city baseline, urban location, and spot location were manipulated in Excel using VBA macros to create the following metrics:

- Sky View Factor (SVF): Per spot location. SVF shows the percentage of the view from that location that is obstructed by buildings and/or trees. Trees are given partial credit for this metric, reflecting the same transparency requirements as during the analysis.
- Annual Hours Of Direct Sunlight: This value was compared to the city baseline, resulting in the percentage of time that the spot receives direct daylight compared to an unobstructed location.
- Annual Klux-Hrs: This metric multiplies illuminance values by time, producing one number to represent how much light a space receives annually. This too was compared to the city baseline and referenced as “klux-hrs (% of city).”
- Daylight Autonomy (DA) is the percent of time throughout the year (during the relevant time range) that each point reaches the threshold. Here, the threshold used is 2500 lux to match both human health (SAD reversal) and tree growth needs.
- Continuous Daylight Autonomy (cDA) is calculated by giving partial credit to those values below the DA threshold (here, 10,000 lux). This was used to give a snapshot of annual exterior daylighting conditions, with

the most important variations in light conditions in the studied areas falling within this range of visible differentiation.

- Average Illuminance Values: Average illuminance values were calculated separately for morning (8AM-11AM), evening (4PM-7PM), summer (April-September), and winter (October-March). This data was also directly compared to their counterparts using their coefficient of variation (CV) and then comparing this to the city baseline CV. Each spot location data-group was similarly compared both to its immediate surroundings (represented by the average urban location data) and its city baseline in order to understand the variation between points and test for unexpected correlations.

Average values rather than total percentage above 50% were used for these DA metrics in order to compare directly to point values at spot locations. Both DA and cDA used 8AM-6PM as the timeframes for consideration due to the primary daylit urban activity falling within this range. Finally, all results were statistically analyzed using various comparisons in R.

3 RESULTS

3.1 Data

The following chart was created with Tableau and is associated with findings confirmed in R.

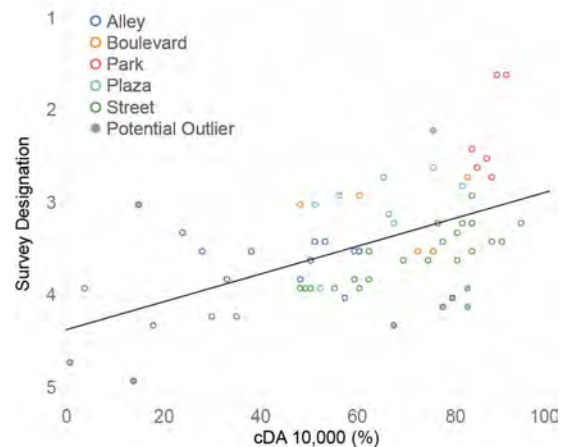


Figure 2. cDA10000 – survey relationship by space type

While general trends clearly indicate a preference for more daylight when experiencing public spaces, more sophisticated data analysis was able to produce further, more nuanced conclusions. Figure 2 separates the simulation points by use type for reference. Due to the number of “street” type points, these were also analyzed separately (slope=-1.322) due to their proven reliability (p -value <.0001). Grey fill indicates an outlier as explained in 3.2 but still incorporated in all data analysis due to the qualitative method used for identifying outliers.

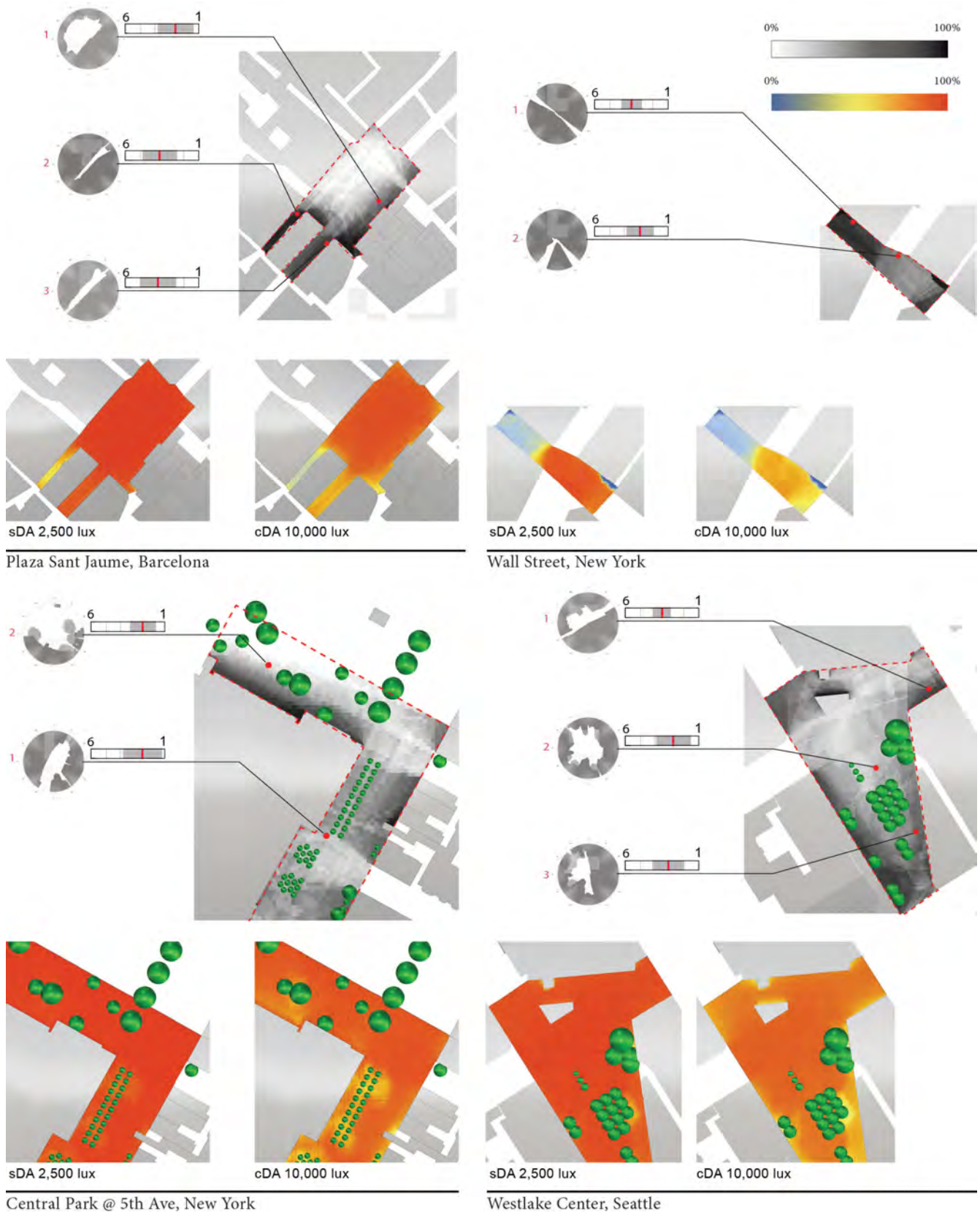


Figure 3. Sampling of graphic simulations: Barcelona’s Plaza Sant Jaume (plaza, alley, and street points), New York’s Wall Street (street and plaza points), NYC’s Met. Museum of Art (Park and Boulevard points), and Seattle’s Westlake Center (Street and Plaza points)

Were clear outliers removed, alleys and plazas would indicate a similar clustering and correlation but with varying slopes. Figure 2 may therefore be used to begin to identify an expected user experience for these use types based on simulated daylight exposure as measured in cDA10000. Boulevards and parks did not include enough points to produce reliable findings when separated by use type but suggest a potential variation in slope by use type. Parks, for instance, may require brighter daylight for a similar user response than another use type.

Figure 3 displays the graphic output from 4 locations in the study. These analyses give designers benchmark locations with which to compare their designs. The rectangular graphic at each point location in figure 3 (notated with a 6 and a 1) is used to represent the survey values. The red line shows the average response, while the grey shading shows the approximate variation based on the standard deviation. The primary graphic at the upper right of each image cluster represents a new graphic not currently available using Diva for Grasshopper. This shows percentage of otherwise daylight time that the area receives direct daylight. This was created by manipulating the .ill file using an Excel Macro, then feeding this new file back into Diva for a graphic display.

3.2 Outliers

Calculations presented in this paper include all data points, but the following outliers may have qualitative explanations for their inconsistencies and have been highlighted in order to explain potential variations in future area design and simulation. Although respondents were asked to only include daylight in their observations, some spaces have such strong effects (both positive and negative) that respondents still unconsciously let these associations impact their ratings of spot locations.

Some of these effects had a positive impact on respondents' experience of space that had little to do with daylighting. For example, Seattle's Chophouse Row and Portland's Director Park both include human scale details that improve the quality of the space and a high level of activity throughout the week. Despite the lower level of light than other locations, these spaces were rated highly.

This study also showed points that seemed to have other influences negatively impacting respondents' answers. Most of these spaces display urban design factors typically associated with negative experiences. For instance, all three points within Prefontaine Place in Seattle are rated significantly lower than one would expect given their daylighting. Seattle's Convention Center tunnel, New York's Exchange Alley, and the two points at the edges of Cal Anderson Park in Seattle all fall below the expected ratings. These areas display negative urban design features, primarily blank walls and a lack of activation. In addition, some of these spaces are known for large transient populations, high litter rate, or other

elements that likely negatively impacted respondents' answers.

3.3 Data Analysis

Using the point data explained in section 2.4, further investigations were made regarding the relationships between spaces and survey results as well as any more nuanced effects. For instance, when separating those points heavily impacted by the presence of trees, the relationship between kLux-hrs (% of city) and survey designation shifted from -1.24 (no trees) to -1.57 (trees). This suggests that humans perceive areas shaded by trees as brighter than they would were the area shaded instead by a building or other obstruction. This difference is small and does not yield a significant statistical result but instead suggests the possibility for further study regarding the impact of trees on daylight perception and urban experience.

Further robust correlations were analyzed in R, using Spearman's rho (r_s) and Kendall's tau. This was determined because of the 6-point Likert scale used for survey responses (1=best, 6=worst), meaning that the assumptions under Pearson's correlation have not been met. In the following findings, we report Spearman's rho, as it can be squared to give an effect size. In all cases, however, Kendall's tau produced significance levels that were identical with Spearman, providing an important cross-validation of results.

The initial correlation analysis analyzed the relationship shown in figure 2. This compares cDA10000 with survey designation (mean survey response). The analysis found the survey designation to be significantly negatively correlated with cDA 10000, per the values below. This represents a large effect, as $r_s^2 = -0.25$, and means that more daylight is correlated with better (lower number) survey responses.

Data collected also measured daylight access in a number of other ways as shown in Table 1. Each of these metrics was found to have nearly identical correlation strength to cDA10000. This suggests a clear correlation to daylight access without a strong preference for any specific measurement. DA at 2500 lux had the lowest correlation, showing that the daylight above 2500 lux is more relevant in our perceptions of outdoor spaces.

	r_s	p	r_s^2
kLux-hrs (% of city)	-.493	<.0001	-.24
kLux-hrs	-.500	<.0001	-.25
DA 2500	-.474	<.0001	-.22
cDA10000	-.508	<.0001	-.25

Table 1. Data Correlations

In order to understand whether enclosure magnitude affects experience more than daylight itself, the same

analysis was performed for SVF as well. While these were found to be significantly positively correlated at $r_s = 0.406$ $p = <.001$, this represents only a medium effect, as $r_s^2 = 0.17$. This suggests that daylight access affects survey results more than enclosure amount. This result was further explored using a regression analysis to determine if SVF had any additional impact on survey results over daylight access itself. No statistically significant impact was found, suggesting that SVF is only related to survey responses in how it affects daylighting.

Following this finding, a number of other regression analyses were also tested in order to determine any other significant impacts on survey results in addition to daylight access. The variation between morning and evening daylighting (normalized for city daylight access), as well as a similar variation between summer and winter daylighting, was found to have no significant impact.

Similarly, a regression analysis adding hours of direct light to the kLux-hrs (% of city) relationship to survey response yielded no significant impact. This was an unexpected result, meaning that direct daylight was only relevant to occupant experience in that it increased the total amount of daylight in a space.

The last regression analysis tested if a spot's relationship to its immediate surroundings (represented by the average values for that location) has any further impact on survey results than that shown by kLux-hrs (% of city). This comparison also yielded no significant additional impact, meaning that, in most cases, an area's immediate surroundings do not impact experience; only daylight access itself does. This result was unexpected. Human eyes adjust to see light in relationship to its surroundings, leading to the expectation that visual experience would be impacted by that relationship. This analysis contradicted this assumption.

In addition to effects impacting survey response designation, the standard deviation of those responses was also analyzed. On average, there is a statistically significant and greater standard deviation for "place" locations, such as parks and plazas (median = .90, standard error = .03) than for "path" locations, such as streets and alleys (median = .66, standard error = .02), $t(24) = -5.55$, $p = <.0001$, $r = .75$. This represents a large effect on standard deviation due to a spot's type as either place or path. This suggests that there is less agreement regarding a spot's survey designation (and therefore occupant experience) when that spot is a place rather than a path. Daylight analysis may therefore be more subjective within courtyards, parks, and plazas than along streets and alleys.

4 CONCLUSION

Results demonstrate clear correlations between individuals' experiences in a space and that area's

daylighting. Figure 2 may be used to understand the lighting expectations for specific uses, particularly when generating design goals regarding exterior daylighting in both public and private spaces. Similarly, the data calculated for each point may be used to determine targets for any one of the daylighting methods used in this study. In particular, DA2500 may be used for plant selection, while cDA10000 appears to be the most appropriate for determining user experience.

These graphics and the related data help designers associate their own analysis with familiar spaces, providing intuitive benchmarks for daylight analysis. These results create a framework for comparing potential designs to existing spaces in order to make more informed design decisions. More nuanced metrics, such as SVF or a spot's immediate surroundings as measured in kLuxHrs (% of location), may help a designer understand spatial conditions.

Using the new metrics created through this study, designers may make more informed decisions regarding building massing and zoning requirements, the placement of exterior programming, and spacing of buildings. These metrics have also led to the ability to analyze daylight for plant specifications, allowing for design decisions to ensure green environments to thrive. Such influences on the public realm allow for more livable communities to grow and thrive in urban environments.

The results outlined in this paper rely on qualitative survey responses. These were made as accurate as possible by filtering responders to only those who were familiar with the location in question. The reliance on survey respondents' memories and the small sample size indicates that further study may be required to confirm and further explore some of these findings, particularly those results that may contradict existing urban design attitudes.

Further study regarding the impact of enclosure (SVF and height-to-width ratios), direct versus total daylight exposure, and the influence of an area's immediate surroundings would further this line of research. Research could delve into these phenomena on a larger scale. One could explore whether a similarly lit street in New York is perceived as the same brightness as its counterpart in Portland, given the former's height and density and the latter's tendency for a lower height to width ratio in its streets. These ratios in particular require further study to determine if they or their resulting daylight impacts drive urban experience.

Urban designers have often tried to pinpoint this ideal height to width ratio for streets. In doing so, they have either passively or actively assumed a relationship between height of enclosure and pedestrian experience that surpasses daylighting alone. This relationship was explored with the SVF metric, suggesting that enclosure

quantity, represented by SVF, only impacts pedestrian experience in as far as it affects daylight access to the street.

If further explored using the above methods, these findings may have meaningful ramifications in how zoning codes may be designed. Current building codes rarely take solar orientation into account in dictating envelope restrictions. The north side of the street may need far fewer requirements for upper level setbacks than many codes currently require. In contrast, the south side of the street should be designed to ensure adequate daylight reaches both the lower levels of buildings and adjacent public spaces. The lack of additional correspondence between SVF and urban experience found in this study supports this approach. It suggests that zoning requirements that lessen restrictions at the north side of streets may be as effective at curating urban experience as those that prescribe detailed setbacks throughout.

New studies would be advantageous to further an understanding of the impact of zoning typologies' on the public realm. While some have been studied with regard to their impact on lower level interior floorplates, there is much room for growth in the understanding of zoning massing requirements' impact on exterior spaces. Human health requires access to these brighter exterior spaces. Further research could identify the necessary benchmarks for public health. This work allows for a potential performance option to replace current prescriptive requirements, such as upper level setbacks, angled skyplanes, and other massing moves intended to allow light into the street. Extended study of these common prescriptive methods could yield a more efficient approach to ensuring equitable daylight access within the public realm.

ACKNOWLEDGMENTS

This research was made possible by the ZGF Idea Foundry research grant. The authors thank the Idea Foundry support team in particular, Scott Blakemore, Jake Jones, Craig Rizzo, Irene Song, Todd Stine, Dane Stokes, and Henry Zimmerman. Their assistance and encouragement was greatly appreciated.

REFERENCES

1. Baker, Nick V., A. Fanchiotti and K. Steemers. *Daylighting in Architecture: A European Reference Book*. Routledge, 2015.

2. Balakrishnan, Priji and Jakubiec, John. "Measuring Light Through Trees for Daylight Simulations: A Photographic and Photometric method." Presented at: Building Simulation and Optimization, September 2016.
3. Boubekri, M., I., C., Reid, K., Kuo, N., Wang, C., & Zee, P. "Impact of Windows and Daylight Exposure on Overall Health and Sleep Quality of Office Workers." Presented at: 27th Annual Meeting of the Associated Professional Sleep Societies, Baltimore, June 2013.
4. "Childcare Design Guidelines." *Land Use and Development Policies and Guidelines*. 4 Feb 1993. <https://vancouver.ca/docs/planning/childcare-design-guideline-1993-February-4.pdf>. Accessed 26 Nov 2018.
5. DeKay, R. M. "Climatic Urban Design: configuring the urban fabric to support daylighting, passive cooling, and solar heating." *The Sustainable City VII, vol. 2*, pp. 619-630. 2012.
6. DeKay, Mark. "Urban Development Patterns for Daylighting." Presented at: 18th National passive Solar Conference, American Solar Energy Society, April 1993.
7. Ewing, Reid and Keith Bartholomew. *Pedestrian- & Transit-Oriented Design*. Urban Land Institute and American Planning Association, 2013.
8. IESNA. "Lighting for Exterior Environments." Illuminating Engineering Society, 2014.
9. McAuliffe, Heather. *Beating Seattle's Grey*. 2016, Seattle.
10. Metry. <https://metry.io/en/collect-data/utility-company-data/>. Accessed 7 November 2018.
11. San Francisco Planning Department. *Central SoMa Plan Adoption Packet*. 10 May 2018. http://commissions.sfplanning.org/cpcpackets/2011.1356EMTZU_Central%20SoMa.pdf. Accessed 28 July 2018.
12. Saratsis, Emmanouil. "Daylight Density: A simulation-based framework towards performance-aware zoning and real-estate development." SMArchS Thesis, Massachusetts Institute of Technology, 2015.
13. Saratsis, Emmanouil, Timur Dogan, and Christoph Reinhart. "Simulation-based daylighting analysis procedure for developing urban zoning rules." *Building Research & Information*, 5 May 2016.

Retrofitting Analysis

Unleashing the Diversity of Conceptual Building Renovation Design: Integrating High-Fidelity Simulation with Rapid Constraint-Based Scenario Generation 29

Aliakbar Kamari, Carl Peter Leslie Schultz and Poul Henning Kirkegaard

Application of Surrogate Modeling to Multi-Objective Optimization for Residential Retrofit Design. 37

Arfa N. Aijazi and Leon Glicksman

Aerial Thermography as a Tool to Inform Building Envelope Simulation Models 45

Norhan Bayomi, Shreshth Nagpal, Tarek Rakha, Christoph Reinhart and John Fernandez



Unleashing the Diversity of Conceptual Building Renovation Design: Integrating High-Fidelity Simulation with Rapid Constraint-Based Scenario Generation

Aliakbar Kamari, Carl Peter Leslie Schultz and Poul Henning Kirkegaard

Department of Engineering, Aarhus University
Aarhus, Denmark
{ak, cschultz, phk}@eng.au.dk

ABSTRACT

Designing a renovation plan for a building is a highly complex task: during this planning process, the design team needs to explore an enormous “design space” of possible renovation actions, and on the other hand, must evaluate the efficacy of each candidate design using computationally expensive simulations. Moreover, the design team seeks to balance a range of competing key performance indicators (KPI) as demanded by clients and the real conditions of the existing buildings, which are unique for every project (e.g. energy consumption, daylight, and thermal comfort).

We present an innovative renovation decision support framework that provides the design team with broad coverage of the design space in conjunction with limited, careful use of precise simulations for KPI evaluation. Our approach integrates logic-based domain model querying and multi-objective optimization based on Answer Set Programming and the KPI simulation system. We empirically evaluate our system in a large residential building case study in Denmark.

Author Keywords

Building Renovation; Holistic Renovation Scenarios; Renovation Typologies; Rapid Scenario Generation; Answer Set Programming.

ACM Classification Keywords

I.6.1 SIMULATION AND MODELING (Model Development and analysis)

1 INTRODUCTION

The topic of renovation of existing buildings is receiving ever-increasing attention in European countries [9] towards the development of more holistic renovation decisions [13] that align with core sustainability objectives [8]. Moreover, there is a growing need to involve stakeholders in earlier stages of the renovation design process [12] where many numerical details may not be available, and where soft

criteria play a key role such as “a sense of privacy”, “spatial quality”, etc.

A renovation *scenario* is a set of particular design changes that will be made to a building, e.g. replacing all north-facing windows with triple glazing, and adding a layer of insulation or replacing the final finish on façades with architectural aluminum panels. From a *scenario search and optimization* perspective, the challenge is to select a scenario that satisfies many competing soft and hard criteria such as energy consumption, indoor thermal comfort, daylight comfort etc., see [11]; we refer to these criteria as sustainability *Key Performance Indicators* (KPIs).

However, as a *design task* the challenge is not to simply find a single optimal scenario, but rather to identify and present meaningful renovation decisions that represent real tradeoffs between different KPIs, i.e. to find a set of *diverse* optimal scenarios that each prioritize *different* KPIs. Moreover, the user must be able to specify scenario *constraints* that all returned scenarios satisfy, e.g. “add a balcony to all exposed north-facing walls”. The designer can then engage in dialogue with stakeholders to incrementally refine the renovation design, from an early stage through to the more detailed final stages.

We present an innovative renovation decision support framework that provides design team with broad coverage of the design space in conjunction with limited, careful use of precise simulations for KPI evaluation. We build upon previous work in [16], on developing a formal (logic-based) domain specific renovation modeling language, named NovaDM, which enables design team to readily express their project-specific renovation design space at a range of abstraction levels.

Our key contributions are:

- we formalize NovaDM based on a software programming paradigm from artificial intelligence,

Answer Set Programming (ASP) [4] (Sections 2.3 and 2.4). We show how this provides an elegant mechanism for querying the *design space* of scenarios, for expressing semantically-rich design constraints, and for rapid, high-level constraint-based optimization [19];

- we integrate high-fidelity simulations to assess KPI values for given scenarios, using a simulation tool (Sections 2.1 and 3.1);
- we evaluate our approach on a real-world, large residential renovation case study in Denmark (Section 3).

2 THE RENOVATION DESIGN TASK AND NOVADM

The renovation design task is as follows: given a built environment, we can repair, replace, remove, refurbish, modify and add building facilities and architectural elements. The particular details of exactly *what* can be repaired, replaced, etc., and *how*, varies drastically between renovation projects. Thus, design team require a suitable “language” to express the particular renovation choices available, and this language should be *formal* so that software tools can be developed that can read and process such renovation information. We have developed NovaDM, a formal domain model to structure these concepts, as a basis for our renovation scenario generation system.

2.1 Scenario Generation System Overview

Figure 1 illustrates the workflow of our scenario generation system. First the design team specify the (a) project-specific renovation options in the form of a NovaDM action tree, (b) renovation scenario constraints, and (c) the Building Information Model (BIM) of the design to be renovated. Our scenario generator parses the action tree into Answer Set Programming (ASP) facts (Section 2.4) and generates (optimal) scenarios that are consistent with the given constraints using an ASP reasoning engine. Each scenario is then evaluated according to user-specified KPIs using a high-fidelity simulator ICEbear [20] (Section 3.1).

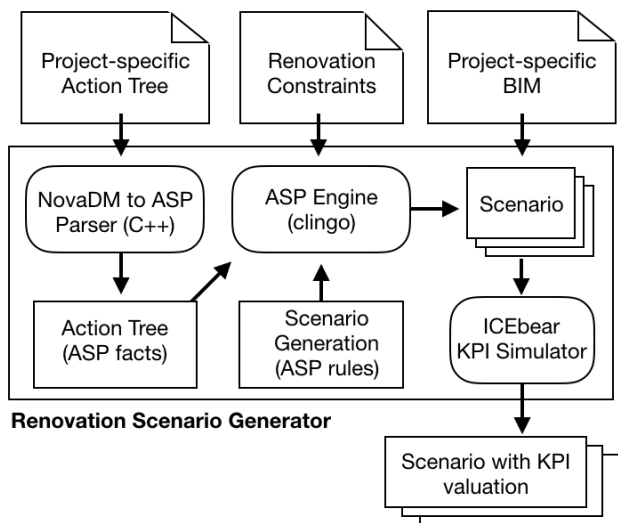


Figure 1. Workflow of renovation generation system.

2.2 Source Material for NovaDM

NovaDM is being developed based on many years of research in the topic of renovation, and through many use cases of renovation projects. Here, the meaning of the terms ‘holistic scenario’ and ‘sustainable renovation’ used in this paper is adopted from [13]. They serve as a means to unify the field for renovation strategies for refining and improving the contemporary building sector seen in the light of sustainability, ahead of generating renovation scenarios as holistically as possible.

There are a broad range of ‘renovation approaches’ that can be applied for the renovation of existing buildings including: insulation approaches, replacement of existing windows, integration or replacement of existing equipment, heating/cooling system, building envelope implementation of roof and partially of facades to avoid thermal bridges, total building envelope implementation, volumetric additions, partial replacement of existing windows, partial building envelope implementation, integration of PV and solar collectors on the roof/facades etc. [2].

Following previous work in [15], for development of the knowledge base of renovation approaches, we have extracted concepts from literature [1, 2, 5], from 10 European renovation research projects [14], and from the SIGMA database by Molio [17]. Moreover, as we present in Section 3, we studied a renovated building project case (Skovgårdsparken located in 8220 Brabrand, Denmark). The project was a residential building consisting of nine blocks built during 1968/72, and “modernistic” in terms of architectural typology. It was renovated by the Brabrand Housing Association. We selected this case to provide us with a real-world, comprehensive ‘renovation scenario’ (i.e. insulation of walls, renovation of foundation, installation of PV etc.) that has been applied for renovation in practice.

2.3 NovaDM Renovation Concepts

In this section we present the key concepts in NovaDM (see Figure 2). We use the term *renovation domain model*, (NovaDM [16]) to refer to a structured collection of renovation concepts and relationships between those concepts, similar to the notion of a “schema”. Concepts include cultural, technological, spatial, environmental, societal notions that have either a direct or indirect impact on building renovation. NovaDM is a first step towards formally structuring this information in a general, extensible manner.

Renovation Subject is: the object being renovated, e.g. windows. Subjects have a *type* (e.g. architectural element) and a *value* (e.g. window). Subject types correspond to categories of building elements in alignment with existing Building Information Models such as Industry Foundation Classes – IFC [21] including: Architectural Elements, Mechanical Elements, Individual Elements, Structural Elements, Electrical Elements, Interior Elements, Landscape Elements.

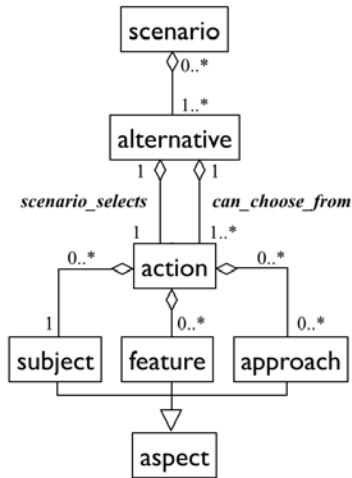


Figure 2. UML diagram illustrating relationships between concepts in NovaDM.

Renovation Approach is: the way that the subject will be renovated, e.g. repair, replace, remove, refurbish, or modify, e.g. see [14].

Renovation Feature is: the aspect of the subject being renovated, e.g. window frame material. Features have *types* (e.g. material) and *values* (e.g. fiberglass, uPVC, etc.).

Renovation Action is: an instance of a subject, an approach, and a set of feature types and values, e.g. “window frames will be replaced with fiberglass material”.

Renovation Alternative is: the set of (mutually exclusive) actions for a given subject, e.g. all the ways that windows can be renovated according to the specified approaches and features.

Renovation Scenario is: a set of actions such that each action belongs to a different alternative, e.g. one action for windows and one action for floors.

Action Trees. For each renovation project, the architect needs a way of specifying the particular *subjects*, *features* and *approaches* that are available; collectively, subjects, features and approaches are referred to as *aspects*. For this we have developed a formal action tree language for compactly specifying sets of actions has (see [16]).

Each action tree (see Figure 3) corresponds to a renovation *alternative*. Traversing an action tree corresponds to generating an action in a scenario, starting from the root node. Each node assigns zero or more *aspects* (subject, feature or approach) to the action. Tree nodes can be either *xor*-nodes “-” (meaning that the current action must be built by traversing **exactly one** child), or *and*-nodes “+” (meaning that the current action must be built by traversing **all** children). Figure 3 illustrates an action tree for describing the set of mutually exclusive actions for renovating windows.

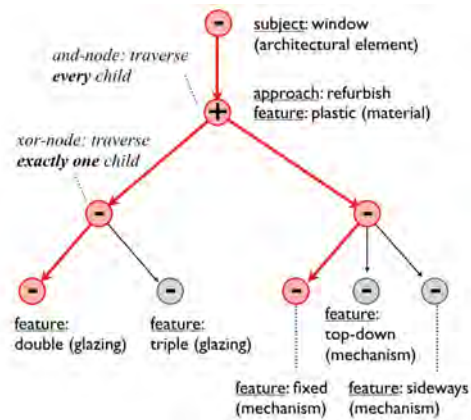


Figure 3. Example of an action tree describing six mutually exclusive actions. The red edges correspond to one particular action with: subject=window; approach=refurbish; features=upvc material, double glazing, fixed mechanism.

2.4 Generating Scenarios with ASP

A key innovation in our approach is the integration of Answer Set Programming (ASP) and high-fidelity simulations. ASP is a logic-programming paradigm developed within the artificial intelligence community that has its foundations in first-order logic [4]. Similar to Prolog, ASP has a knowledge base of *facts* and *rules* of the form “Head :- Body” meaning that, if the Body is true, then the Head must also be true. Rules with no Head are ASP *constraints*, written “:- Body” meaning that the Body must not be true (i.e. as a logical expression: *Body* implies *False*). *Choice rules* enable one to express that the “Head” may, or may not, be deduced, written “{Head}:- Body”, meaning that we can now define *combinations* of valid deduced facts. ASP *reasoning engines* are specifically designed to rapidly find combinations of deduced facts that are consistent with all given domain rules (referred to as *models* or *answer sets*), and can perform multi-criteria optimization by minimizing cost valuations that are assigned to deduced facts.

We have implemented our renovation domain model NovaDM as ASP *rules*, *constraints*, and *choice rules* such that valid combinations of deduced facts correspond to complete renovation scenarios. We encode project-specific renovation options as ASP *facts*. We encode project-specific renovation constraints as ASP *constraints*. We use the ASP solver (i.e. ASP reasoning engine) Clingo [24].

For example, the following ASP facts specify that node $t0_n0$ is an *xor*-node, and that it is a parent of node $t0_0_n0_n0$. This “child” node is an *and*-node with the subject “HVAC_systems” which is a subject type of “mechanical_elements” (this code is automatically generated from our NovaDM parser):¹

¹ We emphasize that we do not intend end-users to directly write ASP code. Instead, our system provides text-based and graphical interfaces and


```
node_type(t0_n0,xor).
parent(t0_n0,t0_n0_n0).
node_Type(t0_n0_n0,and).
subject(t0_n0_n0,"mechanical_elements","HVAC_systems").
. . .
```

Scenarios are generated by selecting action tree nodes. E.g. to select node *t0_n0_n0* we could assert the following fact:

```
select(t0_n0_n0).
```

Rather than referring explicitly to the node ID we can select nodes based on their aspects, e.g. select node N with a subject “HVAC_systems”:

```
select(N) :- subject(N,_, "HVAC_systems").
```

Words beginning with capital letters (and not in string quotes) are ASP variables, and the underscore “_” indicates variables whose values we do not care about. ASP will find all node IDs that satisfy this rule (i.e. substituting the N variable with valid terms such as *t0_n0_n0*) and deduce the corresponding *select* facts. Similarly we can generate scenarios that necessarily do *not* renovate HVAC systems by adding a constraint:

```
:- subject(N,_, "HVAC_systems"), select(N).
```

..or more generally, we can constrain scenarios to not renovate *any* mechanical elements:

```
:- subject(N, "mechanical_elements",_), select(N).
```

These rules can be complex logical expressions giving us significant flexibility and control over the types of scenarios that are generated. Importantly, we can use constraints to easily define rich renovation *typologies*. E.g. we might define a typology that represents minor renovation requiring that windows are renovated and that mechanical elements are not renovated:

```
select(N) :- typology(minor_renovation),
             subject(N, "architectural_elements", "windows").
:- typology(minor_renovation),
   subject(N, "mechanical_elements",_), select(N).
```

To select this typology in scenario generation we then simply assert the fact:

```
typology(minor_renovation).
```

For our case study in Section 3 we have formalized and implemented the Horizon2020 NeZBR [23] renovation typology framework.

Our domain rules that implement action trees include: (a) “if a node is selected then its parent must be selected”:

```
select(N1) :- select(N2), parent(N1,N2).
```

(b) “for each selected node N1, if N1 is an *xor*-node then *exactly one* child must be selected”:

```
1{select(N2) : parent(N1, N2)}1 :-
   select(N1), node_type(N1, xor), parent(N1,_).
```

the corresponding ASP code is automatically generated by our internal parsers.

(c) “for each selected node N1, if N1 is an *and*-node with a child N2 then N2 must be selected”:

```
select(N2) :- select(N1), node_type(N1, and), parent(N1,N2).
```

Generating Optimal Scenarios. We assign valuations to facts that can *order* scenarios with respect to individual KPIs without needing to compute the precise KPI values. In this manner we can rapidly generate optimal scenarios that lie on the pareto front [19], i.e. by pruning scenarios that are dominated by other scenarios, thus significantly reducing the search space.

For example, to minimize energy efficiency we need to minimize a u-value attribute assigned to various features. Single glazing windows necessarily have a higher u-value than double and triple glazing, and thus if all other aspects remain constant (such as window area) then we can *order* scenarios with respect to energy efficiency and glazing without deriving the exact u-value or computing the final energy efficiency KPI. E.g. the following rules expresses that if a scenario includes triple glazing for windows then the scenario gains a u-value attribute cost of 10:

```
attribute("u_value", N2, 10) :-
   subject(N, "architectural_elements", "window"),
   ancestor(N,N2),
   feature(N2, "glazing", "triple"), select(N2).
```

We then ask the ASP reasoning engine to not only find consistent scenarios, but scenarios that *minimize* this cumulative attribute cost:

```
#minimize(Cost,"u_value",N : attribute("u_value",N,Cost)).
```

We can minimize multiple attributes simultaneously; ASP will return dominating scenarios on the pareto front. Moreover, because the ASP search seamlessly incorporates constraints we can rapidly generate optimal *diverse* scenarios by optionally applying various combinations of renovation constraints and typologies. Once we have generated a set of optimal diverse scenarios, we then compute their precise KPI values using more computationally intensive simulators. Currently we are using the ICEbear simulator.

3 CASE STUDY – RESIDENTIAL DANISH BUILDINGS

In this section we present a case study where we empirically evaluate our system by applying it to real renovation tasks for a large residential building case in Denmark. The scenarios are built on the basis of different typologies, primarily related to the renovation depths and level of interventions that illustrate the impact of different ambition levels regarding the European environment and economy [3, 23]. The second level of typologies link to the typologies of the existing building according to [22]. Likewise, the third level of typologies target the architectural aspects and the appearance of the renovation scenario [2], especially related to the buildings’ facades.

Typologies for Renovation Depth / Intervention. The depth of renovation refers to the extent and size of measures applied as well as level of resulting energy and emissions

reduction. It is used to generate scenarios with various depths of renovation including Minor, Moderate, Deep, and Nearly Zero Energy (NZEB) [23]. The Minor is the least ambitious and represents renovation of only the exterior walls and windows. The second is Moderate that denotes basic interventions but, at the same time, tends to be a complete renovation, including the three types of energy efficient solutions (passive, active and Renewable Energy Sources - RES solutions). The next renovation level named Deep Renovation is more ambitious than the previous two and it is aligned with renovation of the building envelope and interior elements, which has a significant result in saving Energy. Finally, the last one is the most ambitious intervention representing a NZEB Renovation and it is in line with significant use of the Renewable Energy Sources in the renovation scenario.

Existing Buildings. Typology of the existing buildings encompasses the actual conditions of the existing buildings, which are different from project to project in connection to the location and climate regions, construction class, buildings operations, building's type and size classes, and their Heat Supply System, see [22].

Architectural Aspects. Architectural aspects are related to the typology of the façades, in connection to the major elements of the building facades. It refers to selection of the final finish material on the façade (i.e. Brick, Concrete, Wood etc.), size of the windows, add or refurbish the balconies, and also use of the sun control and shadings devices (overhangs) on the façade.

Table 1 lists the statistics of the number of concepts we defined using our action tree language, based on the above typologies. We defined 12 subjects (i.e. 12 action trees), each with a feature value count ranging from 4 to 51 values. This resulted in the number of mutually exclusive actions per subject ranging from 4 to 10.8 million actions. The very large number of actions is due to the combinatorial character of features, i.e. introducing a new feature type with just two values can double the number of actions (when those feature values are compatible with all combinations of previously defined feature values). We then assigned attributes of production cost and u-value to feature values, ranging from 4 to 24 assigned values per subject.

The size of the *scenario search space* that results from these actions trees is enormous. A renovation scenario consists of, at most, one action per subject. Thus, the number of scenarios where *only* exterior walls are renovated is 933,120 according to Table 1. The number of renovation scenarios where *every* subject is renovated is calculated by multiplying the number of all action counts, i.e. approximately 3.6×10^{42} . The complete scenario search space is much larger still, because not every subject is necessarily renovated, and thus we first need to count all combinations of 12 subjects, and then for each combination

of subjects multiply the number of actions of each selected subject.

Subject	Number of Feature Values	Number of Actions	Number of Attributes
Exterior walls	41	933,120	12
Interior walls	10	16	6
Curtain walls	31	36,288	10
Roof	51	10,886,400	24
Ground floor	16	126	8
Upper floor	15	126	7
Ceiling	16	90	6
Windows	46	4,717,144	18
Exterior doors	40	290,306	12
Interior doors	25	8,748	8
HVAC system	9	9	9
RES-Renewable energy sources	4	4	4

Table 1. Statistics of the action trees defined for the empirical evaluation of the Danish residential case study.

By using ASP we provide a mechanism to not only search through this enormous search space for optimal scenarios, but can readily incorporate constraints that refine the desired scenarios, e.g. forcing window material to be uPVC or only considering scenarios with total production costs below a given threshold.

3.1 KPIs for evaluation

Table 2 summarizes the evaluating KPIs for generated renovation scenarios in this study. We use an extended version of the hourly dynamic simulation tool ICEbear [20] to simulate the generating renovation scenarios for the listed KPIs in Table 2. ICEbear is a tool that strives to facilitate design buildings for architects and engineers, evaluating the impact of the geometry on the indoor climate and energy demand at the same time. It is based upon algorithms for auto-generating hourly building performance data at a room level basis.

KPIs	Evaluation
Energy consumption	kWh/m ² /year [less better]
Energy frames defined in BR18 (Danish building regulation 2018)	kWh/m ² /year [less better]
Indoor Thermal Comfort	% in Class I, II, III according to EN 15251 [bigger better]
Discomfort hours above 27 and 28 (°C)	Number of hours [less better]
Indoor Air Quality	% out of Class III according to EN 15251 [less better]
Investment Cost	Price of the procurement in DKK (Danish Krone) [less better]
DF (daylight factor)	0<DF<5 [bigger better]
Daylight requirements acco. to BR18	% >= 10 [bigger better]
View-out quality	% of openings area on façade regarding adjacent buildings [client dependent]
Degree of privacy	% of openings area on façade

	regarding adjacent buildings [client dependent]
Degree of Satisfaction	% regarding indoor thermal comfort & air quality [bigger better]
Health & Well-being	% regarding Energy improvement, indoor thermal comfort, air quality and their effects on Asthma, Allergy, and Eczema diseases [bigger better]

Table 2. Outline for the selecting criteria for evaluation of holistic renovation scenarios

3.2 Case Study Description

The selected case study is the renovation of a dwelling apartment block located in Aarhus, Denmark. The apartment block is a part of a dwelling area (see Figure 4) consisting of 27 identical apartment blocks built in 1967–1970. The blocks and common areas went through a renovation in the period of February 2014 to September 2017. The renovation included a refurbishment of all apartment blocks, new terraced houses, and common areas. The blocks were renovated in different styles, so they became a unit of two similar blocks. The façade types are, respectively, concrete/wood combination, and natural slate and zinc/aluminum/wood combination. The budget for the renovation of the blocks was estimated at 880 Mio. DKK.

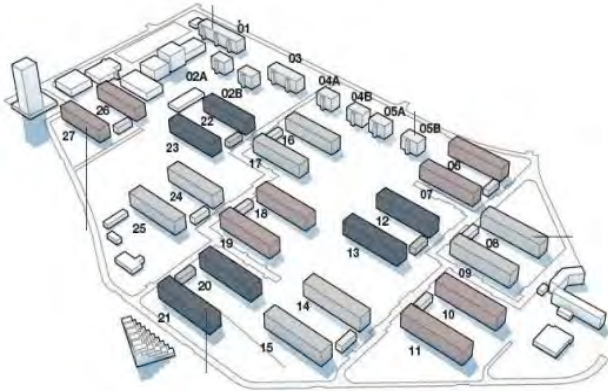


Figure 4. The dwelling area located in Aarhus, Denmark

Each apartment block consists of 32 unit apartments with similar layout, total heated floor area of 2700 m², 340 doors, and 129 windows. Prior to performance simulations of the generating renovation scenarios, the apartment block is separated into six different types of units (as demonstrated in Figure 5), as some units are placed on different floors as well as at the gables of the block and thereby have a larger exterior wall area or roof.

Table 3 provides the surface area and u-values for walls, floor, and roof of the existing apartment. These data related to the existing condition of the renovation project are used as the required input to ICEbear [20] to simulate the energy consumption and evaluate the thermal indoor comfort.

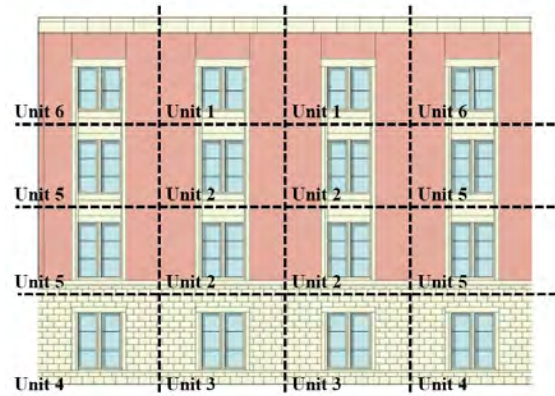


Figure 5. Placement of the unit types (the elevation view)

Unit 1	Floor	Roof	Windows	Walls
Area (m)	83.74	85.64	21.95	27.54
u-value	0.66	0.41	2.97	0.60
g-value	-	-	0.55	-
glass LT	-	-	0.65	-
frame width	-	-	0.06	-
frame spacer U	-	-	0.03	-
window loss	-	-	0.06	-

Table 3. The ‘unit 1’ apartment with coherent areas and attributes

3.3 Empirical Evaluation Results

For the empirical evaluation we defined 8 cases presented in Table 4. These cases correspond to realistic scenario typologies that clients and architects deem to be plausible in the context of Danish residential renovation. We defined all categories of the NeZeR renovation depth typologies, however in the Danish context only moderate renovation depth is realistic and thus we focused on this for cases 1-5.

For each case we generated 10 optimal scenarios using ASP, and then evaluated these 10 scenarios using ICEbear to get the exact KPI valuation (see Table 5).² The results show that this integration is highly effective and practical for semantic querying and constrained search (i.e. scenario generation with ASP) thus facilitating more effective renovation design support. The run-time for generating and evaluating 10 scenarios with a combination of typology constraints is approximately 9 seconds, with ~30% of run-time on ASP and ~70% on ICEbear.

To demonstrate the scalability of our approach with respect to semantic querying and constrained-search (i.e. before exact KPI evaluation) we ran a second round of experiments where we generated 1000 scenarios for each case. As presented in Table 6, run-time ranged between approximately 5-7 seconds per case.

² Experiments were run on an Intel Xeon(R) CPU E5-2620 v4 desktop computer running Windows 10, with 64 GB RAM and 2.10 GHz 2.10 GHz (2) processors








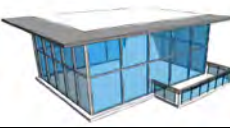
Case	Illustration	Description
1		Moderate, Replace, (1 side) Masonry façade-Brick, Small-scale window, with balcony + overhang, flat roof, non-ground floor
2		Moderate, Refurbish, (1 side) Masonry façade-Concrete, Large scale window, with balcony + overhang, flat roof, non-ground floor
3		Moderate, Replace, (2 side) Masonry façade-Architect panels, Small scale window, with overhang, flat roof, non-ground floor
4		Moderate, Replace, (1 side) Glass façade, with balcony as volume addition, flat roof, non-ground floor
5		Moderate, Refurbish, (2 side) Glass + Masonry façade-Concrete, Small-scale window, with balcony as volume addition + overhang, flat roof, non-ground floor
6		Minor, Replace, (1 side) Masonry façade-Brick, Small-scale window, with balcony, flat roof, non-ground floor
7		Deep, Replace, (1 side) Masonry façade-Concrete, Large scale window, with balcony as volume addition + overhang, flat roof, non-ground floor
8		NZEB, Replace, (2 side) Glass façade, with balcony + overhang, flat roof, non-ground floor

Table 4. Cases used in the empirical evaluation.

4 RELATED WORK

Recent research in building renovation seeks methods and decision support systems - DSSs for formulation of upgrade strategies, proposing renovation solutions via development of efficient renovation scenarios [10].

Various DSSs for building renovation already exist [6]. Forty-three decision support tools were considered in a literature review by the authors [18]. Some of the tools encompass the aspect of setting goals for sustainability, some focusing explicitly on the discussion of objectives among the decision-makers, and the rest providing a fixed set of criteria but leaving the weighting of the criteria open to the decision-makers.

The emerging development of new DSSs reflects the growing focus on renovation, and the need for efficient tools to support dialogue, communication, and decision-making in the early stages of renovation projects [7]. However, the majority of the existing tools in the design stage of renovation projects focus primarily to set up, evaluate, or optimize the sustainability KPIs [15], whereas a few support the decision-makers (in this case the architects/designers) to deal with the appropriate selection and formulation of the renovation scenarios, exploring an enormous “design space” of possible realistic renovation actions. Likewise, this entails evaluating the efficacy of each candidate design for a range of competing KPIs, using computationally expensive simulations (e.g. daylight parameters such as Daylight Autonomy, Useful Daylight Illuminance etc.), while the renovation scenarios are being formulated and generated[15].

Case	Time to generate 10 scenarios (seconds)	Time to evaluate 10 scenarios (seconds)	Total time (seconds)
1	2.80	6.35	9.10
2	2.41	6.81	9.22
3	2.83	6.36	9.19
4	2.79	6.38	9.35
5	2.97	6.70	9.67
6	1.59	6.62	8.21
7	2.91	6.81	9.72
8	3.02	6.98	10.00

Table 5. Run-time for generating 10 scenarios (using ASP) and evaluating 10 scenarios (using ICEbear) per case.

Case	1	2	3	4	5	6	7	8
Time seconds	6.14	5.87	6.68	5.71	6.28	4.37	6.54	6.82

Table 6. Run-time to generate 1000 scenarios.

5 CONCLUSION

We have presented a renovation design support system that provides formal language NovaDM for quickly defining project-specific renovation options (valid combinations of subjects, features, approaches), and generates and evaluates renovation scenarios under constraints based on an integration of Answer Set Programming and ICEbear³.

Our approach is a significant departure from existing optimization approaches in renovation design that deliver a small number of similar, optimal designs with no intermediate layers of abstraction, and no support in analyzing and exploring the diversity of the design space. In future work we are looking to utilize regression and surrogate methods for capturing more complex

³ A video of our prototype which is developed as a part of a tool named PARDIS, can be watched in the following link: <https://www.dropbox.com/s/rabym5ys3b63thw/PARDIS%200.0.6%20-%20Demo.mp4?dl=0>

relationships between KPIs and expressing these as ASP rules for rapid renovation scenario search space exploration. This will be particularly valuable when more computationally expensive KPI simulators are employed.

REFERENCES

1. Baker, N. *The Handbook of Sustainable Refurbishment: Nondomestic Buildings*. Earthscan, London, UK, 2009.
2. Boeri, A., Antonin, E., Gaspari, J., & Longo, D. *Energy Design Strategies for Retrofitting: Methodology, Technologies, Renovation Options and Applications*. WIT Press, Southampton, 2014.
3. BPIE - Buildings Performance Institute Europe, Europe's buildings under the microscope. <http://bpie.eu/wp-content/uploads>. As of 10 November 2011.
4. Brewka, G., Eiter, T., & Truszczynski, M. Answer set programming at a glance. *Communication ACM* 54, 12 (2011), 92–103.
5. Burton, S. *The Handbook of Sustainable Refurbishment: Housing*. Earthscan, Abingdon, 2012.
6. Ferreira, J., Pinheiro, M.D., de Brito, J. Refurbishment decision support tools review—energy and life cycle as key aspects to sustainable refurbishment projects. *Energy Policy*, 62 (2013), 1453–1460.
7. Gade, A.N., Larsen, T.S., Nissen, S.B., & Jensen, R.L. REDIS: A value-based decision support tool for renovation of building portfolios. *Building and environment*, 142 (2018), 107-118.
8. International Living Future Institute. Living Building Challenges. <https://living-future.org/wpcontent/uploads/2016/12/Living-Building-Challenge-3.0-Standard.pdf>. As of February 2014.
9. Jensen, P.A., & Maslesa, E. Value based building renovation – A tool for decision making and evaluation. *Building and Environment*, 92 (2015), 1-9.
10. Juan, Y., Gaob, P., & Wangc, J. A hybrid decision support system for sustainable office building renovation and energy performance improvement. *Energy and Buildings* 42, 3 (2010), 290–297.
11. Kamari, A., Corrao, R., & Kirkegaard, P.H. Sustainability focused Decision-making in Building Renovation. *International Journal of Sustainable Built Environment* 6, 2(2017), 330-350.
12. Kamari, A., Jensen, S. R., Corrao, R., & Kirkegaard, P. H. A Holistic Multi-methodology for Sustainable Renovation. *International Journal of Strategic Property Management* 23, 1(2019). Manuscript has been accepted ahead of publication.
13. Kamari, A., Corrao, R., Petersen, S., & Kirkegaard, P.H. Tectonic Sustainable Building Design for the development of renovation scenarios – Analysis of ten European renovation research projects. *SER4SE 2018 (seismic and Energy Renovation for Sustainable Cities) conference*, Catania, Italy (2018), 645-656.
14. Kamari, A., Corrao, R., Petersen, S., & Kirkegaard, P.H. Towards the development of a Decision Support System (DSS) for building renovation: Dependency Structure Matrix (DSM) for sustainability renovation criteria and alternative renovation solutions. *SER4SE 2018 (seismic and Energy Renovation for Sustainable Cities) conference*, Catania, Italy (2018), 564-576.
15. Kamari, A., Jensen, S., Christensen, M.L., Petersen, S., & Kirkegaard, P.H. A hybrid Decision Support System for Generation of Holistic Renovation Scenarios—Cases of Energy Consumption, Investment Cost, and Thermal Indoor Comfort. *Sustainability* 10, 4 (2018), 1255-1278.
16. Kamari, A., Schultz, C., & Kirkegaard, P.H. NovaDM: Towards a formal, unified Renovation Domain Model for the generation of holistic renovation scenarios. *ECPPM 2018 (12th European Conference on Product & Process Modelling) conference*, Copenhagen, Denmark (2018), 197-205.
17. Molio 2016. Molio Price data. <https://molio.dk/molio-prisdata/prisdata-footer/brug-molioprisdata/>. As of 21 March 2016.
18. Nielsen, A.N., Jensen, R.L., Larsen, T.S., & Nissen, S.B. Early stage decision support for sustainable building renovation—A review. *Building and environment*, 103(2016), 165-181.
19. Pareto, V. *Cours d'Economie Politique*. Droz.olio-prisdata, Geneva, 1896.
20. Purup, P.B., & Petersen, S. Rapid Simulation of Various Types of HVAC Systems in the Early Design Stage. *Energy Procedia*, 122(2017), 469-474.
21. Schultz, C., & Bhatt, M. InSpace3D: A Middleware for Built Environment Data Access and Analytics. *ICCS 2013 (International Conference on Computational Science)*, Barcelona, Spain (2013), 80–89.
22. TABULA. Typology Approach for Building Stock Energy Assessment. <http://episcopes.eu/building-typology>. As of 18 May 2017.
23. TECNALIA. Intervention criteria and packaged solutions for buildings renovation towards a NZEBR. <http://www.nezer-project.eu/download>
24. Tgebser, M., Kaminski, R., Kaufmann, B., Ostrowski, M., Schaub, T., & Wanko, P. Theory solving made easy with clingo 5. In OASICs-OpenAccess Series in Informatics 52. Schloss Dagstuhl-Leibniz-Zentrum fuer Informatik (2016).



Application of Surrogate Modeling to Multi-Objective Optimization for Residential Retrofit Design

Arfa N. Aijazi^{1,2} and Leon R. Glicksman²

¹Center for the Built Environment,
University of California
Berkeley, CA USA
arfa@berkeley.edu

²Building Technology Group,
Massachusetts Institute of Technology
Cambridge, MA USA
glicks@mit.edu

ABSTRACT

This project combines surrogate modeling, a supervised machine learning technique, to bypass whole building energy simulations to enable multi-objective design optimization. We applied this method to identify Pareto optimal retrofit designs that are energy and cost effective for three residential apartments in Lisbon, Portugal. As part of our validation of this approach, we compared the surrogate model error for these Pareto optimal designs to the error in the rest of the design space when compared to a detailed energy simulation. Surrogate model error is higher towards the minimum and maximum energy consumption within the Pareto optimal designs compared to the rest of the design space. We also find that in the Pareto optimal set some design variable values are near their minimum or maximum value, which could be driving higher surrogate model error. We propose that future research should retrain the surrogate model after identifying design variable values of interest from an initial optimization run.

1 INTRODUCTION

The age and quality of residential buildings in Portugal presents a unique opportunity for rehabilitation of the building stock. According to the 2001 national census, the average Portuguese building is 34 years old and over half of residential buildings constructed between 1960-1980 need some kind of repair [19]. These buildings also predate national energy efficiency requirements, introduced in 1991 for residential buildings and 1998 for commercial buildings [8]. So it is not surprising that the vast majority of existing buildings lack common energy conservation measures, for example among residential buildings, 79% lack exterior wall insulation, 89% lack roof insulation, and 75% have single-glazed windows on the south façade [20].

To address deficiencies in the Portuguese building stock, *SusCity: Urban data driven models for creative and resourceful urban transitions* (SusCity) aims to develop

and integrate new tools and services to improve energy efficiency by focusing on urban interventions in Lisbon, Portugal at the Parque das Nações testbed. The project is a consortium between 13 government, industry, and university partners. In this paper, the SusCity test bed serves as a case study to apply computational techniques to make retrofit recommendations that can guide policy to encourage building energy efficiency.

In recent years, data analysts and engineers have applied machine learning techniques to a variety of problems from bioinformatics to online advertising. Applications in building performance include mechanical system controls, model calibration, and building energy consumption [1,14,17]. This research focuses on a general class of machine learning techniques called supervised machine learning, where paired input and output data train the machine learning model. In surrogate models the output data is a performance metric obtained from a detailed simulation. Other areas of research refer to these models as meta-models or emulators.

One of the most exciting applications of surrogate modeling is the potential to apply gradient-based multi-objective optimization techniques to inform building design. The maturation of building energy performance simulations and the advent of more powerful computers now allow application of design optimization processes to inform building design.

The goal of this research is to apply surrogate models to multi-objective optimization to select building retrofit designs that balance energy consumption and the capital cost, which are two important factors of consideration for a residential unit owner. A unique contribution of this work is that we compare the surrogate model error for optimal designs versus the error in the overall design space. This is important for informing how we should train such models for computational optimization applications. Though these methods rely on the difference in slope of the performance

objective, we cannot assume a uniform error between the surrogate model and the detailed simulation.

2 PRIOR WORK

There is significant research and interest in applying computational optimization methods to the building design process as it provides a rigorous way to explore tradeoffs between large numbers of design options. Evins provides a comprehensive review of computational optimization for sustainable building design [10]. The greatest limitation is the speed of building performance simulations, which surrogate models can help overcome.

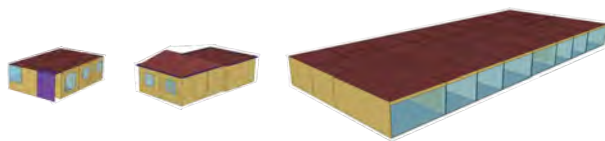
There are several examples of applying surrogate models for predicting energy performance of newly designed buildings. One study used multivariate linear regression to build a surrogate model with 27 design parameters as model inputs [12]. Another study trained a surrogate model from randomly generated floor plates, using 22 form-related building parameters to train the model [7]. Compared to new design, retrofit design is highly constrained due to the nature of working within an existing building.

There are two examples of work utilizing Artificial Neural Networks (ANN) to bypass building energy simulations to predict energy consumption of existing buildings [5,6]. In Asadi et al. the ANN model bypasses a model of an existing building in TRNSYS, an energy simulation engine, and joins with a multi-objective optimization algorithm to minimize energy consumption, retrofit cost, and thermal discomfort hours.

This paper builds on previous work by including additional retrofit parameters such as air infiltration and lighting, which both have significant impact on energy consumption [3]. Finally, we compare surrogate model performance for optimization results to that in the overall design space.

3 METHODS

3.1 Surrogate Model Development



(a) Pedro Sousa (b) João Barata (c) Carlos Camelo

Figure 1. SusCity apartment building energy models visualized in OpenStudio. Large shading surfaces omitted for clarity.

Three SusCity apartments serve as case studies for this research, visualized in Figure 1. SusCity project partners at the Instituto Superior Técnico (IST) and the Laboratório Nacional de Energia e Geologia (LNEG) developed whole-building energy models in EnergyPlus, which form the basis for the surrogate models and calibrated model inputs, namely internal gains and occupancy schedules, using

monitored data for energy consumption in each apartment. EnergyPlus is a whole-building energy simulation program developed and funded by the U.S. Department of Energy’s Building Technology Office and is the industry standard building energy simulation platform [21]

Table 1 summarizes select energy model inputs for the three apartment buildings, which represents the existing condition. The Pedro Sousa apartment is on the ground floor, while the João Barata and Carlos Camelo apartments are on the top floor. Ground floor apartments require a floor U-factor and top floor apartments a roof U-factor. Otherwise, we consider surfaces adjacent to other apartment units as adiabatic. The zone heating and cooling needs are met by an ideal loads air system in EnergyPlus, which corresponds to an ideal VAV terminal unit. In these models the capacity is autosized to meet the zone heating and cooling demand.

Model Parameter	Units	Pedro Sousa	João Barata	Carlos Camelo
Area	m ²	47.11	97.97	486.92
Construction Period	Year	1961-1990	1946-1960	1991-2005
Thermal Zones	No.	6	7	42
EnergyPlus Runtime	Seconds	9.5	14.1	35.9
Window-to-Wall Ratio	%	29	31	42
Lighting	W/m ²	11.5	6.9	3.3
People	m ² /person	11.8	16.3	15.2
Plug Loads	W/m ²	99.6	85.7	65.2
Window U-Factor	W/m ² -K	2.7	2.7	2.8
Window SHGC ^a	-	0.7	0.7	0.7
Wall U-Factor	W/m ² -K	1.1	3.1	0.5
Roof U-Factor	W/m ² -K	-	3.9	0.5
Floor U-Factor	W/m ² -K	2.2	-	-
Infiltration	ACH ^b	0.9	1.0	0.6

^a Solar heat gain coefficient

^b Air changes per hour

Table 1. Energy model inputs for SusCity apartments

The design space for multi-objective optimization represents possible retrofits for SusCity apartments. SusCity project partners helped to ensure the range of performance is realistic for residential construction in Portugal. Table 2 summarizes the minimum and maximum value for each retrofit parameter.

Retrofit Variable	Units	Min	Max
Window U-Factor	W/m ² -K	1.1	6.0
Window SHGC ^a	-	0.35	0.80
Infiltration	ACH ^b	0.35	1.00
Wall Insulation	m	0	0.12
Floor Insulation	m	0	0.12
Roof Insulation	m	0	0.12
Lighting ^c	-	LED	Fluorescent

^a Solar heat gain coefficient

^b Air changes per hour

^c Lighting power calculated individually for each apartment based on target illuminance by space type.

Table 2. Retrofit design variables and ranges.

In general the steps to build a surrogate model are 1) develop a detailed simulation model 2) generate a library of results over the design space 3) fit the results to a statistical function and 4) test model performance [11]. We used EnergyPlus as the detailed simulation engine for this analysis..

For surrogate modeling, we generate data points deliberately as opposed to relying on pre-existing data sets. Therefore, we can explicitly control the sampling plan for the training data set. In general, the surrogate model is most accurate near points in the training data set used to build the model. Standard practice is to ensure a uniform level of accuracy throughout the design space by sampling a uniform spread of points throughout the design space [11]. One example of such a stratified sampling method is the Latin hypercube, where we divide the range of each variable into bins and randomly select one value from each bin. We used the MATLAB implementation of the Latin hypercube, lhsdesign, in the Statistics and Machine Learning Toolbox [15].

Based on prior study of surrogate model regression techniques, we used the Kriging technique due to high accuracy and fidelity for predicting building energy consumption [2,4]. We trained the surrogate model from the total energy consumption, which is the sum of heating, cooling, interior lighting, and interior equipment loads calculated from a detailed simulation. The total energy consumption is also an objective in multi-objective optimization.

3.2 Retrofit Cost Model

In addition to total energy consumption, retrofit cost serves as a second performance objective in multi-objective optimization. Gerador de Precos, an online software tool for estimating engineering and construction costs in Portugal, provided the retrofit cost all design variables except lighting [9]. The reported cost includes estimates for surface preparation, installation, and materials. Figure 2 shows how retrofit cost varies by performance for each design variable.

We treated the cost of each design variable as independent of one another except for window U-value and SHGC. To prevent double counting the cost of window replacement, for a given retrofit design we compared the window U-value and SHGCC to those of windows in Gerador de Precos and assigned the cost with the minimum Euclidean distance. For infiltration, Gerador de Precos provided three levels of weatherization by sealing window frames based on linear feet. We approximated these three levels of rehabilitation to three air infiltration rates and computed the total cost per apartment based on the total perimeter of glazed openings.

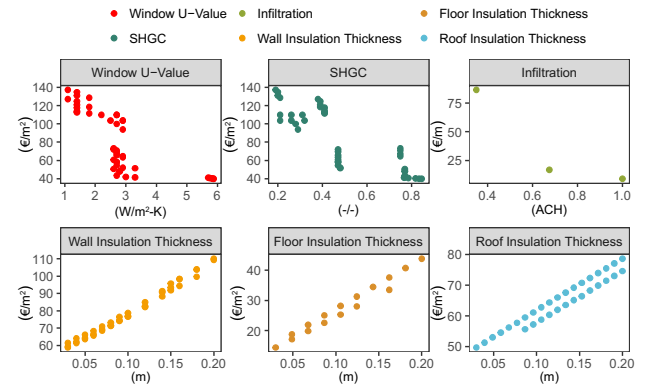


Figure 2. Relationship between design variable performance and retrofit cost in Lisbon [9].

For other design variables, we fit a continuous function between data points obtained from Gerador de Precos to interpolate the cost for any value within the retrofit design space, summarized in Table 3. Although the continuous functions have high values for the correlation coefficient, i.e. greater than 0.9, there are few data points in Gerador de Precos for the retrofit cost of infiltration.

Retrofit Variable, x	n	Continuous Function, $y(x)$	R ²
Infiltration	3	$y(x) = 8.35x^{-2.17}$	0.99
Wall Insulation	41	$y(x) = 292.20x + 49.57$	0.99
Floor Insulation	16	$y(x) = 317.57x + 4.83$	0.97
Roof Insulation	32	$y(x) = 298.53 + 34.44$	0.94

Table 3. Continuous functions to interpolate retrofit cost.

We obtained the cost of an LED lighting replacement from IKEA Portugal summarized in Table 4 [22]. We selected the minimum number of LED lightbulbs to meet the required lumens for each space type in each apartment.

The total retrofit cost is the sum of the cost of each individual design variable and is an objective for multi-objective optimization.

Lumens	Power (W)	Cost (€/bulb)
400	5	4
600	8	8
1000	13	10

Table 4. Lumen, average power, and average cost of LED lightbulbs from IKEA Portugal [22].

3.3 Multi-Objective Optimization

The overall goal is to find retrofit designs that are both energy efficient and cost effective. We used computational optimization methods to identify combinations of variables in Table 2 that minimize total energy consumption and total retrofit cost. In multi-objective optimization, rather than a single optimum solution, the result is a set of solutions called the Pareto set or Pareto front. For designs in the Pareto set, the performance of one objective cannot improve without sacrificing performance of another. We used the MATLAB implementation of the genetic algorithm, `gamultiobj`, in the Global Optimization Toolbox with a function tolerance of $1e-4$ to search the design space. The optimization solved for the minimum of total energy consumption and total retrofit cost subject to an inequality constraint of the minimum and maximum value for each design variable listed in Table 2.

Computational optimization algorithms traditionally evaluate thousands of design combinations before converging to the Pareto set. For each iteration, the algorithm must evaluate the performance objective, one of which is output of a building energy simulation. For the SusCity apartments, each simulation takes between 10-30 seconds to compute, which is still too computationally expensive. The surrogate model for each apartment, as described in Section 3.1, allows the optimization to bypass direct energy simulations and predict total energy consumption in a fraction of a second, greatly accelerating the search for Pareto optimal designs.

3.4 Model Error

We can use multi-objective optimization because we used a Kriging surrogate model to bypass detailed energy simulations. This approach is only reasonable if the surrogate model is accurate relative to the detailed simulation. We computed global surrogate model error as the coefficient of variation (CV) of the root mean square error (RMSE). We define RMSE in Equation (1) where N is the number of design points, y_i is the simulated performance, and \hat{y}_i is the predicted performance [16]. The CV is the RMSE divided by \bar{y} , the mean value of simulated performance, and allows us to compare surrogate model error among different groups.

$$\text{RMSE} = \sqrt{\frac{1}{N} \sum_{i=1}^N (\hat{y}_i - y_i)^2} \quad (1)$$

$$\text{CV} = \frac{\text{RMSE}}{\bar{y}} \times 100 \quad (2)$$

Prior work suggests that the error is higher at the extremes of the design space for a linear-regression based model [13]. We compared surrogate model error relative to the detailed simulation for Pareto optimal designs and the whole design space for each SusCity apartment. We then evaluated the distribution of Pareto optimal retrofit variables to see if extreme values in the design space could be driving model error.

4 RESULTS AND DISCUSSION

4.1 Existing Building Energy Consumption

To better understand the results from multi-objective optimization, Figure 3 breaks down the energy consumption by end use for each apartment building. In all three apartments, interior equipment loads dominate, constituting as much as 76% of total energy consumption.

None of the retrofit options considered in this study address the interior equipment loads, which limits performance improvements. The apartments differ in the relative contribution of heating, cooling, and lighting energy consumption. The second largest contributor to the total load, is heating energy in the Pedro Sousa apartment but cooling energy in the João Barata and Carlos Camelo apartments. Overall, interior lighting represents the smallest contributor to total energy consumption.

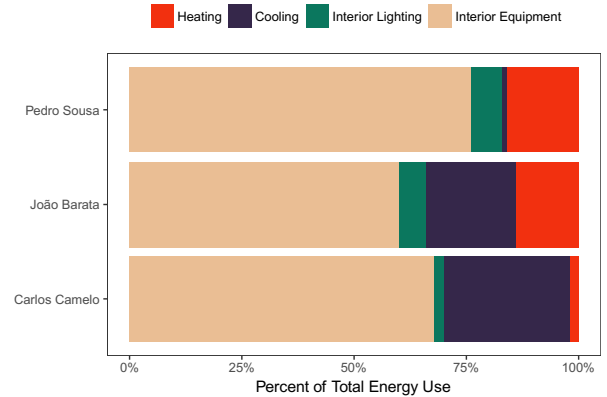


Figure 3. Breakdown of energy consumption by end use for existing apartments.

4.2 Multi-Objective Optimization

Figure 4 shows the resulting Pareto optimal designs as well as a stratified sample within the design space for each apartment. The Pareto optimal designs for each apartment are the result of approximately 7,000 evaluations of the surrogate model as part of the genetic algorithm. Using a detailed energy simulation that takes 10-30 seconds per iteration, each plot would take 1-3 days to produce. Each iteration with a Kriging surrogate model takes 0.0006 seconds, so each plot took less than 4 minutes to produce.

The results show that some retrofits within the design space result in increased total energy use relative to the existing building. However, all the Pareto optimal designs use less energy than the existing building. The normalized total energy use and retrofit cost vary by apartment.

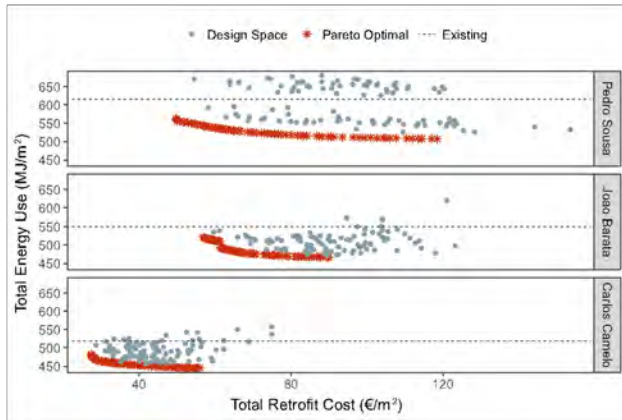


Figure 4. Multi-objective performance for a stratified sample and Pareto optimal designs for each SusCity apartment.

4.3 Model Error

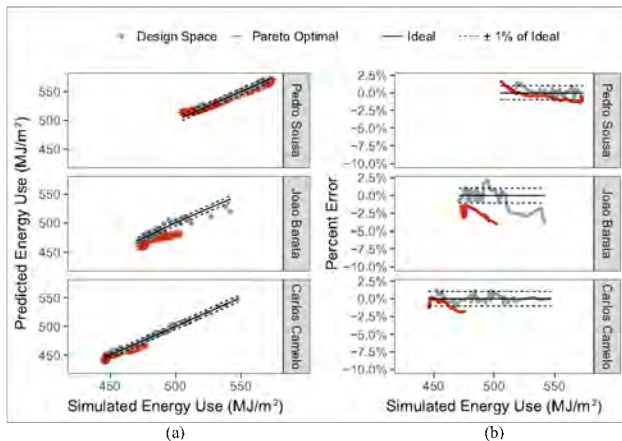


Figure 5. a) Surrogate model predictions (b) percent difference as a function of simulated energy use.

Figure 5a shows the surrogate model predictions for total energy use relative to a detailed simulation in EnergyPlus for a stratified sample in the design space and the Pareto optimal designs. The ideal case is when the surrogate model prediction exactly matches the simulated value and is represented by a solid line with a slope of 1. Dashed lines representing $\pm 1\%$ of the ideal case are included for reference. Figure 5b shows the percent error as a function of the simulated total energy use to give a sense of how error varies through the design space. Surrogate model error in Pareto optimal designs tends to be higher for extremely low and high values of total energy represented in that set of designs. Error within the design space can also be higher at extreme values for energy use – such as the for energy use larger than 500 MJ/m^2 in the Joao Barata apartment. Generally, the percent error within the design space oscillates around 0%. Interestingly, for the similar

values of total energy use, the Pareto optimal design will generally have a larger percent difference relative to the design space.

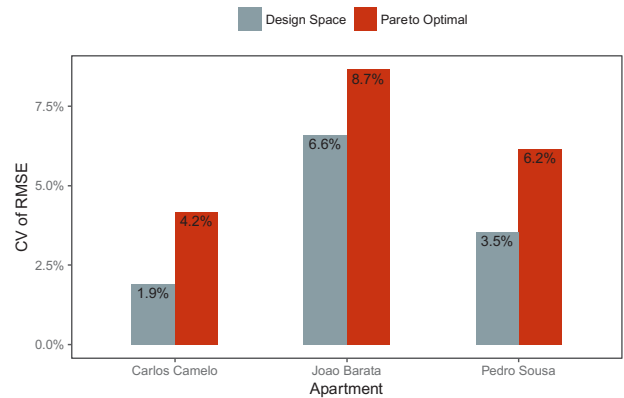


Figure 6. Global model error for a stratified sample and Pareto optimal designs for each SusCity apartment.

Figure 6 shows the CV of the RMSE for a stratified sample within the design space and Pareto optimal designs for each SusCity apartment. For all three apartments the CV is higher in the Pareto optimal set than the general design space. This is consistent with the results found in Figure 5, that surrogate model error is higher in the set of Pareto optimal designs.

The results show that the distribution of values for each design variable varies among the three apartments. Several variables have a bimodal distributions, meaning that the optimal designs are highly concentrated at their minimum or maximum such. These extremes are likely driving the higher surrogate model error for Pareto optimal designs observed in Figures 5 and 6.

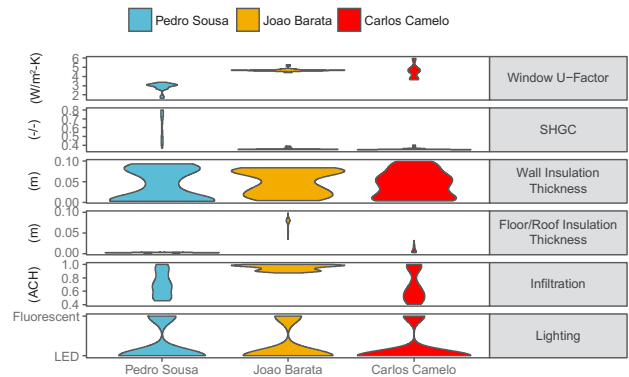


Figure 7. Distribution of design variable values for the Pareto optimal set for each SusCity apartment.

Figure 7 shows the distribution of design variables in the Pareto optimal set as a violin plot. This type of plot is similar to a box plot in that it shows the range of values, but the shape and width is reflective of the probability density of the data at different values. The y-axis scale

reflects the minimum and maximum value of each design variable from Table 2.

This suggests that current practice of stratified sampling for training surrogate models is inadequate for applications to optimization, because we are not interested in a uniform error throughout the design space. In the case of optimization, we are seeking out extreme design values to minimize performance objectives, which increases the error of the surrogate model. The challenge is we do not know the relationship between design variable values and the performance objectives a priori. An approach for future research could be to use optimization outputs to retrain the surrogate model in a narrower region within the design space. This approach to adaptively update the surrogate model has precedent in optimization literature [18].

5 CONCLUSIONS

In this research we combined surrogate modeling with multi-objective optimization to identify energy and cost-effective retrofits for three residential apartments in Lisbon, Portugal. To validate this approach, we reviewed the surrogate model error as a function of the simulated value for total energy and found a higher magnitude of percent error for extremely high or low values. Reviewing the global surrogate model error showed that designs in the Pareto optimal set had higher values of CV, meaning these predictions have greater variance. Further work should explore alternative approaches to sampling and training the surrogate model to reduce error for the Pareto optimal designs, which is the value of interest for multi-objective optimization.

6 REFERENCES

1. Abdul Afram and Farrokh Janabi-Sharifi. 2014. Theory and applications of HVAC control systems – A review of model predictive control (MPC). *Building and Environment* 72: 343–355. <https://doi.org/10.1016/j.buildenv.2013.11.016>
2. Arfa N. Aijazi. 2017. Machine learning paradigms for building energy performance simulations. Massachusetts Institute of Technology. Retrieved February 25, 2018 from <http://dspace.mit.edu/handle/1721.1/111280>
3. Arfa N Aijazi and Leon R Glicksman. 2016. Comparison of Regression Techniques for Surrogate Models of Building Energy Performance. 8.
4. Arfa N. Aijazi and Leon R. Glicksman. 2016. Comparison of Regression Techniques for Surrogate Models of Building Energy Performance. In *Proceedings of SimBuild*.
5. Ehsan Asadi, Manuel Gameiro da Silva, Carlos Henggeler Antunes, Luís Dias, and Leon Glicksman. 2014. Multi-objective optimization for building retrofit: A model using genetic algorithm and artificial neural network and an application. *Energy and Buildings* 81: 444–456. <https://doi.org/10.1016/j.enbuild.2014.06.009>
6. Fabrizio Ascione, Nicola Bianco, Claudio De Stasio, Gerardo Maria Mauro, and Giuseppe Peter Vanoli. 2017. Artificial neural networks to predict energy performance and retrofit scenarios for any member of a building category: A novel approach. *Energy* 118: 999–1017. <https://doi.org/10.1016/j.energy.2016.10.126>
7. Mohammad Rahmani Asl, Weili Xu, Jin Shang, Barry Tsai, and Ian Molloy. 2016. Regression-Based Building Energy Performance Assessment Using Building Information Model (BIM). *Proceedings of SimBuild* 6, 1. Retrieved April 25, 2018 from <http://ibpsa-usa.org/index.php/ibpusa/article/view/379>
8. BCAP. 2018. Portugal | The Building Codes Assistance Project. *Building Codes Assistance Project*. Retrieved April 25, 2018 from <https://bcapcodes.org/code-status/country/portugal/>
9. CYPE Ingenieros, S.A. 2018. Gerador de preços para construção civil. Portugal. Retrieved April 25, 2018 from <http://geradordeprecos.info/>
10. Ralph Evins. 2013. A review of computational optimisation methods applied to sustainable building design. *Renewable and Sustainable Energy Reviews* 22: 230–245. <https://doi.org/10.1016/j.rser.2013.02.004>
11. Alexander Forrester, Andrés Sobester, and Andrew Keane. 2008. *Engineering Design via Surrogate Modeling: A Practical Guide*. J. Wiley.
12. Janelle S. Hygh, Joseph F. DeCarolis, David B. Hill, and S. Ranji Ranjithan. 2012. Multivariate regression as an energy assessment tool in early building design. *Building and Environment* 57: 165–175. <https://doi.org/10.1016/j.buildenv.2012.04.021>
13. Andrew (Andrew Joseph) Mandelbaum. 2014. Improvements to building energy usage modeling during early design stages and retrofits. Massachusetts Institute of Technology. Retrieved April 26, 2018 from <http://dspace.mit.edu/handle/1721.1/912195>
14. Massimiliano Manfren, Niccolò Aste, and Reza Moshksar. 2013. Calibration and uncertainty analysis for computer models – A meta-model based approach for integrated building energy simulation. *Applied Energy* 103: 627–641. <https://doi.org/10.1016/j.apenergy.2012.10.031>
15. MathWorks. 2018. MATLAB - MathWorks - MATLAB & Simulink. Retrieved April 25, 2018 from <https://www.mathworks.com/products/matlab.html>
16. Caitlin T. Mueller. 2014. Computational exploration of the structural design space. Massachusetts Institute of Technology. Retrieved April 26, 2018 from <http://dspace.mit.edu/handle/1721.1/91293>
17. Zhiguang Qian, Carolyn Conner Seepersad, V. Roshan Joseph, Janet K. Allen, and C. F. Jeff Wu. 2006. Building Surrogate Models Based on Detailed and Approximate Simulations. *Journal of Mechanical*

- Design* 128, 4: 668–677.
<https://doi.org/10.1115/1.2179459>
18. David Brian Serafini. 1999. A framework for managing models in nonlinear optimization of computationally expensive functions. Retrieved February 14, 2019 from <https://scholarship.rice.edu/handle/1911/19444>
 19. J. Sousa, L. Bragança, M. Almeida, and P. Silva. 2013. Research on the Portuguese Building Stock and Its Impacts on Energy Consumption – An Average U-Value Approach. *Archives of Civil Engineering* 59, 4. <https://doi.org/10.2478/ace-2013-0029>
 20. Joana Sousa, Sandra Silva, and Manuela Almeida. 2012. Energy Rehabilitation of Portuguese Residential Building Stock Through its Transformation into NZEB. 8.
 21. EnergyPlus | EnergyPlus. Retrieved November 22, 2018 from <https://energyplus.net/>
 22. IKEA - Móveis e decoração, tudo para a sua casa - IKEA. Retrieved November 22, 2018 from <https://www.ikea.com/pt/pt/>



Aerial Thermography as a Tool to Inform Building Envelope Simulation Models

Norhan Bayomi¹, Shreshth Nagpal¹, Tarek Rakha², Christoph Reinhart¹ and John E. Fernandez¹

¹Massachusetts institute of Technology
Cambridge, MA- USA
{nourhan, shreshth, tito_, fernande}@mit.edu

²Georgia Institute of Technology
Atlanta, GA- USA
rakha@design.gatech.edu

ABSTRACT

The building sector consumes more than 33% of global energy use and around 50% of electricity consumption, and is responsible for one third of global carbon emissions [1]. Envelope and windows alone impact over 50% of energy loads in buildings [2]. Thus, understanding building envelopes' thermal performance is critical to the application of energy efficiency retrofits. Through detecting main envelope thermal deficiencies and areas of deterioration, suitable energy management measures can be effectively determined. While simulation models are considered as reliable tools to understand building energy performance, they rely significantly on assumptions related to envelope performance [3,4]. The main contribution of this paper stems from the proposed analysis framework, which integrates Unmanned Aerial Vehicles (UAVs) equipped with thermal cameras in estimating thermal transmittance properties of existing building envelope, specifically opaque walls, and using these data to calibrate energy simulation models for better predictions. Results revealed a significant increase in the accuracy of heating energy use prediction during winter months. With the proposed workflow, simulation errors were reduced from over 20% to less than 1%.

Author Keywords

Aerial Thermal Mapping; Energy Simulation; Drones; Thermal Transmittance; Energy Efficiency.

ACM Classification Keywords

Building Energy Simulation; Experimentation; Performance.

1 INTRODUCTION

Building envelopes play a major role in energy consumption, as they account for 25% of total energy use [5]. Yet, envelope improvements can impact around 57% of commercial buildings' energy use and 42% of residential energy use [1]. Thermal transmittance of buildings' envelopes (also known as U-value) is considered one of the key properties that directly affect a buildings' energy use [6,7]. On the other hand, an envelope's thermal transmittance is not consistent,

as its thermal properties change significantly over time with respect to surrounding environmental conditions, building maintenance and level of deterioration in materials' conditions. It was previously estimated that designed U-values are reduced over time by around 50% or more post occupancy [8]. As a result, this can potentially affect modeling and predicting of energy use for post occupancy conditions.

Infrared thermography (IR) has recently gained significant interest as a reliable tool to analyze building envelopes' existing thermal properties qualitatively. This in addition to the ability of identifying insulation damages. Envelope thermal inspection using hand held IR camera is one common way to identify potential heat losses and areas of deterioration [9,10]. However, this process can be time-intensive in situations where the building skin has a relatively large surface area. This paper examines and validates the applicability of utilizing UAVs equipped with IR camera to estimate building envelope's thermal transmittance. The main objective of this work is to demonstrate how this method can be used to simulate and predict heating energy use more accurately. To verify the applicability of this approach, the paper analyzes two different scenarios: energy use prediction depending solely on designed U-values, and after estimating U-values from the envelope's thermal mapping. The two scenarios are compared against metered energy use to estimate how this method can be deployed to inform building energy simulation models.

2 METHODS

There has been a growing interest in the use of drones in surveillance, and most recently building inspection [11]. their efficiency lies in the ability to collect high-resolution data that is time efficient with minimum human labor [12]. Using aerial thermography provides a comprehensive overview of envelope heat flow as temperature data are collected over the same timeframe, which as a result has a bigger advantage over the point-based data method. The

proposed framework of estimating u-values using aerial thermography is developed through four main steps, as illustrated in figure 1 below. In the proposed framework, we first utilized UAVs equipped with IR camera in the data collection process. Collecting such data will aid in revealing issues such as insulation deficiency, heat losses as well as overall performance of existing conditions. In the following step we applied thermal imaging analysis to investigate envelope's thermal performance through surface temperature examination. Using temperature differences between indoor and outdoor, we numerically estimate the envelope thermal transmittance [9]. Finally, we integrated calculated U-Value into an energy simulation model to estimate heating energy use for the winter months.

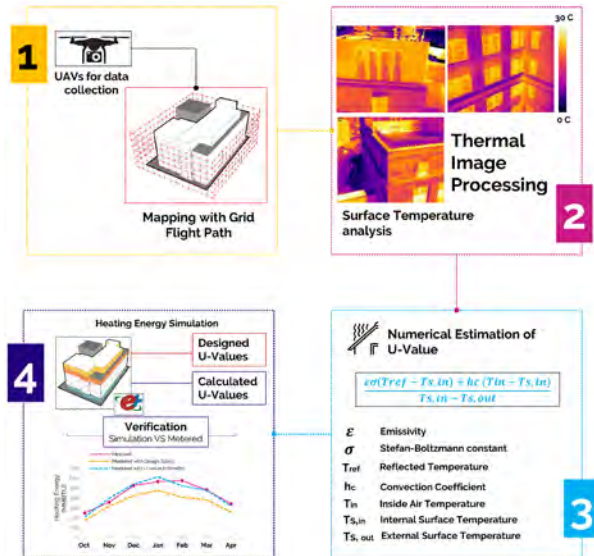


Figure 1. Analysis framework and methods used.

3 EXPERIMENTAL STUDY

An academic building on the MIT campus in Cambridge, MA, is tested for the proposed analysis framework. The selected building's envelope was recently renovated to incorporate materials with lower thermal transmittance to improve energy efficiency (Figure 2). In this study, we used An Inspire 1 drone by DJI, equipped with a FLIR Zenmuse XT thermal for data collection.



Figure 2. Envelope condition prior to retrofitting

The accuracy of data collected from the thermal flight is strongly dependent on two main factors: flight procedures (flying method) and outdoor climate conditions. According to Snell & Spring [13], for more accurate measurements,

there should be a minimum temperature differences of 10 °C between the indoors and outdoors. Thus, we conducted the flight during the early morning of March 31st, 2018 with an outdoor temperature average of 8 °C. There are numerous flight methods while using UAVs in thermography analysis. From reviewed literature [11], we used the strip method for data collection. This method is based on flying the UAV in vertical and horizontal strips perpendicularly facing each façade as illustrated in Figure 3 below. We calculated the flying distance from the façade based on the camera's angle to ensure 90% overlap for each image captured.

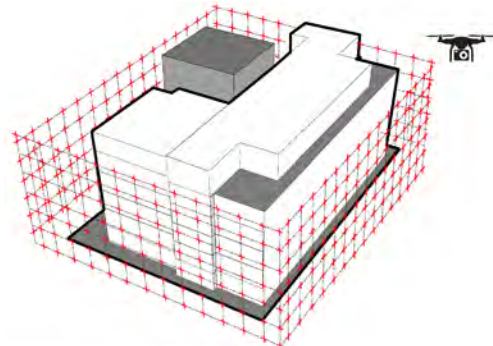


Figure 3. Flying method used for data collection (grid pattern with 90% overlap).

Next, over 500 images were captured and analyzed for each façade using FLIR analysis tool, as shown in Figure 4. From this analysis we identified surface temperature variation in each façade to identify areas of thermal deficiencies and heat losses. The subsequent stage of the analysis is based on measuring heat flow as well as indoor and outdoor air temperature differences. In heat flow calculation, we included thermal conduction, convection and radiation driven by temperature differences between the indoors and outdoors. The average indoor temperature used in the calculation represented typical set points for different spaces (classrooms, conference rooms and offices). Surface temperature indoors was measured using a hand-held thermal camera for each façade instantaneously with the outdoor measurements captured by the UAV's IR camera.

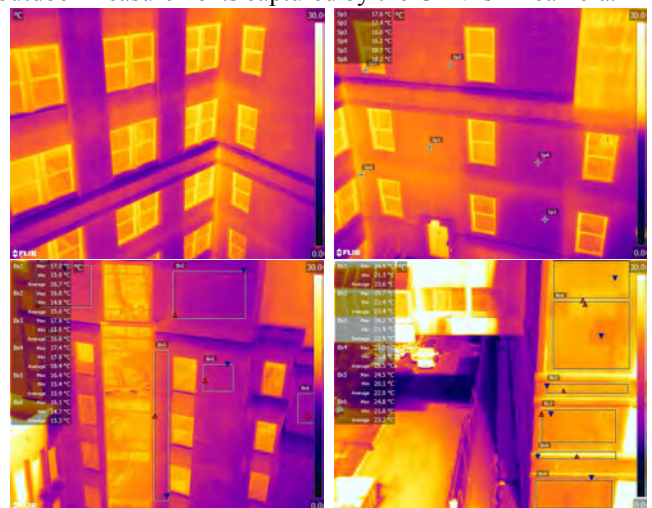


Figure 4. Sample of thermal imaging analysis

In order to calculate U-values, we used the convection coefficient (h_c) derived from Tanner et al. [14] standardized value of $= 8.7 \text{ W/m}^2\text{K}$. The overall heat transfer coefficient is calculated using equation (1) as follows:

$$\frac{\varepsilon\sigma(T_{ref} - T_{s,in}) + h_c(T_{in} - T_{s,in})}{T_{s,in} - T_{s,out}} \quad (1)$$

Where:

ε is the emissivity on the spectrum ranging between 0.1 and 1.0, σ is Stefan-Boltzmann constant that equals to $5.67\text{e-}8 \text{ W}\cdot\text{m}^{-2}\cdot\text{K}^{-4}$, h_c is the convection coefficient, T_{ref} is the reflected temperature, $T_{s,in}$ is internal surface temperature, T_{in} is the indoor ambient air temperature and $T_{s,out}$ represents external surface temperature.

Although wind speed has an effect on convection coefficient estimations, we estimated thermal transmittance numerically depending solely on temperature variation between the indoors and outdoors.

Thermal transmittance of each façade is calculated separately by averaging 500 temperature readings in each façade to calculate the overall U-value of the façade. We calculated areas that are classified as thermal bridges with respect to their average area to the total façade's area using equation (2):

$$U_{avg} = U_1 * \frac{A_1}{A_1 + A_2} + U_2 * \frac{A_2}{A_1 + A_2} \quad (2)$$

Where:

U_1 : U-value calculated for thermal bridge area

U_2 : U-value calculated for total façade area

A_1 : Area of the thermal bridge

A_2 : Non-thermal bridge area.

To examine the applicability of thermography analysis, we developed an energy simulation model in EnergyPlus and incorporated calculated U-values to model heating energy use for two cases. First, an energy model that involves envelope parameters based on retrofitting specifications. A second case that uses U-values calculated from the thermal mapping. Then we compared the two cases against metered energy use data to examine the reliability of the proposed analysis framework.

4 SIMULATION VERIFICATION

A previously developed detailed whole building energy model for the studied building was utilized for this analysis. The model, graphically represented in Figure 5, was generated at the time of building renovation. All envelope thermal performance parameters, internal load densities, operating schedules, lighting power and mechanical system inputs in the energy model were based on the design drawings and specifications.



Figure 5. Graphic rendering of the previously developed energy model (left) and building photograph post renovation (right)

Using the methodology discussed above, the U-Values of exterior walls of the building were numerically estimated based on the data collected by a thermal flight. Table 1 compares these properties with the as-designed values based on design specifications that were previously assumed as inputs in the energy model.

Exterior Wall U-Value (Btu/hr-ft ² -°F)			
Orientation	Designed Opaque	Calculated Opaque	Designed Fenestration
SE, SW	0.053	0.282	0.361
W		0.203	
N, NE		0.142	
E		0.192	

Table 1. As-designed and estimated wall U-Values

Figure 6 compares the simulated winter heating energy use from the previous model with the updated model results after incorporating calculated estimates. These results are juxtaposed against the actual metered heating energy post-renovation and show that the model error reduced from over 20% with previous assumptions (yellow and black lines) to less than 1% with current estimates (green and black lines).

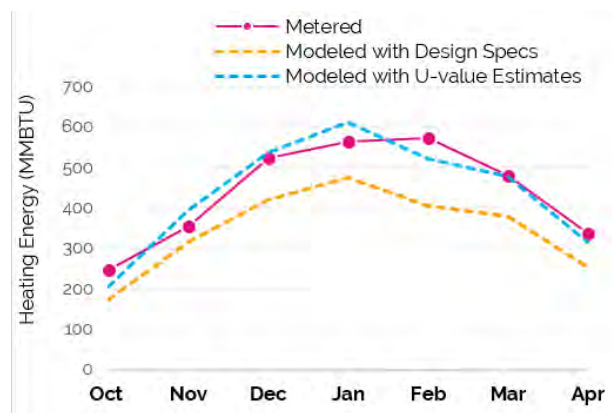


Figure 6. Comparison of metered and modeled heating energy use

5 DISCUSSION AND CONCLUSION

This paper aspires to initiate a framework by which building retrofitting design is informed through a substantial alteration in the methods and modes of performance evaluation. The innovation aims to be on multiple fronts: the use of UAVs makes evaluators experience substantially more limited physical barriers. This is especially evident when accessing multiple buildings and not relying on single-

frame images for inspection; developing 3D models that designers are able to interact and engage with in terms of developing solutions for building vulnerabilities, and finally targeting compromised areas and designing retrofits to address directed, and efficient building skin issues. The presented workflow has demonstrated significantly reduced errors, and further work should demonstrate its applicability (and limitations) in other climates and more sophisticated built environment situations.

Typical energy audits face multiple challenges that the proposed workflow can address, including i) inaccessibility to areas such as roofs, ii) significant time-consuming inspection activities, with possibility of human error, and iii) unsafe and life-threatening settings for detailed inspection. These difficulties in the auditing process create challenges for supporting whole Building Energy Modeling (BEM) practices, and do not inform retrofitting design decisions accurately when accounting for construction defects or degradation. In addition, current retrofit BEM tools face multiple barriers, including time consumption and labor intensity due to manual modeling and calibration processes. Therefore, there is a need to provide institutions, developers and owners with the means to examine buildings safely, accurately and rapidly to build reliable simulation models that inform precise and directed retrofitting design to achieve target savings from existing building envelope improvements.

Future work should further validate the use of UAVs to examine buildings to build reliable models that inform directed retrofitting design. This validation process should include advanced statistical methods to verify the reliability of the models, including measuring errors accurately (using Root Mean Square Error (RMSE) or other robust methods). The process should also expand to measure heat transfer anomalies in other building components other than walls, such as windows and roofs. Finally, the presented process should be incorporated in BEM frameworks to build simulation models that better represent the existing built environment, rather than estimate performance. The process should prove most-useful in the context of multiple buildings. The workflow can then be used as tool to identify the most effective retrofitting solutions at the neighborhood scale, in a fraction of the time that would have been used to assess multiple buildings using traditional means of building performance inspection.

References

1. International Energy Agency (IEA). Technology Roadmap “Energy Efficient Building Envelopes.” 2014. doi:10.1787/9789264118492-en.
2. U.S. Department of Energy. Windows & Building Envelopes R&D: Roadmap for Emerging Technologies. 2014.
3. McCranie KD, Faulkner M, French D, Daddis GA, Gow J, Long A. Analysis Of The Differences In Energy Simulation Results Between Building Information Modeling (Bim)-Based Simulation Method And The Detailed Simulation Method. *J Strateg Stud* 2011;34:281–93. doi:10.1080/01402390.2011.569130.
4. Frayssinet L, Kuznik F, Hubert JL, Milliez M, Roux JJ. Adaptation of building envelope models for energy simulation at district scale. *Energy Procedia* 2017;122:307–12. doi:10.1016/j.egypro.2017.07.327.
5. (DOE) D of E. Quadrennial Technology Review An Assessment Of Energy Technologies And Research, Chapter 2: Energy Sectors And Systems. 2015:39.
6. O’Grady M, Lechowska AA, Harte AM. Quantification of heat losses through building envelope thermal bridges influenced by wind velocity using the outdoor infrared thermography technique. *Appl Energy* 2017;208:1038–52. doi:10.1016/j.apenergy.2017.09.047.
7. Seghier TE, Lim YW, Ahmad MH, Samuel WO. Building Envelope Thermal Performance Assessment Using Visual Programming and BIM, based on ETTV requirement of Green Mark and GreenRE. *Int J Built Environ Sustain* 2017;4:227–35. doi:10.11113/ijbes.v4.n3.216.
8. Foam-Tech. Building Envelope Theory 2015. http://www.foam-tech.com/toc_NEW.htm (accessed October 29, 2018).
9. Danielski I, Fröling M. Diagnosis of buildings’ thermal performance-a quantitative method using thermography under non-steady state heat flow. *Energy Procedia* 2015;83:320–9. doi:10.1016/j.egypro.2015.12.186.
10. Bianchi F, Pisello AL, Baldinelli G, Asdrubali F. Infrared thermography assessment of thermal bridges in building envelope: Experimental validation in a test room setup. *Sustain* 2014;6:7107–20. doi:10.3390/su6107107.
11. Rakha T, Gorodetsky A. Review of Unmanned Aerial System (UAS) applications in the built environment: Towards automated building inspection procedures using drones. *Autom Constr* 2018;93:252–64. doi:10.1016/j.autcon.2018.05.002.
12. Ma L, Li M, Tong L, Wang Y, Cheng L. Using unmanned aerial vehicle for remote sensing application. *Int Conf Geoinformatics* 2014. doi:10.1109/Geoinformatics.2013.6626078.
13. Snell J, Spring R, Montpellier V. Testing Building Envelope Systems Using Infrared Thermography. 2008.
14. C. Tanner, B. Lehmann, T. Frank KGW. A proposal for standardized thermal images. *Bauphysik* 2011;33:345–56.

Data in Mixed Realities

Towards Assembly Information Modeling (AIM) 51

Ayoub Lharchi, Mette Ramsgaard Thomsen and Martin Tamke

Subjective Impressions of a Space Influencing Brightness Satisfaction: an
Experimental Study in Virtual Reality 57

Azadeh Sawyer and Kynthia Chamilothori

Immersive Representation of Urban Data 65

Amber Bartosh and Rongzhu Gu



Towards Assembly Information Modeling (AIM)

Ayoub Lharchi, Mette Ramsgaard Thomsen and Martin Tamke

Centre for IT and Architecture (CITA), Copenhagen, Denmark, alha@kadk.dk

ABSTRACT

Nowadays digital tools support architects, engineers and constructors in many specific tasks in the construction industry. While these tools are covering almost all aspects of design and manufacturing, the planning and design for the assembly of buildings remain an unexplored area. This research aims to lay the foundations of a new framework for the design for assembly in architectural applications entitled Assembly Information Modeling. In practice, it is a central digital model containing the structure architectural design, construction details, three dimensional representations, assembly sequences, issue management and others. This framework forms the base for a multitude of novel applications for assembly design, planning and execution, such as assembly simulation and strategies communication, problem detections in the early design phases and interdisciplinary coordination. This paper describes the specifications of the digital assembly model and illustrate two use cases: collaborative assembly design using AEC cloud-based platforms and Augmented Assembly using Augmented reality devices.

Author Keywords

Design For Assembly; Digital Model; Assembly Modeling

1 INTRODUCTION

For an extended period, many architectural systems were strictly restricted in their general topology and geometrical differentiation because of both technical and economic factors [11]. These limitations increased the need for a toolbox that is adapted for complex geometries and led the architects and engineers to search and develop an entirely new set of methods and tools for design and manufacturing [3]. Today digital tools form the basis of nearly all design, construction, fabrication and management tools in all professions related to the building industry [13].

Overall, computational design tools and digital fabrication processes enabled a higher degree of differentiation between the elements in a single structure [11] and it became possible to design and manufacture large-scale freeform shapes.

However, this new shape emergence posed significant challenges in terms of communication, fabrication, and assembly [9]. Although there are many attempts to standardize the information modeling and data sharing between the different interdisciplinary partners within one project [12], there are more issue that can rise and are not covered by traditional approaches such as Building Information Modeling (BIM).

This research aims to fill the existing gap in the design for assembly field, by suggesting a novel approach for handling assembly information in a construction context. By combining computer science techniques and design practices from other disciplines, this project defines in a first step a scheme by which professionals can describe, analyze and communicate assembly information.

This digital model forms the base for a multitude of novel approaches for assembly design, planning and execution (figure 1): now detailed digital assembly information can be shared and discussed between partners through cloud-based platforms, assembly sequences can be generated and optimized with the help of algorithms and new human-machine interfaces such as augmented reality can be used to assemble constructions. Finally, the model presents the base for future robotic assembly.

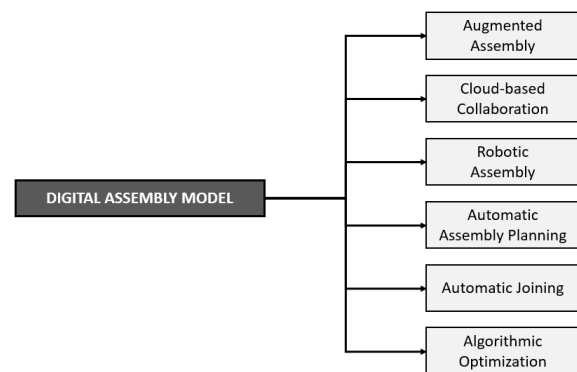


Figure 1. Potential Applications of Assembly Information Modeling

2 DESIGN FOR ASSEMBLY IN ARCHITECTURE

A proficient assembly planning should be part of any successful design. This can reduce assembly time, allow flexibility and improve the quality and reliability of the final product [15]. Design for Assembly (DfA) is a well-established practice in other disciplines since the 80s [2], especially in industrial and mechanical design. It is often combined with Design for Manufacturing (DfM) techniques in order to optimize the manufacturing and assembly within industrial applications. DfA aims to have a full understanding of the assembly process and to extract principles that influence the design iterations. In general, it involves two crucial steps: minimization of the number of the separated parts that constitute the global structure (figure 2), and the improvement of the “Assemblability” of the remaining parts [2]. Research has been conducted on assembly planning, little focus was however set on the integration of questions of assembly in the design phase [14]. Furthermore, the existing approaches to DfA are all rooted in industrial fabrication processes for e.g. machines and consumer products, which makes it difficult to have a direct transfer of these to an architectural context due to material and scale considerations.

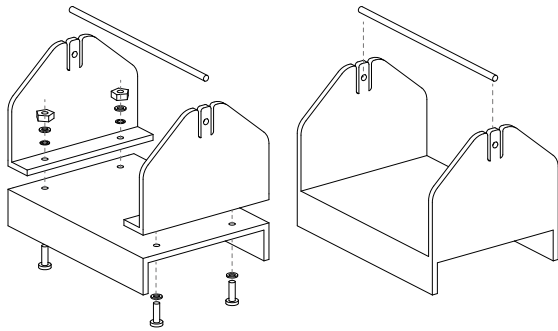


Figure 2. Pieces number reduction for optimized Assembly [2]

3 ASSEMBLY INFORMATION MODELING

An Assembly Information Model (AIM) as described here is a digital framework directed for application in building processes, that aims to include all the necessary data to describe precisely an assembly sequence and at the same time to bridge the different authoring tools used by the stakeholders. The model specifications are freely available online and are covering most of the common needs in a typical architectural assembly planning process, but can be extended as well if needed. In order to assure high interoperability between different software package, the implementation presented in this paper is intentionally software agnostic and is using exclusively open source libraries to allow an eventual use in commercial software.

The AIM implementation we propose is composed of the following elements:

- A library called AIM.Core defining the basic functions and managing the input (geometry and meta-data) and output (files, documentation, etc.).
- A set of plug-ins for different host CAD systems. Each plug-in uses the geometric capabilities of the host software

and the AIM.Core library to generate an Assembly model (.adm).

The AIM.Core library was written in C# [5], which is a powerful object-oriented language and using the .NET Core Framework, which in itself is a further approach to ensure a cross-platform compatibility. For demonstration and testing purposes an AIM.GH - plug-in for the Grasshopper [10] environment was developed. Additional plug-ins to generate, read and manipulate the assembly model can be written easily by persons with a certain knowledge of the host application API, using any .NET programming language [8].

The full model specifications and the implementations source code are available online at: <https://www.github.com/ALharchi/AIM>

The digital model is composed of the following classes:

3.1 Elements

An element refers to any physical element in the structure. It can be either a part of the structure (beam, column) or a fastener (bolt, screw, etc.). The model stores the defined position, orientation and the geometry of all the elements. For each one, there is a corresponding file containing the geometry. Depending on the modeling approach and the software used, a NURBS or MESH description is used. If the used software support both NURBS and Mesh geometries, dual representation can be enabled, and both geometries representation will be stored to maximize the interoperability. The NURBS is stored in a .STEP file, while the MESH is in a .STL file.

For similar elements, only one file (or two if dual representation is enabled) is used to reduce the model size and memory usage.

3.2 Transformations

Transformations are the sequence of geometrical operations that are necessary to get an element from the entry position to the final position. The entry position can be any safe position without collision or obstacles (on the ground for example). The final position corresponds to the correct spatial location and orientation within the structure. Two main types of transformations are defined using simple mathematical concepts:

- Translation: Linear movement in space, defined by a three-dimensional vector.
- Rotation: Circular movement defined by a rotation plane and a rotation angle (expressed in radian).

Using these two transformations, complex spatial movements can be described. When loaded, the appropriate AIM plug-in will convert it to match with the software native spatial library.

3.3 Components

Elements are grouped together in components. Typically, one component includes several parts and the necessary fasteners. Single-element components are also possible. Transformations can also be assigned to components.

3.4 User Manipulation Zone (UMZ)

The user manipulation zone is the necessary area to operate during an assembly step. It is represented by a sphere defined by radius from the fastener element.

3.5 Joints

Joints define the relation between two or more elements (figure 3). The order or the Assembly Sequence (AS) is specified. Each joint is expressed in the necessary number of transformations.

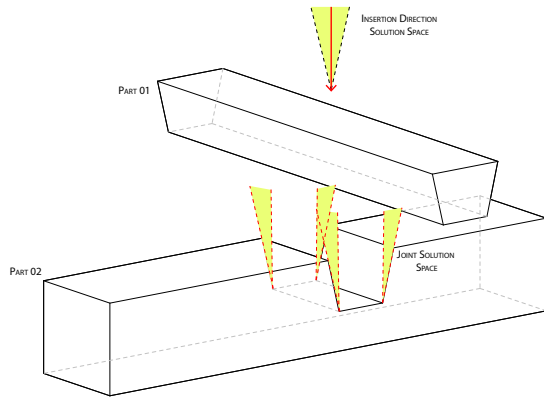


Figure 3. Joints in space with vectors

3.6 Issues

Issues are problems concerning the assembly process that needs to be communicated. It can be either manually defined by the user during the model creation or automatically raised later by the computation engine (as described in 4).

Issues are divided into categories according to the severity and impact on the assembly process:

- Critical: The assembly is impossible.
- Moderate: The assembly is partially possible.
- Suggestion: The assembly is possible, but can be improved.

Every issue is linked to the user that created it, which can be used later for an issue management platform (see 6.1).

3.7 Documentation

Technical drawings of the different elements can be automatically pre-generated and included in the digital model. They are saved in PDF and PNG format (figure 4).

4 MODEL COMPUTATION

One of the main benefits of the assembly modeling approach is to have all the information in one single model, which facilitates any desired analysis or computation. The model computation helps to detect issues in the assembly process in the early stages. Although some of these problems can be detected using 4D simulation of the construction process, the adoption of such techniques remains very slow [4]. They are

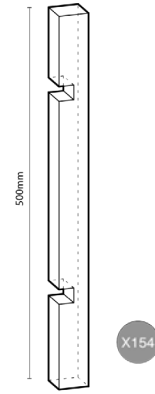


Figure 4. Example of documentation included in the model

usually related to the geometry of the elements [6], for example, if the parts cannot be assembled because of incompatible joints, collision with other elements or due to a wrong assembly sequence order. The problem can also be related to logistics: the assembly is possible in theory but very difficult or impossible to realize in practice. This is often the case if there are some unpredicted constraints on site, such as a smaller crane (only one insertion direction; from above) or existing construction that would prevent the spatial movement of large elements.

Since the AIM.Core does not include any geometrical kernel, the model computation is executed on the software side (using the adequate AIM plug-in).

4.1 Mathematical Conflict Detection

Using the information embedded within the joint definition, issues in the assembly sequence can be detected. Before using computationally expensive Boolean operations to detect collisions, the joints design space are evaluated and conflicting solutions are flagged.

4.2 Physical Collision Detection

Using the transformations, every element in the model is interpolated from the initial entry position until the final position within the structure. The computational Engine is detecting any collision between the current part, and all the previously placed parts during the assembly operation (figure 5). If there is none, the part is marked as safe; otherwise, an issue is raised and recorded in the model as well. A custom collision detection algorithm had to be written based on the existing Boolean operations available in the HCS. The issue with the existing collision detection methods is that they flag two touching solids as intersecting, while in an assembly context, it is accepted or necessary within certain tolerances (such as sliding an element in between two already placed elements).

4.3 Fabrication Constraints

The user can provide additional information about the available logistics. This is intended to be used in coordination and assembly sequence evaluation. All the existing constraints or construction on site are stored within the model. An abstract

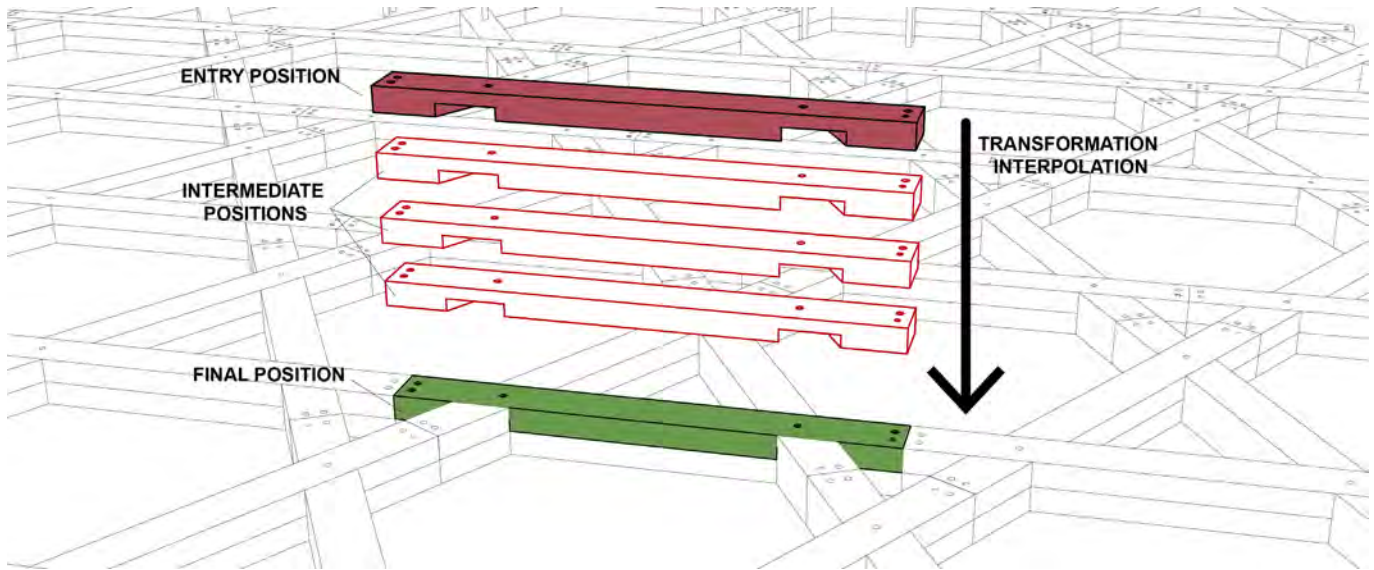


Figure 5. Transformation interpolation from entry to final position.

representation (reduced mesh) is used to reduce the model size.

5 FILE FORMAT

The Assembly Digital Model (ADM) is intended to be used for various applications (see section 6). It is crucial to embed all the information within one comprehensive to allow the desired interoperability. Furthermore, one self-contained file facilitates the exchange with cloud-based platforms, robotic interfaces and other devices. According to the specifications, the information is divided into three categories:

- Geometry data: This includes the elements' geometry. It is a collection of STEP and STL files.
- Graphical data: Technical drawings (PNG or PDF).
- Meta-data: Further data, which provides additional information about the geometry (transformations, issues, joints etc.), relationships to overall project, related models, processes etc.. The metadata is plain text.

The ADM is open-source and the implementation uses freely available libraries that are running on the three majors operating systems (Windows, Linux and MacOS).

5.1 ADM Container

The ADM container we propose is new file format that uses the extension .adm. It is a compressed ZIP file that encapsulates the geometry and graphical files and one single database for the meta-data (see section 5.2). The files are organized in hierarchy using folders (figure 6).

Every element is stored in separated file to allow a quick loading for single elements and to facilitate the replacement/adjustments.

5.2 Meta-Data storage

It was necessary to define a way to store the metadata that is flexible enough to allow an integration of interlinking data

```
filename.adm
  data.db
  geometry/
    part_01.stp
    part_02.stp
    fastener_01.stp
    ...
  docs/
    part_01.pdf
    part_02.pdf
    ...
```

Figure 6. Hierarchy in the .adm file

with the possibility of complex queries. The most commonly used format for this purpose are relational databases and text storage format such as JSON (JavaScript Object Notation) and XML (Extensible Markup Language). While XML and JSON offers the advantages of being human-readable, in this case most of the processing is automated. Therefore the advantage was given to organization querability.

For this purpose, we chose to use a relational database because it is allowing the definition of relations between elements, that once in the system, can be queried using a specific language SQL (Structured Query Language). Common operations queries are already provided with the model and the user can easily write his own query if needed. Among the different relational database systems, we chose to use SQLite because of its advantages as it is a serverless database system so it does not need a server and the generated file can be manipulated directly within the different application (table 1).

6 APPLICATIONS

As we describe a general approach to formalise assembly in a digital model, many promising areas of applications can be imagined. For example the ADM can be a unified base

Name	Advantages	Disadvantages
SQLite	File Based Embedded Applications Serverless Little resource	No User System Single Query
MySQL	Extensible Multi-user support	Requires separated hosting
PostgreSQL	Scalable	Heavy

Table 1. Comparison of relational database systems [7]

for communication between different stakeholders, engineers or architects can receive instant feedback on their assembly strategies through further computation or analysis of the ADM, as the ADM can provide detailed data for robotic assembly.

In this research, we evaluated our approach with two areas of applications, which require an effective communication of assembly strategies and operate at different design stages.

6.1 Collaborative Design for Assembly

The collaborative design for assembly is a platform for the communication, viewing and discussion of assembly data. A web-based platform uses the ADM and makes it available to the different stakeholders with a powerful built-in 3D viewer. The requirement was to create an integrated platform that would run on most modern web browsers without the need of any additional plug-ins. This would include mobile devices such as smartphones and tablets for eventual on-site usage. The presented platform utilize the Autodesk Forge cloud services [1]. We used the Forge Viewer API and Model Derivative API. The application backend was written in ASP.NET using the .NET Core framework; meanwhile, the front-end was mainly in HTML, CSS and JavaScript.

One user can upload an ADM file that is processed by the Autodesk Forge cloud, translated into SVF format. Afterwards, the assembly information is injected into the 3D model. The model is then made available for all the users of the platform for editing and viewing (figures 7 and 8).

Part ID	Description	Status	Actions
1.0.0	1.0.0	Completed	●●●●●
1.0.1	1.0.1	Completed	●●●●●
1.0.2	1.0.2	Completed	●●●●●
1.0.3	1.0.3	Completed	●●●●●
1.0.4	1.0.4	Completed	●●●●●
1.0.5	1.0.5	Completed	●●●●●
1.0.6	1.0.6	Completed	●●●●●
1.0.7	1.0.7	Completed	●●●●●
1.0.8	1.0.8	Completed	●●●●●
1.0.9	1.0.9	Completed	●●●●●
1.0.10	1.0.10	Completed	●●●●●
1.0.11	1.0.11	Completed	●●●●●

Figure 7. Individual elements management

6.2 Augmented Assembly



Figure 8. 3D Viewer

Using the ADM model, it is possible to extract step by step information, which guides a user through an assembly process. Augmented Reality (AR) devices are particularly adapted for this usage as they allow overlaying a digital input onto the user view and thus align the relevant information to the objects of interest [16]. Our tests show (figure 9) that empowered an AR device, an inexperienced user can assemble complex structures without any previous knowledge or training.

The Augmented Assembly interface was implemented for the head mounted device Microsoft HoloLens. Using the autonomous self-tracking features, it was possible to track the user in the space and display assembly information that overlap with the environment (figure 10). The software running on the HoloLens was developed using the Unity 3D Game Engine in C#. The assembly sequence was displayed to the user in sequential order. The assembly was animated in a way that the user can distinguish clearly the orientation of the element as well as the necessary transformations to put it in the correct place.

The user interface uses two input systems of the HoloLens:

- Gesture-Based: To select and manipulate the different elements. It also allows extracting information from the digital assembly model and displaying them directly in the augmented view.
- Vocal commands: This provides a hands-free interface to control the assembly animation (showing the next or previous piece, pausing the animation etc.).

7 CONCLUSION AND FUTURE WORK

We present Assembly Information Modeling (AIM) as a framework to describe, analyze and communicate assembly strategies in the AEC sector. While the current specification of the digital model is covering many typical assembly planning needs (Collision detection, documentation generation, 4D simulation etc.), many technical improvements are necessary to cover more specific cases such as generic joints and interfacing with existing manufacturing techniques. This includes defining the joints class more abstractly and providing additional queries to extract and export data from the model. Furthermore, the implementation of a geometric kernel that would be embedded in the AIM.Core library is envisioned, to unify the geometric operations and to skip the translation phase to the native format within the host CAD software. In



Figure 9. A user performing augmented assembly

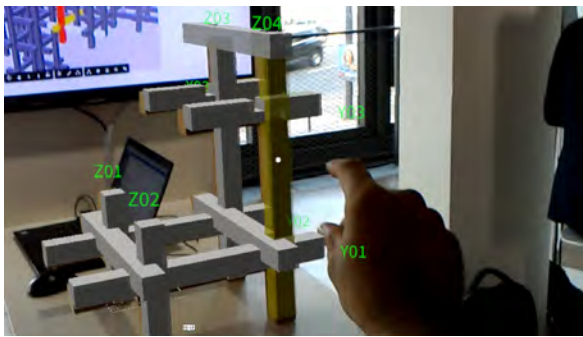


Figure 10. Augmented assembly view

addition, this will speed up the necessary computation time for collision detection.

Two areas of exploration seem especially pressing in respect to the general move of AEC sector:

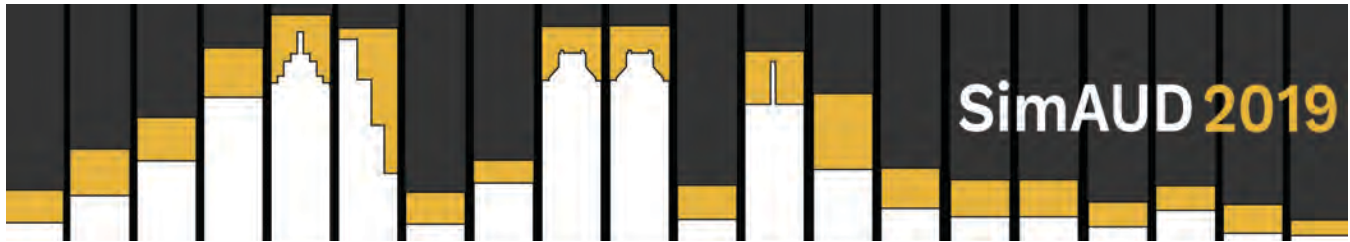
- Mechanization of the construction site, through robotic assembly where the ADM is uploaded directly to a robotic arm for an automatic assembly.
- Integration of simulation tools in early design planning, where AIM can be used for an integrated path planning, using a system capable of generating collision free robotic paths for the construction. Ultimately, the model can serve as a base for machine learning algorithm to assist the designer for assembly choices.

8 ACKNOWLEDGMENTS

This project was undertaken as part of the Innochain Early Training Network. This project has received funding from the European Union's Horizon 2020 research and innovation programme under the Marie Skłodowska-Curie Grant Agreement No. 642877. We would also like to express our gratitude to the industrial partners of this research; Blumer Lehmann and Design-To-Production, as well to Autodesk, especially the Forge development team.

REFERENCES

1. Autodesk Forge: Cloud-based AEC developer tools . <https://forge.autodesk.com>.
2. Boothroyd, G. Design for assembly—the key to design for manufacture. *The International Journal of Advanced Manufacturing Technology* 2, 3 (1987), 3–11.
3. Boothroyd, G. *Assembly automation and product design*. CRC Press, 2005.
4. Boton, C., Kubicki, S., and Halin, G. The challenge of level of development in 4d/bim simulation across aec project lifecycle. a case study. *Procedia Engineering* 123 (2015), 59–67.
5. C# Programming Language. <https://docs.microsoft.com/en-us/dotnet/csharp/>.
6. Czmochn, I., and Pekala, A. Traditional design versus bim based design. *Procedia Engineering* 91 (2014), 210–215.
7. Relational Databases Comparison. <https://www.digitalocean.com/community/tutorials/sqlite-vs-mysqlvs-postgresql-a-comparison-of-relational-database-management-systems>.
8. .NET Framework, a free, cross-platform, open source platform for building apps. <https://www.microsoft.com/net>.
9. Eigensatz, M., Kilian, M., Schiftner, A., Mitra, N. J., Pottmann, H., and Pauly, M. Paneling architectural freeform surfaces. *ACM transactions on graphics (TOG)* 29, 4 (2010), 45.
10. Algorithmic Modeling for Rhinoceros 3D. <https://www.grasshopper3d.com>.
11. Krieg, O. D., Dierichs, K., Reichert, S., Schwinn, T., and Menges, A. Performative architectural morphology: Robotically manufactured biomimetic finger-joined plate structures.
12. Tamke, M. Aware design models. In *Proceedings of the Symposium on Simulation for Architecture & Urban Design*, Society for Computer Simulation International (2015), 213–220.
13. Tamke, M., and Thomsen, M. R. Digital wood craft. *Joining Languages, Cultures and Visions: CAAD Futures* (2009), 673–686.
14. Usai, S., and Stehling, H. *La seine musicale*. In *Humanizing Digital Reality*. Springer, 2018, 201–209.
15. Wilson, R. H. On geometric assembly planning. Tech. rep., STANFORD UNIV CA DEPT OF COMPUTER SCIENCE, 1992.
16. Zollmann, S., Hoppe, C., Kluckner, S., Poglitsch, C., Bischof, H., and Reitmayr, G. Augmented reality for construction site monitoring and documentation. *Proceedings of the IEEE* 102, 2 (2014), 137–154.



Influence of Subjective Impressions of a Space on Brightness Satisfaction: an Experimental Study in Virtual Reality

Azadeh Omidfar Sawyer¹ and Kynthia Chamilothoni²

¹University of Michigan
Ann Arbor, USA
aomidfar@post.harvard.edu

²Laboratory of Integrated Performance in Design
Ecole polytechnique fédérale de Lausanne
Lausanne, Switzerland
kynthia.chamilothoni@epfl.ch

ABSTRACT

This paper investigates the relationship between participants' satisfaction with brightness and other key perceptual attributes of the scene to gain insight in how user satisfaction with brightness is influenced by factors other than brightness levels. In this study, a total of 100 participants were immersed in an office space using virtual reality (VR). The brightness level in all immersive scenes were held constant while the office shading system's design pattern, rendering materials, and furniture were varied to examine how different factors influence the participants' satisfaction with brightness. Statistical analyses indicate that there is a strong association between participants' satisfaction with brightness and other perceptual attributes. Additionally, while the effect of furniture on brightness satisfaction was not statistically significant, the analyses revealed that colored materials had a significant effect on participants' evaluations of their satisfaction with brightness.

Author Keywords

Daylight; brightness; perception; preference; immersive virtual reality.

1 INTRODUCTION

Light has an undeniable influence on our perception of space, as recognized in the fields of architecture [1]–[3] and of lighting [4]–[6]. The design of the luminous conditions in a space aims to address the needs of the occupants, and substantial research effort is devoted to identifying the characteristics of ideal lighting conditions for different social situations and for various tasks. In the case of work environments, lighting is used to ensure that workers can perform their tasks quickly, accurately and easily [7].

In one study people were asked to freely describe the lighting in an office-like room and brightness was the second the most commonly used attribute [8]. Interestingly, the most commonly used description was that the lighting in the room

was dull. Although this finding could be a result of the stimulus range used in the experiment, it raises the question of which features of the luminous environment matter most in occupants' perception.

This question was tackled in a seminal study by Flynn and colleagues in which the appearance of a conference room was examined under different configurations of artificial lighting [4]. Their experiment showed that people prefer lit environments that appear 'bright', an attribute linked to the perception of 'spaciousness', and 'interesting', related to a degree of non-uniformity. They concluded that lighting conditions can be characterized by three dimensions: brightness, uniformity, and the presence of peripheral or overhead lighting. In another study with artificial lighting configurations in an office environment, Hawkes et al. found that the perception of light in the space could be described by the dimensions of brightness and interest, which related to the intensity and the uniformity of the lighting conditions, respectively [5]. Similarly, Loe et al. identified the factors of visual lightness and visual interest as descriptors of the luminous environment, using the same procedure as Flynn [9]. The work of Loe et al. supported the findings of previous research regarding people's preference for their working environment to appear 'bright' and 'interesting', but also noted a key criterion for lighting design, stating that both factors are required to create preferred lighting conditions, i.e. people do not prefer a 'bright' space if it is not 'interesting', or an 'interesting' space that is not 'bright'. In a later study by Veitch and Newsham on the appearance of an open-plan office lit with different lighting systems, the authors found three factors that described the appearance of the space: brightness, visual attraction, and complexity [10]. Brightness is a consistent factor across these studies, which establishes its importance as a central feature of the luminous environment.

Considerable research has been conducted to identify physical measures of the lighting conditions that can predict occupants' impressions of brightness. The perception of brightness in a space has been related to objective indicators such as the average luminance within a 40 degree horizontal band center at the eye height of an observer [9], [11], the logarithm of the vertical illuminance at the eye of the observer [5], and the spectrally-weighted irradiance at the eye of the observer [12].

In related work, numerous studies have investigated the influence of physical properties other than light intensity on the perceived brightness of a space. For instance, Tiller and Veitch investigated the effects of luminance distribution on perceived room brightness in office spaces using brightness matching tasks in offices. Their findings showed that rooms with non-uniform luminance distribution required five to ten percent less working plane illuminance compared to the brightness of the rooms with uniform luminance distribution [13]. The spectrum of the light source has also been consistently shown to affect the perceived brightness of the scene [14]–[17]. The presence of color in the scene in the form of colored objects (in this example, flowers and fruit) was also shown to increase the perception of brightness in the same illuminance [8]. However, other studies showed no or only a negligible effect from the presence of colored objects on the perceived brightness of the scene [14], [17], indicating the need for further investigation.

It is important to note here that a common component of all these studies is the use of artificial lighting. In fact, very few studies have addressed the effect of daylight on occupants' preference and satisfaction. However, sunlight penetration has been shown to increase feelings of relaxation [18] as well as well-being and job satisfaction [19]. In the same vein, in an experimental study where occupants of office environments were asked to control the shading system and create their preferred conditions, the majority of the participants chose to introduce some amount of direct sunlight into the room [20]. Studies investigating the effect of daylight on participants' subjective impressions in virtual environments have shown that the lighting conditions significantly influence the extent to which a space is perceived as pleasant, interesting, and exciting [21]–[23]. Following these findings, a question arises: could occupants' perception and satisfaction with brightness be affected by other perceptual attributes of the space rather than just the actual brightness level of the space? Such a finding could suggest the potential for energy savings if the same level of satisfaction with brightness can be achieved at lower actual levels of illuminance by manipulating other attributes of the luminous environment.

This paper investigates the influence of perceptual attributes—such as the perceived pleasantness or complexity of the scene—on occupants' satisfaction with the brightness in a daylight office space through subjective experiments. The visual stimuli in these experiments are shown to the

participants using a novel experimental method which combines physically-based renderings from Radiance with projection in immersive virtual reality, and has been shown to be a promising surrogate to real daylight spaces for experiments investigating occupant perception [24]. Specifically, an experimental study comparing this method against real environments demonstrated its adequacy in terms of perceptual accuracy, as well as reported presence and physical symptoms of the users of the VR headset [24]. The use of virtual reality allows the control of the brightness to the same level across multiple presented scenes, and the simultaneous variation of the shading system applied to the same space to create different impressions of visual interest and complexity. Controlling the brightness level of the scene across conditions that trigger widely different perceptual impressions allowed us to examine the interrelationship between the satisfaction with brightness and some of the key attributes related to office preference. Additionally, the presence of color and furniture in the virtual environment was varied to investigate the influence of these factors on participant satisfaction with brightness.

2 METHOD

2.1 Visual Stimuli

The scenes used as visual stimuli in this experimental study correspond to six variations of a typical office space with one large window facing south. In these variations, developed in previous work [26], a different shading system was applied to the façade of the space, shown in **Figure 1**. Each façade variation was based on designs from existing buildings, ranging from simple vertical or horizontal louvers to an asymmetrical complex pattern. These variations of the scenes were used to impart different subjective impressions, following existing work which demonstrated the influence of shading system geometry on occupant perception [25], [26]. Although the shading systems varied in design, all were modified to have a 40% perforation in order to create scenes with the same amount of brightness and with distinct perceptual attributes. A 3D model of the office space with six shading system variations was created in Rhinoceros (Rhino, version 5.0) modelling software. Six different spaces were modeled both with and without furniture. Each was rendered in three different color modes—fully colored, partly colored (using the default materials in DIVA-for-Rhino v. 4.0), and grayscale. A view position in the center of the room was established at approximately 2.5 meters from the window and 1.63 meters from the floor, corresponding to the eye height of a standing person. Each model was exported to Radiance [27], an extensively validated physically based lighting simulation tool, using the DIVA-for-Rhino (v. 4.0) simulation toolbar [28]. Immersive scenes were generated in Radiance by rendering a 360° over-under equirectangular HDR image using the script `view360stereo.cal`.

The parameters for the Radiance simulation are provided in Table 1. This procedure resulted in a total of 30 images, which were tone-mapped to a low dynamic range using the

Reinhart02 tone-mapping operator [29] and shown to participants using the Oculus Go virtual reality headset. The resulting scenes are automatically mapped to a sphere in Oculus Go and are perceived as a fully immersive 360° stereoscopic scene (**Figure 2**). The vertical illuminance of the projected scenes was measured at the level of the lens of the VR headset with a Konica Minolta T-10 Illuminance Meter from the viewpoint of a participant looking towards

the main view direction, to provide a measure of similarity in terms of actual brightness. These measurements show that the studied scenes differ between them in vertical illuminance with a maximum factor of 1.13, which is well below the threshold of a noticeable change in illuminance [30], and thus is not expected to result in a difference in the participants' judgements regarding their satisfaction with the brightness of the space.

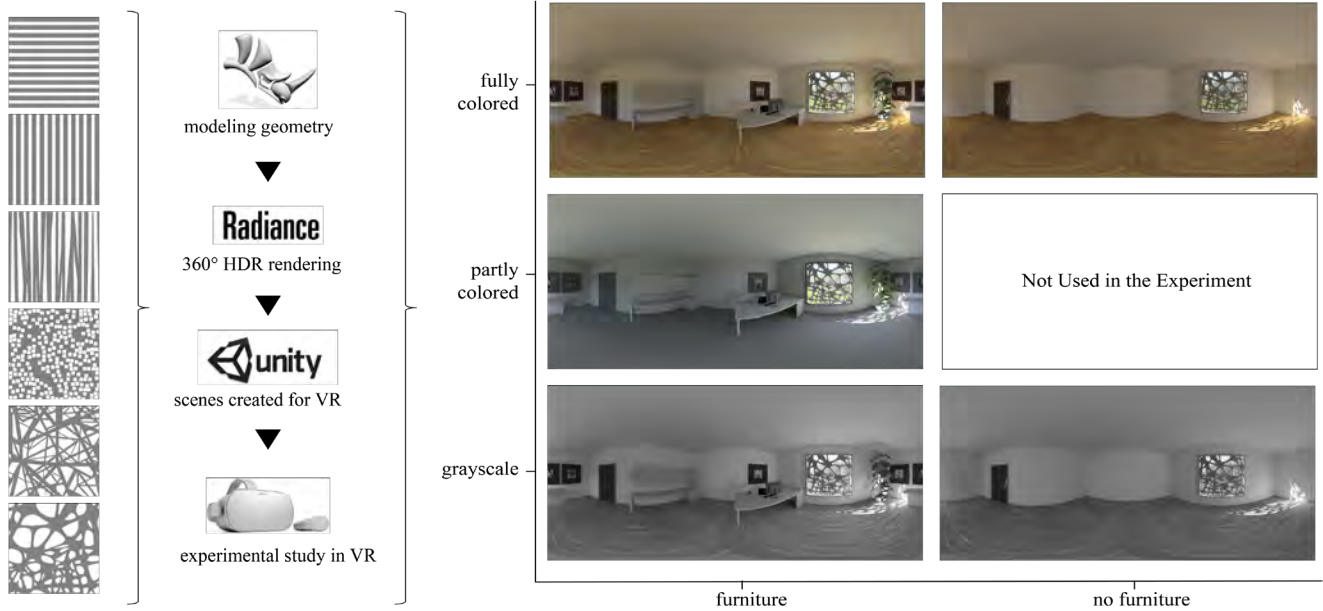


Figure 1. Example scene variations for one window treatment across different levels of scene materials (fully colored, partly colored, grayscale) and simulation level of detail (with/without furniture). Each participant saw a random selection of scenes.

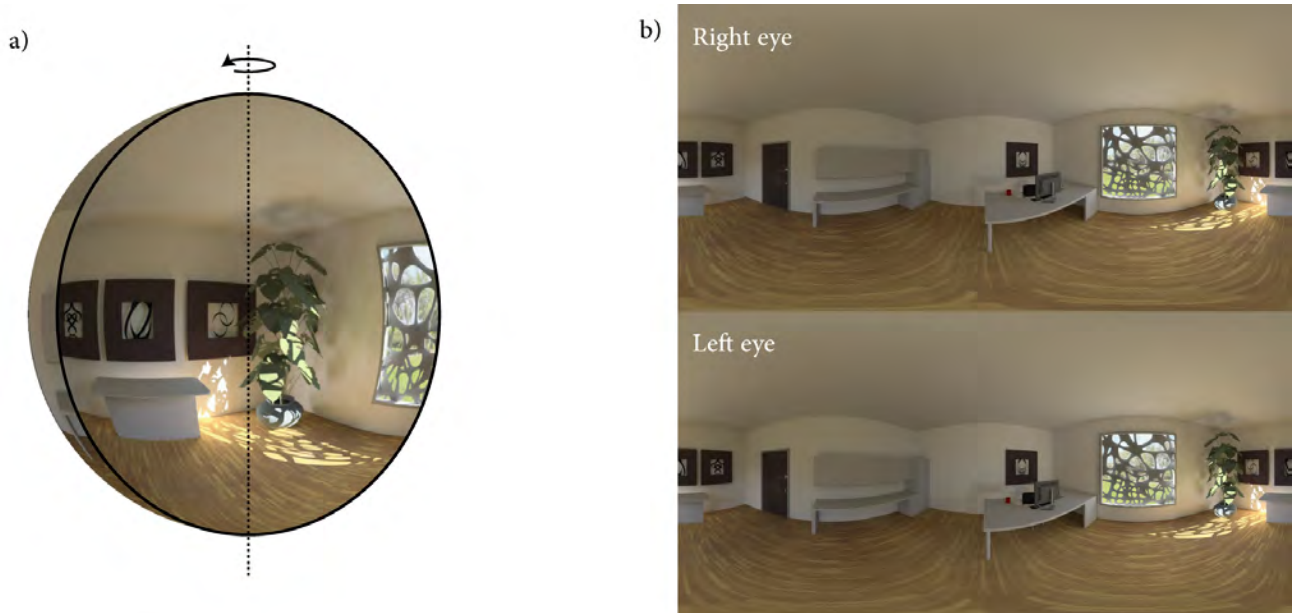


Figure 2. Illustration of participant perception (a) and example of immersive scenes rendered for each eye (b).

dj	ds	dt	dc	dp	St	ab	aa	ar	ad	as	Lr	lw
0.02	0.05	0.05	0.5	256	0.5	4	0.02	32	25000	12500	4	0.000004

Table 1: Radiance parameters for the 360° HDR renderings for viewing in Oculus Go

2.2 Verbal Questionnaire

A verbal questionnaire consisting of 11-point unipolar rating scales was used to collect participants' subjective impressions while they were immersed in each scene. In this paper, we focus on the participants' satisfaction with brightness and its association with a selection of rating scales: how pleasant, interesting, and complex the scene was perceived, as well as their satisfaction with the view out and the ambiance of the space, shown in **Table 2**. It is important to note here that the question on brightness was specifically framed to assess the participants' satisfaction with brightness as an indicator for acceptable range of brightness rather than their perception of brightness levels.

Independent Variables

IV1. Façade variations (six different shading systems of an equal perforation ratio applied to the window of the office room).

IV2. Scene materials (fully colored, partly colored (with default materials in DIVA-for-Rhino), and grayscale).

IV3. Level of detail (simple room without furniture, simple room with furniture).

Dependent Variables

DV1. On a scale of 0 to 10, how pleasant is this space?

DV2. On a scale of 0 to 10, how interesting is this space?

DV3. On a scale of 0 to 10, how complex is this space?

DV4. On a scale of 0 to 10, how satisfied are you with the brightness of the space?

DV5. On a scale of 0 to 10, how satisfied are you with how much you can see of the view outside?

DV6. On a scale of 0 to 10, how satisfied are you with the ambiance of the space?

Table 2. Overview of the experimental variables

2.3 Equipment

An Oculus Go VR headset was used in this study. This is a standalone headset that works without a computer or a phone. Its screen measures 5.5 inches, 538 ppi, at 2560 x 1440 Wide Quad High Definition (WQHD) resolution. The display can run at a maximum refresh rate of 72 Hz, delivering enhanced brightness and colors. The maximum vertical illuminance of a white scene displayed in Oculus Go measured at the level of the lens is 44 lux (lm/m²).

2.4 Experimental Design and Participants

Each participant was presented with a total of six scenes in a randomized order, from the pool of 30 combinations of shading system, color, and furniture variations. Due to the randomization of the scenes, not all participants viewed all six shading patterns used in the study. Analysis of the effect of the shading system on subjective impressions exceeds the scope of this paper and will be reported in a future publication.

The VR experimental study was conducted in Ann Arbor, Michigan over the course of four weeks during the summer of 2018. A total of 100 participants (63 female, 37 male) took part in the study. Participants were unpaid volunteers over 18 years of age, recruited by email or in person. Each experimental session lasted no more than 20 minutes.

Prior to the start of the experimental session the interviewer discussed with the participant possible associated risk with wearing the headset. When they were ready to start the experiment, they were instructed on how to use the Oculus headset and how to customize its fit for comfort. Participant were informed that they would view a total of six scenes of an office space. The scenes were presented in a randomized order and were preceded by a number identifying the condition to the interviewer. Participants were instructed to report this number and were then immersed in an office scene. When the participant was ready, the interviewer verbally asked the questions in a randomized order.

This research was approved by the University of Michigan Health Sciences and Behavioral Sciences Institutional Review Board (IRB-HSBS).

2.5 Statistical Analysis

A linear mixed effects model was used for statistical analysis of the data to account for the repeated measures design in which each participant was asked to rate multiple images. Model analyses were conducted in R [31] for each of the dependent variables using the R software package *lmerTest* [32]. The linear mixed effects model describes the conditional associations between the participants' satisfaction with brightness and the five other perceptual attributes, while controlling for latent participant attributes such as positivity. Statistical analyses were performed by specifying a 0.05 significance level.

Additionally, following the results regarding the associations between the participants' satisfaction with brightness and the other studied dependent variables, a composite index of *satisfaction with selected attributes* was constructed in R by averaging the responses of the attributes *pleasant*, *interesting*, *satisfaction with access to the view outside*, and *satisfaction with ambiance*. This composite index is used to quantify a potential effect on satisfaction with brightness that could stem from a change in the participants' perception of these four attributes, rather than a change in the actual brightness of the scene.

3 RESULTS

The following subsections present the results of the statistical analyses used to study the subjective responses related to the effect of color and furniture on participants' satisfaction with brightness, the associations between satisfaction with brightness and other perceptual attributes, and the comparison of satisfaction with brightness with a composite index of satisfaction with perceptual attributes in the space.

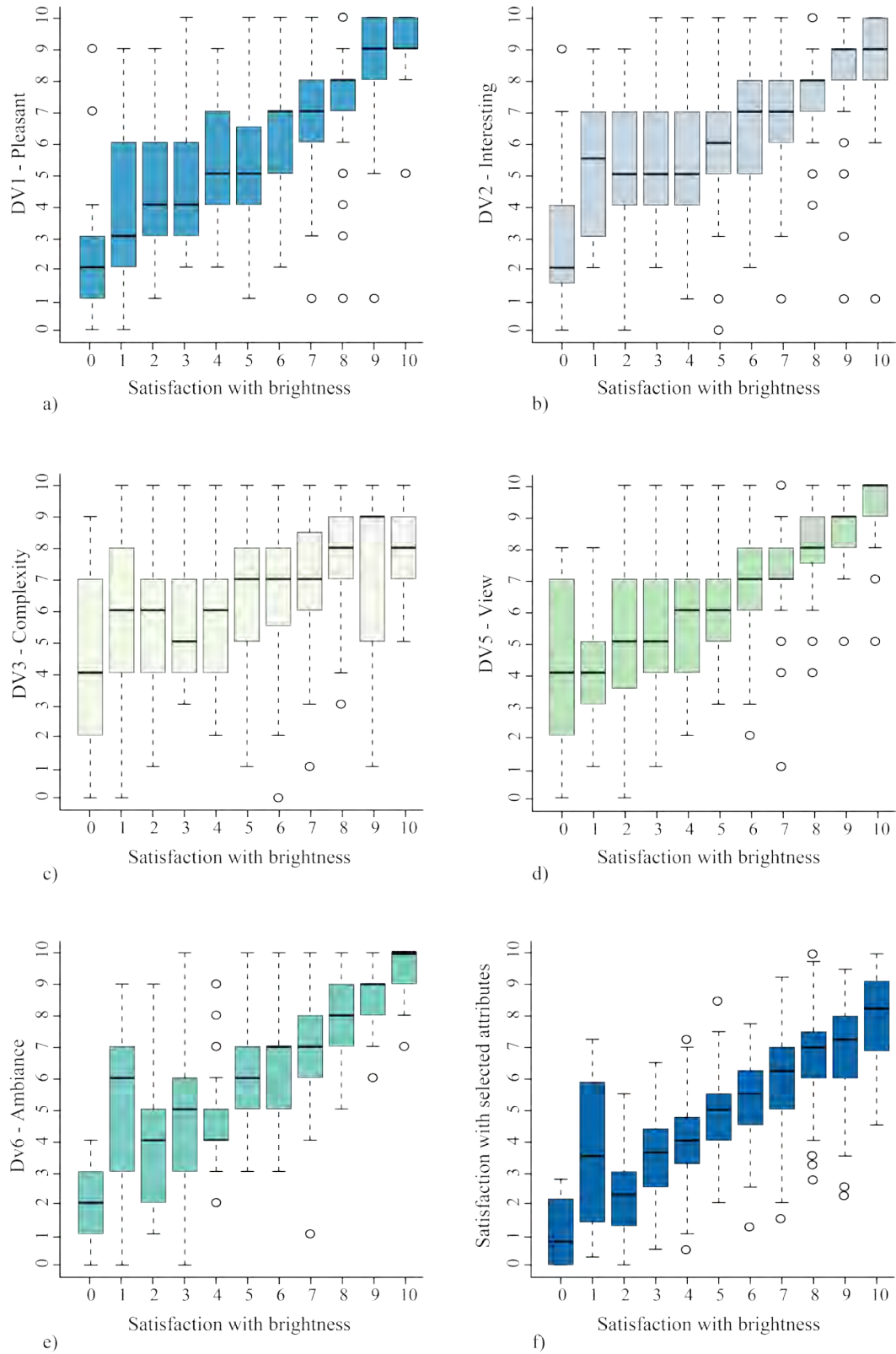


Figure 3. (a)-(e) Boxplots of evaluations of participants' perceptual impressions of the space (y axis), plotted against the equivalent ratings of satisfaction with brightness (x axis), and (f) ratings of the composite index of satisfaction with selected attributes (y axis) plotted against the equivalent ratings of satisfaction with the brightness of the space (x axis).

3.1 Influence of Color and Furniture on Satisfaction with Brightness

Although the actual brightness level of all scenes was the same, participants' evaluations of their satisfaction with brightness spanned the full range of the rating scale (0 to 10 units), with a mean of 6.1 and a standard deviation of 2.18. Linear mixed model analyses were conducted to investigate separately the effect of color and of furniture on the participants' responses. For these analyses, a Bonferroni-corrected significance level of $0.05/2=0.025$ is used to account for the multiple comparisons. Results show a statistically significant main effect of color ($F(2,600) = 75.33$, $p<0.001$) on participants' evaluations of their satisfaction with the brightness in the space. In particular, participants' satisfaction with brightness in the scenes with fully colored materials were on average 1.3 units higher than the ratings in the corresponding grayscale scenes. The effect of furniture was not statistically significant on participants' satisfaction with brightness ($F(1,601) = 4.80$, $p=0.028$).

3.2 Associations Between Satisfaction with Brightness and Subjective Impressions of the Space

Further analyses were performed to investigate the association between satisfaction with brightness and the perceptual impressions of other attributes examined in the study. Positive statistically significant associations were found between the evaluations of *satisfaction with brightness* and evaluations of how *pleasant* ($b=0.16$, $p<0.001$) and *complex* ($b=0.08$, $p<0.05$) the space is perceived, as well as with the ratings of the *satisfaction with access to the view outside* ($b=0.11$, $p<0.01$), and the *satisfaction with the ambiance of the space* ($b=0.24$, $p<0.001$). No statistically significant association was found between the *satisfaction with brightness* and how *interesting* the space was perceived ($b= -0.04$, $p=0.35$). These associations can be observed in the plots (a) to (e) in Figure 3, showing the distribution of participants' evaluations of the space plotted against the corresponding ratings of satisfaction with brightness.

3.3 Composite Index of Satisfaction with Perceptual Attributes

Following the findings of positive statistically significant associations, we constructed a composite index representing participants' *satisfaction with selected attributes* (as described in section 2) to understand its association with participants' perception more broadly. To visualize this index using unadjusted data, we constructed a box plot of satisfaction with brightness in terms of *satisfaction with selected attributes* (Figure 3f). This plot shows a strong positive relationship between these two attributes, suggesting a possible effect on satisfaction with brightness that could be due to the participants' satisfaction with the selected attributes in the composite index. We then used a linear mixed effect model to statistically assess the strength of this relationship. We found that a one-unit difference in overall satisfaction corresponds to a 0.7-unit increase in perceived brightness ($p<0.001$).

4 CONCLUSION

This experimental study investigates the influence of key aspects of participants' perceptual impressions of a scene, such as the pleasantness, the satisfaction with the access to the view or the ambiance of the space, on ratings of satisfaction with the brightness of that scene. Through the use of an experimental method which couples physically-based renderings with projection in virtual reality, a total of 100 participants were immersed in virtual scenes of an interior an office space with different façade shading systems, colored materials and with or without furniture.

Although the studied scenes were similar in terms of illuminance levels, findings demonstrate a significant effect of colored materials on the participants' satisfaction with brightness. Although the addition of colored materials in virtual environments adds a layer of complexity in the simulation workflow, this finding highlights the importance of colored materials in assessing user's satisfaction with the brightness in the scene.

The results of this experimental study also demonstrate that there is a clear association between participants' satisfaction with brightness and other perceptual impressions, such as the access to the view outside, perceived pleasantness, interest, complexity and the overall ambiance. This indicates that our perception and satisfaction with brightness cannot be studied on its own without understanding how the overall design of the environment affects occupants' perception and visual impressions.

Our fitted regression model quantifies how people perceive brightness in a range of settings in which other perceptual attributes are varied while actual brightness is held constant. While we cannot directly control the perceptual impressions of people in a space, we can use this model to investigate how their satisfaction with brightness might change if we were able to design for the other attributes, again without changing the actual brightness of the scene. To do this, we used our fitted mixed effects model to investigate the satisfaction with brightness for a range of hypothetical scenarios, when all four other attributes are scored equally at levels ranging from 0 to 10. The relation between the two ratings indicates that the participants' satisfaction with brightness could potentially be shifted by five units, contrasting a building with minimal ratings on all other perceptual categories with a building with maximal ratings on all other perceptual categories. This result is important in the realm of design, especially in designing 'green' buildings, as post-occupancy surveys on occupants' satisfaction with lighting may be less related to the actual light levels and more to the overall quality and the ambiance of the building. Additional studies with a wider range of stimuli are needed to investigate the validity of the presented findings in different types of spaces, and with different brightness levels. Further research is encouraged to investigate the replicability of these results in a real environment.

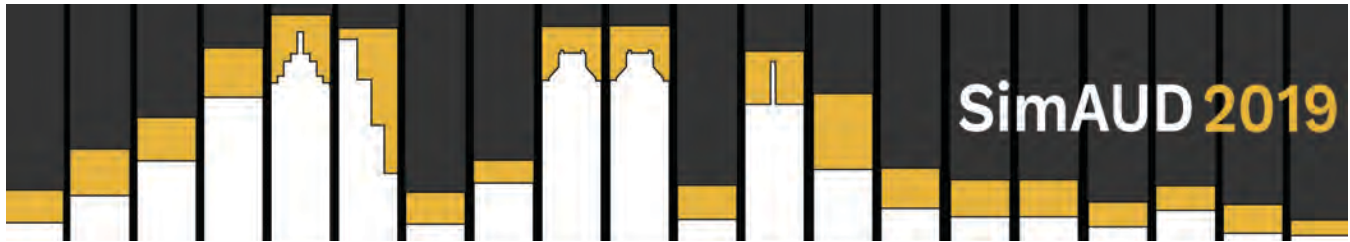
ACKNOWLEDGMENTS

The authors would like to thank professors Mojtaba Navvab and MaryCarol Hunter (University of Michigan) for their valuable support and feedback. We are grateful for the technical support provided by Alstan Jakubiec (University of Toronto) and, Dan Weissman (Lam Partners). We would also like to thank Jan Wienold and Marilyne Andersen (Laboratory of Integrated Performance in Design, Ecole polytechnique fédérale de Lausanne) for their continuous support and advice. We thank Craig Wilkins (University of Michigan) for comments that greatly improved the paper.

REFERENCES

1. S. Holl, S. Kwinter, and J. Safont-Tria, *Color, Light, Time*, 1 edition. Zurich, Switzerland: Müller, Lars, 2011.
2. P. Zumthor, *Atmospheres: architectural environments - surrounding objects*. Basel: Birkhäuser, 2006.
3. J. Pallasmaa, *The Eyes of the Skin: Architecture and the Senses*, 3 edition. Chichester: Wiley, 2012.
4. J. E. Flynn, T. J. Spencer, O. Martyniuk, and C. Hendrick, "Interim Study of Procedures for Investigating the Effect of Light on Impression and Behavior," *J. Illum. Eng. Soc.*, vol. 3, no. 1, pp. 87–94, Oct. 1973.
5. R. J. Hawkes, D. L. Loe, and E. Rowlands, "A Note towards the Understanding of Lighting Quality," *J. Illum. Eng. Soc.*, vol. 8, no. 2, pp. 111–120, Jan. 1979.
6. J. a. Veitch and G. R. Newsham, "Preferred luminous conditions in open-plan offices: research and practice recommendations," *Light. Res. Technol.*, vol. 32, no. 4, pp. 199–212, 2000.
7. P. R. Boyce, *Human Factors in Lighting, Third Edition*. CRC Press, 2014.
8. P. R. Boyce and C. Cuttle, "Effect of correlated colour temperature on the perception of interiors and colour discrimination performance," *Light. Res. Technol.*, vol. 22, no. 1, pp. 19–36, Mar. 1990.
9. L. Loe, K. P. Mansfield, and E. Rowlands, "Appearance of lit environment and its relevance in lighting design: Experimental study," *Light. Res. Technol.*, vol. 26, no. 3, pp. 119–133, 1994.
10. G. R. Veitch, Jennifer a., Newsham, "Lighting Quality and Energy-Efficiency Effects on Task Performance, Mood, Health, Satisfaction and Comfort," no. August, pp. 1–37, 1997.
11. M. Stokkermans, I. Vogels, Y. de Kort, and I. Heynderickx, "Relation between the perceived atmosphere of a lit environment and perceptual attributes of light," *Light. Res. Technol.*, pp. 1–15, 2017.
12. M. Rea, X. Mou, and J. Bullough, "Scene brightness of illuminated interiors," *Light. Res. Technol.*, vol. 48, no. 7, pp. 823–831, Nov. 2016.
13. D. Tiller and J. A. Veitch, "Perceived room brightness: Pilot study on the effect of luminance distribution," *Light. Res. Technol.*, vol. 27, no. 2, pp. 93–101, 1995.
14. J. Bullough, L. Radetsky, and M. Rea, "Testing a provisional model of scene brightness with and without objects of different colours," *Light. Res. Technol.*, vol. 43, no. 2, pp. 173–184, 2011.
15. J. D. Bullough, L. C. Radetsky, U. C. Besenecker, and M. S. Rea, "Influence of spectral power distribution on scene brightness at different light levels," *LEUKOS - J. Illum. Eng. Soc. North Am.*, vol. 10, no. 1, pp. 3–9, 2014.
16. S. A. Fotios and C. Cheal, "Lighting for subsidiary streets: investigation of lamps of different SPD. Part 2—Brightness," *Light. Res. Technol.*, vol. 39, no. 3, pp. 233–249, Sep. 2007.
17. S. Fotios and C. Cheal, "Brightness matching with visual fields of different types," *Light. Res. Technol.*, vol. 43, no. 1, pp. 73–85, Mar. 2011.
18. M. Boubekri, R. B. Hull, and L. L. Boyer, "Impact of Window Size and Sunlight Penetration on Office Workers' Mood and Satisfaction A Novel Way of Assessing Sunlight," *Environ. Behav.*, vol. 23, no. 4, pp. 474–493, Jul. 1991.
19. M. Boubekri and L. L. Boyer, "Effect of window size and sunlight presence on glare," *Light. Res. Technol.*, vol. 24, no. 2, pp. 69–74, Jun. 1992.
20. K. Van Den Wymelenberg, M. Inanici, and P. Johnson, "The effect of luminance distribution patterns on occupant preference in a daylight office environment," *LEUKOS - J. Illum. Eng. Soc. North Am.*, vol. 7, no. 2, pp. 103–122, 2010.
21. K. Chamilothoni, G. Chinazzo, J. Rodrigues, E. S. Dan-Glauser, J. Wienold, and M. Andersen, "Subjective and physiological responses to façade and sunlight pattern geometry in virtual reality," *Building and Environment*, vol. 150, pp. 144–155, 2019.
22. S. Rockcastle, M. L. Amundadottir, and M. Andersen, "Contrast measures for predicting perceptual effects of daylight in architectural renderings," *Light. Res. Technol.*, vol. 49, no. 7, pp. 882–903, Apr. 2017.
23. S. Rockcastle, K. Chamilothoni, and M. Andersen, "An Experiment in Virtual Reality to Measure Daylight-Driven Interest in Rendered Architectural Scenes," in *International Building Performance Simulation Association (IBPSA)*, 2017.
24. K. Chamilothoni, J. Wienold, and M. Andersen, "Adequacy of Immersive Virtual Reality for the Perception of Daylit Spaces: Comparison of Real and Virtual Environments," *LEUKOS - J. Illum. Eng. Soc. North Am.*, vol. 00, no. 00, pp. 1–24, 2018.
25. A. Omidfar, M. Niermann, and L. N. Groat, "The Use of Environmental Aesthetics in Subjective Evaluation

- of Daylight Quality in Office Buildings,” in *Proceedings of IES Annual Conference*, Indianapolis, USA, 2015.
26. K. Chamilothoni, J. Wienold, and M. Andersen, “Façade design and our experience of space: the joint impact of architecture and daylight on human perception and physiological responses,” in *Proceedings of the Light Symposium 2018 Conference*, Stockholm, Sweden, 2018.
 27. G. Ward Larson and R. Shakespeare, *Rendering with radiance: the art and science of lighting visualization*. San Francisco, CA: Morgan Kaufmann Publishers Inc., 1998.
 28. DIVA-for-Rhino, “Solemma LLC.” 2018.
 29. E. Reinhard, M. Stark, P. Shirley, and J. Ferwerda, “Photographic tone reproduction for digital images,” *ACM Trans. Graph.*, vol. 21, no. 3, 2002.
 30. European Committee for Standardization, “Light and lighting - Lighting of work places - Part 1: Indoor work,” *Eur. Stand.*, pp. 1–43, 2002.
 31. R. C. Team, “R: A Language and Environment for Statistical Computing.” R Foundation for Statistical Computing, Vienna, Austria, 2018.
 32. A. Kuznetsova, P. B. Brockhoff, and R. H. B. Christensen, “{lmerTest} Package: Tests in Linear Mixed Effects Models,” *J. Stat. Softw.*, vol. 82, no. 13, pp. 1–26, 2017.



Immersive Representation of Urban Data

Amber Bartosh and Rongzhu Gu

Syracuse University
Syracuse, NY USA
{Abartosh, rg104}@syr.edu

ABSTRACT

Urban environments are not comprised solely of physical objects like buildings, infrastructure, and landscapes, but also invisible, but critically influential, information like traffic patterns, economic values, and energy use. This intangible overlay of quantifiable urban behavior is essential to understanding how cities function. Vast quantities of urban data are now widely available through online open source data repositories, but the raw data remains limited in its value to support informed decision-making unless it can be synthesized and represented in a meaningful fashion. This paper describes in-progress research exploring the spatialization and representation of urban data using virtual reality (VR). This research uses Manhattan as a test case for enabling users to access urban data immersively and interactively from multiple vantage points and scales. It describes the process for visualizing the city in VR, representing urban data three-dimensionally, and creating a user interface for data interaction while in the virtual environment. The paper identifies initial steps towards creating an immersive representation of urban data to effectively inform future urban planning initiatives and design decisions.

Author Keywords

Data visualization; urban data; mixed reality; smart cities; virtual environments; users interface.

ACM Classification Keywords

J.2: Physical Sciences & Engineering

1 INTRODUCTION

The industrial adoption of virtual reality technology extends beyond its obvious application for gaming and recreation. Initial industrial implementation was in defense and medical training, but architectural practices have been quick to take advantage of the rapid rendering capabilities of VR to facilitate communication between designer, consultants, stakeholders and clients. Management, operations and business administration are also using VR for project demonstration and simulation. Such examples of industry-relevant applications which act as precedents for this project include, the Roames project, developed by Fugro and

presented at the United 2017 International Conference of Virtual Reality Software Developers. This platform uses sophisticated artificial intelligence and cloud computing technology to map geographic space. Complex three-dimensional objects, such as structures of buildings and bridges, poles, city accessories, and wires, trees, and streetlights, can be compiled with less than centimeters of accuracy and generated on a visible scale in the virtual world. Intended to help facilitate managerial understanding of complex systems, the Roames platform enables users to remotely check systems status and realistic simulate infrastructure and environmental conditions. In this way, users can view the status of the entire network in real time [1].

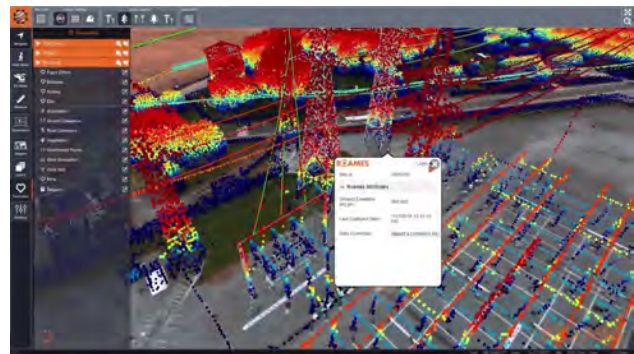


Figure 1 Fugro Roames 3D Simulation Virtual World

The Roames analytics is a platform for data visualization with certain advantages that might be translated for application to visualizing open source urban data. First, Roames uses a video-game interface and within it a 3D virtual world can be freely navigated by mouse or controller (Figure 1). Second, the location and form of the data icons are similar to those used by Google maps and other geographic information system (GIS) software, and the user can toggle on and off relevant data via a simple click which facilitates large-scale information loading and layering.

Despite its sophisticated modeling and video game based interface, the Roames system is still intended to be interacted with through a 2D screen which potential limits its

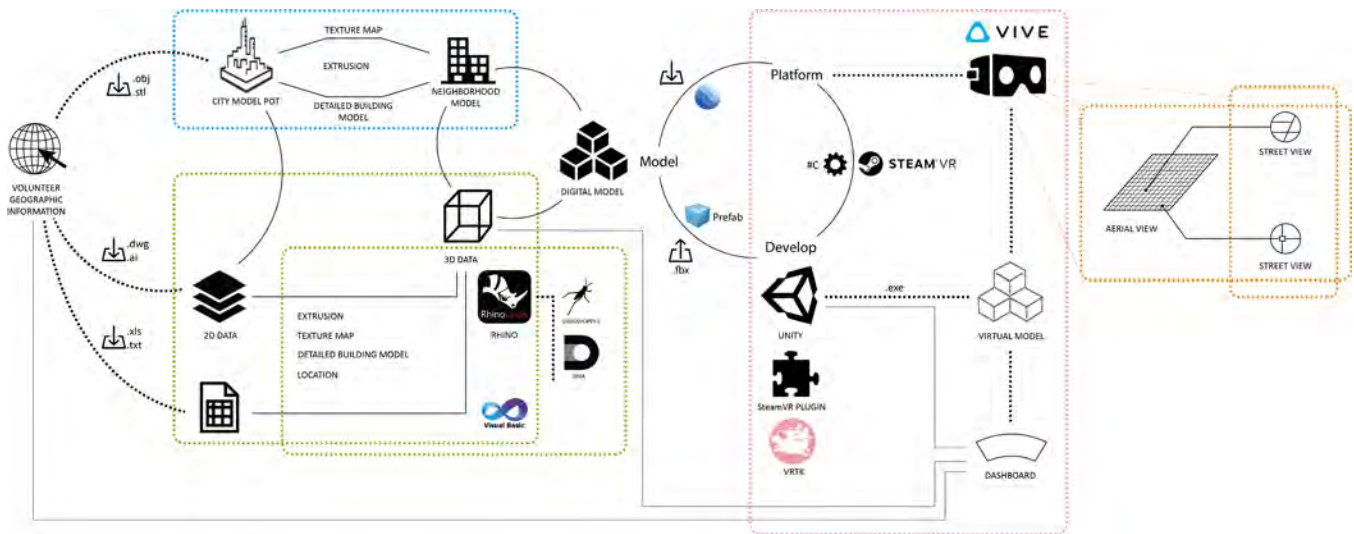


Figure 2 Diagram of work flow from digital model to data integrated virtual urban environment

communicative impact. Users interacting with 3D data visualizations within virtual reality platforms have demonstrated that immersion provides better retention of perceived relationships and more intuitive data understanding than traditional desktop visualization tools. [2]. Perhaps the most pervasive VR application for urban visualization is Google Earth VR which gives the user the ability to zoom in and out from a global perspective down to birds-eye view, and in specific locations and for limited distances even allows the user to virtually walk through the city at street-level [3]. Google Earth VR is impressive in the volume and detail of its model, but it does not integrate additional data beyond the city’s visual appearance and massing.

Other relevant work has attempted to link data visualization to VR representation, with varying degrees of success. Notably relevant work which merges urban data with VR includes the Urban Fusion project conducted at the Future Cities Laboratory at the Singapore-ETH Centre which has an impressive user interface that tracks hand movement and allows for gradient control of data representations, but doesn’t provide a multi-scalar view of the city [4]. Alternate VR urban data visualizations remove the form of the city altogether [5].

With this project the authors have created a multi-scale representation of urban data using VR which couples the geo-physical aspects of the city with the invisible but relevant urban data related to it. The representation is immersive by nature of the head-mounted VR display and designed to be interactive using video game platform mechanics.

2 METHOD

The process of creating our test case for interactive and immersive urban data representation required modeling the city digitally, collecting and spatializing urban data, and creating a VR user interface.

2.1 City Modeling and VR Integration

Digital city models are becoming increasingly easy to find or generate thanks to the development of GIS tools such as ESRI CityEngine. Once generated, the city model was exported from 3D digital modeling software as an .fbx file. This file was then imported into the video game engine, Unity, where the open-source asset package “Virtual Reality Tool Kit” (VRTK) and SteamVR were used to visualize the model in VR. An HTC Vive system was used as the virtual reality display system. It includes a room-scale “play space” of approximately 9’ by 15’ with infrared lighthouses, head-mounted display, and hand controllers.

The VR system allows for a multi-scale view of the city—from a zoomed-out aerial perspective and from street-view at full-scale. The initial system prototype allows the user to choose between three different scenes of Manhattan: the aerial overview, a street-view of the Columbus Circle neighborhood, and World Trade Center area. A different degrees of modeling complexity was implemented with the change in scale between scenes. Due to both computer processing constraints and the need for a simpler backdrop for data visualization when zoomed out, the aerial overview used a simple untextured massing model to represent the physical aspects of the city. However, for the street view scenes a more detailed modeling of the surrounding buildings was both appropriate visually and necessary for user orientation. (Figure 2)

2.2 Urban Data

Open source urban data, like that found on the NYC Open Data website [x], is often one-dimensional in nature – a collection of numerical values without a compelling or obvious mode for graphic interpretation. Data that is mapped two-dimensionally, like most of the data from OpenStreetMap (OSM) or GIS, is more visually interpretable, but is still subject to the limitations and bias of Cartesian logic. The representation of such data in a 3-

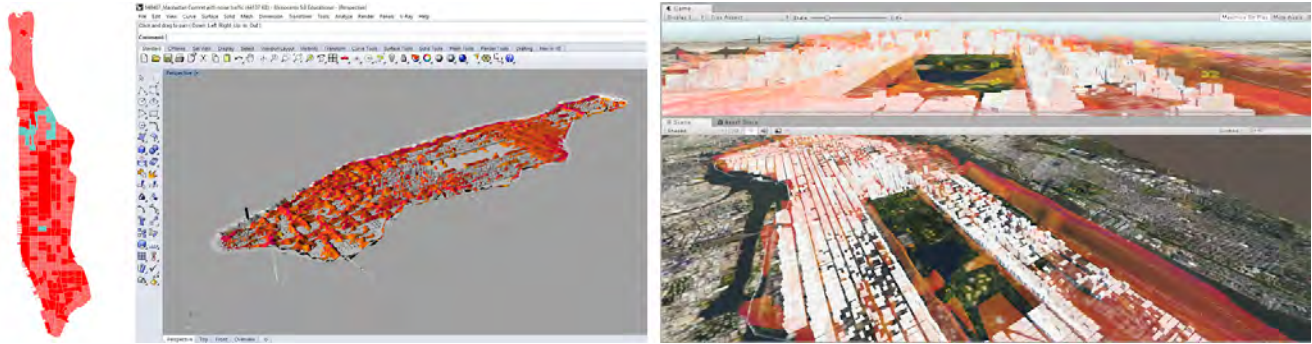


Figure 3 Traffic noise in ArcGIS, Rhinoceros & Unity3D

dimensional virtual environment requires that the data be “spatialized” or given additional dimensionality. This data spatialization required translation and interpretation by the design team. Tested means for spatializing the data for 3D visualization included piping, extrusion, point clouds, and point markers. Spatialized data included public transportation locations (subway and metro), noise levels, and energy use by block.

2.3 User Interface (UI)

By using precedent UI systems, like that of Google Earth VR, as a model, the user interface was designed to take advantage of the video game inclination of Unity to create an interactive UI that allows the user to toggle on and off data sets to create novel overlays of information. Two key aspects to an effective UI, is that it reduce user memory load, the amount of effort the user has to repeatedly input to understand the interface, and supports clear interaction with the “game’s” intent. Attempts to keep user memory load levels low were manifest through hand control button labels which were visible in the virtual environment and a menu/instruction panel which could be easily accessed through the touch of a button. (Figure 4) Users can toggle on and off the data sets by pointing a laser-pointer like extension at the end of one of the hand controllers at menu options and pulling the trigger to select. Similar mechanics are used to move between the aerial perspective and the two street view scenes.



Figure 4 Controller labels are part of User Interface

3 ITERATION & IMPLICATIONS

Varying data spatialization methods were tested for graphic clarity and comprehension. Traffic noise for example was visualized as a height map, where the noise volume was

represented by both the color and height of the resulting topographic surface. Extrusions, piping and height map data visualization methods worked sufficiently in the aerial perspective. However, there is no uniform standard for 3D representation of urban data which makes user interpretation of the data difficult to predict. After completing the initial prototyping phase, iterative evolution of the data representation showed that those with both color and formal differentiation gave mappable data the most visual clarity in the aerial view. By adding transparency, multiple data sets could be layered on one another adding novel comparative possibilities while remain individually coherent (Figure 5).

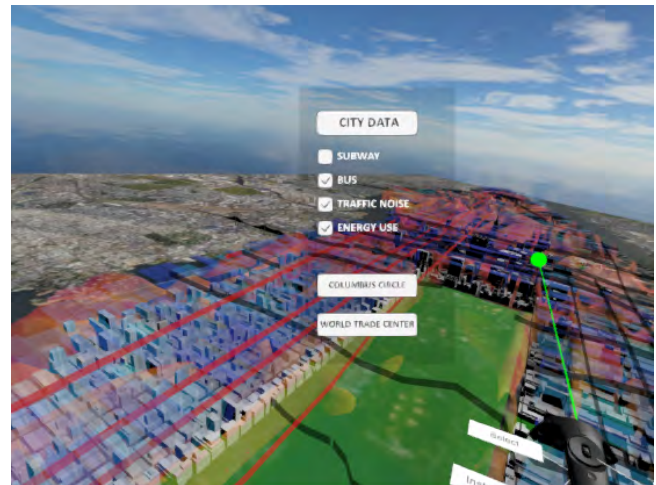


Figure 5 Layers of data visualized as overlays on the city

However, at street level, the same data visualization methods resulted in misinterpretations of the data as architectural objects. Therefore, a new dashboard method was developed for data visualization in the full-scale perspectives. This dashboard linked to the data in a manner which allows color and indicator changes related to user position in space. Even though the data itself is static, the user’s relation to it via position is changing, and the visualization of this results in a dynamic display. (Figure 6)

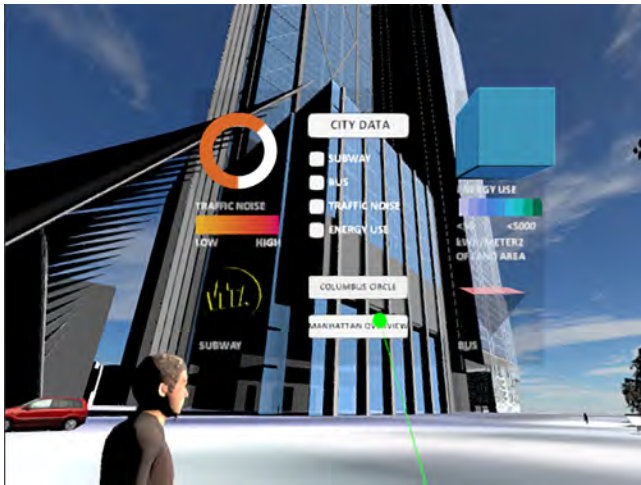


Figure 6 Street Level Perspective Data Dashboard

Additionally, data representations were limited by the rendering capacity of the program and the computer. Overly complex geometries or representations with high face counts or material textures would inhibit the picture in VR and result in a flashing picture inside the headset. This flashing could cause a detrimental effect on the user's experience. Special attention was given thereafter to performatively optimizing both the city and data models.

And lastly, while the full-scale capacity of the HTC Vive allows for user movement to be matched one to one between the physical play space and the virtual environment, the scale of the city neighborhood was so large that users defaulted to "teleporting" through the environment virtually while standing fairly still in the physical space. Such observations suggest that the perception of extent or understanding of potential travel distance within the 1:1 scale experience is undermined by the fact that the user is not really moving their body in a manner that replicates a city pedestrian.

4 CONCLUSION

This paper presents in-progress research aiming to contribute to a body of explorations collaboratively done by architects, engineers, urban planners, and computer scientists to represent, understand, and engage the urban condition through virtual modelling and simulation.

This specific project used the gaming engine Unity3D as a platform for providing both VR visualization and an interactive user interface. Key contributions of the work in its present state include a multi-scalar visualization of data for both aerial and street-view perspectives and an exploration of methods for translating data from 2D to 3D. Future work will apply and test this representation tool as an urban planning communication device between designers and community leaders. Next iterations will add more data sets related to energy and environmental conditions and experiment with in situ augmented reality data representations which would blend the 1:1 street scale data representations with the actual street.

ACKNOWLEDGMENTS

Funding and support of this project was provided through the Syracuse Center of Excellence and Syracuse University School of Architecture.

REFERENCES

1. Roames. Fugro. Accessed December 1, 2018. <https://www.fugro.com/our-services/asset-integrity/roames-power>.
2. C. Donalek et al., "Immersive and collaborative data visualization using virtual reality platforms", Proc. IEEE Int. Conf. Big Data (USA Big Data), pp. 609-614, Oct. 2014.
3. Joanna Kim, "Get a Closer Look with Street View in Google Earth VR," Google, September 14, 2017, , accessed October 22, 2018, <https://www.blog.google/products/earth-vr/get-closer-look-street-view-google-earth-vr/>.
4. Jan Perhac, Wei Zeng, Shiho Asada, Stefan Mueller Arisona, Simon Schubiger, Remo Burkhard, and Bernhard Klein. "Urban Fusion: Visualizing Urban Data Fused with Social Feeds via a Game Engine." *2017 21st International Conference Information Visualisation (IV)*, 2017. doi:10.1109/iv.2017.33.
5. Al Bondakji, Louna, Anna-Maria Chatzi, Minoos Heidari Tabar, Lisa-Marie Wesseler, and Liss C. Werner. "VR-visualization of High-dimensional Urban Data." 2018

Modeling Urban Energies

A Data-driven Framework For Urban Building Operational Energy Use Modeling.71

Narjes Abbasabadi

An Integrated Urban Planning and Simulation Method To Enforce Spatial Resilience
Towards Flooding Hazards. 79

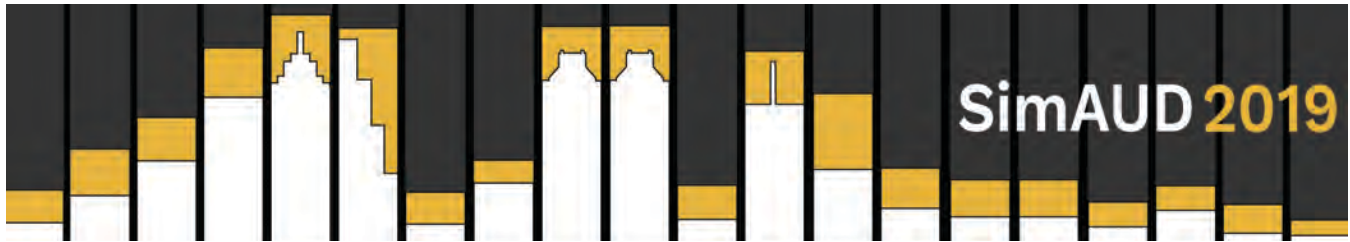
Julius Morschek, Reinhard Konig and Sven Schneider

A Method for Integrating an Ubem with Gis for Spatiotemporal Visualization and Analysis 87

Bess Krietemeyer and Rawad El Kontar

A Technique for Developing High-Resolution Residential Occupancy Schedules for
Urban Energy Models 95

Diba Malekpour, Farzad Hashem, Vinciane Tabard-Fortecoef and Ulrike Passe



A Data-driven Framework For Urban Building Operational Energy Use Modeling

Narjes Abbasabadi and Rahman Azari

College of Architecture, Illinois Institute of Technology
Chicago, USA
{nabbasab, razari}@hawk.iit.edu

ABSTRACT

Accurate measurement and analysis of urban energy use is an essential step in development of low-carbon cities. However, there is a limited number of methods and tools for energy use modeling and prediction at urban or neighborhood scales. This article proposes a bottom-up data-driven framework for urban energy use modeling (UEUM) which localizes energy performance measurements and considers urban context. The framework addresses the urban building operational energy estimation through the use of disaggregated energy use data and allows for an accurate urban energy performance measurement at building-level. A machine learning approach is applied to mathematically associate building characteristics and urban context attributes; i.e., building height, as an urban intensity metric, and sprawl indices representing compactness and connectivity of neighborhoods with urban building operational energy use intensity (EUI). Once the mathematical relationship is identified, the model predicts the energy consumption of individual buildings that represent a particular end-user. Chicago as a pilot case study was selected to test the framework. Several algorithms are tested and then the improved model was used to predict energy use for around 820,000 buildings in the city. The framework has the potential to aid designers, planners, and policymakers in a better understanding of the existing urban energy use profile, and the environmental impacts of alternative scenarios of urban development.

Keywords:

Urban energy use modeling; building energy; data-driven; machine learning method.

1 INTRODUCTION

Over half the world's population lives in cities and this is predicted to increase to over 68 percent by 2050 [1]. Cities consume 67-76% of the primary energy resources and account for 71-76% of GHG emissions [2] and buildings account for the most significant contributions in urban energy use and associated emissions [3]. Therefore,

understanding and managing the energy use in cities is a key challenge to achieve more sustainable and low carbon cities.

While, urban energy use modeling and prediction are essential in urban energy management and understanding of energy performance of cities, there are limited number of methods and tools to accurately predict urban energy use. There is a lack of an integrated approach to incorporate actual urban spatial patterns with urban energy use models. Common urban energy use modeling approaches are classified into two main groups: engineering or simulation models and data-driven or statistical models [4,5]. Either simulation or data-driven models have their own limitations and methodological uncertainties with regard to urban energy quantification. The simulation methods often suffer from oversimplification of building and system data. They rely on limited number of typologies or archetypes to achieve time and computational efficiency.

The data-driven models could present more accurate urban energy modeling if data would be available and sufficient variables would capture in the model [6,7]. The limitation of data-driven models stem from often relying on the aggregated data; yet, limited number of surveys provide local energy data at building level. Recently, as a part of disclosure law which adopted by many cities in the US, energy benchmarking was released. Energy benchmarking provides more transparency and provides disaggregated building level energy data. However, it has limitations regarding data availability for all buildings in the city. For example, for Chicago, it covers less than 1% of Chicago's buildings, which account for approximately 20% of total energy used by all buildings [8].

The main objectives of this research is to develop a data-driven framework for urban energy use modeling (UEUM). This model would predict urban energy use at multiple scales of building, block, neighborhood, and city scales. Also, the model is used to quantify and examine the association between urban spatial patterns and energy use at city scale. Finally, to develop a GIS web-based platform to

communicate and visualize the predicted urban building energy use.

2 METHODOLOGY

2.1 Conceptual Framework

In this research, the urban energy use is outlined as building operational energy use at city scale. The following steps are followed in modeling urban building energy use:

As the first step, the model incorporates the actual urban spatial patterns to define the variables in the model. The key attributes of urban spatial patterns in the model include: a) *Building Characteristics (BC)* consisting of variables such as number of floors, building type, building size, and construction year, b) *Urban Attributes (UA)* such as density, connectivity and land use mix which are captured via urban sprawl index [9], and c) *Occupancy Characteristics (OC)* including total population, household size in residential buildings, worker density in commercial buildings, and percentage of occupied units. Then it analyzes actual spatial patterns of the city to extract new features and add new variables in the model. As an example, building height typology is defined through the actual building height pattern extraction of the buildings in the city. In the next step, the model predicts urban energy use through learning the mathematical relationship between variables. Then the model is used to explain the association between variables. It quantifies how key attributes of urban spatial patterns at neighborhood scale; i.e., building height and sprawl index affect urban energy use. Finally, the model provides a multi-scale analysis and prediction at neighborhood, census tract, census block, and building scales. A multi-scale analysis could provide a more accurate and holistic image of urban energy use and the impact of different design decisions on energy consumption.

The framework is generalizable for all cities with similar datasets. Chicago as major city in the US has been selected as a pilot case study to test the framework.

2.2 The UEUM framework

This framework is outlined as a two-step model:

1. *Pattern Extraction*: The first step analyzes actual spatial patterns of the city to learn and extract new features and add new variables in the model

2. *Prediction*: In the next step, it tests different algorithms to propose an enhanced prediction model.

The model for building energy use prediction framework is split up into four sub-sections:

2.2.1. Data Preparation

Data preparation includes: locate data, treat missing data, process and clean data, and finally merge data.

a) Locate data

Several datasets were used as the basis for the statistical model including urban spatial data, building characteristics,

and operational energy data. The building characteristics are captured from the Chicago building footprints dataset [10] which is a GIS-based dataset and represents a compilation of land use and geographic data for Chicago. This dataset provides building-level data for around 820,000 buildings in Chicago. The geo-referenced urban attributes was built based on the U.S. Urban Sprawl Data [11] developed by Ewing [9,12] which are captured multidimensionally using density, land use, activity centering, and accessibility indicators. This database is available at census tract, urbanized areas, Metropolitan Statistical Area (MSA), and county level. For building energy data, the recently released Chicago Energy Benchmarking data [13] was used. This dataset provides energy data for buildings of certain sizes, greater than 50,000 sq.ft. And for buildings with smaller sizes, this research used Chicago Energy Usage (2010) dataset [14] which provides energy data for buildings of all sizes. This dataset does not provide exact geographical location and provides location at block level because of privacy issues.

b) Treat missing data

In order to maximize use of available information and handle missing data, several statistical methods was done including multiple imputation methods with linear regression, multivariate normal regression, and predictive mean matching algorithms. The objective of Multiple imputation (MI) is to analyze missing data and replace missing values to complete the data based on valid frequency inference [15]. The Chicago Building Footprint (CBF) dataset has limitations such as an extensive amount of errors and missing data such as building height information. The multiple imputations were employed to fill the missing information in the CBF dataset. Several algorithms were tested for handling missing data. For continuous variables such building height, this research tested several multiple imputation methods with linear regression, multivariate normal regression, and predictive mean matching algorithms. The results show that the predictive mean matching algorithm provides a higher accuracy level for handling missing data for building heights.

c) Process & clean data

The building energy data have limitations regarding having errors in data, and outliers as extreme observations. Then, the potential outliers were identified through statistical tests [16]. In the next phase, those potential outliers was assessed in terms of how being influential on individual regression parameters through the Cook's Distance test [17]. Finally, extreme outliers with significant influence were dropped out of the datasets. To test the model regarding normal distribution, evaluating the shape of residuals and the distribution of errors, we used Quantile-normal (q-norm) plot which is considered as a common normality test [18] as well as well as p-norm and Kornel Density plots.

d) Merge data

Then all the datasets including urban spatial data, building characteristics data, and operational energy data were

merged to build the Urban Spatial and Energy (USE) dataset as the basis for the statistical model.

2.2.2. Pattern Extraction: Cluster

The most promising Machine Learning clustering algorithm, k-means, [19–21] was applied to extract the actual archetypes/typologies of buildings with certain similarities together and learn underlying patterns. “The aim of the K-means algorithm is to divide M points in N dimensions into K clusters so that the within-cluster sum of squares is minimized” [22]. Then new variables such as building height typologies were added into the model. Incorporating the actual urban spatial patterns, building characteristics and urban context would improve the prediction accuracy for a city scale energy use.

2.2.3. Prediction

This section includes: train models; validate; compare the trained models and predict based on the enhanced model; and finally analyze.

In this research, a machine learning approach is applied to model and predict urban building energy use by “learning” the patterns present in the merged dataset, to fit the model, and to find the mathematical relationship between energy use and key urban attributes, and then to predict energy consumption for all buildings in the city where the energy use data is not available. This is a regression problem as it is the task of approximating a mapping function (f) from input variables (X including urban attributes, building characteristics, and residents characteristics) to a continuous output variable (y which is building operational energy consumption). The energy prediction was done for almost all buildings, around 820,000 buildings, in the city of Chicago.

In this section, six promising machine learning models including Multiple linear regression (MLR), Nonlinear Regression (NLR), Random Decision Forest (RDF), Classification and Regression Trees (C&RT), K-Nearest Neighbors (K-NN), and Artificial Neural Networks (ANNs) [19–21] were trained on the merged dataset to test and propose an enhanced model.

The MLR algorithm as a most common technique is utilized widely for both building and transportation energy use modeling and prediction [31,50]. This method is widely applied in the energy consumption prediction models for its simple design, and computationally effecting while it is still sufficiently precise [9,62–64]. Also, it has advantages such as being easily interpretable and suitable for modeling the complex relationships [49]. MLR uses the ordinary linear least square (OLS) method to estimate the coefficient and minimizes the sum of squared residuals (SSR) between the prediction and observed values [149].

ANNs is one of the most promising methods in energy use prediction. ANNs generate and connect a network of input nodes, hidden nodes, and output nodes by weighted links which has remarkable capability in modeling nonlinear patterns [56] [42]. ANNs have been commonly used for short

term energy use forecasting and time series data at a building scale [55]. Limited number of studies used ANNs for energy use prediction at urban scale and an annual resolution [150].

2.2.4. Validation

The validation process was done to achieve solid results. The cross-validation method as a most effective validation technique [23,24] based on Random Sub-sampling was applied to avoid biased results. Data was split to train and test of 80% / 20%.

2.2.5. Prediction Performance Measurement

Then the models were compared in terms of their prediction performance which is calculated based on measuring the errors between the predicted and actual values. There are many ways to estimate the performance of a regression predictive model, the most widely used evaluation metrics are the mean absolute deviation (MAD), Mean Square error (MSE), Root Mean Square Error (RMSE), and Mean Absolute Percentage Error (MAPE). The lower the values of MAD, MSE, RMSE, and MAPE show the better performance of the model.

2.2.6. Model to Explain the Association Between Variables

The MLR algorithm with the OLS method was applied on the merged USE dataset to model the urban energy use of buildings and transportation in Chicago neighborhoods and use the model to explain the association between variables. Then the PR algorithm was applied to capture the non-linear patterns and draw the polynomial fitting curves on data points plotting the two variables of building height and sprawl index and energy use. These algorithms were selected because of their effectiveness and ability to provide interpretable predictive models. While, they can provide an accuracy level, as good as their counterparts such as ANNs, they do not depend on extensive historical data and are not computationally expensive [25]. In addition, the MLR algorithm are easily adaptable to energy consumption prediction models for other cities [4,26–28]. It should be noted that, although fairly robust, OLS has limitations when the relationships between variables are non-linear which may lead to over-fitting. Furthermore, OLS is sensitive to outliers which can significantly affect the fitness of regression line. On the other hand, polynomial regression fits nonlinear relationship. It is statistically a specific type of multiple linear regression due to the linear statistical estimation $E(y|X)$ in the unknown factors that are estimated from data.

2.2.7. Visualization

The urban energy use visualization is at multi-scales of building, block, neighborhood, and city scales. A GIS web-based platform was developed to communicate and visualize the predicted urban energy use.

3 RESULTS

3.1 Predictive Model

The six machine learning models including the Multiple linear regression (MLR), Nonlinear Regression (NLR),

Random Decision Forest (RDF), Classification and Regression Trees (C&RT), K-Nearest Neighbors (K-NN), and Artificial Neural Networks (ANNs) algorithms were employed to predict energy use at multi-scale for buildings in Chicago. The most widely used predictive model evaluation metrics including: Mean absolute Error (MAE), Mean Square error (MSE), Root Mean Square Error (RMSE), and Mean Absolute Percentage Error (MAPE) were used to compare the models in terms of their prediction performance (Figure 1).

The results shows that among the six promising algorithms modeled in this research, K-NN provides the best predictive performance with mean absolute error (MAE) of 0.08; while MLR provides the weakest predictive model with MAE of 0.22. The results show that the K-NN model performs best. The results of this research indicating the high accuracy of the K-NN algorithm in urban building energy use prediction confirm the findings of previous studies. The findings of this dissertation suggest that using K-NN model compared with MLR enhances the accuracy of the model through decreasing MAPE around 65%. However, it should be noted that the K-NN model has been applied in the literature scarcely [3].

The results of this dissertation also suggest that the CART (C&RT) model is able to predict building energy use at urban scale fairly well and displays the next high-performance model after K-NN algorithm and provides better performance relative to the MLR and MLP-ANN modes. This result confirms the finding of previous studies such as Tso et al. [5] which use CART model to predict the electricity demand for four types of residential building in Hong Kong, China based on a survey based data. The results show the CART model has better performance relative to those captured through the regression and MLP-ANN models.

The other algorithms provide results at least better than, MLR. However, no significant difference observed between RDF, ANNs, C&RT models and MLR model. The result suggest that MLR model is able to predict the energy use fairly well with not significant difference, compared to RDF, ANNs, C&RT which are computationally expensive and time consuming models when generalizing to the city level.

Then the improved model was used to predict energy use for all 820,000 buildings in the city. The model evaluates energy performance of city in a multi-scale resolution analysis which maximizes the use cases and allow for a more comprehensive energy decision-making and policy (Figure 2).

3.2 Model to explain the association between variables

The overall results show that building height does not have a linear effect on building energy use, rather a polynomial curve best explains the relationship (Figure 4).

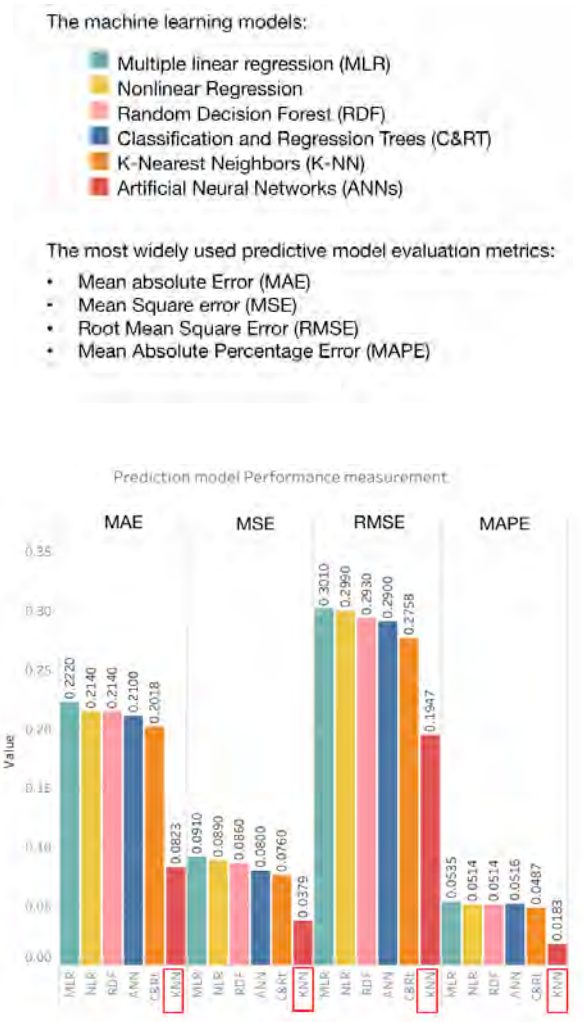


Figure 1. Models Prediction Performance

The findings of this study also suggest that building height, has a negative relationship with building energy use in building typology of lower than 12-stories. This pattern then changes to a positive effect. The results imply that increasing density through increasing building height will not lead to more energy efficiency. Also, a negative relationship is found between sprawl variable in the model and building energy use.

The maps in Figure 3 illustrate how sprawl, height, and energy use vary across Chicago neighborhoods. The highest site energy use intensity values per unit of building floor area (kBtu/sq.ft) are observed at neighborhoods on the western and southern outer edge of the Chicago region such as Riverdale, West Pullman, Ashburn, and O'hare.

These neighborhoods also represent the lowest sprawl index score, i.e., the lowest compactness and connectivity, with buildings of one to two floor as single family detached or attached building typologies.

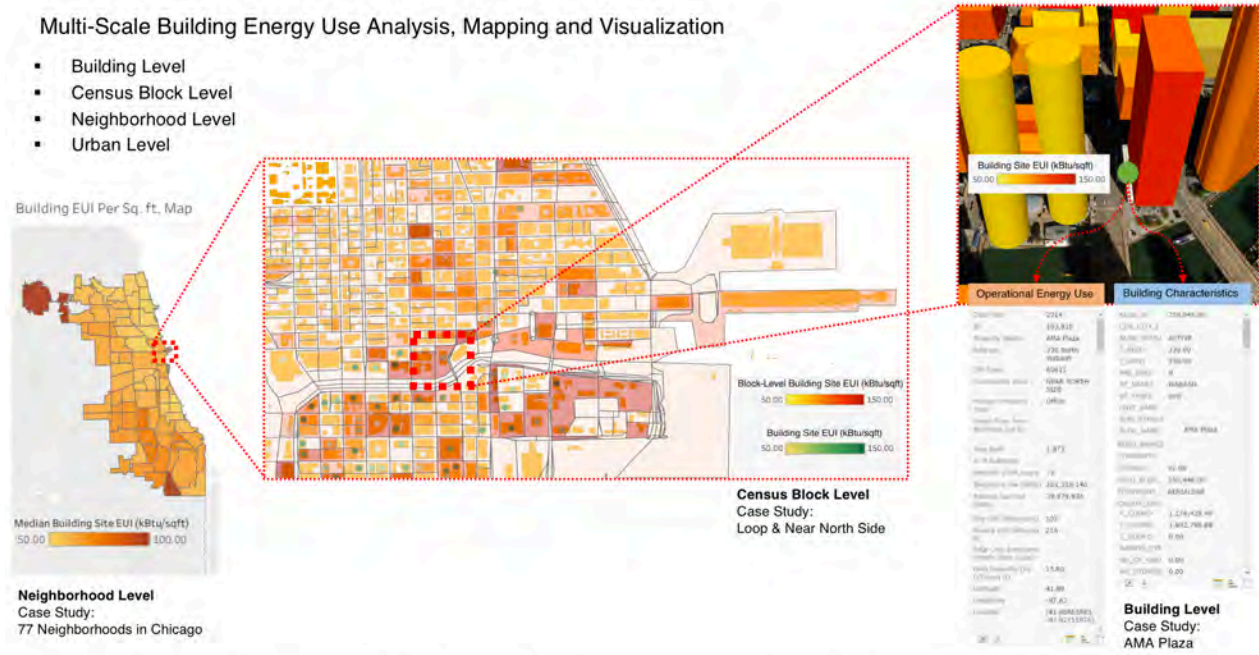


Figure 2. Multi-Scale Building Energy Use Analysis, Mapping and Visualization

The neighborhoods located at urban core including Loop, Near South Side, Near North Side, and Near West Side reflect medium energy use intensity. These neighborhoods represent the highest sprawl index score, i.e., highest compactness and connectivity, but incorporate buildings in ‘high’ and ‘very high’ building height classification. On the other hand, some neighborhoods in between the core and the outer edge and northern neighborhoods such as Lincoln Park, West Town, Lake View, Up Town, and Kenwood represent lowest levels of energy use intensity per floor area. These neighborhoods are among the neighborhoods with high

sprawl index score representing higher density and connectivity. They also include buildings in ‘medium’ and ‘medium-high’ building height classification.

With regard to energy use intensity per unit (kBTu/Unit), the neighborhoods on the southern and northwestern the outer edge of the Chicago region such as Beverly, Mount Greenwood, West Pullman, Ashburn, Garfield Ridge, Forest Glen, Norwood Park, and Dunning neighborhoods, and the Central Business District (CBD) and the Loop neighborhood represent high energy use intensity values.

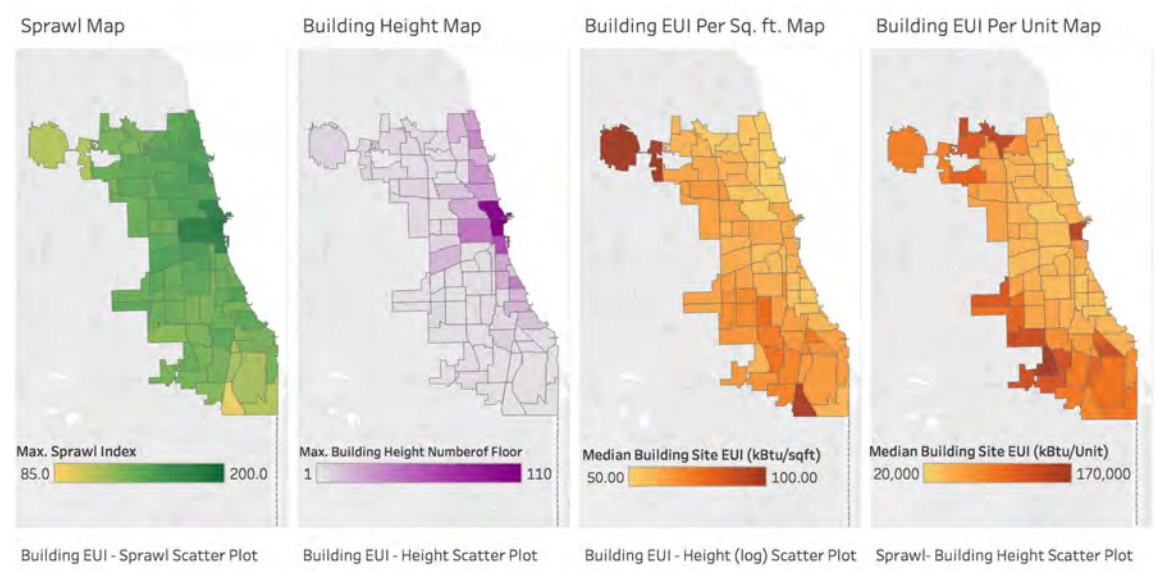


Figure 3. (left to right) Sprawl index map, building height map, transport energy use intensity per household map and building energy use intensity per unit map.

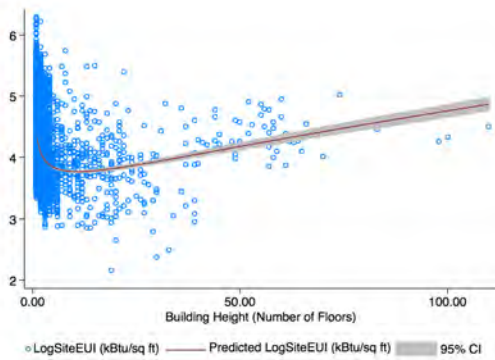


Figure 4. The scatter plot of Building Height and Log Site EUI, with polynomial fit line

These neighborhoods, except the Loop, also represent low sprawl index and incorporate low-rise buildings, as single-family detached or attached building typologies. On the other hand, the Loop reflects a high sprawl index score and incorporates buildings in ‘high’ and ‘very high’ building height typologies. The high energy consumption associated with a downtown neighborhood such as the Loop could be the large-size commercial units present in the Loop. The neighborhoods in between the core and the outer edge of the city, such as Uptown, Lincoln Park, West Town, Lake View, and Kenwood are observed as having low energy use intensity per unit. These neighborhoods are also among the neighborhoods with high sprawl index score representing higher density and connectivity and include buildings in ‘medium’ and ‘medium-high’ building typologies.

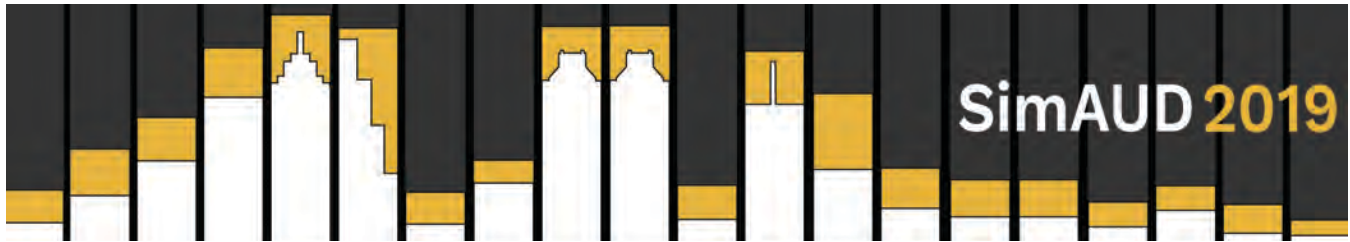
4 CONCLUSION

The UEUM framework is able to predict energy use at multiple scales of building, block, neighborhood, and city scales. This model captures the urban building operational energy use. The results of this research suggest that the urban energy prediction accuracy can be increased by using disaggregated data at building level and incorporating the actual urban spatial patterns. Also, the more advanced machine learning methods enable an improved prediction model. Among the six promising machine learning algorithms tested in this research, K-NN showed the best predictive performance. The finding of this study also provides empirical evidence on how spatial characteristics of neighborhoods impact the building and transport energy performance. The results imply that increasing density through applying an optimal building height would lead to higher energy performance. However, considering other influencing factors such as occupancy contexts and construction systems, buildings of certain heights in a denser urban context could contribute to more comprehensive low carbon urban policies.

REFERENCES

1. UN-DoESA, World Urbanization Prospects, 2014. <https://esa.un.org/unpd/wup/Publications/Files/WUP2014-Report.pdf>.
2. IPCC, Climate Change 2014: Synthesis Report. Contribution of Working Groups I, II and III to the Fifth Assessment Report of the Intergovernmental Panel on Climate Change, Geneva, Switzerland, 2014. doi:10.1017/CBO9781107415324.
3. EIA, Annual Energy Review, US Energy Information Administration (EIA), (2012). <https://www.eia.gov/totalenergy/data/annual/showtext.php?t=ptb0201a> (accessed June 27, 2018).
4. L.G. Swan, V.I. Ugursal, Modeling of end-use energy consumption in the residential sector: A review of modeling techniques, *Renew. Sustain. Energy Rev.* 13 (2009) 1819–1835. doi:10.1016/j.rser.2008.09.033.
5. M. Kavacic, A. Mavrogiani, D. Mumovic, A. Summerfield, Z. Stevanovic, M. Djurovic-Petrovic, A review of bottom-up building stock models for energy consumption in the residential sector, *Build. Environ.* 45 (2010) 1683–1697. doi:10.1016/J.BUILDENV.2010.01.021.
6. D. Hsu, Identifying key variables and interactions in statistical models of building energy consumption using regularization, *Energy.* 83 (2015) 144–155. doi:10.1016/J.ENERGY.2015.02.008.
7. C. Kontokosta, B. Bonczak, M. Duer-balkind, DataIQ – A Machine Learning Approach to Anomaly Detection for Energy Performance Data Quality and Reliability, (2016).
8. Chicago Energy Benchmarking | City of Chicago | Data Portal, (n.d.). <https://data.cityofchicago.org/Environment-Sustainable-Development/Chicago-Energy-Benchmarking/xq83-jr8c> (accessed October 10, 2018).
9. R. Ewing, S. Hamidi, Measuring Urban Sprawl and Validating Sprawl Measures, *Metrop. Res. Center, Univ. Utah.* (2014). doi:10.1017/CBO9781107415324.004.
10. City of Chicago, Building Footprints (current), City of Chicago, Data Portal, (n.d.). https://data.cityofchicago.org/Buildings/Building-Footprints-current-/hz9b-7nh8?category=Buildings&view_name=Building-Footprints-current- (accessed June 27, 2018).
11. National Cancer Institute, Urban Sprawl Data for the United States- Geographic Information Systems & Science, (n.d.). <https://gis.cancer.gov/tools/urban-sprawl/> (accessed June 27, 2018).

12. R. Ewing, T. Schmid, R. Killingsworth, A.Z.-U. Ecology, undefined 2008, Relationship between urban sprawl and physical activity, obesity, and morbidity, Springer. (n.d.). https://link.springer.com/chapter/10.1007/978-0-387-73412-5_37 (accessed June 22, 2018).
13. City of Chicago, Chicago Energy Benchmarking - 2016 Data Reported in 2017, City of Chicago, Data Portal, (n.d.). <https://data.cityofchicago.org/Environment-Sustainable-Development/Chicago-Energy-Benchmarking-2016-Data-Reported-in-/fpwt-snya> (accessed June 27, 2018).
14. City of Chicago, Energy Usage 2010, City of Chicago, Data Portal, (n.d.). <https://data.cityofchicago.org/Environment-Sustainable-Development/Energy-Usage-2010/8yq3-m6wp> (accessed June 27, 2018).
15. D.B. Rubin, Multiple Imputation after 18+ Years, *J. Am. Stat. Assoc.* 91 (1996) 473–489. doi:10.1080/01621459.1996.10476908.
16. M.H. Kutner, C. Nachtsheim, J. Neter, *Applied linear regression models.*, McGraw-Hill/Irwin, 2004.
17. D. Cook, Detection of influential observation in linear regression, *SAGE Handb. Regres. Anal. Causal Inference.* 19 (1977) 15–8. doi:<http://dx.doi.org/10.4135/9781446288146>.
18. B. Miller 1997 Of, *A. Statistics, BEYOND*, n.d.
19. T. Ahmad, H. Chen, Y. Guo, J. Wang, A comprehensive overview on the data driven and large scale based approaches for forecasting of building energy demand: A review, *Energy Build.* 165 (2018) 301–320. doi:10.1016/j.enbuild.2018.01.017.
20. R.Ž. Jovanović, A.A. Sretenović, B.D. Živković, Ensemble of various neural networks for prediction of heating energy consumption, *Energy Build.* 94 (2015) 189–199. doi:10.1016/J.ENBUILD.2015.02.052.
21. K. Amasyali, N.M. El-Gohary, A review of data-driven building energy consumption prediction studies, *Renew. Sustain. Energy Rev.* 81 (2018) 1192–1205. doi:10.1016/j.rser.2017.04.095.
22. J.A. Hartigan, M.A. Wong, Algorithm AS 136: A K-Means Clustering Algorithm, *Appl. Stat.* 28 (1979) 100. doi:10.2307/2346830.
23. S. Torabi Moghadam, J. Toniolo, G. Mutani, P. Lombardi, A GIS-statistical approach for assessing built environment energy use at urban scale, *Sustain. Cities Soc.* 37 (2018) 70–84. doi:10.1016/J.SCS.2017.10.002.
24. K. Amasyali, N.M. El-Gohary, A review of data-driven building energy consumption prediction studies, *Renew. Sustain. Energy Rev.* 81 (2018) 1192–1205. doi:10.1016/j.rser.2017.04.095.
25. X. Cheng, B. Khomtchouk, N. Matloff, P. Mohanty, Polynomial Regression As an Alternative to Neural Nets, (2018). <http://arxiv.org/abs/1806.06850> (accessed August 22, 2018).
26. C.E. Kontokosta, C. Tull, A data-driven predictive model of city-scale energy use in buildings, *Appl. Energy.* 197 (2017) 303–317. doi:10.1016/j.apenergy.2017.04.005.
27. S.K. Park, H.J. Moon, K.C. Min, C. Hwang, S. Kim, Application of a multiple linear regression and an artificial neural network model for the heating performance analysis and hourly prediction of a large-scale ground source heat pump system, *Energy Build.* 165 (2018) 206–215. doi:10.1016/j.enbuild.2018.01.029.
28. S. Papadopoulos, E. Azar, W.-L. Woon, C.E. Kontokosta, Evaluation of tree-based ensemble learning algorithms for building energy performance estimation, *J. Build. Perform. Simul.* 11 (2018) 322–332. doi:10.1080/19401493.2017.1354919.



An Integrated Urban Planning and Simulation Method to Enforce Spatial Resilience Towards Flooding Hazards

Julius Morschek^{1,2}, Reinhard König^{1,2} and Sven Schneider

¹Bauhaus-University Weimar
Professorship for Computational
Architecture,
Weimar, Germany
reinhard.koenig@uni-weimar.de

²AIT Austrian Institute of
Technology,
Smart and Resilient Cities,
Vienna, Austria
julius.morschek.fl@ait.ac.at
reinhard.koenig@ait.ac.at

³Bauhaus-University Weimar
Chair of Computer Science in
Architecture, Weimar, Germany
sven.schneider@uni-weimar.de

ABSTRACT

Urban development projects in flood-prone areas are usually complex tasks where failures can cause disastrous outcomes. To tackle this problem, we introduce a toolbox (Spatial Resilience Toolbox – Flooding, short: SRTF) to integrate flooding related aspects into the planning process. This, so called toolbox enables stakeholders to assess risks, evaluate designs and identify possible mitigations of flood-related causes within the planning software environment Rhinoceros 3D and Grasshopper. The paper presents a convenient approach to integrate flooding simulation and analysis at various scales and abstractions into the planning process. The toolbox conducts physically based simulations to give the user feedback about the current state of flooding resilience within an urban fabric. It is possible to evaluate existing structures, ongoing developments as well as future plans. The toolbox is designed to handle structures in a building scale as well as entire neighborhood developments or cities. Urban designers can optimize the spatial layout according to flood resilience in an early phase of the planning process. In this way, the toolbox can help to minimize the risk of flooding and simultaneously reduces the cost arising from the implementation and maintenance of drainage infrastructure.

Author Keywords

Fluid dynamics; flood simulation; spatial resilience; Grasshopper for Rhino.

ACM Classification Keywords

I.6.1 SIMULATION AND MODELING

1 INTRODUCTION

A modern city's ability to thrive is compromised by many factors. Flooding and insufficient storm drainage systems in combination with rapid urbanization can have disastrous effects to the inhabitants [6]. Flood modeling is adopted by stakeholders to enforce an integrated water management to

mitigate the risk of damage caused by flooding. A relatively new but promising approach in this field of research is flood resilience. A flood is typically a common event that needs to be considered as such. Furthermore, the number and severity of flooding events will increase: Experts from the United Nations University warn that due to climate change, deforestation, rising sea levels and population growth in flood-prone lands, the number of people vulnerable to a devastating flood will rise to two billion by 2050 [1,11]. Extreme natural disasters, such as tropical storms, are expected to become more frequent while rainfall events are predicted to become more intense. Modern planners and developers must adapt to new challenges in order to facilitate sustainable and resilience-focused urban planning. Conventional planning techniques are reaching their limits in such a context [9]. This paper demonstrates how the Spatial Resilience Toolbox – Flooding (SRTF) can be used as a flexible integrated urban planning and simulation framework to enforce flood resilience for urban developments. For this purpose, it evaluates any site plan regarding three different types of flood: (1) urban inundation, (2) tidal flooding and (3) river flooding. The toolbox then assesses the individual risks of a given spatial layout. During the planning process, it is possible to exclude insufficient proposals right at the beginning. As a result, the SRTF encourages stakeholders to develop the most suitable spatial solution for a specific area.

The toolbox combines several computer-generated processes such as physically based simulation and evaluation models to visualize the current state of flooding resilience. It is construed to facilitate an integrated urban development workflow with the focus on flooding resilience to mitigate flooding outcomes, to minimize damages and most important to improve the life of the inhabitants.

The SRTF is designed to provide valuable information about the status of resilience to support an integrated and

streamlined workflow. The main benefits of using the toolbox can be summarized with visibility and transparency, interactivity, flexibility and adaptability while using it during the urban design process. Thereby the most important outcome of the toolbox constitutes specific information pertaining to flood-resilience that allows the designer to rank different options of an urban development. To achieve this, we determined data visualization as one of the main goals of the toolbox. All necessary information is directly presented in the viewport as alphanumeric values and 3D scenario maps. Interactivity means it allows the user to directly work on the spatial layout, the terrain and the anti-flooding measures within the program to test out several options. Furthermore, the toolbox is construed to handle several scales, starting with for example simulating the risk of the rain-runoff inundation for one hospital to evaluating the tidal flooding risk for a whole city. Eventually, it is possible due to the program environment of Grasshopper to use the outcome of the SRTF to conduct other simulation and evaluation models.

2 STATE OF THE ART

Since the 1970s, the research community put systematic effort into developing and improving flood modeling techniques to forecast and to predict the outcome of flooding events for rural and urban contexts [4]. Two groups of methodologies emerged in the past century that are now the subject of ongoing research: Empirical methods and physically based hydrodynamic models [4]. Today, it is widely acknowledged that using physically based hydrodynamic models for predicting flood outcomes in an urban context constitutes the most realistic approach [8]. These models are well established in commercial packages. HEC-RAS [14], MIKE FLOOD [15] and Hydro-Bid [16] are amongst others, software tools to simulate, to present preceded flooding events or to present the probability of a flooding event for a specific location. These tools are mainly physically based, however, use different approaches to model urban flooding. Physical models are based on the understanding of the physics related to the hydrological processes [13]. They use physically-based equations to govern multiple parts of real hydrologic characteristics that represent realistic responses in the catchment area. The behavior is reproduced based on general physics laws and principles including water balance equations, conservation of mass and energy, momentum, and kinematics. Saint-Venant, Boussinesq, Darcy, and Richard have developed some of the equations that physical models utilize [8].

Spatial and temporal variations within the evaluation perimeter can be adopted by physical models. They are organized like the real-world system. One of the main advantages of a physical model is the interaction between model parameters and physical catchment characteristics. This approach leads to a more realistic scenario. Physical models produce accurate results when precise data are available and the physical properties of the hydrological processes are correctly understood and applied. To function

properly, the model requires the calibration of many individual physical and process parameters. Physical parameters are properties of the evaluation perimeter that can be measured; process parameters represent physical properties including average water storage capacity [8]. Therefore, physical models are site-specific. Most of them represent a three-dimensional system of the water exchange within the soil, surface, and air. Besides that, they are suitable to simulate groundwater movement, and the site's interactions with sediments, nutrients, and chemicals.

Logic dictates that the more advanced a model is, the more expensive it is in terms of data and computational resources. When physical data is hardly available, historical statistics in combination with simple black box models, such as hydrological models, can still produce valuable information. A 1D hydraulic model is helpful to understand and manage drainage networks in a relatively short amount of time (1 min to 1h) [3]. Therefore, these models are suitable for real-time applications. However, 1D models are not able to evaluate the effects when the network overflows and inundation is affecting the city surface. By contrast, two-dimensional hydrodynamic models have proven suitable and precise to simulate urban flooding. Due to the characteristics of urban areas and its inherent complexity, 2D models require long computation time (1h to several hours) [3], opposing real-time applications. Combining storm drainage systems and urban inundation requires a 1D-2D coupling. The computation time (1h to several hours) [3] of this model is not sufficient for real-time purposes.

Summarizing, there are very powerful tools (commercial and open source) available on the market. Most of them are characterized by a high level of accuracy and versatile configurations. Alongside with the great functionality comes an operation that demands profound knowledge and a detailed input of data. Besides that, the usage of 1D-2D models involves a substantial amount of computational time [3]. During the concept phase, where planners want to quickly compare a proposal with another, this is impracticable.

3 FLOODING SIMULATION

The objective of the SRTF is to offer an adaptable framework for stakeholders that are involved in a development project such as urban planners, investors, developers etc. to evaluate planning proposals according to its flooding resilience status. In the following, the methods that are used in the toolbox are explained based on a case study. The Toolbox was developed within the software environment of Rhinoceros3D and its Plugin Grasshopper for visual programming.

The flooding component forms the main part of the SRTF. It can be further divided into a simulation phase and an evaluation phase. The simulation phase consists of two simulations, the rain runoff simulation, and the tidal and river flooding simulation. When the simulations are completed, the output information of each simulation is then evaluated and visualized. This includes the rain-runoff inundation risk,

the rain-runoff erosion risk, and the tidal or river flooding risk for a specific level of water and the average risk value. The simulations can be conducted individually for example by evaluating only the urban inundation that is caused by rainfall. The evaluations in this paper are conducted for a newly planned neighborhood of a tropical town.

3.1 Rain Runoff Simulation

The rain runoff simulation is conducted with the help of the interactive physics/constraint solver Kangaroo for Grasshopper by Daniel Piker. The toolbox can represent a rainfall event by equipping particles with a certain mass and gravitation force. During the simulation, the particles are attracted by the external gravitational force, which results in runoff. Thereby, the particles search for ways downwards comparable to rain runoff. They behave as spherules running off the 3D geometry (Figure 1).

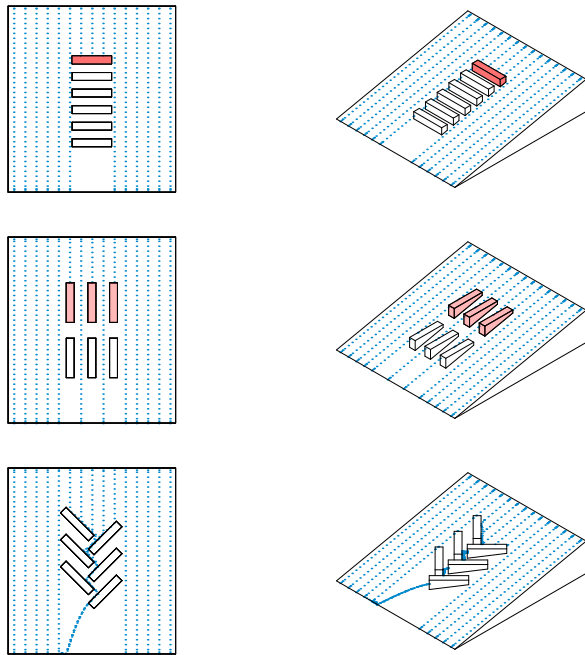


Figure 1. Using the rain-runoff simulation to compare different spatial configurations according to its behavior during rainfall

They pick up velocity when running unhindered and accumulate at bottlenecks or depressions. There are three parameters that can be set individually to match several different rainfall events: (1) the number of particles, (2) the size of particles and (3) the number of iterations. The simulation gets more realistic by increasing the number of particles and simultaneously decreasing the size of each particle. Obviously, a simulation with the number and size of actual raindrops constitutes the most realistic scenario. However, due the immense consumption of processing power for billions of particles, such an approach is not a realistic option for common users with limited technological possibilities. The rain runoff inundation simulation for the case study was conducted with 10,000 particles with a

diameter of 30 centimeters for each particle. The value of 30 centimeters is used to reach the same volume with spherules as around four liters of water per square meter. This amount reflects approximately one hour of rain during a day with excessive rainfall (> 100 mm per day). For comparison, in February 2015, during an excessive rainfall event, the city of Jakarta (c. 450km from Semarang) recorded a precipitation of 277 mm on one day [12].

The number of iterations is based on the situation that is being evaluated. A smaller amount of iterations represents the situation during a rainfall event and shows bottlenecks within the urban layout whereas more iterations are used to evaluate local inundation that appears after a rainfall event. The simulation in this paper is carried out with 3000 iterations. The most accurate practice for inundation would be achieved by letting the simulation run as long as there is movement in the scene. The results of further attempts had shown that in this case, the results are very similar after 3000 iterations. During the simulation, the toolbox saves the locations for each particle after every 10 iterations. These locations are then being connected with curves to show the flow paths. Additionally, it saves a screenshot after 10 iterations that can be merged afterward into a video, which shows the course of the simulation. The interval between iterations can be adjusted as needed. The value that is used in this paper is explained in the section of the erosion risk since it is also dependent on the number of flow-path segments.

3.2 Rain Runoff Evaluation

The risk assessment of the rain runoff inundation is conducted based on the location of each particle after the simulation. The toolbox counts the number of particles that are in a specific range within every building. The range is set to two meters by default. This allows to compromise the rating of a building in a negative way when it is surrounded by water under pressure. The value of the range distinguishes water that is running along the housing units from water that accumulates and pushes against buildings. Then the number is divided by the footprint area of each building. The higher the value the greater the risk of damages through flooding. This means that the density of particles near or at the buildings is responsible for the outcome of the evaluation. Buildings with a high risk of inundation are always characterized by an accumulation of particles nearby. The street network is treated similarly. Each street is further divided into segments at junctions or bends. Then the number of particles measured that are within a specific range near each street segment. The value is the same that is used for the housing units. The number is then divided by the area of the range. Now each building and each street segment is assigned with specific risk value. The information is visualized with color gradation in the viewport (Figure 2).

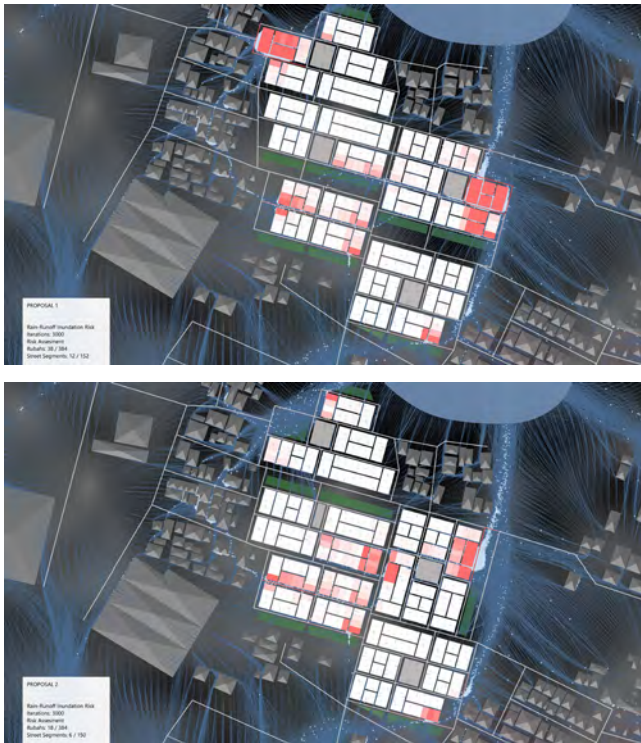


Figure 2. Comparing two proposals from the case study according to the rain-runoff inundation risk after 3000 iterations. Red buildings are considered flooded; proposal I - 38 vs. proposal II - 18

The darker the tone, the higher is the risk of inundation for a specific home. Furthermore, there is a legend in the viewport that indicates the number of housing units and street segments affected by flooding (Figure 2 and Figure 3, bottom left). With the outcome of the rain runoff simulation, one can also conduct the rain runoff erosion risk evaluation (Figure 3). Hereby the path of each particle is used to evaluate the runoff erosion risk. The toolbox creates the paths by recording the locations of the particles after a given amount of iterations. For the case study, the interpolation between locations is set to 10. So, the simulation with 3000 iterations produces paths with 300 segments for each particle. The value of the recording can be changed as needed. A smaller number constitutes a more accurate representation of reality. Nevertheless, it also affects the processing time in a negative way.

In the next step, the toolbox measures the distance of each segment. This distance gives information about the velocity of each particle at a specific location. It is possible to cull segments with a low value, so the outcome shows only places that are subject to the risk of erosion. The algorithm automatically culls those paths where the travel distance is lower than a given value. For the presented case study, the value is set to 1.5 m. This means that only those paths are visible in the evaluation where its particles traveled with a velocity of 1.5 m or higher per 10 iterations. This procedure ensures a clear picture of the situation because there are

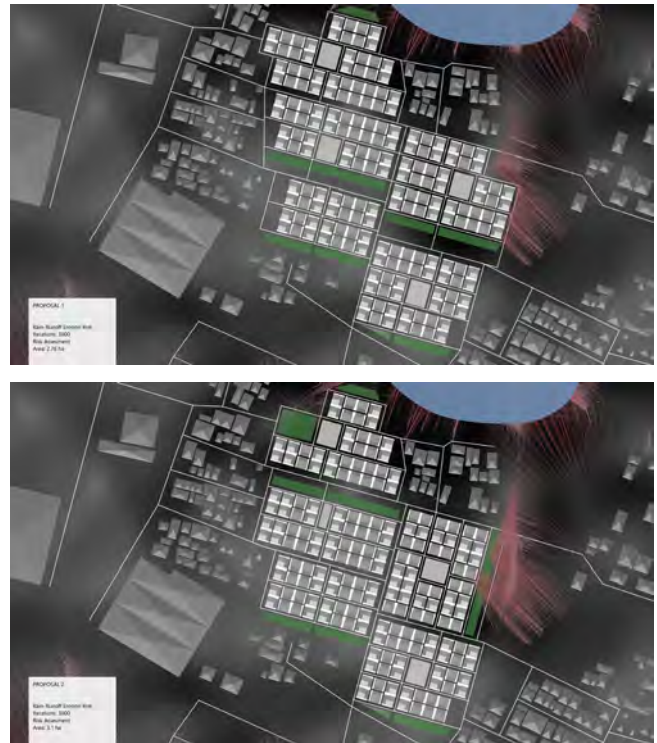


Figure 3. Comparing two proposals from the case study according to the rain-runoff erosion risk after 3000 iterations. Red flow paths mark areas that are likely to face erosion; proposal I – 2.76 ha vs. proposal II – 3.1 ha

3.000.000 flow-path segments in the scene. The remaining paths are displayed in the viewport with a gradient that shows the risk level of erosion caused by runoff (Figure 3). The algorithm also measures the area that is affected by the risk of runoff erosion. Therefore, it groups several flow-paths that are near each other with a given density threshold into a patch. The threshold is set to 1.5 m. Then it uses the segments located on the edge of the patch to span an area. This area is then measured and rated as prone to erosion.

3.3 Tidal and River Flooding Simulation

The second simulation the toolbox is capable of is the tidal and river flooding simulation. It illustrates and evaluates the impact of different water levels in the area. To measure the inundation, a plane is moved from a given altitude up to a predetermined value. The plane is considered as the surface area of a river, lake or the sea. To get precise information about which part of the geometry is flooded, the toolbox calculates the intersection between the plane and the surroundings (Figure 4).

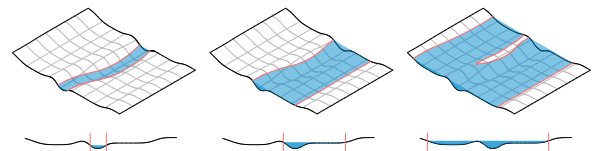


Figure 4. Using the tidal & river flooding simulation to compare three different water levels for a river flooding scenario

Everything inside the intersection area is perceived as flooded. Hereby, the toolbox culls areas that are not directly connected to the original surface. In this way, it is possible to evaluate the impact of, for example, dams where the terrain behind it can be lower than the level of water (Figure 5). The simulation computes several water levels one after the other according to the input parameters. The altitude of the water level indicates the peak.

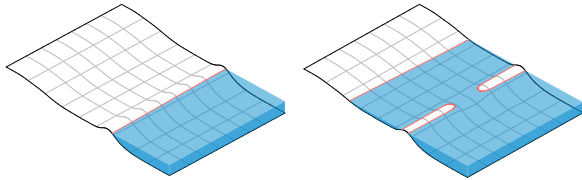
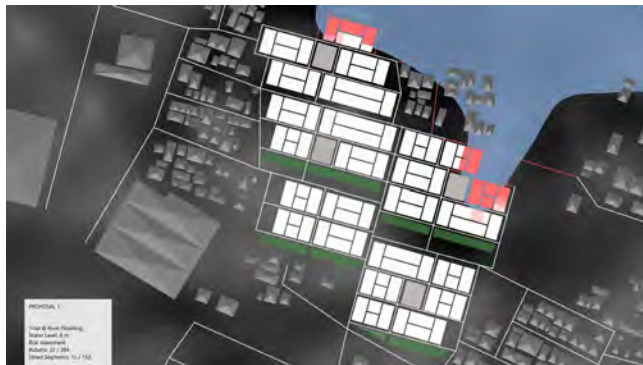


Figure 5. Using the tidal & river flooding simulation to evaluate the outcome of an open dam for the same water level

The frame count states the number of iterations between the lowest and the highest value. This case study was evaluated within a range from zero to eight meters. Although it is very uncommon in this region, this scenario is comparable to an intense storm surge like the one the hurricane Katrina produced in August 2005 [2].



3.4 Tidal and River Flooding Evaluation

During the simulation, the risk assessment for the houses and the street network is presented in Figure 6. The legend (Figure 6, bottom left) provides details about the number of affected buildings and street segments. When the water level reaches the top of a platform of a building, it is marked with a red color. The toolbox applies a darker tone of red according to the depth of water. The depth is computed by iteration so each frame represents a depth of eight centimeters. It counts the number of iterations after a building is considered as flooded. In this case, the water levels that are deeper than 24 centimeters are considered equal. The values can be adjusted as needed. For this case study, the value is set to balance imprecisions and to match the threshold of lasting damages. The same methodology for assessing the risk applies to the city network. Hereby the lowest point of the street segment is evaluated. When the water reaches it, it is marked with a red color in the same manner as the risk assessment for the buildings.

The last part of the evaluation phase is called the mean risk assessment (Figure 7). It is related to the tidal and river flooding simulation and gives an understanding of the risk distribution in the area. Whereas the prior evaluation is useful for evaluating the site for specific water levels, the mean risk assessment shows the risk of all scenarios combined.

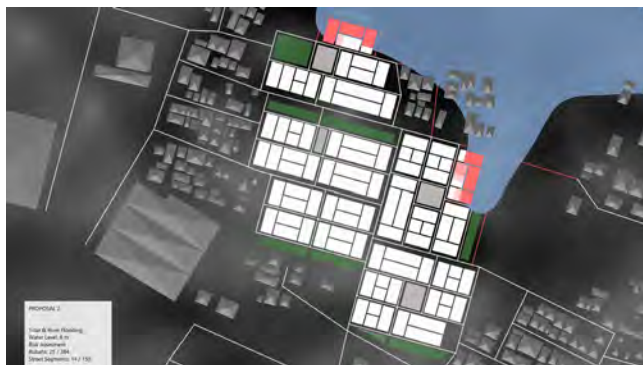
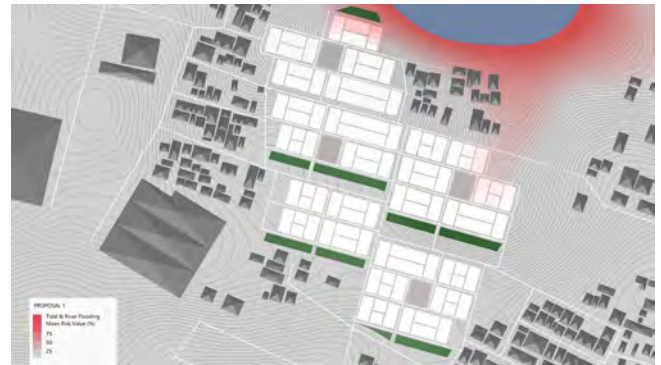


Figure 6. Comparing two proposals from the case study according to the tidal & river flooding simulation for a level of water of 8 m. Red buildings are considered flooded; proposal I - 32 vs. proposal II - 25

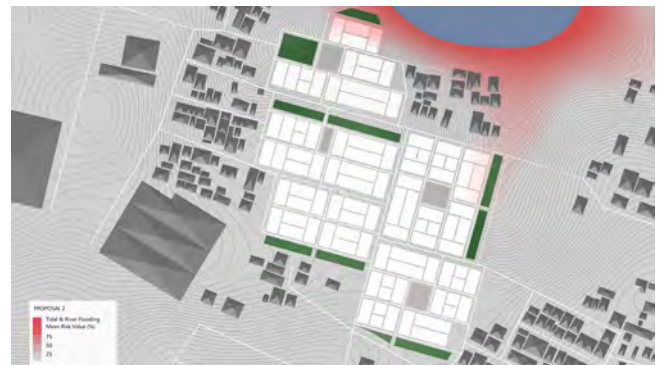


Figure 7. Evaluating the mean risk of two proposals from the case study according to the tidal & river flooding simulation. The color gradient reaches from red (high risk) to grey (low risk).

In this case, every single state of the tidal and river flooding simulation is recorded to compute the mean value. The toolbox then colors all affected buildings and street segments according to its mean associated risk from low to high (Figure 7). The algorithm behind that works as follows: Every building in the area is reduced to one point. As in the evaluation before the point is located on the foundation of a building. This point marks the threshold that distinguishes vulnerable from not vulnerable. The space above the point is considered vulnerable. To measure the mean risk, the algorithm counts every iteration when the point is flooded. In the end, this number is divided by the number of iterations that are used to conduct the simulation to get the mean risk. The same methodology applies to the street network and the terrain. Therefore, the terrain is interpolated to a grid, in this case, approximately three by three meters (the value is set by default but can be adjusted as needed). The surface consists now of several faces with one center point. The center point is used to define the risk value with the method explained above. The value of the center point is used for the corresponding face. Finally, the information is visualized by means of a gradient that shows the mean risk level of flooding (Figure 7).

4 RESULTS & DISCUSSION

In the presented case study, several parameters have been analyzed that affect the outcome of the SRTF. First, the accuracy of the results depends on the accuracy of the input data. A more detailed terrain surface can produce a more realistic rainfall runoff outcome than a less detailed surface. Furthermore, the accuracy can be increased by raising the level of complexity of the simulations. Technically, there are no limits to the richness of detail, e.g. the number of particles, or building geometry. However, the complexity goes along with processing power and time. The 3000 frames of the rain runoff simulation used in this case study take about two minutes to finish with a customary computer (i7, 4.0GHz). If one would increase the number of particles to get more accurate results, the simulation would take longer. The number of particles exponentially increases the processing time of the evaluations as well. Therefore, it is important to find the right balance between accuracy and speed. At least when the toolbox is used in a form finding process where fast feedback is essential for evaluating many different options. Nevertheless, on the same hand, it makes sense to increase the level of complexity for the simulation when the variety of proposals has shrunk.

Another aspect one needs to consider is the size of the investigated area. To get precise results one may use a terrain that is larger than the actual site. In fact, the results become more accurate by increasing the investigated area. The surroundings have a direct impact on the investigated design (see Figure 2; the blue flow-paths are directed along the terrain and the layout of the buildings). Terrain and other solid geometry like buildings channel the runoff into a certain direction and therefore affect everything beneath. For

the case study, we used a terrain that is about 80% larger than the design proposal.

As it is commonly known, water is a fluid. For the evaluation of the rain-runoff inundation, this means that the situation is always changing until it settles. To represent reality, it would be necessary to evaluate every stage. Since this approach would take too long, one must find the balance between time and accuracy. As stated above, we used two stages to evaluate the proposals of the case study. The simulation is executed with 1000 respectively 3000 iterations to perceive the conditions after two different periods of time. After 1000 iterations, the toolbox presents the situation during a rainfall event. After 3000 iterations, the simulation has progressed so far to represent the situation after a rainfall event.

Comparing the two planning proposals described above in more detail, the major shortfall of the second proposal can be found at the T-junction in the middle of the neighborhood (Figure 8). It is evident, that the arrangement of the buildings in the first proposal is more convenient at this place because the excess water can runoff along the street.

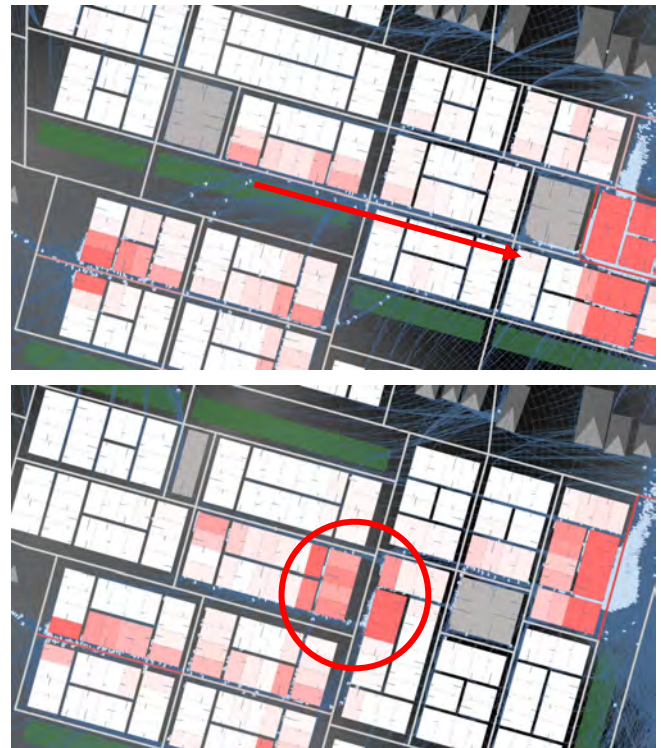


Figure 8. Comparing two identical extracts of the two proposals (presented in Figure 6) according to the rain-runoff simulation. The figure shows the situation amid the neighborhood. In the first proposal, the water runs downwards to east along within the street network (see arrow). In the second proposal, the water accumulates amid the neighborhood because it is blocked by the housing units (see circle).

Therefore, to ensure the discharge of rainwater, planners can adopt the layout of the first proposal because it provides a better drainage in this area.

Both examples prove that the SRTF provides information about the status of flooding-resilience for urban inundation. Combined with the evaluation of the street network one can assess the functional capacity of a city's infrastructure. In the viewport, it is visible, which parts of the neighborhood are cut off due to inundation. This information is essential to evaluate the resilience status of a city since the street network facilitates its operability. Moreover, the toolbox reflects the situation on site and provides feedback about the spatial layout. The outcome of the rain-runoff inundation evaluation constitutes essential information for further planning intentions.

Besides urban inundation, the toolbox is also developed to evaluate the risk of erosion due to rain-runoff. This helps to mitigate fast runoff and therefore the risk of damages caused by erosion, debris, and landslides. Urban planners can take this information into account when developing buildings, neighborhoods or cities. The toolbox visualizes the evaluation by means of the flow paths. Combined with the description of the velocity the user gets profound data for the area. For example, at first sight, the situation looks in favor of the first concept when comparing the proposals about the rain runoff erosion risk. Hereby, the first concept seems to perform better because the affected area is smaller. But as it is visible in Figure 3, the runoff in the east gets slowed down by the green space in front of the houses. That means that the buildings are not harmed by the debris. By contrast, in the first proposal, the overall area at risk is less but the buildings that are affected are hit directly by the fast runoff.

Additionally, Figures 6-7 depict the outcome of the tidal & river flooding simulation. The legend in Figure 6 states, that the first concept hosts its housing units in a way that during a high tide of 8 meters, there are 32 buildings flooded. At the same water level, there are only 25 buildings at stake in the second concept. This means that 7 homes can be saved from severe damages due to flooding by changing the spatial layout. Combined with the results of the mean risk assessment, the findings demonstrate that the second concept is not perfect but more suitable a tropical town in case of a tidal flooding event.

5 CONCLUSION

The SRTF provides information about the status of flooding-resilience for urban inundation, tidal and river flooding. The rain-runoff simulation provides information about the status of inundation and the level of erosion in the area. On the one hand, this information is valuable because it enables the user to foresee the properties of a specific spatial layout during or after a rainfall event. One benefit is obvious: In order to eradicate insufficiencies within an urban system, it is necessary to detect them. The toolbox presents all necessary information visually so the user can get an exact image of the advantages and deficiencies of a design concept. In the same manner, the user is provided with information that allows rating certain layouts according to its characteristics towards rain-runoff. As shown in the case study, the second layout is

more suitable for the area regarding the rain-runoff inundation risk. As it is shown in the images (Figure 2), the second neighborhood would suffer less during a heavy rainfall event. After 3000 iterations, the number of housing units that encounter a risk of inundation decreases about 20. A similar discrepancy applies to the street network. There are 6 segments fewer affected in the second proposal. Hence, by choosing the second proposal over the first one, the damage caused by a heavy rainfall event could be reduced by more than 50 percent. It also indicates that the effort of implementing stormwater infrastructure is higher in the first concept because there are more insufficiencies within the urban system.

We want to clarify that the approach that is presented in this paper is not intended and able to replace the actions carried out by hydraulic engineers but instead it should assist the urban designer or other non-hydrologists to analyze a site plan quickly and effectively or to implement measures for enforcing resilience during an early phase of the planning process. This means that urban designers can develop a concept with a realistic focus on flooding hazards.

The findings that are presented in this paper prove that the SRTF is construed to support decision making during the planning process of an urban development. It enables decision-makers to foresee the impact in advance which gives them the means to act when it is still possible. For example, the mean risk evaluation provides useful information about locations that are not endangered by flooding and therefore suitable for e.g. housing units. Alongside comes the ability to divide a plot into parcels with different functions. For example, locations with a high risk of inundation are not suitable for housing or commercial estates but rather can be used for green spaces or public spaces with mobile structures such as markets. With the SRTF, it is easy and fast to locate such places.

In conclusion, it can be said planning in flood-prone areas is a complex task. There are many issues that need to be taken into account in order to plan a site effectively. One crucial factor hereby constitutes the orientation and the arrangement of the buildings. Conventional planning techniques without computational assistance are reaching their limits in such a context. The SRTF overcomes this issue. The findings prove, that its usage provides a convenient approach that assists users to enforce flooding resilience for future urban developments.

ACKNOWLEDGMENTS

The idea of creating an integrated urban planning and simulation method to enforce spatial resilience towards flooding hazards originated by dealing with the case study Tropical Town. The research teams "Urban-Rural Systems" and "Big Data Informed Urban Design and Governance" of the Future Cities Lab in Singapore developed Tropical Town under the archipelago cities project. We wish to express our sincere thanks to Kateryna Konvieva from the Future Cities

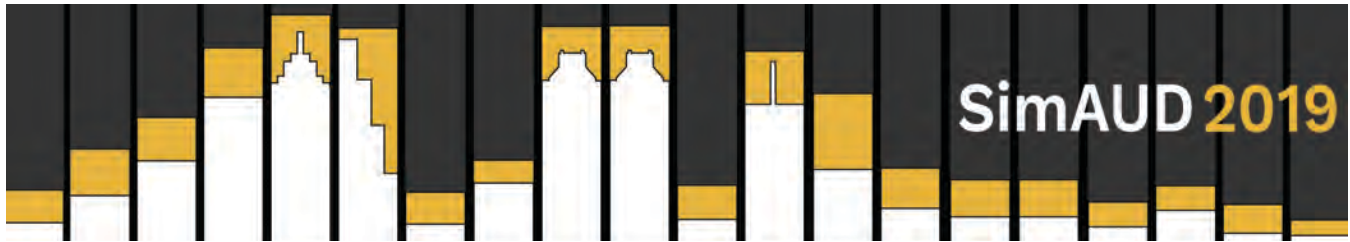
Lab who made important contributions for providing the case study, helpful feedback and inspiring comments.

Further information and videos of the simulations can be found at:

<https://toolbox.decodingspaces.net/spatial-resilience-towards-flooding-hazards>

REFERENCES

1. European Academies' Science Advisory Council. New data confirm increased frequency of extreme weather events: European national science academies urge further action on climate change adaptation. www.sciencedaily.com/releases/2018/03/180321130859.htm. As of 21 March 2018.
2. Fritz, H.M., Blount, C., Sokoloski, R., Singleton, J., Fuggle, A., McAdoo, B.G., Moore, A., Grass, C., Tate, B. Hurricane Katrina storm surge reconnaissance. *J. Geotech. Geoenviron.* 134 (2008), 644–656.
3. Henonin, J., Russo, B., Mark, O. Gourbesville, P. Real-time urban flood forecasting and modelling – a state of the art. *Journal of Hydroinformatics.* 15, 3 (2013). 717–736.
4. Hurlimann, A., Wilson, E. Sustainable Urban Water Management under a Changing Climate: The Role of Spatial Planning. *Water* 10, 4 (2018), 0-22.
5. Marfai, M. GIS Modelling of River and Tidal Flood Hazards in a Waterfront City. International Institute for Geo-Information Science and Earth Observation Amsterdam. 2003
6. Münchener Rückversicherungs-Gesellschaft. Relevant hydrological events worldwide 2012 – 2017. Report. 2018
7. Parkinson, J., Mark, O. Urban Stormwater Management in Developing Countries. 2nd edition. IWA Publishing, London. 2005.
8. Pechlivanidis, I. G., Jackson, B. M., McIntyre, N. R., & Wheater, H. S. Catchment Scale Hydrological Modelling: A Review of Model Types, Calibration Approaches and Uncertainty Analysis Methods in the Context of Recent Developments in Technology and Applications. *Global NEST Journal*, 13, 3 (2011), 193-214.
9. Restemeyer B., Woltjer J., van den Brink, M., A strategy-based framework for assessing the flood resilience of cities – A Hamburg case study. *Planning Theory & Practice*, 23, 2 (2015) 45-62.
10. Teng, J., Jakeman, A.J., Vaze, J., Croke, B.F.W., Dutta, D., Kim S. Flood inundation modelling: A review of methods, recent advances and uncertainty analysis. *Environmental Modelling and Software.* 90 (2017) 201-216.
11. United Nations University. "Two Billion Vulnerable To Floods By 2050; Number Expected To Double Or More In Two Generations." *ScienceDaily*. www.sciencedaily.com/releases/2004/06/040614081820.htm. As of November 20 2018.
12. Van der Schrier, G., van Oldenborgh, G., van den Hurk B., Aldrian, E., Swarinoto, Y., Sulistya, W., Sakya, A. A very unusual precipitation event associated with the 2015 floods in Jakarta: an analysis of the meteorological factors. *Weather and Climate Extremes.* *Weather and Climate Extremes* 16 (2017) 23–28.
13. Vaze, J., Jordan, P., Beecham, R., Frost, A., Summerell, G. Guidelines for Rainfall- Runoff Modelling: Towards best practice model application (pp. 47). 2012.
14. <http://www.hec.usace.army.mil/software/hecras/>
15. <https://www.mikepoweredbydhi.com/products/mike-flood>
16. <http://hydrobidlac.org>



A Method for Integrating an UBEM with GIS for Spatiotemporal Visualization and Analysis

Bess Krietemeyer¹ and Rawad El Kontar²

¹Syracuse University
Syracuse, NY, USA
eakriete@syr.edu

²National Renewable Energy Laboratory
Golden, CO, USA
rawad.elkontar@nrel.gov

ABSTRACT

Leveraging Geographic Information Systems (GIS) for spatiotemporal visualization and analysis of simulated UBEM datasets and real-world data simultaneously can assist in identifying opportunities, as well as potential barriers, to energy efficient and climate adaptation strategies. However, current GIS-based models that support interactive exploration of adaptation strategies and future scenarios are scarce and do not easily incorporate building energy use data for visual analysis over time. This paper describes a workflow to integrate simulated building energy consumption data associated with variable energy efficiency scenarios within a GIS platform for interactive spatiotemporal visualization to support climate adaptation decision-making. The contribution of the work presented is in the ability to selectively view and analyze simulated building energy performance data layered with other real-world geospatial data through an automated feedback loop between an UBEM and ArcGIS. An interactive interface is designed in ArcGIS to enable users to explore building performance scenarios spatially and over time. Using a downtown neighborhood in Syracuse, New York, USA, as a case study, preliminary results demonstrate how the workflow provides insight into existing energy use issues and potential for implementing strategies such as energy load shifting or building retrofits. A discussion includes opportunities as well as challenges to the workflow in facilitating understanding of urban energy model outputs by multiple stakeholders in evaluating potential energy efficient strategies.

Author Keywords

UBEMs; GIS; Visualization.

1 INTRODUCTION

In the context of sustainable urban planning and resource management, the integration of energy modeling and real-world data into decision support tools is becoming increasingly important for stakeholder involvement in determining climate adaptation measures. Developing neighborhood-scale energy efficiency strategies for building

stocks is a key component to meeting GHG emission reduction targets, since a majority of near-term implementation of sustainable measures often occur at the municipal level [19]. Common practices for energy efficiency strategies include building retrofits such as glazing replacement or enhanced insulation, advanced conversion and storage technologies integrated with smart grid systems, energy load-shifting, and distributed generation schemes [9]. Whereas an understanding of building performance is a key factor to address the implementation of strategies such as building retrofits, conversion technologies, and energy use load-shifting, the spatiotemporal characterization of building demands in the context of other information, such as demographic data and renewable resources, is especially necessary to assess the effectiveness and economic viability of adaptation measures. The characterization of renewable resources is important for sizing and operation of technologies such as heat pumps, combined heat and power, and thermal storage, whose efficiencies are time- and temperature-dependent [8].

1.1 UBEMs in Sustainable Planning

Visualizing and forecasting impacts of various building adaptation measures can assist city governments and community stakeholders in creating a net-positive environmental impact while enhancing their resilience to climate change. Urban building energy models (UBEMs) are being developed to support forecasting of climate adaptation strategies at the building level by estimating neighborhood-scale hourly energy demand loads. The goal for such models is to explore future scenarios for various design strategies, and to prioritize the most effective solutions. UBEMs can be used by urban planners to evaluate and quantify the efficiency of urban design policies by comparing different proposed strategies and understanding implications at a community level. Furthermore, they can be used to inform individual citizens about estimated energy consumption behaviors in order to reduce electricity bills and to contribute to energy efficient targets on the community scale. UBEMs thus provide a pathway between municipality or city goals,

and the specific proposed strategies or design interventions required at the scale of a district or the whole city. While urban modeling approaches allow trained users of the tool to assess potential impacts of multiple climate adaptation strategies, their engagement with non-expert stakeholders is limited to the evaluation of static proposals in a single moment of time [16]. Techniques for visualizing UBEM outputs are typically in the form of 2D graphics with fixed 3D views of the context. Recent developments in 4D interfaces for urban models seek to convey spatial and temporal dynamics of energy services at the urban scale by offering the simultaneous comparison of both power and temperature requirements in both individual and clusters of buildings [8]. Despite advances in generating multidimensional views of simulation results, current interfaces are still expert-driven, privileging the designer or building scientist's perspective. Further, the simulation data tend to be viewed in isolation, requiring additional tools for analysis with other geospatial information. One of the major challenges to current UBEMs is the need for GIS-based visualization of UBEM results to ensure that stakeholders easily understand key takeaways, such that results can inform decision making in a seamless workflow [10]. When cleaned and layered in a GIS platform, geospatial information can be used to illustrate, analyze and draw conclusions about important urban features such as energy usage, capacity, and potential [14]. In order for policy makers and other non-experts to utilize UBEMs for evaluating a range of possible strategies over time, the communication of their outputs should be in a form that is spatial, variable, and comparable to other types of relevant environmental, socio-economic, and demographic information for a holistic view on the potential of such strategies.

1.2 UBEMs Informed by GIS

Geographic Information Systems (GIS) can be powerful platforms for interactively visualizing layered spatiotemporal datasets, including building and urban energy data, and for gaining a holistic view of past trends, current conditions, and future scenarios related to the physical, ecological, political, and cultural aspects of the built environment. GIS systems are designed to store, retrieve and analyze geographically referenced data. In GIS platforms such as ESRI's ArcGIS, information is contained as a spatial data layer, and data are spatially referenced through map projections using coordinate systems. Spatial data layers can be overlaid, manipulated, and combined to form composite layers. This offers the ability to perform overlay analysis, and hence, the ability to analyze the trends and patterns of a geographically defined area by exploring the relationships between spatial data layers.

Many UBEMs rely on GIS databases to generate 3D massing models for urban energy modeling and analysis [19]. Recent research in urban energy models and tools have utilized GIS capabilities to enhance understanding, analysis and dissemination of neighborhood and city-scale energy

systems and strategies. Fonseca and Schlueter [8] developed a framework to input geo-referenced data of existing or foreseeable urban scenarios that also calculates the hourly power and temperature requirements of energy services in buildings. Kim et al. [12] developed a BIM-GIS integrated web-based building energy data visualization system to monitor and manage energy use on a city-wide level. Ma and Cheng [15] used a GIS integrated data mining framework for estimating the building energy use intensity (EUI) at the urban scale. Kontokosta and Tull [13] designed a web-based tool to enable building stakeholders and the general public to explore and compare patterns of building energy use across New York City, whereby users can query the energy consumption of individual buildings and compare that against buildings of similar type, age, size, or location. Alhamwi et al. [2] developed a GIS-based model where electricity demand is represented as a function of space and time at the distribution level in order to investigate the deployment of renewable energy sources at the city level. The Smart City Energy platform is yet another example of a web-based GIS interface used to explore potentials for renewable energy, green roofs, and risks associated with urban heat island and energy poverty [22].

The deployment of renewable energy resources, such as solar, requires a deep understanding of its spatiotemporal characteristics for the design and evaluation of solar application systems. In order to assess potential locations and feasibility of such energy efficiency strategies, the environmental and socio-economic conditions must be considered for adequate support decision-making [20]. The ability for GIS-based tools to facilitate the deployment of energy efficient strategies and renewable energy resources in the context of other geographic data has been investigated for several decades [23]. The recent developments in ESRI'S GIS software include solar radiation analysis tools in the ArcGIS Spatial Analyst extension, which allow the calculation and analysis of the effects of the sun over selected geographic area and for specific periods of time [5]. These tools and extensions begin to address growing interest and opportunities for visualizing energy-related data within a GIS platform.

Recent work demonstrates how GIS data can significantly inform the development and use of urban energy models. However, GIS-based models offering flexibilization options and strategies are still scarce [2], and downscaled microclimate data is not easily viewed in GIS at the neighborhood level [5]. Further, the GIS platform itself is not typically used as the primary interface for viewing urban energy model outputs, thus missing an opportunity to view energy consumption data and proposed energy efficient strategies in the context of other relevant geospatial data. Data related to land use, building age, and income can shed light on the socio-economic conditions that may either support or require alternative approaches to implementation of climate adaptation strategies. These challenges, combined with current issues with visualizing UBEM outputs in a way

that is accessible by non-expert users, demonstrate the need for methods to facilitate the spatiotemporal visualization of current and future building performance and energy behavioral scenarios in association with other geo-referenced datasets. Understanding the complex spatiotemporal relationship between hourly building energy use in the context of other real-world geo-referenced datasets has only recently become possible through the advancement of UBEMs and GIS platforms and interfaces, making this valuable territory for sustainable design and urban planning.

1.3 Research Objectives

Leveraging the GIS platform for spatiotemporal visualization of real-world and simulated UBEM datasets simultaneously can assist in identifying opportunities, as well as potential barriers, to climate adaptation strategies in the context of other relevant geospatial data. Information such as building age, land use, and income can be valuable when inputting parameters and testing strategies through an UBEM. For instance, we may recognize that design retrofits and load-shifting strategies can be effective, but in what areas and to which buildings are they most likely to have the greatest impact?

The objective of this work is to investigate how a GIS platform can enable more informed decision-making when constructing an UBEM and viewing its results. A method is developed to integrate simulated building energy consumption data associated with variable energy efficiency scenarios within a GIS platform for interactive spatiotemporal visualization of multiple building and urban datasets. Datasets include building age, type, and occupancy, to inform how and where load-shifting strategies might best be implemented, thus informing the UBEM itself. A feedback loop is created between an UBEM and ArcGIS that supports iterative testing of load-shifting scenarios to facilitate the spatiotemporal visualization of various UBEM outputs spatially and over time. A downtown neighborhood in Syracuse, New York, USA is used as a case study to test the viability of our workflow, specifically to identify existing energy use issues and opportunities for implementing strategies such as retrofits and energy load-shifting. Designs for a graphical user interface (GUI) support exploration of strategies over time within a web-based application. The broader aims are to facilitate better understanding by non-expert stakeholders of existing energy use issues, such as peak energy use demand, and to identify the viable opportunities and potential barriers for adaptation strategies in the context of various physical, demographic, and environmental data.

2 METHODOLOGY

The proposed workflow was implemented on a downtown neighborhood in Syracuse, New York, to analyze existing energy use behaviors, highlight issues of energy consumption, and propose behavioral strategies and analyze their effect on reducing peak energy demands at a neighborhood scale.

The workflow is illustrated in Figure 1. The first step was the development of a base model UBEM to simulate energy use patterns and behaviors for the Syracuse neighborhood case study. The second step involved acquisition of simulated energy use data and real-world data and integration within the ArcGIS platform, where data layers could be overlaid and visualized spatiotemporally. The third step involved the design of the GUI to visualize and analyze UBEM scenarios in hourly timesteps and in association with other building data. By creating a feedback loop between UBEM outputs and ArcGIS, hourly energy use results of alternative scenarios could easily be tested and viewed spatiotemporally in ArcGIS. The following sections of the Methodology describe the development of this workflow.

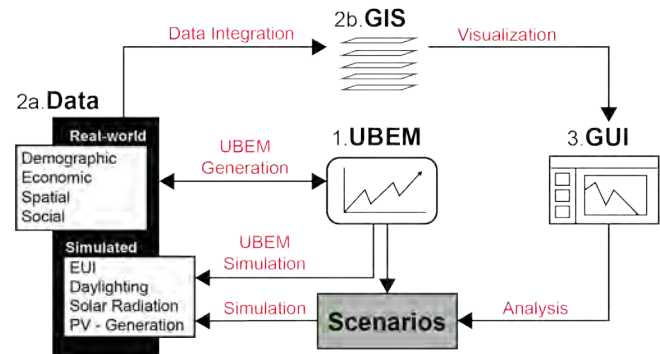


Figure 1. Diagram of the proposed workflow.

2.1 UBEM Development and Simulation

A baseline UBEM for this case study was generated using the Urban Modeling Interface (UMI) [18] plugin for the Rhino3D CAD software. Syracuse Hancock Typical Meteorological Year (TMY3) weather file was used in this study. The generation of the UBEM required a definition on geometric and non-geometric properties for each building in the model. GIS data provided information on building footprint and height to generate 3D massing, which was used to calculate areas and orientation. Information for building construction, material properties, and Window to Wall Ratio (WWR) are usually provided from a survey of existing construction or from the district municipality archives; in our case we used geospatial vector data, or shapefiles, for determining building orientation, size, and WWR.

Non-geometric buildings and occupant inputs included envelope construction details, HVAC systems properties, occupancy schedules, and dominating schedules of energy use for each building type. These factors influence energy demand and should be defined to reflect the existing properties and behaviors that represent the energy use patterns of the urban context. Since energy use behaviors are uncertain and difficult to define, calibration methods can be utilized to generate more accurate behavioral inputs and outputs, provided that the measured data is available [7,21].

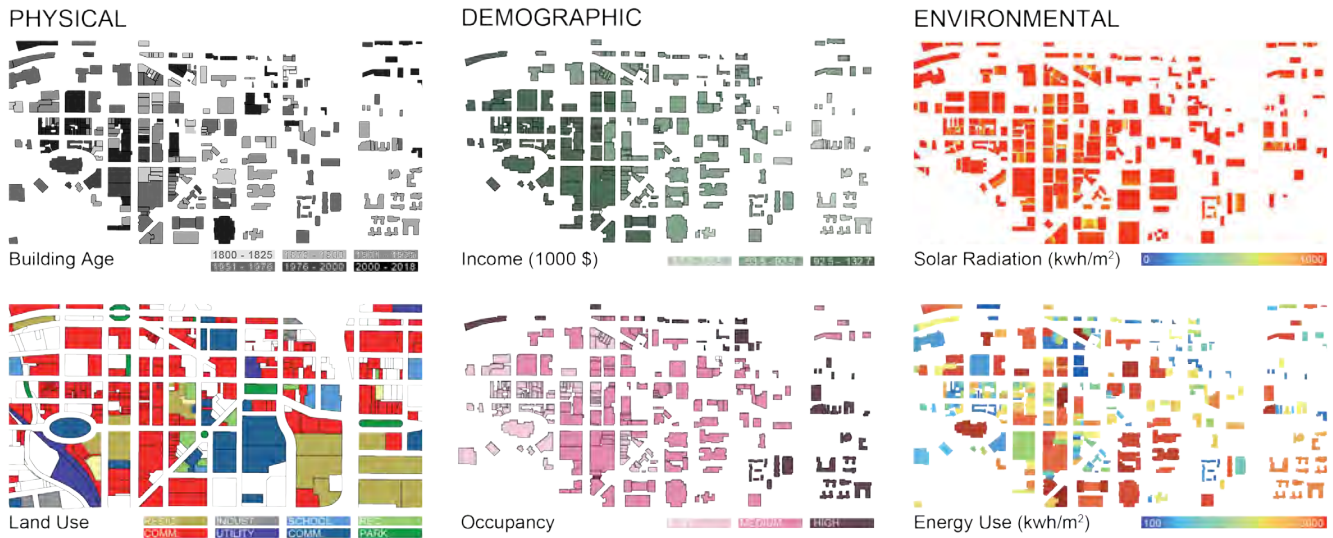


Figure 2. Examples of publicly available and simulated geospatial data related to physical, demographic, and environmental conditions within the Syracuse, NY, case study.

In the absence of detailed behavioral information, the process relies on deterministic assumptions and the expertise of the modeler. This deterministic simplification of unknown occupant related parameters is relevant in energy modelling [24]. In our baseline UBE, we needed to define behavioral information such as cooling and heating setpoints and illuminance targets, which we defined as single values using ASHRAE 90.1 [1] and IESNA standards [17]. Building construction details and building systems properties were also defined according to ASHRAE 90.1 guidelines for the Syracuse Climate Zone 5A, Cool-Humid. All schedule, construction, and HVAC system inputs were then combined into a template that characterized each specific building type and were used to detail a thermal simulation model.

UMI’s operational energy simulation was based on an algorithm that abstracts an arbitrarily shaped set of building volumes into a group of simplified “shoebox” energy models [6] and uses EnergyPlus as an underlying simulation engine [4]. A single dominating energy use schedule for each building type was defined empirically using the data collected for commercial, school and offices and residential operational hours. After assigning the detailed templates to the buildings in our model, simulations were performed to generate Energy Use Intensity (EUI) data (energy per square foot per year) for each of the buildings. Hourly data for heating, cooling, lighting and equipment energy use was extracted.

With the UBE simulation, we could predict the impact of different scenarios and sustainable strategies on building energy use, such as building design and retrofit proposals or load shifting and shedding strategies, by adjusting geometric and non-geometric inputs. For example, we could manipulate geometric parameters such as shading devices, or

the choice of materials, and run the simulation to get outputs for hourly energy use. We could also simulate the impacts of load shedding / shifting strategies to compare the effects of different heating or cooling setpoints, and illuminance targets, as well as the effect of different occupancy and usage schedules to the existing behavioral patterns of energy use. For our case study UBE we focused on simulating the impacts of behavioral load shifting strategies on reducing the energy use demand during peak hours. In this case UBE behavioral inputs were represented as schedules that reflect the percentage of energy use at each hour of the day. These inputs can be modified to represent a precooling/preheating strategy or the scheduling of heavy equipment use during off-peak hours to save energy and cost.

2.2 Integration of Hourly Energy Use Data with ArcGIS

Similar to UBE templates that combine a list of inputs (properties), GIS can spatially combine information in the form of attribute tables (text files/spreadsheet) that contain features that are linked to the tabular data and a specific location. Attributes for individual buildings can be modified to include features that contain both publicly available geospatial data as well as simulated data. Geospatial datasets can be imported to ArcGIS in the form of vector data, or shapefiles, with information related to the physical characteristics of the built environment, such as building height, type, age, and number of floors or overall square footage. Demographic data can include income, population density, and occupancy. Simulated data related directly to energy and the environment can include solar radiation, existing building energy use, and proposed energy use under different scenarios (Figure 2).

In our process, the energy use results simulated from our UBE included hourly values for lighting, heating, cooling,

and equipment energy use. These results were exported as comma-separated values (CSV) files, which were then imported as a text file into the ArcGIS platform. The hourly energy use values were assigned as customized attributes, or energy use features, to individual building object IDs via a master CSV file. Geospatial data was collected from an ArcGIS database and from site surveys for building age, land use, number of occupants, and building properties. This data was combined into the master CSV file using the corresponding building IDs. Once the CSV file was linked to each of the building features, then the simulated energy data could be directly viewed, manipulated, and analyzed in ArcGIS alongside multiple real-world geospatial datasets. This CSV file could be linked to the attribute table in GIS, hence an update in the simulation results would update GIS inputs and the visualization through the GUI.

3 EXPERIMENTAL RESULTS

Once all physical, demographic, and energy-related datasets were integrated into ArcGIS, filtering analysis was applied using all the data layers to provide insights into existing energy use issues and opportunities for energy efficient strategies to reduce energy use during peak demand hours. Preliminary studies utilized the selective filtering of real-world and simulated energy use datasets in ArcGIS to examine factors that could inform strategies related to building retrofits, and load shifting through changes in energy use behavior.

3.1 Building Retrofits

The first phase of analysis sought to identify which, if any, buildings had potential for building envelope and equipment retrofits. Data used for analysis included building type, building age, income level, and simulated energy use data through the UBEM. Buildings were grouped into age ranges for every 25 years then mapped in ArcGIS accordingly. Filtering analysis was used to visualize the relationship between specific age ranges and energy use. Visualizations of each age range illustrated which of these buildings were consumers of high energy based on occupancy, size, and simulated energy use (Figure 3). Furthermore, this multi-dimensional visualization allows us to identify the relationship between users' energy use intensity and building types, occupancy level, building size and income. The different layers that are used for our analysis are illustrated in FIGURE 3. Visualizations also showed that the majority of the offices and residential buildings in this area were built prior to 1950, indicating the likelihood that these buildings have inefficient envelopes, heating, and cooling equipment. The analysis provided several insights as to which subset of aged buildings with high energy consumption might require different energy efficient strategies. It also suggested that focusing on energy efficient strategies for aged buildings could have a greater impact on reducing the overall energy use of the neighborhood than if applied to newer buildings.

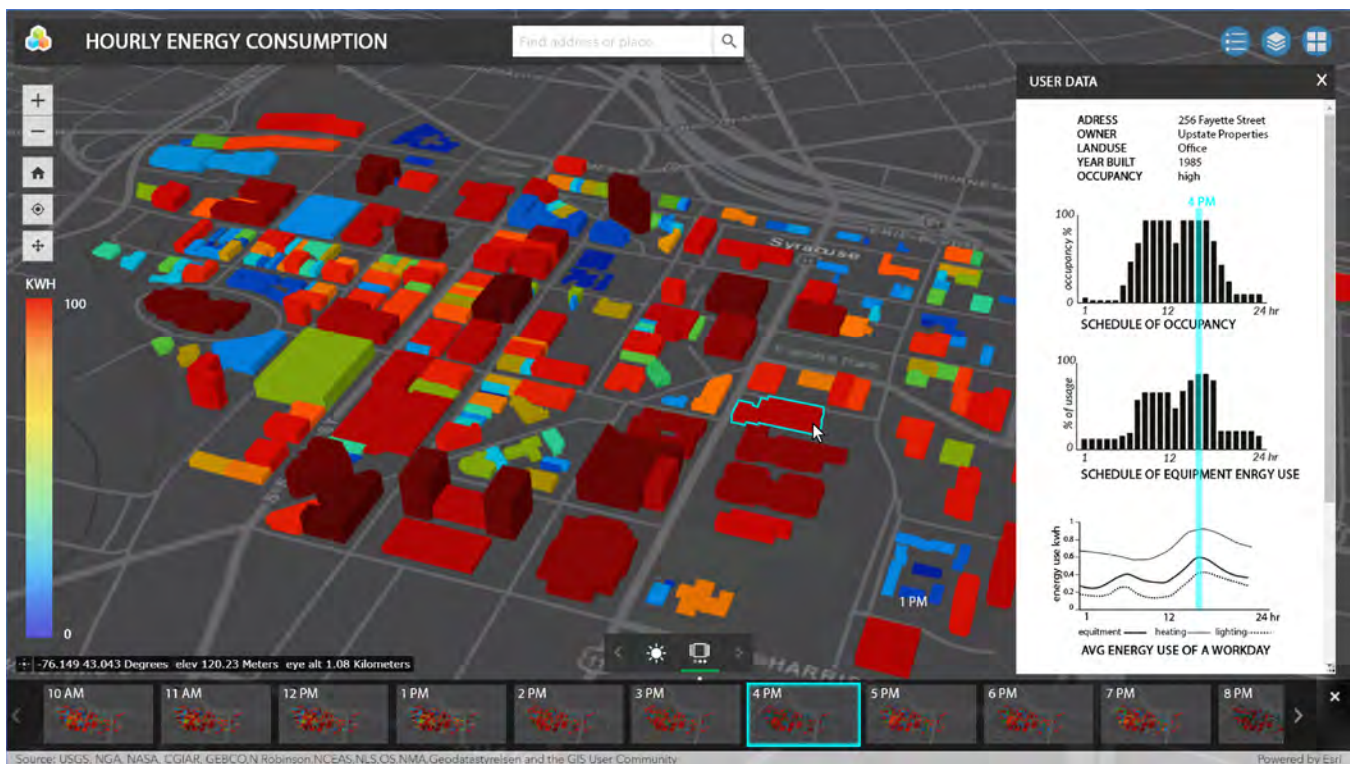


Figure 3. False color simulated hourly energy use for buildings in the Syracuse downtown neighborhood. Users can select a building and view a GUI that presents detailed information about the selected building, including age, types with their dominating energy use schedules, and total energy use over a typical 24-hour period.

Layered onto the analysis was demographic data related to income, to factor in potential barriers to building retrofit solutions such as upgrading the building envelopes or equipment. A majority of aged buildings with high energy consumption predictions were located in areas with lower income, raising concerns as to the economic feasibility of such upgrades and pointing to the investigation of alternative strategies. In this situation, behavioral adjustments presented a possible alternative approach that could be effective in stabilizing the energy demand during peak demand hours. This would require shifting heavy duty equipment use to evening hours and applying pre-heating strategies.

3.2 Energy Load Shifting

The next phase of analysis identified aged buildings that were likely to contribute to high energy use specifically during peak demand hours, in order to implement possible load shifting strategies to offset grid pressures. This analysis layered geospatial data for building type, hourly occupancy, and simulated hourly energy use data. The spatiotemporal visualizations illustrated that peak energy demand for commercial and office buildings built prior to 1950 surpassed the grid energy supply during late afternoon hours. During this high demand period, the city is obliged to depend on peaker plants, which typically are expensive to operate and use more fossil fuels than non-peaker plants [3]. To avoid use of peaker plants, load shifting strategies were proposed to analyze their potential impacts on overall building energy use for the downtown neighborhood.

Strategies included energy use behavioral adjustment by shifting heavy-duty equipment use to evening or early morning hours, when energy demand is lower. Load-shifting was also applied by implementing pre-heating and pre-cooling strategies. In this case, HVAC systems schedules and setpoints were modified to operate at a higher level in hours that preceded the afternoon peaks; this would require building inhabitants to turn-off the HVAC systems or set an energy efficient setpoint during the peak hours while maintaining comfort levels.

In order to test and visualize the effect of the proposed load-shifting strategies, behavioral inputs of our baseline UBEM were modified to reflect these updated behaviors. We modified the operational schedule inputs of HVAC equipment, and modified the intensity inputs such as heating/cooling setpoints to reflect the proposed strategies. Schedules of energy use in the UBEM represent a percentage of energy use for each hour of the day. New simulations were generated and their outputs updated directly to the ArcGIS hourly geodatabase for building energy use features. These results were then compared with the existing conditions in an interactive GIS interface (Figure 4).

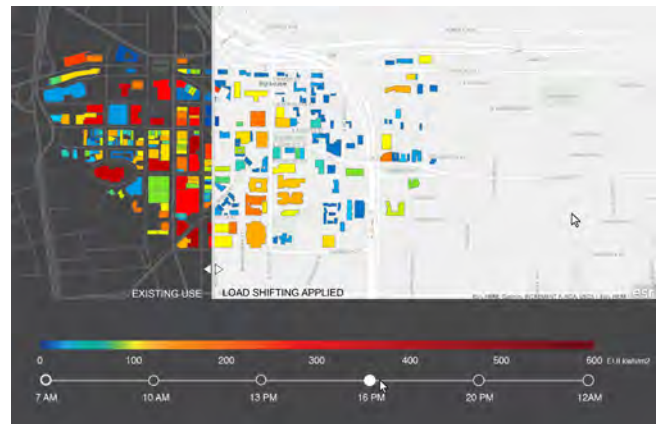


Figure 4. Example of interactive slider viewer comparing energy use before and after load shifting strategies are applied.

4 DISCUSSION

4.1 Summary of Findings

Through the use of ArcGIS as a primary interface for analyses, we were able to visualize the peak energy use demands spatiotemporally by layering together simulated energy use data, land use, building type, building age, and occupancy. Patterns of energy use for specific building types and ages were easily filtered and isolated for spatiotemporal analysis, which enabled a more holistic understanding of the potential feasibility, as well as possible barriers, to implementing strategies such as retrofits or load shifting. These preliminary analyses are modest examples of what could be further studied for the future of urban energy systems. Many other physical, environmental, and socioeconomic factors are important to consider in the evaluation of scenarios and strategies. Layering this information might reveal unexpected concerns but also potential solutions.

The workflow presented creates a useful feedback loop between UBEM and ArcGIS, making the iterative testing of urban energy strategies in the context of other data more easily achieved. When the UBEM gets modified and results updated, the data is easily integrated to the ArcGIS building objects and attributes. This process of integrating simulation results and GIS is automated, so that changes made to an UBEM can be immediately simulated and results viewed interactively in ArcGIS. The feedback loop works in both directions; the UBEM produces data for ArcGIS visualization and analysis, and the layered information coming out of GIS can produce important insights and new parameters that inform the UBEM development.

4.2 Opportunities for Visual Analysis and Dissemination

In contrast to existing methods for visualizing outputs from UBEMs, which tend to be static 2D or 3D views, our approach enables the user to spatialize the building energy use data layered with other relevant information. The spatiotemporal visualization of multidimensional datasets

through an interactive GIS platform facilitates analyses of energy efficient strategies, not in the black box of an energy model, but in the open-ended context of real-world data. In our process, interactive visualization in ArcGIS is the primary method for exploring datasets, interpreting and investigating analysis results, and communicating valuable findings. Since each data layer can include attributes with high granularity, the user can visually explore and manipulate the data at different levels. Data is spatially located and can be identified using dynamic selection, which can also be used to filter data sets for analysis; by selecting specific layers, the user can isolate and compare layers of data/outputs. Within the ArcGIS platform users can also create dashboard charts which are dynamically connected to the spatial data. This aspect allows users to run hot spot analysis by selecting specific results in the dashboard charts that link the user to specific areas in the map. Datasets with temporal components can be visualized spatially through sliders and in a dashboard through line charts. To spatially visualize time series data, data should be summarized in time step layers and linked to a timeline slider. The user can also visualize temporal spatial-data overlaid with other data layers. This temporal visualization can be used to identify anomalies in behaviors and patterns.

Custom generated data layers can be exported to a GUI, where the layout can be edited, and some visualization features can be added to make the interface user friendly. This interface can be then published and shared with various stakeholders (urban planners, utility companies, policy makers, etc.) to facilitate evaluation and communication of sustainable urban planning and resource management strategies.

4.3 Limitations and Future Work

As with any creation and use of data, there are limitations to the accuracy and assumptions behind the data, including that which is simulated. Understanding the bias behind data and how data can be manipulated are also important considerations when maps are generated for communicating a position or set of strategies. In our examples, there are conclusions drawn between income level and economic feasibility, or between the outdated conditions of HVAC systems and older buildings that would require further research to verify the state of individual buildings and their systems. However, the workflow is not intended to solve problems directly, but rather assist with clarifying questions, and identifying issues and opportunities that could benefit from further investigation.

Future work focuses on implementing this process as a plugin to UBEMs for a user-friendly exploration, analysis, and visualization interface. Further development of a GUI could be action-based to enable users to easily explore a library of energy efficient strategies, generate input for an UBEM, and obtain updated results through the automated process for quick viewing in the context of other socioeconomic information. Incorporating benchmarking

data as a GIS layer would also be beneficial for calibrating the UBEM and for evaluating strategies in the context of city-wide policies for building energy use. With 24 U.S. cities with benchmarking policies in place, workflows with GIS interfaces such as this one could address challenges related to communicating the complex data to those outside the building energy efficiency community. Finally, testing the workflow and interface with stakeholders will provide valuable feedback for improving its usability and application in real-world settings and communities. This is especially important for enabling those who live in disadvantaged neighborhoods to articulate how their own communities might be understood by the interface, in light of investment and development of sustainable strategies.

5 CONCLUSION

This paper described a workflow to integrate simulated building energy consumption data associated with variable energy efficiency scenarios within a GIS platform for interactive spatiotemporal visualization to support energy efficient strategies and climate adaptation decision-making. A feedback loop was developed to link UBEM hourly simulation results to building attributes in ArcGIS for visualization and analysis of energy efficient strategies over time and in the context of other georeferenced data. This work addresses current challenges with UBEMs by developing an automated process to integrate simulated building energy performance data layered with GIS, enabling users to selectively view, analyze, and update composite data layers for a more holistic understanding of the potential feasibility, as well as possible barriers, to implementing strategies. Analysis of a case study of downtown Syracuse, New York, demonstrated how the workflow provided insight into existing energy use issues and preliminary evaluation of load-shifting strategies. Future work points toward implementing this process as a plugin to UBEMs, further development of the GUI, and testing for stakeholder input.

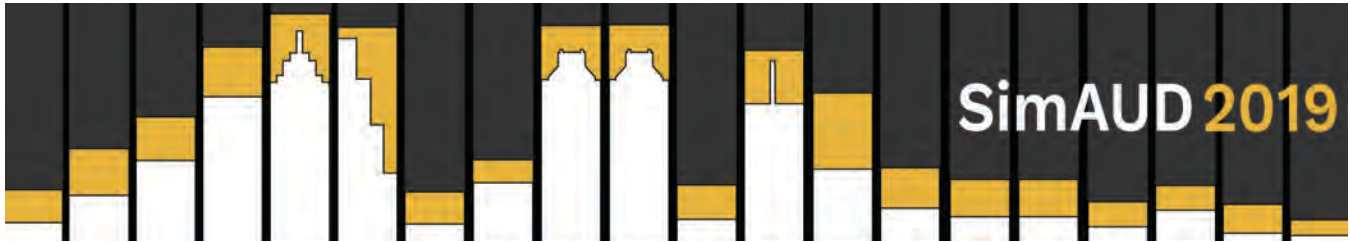
ACKNOWLEDGMENTS

This work is funded in part by the Syracuse University School of Architecture and the Syracuse Center of Excellence Faculty Fellows program. The authors would like to thank student collaborators Katharina Koerber, Chenxie Li, and Harshita Kataria for their contributions to the research.

REFERENCES

1. ASHRAE (American Society of Heating, Refrigerating and Air Conditioning Engineers). 1989. 90.1: Energy Efficient Design of New Buildings Except New Low Rise Residential Buildings. Atlanta, GA: ASHRAE.
2. Alaa Alhamwi, Wided Medjroubi, Thomas Vogt and Carsten Agert. 2017. "GIS-based urban energy systems models and tools: Introducing a model for the optimisation of flexibilisation technologies in urban areas." *Applied Energy* 191:1-9.

3. Arababadi, R., 2016. Operational and Technological Peak Load Shifting Strategies for Residential Buildings. Arizona State University.
4. Crawley, D.B., Lawrie, L.K., Winkelmann, F.C., Buhl, W.F., Huang, Y.J., Pedersen, C.O., Strand, R.K., Liesen, R.J., Fisher, D.E., Witte, M.J. and Glazer, J., 2001. EnergyPlus: creating a new-generation building energy simulation program. *Energy and buildings*, 33(4), pp.319-331.
5. Charabi, Yassine, Gastli, Adel, Al-Yahyai, Sultan. 2016. Production of solar radiation bankable datasets from high-resolution solar irradiance derived with dynamical downscaling Numerical Weather prediction model. *Energy Reports* 2: 67-73.
6. Dogan, T. and Reinhart, C., 2017. Shoeboxer: An algorithm for abstracted rapid multi-zone urban building energy model generation and simulation. *Energy and Buildings*, 140, pp.140-153.
7. Rawad El Kontar & Tarek Rakha. 2018. Profiling Occupancy Patterns to Calibrate Urban Building Energy Models (UBEMs) Using Measured Data Clustering, *Technology|Architecture + Design*, 2:2, 206-217, DOI: 10.1080/24751448.2018.1497369
8. J.A. Fonseca, A. Schlueter. 2015. Integrated model for characterization of spatiotemporal building energy consumption patterns in neighborhoods and city districts. *Applied Energy* 142: 247-265.
9. Girardin L, Marechal F, Dubuis M, Calame-Darbellay N, Favrat D. EnerGis: a geographical information based system for the evaluation of integrated energy conversion systems in urban areas. *Energy* 35:830-40. <http://dx.doi.org/10.1016/j.energy.2009.08.018>.
10. Hong, Tianzhen, Langevin, Jared, Sun, Kalyu. 2018. Building simulation: Ten challenges. *Building Simulation* 11(5): 871-898.
11. Hong T, Chen Y, Lee SH, Piette MA (2016a). CityBES: A web-based platform to support city-scale building energy efficiency. In: *Proceedings of the 5th International Urban Computing Workshop*, San Francisco, USA.
12. Kim, S. A., Shin, D., Choe, Y., Seibert, T., & Walz, S. P. (2012). Integrated energy monitoring and visualization system for Smart Green City development: Designing a spatial information integrated energy monitoring model in the context of massive data management on a web based platform. *Automation in Construction*, 22, 51-59.
13. Kontokosta, C., & Tull, C. (2016). EnergyViz: Web-Based Eco-Visualization of Urban Energy Use from Building Benchmarking Data. In *Proceedings of the International Conference on Computing in Civil and Building Engineering*
14. C. Li, GIS for urban energy analysis, in: B. Huang (Ed.), *Comprehensive Geographic Information Systems*, Elsevier, Oxford, 2018, pp. 187-195
<https://doi.org/10.1016/B978-0-12-409548-9.09652-4>.
15. Ma, June and Jack C.P. Cheng. 2016. "Estimation of the building energy use intensity in the urban scale by integrating GIS and big data technology." *Applied Energy* 183(1): 182-192.
<https://www.sciencedirect.com/science/article/pii/S0306261916311679>
16. Nagpal, Shreshth, Hanson, Jared, Reinhart, Christoph. 2018. Auto-Calibrated Urban Building Energy Models as Continuous Planning Tools. *Proceedings of the 2018 SimAUD Conference*: 309-312.
17. Rea, M.S., 2000. *The IESNA lighting handbook: reference & application* (p. 1000). New York: Illuminating Engineering Society of North America.
18. Reinhart, C.F., Dogan, T., Jakubiec, J.A., Rakha, T. and Sang, A., 2013, August. Umi-an urban simulation environment for building energy use, daylighting and walkability. In *13th Conference of International Building Performance Simulation Association*, Chambéry, France.
19. Reinhart, C., and Cerezo Davila. 2016. Urban building energy modeling – A review of a nascent field. *Building and Environment* 97: 196-202.
20. Sarmiento, Nilsa, Belmonte, Silvina, Dellicompagni, Pablo, Franco, Judith, Escalante, Joaquin Sarmiento. 2019. A solar irradiation GIS as decision support tool for the Province of Salta, Argentina. *Renewable Energy* 132: 68-80.
21. Sokol, J., Davila, C.C. and Reinhart, C.F., 2017. Validation of a Bayesian-based method for defining residential archetypes in urban building energy models. *Energy and Buildings*, 134, pp.11-24.
22. Smart City Energy. 2018. Accessed November 26, 2018. <http://iguess.tudor.lu/about>
23. D. Voivontas, D. Assimacopoulos, A. Mourelatos, J. Corominas, Evaluation of renewable energy potential using GIS decision support system, *Renewable Energy* 13 (1998) 333e344.



A Technique for Developing High-Resolution Residential Occupancy Schedules for Urban Energy Models

Diba Malekpour Koupaei¹, Farzad Hashemi², Vinciane Tabard-Fortecoëf³ and Ulrike Passe¹

¹Iowa State University
Ames, USA
{malek, upasse}@iastate.edu

²Penn State University
State College, USA
fxh99@psu.edu

³INSA Lyon
Lyon, France
vinciane.tabard-fortecoef@insa-lyon.fr

ABSTRACT

Occupants' presence and activity schedules directly influence residential energy consumption loads. Regardless of their widely acknowledged importance, developing proper representative occupancy inputs for urban energy use studies of residential neighborhoods remains to be a challenge to overcome. The presented work aims to balance between accuracy and complexity of such occupancy models by developing a technique that takes advantage of a previously proposed sophisticated method for schedule generation and attempts to refine and simplify its results for practicality purposes.

Here, we used a Markov chain transition probability matrix based on the American Time-Use Survey (ATUS) database and selectively refined its outputs according to the data collected from our own designated population of study. The resulting refined schedules were incorporated into the Urban Modeling Interface (*umi*) interface and were then tested on our pilot case study, a relatively low-income dense neighborhood in the Midwestern United States composed of 272 residential buildings. An initial investigation of this technique's performance suggests that while the use of the ATUS based model provided a high level of variability and sophistication, the customization step ensured that the resulting schedules are representative of our population and its characteristics. More importantly, we were able to maintain simplicity and practicality.

Author Keywords

Urban Building Energy Simulation, Occupancy Schedules, Markov Chain, Time-Use Data.

ACM Classification Keywords

I.6.5 SIMULATION AND MODELING; I.6.5 MODEL DEVELOPMENT

1 INTRODUCTION

According to the 2018 Annual Energy Outlook [13], the building sector (both residential and commercial) accounted for more than 27% of total U.S. delivered energy in 2017. Unfortunately, projections for the future are not decreasing

and are in fact predicted to be growing by about 0.3% per year. As a consequence, energy use in buildings has become a growing concern of both the public and professionals in the field [14]. However, a key concept that historically had been neglected for too long is that "Buildings don't use energy: people do" [7]. It is now an established fact that whether one is concerned with studying the current state of energy use in buildings or is proposing energy saving measures for improvement, an understanding of occupancy behavior and its implications for energy use is vital [8]. Some researchers even go as far as suggesting that residential demand profiles are for the most part shaped by their corresponding occupancy patterns. For instance, the Tyndall Center's report on microgrids (2005) states that "electricity load profile depends mainly on the household size and occupancy pattern." [1]

Hence, in the recent years, there has been an increase in the body of literature concerned with energy-related occupant behavior in buildings [14]. As a result, today almost all energy modelling and simulation software tools use some sort of data linked to occupant behavior and treat it as a defining factor in their calculations of yearly profiles for heating, cooling, lighting ventilation and even plug loads. The most common form of this data is known as "diversity profiles," which is a schematic occupant presence profile of a space or thermal zone over a given period of time. Such profiles intend to reproduce the real occupancy of the space in order to accurately estimate the impact of peoples' presence and activity levels on energy load demand calculations of buildings [2].

These profiles usually consist of a combination of weekday and weekend schedules for the particular type of building (for instance residential or commercial) in discussion. Software users are often given the choice of using the predefined generic schedules in the simulation tool's default library or defining their own profiles instead. While the second option is meant to give the user flexibility and higher precision, the reality is that high quality occupancy data in all its stochastic variety is scarce, and often times, the user is

left with no choice but to use the predefined generic schedules. Given that occupancy is understood to have a considerable influence on internal loads, ventilation requirements and thus building energy consumption [15]; the use of such generic schedules in energy models results in large gaps between the predicted and actual energy use of buildings [10].

Accordingly, with the global aim of enhancing simulation approaches and increasing energy efficiency in buildings, multiple efforts have been made to generate high-resolution occupancy schedules and use them as a substitute for generic predefined universal schedules. For instance, some newer models utilize Time-Use Survey (TUS) dataset to produce realistic occupancy data. A TUS is a large survey of how people use their time and includes detailed 24-hour diaries, completed at predefined intervals by many thousands of participants. The TUS data includes the location of the participants at each time step in the diary, and can thus be used to identify the number of active occupants in a building. A fine example of such efforts is the Markov chain transition probability matrix that Richardson et al. (2008) have developed based on the UK's 2000 TUS data [12].

If we were to put all the occupancy behavioral models on a spectrum of accuracy, previously discussed generic and simplified occupancy schedules would land on one end, while TUS based models would probably land on the opposing end of the spectrum. However, the latter models' accuracy and precision, comes at the not so cheap price of them being overwhelming, complicated and in uncompromising need for a high-resolution database of large magnitude. All of this means that such techniques are still far from being practical enough to become part of the common practice. Moreover, since TUS surveys are often conducted on a national level, such models can only represent the typical lifestyle in the same scale and are hence in need of serious revision if their intended use is for a specific population with unique characteristics, which is the case in this study. The unique characteristics of our population will be discussed in the following sections of this manuscript.

When faced with this wide range of occupancy behavioral models and considering the shortcomings of each type, the question that arises with every choice is that of efficiency. It should not come as surprising that all users hope to use high-resolution and accurate data as the input to their energy use models. Acquiring such data is now possible with the use of sophisticated methods, such as the one discussed above. However, maintaining practicality and thus simplicity is also crucial, especially if efficiency is desired. Given that simplicity and accuracy often go in opposite directions, the main task ahead is that of finding the balance between these two opposing factors somewhere on this wide spectrum of occupancy behavioral models.

In the following sections, the researchers will propose a conscious strategy to find this point of balance. Our goal is to propose a technique that is simplified (and hence practical)

without jeopardizing its accuracy and precision in terms of predicting occupant presence profiles and all their stochasticity. We then follow on by testing the performance of our proposed technique in a pilot case study, the Capitol East neighborhood in Des Moines, Iowa, USA (population 217,521) with the help of Urban Modeling Interface (*umi*) [11].

2 CASE STUDY AND DATA COLLECTION

This study focuses on the use of occupancy presence schedules in the energy use simulation of a predominantly residential neighborhood in Des Moines, Iowa. The Capitol East neighborhood, which is the pilot study area for this urban energy simulation is located just east of the State of Iowa Capitol complex, near downtown Des Moines. Capitol East community is primarily low income, and their settlement pattern in this neighborhood is quite compact when compared with other parts of the city [6].

The main reference for this study is a survey that has been conducted by the Sustainable Cities Research Group at Iowa State University [5] in this neighborhood to understand how residents make energy related decisions around their houses and make use of HVAC and lighting systems. The survey has been sent to about 1,000 household addresses in three Des Moines neighborhoods (i.e., Capitol East, Capitol Park, and MLK Jr Park). Although the sample size seems reasonably large, the response rate for this survey, calculated as the

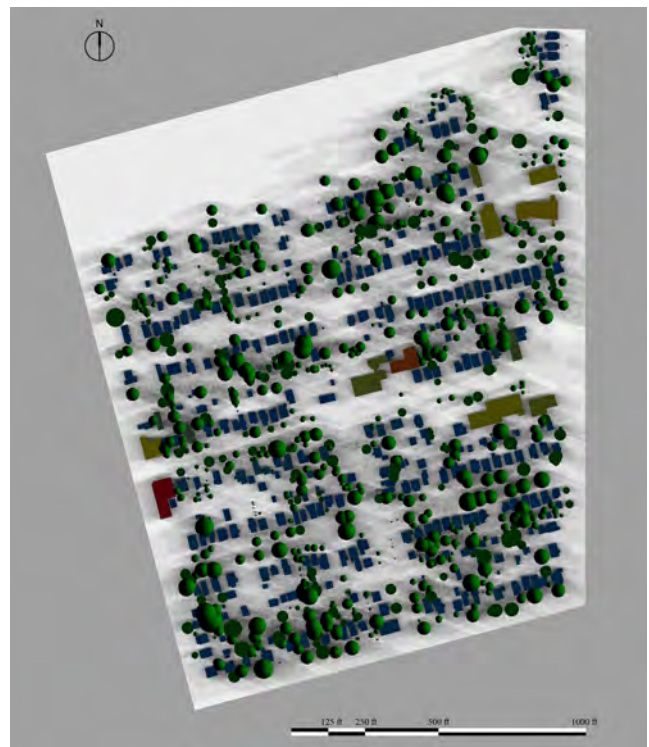


Figure 1. Top view of the neighborhood model in the *umi* environment.

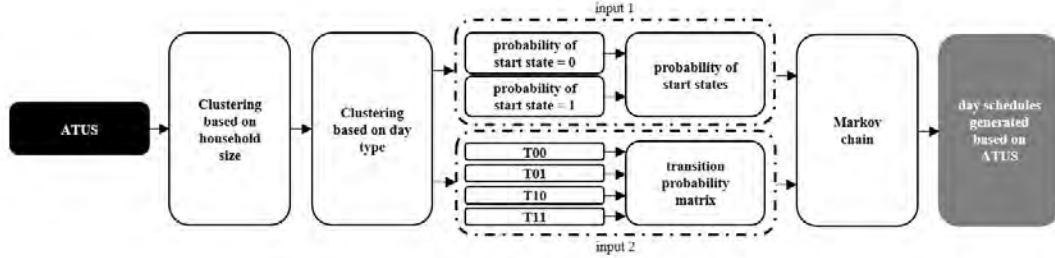


Figure 2. A schematic diagram of the original method.

number of completed forms divided by the eligible sample size, was only 6.3%. This is surprisingly low, given the fact that this survey was purposefully designed to be simple, straight forward and quick. Moreover, this rather low response rate further emphasizes the importance of finding a technique that requires a smaller database as its input, and it is clear that acquiring enough data for building a customized TUS based model from scratch is time consuming, expensive and in short, impossible for smaller projects like this.

3 SCHEDULE DEVELOPMENT

3.1 Developing Schedules Based on ATUS

In the previous sections, we mentioned that our intention was to refine and customize the results of a previously proposed Markov chain transition probability matrix. Hence, this section is an adaptation of the work done by Richardson et al. (2008) in their widely acknowledge paper “A high-resolution domestic building occupancy model for energy demand simulations” [12]. The main difference between the two studies is in that Richardson et al.’s method was applied to the British TUS database, while we followed their guidelines to generate occupancy presence schedules based on the ATUS database instead.

To that end, we classified the ATUS database into different groups based on the respondents’ household size and then divided each one of those groups into two different subgroups: diaries filled in weekdays and those that were captured in weekends. For each one of our subgroups, two inputs were required to make the Markov chain transition probability matrix:

- **Input 1:** The probability that a respondent belonging to that group was present in the house at 00:00 (midnight);
- **Input 2:** A matrix that included probabilities of their presence state changing in every time step (here each time step is 10 minutes)

The first input was calculated as the number of present respondents in each subgroup divided by the total number of respondents in that subgroup. For instance, of all the 816 diaries filled by people coming from three-person households in the weekend days, 43 of them indicated 0 as their state at 00:00, while the other 773 were actually present in their homes at midnight. Accordingly, the chance of a

respondent from a three-person household being present in the house at 00:00 in a weekend night was set to be 95% ($773/816=0.95$). This means that the chance for someone from that same subgroup not being present in the house at that time was set to be 5% ($43/816=0.05$) only.

As for the second input, first all of the diaries were divided into a sequence of ten minute time steps. This extra step was unavoidable, because unlike the British TUS database, ATUS is not filled in predefined regulated time steps. Instead, a diary input in ATUS starts with an activity and ends when the respondent is done with that specific activity. Following that classification step, a state of 0 or 1 was allocated to each diary entry according to the respondents availability at their house in that specific time step. A state of 0 stands for “not present” while a state equal to 1 has the connotation that the respondent is indeed “present”.

Then, in every subgroup, the chance of a state changing or remaining the same was calculated by defining the following variables for each one of the 144 defined time steps (6 time steps per hour in 24-hour diaries):

$$T_{00} = \frac{\text{\# of cases where start state \& end state are both} = 0}{\text{\# of cases where start state} = 0}$$

$$T_{01} = \frac{\text{\# of cases where start state is} = 0 \text{\& end state is} = 1}{\text{\# of cases where start state is} = 0}$$

$$T_{10} = \frac{\text{\# of cases where start state is} = 1 \text{\& end state is} = 0}{\text{\# of cases where start state is} = 1}$$

$$T_{11} = \frac{\text{\# of cases where start state \& end state are both} = 1}{\text{\# of cases where start state is} = 1}$$

Equations 1-4. Probability inputs to be used in the transition probability matrix.

For instance, if we go back to the three-person household weekend subgroup example discussed before, of all the 43 respondents absent in the house at 00:00, 3 of them reported that they were present in their houses at 00:10. This means that T_{01} for this subgroup was 6% ($3/73=0.06$) and therefore their T_{00} at this time step was equal to 94%.

These sets of calculations were repeated for all the subgroups and then organized into a transition probability matrix. Finally, a start state (0 or 1) was chosen randomly, taking the probability distribution (the first input) derived from the ATUS dataset into account. Subsequent states in the Markov chain were then determined by using the randomly defined

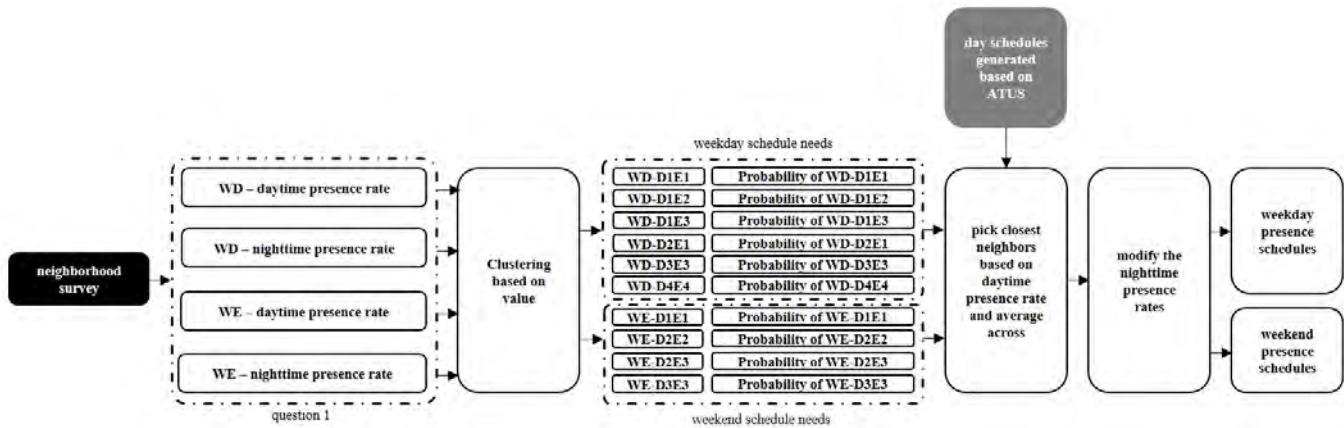


Figure 3. A schematic diagram of the refinement process.

start state with the appropriate transition probability matrix (the second input). As a result, our chain was able to produce occupancy presence schedules based on the type of the day (weekend or weekday) and household size (Figure 2).

In our selected pilot case study, average household size is determined to be about 2.5 people [6]. Hence, we used our chain to generate occupancy presence profiles for three-person households in both weekdays and weekend days. These generated profiles were then refined and customized to represent our population’s distinctive characteristics.

3.2 The Refinement Process

To refine the schedules generated by the last step, we needed to have occupancy data specific to our population. The only source of data available in this regard was our own energy use survey results discussed in previous sections. Hence, we decided to use it as the basis for this refinement procedure, regardless of its low response rate.

In our survey, one question (and its corresponding answers) is particularly relevant to occupancy profiles and thus of interest for the research project at hand. The aforementioned question was:

“Question 1: In an average week:

- What percent of your Monday-Friday daytime hours is spend at home?
- What percent of your Monday-Friday evening hours is spend at home?
- What percent of your weekend daytime hours is spend at home?
- What percent of your weekend evening hours is spend at home?”

Responses to this question (questions 1) were shown to be diverse, covering a range of all the possible values between 0% and 100%. Therefore, making one typical aggregated schedule with the help of an arithmetic average of the reported percentile numbers would have sacrificed this witnessed diversity in behavior among the residents. Accordingly, what we needed here was a number of reliable and representative common schedules generated by a clustering/classification method and not a single schedule

generated by averaging all the answers. Our initial concept for this clustering step was to find the link between the respondents’ answers to this question and some of their general characteristics as reflected in other parts of the survey. These characteristics, which included respondents’ ages, genders, economic activities and education levels, were addressed with the following questions in our survey:

“Question 2: What is your gender?

- 1 = Male
- 2 = Female
- 3 = Other, Non-binary”

Question 3: What is your age category?

- 1 = 18-30
- 2 = 31-40
- 3 = 41-50
- 4 = 51-60
- 5 = 61-70
- 6 = 71-80
- 7 = 81 or older

Question 4: What is the highest degree or level of school you have completed?

- 1 = Did not complete High School
- 2 = High School or equivalent (GED)
- 3 = Some College, no degree
- 4 = Trade/Technical/Vocational training
- 5 = Associate degree (2-year)
- 6 = Bachelors degree (4-year)
- 7 = Masters degree
- 8 = Professional or Doctorate degree

Question 5: What is your current employment status?

- 1 = Employed for wages
- 2 = Self-employed
- 3 = Unemployed and looking for work
- 4 = Unemployed but not looking for work
- 5 = Homemaker
- 6 = Student
- 7 = Military
- 8 = Retired”
- 9 = Unable to work”

As can be seen here, these questions (questions 2-5) were all of a multiple-choice nature and finding any type of link between these answers and that of the presence rate question (question 1) would have facilitated this desired clustering. However, none of the general characteristics addressed by the questions above (questions 2-5) seemed appropriate and relevant in terms of explaining the differences between presence rates on its own. In other words, we were not able to identify a simple direct correlation between any of the respondents' pre-clustered groups (as defined by questions 2-5) and their answers to the presence rate question (question 1). For instance, Figure 4 shows the relationship between daytime presence rates against employment and education levels for the sake of comparison. As can be seen here, no direct link can be detected between these factors and presence rates. This holds true for all other presence rates when compared with respondent characteristics.

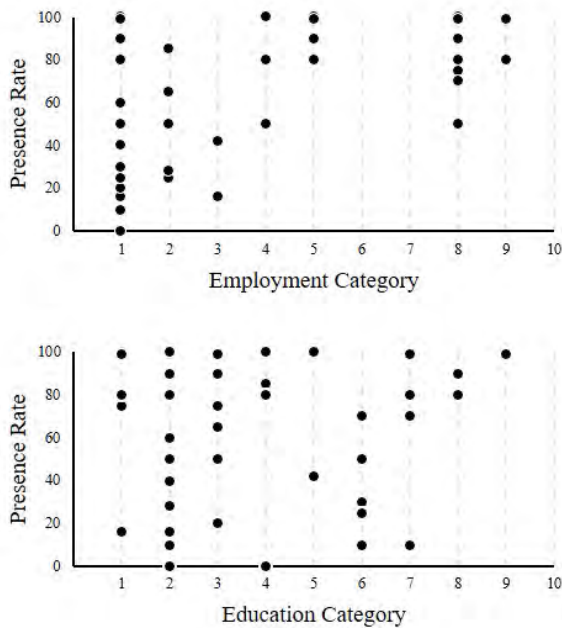


Figure 4. Correlation between weekday daytime presence rates and select respondents' characteristics.

Accordingly, we decided to cluster our data into concentrated homogeneous groups based on the presence rate values, without taking into account other respondent characteristics. The defined criteria for clustering in this step were set on the basis of maintaining group consistency, while keeping the number of groups limited. This was deemed necessary for keeping the overall accuracy and precision of the technique. Our proposed clustering criteria for this dataset were:

- Maximum group value range cannot exceed thirty percentage points.
- Maximum difference between two consecutive values in the same group should not go beyond ten percentage points.

- A presence rate value is always in the group with which it has the smallest difference.
- When a presence rate value can go in either the upper or lower group closest to its value, it should be assigned to the group that has the smallest range.
- The number of groups is limited to six.

Note that these thresholds are arbitrary criteria to create a practical number of homogeneous and concentrated groups and can be modified and adjusted according to the collected data for different projects.

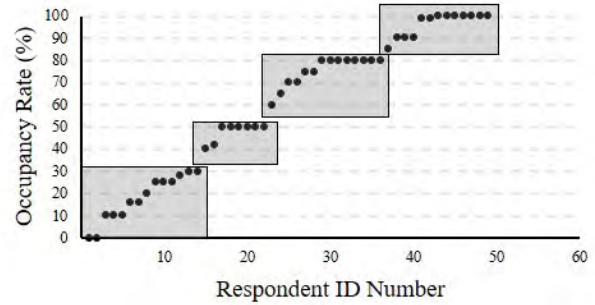


Figure 5. Clustering survey responses into schedule groups based on predefined arbitrary criteria for weekdays daytime period.

Following this procedure, the collected data from the neighborhood survey was clustered into different groups depending on day type (weekday or weekend day) and time period (daytime or nighttime). For instance, Figure 5 above shows an example of this clustering step for our weekday schedules during the daytime period.

This step resulted in 6 weekday and 4 weekend schedule types. Table 1 summarizes the characteristics of each of these ten daily schedules.

Type	Name	Presence Rate (%)		Probability (%)
		Daytime	Nighttime	
Weekday (WD)	D1	17.5	44.1	12.5
	D2		72.0	12.5
	D3		96.5	7.5
	D4	47.8	44.1	12.5
	D5	75.4	96.5	27.5
	D6	96.4	96.5	27.5
Weekend (WE)	D1	49.0	46.6	26.3
	D2	71.7	72.3	23.8
	D3		98.1	18.5
	D4	96.0	98.1	31.5

Table 1. Clustered day schedule types and their characteristics.

All ten of these day schedule types now need to be translated into hourly presence rate values, which is the format that most software tools, including *umi*, use as their data input for

occupancy schedules. This is where the schedules generated based on ATUS in the last section will be utilized.

The following procedure describes the refinement process applied to the ATUS generated schedules:

- First, for ease of use all the desired presence rates introduced in Table 1 were rounded up to their closest multiple of five. Now, each one of the desired day type schedules is recognized by two variables: daytime presence rate and nighttime presence rate. If these two were to be translated into hourly values, daytime presence rate would be of a dynamic nature, while nighttime presence rates would probably be static in most cases. This is due to the fact that daytime is usually a vibrant period of time for a household where changes in the hourly presence rates are expected, while the nighttime period is considered to be of a more stable nature. Therefore, we decided to use the ATUS generated schedules and refine them for the daytime period and use appropriate constant values for all hourly rates that fall into the nighttime period.

- To find matches for these desired daytime period presence rates defined in the last step, we first generated 100 ATUS based occupancy profiles for weekday schedules and another 100 for weekend schedules of a three-person household. This was done with the help of the Markov chain transition probability matrix described in the previous section. Then, these were arranged in terms of their calculated daytime presence percentages. To find appropriate matches for our desired presence rates, we used the following criteria:

“IF (desired presence rate – 5%) ≤ desired daytime presence rate < (desired presence rate + 5%)

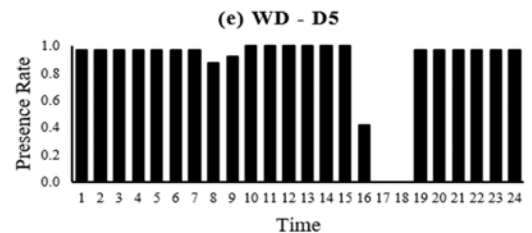
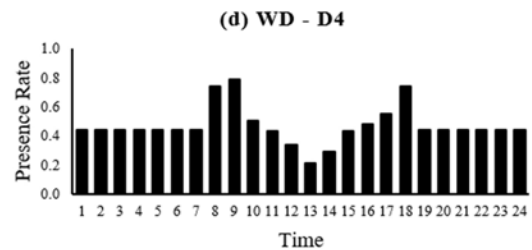
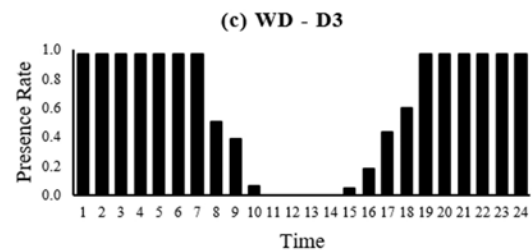
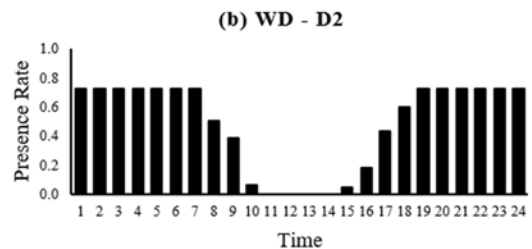
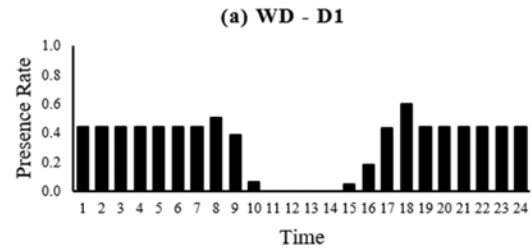
THEN average all”

The logic behind this extra step was to avoid using a rare occurrence of a specific schedule and receive a more common profile instead. This was necessary, since each one of our type schedules was meant to represent the common occupancy profile of its group and not an individual’s.

Accordingly, 10 day presence profiles were developed to match our needs. It is worthy to note here that this method does not work for daytime presence rates smaller than 5% or larger than 95%. This should not come as a surprise, given the fact that such low/high presence rates hardly allow room for any changes in their corresponding hourly presence values. Therefore, when such presence rates were desired, the hourly rates were set as constants equal to the overall mean daytime presence rate instead. Figure 6 showcases these 10 occupancy schedule profiles.

Since we had 6 weekday and 4 weekend schedules types, we were able to define 24 week schedule types by considering all the possible combinations. As a result, for every construction template introduced in the model, 24 building templates were defined in the *umi* template library interface [3] and then, randomly assigned to the residential buildings in our neighborhood with the help of a script developed in

the Grasshopper environment [4]. The probability distribution appointed to this script was set to match the number of cases in our survey that represented a specific schedule (as represented in the last column of Table 1). The only other variable define in this script was a seed point, which allowed us to test the performance of our technique. These evaluation efforts will be discussed in the following section.



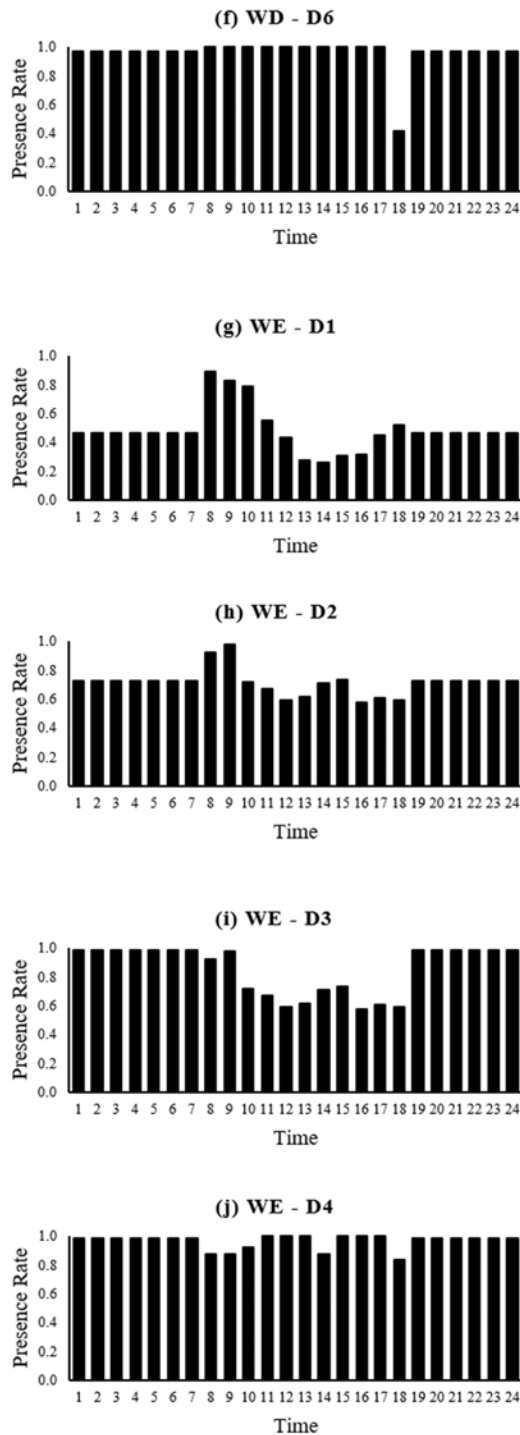


Figure 6 (a-j). Developed schedules for day occupancy profiles.

4 RESULTS AND DISCUSSION

To test the performance of our refined probabilistic occupancy schedules generated with the method described above, three models of the study neighborhood were simulated in the *umi* environment. These three models all shared the same geometry and material inputs but were assigned different occupancy schedules. This assignment of occupancy schedules was based on a single probability

distribution model with the seed (in the randomizing script in Grasshopper) changing for each run.

Overall, the results of these energy simulation runs were very close in terms of both their total yearly energy consumption values and the composition of their operational energies. As can be seen in Figure 7 below, total operational energy loads for each of these models are almost equal in all cases. While equipment, lighting and domestic hot water loads are shown to be not directly impacted by the occupancy schedule changes; of all other load components calculated by the *umi* software, none of them have witnessed a change from their arithmetic mean that is equal to or higher than 1.25%. Therefore, energy load composition also remains the same and hardly changes among different models. This suggests that the randomization process has been successful in creating a homogeneous distribution of the generated schedules based on their assigned probabilities.



Figure 7. A comparison between the changes from the mean.

In another validation effort, we compared the arithmetic mean of the results of the three models discussed above, which were randomly assigned, with a model that uses *umi*'s default schedules as its input. This analogy showed that the total energy consumption of our refined model is down by nearly 9% in comparison. This translates into a 19 kWh/m² gap between the two models (Figure 8). Therefore, since we believe our model is representative of the sample's behavior, this rather simple but crucial adjustment had been a big step towards bridging the gap between simulation results and actual energy use of residential buildings in existing urban neighborhoods. This finding also has the connotation that if those predefined schedules had been used instead, our predictions would have been far off from reality.

Finally, it has been suggested before that there are three major dimensions of model resolution: (1) temporal, (2) spatial, and (3) occupancy [9]. Comparing our presented model against these evaluation criteria, it can be seen that we were able to maintain a relatively high level of temporal, spatial and state resolution for generating our occupancy profiles without jeopardizing the overall simplicity and practicality of the model.

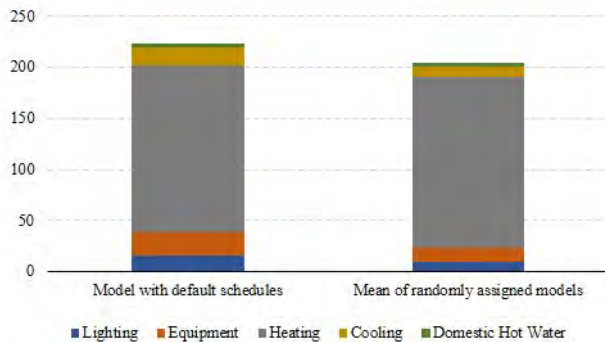


Figure 8. Total energy consumption comparison (normalized kWh/m²).

5 CONCLUSION AND FUTURE WORK

This paper describes a technique to develop occupancy schedules for residential neighborhoods based on their unique behavioral and demographic characteristics. Our primary goal was to balance between accuracy and complexity of occupancy data. This was achieved by taking advantage of a sophisticated Markov chain transition probability model based on the ATUS and refining its outputs according to the project specific collected data. An initial investigation of the developed technique in a pilot case study showed a 9% reduction in annual energy consumption of an urban residential neighborhood, when compared to using the selected software's default occupancy schedules. Since our schedules are developed to be representative of our sample's behavioral pattern, one may consider this effort as a step towards bridging the gap between the predicted and actual energy use of urban models. Current limitations of the proposed technique are related to the missing validation with actual metered energy consumption data. Future studies can use aggregated energy use data per zip code provided by the utilities companies to address this shortcoming. At last, the developed methodology and resulting preliminary data can serve as communication tools for community outreach and become the basis for developing more relevant neighborhood specific retrofit strategies in the future.

ACKNOWLEDGMENTS

This work was funded by the 2016 Iowa State University Presidential Interdisciplinary Research Initiative (PIRI) on Data-Driven Science.

REFERENCES

1. Abu-Sharkh, S., Li, R., Markvart, T., Ross, N., Wilson, P., Yao, R., ... Arnold, R. (2005). *Microgrids: distributed on-site generation*. Tyndall Centre for Climate Change Research.
2. Abushakra, B., Sreshthaputra, A., Haberl, J. S., & Claridge, D. E. (2001). *Compilation of Diversity Factors and Schedules for Energy and Cooling Load*

Calculations, ASHRAE Research Project 1093-RP, Final Report.

3. Cerezo, C., Dogan, T., & Reinhart, C. (2014). Towards standardized building properties template files for early design energy model generation. In *Proceedings of the ASHRAE/IBPSA-USA building simulation conference*.
4. Grasshopper: Algorithmic Modelling For Rhino. (n.d.). Retrieved from <https://www.grasshopper3d.com/>
5. Iowa State University. (n.d.). ISU Sustainable cities. Retrieved from <https://sustainablecities.cber.iastate.edu/>
6. Iowa State University Planning Team. (2014). *Capitol East Neighborhood Plan 2014*.
7. Janda, K. B. (2011). Buildings don't use energy: people do. *Architectural Science Review*, 54(1).
8. Mahdavi, A., Lambeva, L., Mohammadi, A., Kabir, E., & Pröglhöf, C. (2007). Two case studies on user interactions with buildings' environmental systems. *Bauphysik*, 29(1).
9. Melfi, R., Rosenblum, B., Nordman, B., & Christensen, K. (2011). Measuring building occupancy using existing network infrastructure. In *Green Computing Conference and Workshops (IGCC), 2011 International*. IEEE.
10. Menezes, A. C., Cripps, A., Bouchlaghem, D., & Buswell, R. (2012). Predicted vs. actual energy performance of non-domestic buildings: Using post-occupancy evaluation data to reduce the performance gap. *Applied Energy*, 97. <https://doi.org/10.1016/j.apenergy.2011.11.075>
11. Reinhart, C. F., Dogan, T., Jakubiec, J. A., Rakha, T., & Sang, A. (2013). Umi-an urban simulation environment for building energy use, daylighting and walkability. In *13th Conference of International Building Performance Simulation Association, Chambery, France*.
12. Richardson, I., Thomson, M., & Infield, D. (2008). A high-resolution domestic building occupancy model for energy demand simulations. *Energy and Buildings*, 40(8).
13. U.S. Energy Information Administration. (2018). *Annual Energy Outlook 2018: with projections to 2050*.
14. Yan, D., Hong, T., Dong, B., Mahdavi, A., D'Oca, S., Gaetani, I., & Feng, X. (2017). IEA EBC Annex 66: Definition and simulation of occupant behavior in buildings. *Energy and Buildings*, 156.
15. Yan, D., O'Brien, W., Hong, T., Feng, X., Gunay, H. B., Tahmasebi, F., & Mahdavi, A. (2015). Occupant behavior modeling for building performance simulation: Current state and future challenges. *Energy and Buildings*, 107.

Designing Urban Futures

Environmental Data and Land Use: Integration of Site-Specific Ecology and Urban Design 105

Claudio Campanile and Shih Hsin Wu

How to Generate a Thousand Master Plans: A Framework for Computational
Urban Design 113

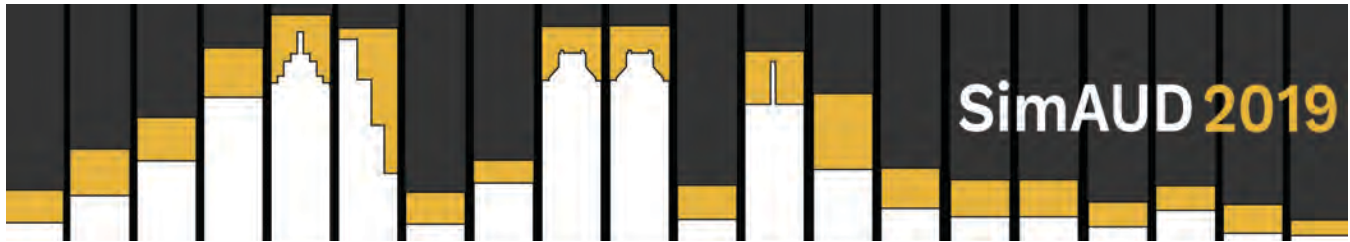
Luc Wilson, Jason Danforth, Carlos Cerezo Davila and Dee Harvey

CityFiction – Scenarios for Densification 121

Henrik Malm and Petra Jenning

Exploring Urban Walkability Models and Pedestrian Movement Trends in a
Vancouver Neighbourhood. 129

Nicholas Martino, Cynthia Girling and Edja Trigueiro



Environmental Data and Land Use: Integration of Site-Specific Ecology and Urban Design

Claudio Campanile and Shih Hsin Wu

Architectural Association School of Architecture
London, UK

{claudio.campanile, shih-hsin.wuu}@aaschool.ac.uk

ABSTRACT

The aim of this research focuses on how site-specific environmental data and programme-defined relationships (land use and their relation) can work collaboratively to design an integral ecological urban fabric. The paper presents a work flow applied to a case study and is formed by three main parts: data collection and elaboration, land use pattern generation and design development for critics and insights. The case study consists of a design proposal for a city for 40,000 dwellers located along the South coast-line of Isle of Grain, UK. The area is mainly made up of marshlands and the project is envisioned in a near-future scenario in the likely event of land shortage and sea level rise. In the first part, design parameters such as areas and functions for hypothetical energy, food and site protection needs are defined. At the same time, environmental data is gathered for tide frequency, topography and water speed. A suitability-based evaluation criterion is introduced to relate land use and environmental conditions at a specific location within the site. In the second part, we investigate two methods for generating design options of land use distribution. As both methods rely on neighbour conditions, a principle of the cellular automata algorithm (CA), their implementations deviate fundamentally from CA, such as that all the land-uses generated within an iteration are quantitatively defined as a design parameter. The first methodology is based on a growing system, while the latter on a competing system. In the third and last part of the workflow, we select and carry forward one generated land-use pattern due to specific evaluation criteria and develop the design at urban scale: different building plots' morphologies are generated depending on their location and degree of clustering. We conclude with critics and potentials, such as the applicability at different scales.

Author Keywords

Environmental Data; Urban Ecology; Generative Design; Land Use Optimisation; Cellular Automata; Growing System; Agent System; Processing; Grasshopper3D.

1 INTRODUCTION

As the impacts of global population growth and climate change increasingly threaten the subsistence of human being, the issues of land consumption and new settlements design increase of significance and urgency. To address such issue, more settlement designs have been considering using lands with high environmental pressure to solve the problems aforementioned. On the other hand, as we are in the century with readily accessibility of data, it is sensible to incorporate it to enhance the performances and efficiencies of targeted design scopes. Upon the convergence of those two scenarios, the paper takes a field of wetland in Kent, south of England, as a case study site to propose a new approach of settlement design, utilizing environmental data as a primary drive to cope with land-use distribution and spatial formation.

Speaking of design engagement with environment, especially within wetland, several existing settlements, such as villages with polders in The Netherlands and the Marsh Arabs in Iraq, can provide advisable approaches about how we can deal with water with different infrastructure or how the design can be subtly integrated into landscape with adaptation to different water condition. However, taking Marsh Arabs as an example, such settlements are either developed spontaneously without any contemporary regulations or relatively low-density with homogeneous land-use types. Apparently, such qualities could not meet the requirement of creating future settlements, as the course of how to integrate environment, land-use, and architectural morphology becomes imperative.

Therefore, the complexity that new settlement design have been facing requires a shift of design paradigm, where the integration of data comes into play. The computational work flow proposed in acquisition, data processing and spatial formation. By such, the system cannot only process the inter-related inputs including the environmental and social ones, but also perform adaptiveness to surroundings and compliance to local spatial relationship. Moreover, such approach expresses scalability for different scales.

2 STATE OF THE ART

One of the first prominent criticisms of urban zoning came from Jane Jacobs with her attack to “Orthodox Urbanism” [8]. It focuses on “four generators of diversity” that “create effective economic pools of use”: mixed primary uses, short blocks, buildings of various ages and states of repair, and, density. Jacobs, with her organicist conception of the city helped to re-frame how cities are both planned and interpreted. Through mixed-used approaches, cluster development and complete communities are fostered through a transit-oriented development, smart growth and the creation of activity centres.

Jacobs’ work, however, focuses more on the city *per se*, whereas the pure relationship between the city and the environment is encompassed by Urban Ecology. Here, any temporal yet socio-economical aspects aren’t part of the discipline. However, later, Jay Forrester developed his “Urban Dynamics” [5], posing his model on the temporal dynamics between socio-economics and residential location. However, any spatial aspects and proximity rules, such those of geography such as Waldo Tobler’s (“everything is related to everything else, but near things are more related than distant things”)[18], were neglected. Therefore, many urban models[1,2,19] rely on the structure proposed by Lawry [12].

Lately, as Koenig et al. reports in their System Dynamics for Modelling Metabolism Mechanisms for Urban Planning[11], there is a segregation of tools for urban planning which creates a gap between general purpose frameworks, such as Netlogo and AnyLogic, and GIS-based systems which are scarcely used due to their “lack of flexibility required for creative urban planning and design”. Moreover, scarce applicability to direct urban planning is evidenced [9,10]. For this research, we focus on environmental pressures and programme-defined functions for a new settlement, which does not consider any pre-existence. This has the scope to run a first test over the applicability of our methodology, then to be potentially applied to more ‘layered’ and complex scenarios, reflecting the increasing availability of data from various source [14], as well as its regulation [20].

Within our workflow, we use two main frameworks at three different stages. For the initial data wrangling, as well as the final urban design phase, the parametric visual programming tool Grasshopper for the CAD system Rhino3D developed by David Rutten. For the urban simulation, the Processing IDE [15]. The first, allows for highly efficient flexibility and interoperability with other software (such as GIS) to wrangle the environmental data relevant to our case study; then, Grasshopper enables us to define a custom Informed Terrain Model (ITM). On the other hand, Processing ensures typical advantages of Object-Oriented Programming (OOP) to write our models and provides an immediate visualization of the results. Then, as a Java-based platform, it is suitable for computationally expensive tasks, provides multithreaded computing, and, ultimately, can be seamlessly exported to professional IDEs such as Eclipse.

It is worth mentioning that per our scope, we lay down a work flow focusing on a case study but looking at its scalability for different scopes. This unlock the potential to asses project-specific data as well as the relationships between the elements of a predefined design programme. More specifically, as our system relies and implement a fuzzy logic, its output requires to be validated against the initial site-specific environmental conditions as well as criteria which are not directly expressed in the design phase, such as the centrality analysis of the generated urban pattern.

3 DATA PREPARATION

To ensure the integral formation of urban fabric, two sets of principles from the global and local scales should be defined respectively. On the one hand, it is of significance to ensure holistic efficiency and performance of the settlement; thus the environmental data across the site become the primary focus to address. As such, the settlement can grow or progress toward areas which are more suitable for the defined land-use types. On the other hand, no settlement can be formed without consideration of its own spatial structure. Accordingly, the local relationship between different land-use types should be stipulated. As the whole system relies on the integration of two scales, the following sections will keep elaborating on both to present a collaborative mechanism between them. The work stream of how the data is prepared for the further computational modelling is as such:

1. Design requirements and ambition from the site

The design proposal aims at fulfilling a self-sufficient settlement. Accordingly, it will address the issue of buildings and urban plots as well as the integration of productive fields. Hence, the three land-use scopes, living spaces, environmental resources, environmental protection, are proposed and break into 8 land-use types (residential area, public space, reeds’ bed, water reservoir, mari-culture, tidal energy, surge barrier, noise barrier). With a total area proposed for a settlement of 40,000 inhabitants [7,17].

2. Data acquisition and site representation

To rationalise the acquired data throughout the site, a grid-based system is adopted, thus the site is discretised by cells (100 x 100 m).

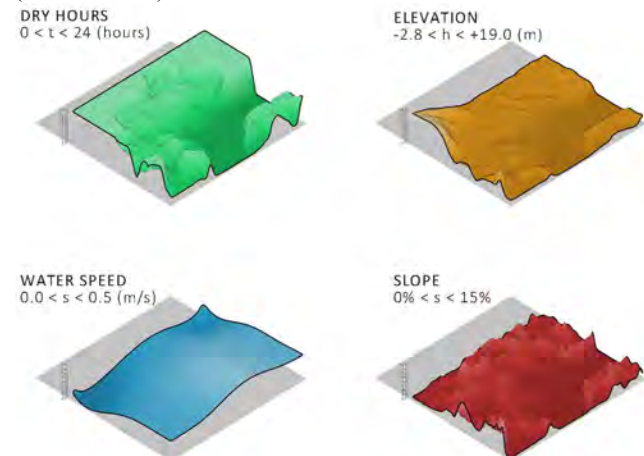


Figure 1. Environmental data throughout the site.

	BUILDING		PUBLIC SPACE		TIDAL ENERGY		WATER RESERVOIR		MARI-CULTURE (OYSTER)		REED BED		SURGE BARRIER		BUFFER ZONE	
	Data	Scoring	Data	Scoring	Data	Scoring	Data	Scoring	Data	Scoring	Data	Scoring	Data	Scoring	Data	Scoring
A.	13	(5-0)	X>20	0	X<1	0	X>20	0	X<12	0	X>20	0	X>15 X<9	10	X>23	0
Dry hours (Hr)	<x<24															
	0<x<12	10	12<X<20	(5-0)	X>=1	10	0<X<20	10	X>=12	10	0<X<20	10	12<X<15	(0-5)	X<22	10
			X<12	10									9<X<12	(5-0)		
B.	0<x<10	(5-0)	0<x<10	(5-0)			X>5	0			X>2	0	-5<X<5	0	0<X<10	(5-0)
Elevation (m)	x<0 ,	10	x<0 ,	10			0<X<5	(5-0)			0<X<2	(0-5)	X>5	10	X<0	10
	x>10		x>10												X>10	0
							X<0	10			X<0	10			X>10	0
C.	0< x	(0-5)	0<X<4%	(0-5)			0<X<4%	(0-5)			0<X<2%	10	X<1%	2	X>0.15%	0
Slope (%)	<8%															
	x>8%	10	X>4%	10			X>4%	10			X>2%	(0-5)	1X<2.5%	(2-0)	X<0.15%	10
													2.5<X<6%	(0-5)		
													X>6%	10		
D.					X>0.35	0			X>0.35	0						
W. Speed (m/s)					X<0.35	10			X<0.35	10						
RANKING	$(0.3*A)+(0.3*B)+(0.3*C)$		$(0.3*A)+(0.3*B)+(0.3*C)$		$(0.5*A)+(0.5*D)$		$(0.3*A)+(0.3*B)+(0.3*C)$		$(0.5*A)+(0.5*D)$		$(0.3*A)+(0.3*B)+(0.3*C)$		$(0.3*A)+(0.3*B)+(0.3*C)$		$(0.3*A)+(0.3*B)+(0.3*C)$	

Table 1. Sequential placement of programmatic units. The first formed household (a1-a8) performs a horizontal distribution.

Four environmental parameters, elevation[4], tidal frequency[3], slope[4] and water flow speed[3], are extracted and stored at each cell location to generate likewise sets of environmental data patterns throughout the site. The data sources referenced are publically accessible and free of use. The next step is to calculate the land-use specific suitability.

3. Land-use suitability and data wrangling

In order to convert the raw environmental data into ones that can be readily used in the later stage, a set of mathematical functions are required to relate the data with land-use types. As a result, we give scores per land-use, namely suitability values, throughout the topography: the multiplication of environmental and land-use-specific parameters (Table 1).

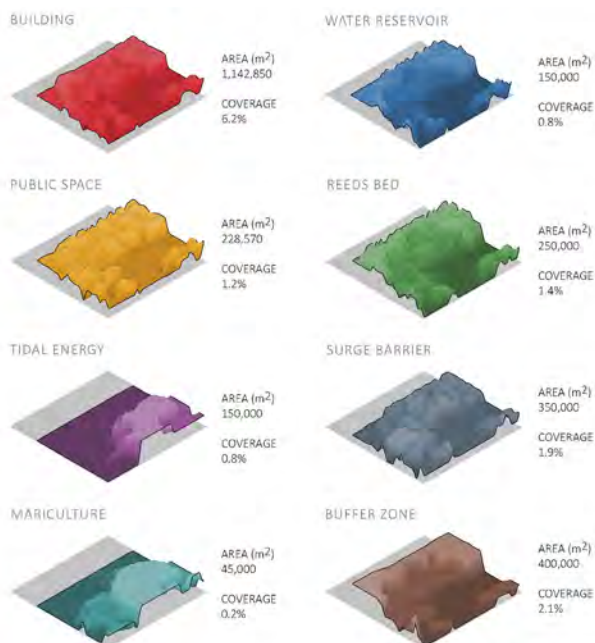


Figure 2. Suitability, area and site coverage for each land-use: the higher, the better suitability.

Similar to the environmental data, each of the land-use suitability is visualized throughout the site with differentiated height (the higher, the better) and saturation (the brighter, the better) depending on the scoring system aforementioned (figure 2). It is immediately noticeable that most of the charts present many local optimums. Finally, the suitability diagram (figure 3) shows the first and second most suitable land-use at each position and gives insights of the final land-use distribution.

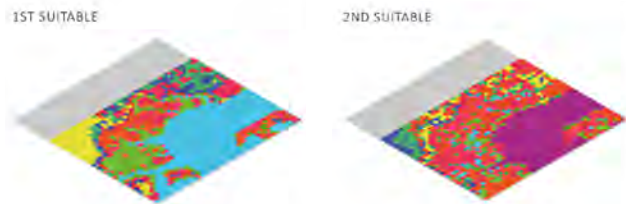


Figure 3. Optimal suitability diagram.

3.1 Local Assembly Logics

As the mechanism of how the data is processed and linked with the site is explicated, this section will elaborate on the stipulation of spatial relationship between the defined land-use types. To ensure the creation of land-use pattern afterwards, two primary rules dictating the local relationship of each land-use type should be conformed to: 1) cluster formation (self-aggregation) and 2) proximity level of different land-use types. Such relations are (figure 4):

1. All the land-use types self-aggregate, except for public spaces.
2. Building, public space, water reservoir and reeds bed should express geographical proximity to form the primary living area.
3. Surge barrier and buffer zone should be arranged closely to the core living area.

- Mari-culture and tidal energy self-aggregate for efficiency purposes.

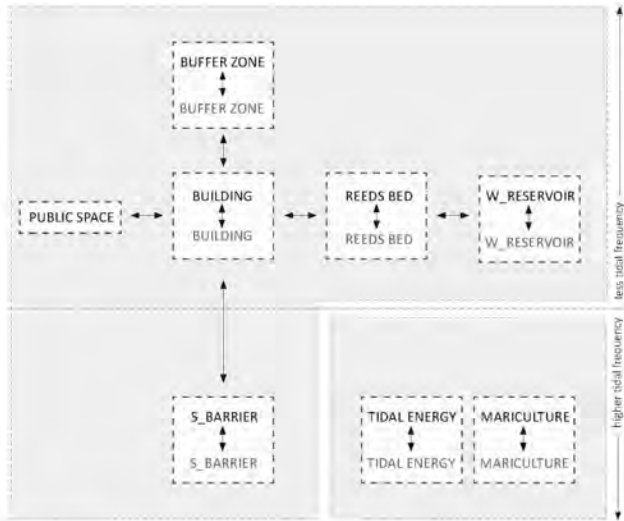


Figure 4. Local assembly logics: self-aggregation and proximity

As the rules on both global and local scales are defined, the following approaches of land-use modelling, though different in computational techniques, can share the same principles to develop variant outputs. On the global scale, the land-use suitability will drive the overall land-use distribution throughout the site. Whereas, on the local scale, the assembly logics between different land-use types will lead to desirable spatial structures. With the collaboration of two forces, the integral urban fabric can be finally proposed.

4 COMPUTATIONAL MODELS

The generation of a land use pattern as an integral urban fabric is “a multi-criteria decision making problem” (MCDM) [13]. A CA is a discrete dynamic system composed of a set of cells in a one-or multidimensional lattice. “The state of each cell in the regular spatial lattice depends on its previous state and the state of the cells in its neighbourhood” [13]. For our case study, the state of a cell (8 land-use types, plus empty cell) leads to $9 \times 9^8 = 387,420,489$ combinations to be modelled, accordingly to the Moore neighbourhood.

Here, we had to overcome such complexity to lower down the reciprocal-position rules. This can be done by skipping all the non-relevant combinations by programming explicitly the ones that matter to the design scope. By looking at the pattern to be generated, not all the possible combinations are relevant. In fact, the quantity of land-use types must be constant by design scope. Even though such a condition is satisfied, it is not possible, nor useful to explore all the possible combinations, therefore we developed our models as two fuzzy systems, to then compare them. Before arguing why two, it is worth summing up the steps both should go through: perception of the suitability data, generation of a (small) range of possibilities, decision and action. Fundamentally, such a process can be performed in two ways

as such are the system’s states, which open to different computational logics as well as emergent behaviours:

Full observation of a state of the system: the land-use cell location depends on the best available suitability and on the cells deployed at a previous stage. This requires the process to drop one cell at each step.

Partial observation of a state of the system: each land-use cell competes for the most suitable position within its surrounding area, until it finds a better one. Relative positioning interferes with the process, fostering self-aggregation. This process is run in parallel between all the cells.

4.1 Growing System

In this section, a computational model performing sequential growth will follow the principles stated as such:

- The entire system starts from one point (cell).
- The local relationship between each land-use type relies on the sequence of placement.
- The system has the tendency to grow toward more suitable location throughout the site.
- After the numbers of each land-use type placed in the cells consist with the initial given numbers, the growth is terminated.
- The partial unpredictability of the final growth pattern is derived from the stochastic growth of each land-use cluster within a given boundary.

The system’s rules apply with a hierarchical scale: the local, the regional and the global scale.

The local rule implies the simplest rules applied to a single land-use, which are 1. the next growth step, 2. the stochastic growth of land-use patch within a given domain and 3. The land-use patch can detect the occupied cells and avoid growing toward them. (Figure 5). As the rules elevated to the regional level, namely the interaction between types of land-uses, the design intentions come in. One attribute of the system is that the growth is performed per living cluster where the regional rules lie. The design intention here is to create a residential cluster where building plots will be

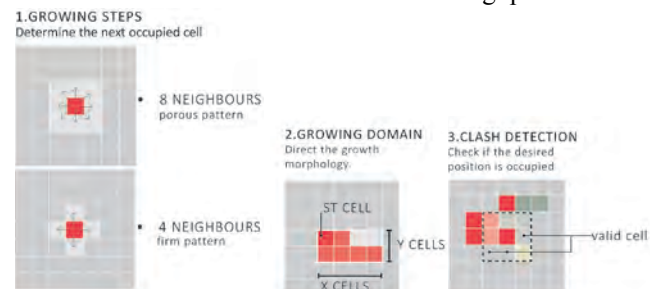


Figure 5. Proximity rules driving the growth locally.

arranged around the centre cluster of reeds bed and water reservoir and the public space will be the interface between reeds bed cluster and the building plots. Moreover, once the growth of a residential cluster is done, the domain regarding the starting cell of next residential cluster will be defined,

and eventually based on which cell contain the best suitability value of building land-use type, the new starting cell will be determined (figure 6). As mentioned before, the new starting cell of residential cluster will depend on the suitability of the building land-use.

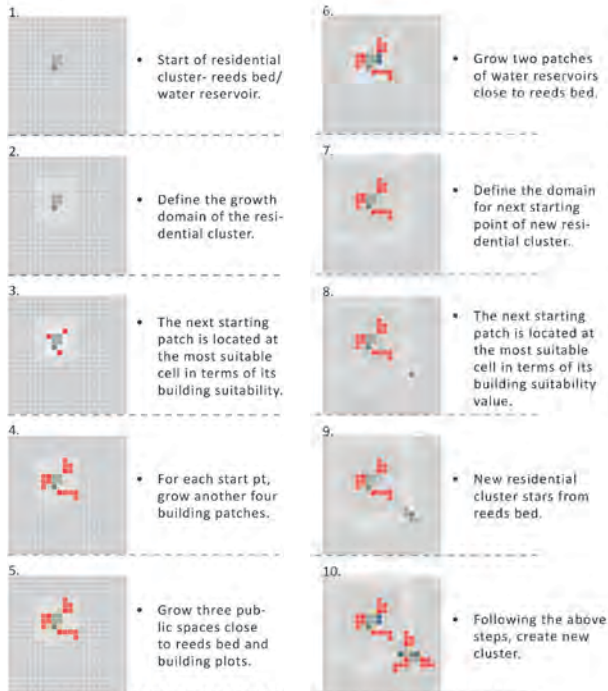


Figure 6. Sequential placement of land-use types

That is, as the procedure iterates over times, the clusters will grow toward the suitable location which meet the global requirement-the location control regarding the suitability values of different land-use types. As the growth of primary area-residential clusters finishes, the peripheral land-use types (buffer zone, surge barrier and tidal energy) will be placed. Different to the growth of primary living cluster, the growth of those peripheral land-uses takes the eight neighbours growth domain (Figure 5), resulting in a pattern with more porosities as compared to those within living area.

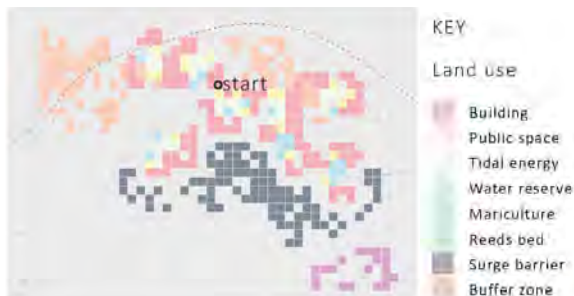


Figure 7. One of output patterns utilizing growth system

Conclusion

With the implementation of the growing system, the final land-use distribution, particularly in the living area, features a clear spatial structure- that the building plots always surround reeds bed (and water reservoir), and form the

continuity between different clusters (Figure 7). Noted that the end result shown here only represents one of possible final land-use patterns given the stochastic growth within the defined boundary as forming each land-use patch.

Yet, as the system lacks the flexibility to vary numbers of land-use types within different residential clusters, the overall land-use pattern appears rather homogeneous without differentiation in density of land-use patch according to different suitability values across the site.

4.2 Competition System

The second model is based on suitability-based competition between land-use patches as well as rules which defines their reciprocal positions. In comparison with the previous model, this computational logic shifts towards a de-centralised decision-making process. In fact, each cell perceives the environment (suitability) and its occupiers (the other cells, in function of the distance), takes a decision and acts accordingly. Such three capabilities endorse it to be classified as an agent-based system [16]. Thus, the system logic here described is applied to each cell independently (in series on the list of cells, shuffled at every loop) to exhibit emergent behaviour due to their short-range relationships [n]. Here, three main relations are considered: 1) the cell and the ground (to address suitability), 2) the cell and its similar cells (same land use, to create same-use clusters), 3) the cell and other cells (different land use, to express the design intention of an integral urban fabric and to avoid zoning). This allows for a simplification of the above-mentioned four-hundreds millions of possible neighbourhood combinations.

For the first rule (figure 8, left), each cell looks for the most suitable position accordingly to its moving distance – equal to Moore’s neighbourhood.

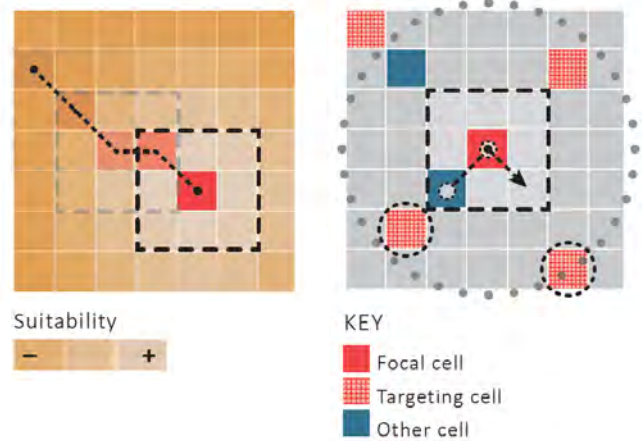


Figure 8. Cells and suitability (left), a cell and other cells (right).

For the second rule (figure 8, right), each cell looks up the similar cell at the most suitable position within a searching distance of ten cells (equal to 1km). A requirement for the system to converge to a solution and promote variation, an alternative route is provided if the cell finds an obstacle on its way. Finally, the third rule aims to foster an integral urban

fabric by providing attraction rules between different land uses, as per design intent. Here, the cells are programmed for looking for either their similar and/or another land use (fig. 8, right). The stepping distance is one cell position, while clash detection avoids land use overlaps (figure 9).

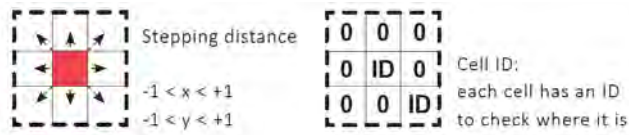


Figure 9. Stepping distance and clash detection system.

Here, some tests were conducted to come up with to a rate of the first rule (which regulates suitability) over the second and third rule (neighbourhood) regarding the model's convergence (figure 10). Tests over the suitability shown at the end of the simulation indicates experiment 2 as the best choice, albeit a sensitivity analysis should be required.



Figure 10. Variance of rate of relationship vs suitability rules (e.g. 25% suitability, 75% neighborhood indicates 1 loop applies suitability and 3 loops apply relational conditions).

For this specific method, a console has been developed to understand how the pattern evolves during time with charts relative to suitability conditions (figure 11). Here, two phases are noticed qualitatively and quantitatively.

- Phase A (steps 1 to 3) Within the first ten seconds of computation time, the cells rapidly gather together and form a cohesive group.
- Phase B (steps 4 to 6) Once the group is formed, the system requires time to adapt to suitability

characteristics as well as to form clusters that express those short-range relationships.

Qualitatively, this sharp separation is because during phase A each cell is less confined from moving around, while in phase B the compaction leads to the lack of moving possibilities. These two actions appear clearly in contrast.

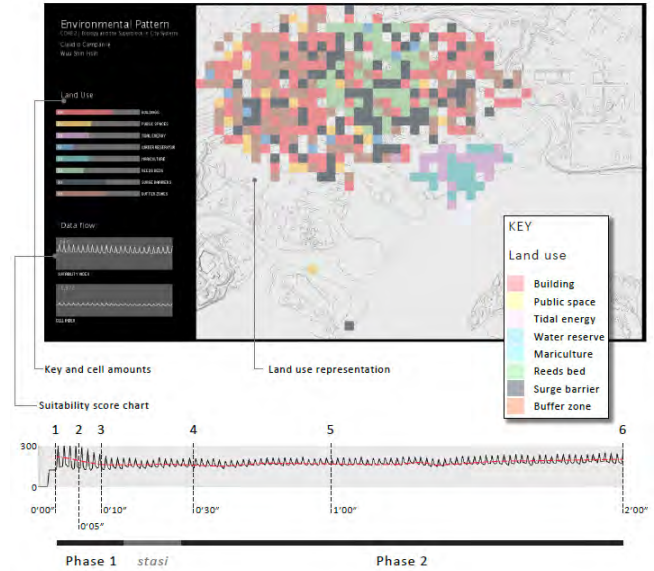


Figure 11. Console (above) and chart representing the cumulative suitability (all the cells, the higher the better) over time (2'00").

During the simulation, the console plots a chart of the suitability score, defined as the sum of all cells' score (the average in red). By comparing the quantitative data to the phases previously evidenced, we observe that, throughout the whole process, the trend is locally volatile. This is due to the alternate actions of the cells of moving alternatively to the most suitable position (the score increases, $\frac{1}{4}$ cases) or proximity cells (the score decreases, $\frac{3}{4}$ cases). By looking at the suitability score chart, phase A shows a remarkably volatile trend. Then, phase A and phase B are separated by a stasis in which the average does not change sensibly. Finally, phase B is characterised by a slow increase of the average.

Conclusion

To conclude, the patterns created need to be evaluated through a different method from the one that has been used to generate the patterns, namely the suitability value. By doing so, design potential as well as a direct comparison to the previous system used can be performed.

5 SYSTEMS COMPARISON AND URBAN DESIGN

Following the elaboration of the methodologies applied, the two systems are compared through two sets of quantitative criteria. Despite the similarities between them, such as the capability of generating various land-use patterns with responsiveness of environmental data, there are still several discrepancies consequent to their logic. 1. The two methods have a different evolution in time: while the competition

system has all the cells deployed throughout the process, this does not happen for the growing system. This requires a comparison at the end of the simulations. 2. The competition system create more compact land-use pattern than the growing system. 3. The growing system has more control over the land-use morphology, but it is also more rigid and difficult to program with several ‘if-else’ conditions. 3. Clear land-use clusters can be read in the growing system, whereas it is relatively vague in the competition system. 4. For each land-use type (can be observed at the design development stage), the competition system varies the density of cluster due to the differentiation of the suitability value, which is rarely achieved by growing system (figure 12).

5.1 Land-Use Pattern Evaluation

We want to investigate how the two system perform and pick one of the two outputs to proceed to design development. In order to assess the environmental performances, it is necessary to check again the results against our initial suitability criteria because both computational models rely on fuzzy logic. Then, the integrity of the pattern is evaluated through graph centrality’s betweenness. Therefore, two numerical values are introduced. The first one is the percentage of cells that present a suitability score above 50%, which has the scope of avoiding strongly unsuitable positions and measuring the effectiveness of the MCDM. The other value the node betweenness[6] from the graph, whose nodes are the building sites and public spaces, connected through a Delaunay triangulation. Thus, it is possible to compare the land use patterns against their potential for providing a space continuity and connectivity. After running 20 iterations per system, we pick the individuals at the 50% percentile. For the betweenness, the growing system present a modest better value (+5%), whereas the migration system reports better values for non-critic land use positioning (+13%) (Table 2).



Figure 12. Growing System, Competition System.

	Suitability	Betweenness (mean)
Growing	64%	205
Competition	77%	195

Table 2. Comparison: betweenness, satisfied suitability.

In fact, a high number of unsuitable cells would lead the process to fail, as this would require reconsidering entirely the environmental pattern at the design development. Thus, the output of the competition system is selected, albeit the pattern requires further investigation at the design

development stage to strategically inform the urban tissue with environmental conditions.

5.2 Procedural Design

A sample design proposal based on the land-use pattern generated by the competition system will be demonstrated. The building design is based on a primitive cell split as a sub-grid 3x3 and developed due to the suitability of each cell and their density gradient. Firstly, the building cells that stay on an unsuitable position (characterised by values of dry hours <51%) are developed as pile dwellings for this case, to facilitate water flow and respond to unsuitable conditions.

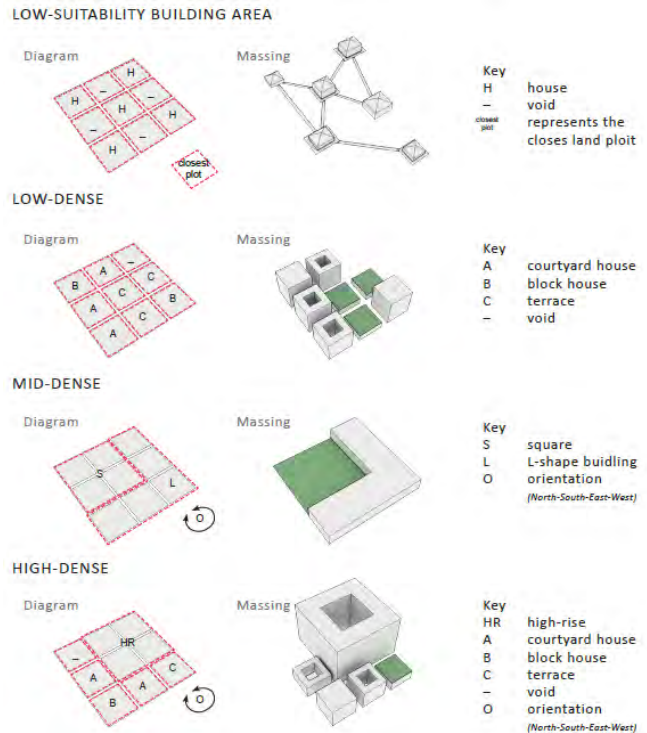


Figure 13. Building morphologies

Then, three building morphologies are developed according to the density of building and public space cells (Figure 13): (low-density) a 3x3 blocks which incorporates buildings and in-block common areas, (mid-dense) a secondary public space and presents a bigger open space and a low-rise building which surrounds it on two sides, (high-dense) a medium-high rise building plus low rise ones aside block’s common areas. Other land-uses are analysed against their suitability and developed accordingly (figure 14).



Figure 14. Procedural design based on the land-use pattern generated through competition system

6 DISCUSSION, CONCLUSION AND OUTLOOK

The simulations presented here are far from being realistic. The two computational models developed, the growth system and the competition system present both advantages and disadvantages. The former is a powerful tool upon strict or complex spatial stipulations, which can be demonstrated by the clear spatial structure of land-use types presented in the results. Yet, its rigidity and less efficiency on land-use distribution require further development. The latter, on the other side, presents stronger capability of integrating environmental data, which leads to more optimized and efficient distribution of land-use types across the site. Yet, given the fact that both systems allow for a degree of flexibility applied upon the process of pattern forming, leading to unpredictability of results, it is of significance to further prove the robustness of the proposed models via sensitivity analyses. Thereby, the systems' capacities of addressing certain tasks can be verified and we can further understand the relationships between input and output variables in both systems. We mentioned at the beginning that the overall design research presents a work flow as approach of new settlement design via computational models and simulations, which can potentially more efficiently integrate natural environment, land-use pattern and building morphologies. Moreover, the research includes a good level of abstraction which introduces different level of spatial conditions at several steps. The approach itself can be applied at different scales, narrowing down from the city level to the district level, until the building scale.

REFERENCES

1. Batty, M. 2005. *Cities and Complexity: Understanding Cities with Cellular Automata, Agent-Based Models and Fractals*. Mit Press.
2. Batty, M. 2013. *The New Science of Cities*. The MIT Press
3. British Oceanography Data Centre <url: https://www.bodc.ac.uk/resources/delivery_formats/sea_level/ntslf_format/1>
4. Digital Terrain Model <url:<http://environment.data.gov.uk/ds/survey/index.jsp#/survey?grid=TQ87>>
5. Forrester, J.W. 1969. *Urban Dynamics*. MIT Press.
6. Freeman, L. (1977). A set of Measures of Centrality Based on Betweenness. *Sociometry*. 40:35&ndash, 41. DOI: <https://doi.org/10.2307%2F3033543>.
7. United Nations Task Team, 11 - Public Space, *UN-Habitat III issue papers*. III, 11 (2015).
url: http://habitat3.org/wp-content/uploads/Habitat-III-Issue-Paper-11_Public-Space-2.0.compressed.pdf
8. Jacobs, J. 1961. *The Death and Life of Great American Cities*. Random House.
9. Koenig, R. and Bauriadel, C. 2009. Generating settlements structures: a method for urban planning and analysis supported by cellular automata. *Environment and Planning B Planning and Design*. 36, 4 (2009), 602 - 624. DOI: <https://doi.org/10.1068/b34025>.
10. Koenig, R. and Mueller, D. 2011. Cellular automata-based simulation of the settlement development in Vienna. *Cellular Automata: Simplicity behind Complexity*. A Salcido, ed. INTECH 23-46.
11. Koenig, R. Bielik, M. Schneider, S. 2018. System Dynamics for Modeling Metabolism for Urban Planning. *Proceedings to SimAUD 2018, (2018)*, 293-300.
12. Lowry, I.S. 1964. *A Model of Metropolis*. Rand Corporation.
13. Malczewski, J. 2004. GIS-based land-use suitability analysis: a critical overview. *Progress in Planning*. 62, 1 (Jul. 2004), 3-65. doi:10.1016/j.progress.2003.09.002.
14. McKinsey Global Institute, 2016. *The Age of Analytics: Competing in a Data-Driven World*. McKinsey & Company.
15. Reas, C. and Fry, B. 2006. Processing: programming for the media arts. *Journal AI & Society*, 20,4 (Apr. 2006), Springer 526-538.
16. Shiffman, D., *The Nature of Code* (2012), Shiffman D.(2012).
17. The London plan (2016), Policy 3.5 Quality and design of housing developments. <url : <https://www.london.gov.uk/what-we-do/planning/london-plan/current-london-plan/london-plan-chapter-3/policy-35-quality-and>>
18. Tobler, W.R. 1970. A computer Movie Simulating Urban Growth in the Detroit Region. *Economic Geography*. 46, (1970), 234-240.
19. Wegener, M. 2004. *Urban Land-Use Transportation Models. GIS, Spatial Analysis and Modeling*. D. Maguire, M. Batty, and M.F. GoodChild, eds ESRI Press. 203-220.
20. Regulation (EU) 2016/679.



How to Generate a Thousand Master Plans: A Framework for Computational Urban Design

Luc Wilson, Jason Danforth, Carlos Cerezo Davila, and Dee Harvey

KPF
New York, USA
lwilson@kpf.com

ABSTRACT

The current process for the design of an urban master plan typically involves a team of architects and urban planners that conceive and develop a handful of schemes based on zoning requirements with the help of CAD software. They may intend for the plan to achieve a set of performance goals (economic, environmental, etc.), but quantitative performance analysis is rarely conducted early and consistently through the design process. This makes it difficult to understand the full range of approaches that are possible on the site, and the relative performance of each scheme. In order to best accommodate rapid urbanization while making cities more sustainable, livable, and equitable, designers must utilize quantitative tools to make informed decisions about their designs. Computational design techniques have been successfully used at the building scale to test numerous designs and quantify their performance, but are challenging to apply at the urban scale due to increased computational expense, difficulty in limiting inputs, and more stakeholders involved in the process. This paper outlines a methodology developed in practice for applying computational design at the urban scale through four steps: 1) Define Inputs & Design Space 2) Procedural Geometry Generation, 3) Performance Evaluation and 4) Analysis, Communication & Stakeholder Engagement to generate and test thousands of master planning scenarios.

Author Keywords

Computational Urban Design, Generative Urban Design, Master planning, Urban Planning

1 INTRODUCTION

Issues as diverse as population growth, transportation, and climate change, all present significant challenges for 21st century cities, and require an approach to urban development that is data-driven, iterative, and most importantly, engages the broadest possible audience of stakeholders. Unfortunately, the design tools traditionally available to the architects and urban planners shaping such developments struggle to integrate

these needs. In design practice, decisions regarding key urban performance drivers, such as land use, density, and building morphology [16], are often made by refining a small number of schemes, developed through manual iteration, without systematically analyzing the full range of possible designs and their performance implications.

This designer-led time intensive process, can hardly integrate the perspectives of the multitude of involved stakeholders with differing, and often misaligned objectives and expertise. Expert consultants, developers, planning agencies, city councils, community boards, and the general public all bring valid perspectives that must be synthesized into a coherent vision¹). The authors, through their practice, have worked on 28 master plans over the past 10 years and have experienced these challenges first-hand: key performance metrics must be agreed upon before meaningful design work can commence (a process significantly more complex at the urban-scale, compared with developer-driven, architectural-scale projects); the long timescale of master planning work requires adapting to shifting political priorities²); and the final product of the master planning process is not a finished urban form, but rather a series of rules which must be flexible enough to accommodate a range of future development scenarios. Practicing architects and planners require computational tools capable of evaluating performance goals based on the information available at each step of the development of a master plan, and communicating the impacts on those goals of any decisions regarding land use, density and form.

This paper introduces a flexible methodology for Computational Urban Design (CURbD) as a response to these limitations in current practice, details its application within the Rhino3d CAD environment for the design of a hypothetical district scale development, and discusses three case studies

¹The planning process in New York City includes the Community Board, Borough President, City Planning Commission, City Council and Mayor, in addition to the designers, consultants and client [9]

²The authors worked on the master plan of Hudson Yards in New York City: started in 1997, initial master plan released in 2001 [24], and last revisions occurring in 2009 [8].

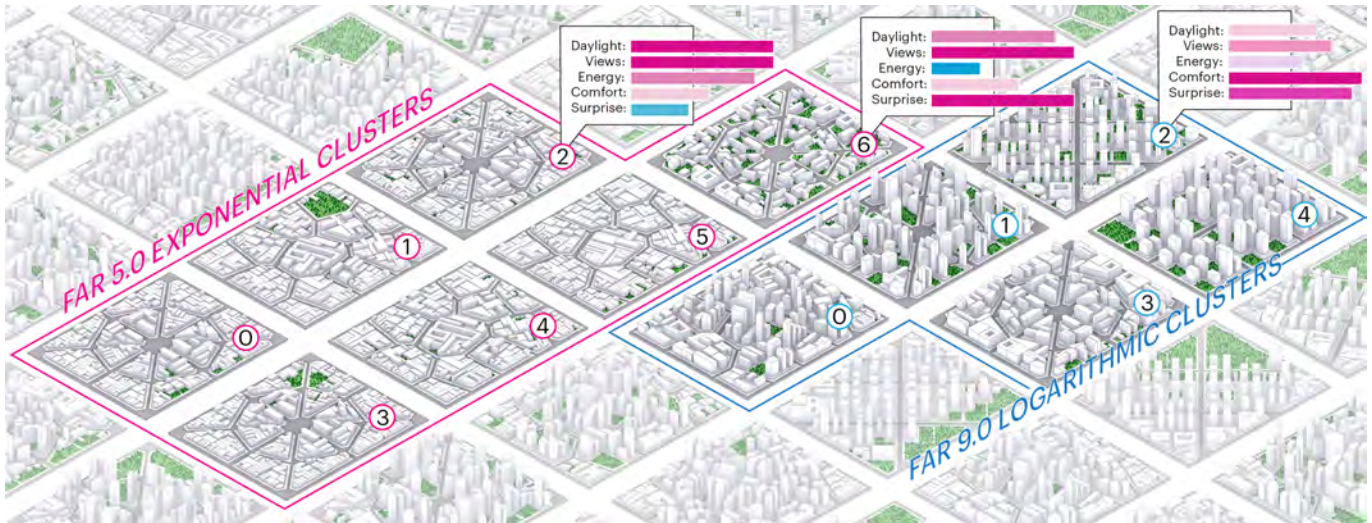


Figure 1. Partial design space of generated master plans, showing representative schemes for each cluster and scores associated with select clusters.

related to urban design and stakeholder engagement. The methodology, described in section 2, is structured in four main steps: 1) Input and Design Space Definition, based on generic data formats such as raster images and vector networks, 2) Procedural Geometry Generation of building and block types, 3) Performance Evaluation and 4) Analysis, Communication and Stakeholder Engagement, through visual interfaces and statistical models.

1.1 Related Work

In contrast to traditional approaches to design, where solutions are refined through manual iteration and experience, computational design methods take advantage of parametric CAD tools to explore larger design spaces. They are routinely utilized in architecture and engineering, typically for the optimization of discrete problems, such as building form and faade geometry for structural and environmental performance, and primarily to address the needs of a single stakeholder, the client [4]. More recently, parametric and generative computational models have been proposed as a tool for urban design and planning [12], [22], but their adoption in practice is still very limited [6]. Documented case studies mainly focus on modeling individual aspects of a design [19], rarely tackle the full scale of a master plan [18], and lack the geometric complexity required for their application in practice [3]. To address the problem of generating a sufficiently complex model out of easy to communicate design inputs at a sufficiently large scale, the method here presented proposes to use simple generic raster inputs, rather than full architectural models, to prescribe land use and density, a variation on the Cellular Automata approach to urban form generation by Batty et al [2]. A similar technique is proposed by Stouffs et al, in the design of large project representative of the full master plan scale often found in practice [23], and by Beirao et al [Beirao 2011] as a tool for interacting with a design team. However, the resulting modeling workflow does not offer a way to incorporate the necessary stakeholder engagement in an urban project.

In addition, most published computational methods are built around urban form optimization, a technique not well suited to accommodate the changing priorities of the many stakeholders involved in the planning process. Nagy et al, present one of the few examples where this approach is applied in practice, presenting a generative design case study for the planning of a multi block cluster optimized for profitability and solar energy generation [18]. While necessary for understanding technical requirements in an urban project, this and any similar optimization take on computational urban design suggests a zero-sum game that eventually benefit a single party [14].

An alternative solution to the optimization of multi stakeholder urban design projects is that proposed in the Urban Simulation Big Data" (URB) method [5]. In it, Cajot et al introduce a multivariate optimization algorithm attempting to balance the goals of all decision makers for the purpose of energy planning, and approximating their likely decisions once the design is complete. However, it still focuses on finding a single best design solution, rather than providing a sufficiently adaptive computational workflow that remains in use throughout an unpredictable, time-intensive master planning process [16]. The methodology introduced in the following sections, takes a different approach, by applying statistical analysis and interactive visualization tools to present stakeholders with families of solutions with distinct pros and cons. This approach, new in an urban application, has been proposed by Mueller for the exploration of structural design solutions as an alternative to pure optimization [15].

2 METHODOLOGY

This section provides an overview of the CURbD methodology, which can be executed by computational experts separate from the design team, or a computation designer embedded on the design team, with engagement from stakeholders at each step of the process.

1. Define Inputs & Design Space
2. Procedural Geometry Generation

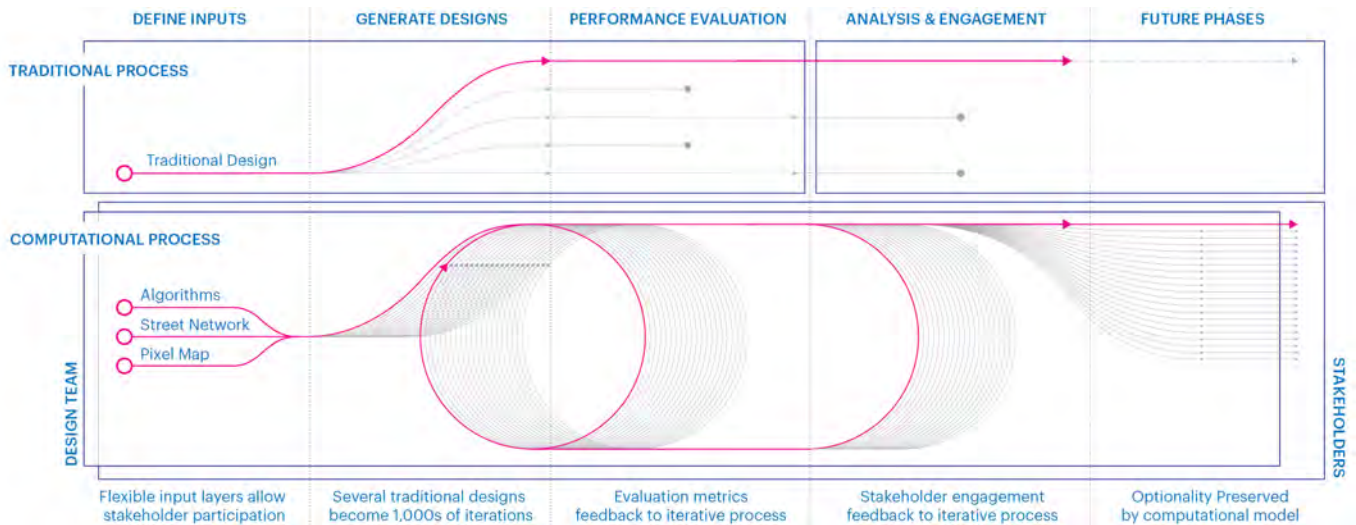


Figure 2. Comparison of traditional master planning process (top) with CURbD methodology (bottom).

3. Performance Evaluation

4. Analysis, Communication & Engagement

2.1 Inputs & Design Space

In the first step a set of input form related variables are defined to drive variation in a "design space" of thousands of master plan iterations³. Initial inputs are grouped in 2 streams that provide all necessary data for design variation while maintaining computational efficiency; one conveying use and density, and another varying street grid, block size, shape and orientation. If instead each building was defined individually by more complex inputs, the design space would quickly get too large to solve reaching millions of options for just one hundred structures⁴. A more complex variation of individual building sis tackled in the procedural modeling step.

The first input, the pixel map (Figure 3) represents a grid of points applied to the urban site, with each point storing attributes for use (e.g. "residential") and density (e.g. Floor Area Ratio (FAR) of 4). This map can be generated both computationally or by hand, sketching the combinations of density and uses to be tested, adding flexibility to explore different patterns through the site with minimal drawing work in an accessible format for non-designer stakeholders to contribute in. The second input, the street network (Figure 3) can also be generated analytically or manually, becoming a useful tool during stakeholder meetings where main streets(associated with a hierarchical traffic class and width) and block sizes can be discussed, and directly loaded into the CURbD model. As opposed to the latter procedural generation step, the specification of both maps requires input from the designers.

Once the pixel map and network are defined, pixels values are aggregated by block polygon defined by the streets. Pixel

³A design space is the combination of all input variables.

⁴If a master plan has 100 buildings, each with 2 inputs (ex. height and orientation) that would result in 2 to the 150 combinations. attributes are then assigned to the block with the closest centroid. For this process, the pixels dimensions must be small

enough so that blocks can contain a mix of uses and should be defined in advance. Next, density and use values are added together to get the total each use type within the block. Parks and open spaces are the only use treated differently, as they are aggregated to the blocks as a percent coverage of the total area (Figure 3).

2.2 Procedural Geometry Generation

Procedural generation allows for geometry with the complexity required in practice while maintaining a reasonably sized design space, by defining buildings based on dependant relationships rather than independent inputs. The procedural generation approach outlined in this section is representative of a large family of methods that have been applied in urban modeling in the past [13] [11], but offers a level of complexity appropriate for the application based on the authors experience.

In the proposed approach, after the aggregation of the pixel map within the street network, the blocks are split into parcels, by applying a readily available algorithm as part of the Decoding Spaces tool kit [1]. The size and shape of the parcels are generated procedurally based on the density and uses of the block or proximity to other elements of the plan, such as transit or landscape features. For example, low density residential may result in small parcels, while high density residential may result in large parcels. Once the parcels are generated, each one is allocated a portion of the density proportional to it's lot area. They are then populated with building types procedurally generated based on the shape of the parcel, density, and use(Figure 3). Building typologies for different densities are defined or sketched out in advance with stakeholders to include desired formal characteristics appropriate the project. in the experience of the authors, it is especially important to develop a library of generic low, mid and high density building types that can be modified for each project to avoid generating completely new procedural types. Each iteration resulting from this process is stored as a

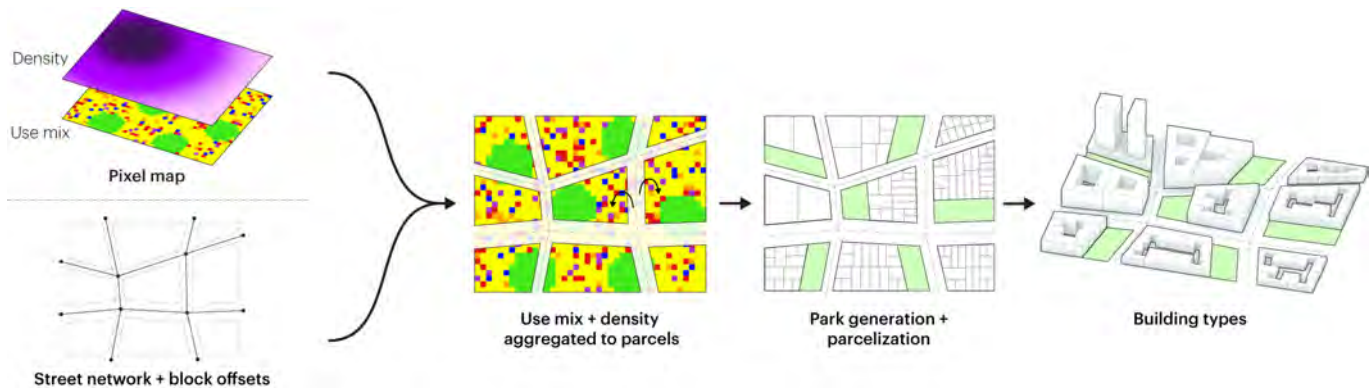


Figure 3. Inputs and procedural generation.

packaged file that includes pixel map, street network, blocks, parcels, parks, and procedurally generated 3D building geometry. Geometry generation is often much faster than performance evaluation, and separating the two allows the next step to be processed in batches distributed across multiple instance of the modeling environment of choice; in this case Rhino.

2.3 Performance Evaluation

Once the design space has been generated and the geometry exported, performance evaluation tools are applied on each iteration to produce a set of analysis metrics. Any type of evaluation (environmental, economic, mobility) can be used based on location specific data (climate, transit, real estate value, etc.) as long as the necessary geometry was generated by the procedural generation model.

Although exploring the optimal analysis tool for each possible urban performance metric is not the purpose of this paper, the authors have found in practice that it is best to select them based on the following criteria: First, tools and metrics should be chosen based on consultation with stakeholders and their specific goals. Second, performance metrics that have direct correlation (e.g. daylight access and views in buildings) should be avoided to reduce computation time while maintaining performance trends. Finally, and the converse to the previous point, metrics that are inversely correlated should be favored for a better understanding of the design (e.g. daylight access VS public space shading ratios). Working with performance tools and metrics at the urban scale produces a unique challenge due to the computation expense of simulation where hundreds of buildings are evaluated. Since CUrbanD generates many options for comparison, often relative performance is more important than absolute accuracy as the performance trends will remain the same in either scenario. Computational expense can be addressed by reducing the resolution of the simulation or through the use of proxies, such as the one for urban daylighting established by Dogan, et al. [10].

2.4 Analysis and Interpretation

Results produced by the evaluation tools are dense, multivariate, and challenging to disentangle. However, there are several analysis methods available that can derive actionable insights and drive the design process forward, all while engag-

ing the myriad stakeholders and conflicting agendas typically associated in large urban projects (clients, city governments, designers, and the public).

Filtering & Visual Exploration. The most rudimentary approach to analysis is to export results into a spreadsheet and sort the metrics for minima or maxima. This allows the user to filter out low performing options, but is insufficient for multivariate trends, and ineffective for graphic communication. Visual Interfaces, such as web-based data visualization tools like Core Studio's Thread [7] and Scout, which was developed by the authors, allows users to explore, sort, and filter the design space of iterations based on their relative performance. Scout features two interfaces that anticipate different levels of user sophistication. The first has a side menu containing sliders that allow the user to set the input values and view each iteration one by one. Metrics are displayed below the inputs so the user can understand the performance of one option at a time, hiding the complexity of the design space and making exploration more accessible. The second interface introduces a parallel coordinates plot that provides dynamic exploration, allowing users to set bounds for an individual metric, and then revealing the remaining iterations and their scores across the other criteria (Figure 4).

These tools quickly surface strong trends in the results, and engage a broad audience of non-experts in exploring the data. At the same time, the emphasis on accessibility and intuitive user experience does limit the sophistication of the analysis, particularly regarding weak, or inconsistent trends that hold for one subset of the data but dissipate elsewhere.

Correlation & High Performance Design Trends. Of the many tools available within descriptive statistics, Correlation Matrices produce a visual summary of the relationship between every parameter of the model, giving designers immediate insights into the association of each input (form) to each output (performance), as well as each output to each output (the association of inputs with inputs is predetermined by the design of the model). Rather than using a Visual Interface to filter through every value for a given input and tracking the results for each output metric, the viewer can simply scan across the relevant row in the matrix and see the numerical correlations. This approach can be used to establish a framework of performance-based design guidelines that can then

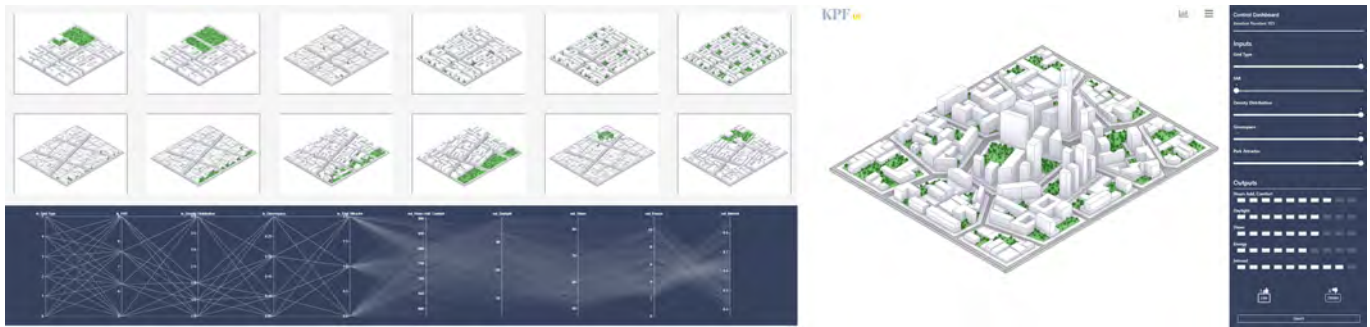


Figure 4. Scout parallel coordinate plots (left) and "explorer" mode (right)

be graphically communicated to the team, but is worse suited for engage non expert stakeholders (Figure 5).

Clustering & Establishing Design Schemes. Moving one step beyond performance-based guidelines, Unsupervised Learning (a subset of machine learning methods), allows the data-set to speak for itself [25], auto-generating trends based on myriad relationships in the results, both strong and weak. The most common form of unsupervised learning is clustering, which groups iterations together into coherent sets of relationships (i.e. a combination of particular inputs that lead to a consistent sets of results). Designers can then use each cluster as a starting point to direct the early stages of a project, or a family of similar urban solutions which can be easily communicated to stakeholders.

The Scikit-Learn implementation of the k-Means algorithm is both user-friendly and broadly applicable to computational design, but it is also fairly generic, and several steps should be taken to ensure meaningful results. First, breaking the data into subsets will generate more specific trends. These subsets can be based on whichever criteria is most relevant to the project, and since density (FAR) is the central driver of building typology in the CUrbD model (and a prime concern for cities and developers alike), it is used here to separate the data. Second, it is important to recognize that k-Means clustering will include every iteration in one of the clusters, so filtering out low-performing options will increase the clarity of relevant trends. Given that overall performance should be relative to all the evaluation metrics, this filtering can be accomplished one of two ways: either a "most-of-the-best" approach that applies an exponential function to identify candidates with the highest possible scores across the greatest number of metrics, or a "least-of-the-worst" approach that applies a logarithmic function to avoid candidates with low scores on any single metric. Lastly, k-Means does not determine the optimal number of clusters automatically, but this can be found by testing a range of options and solving for the best balance of the Silhouette parameter, which indicates the degree of separation between each cluster, and Distortion parameter, which measures the distance between each observation and the centroid of the cluster.

3 DEMONSTRATION

In order to demonstrate the CUrbD methodology, we applied it to a hypothetical, rectangular site with the climate

profile of Toronto, Canada, and produced a design space of 1,152 iterations. For the procedural generation of these iterations we used Rhinoceros, a computer-aided drafting program, and Grasshopper, which is a graphical scripting plugin for Rhinoceros [21] [20]. We augmented Grasshopper with python scripts to handle some of the more complex geometry and file management. The parcelization algorithm was supplied by the plugin Decoding Spaces [1].

Define Inputs & Design Space. In order to generate variation across the master plans, we varied 5 of the inputs (street network, density, density distribution, park space %, and park attractor), and applied a "brute force" method of cross referencing the variables in Grasshopper to ensure every possible permutation of inputs was tested. This is a markedly different approach than optimizing for top performing designs (i.e. using a genetic algorithm or similar method), and while it has a significantly higher compute time, it creates the potential for a far more engaging exploration of the results, particularly for a general audience whose design preferences are not known beforehand.

Some input values, like "street network" and "park attractor" are simply an index that tells the script to import manually drawn geometry. For instance, there were 6 options for the street network. Choosing one of the indices from the range 0-5 would determine which of these street networks would be imported. The same was done for the park attractor. The park attractors were simply geometry that the parks would cluster around. We used 3 park attractors: the first were dozens of points distributed evenly across the site to simulate a distributed park scheme, the second was a single point that would generate a centralized park, the last was a line along one edge of the site simulating a linear park. The rest of the inputs represented specific values that were communicated to the model. "Density" was the total FAR for the site. This was communicated to the pixel map by providing an even FAR across the entire site. "Density distribution" redistributed this density so that it peaked in the center of the site. The value for this input represented the ratio of the least dense pixel, to the most dense pixel in the center of the site. The park space % represented the percent of pixels that would be designated as park space.

Procedural Geometry Generation. We then ran the procedural generation algorithm on each design iteration to produce a design space. In order to demonstrate how buildings

could populate the site, we used a diversity of building types that we distributed based on 3 density categories. High density blocks were populated with either a tower/podium type, or a simple lot-line extrusion if the lot was too small. Medium density parcels were given either a courtyard building, or a simple extrusion if the lot was too small. Small parcels all received a simple extrusion with a rear setback. While these are the particular rules and building types we implemented for this example, the methodology is exible and can be implemented with any rule based building type and distribution logic. Once the procedural geometry generation was complete, we saved each iteration as CSV for the pixel map, json for the street network, and a 3dm file for blocks, parks, parcels, and buildings.

summary scores (both the most-of-the-best exponential score, and the least-of-the-worst logarithmic score) to filter out low-performing iterations; finally, we implemented k-Means clustering to group observations together into the most relevant trends allowing for categorization of high-performing and distinct design schemes.

The results for the 5.0 FAR clusters (Figure 1) show that while there were seven clusters, there were only three main trends: Clusters 1, 4, and 5 all had a low Density Distribution and the voronoi-based Grid 5, while clusters 0, 2, and 3 had a higher Density Distribution and the radial Grid 4. All six of these clusters had the lowest possible amount of parks (5%), and all six scored similarly across the evaluation metrics. This strongly suggested that the best performing low-density iterations would privilege Daylighting, Unobstructed Views, and Energy Efficiency, with above average scores for Outdoor Comfort, and low scores for Visual Interest. In terms of inputs, we could be confident that minimal parks, and either 1.0 Density Distribution / Grid 5, or 2.0 Density Distribution / Grid 4 would return the best results. Contrariwise, Cluster 6 provided an interesting alternative strategy to privilege Visual Interest and Views at the cost of Energy Efficiency, but it should be noted that it contained only a single observation out of the twenty represented across all seven clusters. This made it a much less robust trend, and therefore far less likely to preserve its performance as the final design inevitably deviates from the simplifications of the iterative model. Taken together, this data-driven analysis, combined with the 3-D geometry and visualizations produced by the model, provided clear design direction for any low-density scheme on this site, while preserving optionality and setting expectations for performance.



Figure 5. Correlation Matrix showing relationship between all inputs and evaluation metrics.

Performance Evaluation. For this study, we produced a score for each of the following: views, daylighting, comfort, energy efficiency, and visual interest⁵. For facade based evaluation tools, like views and daylighting, we created a grid of sensor points on each facade. Energy efficiency, which measures PV potential, generates this grid only on building roofs and the outdoor comfort tool produced a grid across the entire public realm. We then export the scores from each metric, along with their associated inputs, to a CSV of results that can be used for analysis.

Analysis. To analyze the results of the study, we followed the steps outlined above in the Methodology section: first we uploaded the results into a visual interface for initial exploration and testing⁶. Second we produced a correlation matrix to understand the fundamental relationships between features, and to either confirm macro assumptions, or identify areas of interest within the data; next we created subsets

To fully explore the trends, the k-means clustering process was repeated for each density (FAR 5.0, 6.3, 7.6, and 9.0) and for each scoring approach (i.e. the Logarithmic and Exponential methods). While it is beyond the scope of this paper to report on the full conclusions of this analysis, the results for the Logarithmic scoring of FAR 9.0 are included for comparison, and it is worth noting both the extreme variation in the geometry of each cluster, as well as the more balanced results (Figure 1.)

4 APPLICATION IN PRACTICE

This section illustrates the CURbD methodology through its application in three real projects, and outlines best practices for successful implementation.

A new district in Hangzhou. We used CURbD to create a design tool for a 620 acre master plan in Hangzhou, China to create a new mixed-use district. Here CURbD was used to address a discrete challenge in the planning process. Federal regulations require a minimum duration of direct sun on the winter solstice for residential units (two hours in Hangzhou). Typically, this regulation results in a modernist tower-in-the-park building type, making it difficult for the design team to achieve their intent to create smaller blocks, continuous street walls and narrower streets. To address this challenge, we defined inputs as a range of block size, street width, gross floor area, and street wall height resulting in a design space of

⁵Views= % unobstructed within a human field of view, Daylighting= Vertical Sky Component, Comfort= Universal Thermal Climate Index, and Visual Interest= visual spatial variation between adjacent sensor points.
⁶kpfui-scout.s3-website-us-east-1.amazonaws.com/SimAUD2019 of the data based on the density values; we then generated



Figure 6. Interactive interface for Sidewalk Toronto

7,400 options. (A pixel map was not used since it was a single use.) From those inputs we applied a procedurally generated a courtyard with towers block type, which was then evaluated for compliance with the direct sun regulations. We uploaded the results into Scout and provided the app as a tool for the design team. They used the parallel coordinates chart to filter for the desired inputs, such as street width and target GFA, and picked from the complying options. It allowed them to find solutions that achieved the kind of urban character they desired while meeting the regulations without defaulting to the tower in the park building type.

Stakeholder engagement for Sidewalk Toronto. Working with Sidewalk Labs, we developed a CURbD model to assist with the master planning of Sidewalk Toronto ⁷. As part of a public-facing exhibition at their Toronto workspace we ran the model for an abstract site with inputs that included a representative sampling of options under consideration for the waterfront development, as well as more experimental edges cases that featured lower and higher densities, abstract street grids, and ambitiously large green spaces. (The model was very similar to the example in the demonstration section and with the same performance evaluation criteria.) The results of this model were used for a physical interface that allowed the public to engage with the CURbD process (Figure 6). Visitors explored combinations of density, public space and street grids by toggling wooden knobs to change design inputs. This allowed users to create the type of neighborhood they wanted and to then understand how those design decisions impact the functioning of a complex system like a city, encouraging design and introspection in equal measure. For example, one participant started with the lowest population and the most green space (she wanted a backyard of her own), but quickly realized that this led to low scores for outdoor comfort and energy efficiency (two things she valued). By making a few quick adjustments she found an option that performed well for those two priorities. Looking ahead to future implementations, this sort of user engagement could also be recorded, aggregating participant feedback into implicit, qualitative metrics which could, in turn be used to drive further generation of additional design options. [17]

Technology Campus in Southern China. We applied CURbD in the design of a 30 million sq ft master plan (mostly RD and residential with some retail and event space) in a hot, humid city in southern China (the actual location and client are confidential). The application of the methodology happened in parallel with the design team. Ideally, the methodology is used prior to the design team starting on a project, which is often not possible. This example will outline approaches for application in the often not ideal circumstances that occur in practice.

To compliment the design as it developed in parallel to our work, we focused the analysis of the CURbD process on recommendations specific what was still flexible in the design scheme, such as changing massing orientation and program distribution in order to reduce solar radiation and decrease

⁷<https://sidewalktoronto.ca/>

average trip duration. To do this we established a combination of inputs that were computationally derived and manually drawn by the designers. Next, we developed procedural versions of the building types being developed by the design team. This allowed us to tailor design guidelines (using the correlation approach in section 2.4) to the design issues that could still change within in the design. When they integrated our guidelines into their scheme, they resulted in increasing outdoor comfort by 33.7%, decreasing average trip duration 24.7%, and decrease solar radiation on buildings by 15.2 % when compared to initial design.

As illustrated through application in practice, effective communication of the results of a CURbD can be difficult, but is crucial for it to have meaningful impact in the master planning process.

5 DISCUSSION & NEXT STEPS

5.1 Challenges

A challenge of this methodology that requires further work is the relationship between form and performance. At the building scale, if you change height, orientation, or location, the link to the resulting performance is clear. At the urban scale, performance is being analyzed across a heterogeneous urban fabric. This means different parts of the master plan can perform differently. When you distill the analysis of the master plan to a single metric, most of this variation is lost. For instance, in the same master plan there may be one group of short buildings which score poorly for the view score, whereas a group of tall, widely spaced buildings score extremely well. An average of these view scores would not reflect the variation of the site or the equity of the score. Further development of analysis tools will focus on addressing the spatial distribution of the performance evaluation.

Because the CURbD process is composed of algorithms, it would be a mistake to think that its unbiased. The range of values supplied for inputs could exclude certain possibilities that might be desirable to some stakeholders. One solution to limit bias is to provide a much larger range of options in terms of the inputs and logic upon which the model is built. Another solution is to solicit specific inputs from all stakeholder since

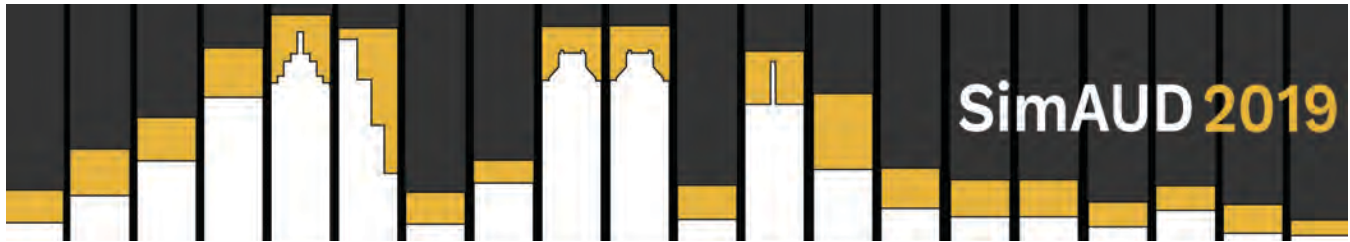
this methodology allows for manually generated inputs. The potential for bias also illustrates the need for design and judgment in the CURbD process and the active engagement in with stakeholders so that, while not every option is explored, the critical ones are represented.

6 CONCLUSION

While computational urban design shows much promise for providing an iterative, quantitative approach to master planning, its place within the master planning process remains in question. While we've shown how the CURbD process can generate useful insights in real projects, how these insights influence what actually gets built is unknown. These insights must be utilized within the complex, multi-stakeholder environment of both the design process, and the implementation of the master plan over the long term. As a result, computational urban design, at least initially, needs to work in coordination with the traditional master planning process. However, with the increasing challenges of population growth, transportation, and climate change, master planning must take advantage of iterative and quantitative approaches to urban design. A process such as CURbD provides an opportunity to navigate the myriad of seemingly contradictory constraints and stakeholder interests of a master planning project.

REFERENCES

1. Abdulmawla, A., Bielik, M., Buš, P., Mei-Chih, C., Dennemark, M., Fuchkina, E., Miao, Y., Knecht, K., König, R., and Schneider, S. *Decoding Spaces*, 2017.
2. Batty, M. Cellular automata and urban form: A primer. *Journal of the American Planning Association* 63 (06 1997), 266–274.
3. Beiro, J., Mendes, G., Duarte, J., and Stouffs, R. Implementing a generative urban design model: Grammar-based design patterns for urban design. *28th eCAADe*, pp.265-274 (09 2010).
4. Brown, N. C., and Mueller, C. T. Design for structural and energy performance of long span buildings using geometric multi-objective optimization. *Energy and Buildings* 127 (2016), 748–761.
5. Cajot, S., Schüler, N., Peter, M., Koch, A., and Maréchal, F. Interactive optimization for the planning of urban systems. *Energy Procedia* 122 (2017), 445–450.
6. Calskan, O. Parametric design in urbanism: A critical reflection. *Planning Practice & Research* 32, 4 (2017), 417–443.
7. Core Studio. Thread. <http://core.thorntontomasetti.com/thread/>, 2019.
8. Department of City Planning, City of New York. Hudson Yards. <https://www1.nyc.gov/assets/planning/download/pdf/about/press-releases/pr121201.pdf>, Jan 2009.
9. Department of City Planning, City of New York. Uniform Land Use Review Procedure (ULURP). <https://www1.nyc.gov/site/planning/applicants/applicant-portal/step5-ulurp-process.page>, Accessed: February 2018.
10. Dogan, T., Reinhart, C., and Michalatos, P. Urban daylight simulation calculating the daylit area of urban designs. *SimBuild 2012* (01 2012), 613 – 620.
11. Esri. Esri City Engine.
12. Fusero, P., Massimiano, L., Tedeschi, A., and Sarah, L. Parametric urbanism: A new frontier for smart cities. *Planum. The Journal of Urbanism* 2 (September 2013), 1 – 13.
13. Halatsch, J., Kunze, A., and Schmitt, G. *Using Shape Grammars for Master Planning*. 01 2008, 655–673.
14. Lindblom, C. E. The Science of “Muddling Through”. *Public Administration Review* 19, 2 (1959), 79–88.
15. Mueller, C. T., and Ochsendorf, J. A. Combining structural performance and designer preferences in evolutionary design space exploration. *Automation in Construction* 52 (2015), 70 – 82.
16. Mueller, J., Lu, H., Chirkin, A., Klein, B., and Schmitt, G. Citizen Design Science: A strategy for crowd-creative urban design. *Cities* 72, August 2017 (2018), 181–188.
17. Nagakura, T. *Acadia 2017*. Acadia Publishing Company, 2017.
18. Nagy, D., Villaggi, L., and Benjamin, D. Generative urban design: Integrating financial and energy goals for automated neighborhood layout. *SimAUD 2018* (06 2018), 25.
19. Rakha, T., and Reinhart, C. Generative urban modeling : A design work flow for walkability-optimized cities. *SimBuild 2012* (2012).
20. Robert McNeel & Associates. Grasshopper, 2014.
21. Robert McNeel & Associates. Rhinoceros 5.0, 2018.
22. Schnabel, M. A., Zhang, Y., and Aydin, S. Using parametric modelling in form-based code design for high-dense cities. *Procedia Engineering* 180 (2017), 1379 – 1387. iHBE Conference 2016.
23. Stouffs, R., and Janssen, P. *A Rule-Based Generative Analysis Approach for Urban Planning*. 10 2016, 125–136.
24. The Office of the Mayor, City of New York. Mayor Giuliani Unveils Plan For Development Of Far West Side In Manhattan. <https://www1.nyc.gov/assets/planning/download/pdf/about/press-releases/pr121201.pdf>, feb 2001.
25. VanderPlas, J. *Python Data Science Handbook*, 1st ed. O'Reilly Media, Inc., 2016.



CityFiction – Scenarios for Densification

Henrik Malm and Petra Jenning

FOJAB

Malmö, Sweden

{henrik.malm,petra.jenning}@fojab.se

ABSTRACT

The aim of the research presented in this paper is to find new ways of understanding and visualising relationships between different types of city data, and thereby support decision making regarding city growth and densification based on desires and values. To this end, a new software tool called CityFiction has been developed. This analysis tool is intended to work as a laboratory for understanding city data, and it will be shown that by interactively weighting, or prioritizing, different measures on the available input data, scenarios for the future development of a city can be efficiently and pedagogically explored. By using the city of Malmö, Sweden, as a pilot study, the tool has been applied to test the placement of e.g. new parks and train stations, and it has aided in the understanding of how the available city data interacts, and possibly conflicts, in the search for a sustainable development of the city.

Author Keywords

Data exploration; data visualisation; city analysis software; city growth; urban development; GIS.

1 INTRODUCTION

The amount of data that we collectively are creating and storing in the world today is doubling every second year, according to a recent analysis by IDC [1]. This enormous wealth of information can be of tremendous value, but can also be overwhelming when it comes to quickly parsing out relevant information and understanding how different data sources correlates, connects or conflicts.

With the increase in the implementation of Smart Cities and Smart Buildings, the rapid rate of data growth is especially true for our urban environments [2]. Here, data collected by sensors and by online devices is used to increase operational efficiency in the city, share information to the public and to improve the quality of government services and citizen welfare. Relating to this is the large increase in mapping of data and the availability of this to the public, like through well-known Google Maps [3] or by more advanced initiatives, such as computer vision driven dense city information mapping [4], or wiki-based open source initiatives [5]. However, most data collected and stored about

our cities is still not openly available and can be both difficult and expensive to obtain, although there exist initiatives to change this [6].

In the current work, the focus has been on city data that can be related to the fitness of an area for potential future urban development. This can be pure geometrical GIS data on the location of e.g. buildings, parks, roads and waterways, but also the density of inhabitants, the plot ratio and the location of different programs and services, such as offices, retail, schools, health centers etc. Sensor data on noise, pollution, traffic etc. is also of primary interest. At least for correlation, economic and social data, such as real estate prices or crime rates can also be relevant. The developed tool is fundamentally open to many different types of data, and can be adjusted to local scenarios and questions. Its big benefit is the capacity to efficiently and interactively find out in which way any kind of input data affects the results. The only requirement on the data is that there is a reasonable way of combining the different data sources to a single fitness value, which describes the suitability of urban development at a specific spatial location, according to the user's preferences.

2 BACKGROUND

The current work was initiated in collaboration with the city of Malmö in Sweden, regarding a visionary city development study on the city. Malmö is Sweden's third largest city and has during the last two to three decades gone through a rapid transition from an industrial harbour city to a city focusing more on education and culture. The city is evolving rapidly and the current project was specifically set up to study how Malmö could grow from its current approx. 300.000 inhabitants to 500.000 during the next few decades, preferably without too much development outside the outer beltway. This poses a major challenge, which calls for inventive approaches to city development and densification.

To this end, we have developed a new type of city data analysis software, which could aid the city planners in exploring different scenarios for developing the city, in order to host almost double its current number of inhabitants.

2.1 Related Work

The approach first researched, for the task at hand, was to create a computer simulation algorithm for city growth. This area has been studied extensively, with pioneering work on mathematical and computational modelling of land-use and urban growth already appearing in the late fifties and through the sixties and seventies [7, 8, 9, 10]. Many authors have since then continued this work, where especially approaches based on Cellular Automata (CA) has been a very active research direction. Influential work along these lines has been published by e.g. Clarke [11, 12] and Batty [13], with the latter also looking extensively at agent-based models and networks for city modelling [14].

Several authors have, along with their theoretical work, also developed and released software packages for land-use simulation, city growth and urban planning such as UrbanSim [15, 16], UrbanFootprint [17], FUTURES [18] and LanduseSim [19]. UrbanSim and UrbanFootprint are comprehensive city planning tools based on large mapped databases (currently mainly focused on the US). UrbanSim is mostly aimed for the real estate market and lets the user evaluate different transportation and land use policies. It also includes procedural city modelling. UrbanFootprint has advanced ways of filtering, visualising and analysing large amounts of available city data, where the analyses includes reports on e.g. transit accessibility or energy use for a set of plots given by the filtering. The user can also choose new programmes, such as parks, high-rise residential etc, for the selected plots and evaluate how this change affects the

analyses. In contrast to these tools, CityFiction is working with general areas instead of sets of plots, and is aiming mostly at larger masterplanning tasks and visions. Specifically, it works by finding suitable areas for new development when the user has chosen a certain weighting (or prioritisation) of different measures on the available data, and shows how new urban intervention affects these results. The weighting could for example be set based on what the city regards as its common values for a good residential area.

In LanduseSim, functions for the fitness for developing different programs at a specific spatial location is approximated, before a CA-based city growth simulation is run, however, it is not clearly documented how this is done in practice. In the current paper, the focus is on the creation and analysis of these kinds of fitness functions. By using the software presented here, we can input a large amount of data, make measurements on the data and then interactively design different fitness functions for different programs (e.g. residential or commercial). By the laboratory style of the program, users can easily understand how the data interacts to create different fitness landscapes. After finding reasonable functions for each studied program, a city growth algorithm could possibly be applied in order to see how the land use develop and change over time. However, this later stage is not the focus of the current paper. Both the creation of the fitness function and the succeeding program distribution simulation has been previously studied by the current authors, but then in the setting of program distribution in a single building [20].



Figure 1. The Graphical User Interface of CityFiction, with the Data Control Interface to the left and the Map Viewport to the right.

Another interesting, and related, area in urban analysis is the field of spatial statistics. Statistics of global autocorrelation, such as Moran's I index, or measures of local spatial association, such as Getis and Ord's $G_i(d)$ or Anselin's LISA (Local Indicators of Spatial Association) has been extensively used to analyse urban spatial patterns, c.f. [21,22,23]. These statistics could for example be used to together with CityFiction in order to measure the amount of clustering created by our weighted fitness function, or to compare the output of the fitness analysis with the spatial patterns of the actual current distribution of building programs and land prices. However, these approaches to spatial analysis lies outside the scope of the current paper.

3 THE TOOL

In this section, the developed tool will be presented in detail. The tool is a stand-alone executable program, however, currently there is a pre-processing and configuration step required before the program is run on a new set of data. The current section will start with a brief description of this first step, and then give a full overview of the developed software.

3.1 Pre-processing

The tool works with rasterised map data as input, i.e. pixelated bitmap images. For the calculations to work properly, all data therefore needs to be translated to this format before the program is run. This means that if e.g. GIS (Geographic Information System) data is used, the vector-based format first needs to be rasterised, which can be done within standard GIS packages such as QGIS [24] or ArcGIS [25]. Furthermore, all resulting images needs to be registered to match in scale and location, and have the same resolution and format. Currently, this pre-processing step has been implemented conveniently by a Python-script in QGIS which preforms the rasterization and sets the right format of the resulting images.

The next step is to tell the software to load the correct data as input, and where to find it. This is done by writing a simple configuration file, as a standard text file, which lists the location of each of the input images in question. For each set of input data listed in the file, a few default settings should also be given. These settings will be explained in more detail

below, when going through the workings of the actual program. In order to control the visualisation of the data in the viewport of the program, there is also a possibility to set a color for each input data entry in the configuration file.

3.2 Interface Overview

When CityFiction is started up, the user is met by a graphical interface as illustrated in Figure 1, which shows the program run on map data of the city of Malmö. The two main parts of this window is the Data Control Interface to the left, and the Map Viewport to the right, the latter filling up the main part of the window. In the top left of the Map Viewport, there is a pie chart giving some more detail on the current analysis results. For further information on this diagram, see Section 3.5 below.

3.3 Data and Controls

As mentioned earlier, the aim of the program is to help the user create a fitness function that shows the suitability of e.g. residential development in different areas of the city. This two-dimensional fitness function is shown in the Map Viewport as shades of brown, where a lighter shade means a higher fitness, c.f. Figure 2 where the map information is removed and only the 2D fitness function is shown. At the top of the Data Control Interface, the 2D fitness function $F(x, y)$ is interactively constructed by the user. Let

$$d_i(x, y), \quad i = 1, \dots, N$$

be N different 2D data sets loaded into the program. Let then $M(d)$ be a measurement function on the data d . A simple and common example of a measurement function is the minimum distance function, let us call this $M_D(d)$. Let the data $d_i(x, y)$ be a binary image marking the location of a specific geographic area, such as the sea, or the location of point objects, such as train stations. $M_D(d_i(x, y))$ is then constructed by calculating the smallest distance in every point (x, y) to this area or set of points. This value is then inverted and normalised to a value between 0 and 1, so that M_D has the maximum value of 1 closest to the area or point in question. The fitness function F is then the weighted sum of a number of these measurements on the data.



Figure 2. If the map data showed in the left panel is removed, we can view only the underlying fitness function, as in the right panel.

Let

$$w_i(x, y), \quad i = 1, \dots, N$$

be N different weights, where $0 < w_i < 1$. Then, the fitness function is constructed as

$$F(x, y) = \sum_{i=0}^N w_i M(d_i(x, y)).$$

In the Data Control Interface, the loaded input data in the current execution of CityFiction is listed consecutively, see Figure 3. Each set of loaded data is also marked with a unique color. In the section for each data item i , the corresponding weight w_i is set by a slider called *Weight*, or by the spin box next to it. In the current version of the program, there is also a slider called *Fall-Off* for each loaded data set. If the minimum distance measure is used as measurement function (M_D), the *Fall-Off* slider controls an exponential transformation of this measurement, so that it can be set how quickly the distance measure should fall off to zero. The higher the value, the quicker the fall-off. This is, for example, useful if we want the distance to the sea to affect the fitness function up to approx. a distance of 2km, while a smaller park only affects the fitness up to a distance of, say, 300m. The default value of the sliders in this section is set in configuration text file, as mentioned earlier. Future developments of CityFiction could also include an easy possibility to add a sharp distance threshold, i.e. so that the fitness value is 1 (normalized) up to the threshold and 0 at larger distances. Another possibility is a feature to let the user set the fall-off function more generally, via a manipulating a graph function in the GUI.

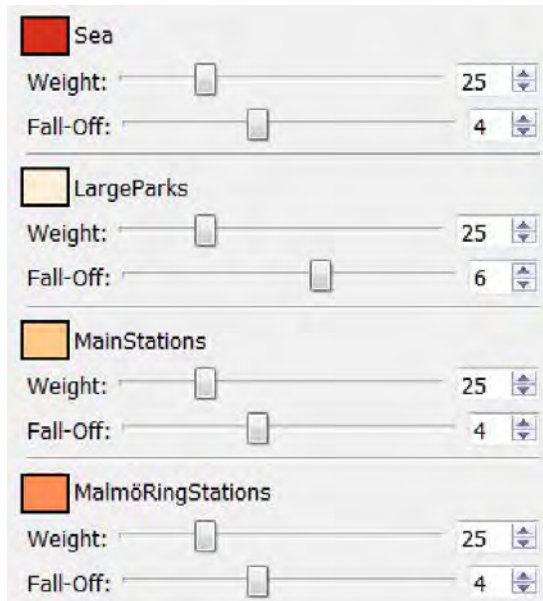


Figure 3. The area of the Data Control Interface where the weights are set in order to construct the fitness function.

By pressing the button *Show Highest Fitness Areas*, further down on the Data Control Interface, the areas with the highest fitness according to the weight settings, are marked with a white field. By changing the value of the slider *Area Size*, we can set how many square kilometers that are marked in white, c.f. Figure 4. As can be noticed, the white area is partially transparent, and this transparency value actually has a quite important meaning. If we consider the complete white field as totally buildable, this area would be totally opaque white. However, this field is also covering areas representing e.g. water, buildings, parks and streets. For maximum flexibility, it is possible to set the probability of development, also in these areas, to larger than 0. For example, while densifying the city there is a large possibility that some of the new development will be add-ons to, or redevelopment of, existing buildings. Therefore, it is reasonable that the possibility of development at the locations of the current building stock is larger than 0. The sea might, for example, seem like a less obvious area for development. However, reclaimed land has historically been used for development to a quite large degree in sea-side cities, so it not totally unreasonable to also consider water area as an area possible for development, to some degree.

The degree to which areas such as the sea or the location of current buildings should be considered for development is set using the sliders located below the list of sliders for the fitness function. The geographic area data listed here is also loaded when the program is started up, and should therefore also be listed in the configuration text file. By setting the slider value called *Development Probability* for each data item listed here, the possibility of building in the area represented by this data is given a value between 0 and 1. This also controls the transparency with which this data item is shown in the white field representing the highest fitness values on the map.

Among the data listed in this section of the Data Control Interface, we could also include non-binary data, as we have done in our current tests by including noise measures in the city. This data should be normalized to be in the range 0 to 1 and then affects the development probability multiplicatively, so that there is a smaller probability of development in a high noise area. The distance measures presented in the beginning of this section is, however, only applicable to binary data.

Below the *Development Probability* slider for each of the data items above, there is a slider named *Smallest Distance*. This is used in order to set a “buffer area” around the areas covered by these data items. For example, it might not be possible to build a new building closer than 8 meters to an existing building, unless it is considered as an add-on. Further, it might not be reasonable to build a new building closer than 10m to the shoreline. To this end, the *Smallest Distance* slider can be set, in order to offset these listed areas with a distance value.



Figure 4. The white field showing the area with highest fitness. When the area is increased the field grows and morphs into new shapes.



Figure 5. A new area is drawn in green as a polygon in the Map Viewport. This area is then added to the loaded park data which directly changes the fitness function and the white field showing the area with highest fitness.

3.4 Drawing and Adding New Areas

One feature of CityFiction is that areas or point data can be added interactively to existing loaded data in the program, and the effect of this addition can be seen directly on the fitness function. Let's say that a particular area in the city has quite a low fitness for residential development since there is no larger park situated close enough to this area. By then drawing a new park in the Map Viewport we can directly see how this park affects the weighted fitness for building in this area, cf. Figure 5. The drawing is performed by clicking a number of times on the right mouse button in different locations, in order to place the corners of a polygon. If a clicked location is close enough to the starting point, the polygon is automatically closed and filled. In a multiple choice menu in the Data Control Interface we can then choose the loaded data type (parks, water etc) which the area should be added to. By then clicking the button *Add Area*, the area is added to the chosen data type. The fitness function is then directly updated in the Map Viewport, incl. the white field indicating the area with highest fitness value.

3.5 The Pie Chart

The brown shading in the *Map Viewport* shows one value for each location, which represents the weighted fitness. However, in many cases it is of interest to see the specific

composition of the fitness in a particular location. We might, for example, be interested in seeing how large part of the fitness value in this location is related to closeness to parks and how much is related to the closeness to a train station. This is achieved by the pie chart in the *Map Viewport*, c.f. Figure 6. This diagram has as many circle sectors as the number of data items loaded for the fitness calculation. If the number of data items used increase, the pie chart might get a bit too cluttered to read. Currently, there is a limit on 10 sectors in the chart, and if the calculations include more data than this, only the 10 measures with the highest weights are shown in the chart. Further, the circle sectors are coloured according to the colour markers next to the data items listed in the *Data Control Interface*, cf. Figure 3 and Figure 6. When hovering with the mouse over a location on the map, the radius of the sectors is changing according to the value of the different data measures. That is, if the location is very close to the sea, the radius of the sector relating to the sea data is almost at its maximum in the diagram, while if we are very far from any station, the radius of the sector relating to the station data is very small.

The current weighting of the different data measures can also be read in the diagram. If we, for example, increase the *Weight* slider for the sea data, the angle for the sector representing this data is increased accordingly. In order to

see this change in the pie chart properly while changing the slider, we first need to lock the pie chart for a specific location. This is done by clicking the left mouse button at that location in the *Map Viewport*. A red dot will then appear on the map and the pie chart will be locked to this location until the left mouse button is clicked again, releasing the diagram, cf. Figure 6. In future versions of CityFiction, the possibility of marking a larger area, calculating the mean values in this area and then plotting these mean values in the pie chart will also be implemented.

3.6 A Word on the Implementation

As mentioned, CityFiction is a stand-alone executable program, currently only running on the Windows operating system. The program is written in C++, using the Qt SDK library to create the user interface, c.f. [26], and the OpenCV library for the image processing, c.f. [27]. OpenCV is a very powerful resource, which for example made it possible to calculate distance measures in real-time through its Distance Transform filters.

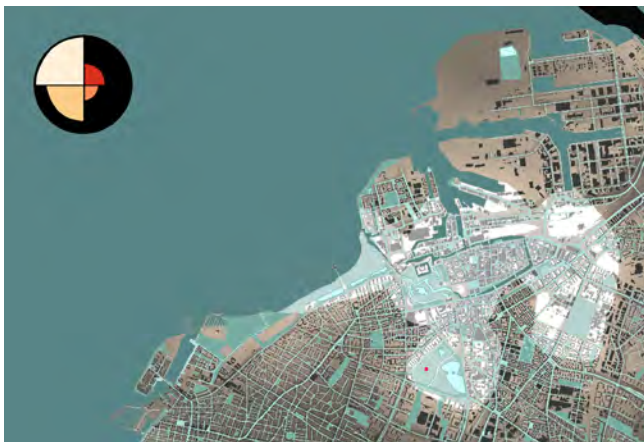


Figure 6. The Pie chart is here locked at the location of the red dot in the map. This point is located in a park and also relatively close to a train station, as the diagram shows.

4 DISCUSSION AND FUTURE WORK

We believe that the analysis software presented in this paper, already in its current state, represents a powerful tool for understanding city data and how it interacts. By changing the weights, or priorities, of the different sets of loaded input data, and by hovering over different locations on the map with the mouse, we can quickly identify locations that are well-suited for development. In contrast, we can also understand what factors are missing at a location for it to be suitable, according to our preferences. Changing the sliders, and simultaneously seeing the white field, which marks the highest fitness area, morph from one shape and location to another is a very pedagogical experience. Also, the ability to draw in new data “on the fly” makes it possible to further test different scenarios for city development, for example to test the location of a new train station or a new park. Generally, we have discovered how important real-time feedback is in

this type of tool and how educational the above mentioned interactivity is. Increasing the resolution and adding more sets of data to the calculation, of course, affects the interactivity, with the complexity scaling to the power of two with the resolution and the linearly with the number of mapped items in the data set. However, running on a mid-range laptop, interactivity has been shown to be working well with a raster resolution of 1600x1200 pixels and up to 10 different data maps in the calculation.

Interestingly, by prioritising the different data measures in a way that feels relevant for residential development, we can in the current project see a rather big correlation with the actual future development plans for Malmö. However, it is of course also interesting when the data interact in ways that wasn’t expected, and when the tool makes us realise aspects of the data that was not obvious from the beginning.

Generally, our discussions with the Malmö planning office has been very beneficial in developing CityFiction. We envision the tool to function as a platform for discussion among different stakeholders in the city’s future (citizens, politicians, planners, etc.) about desires and values and how the relate to city development and densification. This could lead to agreed and common values from where reasonable weighting of the data and measures used by CityFiction can be set as default and the resulting suggested areas for development, based on these values, could easily be visualised. The users could then also quickly find out how a new intervention, such as a new large park, affects these results.

A strength of the software is, however, that these common values can be changed, and that the result of this change is directly visualised by the program. Working with another city, maybe in another country, might e.g. also lead to a quite different set of common values.

4.1 Future Work

There are many ways in which this tool could be further developed. For example, future work could include the ability to in parallel make different settings for a number of different programs, i.e. residential, commercial, offices etc, and overlay the best fitness areas for each program simultaneously in the viewport. This would require that the *Data Control Interface* is made more compact, with different pages for different program setting etc. A more compact interface would also make it easier to load in a larger number of data sets than is currently used.

The usability of the software would also be greatly improved with a tighter association to available GIS software packages. Ideally, the program would be developed as a plug-in to e.g. ArcGIS or QGIS [24,25]. The selection of data to be used in the CityFiction analysis could then easily be done in the main program’s layer window, while the rasterisation would be performed inherently by the GIS package’s internal rasterisation functions.

Another future development of the software could include more intelligence in the analysis results by e.g. generating relational impacts. Greater development in an area might, for example, lead to over-crowding of transit and under-development lead to higher risk of crime. Identifying these kind of negative impacts might impart significant knowledge to the user, if this addition is based on well-documented research findings.

By connecting CityFiction to the research on city growth algorithms presented in Section 2.1, the software could also be used as a first step to set up relevant fitness functions, before a city growth (or land-use) algorithm is run using these fitnesses. The applied growth algorithm could e.g. be based on Cellular Automata, where different programs would compete about the available developable areas, where this competition would be affected by the fitness settings.

Another aspect that needs some more study is the question on how to best approximate how large area needs to be developed in order to reach a certain number of new inhabitants. As detailed in Section 3.3, the size of the white field marking the area with the highest fitness for development is currently set using the *Area Size* slider. But how many new inhabitants could actually fit in this area? Currently, this is approximated by setting a maximum density, say 10000 persons per square kilometer, using the *Max Density* slider in the Data Control Interface. This density will then be true for the opaque white areas, while the density in the transparent areas are multiplied with their transparency value between 0 and 1, i.e. with their probability value for further development. This means that if the probability value for development at the location of current buildings is set to 0.2, it is approximated that on average 2000 persons per square kilometre could be added by redeveloping, or adding on to, the current building stock. A more sophisticated way of approximating the potential for increase of number of inhabitants is probably needed, based on area regulations on building height, current availability of infrastructure and services etc. Further, in order to properly study how much new development that could actually be done in a certain area, we would really need to zoom in on this area and work on a different, more detailed, scale. CityFiction could then be used to roughly map out relevant target areas for development, which then could be studied further by a more detailed tool. This second tool would then need to work in 3D in order to study possible massings and by making analysis on daylighting etc. However, this stretches far outside the topic of this paper.

5 CONCLUSION

In this paper, a new city data analysis tool called CityFiction has been presented in detail. The tool has been developed in order to aid in decision making regarding city growth and densification. By prioritising between different measures on the available input data, scenarios for the future development of a city can be efficiently and pedagogically explored and visualised. The user can also add new data interactively to

the analysis by drawing in the viewport. In this way, the effect of adding a new train station in a specific location, or adding a new park, can analysed “on the fly”. Using the tool for a visionary city development project for the city of Malmö in Sweden, we have found it to give very reasonable outputs and be very educational in helping to understand how different data sets interacts in order to create a measure on the suitability for development and densification in the city.

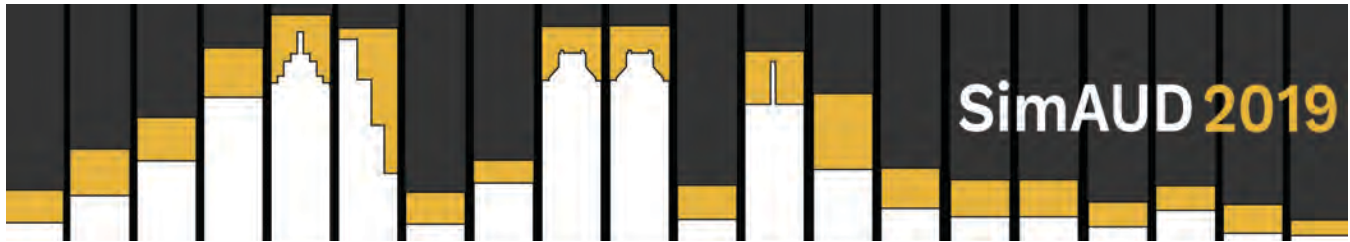
ACKNOWLEDGMENTS

The authors would like to thank the City Planning Office at Malmö City Council for great consultation, an inspiring target project and for the GIS data used to test the developed application. We would also like to thank FOJAB for financing the research and for great discussions with the colleagues at the office regarding the project, not at least with David Kiss. Finally, the authors would like to thank Jens Jul Christensen for contributing substantially in the early stages of this project.

REFERENCES

1. Digital Universe of Opportunities: Rich Data and the Increasing Value of the Internet of Things. *EMC Digital Universe with Research & Analysis by IDC*. <https://www.emc.com/leadership/digital-universe/2014iview/index.htm>. As of 21 Nov 2018.
2. Woetzel, J, et.al. Smart Cities: Digital Solutions for a more Livable Future. *McKinsey Global Institute*. McKinsey&Company. June 2018.
3. Google Maps, Goggle Inc., <https://www.google.com/maps/>. As of 21 Nov 2018.
4. Mapillary, Mapillary AB, <https://www.mapillary.com>. As of 21 Nov 2018.
5. OpenStreetMap, <http://www.openstreetmaps.org/>. As of 21 Nov 2018.
6. Berends, J, et.al. Analytical Report 6: Open Data in Cities 2, *European Data Portal*, June 2017.
7. Lowry, I.S. A Model of Metropolis. Report RM-4035-RC. RAND Corporation, Santa Monica, CA, USA, 1964.
8. Tobler, W. A Computer Movie Simulating Urban Growth in the Detroit Region, *Economic Geography* 46, 2 (1970), 234-240.
9. Batty, M. Modelling Cities as Dynamical System, *Nature* 231, 5303 (1971), 425.
10. Batty, M. Recent developments in Land-use Modelling: A Review of British Research. *Urban Studies* 9, 2 (1972), 151-177.
11. Clarke, K.C., et.al, A Self-Modifying Cellular Automaton Model of Historical Urbanization in the San Francisco Bay Area, *Environmental and Planning B*, 24 (1997)

12. Chaudhuri G., Clarke, K.C, The SLEUTH Land Use Change Model: A Review, *Int. J. Environmental Resources Research* 1, 1 (2013).
13. Batty, M., *Cities and Complexity: Understanding Cities with Cellular Automata, Agent-Based Models, and Fractals*. MIT Press, Boston, USA, 2005.
14. Batty, M., *A New Science of Cities*, MIT Press, Boston, USA, 2013.
15. Teerarojanarat, S., et.al., Urban Growth Simulation with Urban Sim, *Proc. FOSS/GRASS Users Conf.*, Bangkok, Thailand, Sept 2004.
16. UrbanSim, <http://www.urbansim.com>, As of 24 Nov 2018.
17. UrbanFootprint, <http://urbanfootprint.com>, As of 6 Feb 2019.
18. Petrasova, A., et.al., Open Source Approach to Urban Growth Simulation, *Int. Arch. Photogrammetry, Remote Sensing and Spatial Information Sciences*, Prague, Czech Republic, July 2016.
19. LanduseSim, <http://www.landusesim.com>, As of 24 Nov 2018.
20. Malm, H. and Nicholas, P, Re-use and Adaptation of Existing Building Structures using Monte Carlo Simulation, *Proc. Building Simulation and Optimization 2014*, London, UK.
21. Pàez, A, and Scott, DM, Spatial Statistics for Urban Analysis: A Review of Techniques with Examples, *GeoJournal* 61, (2004), 53-67.
22. Getis, A, and Ord, JK, The Analysis of Spatial Association by the Use of Distance Statistics, *Geographical Analysis* 25, (1993), 276.
23. Anselin, L, Local Indicators of Spatial Association – LISA, *Research paper 9331*, Regional Research Institute, West Virginia University, Morgantown, 1995.
24. QGIS, <https://www.qgis.org>, As of 26 Nov 2018.
25. ArcGIS, <https://www.arcgis.com>, As of 26 Nov 2018.
26. Qt, <https://www.qt.io>, As of 25 Nov 2018.
27. OpenCV, <https://opencv.org>, As of 25 Nov 2018.



Exploring Urban Walkability Models and Pedestrian Movement Trends in a Vancouver Neighbourhood

Nicholas Martino¹, Cynthia Girling² and Edja Trigueiro¹

¹Univ. of Rio Grande do Norte
Natal, Brazil
nicholas.martino@hotmail.com
edja_trigueiro@ct.ufrn.br

²University of British Columbia
Vancouver, Canada
c.girling@sala.ubc.ca

ABSTRACT

Walkability, or how inviting a place is to pedestrians, has proven a useful concept for urban decision-makers. Although there are now several methods to measure and evaluate the walkability of streets and neighbourhoods, these are usually dependent on large sets of data, thus making it difficult to apply them in the daily practice of architects and urban designers for evaluating design alternatives. The intention is to compare different measures as indicators of urban walkability based on the study case of the Olympic Village neighbourhood in Vancouver, Canada. Two large-scale walkability indexes were graphically compared with visibility-based measurements and pedestrian movement routes tracked in site. Each method was chosen based on the spatial scale of the variables that compose the measurements: a city-scale walkability index based on the configuration of street grid for the urban whole, a neighbourhood walkability index based on data available at 800m from each building and a pedestrian movement simulation model based on a configurational approach emphasizing visibility and movability in space. Results found similarities between the configurational model and pedestrian movement patterns at the Olympic Village but little agreement between two walkability indexes. Further research is needed to understand why there is little correlation among methods.

Author Keywords

Urban design; walkability; space syntax.

ACM Classification Keywords

I. SIMULATION AND MODELING
I.6.4 Model Validation and Analysis

1 INTRODUCTION

Walkability can be generally defined as “how inviting a certain place is to pedestrians” [1]. Several walkability measurements have been instructive for implementing policies with the goal of increasing the number of people that walk as a main transport mode, but these are mostly based on large scale urban data, which is too time consuming for

quickly evaluating different architectural and urban design alternatives. This paper addresses this need for investigating walkability from an urban design perspective using visibility and spatial configuration as an indicator of walkability.

Studies have objectively measured this urban quality based on a geospatial approach, usually analyzing form and use variables (density, diversity, design, etc.) relative to the surroundings of an urban element (parcels, residences, etc.) [2–5]. Others include a more detailed auditing of physical aspects of the street [6,7] or perceptual variables such as visibility, enclosure [8] or axiality [4]. The Table 1 summarizes approaches towards measuring walkability.

Ref.	Approach	Spatial Scale
[3]	Form and uses	1km network buffer from parcels
[2]	Form and uses	0.4-1.6km network buffer from residences
[7]	Form and uses/ Survey/ Street auditing	Surveyors’ walking routes within street segments network
[4]	Form and uses / Perceptual/ Survey	City grid network simplified into street segments
[8]	Perceptual	Points along streets centerlines
[6]	Form and uses	Blocks’ boundaries at street, neighbourhood and city scales
[5]	Form and uses	Kernel radius from amenities applied to a 80x80m grid

Table 1. Different approaches and scales of walkability analysis.

Few studies links the idea of walkability to the neighbourhood’s spatial configuration – an aspect of architecture inseparable from the design practice – even though the idea that space affects movement and behavior is well established [9–13]. The intention here is to explore a configurational/visibility-based approach [10,14] as an indicator of walkability and compare that to actual behavior.

The Olympic Village was chosen as an example case, because it has a reputation of being a complete walkable community [15]. Two walkability indexes based on the literature and one movement trends model based on space syntax theory [10] were compared with actual pedestrian movement patterns tracked in site.

2 MODELLING WALKABILITY

Neighbourhood/City-based Walkability

Two urban-scale methods for evaluating potential for walkability include: (a) a Neighbourhood Walkability Index, *nwi*, based on land use and floor area data gathered for the surroundings of each parcel – 1km buffer over the street network [3] – and (b) a Space Syntax Walkability index, *ssw*, based on the closeness of every street to all others in the city multiplied by the mean demographic density of the street [4]. Both models have been tested and validated with real world data. The *nwi* was found to correlate with adults’ physical activity [3] and *ssw* with people using walking as a main transportation mode [4]. Here, these indexes were calculated based on data from Open Street Maps and select data from the British Columbia Assessment, processed using QGIS.

Neighbourhood Walkability Index, nwi, mostly based on [3]. Variables are: number of intersections (*Int*), area of 1km network buffer (*BAr*), retail area (*RetAr*), total built area (*TotAr*), bedrooms (*Bedr*) and total residential area (*ResAr*).

$$nwi = 2 * z\left(\frac{Int}{BAr}\right) + z\left(\frac{RetAr}{TotAr}\right) + z(LUM) + z\left(\frac{Bedr}{ResAr}\right)$$

Space Syntax Walkability, ssw, mostly based on [4]. Variables are: space syntax integration (*IntHH*), number of bedrooms (*Bedr*) and total residential area (*ResAr*).

$$ssw = 2 * z(IntHH) + z\left(\frac{Bedr}{ResAr}\right)$$

Visible and Movable Space

Space syntax theory is based on the idea that a significant proportion of pedestrian movement is defined by spatial configuration itself. Hillier et al. [9] defines this configuration-driven movement as “natural movement” and visibility-based studies confirm this correlation among configuration and movement in buildings [16] and cities.

Visibility graph analysis is a method of spatial modelling that “may be closely related to manifestations of spatial perception, such as way-finding, movement and space use” [14]. It consists in abstracting architectural form into a spatial system of barriers and permeabilities, dividing space into grids and calculating relationships of each cell with the system as a whole based on properties of its isovists (see Figure 1). Researchers also applies visibility graph analysis for modelling barriers and permeabilities to movement, which allows for a better understanding of spatial

movability, how people move through spaces and how relations of centrality-periphery are perceived (see Figure 3). The novelty of the proposed approach is on joining visibility and movability measurements in a single indicator.

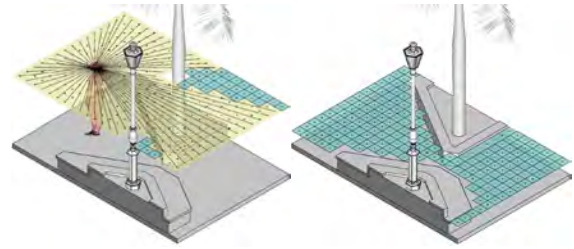


Figure 1. Visible and movable space models.

Each cell then has a set of properties, mostly based on space syntax theory [10] generated with the software Depthmap [17]. These measurements are not deterministic, but rather representations of probable fields of movement and interactions in space. Based on the assumption that people go to where they can see while avoiding corners when moving through space, the measurements applied for the Olympic village case study were modeled by multiplying the isovist area of visible space (see Figure 2) with the convex centrality of movable space (see Figure 3).



Figure 2. Isovist area of visible space¹. The area of visible space from each cell. Proportional to the number of cells directly visible from each cell.

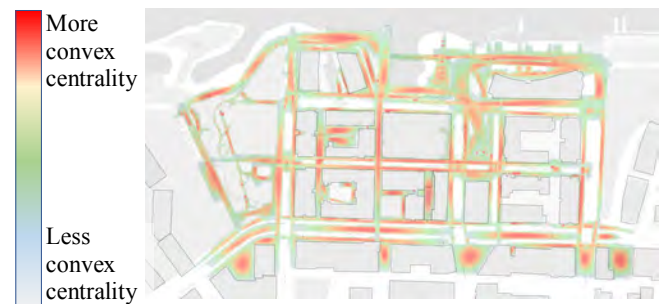


Figure 3. Convex centrality of movable spaces². Standardized measurement based on the amount of times a cell is passed when moving through all the possible origin-destinations in the system.

¹ Isovist Area or Connectivity in Depthmap’s visual graph analysis.

² Though Vision divided by Point Second Moment in Depthmap’s visual graph analysis.

The measure of *configuration-driven movement*, *cdm*, was calculated based on spatial visibility and movability measurements relative to all other accessible spaces in the system [10,13,14]. Graphs were generated using the software DepthmapXnet.

$$cdm = (IsovistArea) * \left(\frac{ThroughVision}{PointFirstMoment} \right)$$

A graphical comparison of the indicator to pedestrian movement data tracked on site [18] provide some validation of *cdm*. Researchers picked up the walkers at they entered the Olympic Village area and unobtrusively followed them until they exited the site, entered a building or stopped for more than 30 seconds. Of 49 people tracked over two days, 84 % walked along the waterfront at some point [19].

3 WALKABLE OLYMPIC VILLAGE

There is low correlation between *nwi* and *ssw* in the analyzed case. Both indexes displays parts of the Olympic Village as relatively walkable, when compared to its urban surroundings (see Figure 4). Only 16% did not walk on the greenway. There seems to be little correlation among the parcel-based *nwi*, the network-based *ssw* and actual pedestrian movement patterns in the Olympic Village neighbourhood (see Figure 5), mostly because these indexes were designed to be indicators of urban walkability instead of pedestrian route predictors.

There is a strong visual correlation between natural movement and pedestrian movement patterns, mainly driven by the generous views to the waterfront and the integration of waterfront with the neighbourhood's central plaza.

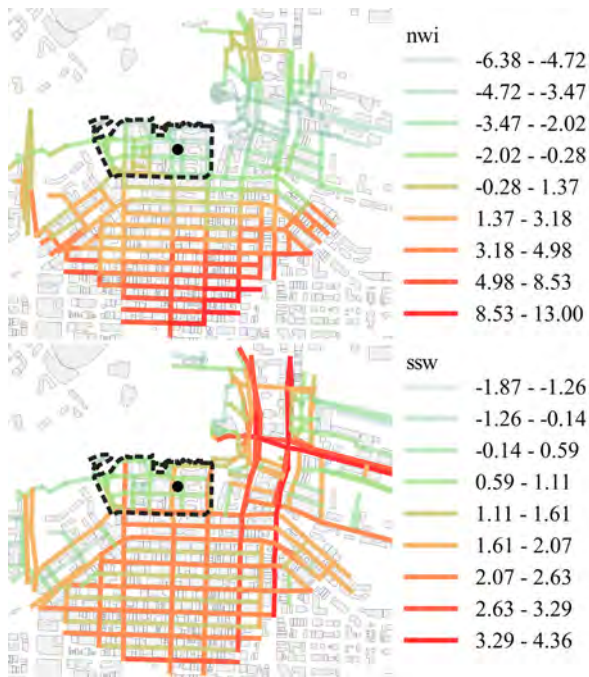


Figure 4. *nwi* and *ssw* within a 10 minute walk from the Olympic Village central plaza (black dot).

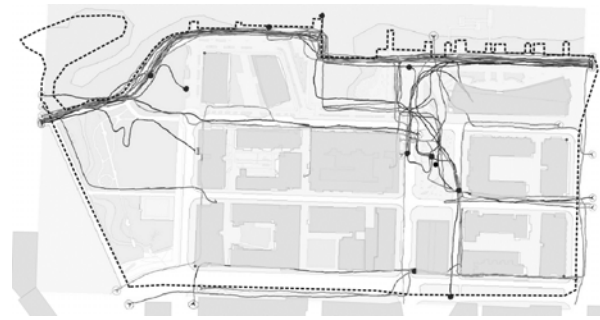
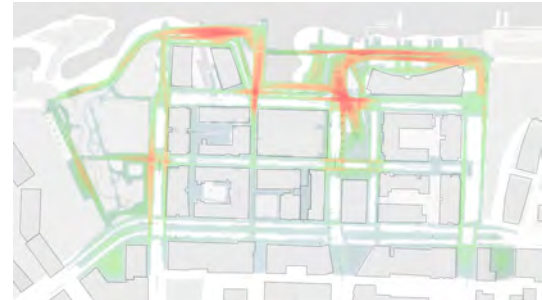


Figure 5. Pedestrian movement patterns tracked in site.



Less potential movement More potential movement

Figure 6. Configuration-driven movement patterns at Olympic Village (isovist area of visible space, Figure 2, multiplied by the convex centrality of movable space, Figure 3).

4 CONCLUSION

The analysis highlights that walkability measurements may serve different purposes and scales, according to its methods of measurement. Firstly, although the large-scale indexes may well indicate neighborhoods that encourage **walking as a main travel mode throughout the city** or to **generally be more physical active**, these measurements do not capture human-scale relationships that may be strongly correlated with actual pedestrian preferences and routes. Secondly, if an aspect of walkability is **how inviting pedestrian spaces are to pedestrians**, the generous views from waterfront at the Olympic village captured by the configurational model closely matched actual walking patterns on the site, even though further research is needed to validate the model as an actual walkability index.

Spatial configuration measurements – such as the *cdm* indicator – does not require land use data and can be easily calculated in parametric design applications [20]. This might facilitate the application of the walkability concept in the daily practice of architects and urban designers when testing different spatial configurations, especially in early stages of the design process. The measure can be refined by including other configurational measurements or other factors that might affect pedestrian movement such as urban design infrastructure, environmental comfort and proximity to amenities or landmarks. Further research could analyze correlations among these variables and actual pedestrian

movement in order to answer what factors are relevant to define a walkability index based on spatial configuration.

Finally, the study confirms spatial configuration and visibility as a potentially relevant variables to be considered in pedestrian movement simulation [15].

REFERENCES

1. Forsyth A. What is a walkable place? The walkability debate in urban design. *Urban Des Int.* 2015;20:274–92.
2. Duncan DT, Aldstadt J, Whalen J, Melly SJ, Gortmaker SL. Validation of Walk Score® for Estimating Neighborhood Walkability: An Analysis of Four US Metropolitan Areas. *International Journal of Environmental Research and Public Health.* 2011;8:4160–79.
3. Frank LD, Schmid TL, Sallis JF, Chapman J, Saelens BE. Linking objectively measured physical activity with objectively measured urban form: Findings from SMARTRAQ. *American Journal of Preventive Medicine.* 2005;28:117–25.
4. Koohsari MJ, Owen N, Cerin E, Giles-Corti B, Sugiyama T. Walkability and walking for transport: characterizing the built environment using space syntax. *International Journal of Behavioral Nutrition and Physical Activity.* 2016;13:121.
5. Lefebvre-Ropars G, Morency C, Singleton PA, Clifton KJ. Spatial transferability assessment of a composite walkability index: The Pedestrian Index of the Environment (PIE). *Transportation Research Part D: Transport and Environment.* 2017;57:378–91.
6. Moura F, Cambra P, Gonçalves AB. Measuring walkability for distinct pedestrian groups with a participatory assessment method: A case study in Lisbon. *Landscape and Urban Planning.* 2017;157:282–96.
7. Park S, Deakin E, Lee JS. Perception-Based Walkability Index to Test Impact of Microlevel Walkability on Sustainable Mode Choice Decisions. *Transportation Research Record: Journal of the Transportation Research Board.* 2014;2464:126–34.
8. Yin L, Wang Z. Measuring visual enclosure for street walkability: Using machine learning algorithms and Google Street View imagery. *Applied Geography.* 2016;76:147–53.
9. Hillier B, Penn A, Hanson J, Grajewski T, Xu J. Natural movement: or, configuration and attraction in urban pedestrian movement. *Environment and Planning B: Planning and Design.* 1993;20:29–66.
10. Hillier B, Hanson J. *The Social Logic of Space.* 1st ed. London: Cambridge University Press; 1984.
11. Marcus L. Spatial Capital: A proposal for an extension of space syntax into a more general urban morphology. *Journal of Space Syntax.* 2010;1:254–257.
12. Turner A. From Axial to Road-Centre Lines: A New Representation for Space Syntax and a New Model of Route Choice for Transport Network Analysis. *Environ Plann B Plann Des.* 2007;34:539–55.
13. Turner A, Penn A. Encoding Natural Movement as an Agent-Based System: An Investigation into Human Pedestrian Behaviour in the Built Environment. *Environment and Planning B: Planning and Design.* 2002;29:473–90.
14. Turner A, Doxa M, O’Sullivan D, Penn A. From Isovists to Visibility Graphs: A Methodology for the Analysis of Architectural Space. *Environment and Planning B: Planning and Design.* 2001;28:103–21.
15. Szibbo NA. *Livability and LEED-ND: The challenges and successes of sustainable neighborhood rating systems.* University of California Berkeley; 2015.
16. Hillier B, Tzortzi K. *Space Syntax: The Language of Museum Space. A Companion to Museum Studies.* 2006.
17. Turner A. *Depthmap: A Program to Perform Visibility Graph Analysis.* 2001.
18. Gehl J, Svarre B. *How to Study Public Life.* Island Press; 2013.
19. Girling C, Zheng K, Monti A, Ebnesahidi M. Walkability vs. walking: Assessing outcomes of walkability at Southeast False Creek, Vancouver, Canada. 2019.
20. Beirão JN, Nourian P, Mashhoodi B. Parametric Urban Design: An interactive sketching system for shaping neighborhoods. *Respecting Fragile Places (29th eCAADe Conference Proceedings).* 2011;225–234.

Mediums of Indoor Comfort

A Simulation-Based Design Analysis for the Assessment of Indoor Comfort Under the Effect of Solar Radiation. 135
Andrea Zani, Henry David Richardson, Alberto Tono, Stefano Schiavon and Edward Arens

Black Globe Free Convection Measurement Error Potentials 143
Eric Teitelbaum, Jovan Pantelic, Adam Rysanek, Kian Wee Chen and Forrest Meggers

Assessing the Performance of UFAD System in an Office Building Located In Various Climate Zones. 147
Roshanak Ashrafi, Mona Azarbayjani, Robert Cox, Benjamin Futrell, Joseph Glass, Amir Zarrabi and Armin Amirazar

Evaluating the Influence of Three Simplifications on Natural Ventilation Rate Simulation 155
Yuchen Shi and Xiaofeg Li



A Simulation-Based Design Analysis for the Assessment of Indoor Comfort Under the Effect of Solar Radiation

Andrea Zani^{1,4}, Henry David Richardson², Alberto Tono³, Stefano Schiavon⁴ and Edward Arens⁴

¹Eckersley O'Callaghan
San Francisco, USA

²WattTime
Oakland, USA

³Hok
San Francisco, USA

⁴CBE, UC Berkeley
Berkeley, USA

sanfrancisco@eocengineers.com

info@watttime.com

sf@hok.com

cbe@berkeley.edu

ABSTRACT

One of the drivers of sustainable design is to maximize daylight across the floor plan in order to decrease electric energy consumption and create more productive and healthy working spaces. However, uncontrolled incoming solar radiation can lead to significant visual and thermal comfort issues. In particular, solar radiation landing on occupants can create thermal discomfort that the HVAC system cannot compensate for, thereby causing intolerable conditions for users close to the façade.

We aim to present a new climate-based annual framework, based on ASHRAE 55 appendix C (2017), to assess radiant discomfort across a space due to direct solar radiation. The framework is calculated using the hourly effective radiant field (ERF) and delta Mean Radiant Temperature (Δ MRT) across the indoor space. The Radiance-based framework coupled with the proposed Annual Radiation Discomfort metric (ARD) provides designers a robust method to assess the performance of complex fenestration systems (CFS) at reducing potential thermal discomfort caused by incoming shortwave radiation.

Author Keywords

Solar radiation; Thermal comfort; Radiance; Complex Fenestration System; Annual Radiation Discomfort index.

1 INTRODUCTION

Controlling incoming solar radiation is one of the main goals for sustainable designers to minimize glare and cooling loads and maximize thermal comfort and usable daylight.

Uncontrolled solar radiation entering the building can introduce significant problems related to visual and thermal comfort. Thermal issues include to heat gains that must be removed by energy-intensive air conditioning, the risk of overcooling from attempting to compensate for the strong local heat gains in sunlit areas and solar radiation landing on occupants directly affects their thermal comfort. However, the third issue has been often overlooked because of the lack of guidelines and the complexity of the problem. The main thermal comfort standards, such as ASHRAE Standard 55 (ASHRAE 2004) or ISO Standard 7730 (ISO 2015),

historically did not even mention shortwave solar radiation in their comfort prediction or evaluation procedures because they were developed assuming occupants would not be exposed to direct solar radiation inside the buildings. Only recently has ASHRAE 55-2017 adopted a method defined by the Center for the Built Environment to calculate discomfort due to shortwave radiation.

In modern glass office buildings where the window-to-wall ratio (WWR) is often close to 80% for aesthetic reasons and to maximize views, the critical design area for thermal comfort is the daylit perimeter zone [10] because of the potential for solar radiation landing on occupants. As proven in different publications [2, 12], shortwave incoming radiation can be the most influential component driving human comfort. The solar radiation that hits the occupant causes a substantial temperature offset which is often beyond the HVAC system's corrective capacity. Even if the HVAC mechanical cooling were capable of counteracting the discomfort of the sunlit occupant, the spatial and temporal variability of the sunlit areas exceeds that of typical HVAC zonal control, and the system will overcool the (usually more numerous) occupants in non-sunlit areas. Different surveys show [9, 10] that in many buildings situated in climates with high solar irradiance throughout the year and characterized by transparent facades the daylit perimeter area is unoccupied or the occupants are forced to deploy the shading for most of the day because of intolerable thermal conditions created by the excess of incoming solar radiation. In addition to the direct effect on human thermal comfort and productivity [1, 18], over deployed shading and the unused floor area near windows has profound impacts on daylight, energy building performance [3, 13] and economic efficiency. For these reasons, in order to help designers account for the direct influence of solar radiation on thermal comfort, ASHRAE 55-2017 Appendix C introduced two approaches to calculate the shortwave MRT.

ASHRAE 55-2017 includes two approaches for estimating the comfort condition when direct beam solar radiation hits the occupant. 1. Prescriptive approach: assume an MRT equal to 2.8 °C above the average air temperature which is

applicable only when prescribed conditions are met including: glazing elements' U-value, maximum outside temperature, maximum window size, blind solar transmission, and spatial room requirements (distance from the facade). 2. Performance approach based on the work of Arens et al. [2]: first compute the long wave and shortwave MRT and then sum the two quantities in order to obtain the adjusted MRT. As explained in the standard, the shortwave MRT is a function of the context, direct and indirect solar transmittance of the fenestration system, occupant position and posture, body exposure, sun position and irradiance value and clothing absorptivity. In the last couple of years, the ASHRAE full calculation method has been implemented in different tools such as SolarCal module of the CBE Thermal Comfort Tool [8] and Ladybug Comfort Component [11, 14] and a new workflow based on Radiance and EnergyPlus [20] that overcome some limitations of previous tools by adding features such as annual evaluations, automatic sky vault estimation, and projected fraction of a representative person exposed to direct beam sunlight in cases with complex fenestration systems (CFS). Compared to a "non-geometric" approach implemented in Trnsys [19] or Ladybug for grid calculation [11], manikin-based method allows to fully capture the distribution and intensity of the incoming radiation on the body. Particular improvements have been noticed [20] for highly directional solar shading system, where only portions of the body are hit by direct radiation. Currently, in architectural practice, facades and floor design solutions are often driven by preliminary daylight and solar heat gain analyses using metrics such as Daylight Autonomy (DA) [15], Useful Daylight Illuminance (UDI) [16], and Annual Sunlight Exposure (ASE). This leads to the question of whether current daylight performance metrics are well suited for the evaluation of the effect of solar radiation on human comfort. The most obvious limitation is that all the metrics are based on illuminance values or targeted toward HVAC system sizing (quantity of solar heat gain). This demonstrates that a thermal-comfort-focused, simulation-based framework and metric is missing from the design process.

In this paper, we present a new simulation framework, based on Zani's paper [20], for predicting the variation in indoor thermal comfort of occupants exposed to solar radiation across the floor plan by computing the change in MRT as a function of the area exposed and of the intensity of solar radiation. Furthermore, we present a new metric to assess the number of annual hours of discomfort caused by solar radiation and their discomfort intensity. Finally, we test the framework and the metric with three different facade system and determine their effect on the Predicted Mean Vote (PMV) near the facade.

2 METHOD

The climate-based shortwave radiation comfort framework used here allows the evaluation of the effect of direct solar radiation on human thermal comfort across indoor spaces over a one-year period. It consists of a refined and extended

workflow based on a validated Radiance and EnergyPlus simulations approach [20] and a novel metric: the Annual Radiation Discomfort (ARD) index (defined in section 2.4). The scope of the new framework is to provide meaningful insight on how well a facade system controls incoming solar radiation to guarantee the thermal comfort of the occupants. It is intended to help quantify the frequency and intensity of the thermal discomfort caused by solar radiation during the year in a commercial building.

2.1 Simulation Framework

The simulation framework is divided into four main components as shown in Figure 1. First, using Rhinoceros 3D and Grasshopper, we create a series of manikins across the space and the subject scene. Second, we import the scene and manikin grid, previously generated, into Radiance. These files were used to calculate the incident solar radiation on the manikins employing the 2-phase Daylight Coefficient method. Third, we compute the long wave MRT for the each specific user's positions near the façade through EnergyPlus (E+). Finally, we analyze the raw output files using a custom Python script to obtain the hourly shortwave MRT and determine the adjusted MRT by coupling the results from the Radiance radiation analysis with E+ thermal analysis. The Annual Radiation Discomfort index is computed directly from the shortwave MRT without accounting for the effect of the long wave MRT. Given the magnitude of the effect of shortwave radiation landing on the occupants, long wave radiation can be overlooked in early design.

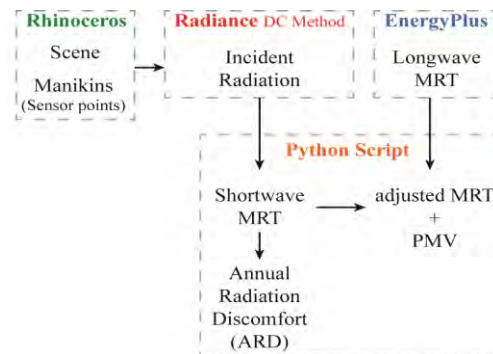


Figure 1. Simulation workflow. In colors the software used and in black each output obtained.

Incident Radiation - Radiance Calculation

The main change introduced in the framework is the automated hourly calculation for the entire year of the incoming radiation falling on the users across the space using Radiance. In particular, given the high resolution required to capture the amount of radiation in a specific portion of the manikin, we selected a modified version of the Daylight Coefficient. This method, in contrast with the traditional method where the luminance of the sun is attributed to the three patches closest to the sun, considers the exact position of the solar disc along the analemma. In the approach we used several Radiance programs in order to compute the incoming radiation landing on the manikin with high accuracy, even through a complex fenestration system. The

Gendaymtx tool generates a sky matrix with luminance values based on direct and diffuse component of the solar radiation using the Perez distribution, plus the Analemma matrix that generates the sun matrix. Rfluxmtx computes the daylight matrixes taking into account sky conditions, scene geometries, and material properties. Dcimestep is used for the matrix multiplication and a modified version of rmtxop is used to convert RGB output file into irradiance [W/m^2]. The manikins tested in this paper are defined by a sensor point placed at the centroid of each mesh face and oriented with a normal perpendicular to the surface centroid. Each sensor captures, for that specific portion of the body, the total solar radiation ($E_{\text{solar},i}$) taking into account all the components of solar radiation (diffuse, reflected and direct).

Long wave MRT - EnergyPlus simulation

Simultaneously, an energy simulation using EnergyPlus can be run in order to calculate the air temperature, humidity and surface temperatures based on the scene properties described in Section 2.2. EnergyPlus' basic output gives the longwave MRT for one point placed in the center of the room. Given that the analyses are focused on the area close to the façade, we decided to compute the longwave MRT for six specific positions in the space located in the first 3 m adjacent to the façade, resulting in a spacing of 0.5 m. The longwave MRT is computed considering the surface temperatures of walls, glazed surfaces and the corresponding view factor for the exact user position, employing the method described in [11]. By adding the hourly MRT to the hourly ΔMRT obtained from the Radiance simulation, it is possible to compute the adjusted MRT with the SolCal method described in ASHRAE 55 appendix C for the performance approach. Finally, the PVM model is fed with the adjusted MRT to assess the thermal comfort and the percentage of potentially dissatisfied people.

Python Script

The Python script has two main functions; first computing the Effective Radiant Field (ERF), shortwave MRT, and ARD for each manikin in the space; second combining the shortwave MRT with the long wave MRT to calculate the adjusted MRT. In the Radiance section of the script, for each hour of the year we first multiply the $E_{\text{solar},i}$ for each point by the equivalent area of the mesh to determine the total radiation on each surface. We then sum the radiation for all the surfaces to determine the total radiation falling on the body. Finally, by dividing the total radiation by the total body area, it is possible to calculate hourly the incoming radiation rate for the whole body (E_{solar}) (W/m^2). Using the formulas described by Arens [2], we compute the hourly ERF and ΔMRT for each manikin in the space and finally, we implement the ARD definition described in 2.4. The script embedded in Grasshopper generates graphs and heat map visualizations automatically.

2.2 Scene and Parameters

The simulated model used in this simulation employs the same geometry as the ASHRAE BESTEST (see Figure 2) office space [7] fully described in Zani's paper for its optical

and thermal properties [20]. In order to guarantee a thermally neutral starting condition, an ideal HVAC has been modeled with a $T_{\text{heating}} = 20\text{ }^\circ\text{C}$, $T_{\text{cooling}} = 26\text{ }^\circ\text{C}$ and minimum relative humidity equal to 30%. For the assessment of the PMV, the following standard values were used during the year: air flow speed of 0.1 m/s, users' metabolic rate of 1.2 met, and a dynamic clothing level based on outdoor temperature [17]. We tested three different façade configurations. Starting with classic insulated glazing units with two different values of solar transmittance, respectively 60% (low-e coating) and 28% (solar control coating). Second, a CFS with medium-low shade density obtained by coupling a glazing unit with 52% solar transmittance with static external louvers. The third configuration was a CFS with high shade density with geometry inspired by NMAAHC museum.

2.3 Spatial Mapping

In comparison with daylight performance metrics, a metric to assess the effective radiant field (ERF) and ΔMRT for the human body requires more than a typical sensor point every 0.45 m as required for LEED simulation and described in LM-83-12. In order to accurately calculate the intensity and direction of solar radiation landing on the occupant, it is necessary to use a more refined array of sensors. As presented in Zani et al. research work [20], a high-resolution manikin with 363 meshes combined with an accurate sky definition is able to fully capture the spatial complexity of the problem and accurately determines the change in MRT due to direct solar radiation. However, in order to create a more flexible framework that is able to investigate the performance of the façade independent of the position and orientation of the occupant, it is necessary to extend the analysis to a grid of locations and remove the directionality of the manikin. A simplification of the manikin has been necessary in order to reduce the calculation time and create a non-directional representation. Starting from the high resolution (HR) manikin with 363 meshes described in [20], we tested a medium resolution (MR) with 120 meshes and a low resolution (LR) with 30 meshes, while maintaining the same total area. As described in Figure 3, we tested the accuracy and calculation analysis time of the simplified manikins (MR and LR) against the high-resolution one (HR), comparing the ΔMRT hourly values for the entire year with three different façade configurations. First, we compared the three manikins in a scene without a shading system (No shade).

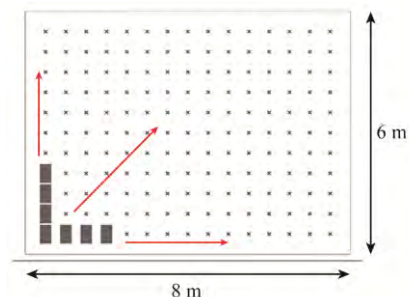


Figure 2. Office space configuration (ASHRAE BESTEST) and spatial distribution of manikins (red arrows).

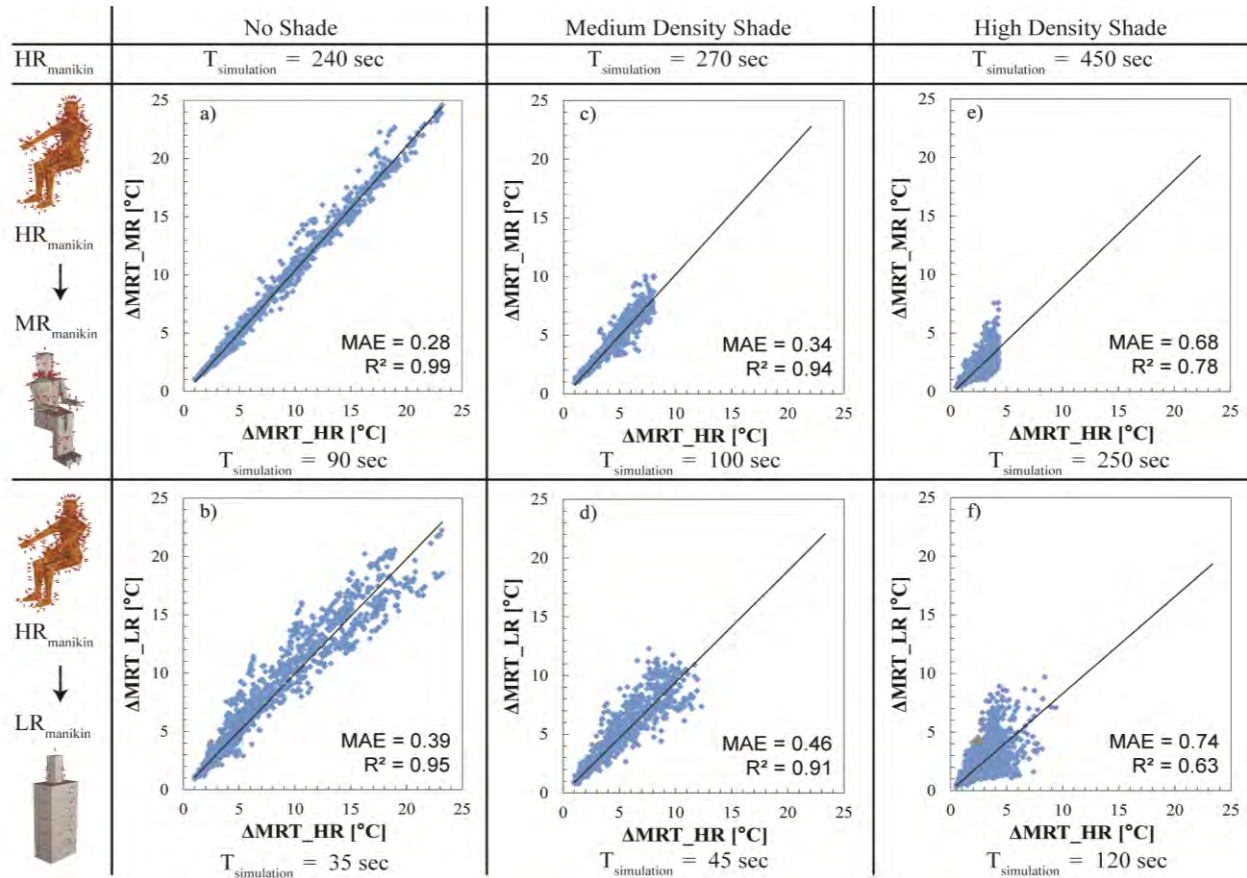


Figure 3. Accuracy and computational time comparison between manikins resolution for three different shading density.

As shown in Figure 3 in the first column, decreasing the number of calculation points does not affect the accuracy of the simulation, with a coefficient of determination (R^2) equal to 0.99 and 0.95 for the simplified manikins and a mean absolute error smaller than 0.4 °C. Meanwhile, we achieved a decrease of calculation time of up to 85% from 240 to 35 s. In the second comparison, we introduced a medium density solar shading system with external louvers characterized by a depth of 0.3 m and a spacing of 0.3 m. As expected, we had a decrease in the explained variance given the coarser meshes with a reduction in R^2 respectively of 0.05 and 0.04 compared to the “No Shade” case. In particular, in the range of ΔMRT between 2 and 5 °C that represents the tolerable range in the thermal comfort zone, the accuracy remains high with a MAE less than half degree. In addition, with a medium density shading system, we were able to reduce the simulation time by 80-85%. Finally, with a high-density solar screen, the scatter-plot graphs in the third column show a larger deviation of results. Both the simplified manikins present a coefficient of determination lower than 0.9, set as a threshold for this analysis, respectively 0.8 for MR and 0.63 for LR manikin.

A visual inspection of the data and the residuals shows that the linear model assumptions are satisfied for the case with no shade and medium density shade. For the high-density shade, there is clear heteroscedasticity of the data, indicating

a larger uncertainty and lower reliability of the errors of the linear model. Given that the objective of these linear regressions is not the prediction of a dependent variable but the assessment of a model, we think that an adjustment (e.g., a Box-Cox transformation) is not needed. Based on the results shown following tests of the framework the LR manikin will be used only with simple glazing and medium shading density configurations.

2.4 Annual Discomfort Radiation Index

The Annual Discomfort Radiation Index (ADR) is based on the concept of annual metric like Daylight Autonomy (DA) [4]. The ADR index is defined as the percentage of the occupied hours (from 8 to 18) of the year when the ΔMRT for each manikin position (see Figure 2) is over the threshold of 4 °C.

$$ARD = \frac{\sum_j (wf_i \cdot t_i)}{\sum_j t_i} \quad wf_i = 1 \text{ if } \Delta MRT_i > 4^\circ\text{C}$$

Where the t_i is each occupied hour in a year; and the ΔMRT_i is the hourly value of shortwave mean radiant temperature for each point of the grid. We selected the 4 °C ΔMRT threshold for ADR because, starting from a neutral thermal condition with a PMV value between -0.1 and 0.1; an MRT increment of this magnitude produces a shift in the occupant's comfort zone, moving the occupant outside the boundaries with a higher PMV, causing slightly warm

conditions (see figure 4). The underlying definition of the ARD index is the assumption that the overall space, and in particular the area close to the façade, is properly thermally controlled by the HVAC system. Specifically, the HVAC system is able to maintain the comfort conditions of occupants when the sun is not striking in the space. The actual definition has not been evaluated for other comfort methods such as the adaptive method [6]. Given the variability in the thermal comfort range based on façade configuration, space activities space subdivision, and sensibility of mechanical systems, the ΔMRT threshold can be adjusted on a case by case basis. By deliberately only using ΔMRT in the calculation of the ARD metric, the results are decoupled from the HVAC system. This allows designers to isolate the effect of direct solar radiation on the comfort of occupants across the spaces they design, providing specific insight that was unavailable before.

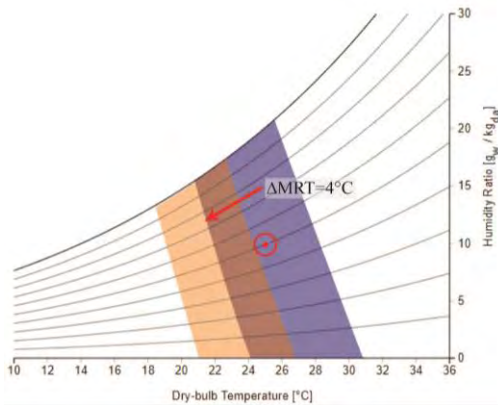


Figure 4. Comfort zone shift due to the increment of MRT caused by incoming solar radiation.

To visualize the ARD index the python script generates two outputs (see Figure 5). The first part (on the left) is an RGB-color scheme that can be used to highlight areas on the floor plan that experience uncomfortable thermal condition over the year. The spatial map reveals the percentage of occupied hours where the ΔMRT is greater than 4°C. A number of uncomfortable hours, in the first three meters of the space, larger than 10% [5] is considered unacceptable.

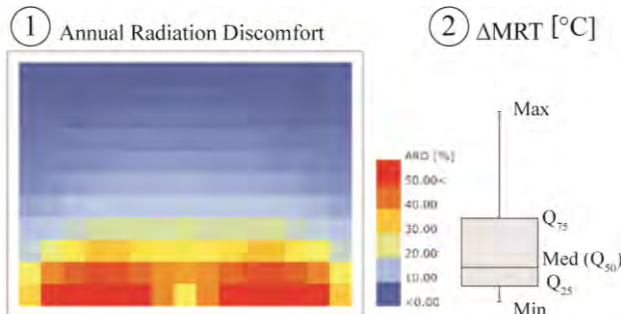


Figure 5. Framework results overview: ARD spatial color map (on the left) and ΔMRT intensity distribution (on the right).

In addition to the spatial heat map, the python script outputs a box-plot chart to visualize the magnitude of ΔMRT in the

first three meters from the façade, considered by ASHRAE 55 in the prescriptive approach as a buffer of unused area in order to guarantee occupants' thermal comfort. In particular, looking at this plot, designers can easily visualize the statistical distribution of ΔMRT during the year and extract median, extreme values. Coupling the two visualizations, we have a spatial, temporal and magnitude understanding of the phenomena and an additional instrument to assess the façade performance.

3 APPLICATION OF ANNUAL DISCOMFORT RADIATION INDEX TO INFORM DESIGN - RESULTS

All the preliminary analyses, simplifications, and assumptions presented so far, have as a final goal the development of a framework that can support the design decision-making side by side with the traditional daylight metrics as DA, sDA, UDI, and ASE. In order to demonstrate the framework we tested and analyzed three façade configurations using the test room and parameters presented in paragraph 2.2. The three façade systems tested, in summary, were two glazing system without shading and with a solar transmittance of 60% and 28% (labeled T60 and T28), and one glazing system with solar transmittance of 52% with shading louvers (labeled T52+L). As indoor conditioning was imposed continuously through the year, additional discomfort for the user would be caused by the increase of MRT due to shortwave radiation. The overall performance criterion for the façade systems takes into account ARD, ΔMRT range, DA_{300} , $UDI_{300-3000}$ and $ASE_{1000Lux, 250h}$. In the second part, we assessed the influence of ΔMRT on the PMV in the first three meters of the floorplate adjacent to the façade in order to understand the occupant's thermal sensation with and without the effect of solar radiation.

3.1 Annual Discomfort Radiation and Daylight

Figure 6 shows the false-color and the box-plot visualization for the three cases analyzed. In the office space with a typical low-e glass (T60_NoShade) the number of uncomfortable hours due to incoming solar radiation falling on building occupants reach peaks of 50-60% in the first 2 meters and around 30-40% in the following meter. As shown in the box-plot representation for T60_NoShade, the median value in the first 3 m is 3.2 °C; close to the critical threshold of 4 °C. In addition, we note a wide variation in the upper quartiles, with a peak of 25 °C. By replacing the glass with high-performance glazing with a solar transmittance of 28% (T28_NoShade), we were able to reduce the number of uncomfortable hours near the façade by 15% with a peak reduction of 30-40% in the first meter.

Case	DA [%h]	UDI [%h]	ASE [%h]	ARD _{3m} [%h]
T60	86.6	69.6	42	28
T28	80.5	74.2	40	15
T52+L	83.9	77.9	13	10

Table 1. Daylight performance scores and average ARD.

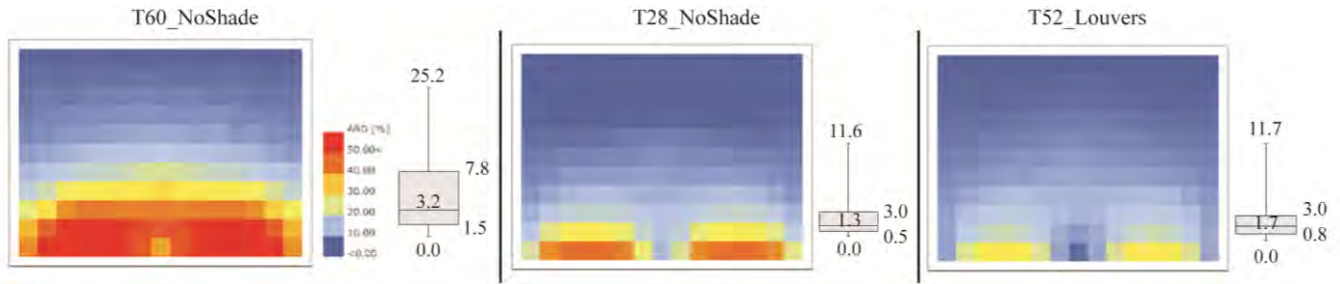


Figure 6. False color plots of Annual Radiation Discomfort (ARD) and box-plot for Δ MRT.

We achieved a consistent reduction also in the peak and median values of Δ MRT. In addition, from the boxplot, we can understand that 75% of Δ MRT values are below the critical threshold of 4 °C. Finally, coupling a low-e glass with external louvers (T52_Louvers), we achieve a further improvement in the “thermal” performance with an average value of ARD in the first three meters equal to 10% and a peak of 25% in the first meter. We found a similar distribution in Δ MRT values with the T28_NoShade, with a slight increase in the median value from 1.3 °C to 1.7 °C.

Table 1 shows for the same cases presented for ARD, the overall daylight performance. Considering the three metrics, we can understand that the glazing plus shading system configuration (T52_Louvers) presents the best daylight performance with the highest level of UDI and the lowest ASE compared to the glazing solutions without shading. In particular, the proposed solution is able to maintain the same level of Daylight Autonomy and reduce the amount of overlit hours. Taking into account both thermal and daylight performance, the T52_Louvers façade configuration performs better, decreasing the number of uncomfortable hours near the glazing while maintaining a good level of illuminance across the space.

3.2 ARD and the Influence on Interior Comfort (PMV)

In addition to the daylight and comfort parameters described above, we also calculated the adjusted PMV for point in time and annual analyses by coupling the outputs from Radiance (Δ MRT) and EnergyPlus (MRT).

Figure 7 shows the PMV values in the office space considering the effect of shortwave radiation on the 21st of December at 9:00 for two different glazing solutions. With 60% solar transmittance, occupants in more than half of the space may experience warm or extremely warm thermal sensation. Additionally, occupants in the other half of the space not directly impacted by direct radiation experience discomfort conditions. With the same outdoor conditions, a solar control glass can guarantee a more comfortable space. PMV over the comfort range is experienced only in the first couple of meters of the floor plate adjacent to the façade and localized only in the portion struck by direct sun. Figure 8 shows the annual variance of PMV and PMV adjusted to include direct solar radiation for the area within the first three meters of the façade for the same three façade configuration assessed before.

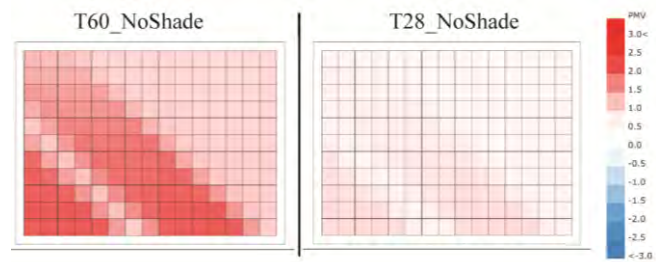


Figure 7. Point in time false color visualization of PMV.

As expected, the glazing system with high solar transmittance (T60_NoShade) that presents the highest ARD also has the wider range in adjusted PMV values. For the T60_NoShade conditions without considering the effect of the incoming shortwave radiation, the median PMV value is slightly above 0. By adding the Δ MRT, the median value rises to 1 and for 50% of the time occupants of the area close to the window experience intolerable thermal conditions. Installing solar control glass or external louvers as shading devices effectively show their effectiveness in decreasing negative thermal comfort conditions. The variance on the thermal sensation after Δ MRT was considered, has been substantially reduced compared to the low-e glazing. Both T28_NoShade and T52_Louvers show a maximum PMV value equal to 2 and a median value close to neutral. More than 50% of the values (first and third quartile) are included in the PMV comfort zone between -0.5 and 0.5.

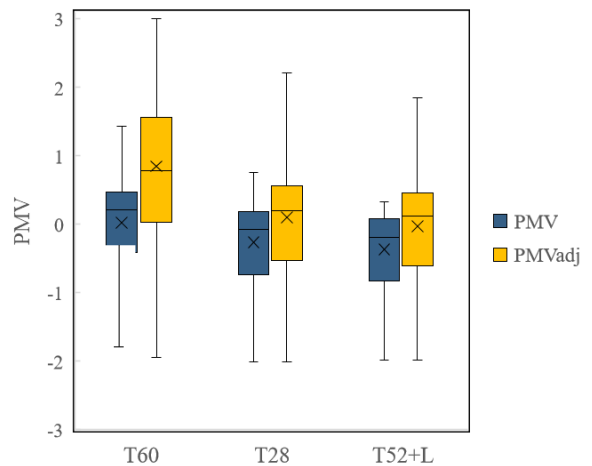


Figure 8. PMV and PMV adjusted variance influenced by façade configuration.

4 DISCUSSION

The results presented in the previous section show that it is feasible to assess the discomfort due to solar radiation landing on occupants across a floor plan. The ARD index calculated using Δ MRT can be used to compare and optimize façade systems to reduce the influence of incoming shortwave radiation on comfort from the first stage of design without the need of complex energy simulations. Energy simulations can be added in subsequent phases to fully understand the overall thermal performance of the system and introduce PMV calculation. The combined results visualization presented in Figure 5 clearly shows the spatial distribution of critical areas of concern and the magnitude of the phenomenon and facilitate the interpretation of results to inform the design process. In the preliminary tests presented in 2.3, we observed a significant variation in the accuracy of the results due to the sensor points density and the complexity of the shading system. For this reason, we suggest selecting the manikin-based on the detail level of the scene and the accuracy required.

The case study results show that significant improvements can be achieved using specific design solutions like solar control glass or external shading systems. ARD results effectively complement classic daylight grid-based metrics, creating a set of holistic metrics that are able to fully describe the performance of a façade system.

From preliminary comparison, between ARD and ASE, it appears that ASE tends to overestimate the amount of space and hours in which occupants are potentially in discomfort condition. Additional comparisons will be carried out in following research studies.

5 CONCLUSIONS AND FUTURE DEVELOPMENTS

This paper introduces a new analysis framework to calculate the number of discomfort hours due to by solar radiation landing directly on occupants. The flexible workflow can be used from the early stages of design or for more detailed analysis when coupled with energy simulations. As shown in the tests, the new Annual Radiation Discomfort (ARD) metric can be employed to estimate the performance of different shading strategies, reduce unused space near the façade caused by increased temperatures, or control roller shade deployment when combined with daylight performance metrics. Furthermore, the ARD metric allows designers to predict the thermal sensations of occupants across the floor at every hour of the year, using a single simulation with the appropriate manikin definition selected based on the complexity of the application.

Although direct solar radiation falling on the user might occur only a few hours during the day, it can generate uncomfortable thermal condition throughout the year that cannot be offset by a HVAC system. This may increase the hours of discomfort experienced by the occupants, potentially leading to the decay of human health and loss of productivity or learning proficiency. Having a framework and a metric that take into account the effect of direct shortwave radiation on comfort can increase the awareness

of the issue and help practitioners design more thermally comfortable spaces.

The framework and analyses described in the paper open the way to new research questions and provide the opportunity to further improve the accuracy and enhance the capacity of the tool:

- Test different manikin-sensor points density to increase the accuracy of simulations for highly complex shading system.
- Investigate the implementation of Bidirectional Scattering Distribution Function (BSDF) in simulations. Given the required spatial resolution, Klems and Tensor-tree BSDF can be tested.
- Thorough comparisons between ARD, UDI and ASE to investigate possible similarities.
- Release a series of open-source Grasshopper components.
- Introduce, for high accuracy simulation, the assessment of overall and local thermal sensations using Machine Learning techniques. Time-series algorithms can be applied in order to make an accurate prediction about what should be the right temperature to apply in a particular room at a specific time.

ACKNOWLEDGMENTS

We thank all the people that provided helpful comments on previous versions of this document. A special thanks to Andrea G. Mainini and Juan Blanco Cadena for the support during the preliminary tests of the workflow.

REFERENCES

1. Akimoto, T., Tanabe, S., Yanai, T., & Sasaki, M. (2010). Thermal comfort and productivity - Evaluation of workplace environment in a task conditioned office. *Building and Environment*, 45, 45–50.
2. Arens, E., Hoyt, T., Zhou, X., Huang, L., Zhang, H., & Schiavon, S. (2015). Modeling the comfort effects of short-wave solar radiation indoors. *Building and Environment*, 88, 3–9.
3. Bessoudo, M., Tzempelikos, A., Athienitis, A.K., & Zmeureanu, R. (2010). Indoor thermal environmental conditions near glazed facades with shading devices - Part I: Experiments and building thermal model. *Building and Environment*, 45(11), 2506–2516.
4. Carlucci, S., Causone, F., De Rosa, F., & Pagliano, L. (2015). A review of indices for assessing visual comfort with a view to their use in optimization processes to support building integrated design. *Renewable and Sustainable Energy Reviews*, 47(7491), 1016–1033.
5. Carlucci, S., Pagliano, L., & Sangalli, A. (2014). Statistical analysis of the ranking capability of long-term thermal discomfort indices and their adoption in optimization processes to support building design. *Building and Environment*, 75, 114–131.

6. De Dear R.J., Brager G. (1998) Developing an Adaptive Model of Thermal Comfort and Preference, Am. Soc. Heating, Refrig. Air Cond. Eng. Inc., Macquarie Res. Ltd. 4106.
7. Henninger, R.H., & Witte, M. J. (2004). EnergyPlus testing with ANSI/ASHRAE standard 140-2001 (BESTEST). *U.S. Department of Energy*
8. Hoyt, T., Schiavon, S., Piccioli, A., Cheung, T., Moon, D., Steinfeld, K. (2017). CBE Thermal Comfort Tool. Retrieved from <http://comfort.cbe.berkeley.edu/>
9. Konis, K. (2013). Evaluating daylighting effectiveness and occupant visual comfort in a side-lit open-plan office building in San Francisco, California. *Building and Environment*, 59, 662–677.
10. Konis, K., & Selkowitz, S. (2017). *Effective Daylighting with High-Performance Facades*. Springer.
11. Mackey, C., Baranova, V., Petermann, L., Menchaca-Brandan, A. (2017) Glazing and Winter Comfort Part 2 : An Advanced Tool for Complex Spatial and Temporal Conditions, *Build Sim.*, 2317–2325.
12. Marino, C., Nucara, A., & Pietrafesa, M. (2017). Thermal comfort in indoor environment: Effect of the solar radiation on the radiant temperature asymmetry. *Solar Energy*, 144, 295–309.
13. Marino, C., Nucara, A., Pietrafesa, M., & Polimeni, E. (2017). The effect of the short wave radiation and its reflected components on the mean radiant temperature: modelling and preliminary experimental results. *Journal of Building Engineering*, 9, 42–51.
14. Sadeghipour M., Pak M. (2013). Ladybug: a Parametric Environmental Plugin for Grasshopper To Help Designers Create an Environmentally-Conscious Design, 13th Conf. Int. Build. Perform. Simul. Assoc.
15. Reinhart, C.F., Mardaljevic, J., & Rogers, Z. (2006). Dynamic daylight performance metrics for sustainable building design. *LEUKOS - J. Illum. Eng. Soc. North Am.* 3
16. Reinhart, C.F., & Walkenhorst, O. (2001). Validation of dynamic RADIANCE-based daylight simulations for a test office with external blinds. *Energy and Buildings*, 33(7), 683–697.
17. Schiavon, S., & Lee, K.H. (2013). Dynamic predictive clothing insulation models based on outdoor air and indoor operative temperatures. *Building and Environment*, 59, 250–260.
18. Wargoeki, P., Frontczak, M., Schiavon, S., Goins, J., Arens, E., & Zhang, H. (2008). Satisfaction and self-estimated performance in relation to indoor environmental parameters and building features. *10th Int. Conf. Heal. Build.* 1–7.
19. Wolfgang, K., Frenzel, C., Hiller, M., Muller, K. (2011). Simulation of thermal comfort in soccer stadia using Trnsys 17. *International Building Performance Simulation Association*.
20. Zani, A., Mainini, A.G., Cadena, J.D.B., Schiavon, S., & Arens, E. (2018). A New Modeling Approach for the Assessment of the Effect of Solar Radiation on Indoor Thermal Comfort. *Building Performance Analysis Conference and SimBuild*.



Black Globe Free Convection Measurement Error Potentials

Eric Teitelbaum,¹² Jovan Pantelic,³ Adam Rysanek,⁴ Kian Wee Chen,⁵ and Forrest Meggers²⁵

¹ETH Zurich, Singapore-ETH Centre, Singapore, SIN

²Princeton University, School of Architecture, New Jersey, USA

³University of California, Center for the Built Environment, Berkeley, USA

⁴University of British Columbia, School of Architecture and Landscape Architecture, Vancouver, CAN

⁵Princeton University, Andlinger Center for Energy and the Environment, New Jersey, USA

ABSTRACT

For thermal comfort research, black globes have become the de facto tool for mean radiant temperature, T_{MRT} , measurement. They provide a quick, cheap means to survey the radiant environment in a space with nearly a century of trials to reassure researchers. However, as more complexity is introduced to built environments, particularly by engineering spaces to separate radiative and convective modes of heat transfer for energy efficiency and comfort, we must reassess the relationship of globe readings in the context of their environments. In particular, corrections for globe readings taking wind into account [1, 4] rely on a forced convection heat transfer coefficient. The simulation proposed in this paper demonstrates the influence of free convection on the instrument's readings. Initial studies show that the T_{MRT} and air temperature separations of 2 K could introduce errors equivalent to 0.1 m/s of air velocity, providing an additional mechanism for globe readings to track air temperatures.

Author Keywords

Black globe; mean radiant temperature; sensors; measurement protocol

1 INTRODUCTION

Heat transfer manipulations for comfort in the built environment have a recent history of being skewed towards convection, i.e. air conditioning, as the majority of thermal comfort research tuned air properties for desired physiological responses [2, 6, 13]. Using air as a medium and the thermostat as its control mechanism, these effective temperature frameworks saw air temperature and humidity as the system side independent variables for comfort. Through today, climate dictates air conditioner or furnace sizing based on the latent and sensible loads, often optimizing form to offset solar radiation gains. However, these systems fail to engage with radiation as an independent mechanism for comfort, despite equal

radiative and convective fluxes in typical office environments [5].

To quantify the radiant environment in a building, black globes are often used to measure a “globe temperature” which is used to back-calculate the environment's perceived mean radiant temperature. The device was originally developed in 1934 [1], and has remained unchanged. Several characterizations of the heat transfer properties characteristics of the globes have been conducted [7, 9], and a widely accepted correction factor for forced air movement was proposed in 1987 by Richard de Dear [4], shown in equations 1 and 2. In these equations, T_{MRT} is the corrected MRT [K], T_g is the measured globe temperature [K], ϵ is the emissivity of the globe [0.95], D is the diameter of the globe [m], T_a is the air temperature [K], h_{cg} is the forced convective heat transfer coefficient [$Wm^{-2}K^{-1}$], and v_a is the air speed [ms^{-1}]

$$T_{MRT} = \sqrt[4]{T_g^4 + \frac{h_{cg}}{\epsilon \cdot D^{0.4}} \cdot (T_g - T_a)} \quad (1)$$

$$h_{cg} = 1.1 \cdot 10^8 \cdot v_a^{0.6} \quad (2)$$

Researchers have noted the limitations of black globes in outdoor environments and windy environments [10, 11], noting the tradeoffs between size and sensitivity to convection and radiation. Importantly, it has been noted that black globes often track air temperature, a phenomenon that can be mitigated in the presence of detectable air motion thanks to the forced convection correction factor in equation 1. Additionally, other researchers have previously noted potential sensitivities of black globe readings to the emissivity of the black coating [8].

However, recent work by the authors in evaluating an outdoor radiant cooling pavilion has elucidated a new issue with black globes - natural convection. In the environment, the radiantly

activated surfaces are convectively separated from the air to create a space with mean radiant temperatures up to 10 K below the air temperature. In the absence of air motion, equation 1 shows the MRT to be equal to T_g , neglecting the potential for free convection that the radiant environment could generate around the sphere. Comparing the mean radiant temperature calculated from globe readings with the ground-truth mean radiant temperature established with a pyrgometer and pyranometer, it was immediately clear that something was wrong since the recorded mean radiant temperature was below the dewpoint, yet no condensation was visible on the globe (Which would have been yet another mechanism skewing the reading).

This paper describes a correlation-based simulation from empirically derived heat transfer equations about spheres to describe the potential contribution to globe measurement errors from free convection. At most in the literature it has been mentioned that “natural convection currents affect heat exchange, and modify the relations” [9], however the corrections have never been directly addressed.

2 METHODS

To assess the basic contributions of forced and free convection about a black globe, Nusselt number correlations were obtained. The Nusselt number, Nu , is a dimensionless parameter that describes the ratio of convective heat transfer to conductive heat transfer, and is shown in equation 3. In this equation, H_c is the convective heat transfer coefficient [$Wm^{-2}K^{-1}$], D is the hydraulic diameter [m], and k is the thermal conductivity of air [$0.02662 Wm^{-1}K^{-1}$]. Therefore if the Nusselt number is known for a globe, the convective heat transfer coefficient can be calculated as in equation 4.

$$Nu = \frac{H_c D}{k} \quad (3)$$

$$H_c = \frac{Nu \cdot k}{D} \quad (4)$$

Updated Nusselt number correlation equations were obtained from the literature. Equation 5 shows the free convection correlation for free convection about a sphere [3].

$$Nu_{free} = 2 + \frac{0.589 Ra_D^{\frac{1}{4}}}{(1 + (0.469/Pr)^{\frac{9}{16}})^{\frac{4}{9}}} \quad (5)$$

In equation 5 Ra is the Rayleigh number, and Pr is the Prandtl number. Equation 5 is valid for $Ra < 10^{11}$ and $Pr \geq 0.7$. Ra is calculated in equation 6 and Pr is calculated in equation 7.

$$Ra = \frac{g\beta}{\nu\alpha}(T_g - T_a)D^3 \quad (6)$$

$$Pr = \frac{c_p\mu}{k} \quad (7)$$

In equations 6 and 7, g is the acceleration due to gravity [$9.81 ms^{-2}$], β is the thermal expansion coefficient of air [$0.0034 K^{-1}$], ν is the kinematic viscosity [$1.48 \cdot 10^{-5} m^2 s^{-1}$], α is the thermal diffusivity of air [$2.591 \cdot 10^{-5} m^2 s^{-1}$], c_p is the specific heat capacity of air [$1005 J kg^{-1} K^{-1}$], and μ is the dynamic viscosity of air [$1.81 \cdot 10^{-5} Pa s$]. For comparison to the free convection case, the same forced convection relationships were derived using a Nusselt correlation provided in equation 8 [12].

$$Nu_{forced} = 2 + (0.4Re^{\frac{1}{2}} + 0.06Re^{\frac{2}{3}})Pr^{0.4} \quad (8)$$

In equation 8, Re is the Reynolds number given in equation 9. Using these convection correlations, the magnitude of each mode of heat transfer was assessed for varying air velocities and globe temperatures. Equation 8 is valid for $3.5 < Re < 7.6 \cdot 10^4$ and $0.7 < Pr < 380$, appropriate for this application.

$$Re = \frac{v_a D}{\nu} \quad (9)$$

To reparametrize a version of equation 1 for free convection effects on the T_g reading in environments with large surface to air temperature gradients, the equilibrium globe description equation, shown as equation 10 from [4], becomes equation 11.

$$\sigma\epsilon(T_g^4 - T_{MRT}^4) = h_{c,free}(T_a - T_g) \quad (10)$$

$$T_{MRT} = \sqrt[4]{T_g^4 + \frac{Nu_{free} \cdot k}{\epsilon\sigma D}(T_g - T_a)} \quad (11)$$

The form of equation 11 is useful since the correction can be applied both for free and forced convection.

3 RESULTS

Comparing the contributions from both free and forced convection to the globe temperature, it is clear that as the air velocity increases, forced convection will dominate the reading for T_g , see figure 2. However, as the difference between T_g and T_a grows as is plotted in figure 1, there is a plateau in the convective response. The magnitude is smaller than air speeds above 0.1 m/s, however the shape of the free convection response presents certain challenges for interpreting the true T_{MRT} from globe readings in a free convection dominated scenario.

For example, the change in h_c for $T_g - T_a$ from 3 to 4 is approximately 8 to $8.2 W m^{-2} K^{-1}$, therefore making the calculation very susceptible to any fluctuations. This is unlike the globe's response to forced convection, which is nearly a linear response to air speed.

However, as h_c is also multiplied by the temperature difference, the effect is not negligible. As shown in figure 3, the

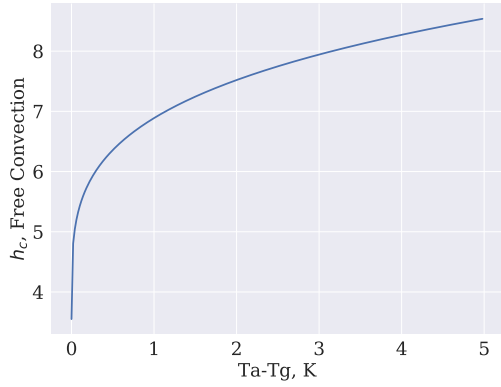


Figure 1. Convective heat transfer coefficient for free convection.

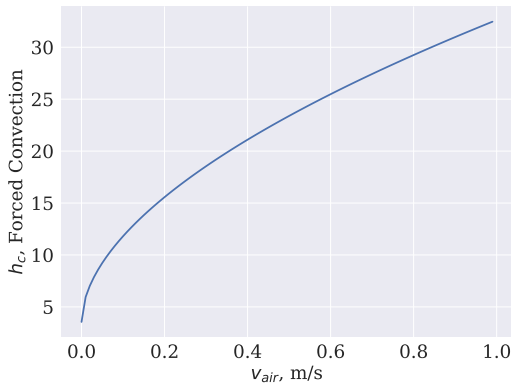


Figure 2. Convective heat transfer coefficient for forced convection.

heat lost due to forced and free convection, $Q_{convection}$ at a low air velocity is larger than the heat lost due to free convection, however the free convection portion is certainly not negligible.

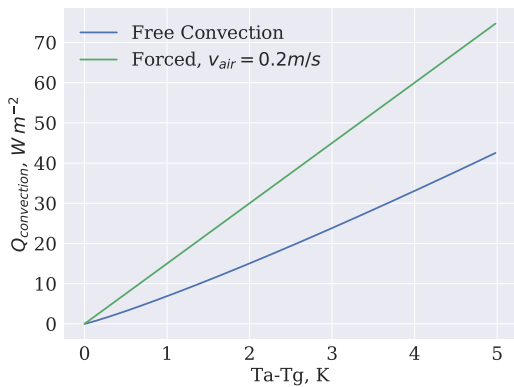


Figure 3. Comparison between heat lost due to free and forced convection.

Reconstructing a potential measurement domain with the free convection correction is shown in figure 4, for differences in

T_a and T_g up to 5 K. A slice of this data is shown in figure 5 with a fixed $T_a = 30^\circ C$.

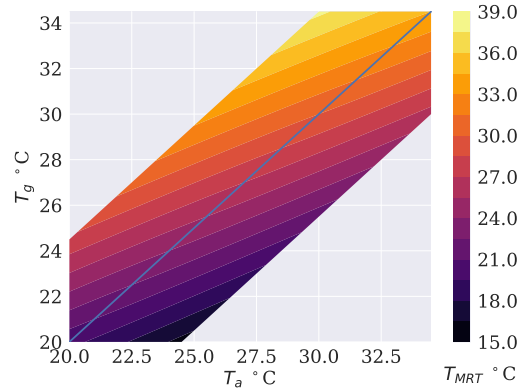


Figure 4. The remapped domain calculating T_{MRT} from T_g and T_a measurements, correcting for free convection.

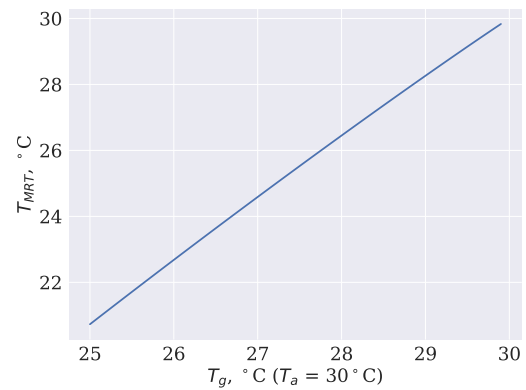


Figure 5. The calculated T_{MRT} using the proposed free convection correction factor from the globe measurement T_g and fixed $T_a = 30^\circ C$.

4 DISCUSSION

Clearly, there is a potential significant contribution to globe temperature from from convection in environments with increasing air/surface gradients. This fact did not go unnoticed from original researchers [7], however the contributions was not further investigated since many real building scenarios do not generate large air temperature to surface temperature separations. However, with new advancements with radiant cooling systems which separate radiative from convective heat transfer, it becomes a valid question to test the limits of black globes, with respect to greater air/surface separations for radiant cooling.

A potential mechanism describing the observed discrepancy in the test radiant cooling pavilion that inspired this study is the fundamental nature of blackbody emission. Proportional to T^4 , at high absolute values the relationship between emitted power and temperature is roughly linear. However, consider a theoretical comparison between the radiative forcing of a black globe from a radiant cooling system with a design

T_{MRT} setback of 5 K from the air temperature with the radiant forcing from a radiant heating system with a T_{MRT} 5 K higher than the air temperature. Compared to the reference “equilibrium” case where $T_g = T_{air}$, the nonlinearity of the blackbody emission is accentuated. This is plotted in figure 6, taking a small office test scenario with a fixed air temperature of $T_a = 30^\circ\text{C}$. The T_{MRT} is modulated from 0.1 to 10K above and below the reference 30°C temperature. Clearly, radiant heat is able to sustain larger T_g gradients due to the additional power of radiant heating compared to radiant cooling. The measured T_g values are much more sensitive in a radiant cooling scenario to small changes in convection than in a radiant heating scenario. This is a potential explanation for why concerns regarding free convection have not needed to be addressed, since most of the literature concerning black globes physics has exclusively been constructed with data from radiant heating.

In fact, figure 6 implies that globes may overestimate the radiant temperature for radiant heating, since the globe’s forced convective losses shown by the blue line are much smaller. The overestimation of radiant heating and associated underestimation of radiant cooling could have impacts on the perceived functionality of both systems.

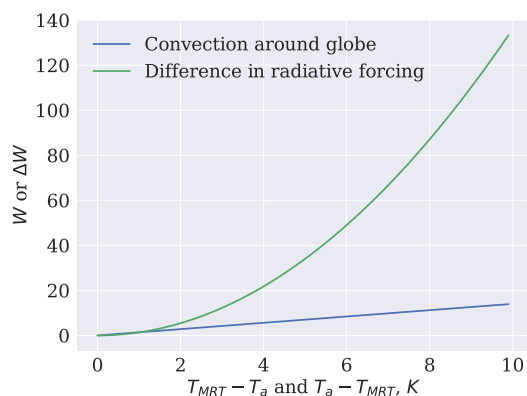


Figure 6. Comparison between radiative forcing of a small office (20m^2 wall area) with radiant heating or cooling above or below the air temperature (x-axis) and the modeled forced convection around a globe at $v_{air} = 0.5\text{m/s}$. Radiant cooling is largely under-powered compared to radiant heating to drive the globe temperature away from the air temperature.

In the future, generating experimental datasets to validate these claims will be necessary. While it is potentially a small contribution to a niche group of radiant comfort researchers, understanding the physics of measurement tools and the self-imposed limitations will quell potential systematic measurement errors in the future.

5 CONCLUSION

The simulations presented in this paper make a compelling argument for the necessity of a free convection correction as the gradient between the air and surface temperatures in a space increases. Free convection effects can introduce a potential measurement error that is not currently accounted for, and is of the same magnitude as forced convection. This

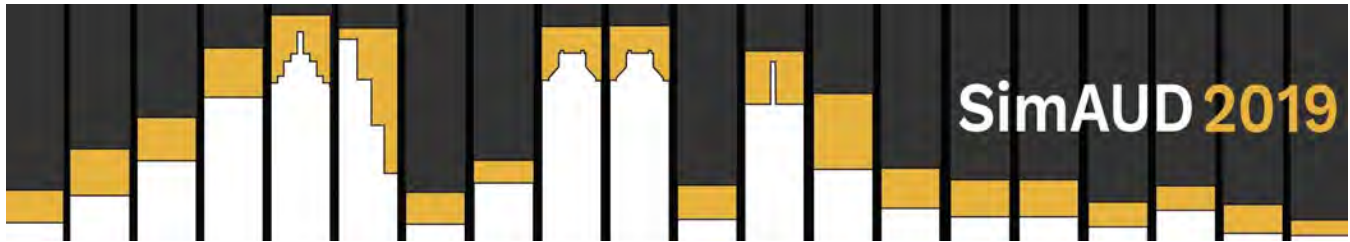
paper presents a simulation-based framework for free convection around a globe, and a correction factor to remap the measurement domain. Future work will be carried out to experimentally validate the framework.

ACKNOWLEDGMENTS

We thank all of the staff and researchers involved in this project, particularly the facilities staff at United World College Southeast Asia for the support in kind of our radiant cooling experiments in the tropics.

REFERENCES

1. Bedford, T., and Warner, C. The globe thermometer in studies of heating and ventilation. *The Journal of Hygiene* 34, 4 (1934), 458–473.
2. Carrier, W. H. Rational psychometric formulae. *Trans Am Soc Mech Eng* 33 (1911), 1005.
3. Churchill, S., and Bernstein, M. A correlating equation for forced convection from gases and liquids to a circular cylinder in crossflow. *Journal of Heat Transfer* 99, 2 (1977), 300–306.
4. De Dear, R. Ping-pong globe thermometers for mean radiant temperatures. *Heating and Ventilation Engineer and Journal of Air Conditioning* 60 (1987), 10–11.
5. Eric Teitelbaum. Expanded psychometrics for novel integrated design of radiant and passive building systems. Master’s thesis, Princeton University, 2017.
6. Fanger, P. O. *Thermal comfort. Analysis and applications in environmental engineering*. Copenhagen: Danish Technical Press., 1970.
7. Fountain, M. Instrumentation for thermal comfort measurements: The globe thermometer. *Internal study, Center for the Built Environment* (1987).
8. Guo, H., Teitelbaum, E., Houchois, N., Bozlar, M., and Meggers, F. Revisiting the use of globe thermometers to estimate radiant temperature in studies of heating and ventilation. *Energy and Buildings* 180 (2018), 83–94.
9. Hey, E. Small globe thermometers. *Journal of Physics E: Scientific Instruments* 1, 9 (1968), 955.
10. Middel, A., Selover, N., Hagen, B., and Chhetri, N. Impact of shade on outdoor thermal comfort: A seasonal field study in tempe, arizona. *International journal of biometeorology* 60, 12 (2016), 1849–1861.
11. Thorsson, S., Lindberg, F., Eliasson, I., and Holmer, B. Different methods for estimating the mean radiant temperature in an outdoor urban setting. *International journal of climatology* 27, 14 (2007), 1983–1993.
12. Whitaker, S. Forced convection heat transfer correlations for flow in pipes, past flat plates, single cylinders, single spheres, and for flow in packed beds and tube bundles. *AIChE Journal* 18, 2 (1972), 361–371.
13. Yagoglou, C. Report of committee to consider the report of the new york state commission on ventilation. *American Society of Heating and Ventilating Engineers* 30 (1924), 254–256.



Assessing the Performance of UFAD System in an Office Building Located In Various Climate Zones

Roshanak Ashrafi, Mona Azarbayjani, Robert Cox, Benjamin Futrell, Joseph Glass, Amir Zarrabi and Armin Amirazar

UNC Charlotte
Charlotte, United States

{Rashrafi, Ahossei3, Aamiraza, Mazarbay, Robert.Cox, Benjamin.Futrell, Jglass10}@UNCC.edu

ABSTRACT

The energy performance of Underfloor Air Distribution (UFAD) system is previously investigated in several studies. Energy saving is known to be one of the benefits of UFAD in comparison to other all-air systems; however, there has been some controversy over the performance of UFAD system in each climate. This paper aims to investigate the role of the climatic condition on the energy behavior of the UFAD, compared to the Over Head (OH) air distribution system. To that end, the effects of temperature and humidity on the energy performance of the system are examined in detail. The overall research plan is based on simulating one story of an existing office building in Phoenix with EnergyPlus. The validated model is then used in different ASHRAE climate zones to predict energy consumption in terms of cooling loads, heating loads and fan energy usage for the two systems: UFAD and OH.

These comparative analyses have led to a comprehensive understanding of the energy performance of UFAD and OH systems under different climatic conditions. The *Results* section highlights the overall efficiency of UFAD system, pointing to different percentages of energy saving in each climate. It is found out that UFAD system works best in San Francisco with 26 percent of energy saving and relatively warm climatic conditions, while climates that were too hot or too cold adversely effected the energy saving performance. The lowest percentage of energy saving is 10.31 percent for Duluth in the very cold climate category. The energy saving percentages were then visualized on the map to provide a better spatial understanding of this system's effectiveness.

Author Keywords

Underfloor Air Distribution (UFAD); climate; energy performance; energy saving.

1 INTRODUCTION

Energy consumption in a building HVAC system is dependent on many factors, such as the building envelopes properties and the HVAC system technology. Climatic conditions can also influence the system energy use by affecting the performance indicators, such as room air stratification and plenum thermal decay [1,11,12,13]. Therefore, we need to have a comprehensive understanding of the performance, proper installation and proper underlying design of the UFAD system to properly evaluate its potential efficiency and energy saving improvements [1,11]. It is argued that the UFAD systems are not as efficient as their early stage designs, which may be due to poor design and operating conditions [2]. So far, little is known about the possible effect of climate on the UFAD design and proper design of this system based on the existing climatic conditions. Some papers have investigated the performance of the UFAD system in a few climates, and others have looked at the effect of the climate on the system cooling loads [3]; however, there is not any research that studies the overall performance of the UFAD system in different climatic conditions. In a research that was conducted by California Build Environment in CBE (2009) they have compared the performance of UFAD in 3 different climates in California and found the total energy saving in San Francisco warm-marine climate is 5.2% higher than Sacramento's Mediterranean climate [4]. Later in 2011, they added more climatic conditions to their investigation, concentrating only on the cooling loads of the building, and found there was not much difference in performance of the UFAD in different climates in terms of cooling loads [3].

In addition, there have not been sufficient studies about the energy saving of the UFAD in humid climates, in comparison to the research that studies the UFAD performance in mild and hot climates [5]. As the supply air temperature is higher in the UFAD system, the dehumidification capability of the air-handling unit deteriorates, causing a higher indoor relative air humidity

[5]. Therefore, considering the occupants thermal comfort we have to provide more dehumidification strategies in UFAD systems, especially in humid regions. This also affects the energy saving of the system, as more energy is demanded for dehumidifying and removing the latent load.

The goal of this study is to investigate the overall energy performance of the UFAD system compared to OH system in different climatic conditions. To that end, we have looked into the annual energy consumption of an existing building in hot and dry climate, and then compared it to the energy consumption of the same building in all ASHRAE defined building climates in the United States.

2 METHOD

In this study, the energy performance of one existing building with its prototypes in 12 other climates is compared in terms of total energy consumption, heating energy, cooling energy and fan energy usage. The results of the energy savings were used to create a visualization map based on the US geographical map. This map is useful, as it graphically displays the areas that have a better energy performance.

Through this comparative and parametric approach, the building and system elements remain the same, except for the cooling coil schedules in cold climate cases.

2.1 Climate Zones

To define the climate content, we have used the standardized climate zones from ASHRAE Standard 169-2013[10]. The classification is based on heating degree-days (HDD) and cooling degree-days (CDD) and precipitation data to determine the moisture zone. The data about the CDD and HDD is provided by National Climatic Data Center (NOAA) with the normal of 1981-2010 [6].

We have selected 14 cities, each representing a unique climate zone that includes 7 thermal zones and 3 humidity zones, which are listed in Table 1.

CITY	ZONE	ZONE NAME	HDD	CDD
Miami	1A	Very Hot-Humid	128	4575
Houston	2A	Hot- Humid	1291	2940
Phoenix	2B	Hot- Humid	935	4607
Charlotte	3A	Warm- Humid	3388	1518
Las Vegas	3B	Warm- Dry	2044	3294
San Francisco	3C	Warm- Marine	2653	164
Baltimore	4A	Mixed- Humid	4764	1164
Albuquerque	4B	Mixed- Dry	4179	1322

Seattle	4C	Mixed-Marin	4370	450
Chicago	5A	Cool- Humid	6340	843
Boulder	5B	Cool- Dry	6011	622
Minneapolis	6A	Cold- Humid	7580	753
Helena	6B	Cold- Dry	7541	406
Duluth	7	Very Cold	9444	204

Table 1. Selected Cities and Climate Zones



Figure 1. Building Overall perspective

2.2 Description of the Simulated Building

Our reference case is the middle floor in a three-story office building in Phoenix, Arizona in a trapezium shape (37m*115) with an aspect ratio of 3 to 1, which is shown in Figure 1. The total floor area is 4544 m² and is divided to three separate sections, each with their own air handling units as they are numbered in Figure 2. Each floor is composed of 3 interiors and 4 perimeter zones, as shown in Figure 2. The pattern of the perimeter and interior zones is based on the effective area of the windows and the diffusers that are attached to the exterior wall of the building, which creates a five feet wide perimeter zone. For the interior zones each thermal zone is defined based on the effective area of the air handling unit for that area. The central interior zone (number 2) had to be divided to 3 subzones as EnergyPlus can't calculate the concave geometries accurately. We have modeled the supply and return plenum as individual thermal zones for the entire floor. In both systems, the plenums are modeled with 60 cm of height. Other specifications of each zone are listed in Table 2 and Table 3. We have also modeled the windows and walls properties, occupancy patterns, lights and equipment loads to get precise cooling and heating loads through the day for a whole year. The construction type of the building in its existing climate could also be used in the other scenarios; however, we had to change the cooling coil schedule for the colder climates to be able to operate in all months of the year. The lighting, occupancy and equipment schedules are based on the real building schedule, which is typically occupied from 6am to 6pm and the equipment are running from 4am to 10pm, as Table 4 indicates.

Walls	Construction	Metal Frame, 2*6, 16 in. O.c.
	Ext Finish/Color	Wood/Plywood 'Medium' (abs= 0.6)
	Exterior Insulation	½ in. fiber board sheathing (R-13)
	Additional Insulation	R-19 batt
Ground Floor	Construction	4 in. Concrete
	Exterior Insulation	3 in. polyurethane (R-18)
Windows	Glass Category	Double Clear/Tint
	Glass Type	Double Clear 1/4in, 1/2in Air
	Frame work	Aluminum/ Fixed
	Frame Width	1.3 in.

Table 2. Building Construction Properties

	Area [m ²]	Height [m]	Wall Area [m ²]
PLENUM-INT	1407	0.60	0
PLENUM-S	1543	0.60	0
PLENUM-N	1594	0.60	0
PERIMETER-SOUTH	41	3.35	80%
PERIMETER-NORTH	57	3.35	80%
PERIMETER-WEST	165	3.35	12%
PERIMETER-EAST	167	3.35	40%
INTERIOR-NORTH	1359	3.35	0
INTERIOR-INT	1062	3.35	0
INTERIOR-SOUTH	1412	3.35	0

Table 3. Thermal Zones Properties

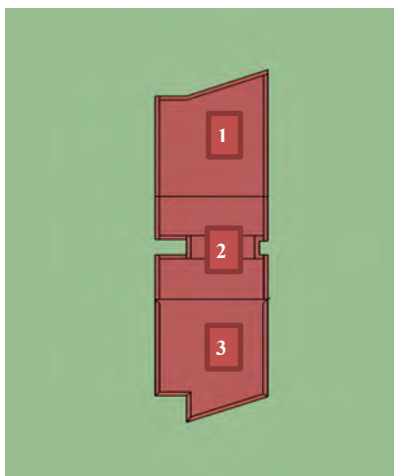


Figure 2. Building Plan

FEATURE	OH	UFAD
Skin/glazing	384 m ²	Same
Window/wall ratio	47.5	Same
Room cooling set point	24°C	Same
Room heating set point	21°C	Same
Equipment	7.6 W/m ²	Same
People	4 m ² /Person	Same
Infiltration	0.0168/Exterior Area	Same

Table 4. Building Load Properties

2.3 Simulated Model

We have used EnergyPlus simulation software, which is currently the most ideal software for simulating the UFAD because of its consideration of the room stratification and simultaneous simulation of zones, systems and plants [7]. The UFAD system in this project is working in a constant air volume (CAV) that relies on the variation of supply air temperature with a constant speed and electric reheat system. The supply air temperature is changing based on the return air temperature and zone temperature to provide the desired thermal comfort. HVAC system parameters and peak occupancy information were gathered from design drawings and meetings with project team members.

On the other hand, the OH system is modeled with a Variable air volume (VAV) air terminal with electric reheat, which uses variable speed fans in the perimeter zone. The SAT for the OH prototype is 12°C; while in the UFAD system the SAT is normally higher than this number as the air is provided directly to the occupied zone. The initial SAT for the UFAD system is 15°C that is changing based on the load of the zone in each time of the day. The AHU fan pressure is also lower for the UFAD system, as shown in Table 5. The HVAC system settings for the UFAD are extracted from the *as built* drawings of the building and the information provided, except for the *Minimum outside air* which is a default amount. For the OH system we have not made any unnecessary changes to have an accurate comparison, other than the basic differences of the UFAD and OH system such as SAT and fan pressure. The fan pressure is 1000 Pa for the OH and 700 Pa for the UFAD system. The supply plenums for both systems are ducted, which decreases the thermal decay effect and results in more fan energy saving, especially in the UFAD. As mentioned before all the HVAC system settings are the same for other climate scenarios except for the cooling coil schedules as they need to run for more months through the year.

HVAC	OH	UFAD
AHU supply air temperature (for OAT range)	12°C	15°C
AHU fan design static pressure	1000 Pa	700 Pa
AHU fan efficiency	0.9	0.9
Minimum outside air rate	0.00944 m ³ /min/person	0.00944 m ³ /min/person
Airside economizer; fixed dry bulb	Yes	Yes
Night cycle control	Yes	Yes
Interior zone reheat	Yes	No
Heating & Cooling Coil	Water	Water
Chiller design COP	5	5
Cooling tower	Single speed	Single speed
Boiler design efficiency	0.9	0.9

Table 5. HVAC System Properties

2.4 Validation

For the validation of our simulations we have compared the indoor air temperature that was measured by the data loggers in the perimeter zones of the Phoenix building to the simulations' average zone air temperature results. The north perimeter zone was selected for the comparisons and the average zone temperature was compared, both for the occupied hours and the whole day. We have selected two business weeks in the winter (January) and the summer (August) for checking the simulation validation in both heating and cooling modes. The measured and simulated average zone temperatures are listed in Figure 3 for the occupied hours and Figure 4 for the whole day average temperature. As it is showed in Figure 5 scattered plot, the simulation results correlate with the temperature measurements for both cooling and heating days with respectively 24°C and 21°C zone set point temperatures. The central blue line fully correlated temperatures while the dotted lines are borders for the accepted ±10% simulation error.

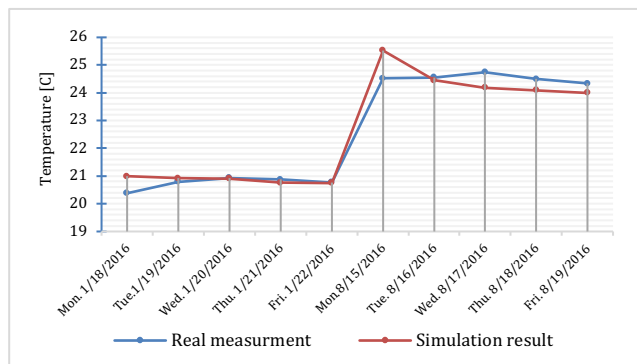


Figure 3. Occupied Hours Zone Average Temperature

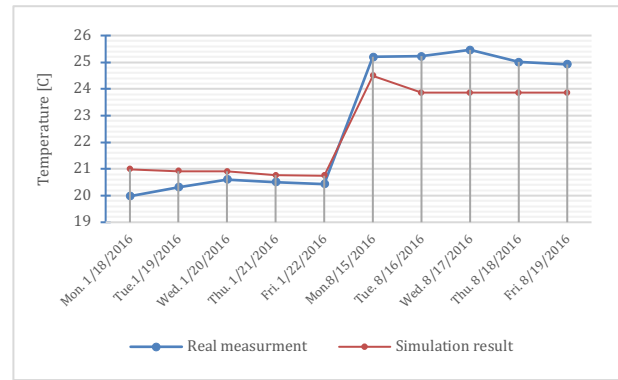


Figure 4. Whole day Zone Average Temperature

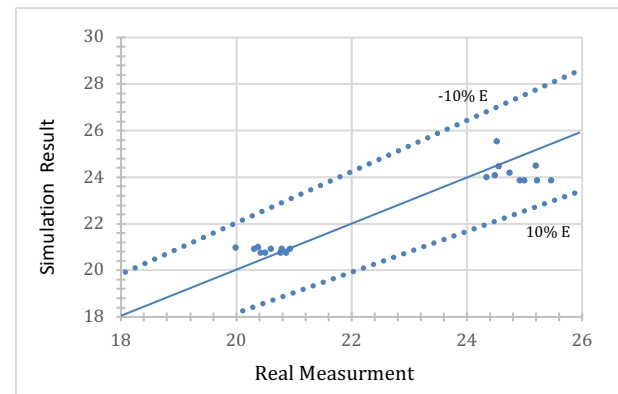


Figure 5. Correlation of the measured and simulated results

3 RESULTS

The net results of the simulation show annual energy consumption of the building in terms of cooling, heating, fan, heat rejection and pump energy. We have compared the energy consumption in each section of the HVAC system for the buildings in different climates in Figure 6. As it is displayed in Figure 6 San Francisco has the lowest energy consumption in both UFAD (331 MJ/m²) and OH(453 MJ/m²) scenarios, while Miami has the highest energy consumption in both of these systems with the numbers of 694 MJ/m² and 852 MJ/m² respectively. Expectedly, cooling and heating energy are the most energy consuming sections in all of the climate, followed by fan energy consumption. The fan energy in the UFAD system has the highest amount in Phoenix (58.33 MJ/m²) and the lowest amount in cold climate of Duluth (34.78 MJ/m²). The pumps energy consumptions is also effected by the climate as in the cold climates there is no need for cooling energy and pumps action. The pump energy consumption can be as high as 72.84 MJ/m² in Miami that decreases down to 5.94 MJ/m² for Helena. We have also investigated the energy saving in all major sections and the total energy saving.

3.1 Total Energy Saving

In the first set of analysis the total energy saving of the system is compared in different climates to identify the best climatic conditions for the UFAD system instead of an OH. The results indicate that the UFAD system has overall energy saving in comparison to OH system for our base case in Phoenix and all other climates. The percentage of the saving was calculated based on the whole building annual energy consumption.

As shown in Figure 7 the UFAD energy saving is different in each climate. Interestingly, the percentages distribution resembles a bell shaped curve at the top with relatively

higher amount in the left side of the chart. The lowest percentage of saving is for the coldest city, Duluth in climate zone 7, which is 10.31percent; while the highest amount is 26 percent for San Francisco in climate zone 3C and warm and marine climate. It is apparent from this chart that the percentage of energy saving is decreasing by getting closer to the extreme weather conditions. Among the hot climates Miami and Houston respectively with very hot and humid, and hot and humid climates have the two lowest amounts of energy saving, which are 18.56 and 18.16 percent. In the cold side of chart is also a clear trend of decreasing that finally ends in 10.43 percent for Minneapolis with cold and humid weather and 10.13 percent for the very cold climate of Duluth.

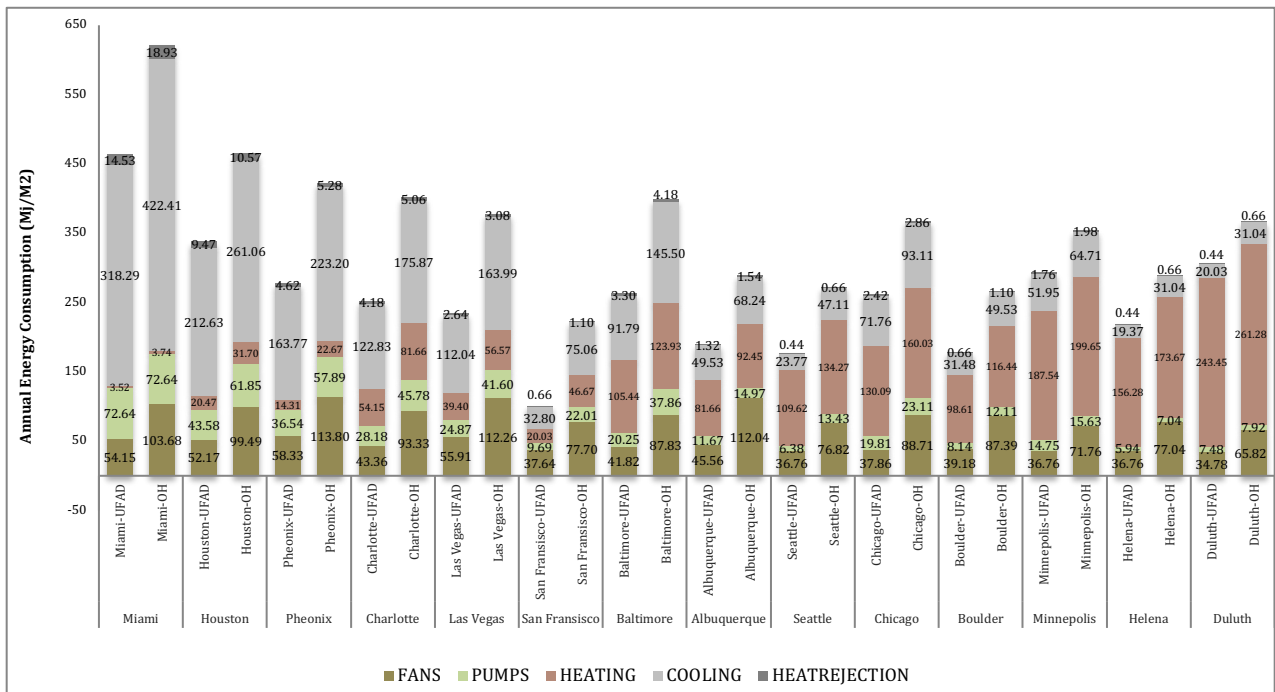


Figure 6. Energy Consumption in All Scenarios

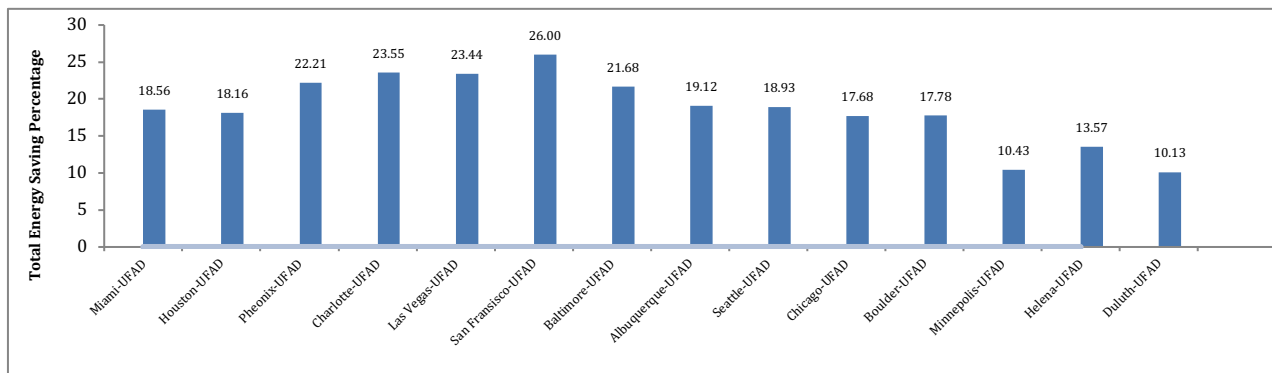


Figure 7. Energy Saving Percentage in Each Climate

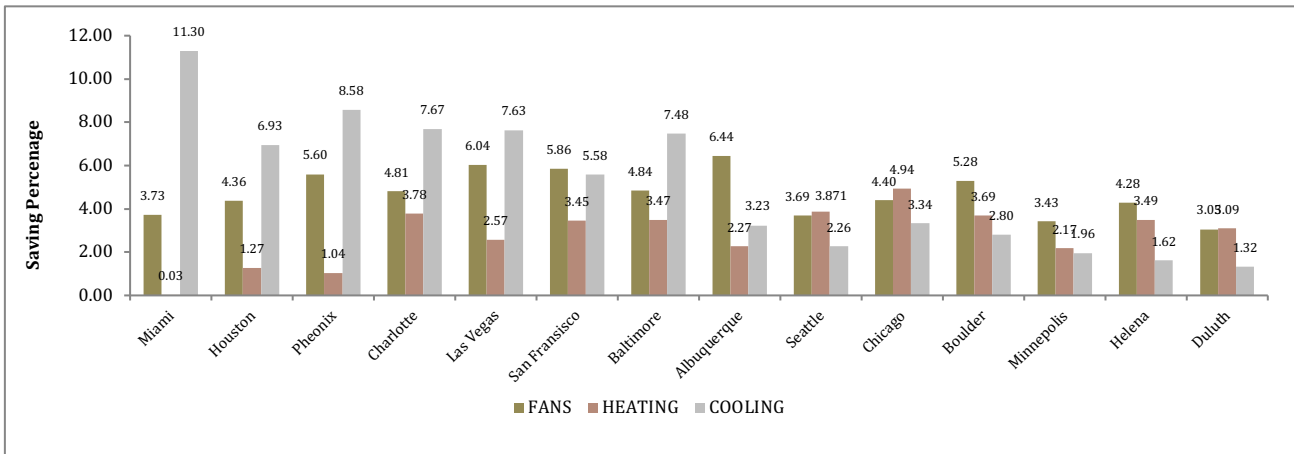


Figure 8. Energy Saving Percentage in Each Section

In the second phase, we looked into the energy saving of the three major sections: heating, cooling and fan energy usages. The UFAD system showed energy savings in all these units. To have a better understanding of the percentage of energy saving in the components, we calculated the weighted contribution of each in the final energy saving. For this purpose, first the contribution ratio (CR) is calculated based on each components energy consumption, and the total energy consumption as it is defined in Equation 1.

$$CR = \frac{\text{Component Energy Consumption}}{\text{Total Energy Consumption}}$$

Equation 1.

The Contribution Ratios for all the cases are listed in Table 6. Finally, we have calculated the weighted saving based on the percentage of saving in each component and its CR as it is shown in Equation 2.

$$\text{Weighted Saving} = CR * \text{Saving Percentage}$$

Equation 2.

The results obtained from this procedure are illustrated in Figure 6 for each unit in all climates.

Scenario	CR _{fan}	CR _{heating}	CR _{cooling}
Miami-UFAD	0.08	0.01	0.46
Miami-OH	0.12	0.00	0.50
Houston-UFAD	0.09	0.04	0.37
Houston-OH	0.14	0.05	0.38
Phoenix-UFAD	0.11	0.03	0.32
Phoenix-OH	0.17	0.03	0.34
Charlotte-UFAD	0.09	0.11	0.25
Charlotte-OH	0.15	0.13	0.28
Las Vegas-UFAD	0.12	0.08	0.24
Las Vegas-OH	0.18	0.09	0.27
San Francisco-UFAD	0.11	0.06	0.10
San Francisco-OH	0.11	0.07	0.11
Baltimore-UFAD	0.09	0.23	0.20
Baltimore-OH	0.13	0.18	0.21
Albuquerque-UFAD	0.11	0.19	0.12
Albuquerque-OH	0.22	0.18	0.13
Seattle-UFAD	0.07	0.21	0.05
Seattle-OH	0.15	0.26	0.09
Chicago-UFAD	0.08	0.26	0.15
Chicago-OH	0.15	0.27	0.16
Boulder-UFAD	0.10	0.24	0.08
Boulder-OH	0.18	0.23	0.10
Minneapolis-UFAD	0.07	0.36	0.10
Minneapolis-OH	0.12	0.34	0.11
Helena-UFAD	0.08	0.35	0.04
Helena-OH	0.15	0.33	0.06
Duluth-UFAD	0.06	0.45	0.04
Duluth-OH	0.11	0.44	0.05

Table 6. Contribution Ratios for Each Scenario

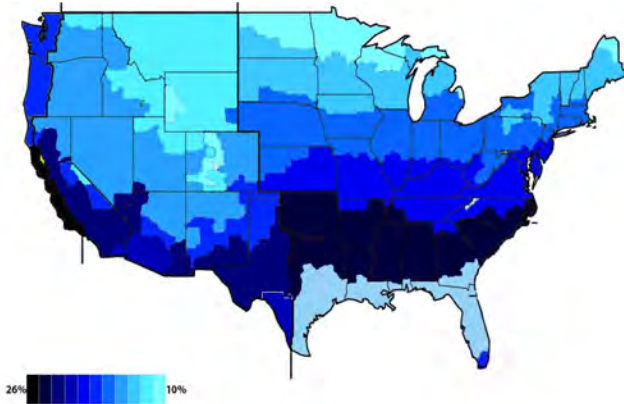


Figure 9. UFAD Energy Saving Visualization

3.2 Cooling Energy

It is expected for the cooling load of the UFAD system to be higher than OH, as the thermal capacity of a room with UFAD is decreased by adding the floor plenum. However, it is shown in Figures 6 and 8 that the cooling energy is still lower than OH, providing cooling energy saving in all climates. Figure 8 indicates that the cooling energy has the highest energy saving of 11.30 percent in Miami with the hottest weather. By moving toward normal weather conditions, an overall decrease in the saving is perceivable. This declining trend continues by getting to the colder areas as we have the lowest cooling energy saving in Duluth with 1.32 percent.

The difference in cooling energy saving can be explained by the difference in both cooling degree days and humidity. High humidity is one of the factors that results in lower efficiency of the UFAD systems; however we are not sure whether it's working better or worse than an OH system. By comparing the energy saving of two cities with approximately the same cooling degree days and different humidity such as Miami and Phoenix we can argue that humidity has less adverse effect on the efficiency of UFAD in comparison to OH. The same result can be understood by comparing Baltimore and Albuquerque with the same cooling degree days and different humidity.

3.3 Heating Energy

During heating days in the underfloor system, the warm returning air reduces heating energy, which results in improved heating performance of the UFAD as Figures 6 and 8 illustrate. This is an important factor for the energy savings in relatively cool climates. According to Figure 8 the highest amount of saving in the heating energy is 4.94 percent in Chicago, and the lowest amount is nearly zero as the heating load itself is negligible in the very hot climate. The amount of energy saving in the heating section mostly results from no reheat setting in the interior zones

of the UFAD. As it is shown in Figure 8, we cannot define any special trend for the saving in heating energy.

3.4 Fan Energy

Fan energy is one of the major energy saving sources in the UFAD as the lower fan energy requirement is a key factor in this system. The results of these simulations are also in line with this characteristic of UFAD system in all climates. The fan unit has relatively high amounts of energy saving in all of our scenarios, which starts from 3.05 percent in Duluth and increases to 6.44 percent in Albuquerque and is illustrated in Figure 8. Interestingly, the fan energy saving in the two extreme weather conditions of hot and cold are almost the same number. This results further support the findings by CBE team at 2009, comparing the energy saving of the UFAD system in three climates of California including San Francisco, Los Angel and Sacramento [4]; however, they have not looked into the other climatic conditions.

4 CONCLUSIONS

This study set out to assess the energy performance of the underfloor air distribution system compared to overhead system in several different climatic conditions. The investigation of energy saving has shown that this amount varies for buildings located in different climates, suggesting further studies should investigate this factor prior to designing a suitable HVAC system.

The second major finding was that UFAD system provides the best energy savings in the normal weather conditions; the energy saving capability declines in too hot or too cold climates. The created energy saving visualization map provides a better understanding of the energy performance through all climates of the United States. Further investigation of the energy saving in each units of fan, heating and cooling shows that the saving capability in each of this sections also varies when we move from hot climates to the cold ones; however, the fan energy saving is always significant in all the systems.

This research extends our knowledge of the energy performance of the UFAD by enhancing our understanding of climatic condition influence on the energy saving of this system, both quantitatively and visually.

5 FUTURE STUDIES

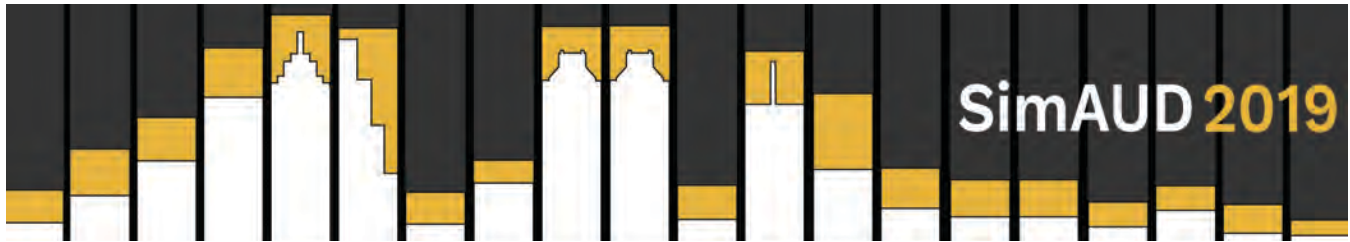
Previous and ongoing research investigates the influence of design and operating conditions on the energy saving capability of the UFAD system. They have found that different system settings can alter the final performance of the system; therefore, it is important to note that changes in UFAD system settings may vary these results.

The findings in this study are subject to two main limitations. First, the investigation was conducted with a constant air volume UFAD system and variable air volume OH system. It would be interesting to look at different

comparison combinations such as CAV to CAV or VAV to VAV comparison to see the influence of airflow type in this process. Second, we have only looked into one city in each ASHRAE climate zone. Further research including multiple cities in each climate would more thoroughly investigate each region. Moreover, the current study has only studied one selected HVAC setting for all the climates. Further research regarding the best design and operating condition in each specific climate is strongly recommended.

REFERENCES

1. D. Webster, Tom Hoyt, Tyler Lee, Edwin Daly, Allen Feng, Dove Bauman, Fred Schiavon, Stefano Lee, Kwang Ho Pasut, Wilmer Fisher, "influence of design and operating conditions on underfloor air distribution (ufad)" *Fifth National Conference of IBPSA-USA* Madison, Wisconsin August 1-3, 2012
2. S. T. Taylor, "Making UFAD systems work," *ASHRAE J.*, vol. 58, no. 3, pp. 44–52, 2016.
3. S. Schiavon, K. H. Lee, F. Bauman, and T. Webster, "Simplified calculation method for design cooling loads in underfloor air distribution (UFAD) systems," *Energy Build.*, vol. 43, no. 2–3, pp. 517–528, 2011.
4. Linden, P F, Yu, Jong Keun, Webster, Tom, Bauman, Fred, Lee, Kwang Ho, Berkeley Schiavon, Stefano, Daly, "Simulation of energy performance of underfloor air distribution (UFAD) systems Author:," *Cent. Built Environ. UC Berkeley*, vol. 94, no. 2, pp. 9–10, 2009.
5. K. Zhang, X. Zhang, S. Li, and X. Jin, "Review of underfloor air distribution technology," *Energy Build.*, vol. 85, pp. 180–186, 2014.
6. N. C. D. Center, "Comparative Climatic Data - United States," 2012. [Online]. Available: <https://www.ggweather.com/ccd/nrmhdd.htm>.
7. T. Webster *et al.*, "Air Distribution (Ufad) System Energy Performance," in *SimBuild 2010*, 2010, pp. 466–473.
8. T. Webster, F. Bauman, F. Buhl, and A. Daly, "Modeling of Underfloor Air Distribution (Ufad) Systems," in *SimBuild 2008*, 2008, no. November, pp. 214–221.
9. P. et al. Bauman, Fred Webster, Tom Linden, "Energy performance of underfloor air distribution systems," *Public Interest Energy Research (PIER) Program California Energy Commission* 2007.
10. Crawley, D. B., Shirey, D. B., Cornick, S. M., Jarrett, P. L., Lott, J. N., Morris, R. J., ... Ferguson, J. M. (2013). ANSI/ASHRAE Standard 169-2013 Climatic Data for Building Design Standards.
11. Khalesi J, Goudarzi N, Thermal Comfort in a Climate-Adaptive Building with Smart Windows and Different Outlet Opening Locations, *Sustainable Cities and Society* (2018), <https://doi.org/10.1016/j.scs.2018.11.029>
12. Ali F. Alajmi, Hosny Z. Abou-Ziyan, Wid El-Amer, Energy analysis of under-floor air distribution (UFAD) system: An office building case study, *Energy Conversion and Management*, Volume 73, 2013, Pages 78-85,
13. Byeong Ho Yu, Byeong-Mo Seo, Sung Hyup Hong, Sanghun Yeon, Kwang Ho Lee, Influences of different operational configurations on combined effects of room air stratification and thermal decay in UFAD system, *Energy and Buildings*, Volume 176, 2018, Pages 262-274



Evaluating the Influence of Three Simplifications on Natural Ventilation Rate Simulation

Yuchen Shi and Xiaofeng Li

Tsinghua University
Beijing, China

{syc17, xfli}@mails.tsinghua.edu.cn

ABSTRACT

Measurement and simulation are two main methods to determine natural ventilation rates in a building. By contrast, the simulation method is widely used in engineering due to its simplicity and convenience. In the practical application of airflow simulation software such as CONTAMW, there exist many simplifications for the actual conditions of simulated buildings. This study focuses on three of the commonly used simplifications and analyses their effects on the simulation results. In addition, for rigorosity, tracer gas decay method is used to verify the reliability of CONTAMW simulation. The conclusions of this study can be used as guidance for airflow simulation software such as CONTAMW.

KEYWORDS

CONTAMW; natural ventilation rate; simplification; simulation.

1 INTRODUCTION

Natural ventilation is an important way to improve indoor air quality and building energy performance [1]. To evaluate the effect of natural ventilation, it is necessary to determine the natural ventilation rate for a building.

Measurement and simulation are two main methods to determine natural ventilation rates in a building. By contrast, the simulation method is widely used in engineering due to its simplicity and convenience [2]. CONTAMW is a software developed by the National Institute of Standards and Technology (NIST) for simulating multi-zone airflow rate in buildings, which has been widely used for natural ventilation simulation [3].

In the practical application of CONTAMW, there exist many simplifications for the actual conditions of simulated buildings. This paper focuses on the following three simplifications:

- Ignore the effects of indoor partitions;
- Ignore the effects of building blockage in the wind flow direction;

- The effective opening area of windows/doors is assumed as maximum openable area of windows/doors.

Natural ventilation rates are simulated and compared when the above simplifications are applied or not. The influence of these simplifications on simulation results is analyzed.

The most commonly used measurement method to determine natural ventilation rate is tracer gas decay method, which has been used in office buildings, residential buildings, and classrooms [4]. The test procedure of tracer gas decay method consists of the release, mixture, and monitor of suitable tracer gas. To verify the reliability of CONTAMW simulation, measurements of natural ventilation rate are conducted in a typical room of the simulated building using the tracer gas decay method. The measured results of tracer gas decay method and the simulated results of CONTAMW are compared with each other to validate the simulation.

This study aims to evaluate the effects of the above simplifications on simulation results and make guidance for the use of airflow simulation software such as CONTAMW.

2 METHODOLOGY

2.1 Simulation

The basic calculation principle of CONTAMW is the following equation, which is for airflow through large intentional openings [5]:

$$Q = C_D A \sqrt{2\Delta p / \rho} \quad (1)$$

where Q is airflow rate, m^3/h ; C_D is discharge coefficient of opening, dimensionless; A is effective opening area of window/door, m^2 ; Δp is pressure difference across opening, Pa; and ρ is air density, kg/m^3 .

The pressure difference across openings is caused by stack effect and wind pressure [5]. The pressure difference caused by stack effect is determined by indoor-outdoor temperature difference. While, the pressure difference caused by wind pressure is an input parameter, which is

generally obtained by simulating outdoor wind field using Computational Fluid Dynamics (CFD) software (such as FLUENT and PHOENICS). In this study, CFD software—PHOENICS—was used to simulate outdoor wind field and determine wind pressure across the window/door openings. The indoor temperatures were determined by iterative computation between indoor-outdoor temperature difference, natural ventilation rate and cooling load (only passive cooling by natural ventilation, air conditioning system off). Outdoor temperature set point is 20 °C.

Then, natural ventilation rates were simulated using CONTAMW when the above three simplifications were applied or not. Results were compared to obtain the main conclusions.

2.2 Verification

Natural ventilation rates were measured in a typical room of the simulated building using tracer gas decay method. Then, the measured results of tracer gas decay method and the simulated results of CONTAMW were compared with each other.

Carbon dioxide (CO₂) was chosen as tracer gas because it is easily available. In the CO₂ decay method, CO₂ was injected into the test room and the decay of CO₂ concentration was measured once a uniform concentration had been reached. The change of indoor CO₂ concentration is expressed as

$$\ln[C_{in}(\tau) - C_{out}(\tau)] = -N\tau + \ln[C_{in}(0) - C_{out}(0)] \quad (2)$$

where C_{in} and C_{out} are indoor and outdoor CO₂ concentrations, ppm; N is air change rate, h⁻¹; and τ is time, h. Based on Eq. (2), N can be determined through the linear fitting between $\ln[C_{in}(\tau) - C_{out}(\tau)]$ and τ .

Then, the natural ventilation rate of the test room is calculated using Eq. (3):

$$Q_{nv} = N \times V \quad (3)$$

where Q_{nv} is natural ventilation rate, m³/h; and V is room volume, m³.

3 RESULTS

3.1 Simulated Building

The simulated building is located in Beijing, China, which has four floors and dimension of 32.5 m×17.8 m×18.3 m (length×width×height). The layout of the third floor is shown in Figure 1. The maximum openable areas of exterior windows and doors on each floor are shown in Table 1. Natural ventilation rate in transition season (April and May) was simulated, during which time the outdoor temperature is lower than that indoor and natural ventilation is used for free cooling.

3.2 Effects of Indoor Partitions

Natural ventilation rate of each floor is simulated under actual building location situations and when the exterior windows and doors are opened to the maximum openable areas.

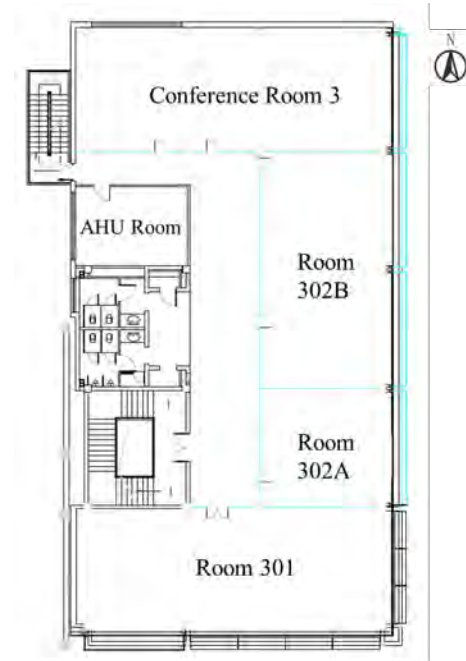


Figure 1. Layout of 3rd floor.

Orientation	Type of window/door	Number of windows/doors	Max openable angle	Max openable area of each window/door (m ²)
East	Top-hung window	10	60°	0.26
West	Balcony door	1	90°	1.60
South	Casement window	2	90°	0.65
North	Casement window	2	90°	0.88

Table 1. Maximum openable areas of exterior windows and doors on each floor

CONTAMW models with or without indoor partitions are shown in Figures 2 and 3 (taking the first floor as an example). Changing the opening areas of inner doors on the partitions to fully open, half open and 1/4 open, the natural ventilation rate simulation results are shown in Figure 4 (air mixing rate: 100%). As shown in this figure, the influence of indoor partitioning on natural ventilation rate is related to the opening area of the partition. The smaller the opening area, the greater the flow resistance and the smaller the natural ventilation rate. When the opening area is large, for example, when the inner doors are opened at 90 degrees, the partition has little effect on natural ventilation rate.

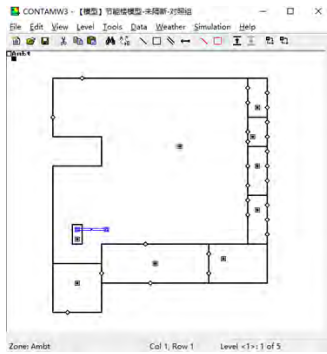


Figure 2. CONTAMW3 model of 1st floor (without partition).

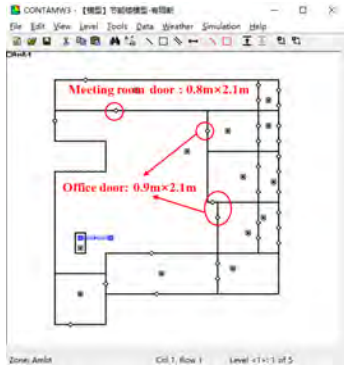


Figure 3. CONTAMW3 model of 1st floor (with partition).

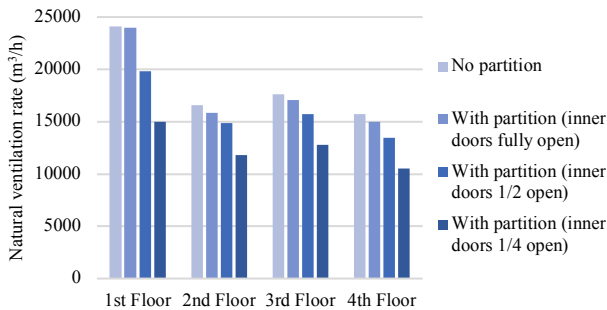


Figure 4. Effects of indoor partitions on natural ventilation rates.

3.3 Effects of Building Blockage in the Wind flow Direction

Natural ventilation rate of each floor is simulated when there is no indoor partition and the exterior windows and doors are opened to the maximum openable areas.

Wind pressure over the building envelop is simulated using PHOENICS under actual building location situations and when removing other buildings blocked on the south side (the wind flow direction). Results are shown in Figures 5 and 6. As shown in these two figures, when removing the building blockage in the wind flow direction, the wind pressure over the building envelop significantly increases on every face.

The natural ventilation rate simulation results when the building is blocked or not are illustrated in Figure 7. The natural ventilation rate is significantly improved when there is no building blockage in the incoming flow direction. Specifically, the natural ventilation rate on each

floor is 8 – 36 % higher than that under actual building location situations. Notably, the lower the floor, the more the natural ventilation rate increases.

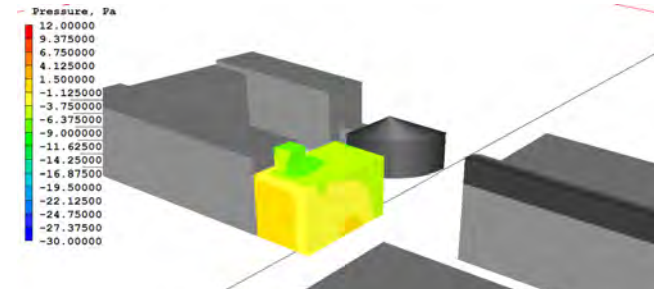


Figure 5. Wind pressure over building envelop when blocked by other buildings in the wind flow direction (grid size: 6m×6m×5m, KEMMK model).

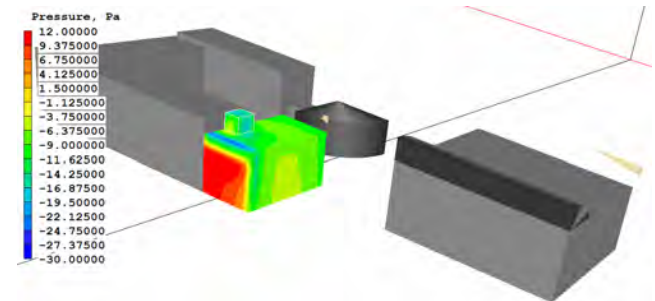


Figure 6. Wind pressure over building envelop when not blocked by other buildings in the wind flow direction (grid size: 4m×5m×4m, KEMMK model).

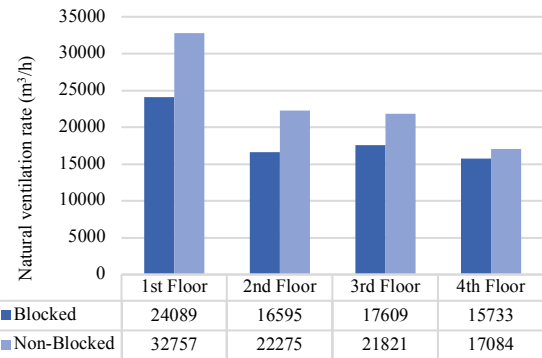


Figure 7. Effects of building blockage in the wind flow direction on natural ventilation rates.

3.4 Effects of Effective Opening Area of Window/Door

Natural ventilation rate of each floor is simulated under actual building location situations and without indoor partition.

Changing the opening areas of exterior windows and doors to maximum openable area and half the maximum openable area, the natural ventilation rate simulation results are compared in Figure 8. When reducing the effective opening areas of exterior windows and doors, the natural ventilation rate significantly decreases. In our case, when the effective opening area is reduced by 50 %, the natural ventilation rate of each floor decreases by 40 – 53 %.

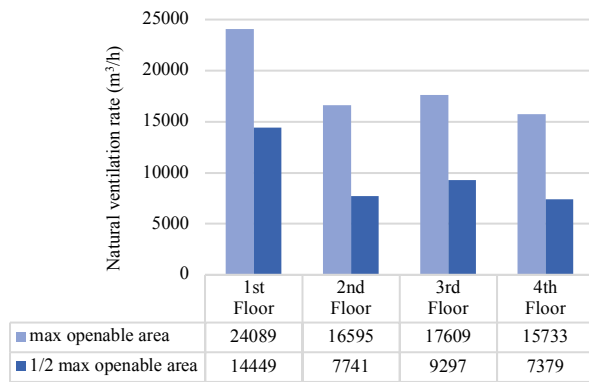


Figure 8. Effects of effective opening area of window/door on natural ventilation rates.

3.5 Verification Results

The validation tests were conducted in the Conference Room on the 3rd floor (Figure 1). The CO₂ decay and liner fitting of Test 1 is illustrated in Figure 9 as an example. The results of CO₂ decay and CONTAMW simulation methods are compared in Table 2. The relative errors between the two methods are no more than 20 %, while the general simulation accuracy of natural ventilation is about 10 – 25 %, which indicates that our simulation method is reliable [6].

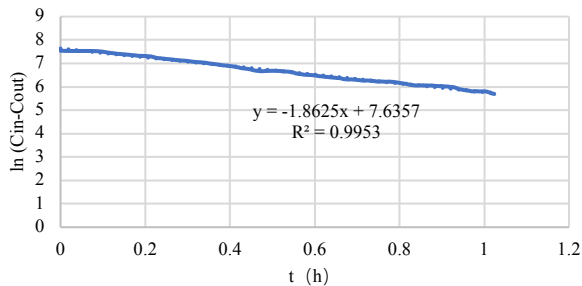


Figure 9. CO₂ decay and liner fitting of Test 1.

Test number	Test 1	Test 2
Effective opening area (m ²)	1.76	0.88
Outdoor wind speed (m/s)	1.27	1.65
Wind direction	ENE	NNE
Indoor temperature (°C)	26.2	26.3
Outdoor temperature (°C)	25.4	27.4
Air change rate by tracer gas measurement (h ⁻¹)	1.86	1.81
Air change rate by CONTAMW simulation (h ⁻¹)	1.50	1.56
Relative error	19.5 %	14.0 %

Table 2. Results of validation tests.

4 CONCLUSION

Simulation method is widely used in engineering to determine natural ventilation rates. However, in the

practical application of airflow simulation software such as CONTAMW, there exist many simplifications for the actual conditions of simulated buildings. This study focuses on three of the commonly used simplifications and analyses their effects on simulation results. In addition, for rigorousness, tracer gas decay method is used to verify the reliability of CONTAMW simulation. The relative error between results of tracer gas measurement and CONTAMW simulation is within 20%, which proves that our simulation is accurate and reliable.

According to this study, in the practical application of CONTAMW, it is necessary to consider the influence of indoor partition, building blockage in the wind flow direction, and effective opening area of windows or doors. By simulation, the following conclusions are obtained:

- The existence of indoor partition will decrease natural ventilation rate; the smaller the opening area on the partition, the greater the flow resistance and the smaller the natural ventilation rate.
- The existence of building blockage in the wind flow direction will significantly decrease the wind pressure and thus decrease natural ventilation rate; the lower the floor, the greater the impact is.
- The reduction of the effective opening area of exterior windows or doors will also decrease natural ventilation rate.

The above conclusions can be used as guidance for the use of airflow simulation software such as CONTAMW.

REFERENCES

- Becker, R., I. Goldberger, and M. Paciuk, *Improving energy performance of school buildings while ensuring indoor air quality ventilation*. Building and Environment, 2007. **42**(9): p. 3261-3276.
- Tan, G. and L.R. Glicksman, *Application of integrating multi-zone model with CFD simulation to natural ventilation prediction*. Energy and Buildings, 2005. **37**(10): p. 1049-1057.
- Walton, G. and W. Dols, *CONTAMW 2.4 user manual*. Gaithersburg, MD, USA, National Institute of Standards and Technology, 2008. **286**.
- ASTM, *Standard Test Method for Determining Air Change in a Single Zone by Means of a Tracer Gas Dilution, ASTM Standard E741, American Society of Testing and Materials, Philadelphia*. 2010.
- ASHRAE, *ASHRAE handbook—Fundamentals: Ventilation and Infiltration*. 2009: American Society of Heating, Refrigerating and Air Conditioning Engineers.
- Jiang, Y. and Q. Chen, *Study of natural ventilation in buildings by large eddy simulation*. Journal of Wind engineering and industrial aerodynamics, 2001. **89**(13): p. 1155-1178.

Simulating People

Adaptive Occupancy Scheduling: Exploiting Microclimate Variations in Buildings 161

Max Marschall and Jane Burry

Toward a Multi-Level and Multi-Paradigm Platform for Building Occupant Simulation. 169

Davide Schaumann, Seonghyeon Moon, Muhammad Usman, Rhys Goldstein, Simon Breslav, Azam Khan and Mubbasir Kapadia

Multi-Constrained Authoring of Occupant Behavior
Narratives in Architectural Design 177

Xun Zhang, Davide Schaumann, Brandon Haworth, Petros Faloutsos and Mubbasir Kapadia

Including Occupant Behavior in Building Simulation: Comparison of a Deterministic vs.
a Stochastic Approach. 185

Max Marschall, Farhang Tahmasebi and Jane Burry



Adaptive Occupancy Scheduling: Exploiting Microclimate Variations in Buildings

Max Marschall¹ and Jane Burry²

¹RMIT University
Melbourne, Australia
marschall.max@rmit.edu.au

²Swinburne University of Technology
Melbourne, Australia
jburry@swin.edu.au

ABSTRACT

Using natural ventilation instead of mechanical building systems to regulate indoor climate can reduce energy consumption while increasing human well-being. The feasibility of natural ventilation depends on outdoor climate conditions as well as the physical and architectural properties of a building. Based on the observation that institutional buildings are rarely occupied to full capacity, this paper proposes a building operation paradigm aimed at increasing the feasibility of natural ventilation. We introduce the concept of adaptive occupancy scheduling, a prescriptive system that allocates occupants in real time to populate only the most environmentally suitable spaces at all times. We exemplify this paradigm in a school design study, in which a fixed room schedule is replaced by a sensor network that assigns classes to classrooms with appropriate microclimatic conditions on-the-go. Our initial results indicate that a higher local architectural diversity generally increases comfort in free-running mode.

Author Keywords

Adaptive occupancy; thermal comfort; school design; campus design; building simulation; ESD; spatial efficiency; computational design.

1 INTRODUCTION

1.1 Background

Occupancy, and therefore spatial redundancy, fluctuates in time. 40% of the schools analyzed in [13] were in use approximately 2200h per year, while [11] reported that US school buildings have historically operated for only 30 percent of available daylight hours. Educational and office buildings incur peak times of maximum occupancy, leaving the building only partially occupied at other times. [13] observed large discrepancies between Finnish school buildings, with available floor area per child ranging from 5 to 35m². While the literature on school building occupancy is scarce, there exist numerous analyses of occupancy patterns in office spaces. The increasing incurrence of flexible work hours in firms has caused a widening of the

range of operational hours per day, often reducing peak occupancy to only 50-70% [7]. The abovementioned figures suggest that spatial efficiency is not, and arguably should not, be the primary driver of architectural design decisions. People seem to welcome procurements of space that go beyond minimum requirements, even if it comes at a cost. This is exemplified by WeWork's research team, who reported that their co-working space users tend to book meeting rooms with higher capacities than the number of attendees, despite the higher rates that this incurs [3].

Victoria currently has 900,000 primary and secondary school students, a number predicted to rise 10% by 2022 [15]. Although there appear to be no Australian building codes specifying minimum spatial requirements for classrooms, the answer to the strong influx of school students cannot be to simply rationalize space; overcrowded classrooms are likely to have direct and indirect impacts on the type and quality of education provided [1]. An appropriate level of occupancy is crucial for the comfort, safety and cost of a building – for construction as well as operation – and affects various stakeholders [2]. The building sector's CO₂ emissions are contributed mostly throughout operational phases [9]. This is mainly due to the use of HVAC systems and indicates an opportunity to save considerable operational costs by minimizing their use. Though spatial efficiency tends to lower the heating energy consumption per person [13], it requires additional efforts to maintain indoor air quality for productivity and health reasons [6]. A Grattan Institute report [16] revealed that wholesale electricity prices have more than doubled across Australia's National Electricity Market since 2015, indicating that operational costs of buildings may become a more crucial factor for consideration in future architectural decision.

Environmentally sustainable design (ESD) approaches generally begin with an assessment of the local climate in which the future building will be located. Climate zone classifications serve as guidelines for the choice of geometry and building materials. Typically, local climate varies considerably over the course of a year or day, therefore

buildings are designed to be trade-offs that perform with time-varying degrees of efficiency. To optimize environmental qualities within buildings, designers introduce both non-energy-consuming measures such as windows and blinds, as well as energy-consuming measures including mechanical ventilation, heating systems and air-conditioning. Decades of comfort research have shown that where possible, non-mechanical means of temperature regulation have a substantial positive effect both on energy expenditure and human well-being [4, 12].

1.2 Objective

This paper explores the potential of adaptive occupancy, that is, the optimized selective use of spaces in response to seasonal and diurnal climatic variation. It is analyzed as a way to increase overall thermal comfort, hence reducing energy consumption through the use of mechanical heating and cooling. The study takes the case of a K-12 year school in the temperate warm climate of Melbourne, Australia with an assumed average occupancy rate of approximately 70%. The experimental methodology engages digital modelling and simulation with optimization approaches to provide a generalized proof of concept. This experimental approach comprises three sub studies:

- a) Parameter study (Section 2.1) to determine spatial modules with high thermal comfort performance in free-running mode, for various analysis periods.
- b) Programming study (section 2.2) to determine configurations of modules that maximize comfort performance by utilizing adaptive occupancy scheduling.
- c) Layout study (section 2.3), entailing environmental simulations for two of the above configurations, by placing modules in actual spatial context to one another and allowing neighboring effects to occur.

This paper suggests a method of providing thermal comfort throughout larger periods of the year without the use of mechanical systems, by designing for spatial redundancies in buildings to offset the energy use and make for more pleasant environments. We introduce the idea of adaptive occupancy scheduling; that is, at sub-maximal building occupancy, room allocation is prescribed on-the-go by an environmental sensor network that assigns occupants to the currently most suitable locations at any given time. In a proof-of-concept design study for a school building, instead of providing a ‘one size fits all’ building typology, we suggest a campus consisting of multiple building types, thereby offering a larger range of microclimatic conditions, as a way of maximally exploiting the anticipated benefits of adaptive occupancy scheduling. We outline our design workflow for a school in the climate of Melbourne, Australia, present initial results and contemplate their implications.

2 METHODS

Implication of Adaptive Occupancy

When not taking adaptive occupancy into account, optimizing a building design for thermal comfort is, as it were, straightforward: various designs are simulated with predefined occupancy patterns, and the variation where comfortable conditions are met for the largest portion of time is chosen. The winning design solution is the one that presents the best tradeoff throughout the entire year. If, however, we assumed that the building will not be occupied to full capacity, and that the occupants can be shifted throughout the available spaces according to time-varying microclimate fluctuations, it is possible that this would result in a different optimal design solution. In particular, this might generate a design that maximizes microclimatic diversity, such that at all times of the year, there are always at least some spaces capable of providing comfortable conditions. The goal of this paper is to provide a framework with which to optimize a design with adaptive occupancy in mind and, in the scope of an initial design study, to explore to which extent adaptive occupancy scheduling could increase the comfort performance of a building.

General assumptions

We limited the number of design variables in this study by making several general decisions and assumptions. The study focused on school buildings, simulated for the climate of Melbourne, Australia. We exclusively considered classrooms and no other programmatic entities of a school building. To simplify the study, teaching spaces were conceived as a small, solitary building (which we refer to as ‘modules’), each containing a single classroom with a single window. The result is a campus-like typology with building sizes reminiscent of portable classrooms common for Victoria. We assumed afterschool utilization, and therefore simulated the school campus to be operated from 9am to 6pm; for simplicity, each lesson was assumed to last 1h, each starting on the hour. Recess times were not considered.

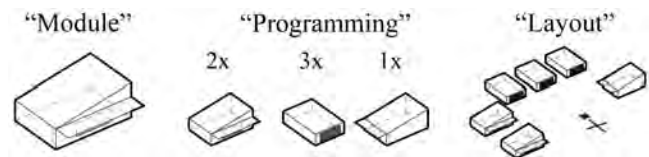


Figure 1. Definitions: In this paper, each classroom was conceived as a solitary building we call “module”. “Programming” involves specifying quantities of module types to be present on a campus, prior to defining their locations on site (i.e., “layout”).

Workflow and Software

We used the Rhinoceros 3D modelling software, along with its algorithmic modelling plugin Grasshopper, to set the parameters of building geometries and automate their generation. Environmental simulations were conducted using the Grasshopper add-ons Ladybug and Honeybee, which serve as user-friendly interfaces to trigger EnergyPlus simulations in the background. Grasshopper’s Colibri add-on was used to conduct the parameter study. The results were

analyzed in a separate Python script to identify high performing modules. Our adaptive occupancy scheduling algorithm was written as a custom GHPython component for Grasshopper. Finally, we conducted evolutionary optimization for the programming study using Grasshopper's plugin Octopus.

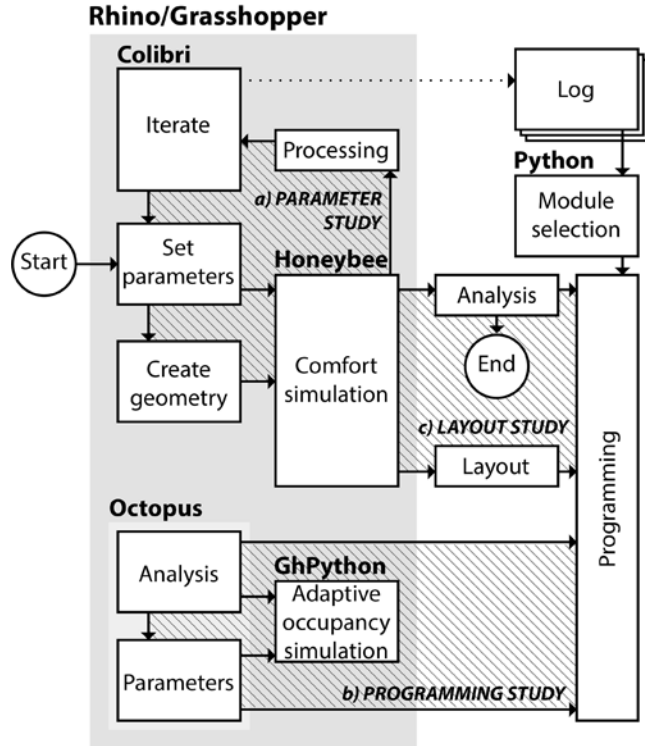


Figure 2. Workflow diagram.

Comfort score

In all three studies, the central performance metric was thermal comfort. Since our goal was to increase natural ventilation, we used adaptive thermal comfort theory to establish optimal indoor temperatures, and compared these to the actual indoor temperatures as measured by EnergyPlus building simulations. As in [12], we considered deviations up to 2K as comfortable conditions, and thereby a region of low likelihood that occupants would use additional energy consuming cooling or heating measures. According to the adaptive thermal comfort theory, humans' desired indoor temperatures in free-running (i.e., not air-conditioned) buildings are driven by outdoor temperatures [4]. As is recommended in [12], we determined design temperatures using a one-month time-weighted running mean outdoor air temperature, expressed in the following formula:

$$Trm = (1-\alpha)\{Tt-1 + \alpha Tt-2 + \dots + \alpha^2 Tt-744\}, \quad (1)$$

where Trm is the weighted running mean outdoor temperature, Tn is the outdoor temperature at a given time-step, t is the current time-step and α is a variable determining the decay of importance of past hours; here, the commonly used value of 0.8 was applied as in [12]. Design temperatures

could then be determined by inserting the Trm values into the adaptive thermal comfort model [4].

$$Td = m \cdot Trm + b \quad (2)$$

where Td is the design temperature, the linear slope is $m = 0.31$ and the intercept is $b = 17.8$ [4]. In this study, the fact that the adaptive comfort model does not apply to outdoor temperatures beyond the domain of 10°C to 33.5°C was not considered, however this case rarely occurred during the analyzed time periods. As in [12], we considered deviations of indoor temperature to comfort temperature of up to 2K as comfortable conditions, and thereby a region of low likelihood that occupants would use additional energy consuming cooling or heating measures:

$$Tdev = |Ti - Td| \quad (3)$$

Where Tdev is the deviation of the indoor temperature (Ti) from the design temperature (Td). To analyze comfort performance over predefined time frames, we calculated the average Tdev in this time frame.

2.1 Parameter Study

We conducted a parameter study to explore the environmental performances of various architectural spaces for school usage in Melbourne, Australia. We refer to each design variation as a module (figure 1).

Assumptions

To simplify the study, all designs were conceived as small, solitary buildings, each containing a single classroom with a single window. The EnergyPlus 'Secondary School' schedules were applied through Honeybee; however, the occupancy, lighting and equipment schedules were simplified and overridden to be active every day of the year between 9am and 6pm, assuming that the buildings would be used for afterschool activities. The 'Secondary School' schedule assumes 0.25 occupants per square meter in classrooms. The average Victorian classroom size is 21 students for primary and 22 students for secondary schools [15]. For this study, we assumed 23 people including a teacher, amounting to 92m² floor area per module. We predefined the dimensions of all modules to be 11.5m length by 8m width by 3m height, excluding an additional 2m height for modules with slanted roofs. The buildings were modelled as not air-conditioned and with default building materials. For natural ventilation via windows or stack effect we set a minimum indoor air temperature of 26 °C, in line with the EN 15251:2007 recommended summer setpoint for indoor operative temperatures. Finally, we defined 50% of window surfaces to be operable, which corresponds to sliding windows common for Australia. The examined variables of the parameter study (figure 3) included orientation (either north-south or east-west); window location (by cardinal direction); glazing fraction (30, 45 or 60%); shading type (either no shading, a single overhang, or horizontal or vertical fins); and roof type (either flat or slanted towards one of the cardinal directions) in; these led to a total of 480 possible parameter combinations.

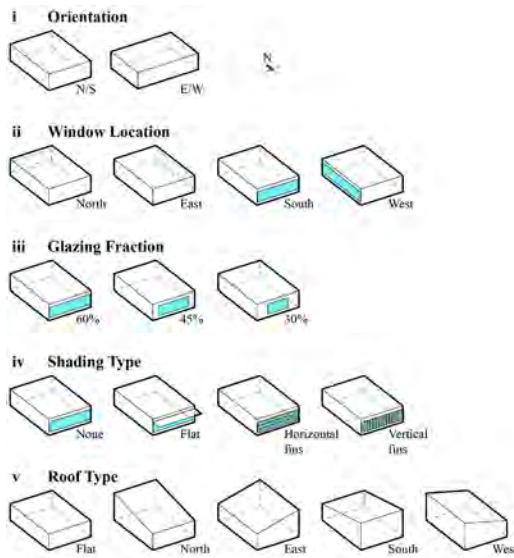


Figure 3. Module parameters.

Evaluation

The goal of the parameter study was to identify high performing modules in terms of thermal comfort. When optimizing a building for environmental metrics, the length of the analysis period plays a crucial role; the smaller the analysis period, the more performative a solution can be found for this narrow time frame. The larger the analysis period is, the less likely it is to find a solution that performs exceptionally all the time, since it is subject to a larger variation of input conditions; the solution increasingly becomes a tradeoff. With these considerations in mind, how might one go about picking modules as building blocks for a campus design? We explored 4 strategies; this resulted in 20 ‘winner’ modules in total, each of which had the best comfort performance for specified analysis periods:

- a) **Baseline:** Only use the overall best performing module. This corresponds to the conventional intuition of environmentally optimizing a building, which is to find the best tradeoff solution considering the entirety of operable hours.
- b) **By Time of Day (TOD):** Divide the operable hours into 3 analysis periods, namely morning (9am-12pm), afternoon (12pm-3pm) and evening (3pm-6pm), and find the best design for each category.
- c) **By Season:** Divide the operable hours by season and choose the 4 best designs for each one.
- d) **By TOD+Season:** As a more granular method, combine the above categories. This results in 12 ‘winner’ modules, each respectively performing best during ‘summer mornings’, ‘summer afternoons’, etc.

2.2 Programming Study

The goal of the programming study was to determine how to combine the ‘winner’ modules from the Parameter Study

(section 2.1) to form a campus that makes most use of the advantages of adaptive occupancy scheduling.

Assumptions

At this stage, neighboring effects were not taken into account. This corresponded to assuming that all buildings were placed at a distance to one another that is large enough to discount the effects of overshadowing and reflection. It must also be noted that dynamic effects were not considered. That is, we used the simulation results from the Parameter Study (section 2.1), which assumed full occupancy for all operational hours. However, a classroom that is vacated for a certain time period can be expected to change its microclimate, in particular to cool down, thereby possibly making it more suitable for occupancy in the following hour. To fully take into account this effect would require a dynamic energy simulation.

In this study, we assumed 70% of available rooms on campus to be occupied at any given time during opening hours. For comparability, we chose to use a consistent number of modules for each campus design variation, and assumed 48 classrooms per school due to its convenient divisibility by 3, 4 and 12.

Strategies

The conventional intuition when optimizing a building for environmental performance is to find the best tradeoff solution considering the entirety of operated hours. Without designing for adaptive occupancy scheduling, and not taking into account the neighboring effects of the modules, the most performative programming based on the available modules would be to only use the overall best performing module. We therefore chose this as a baseline scenario.

However, when taking adaptive occupancy into account, a different strategy is to choose modules that are ‘specialized’ to perform well for complementary time frames. Here, we distinguish three approaches with varying granularity:

- Time Of Day (TOD) approach: The campus consists of the 3 module types that perform best during mornings, afternoons and evenings, respectively
- Season approach: The campus consists of the 4 module types that perform best during summer, autumn, winter and spring, respectively
- TOD+Season approach: The campus consists of the 3 module types that perform best during summer mornings, summer afternoons, etc., respectively

Furthermore, we distinguished two scenarios to determine how many of each module to use:

- Equal amounts: For each above approach, the same numbers of each available module is used. That is, 16 each for the TOD approach, 12 each for the Season approach, and 4 each for the TOD+Season approach

- Comfort optimized: Evolutionary optimization is used to determine the optimal numbers of each available module type to use within each approach

Simulation

We created a custom GHPython component for Grasshopper that identifies the best performing modules on campus for each time step. In our case, it determined around 70% of modules that deviate least from the design temperature. We used the Octopus plugin for Grasshopper to optimize the amounts of each module used.

2.3 Layout Study

The Programming Study in the previous section aimed at finding module configurations that maximized the number of operational hours in which classes could be held on a school campus in comfortable thermal conditions, without the use of mechanical systems. A ‘configuration’ in this case only indicated which modules to use and how many of each, without specifying their spatial relationships to one another, thereby discounting environmental effects that neighboring buildings may have on one another (i.e. over-shadowing and reflection).

Layouting Schemes

The final Layout Study aimed precisely to explore the effects that overshadowing and reflection may have when specifying the geometric context. We chose two configurations from the programming study, namely, the baseline case and the best performing comfort optimized configuration. We arranged both room programs into 4 distinct floor plan schemes (figure 4). We chose layout concepts that we found likely to be explored in an equivalent design project in practice.

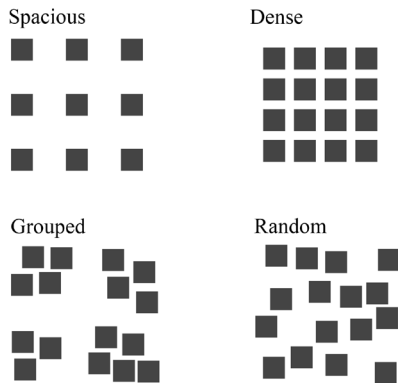


Figure 4. Analyzed layout schemes, to be used both with the baseline case programming and the best performing comfort optimized configuration of modules.

Simulation

An EnergyPlus simulation was run through the Honeybee interface for each layout. As was the case for the Programming Study (section 2.2), at each time step, the model documents the modules on site that lie within the top 70 percentiles in terms of comfort, and assigns these spaces as being occupied.

3 RESULTS

The design study described in this paper consists of three sub-studies: Parameter study (Section 2.1), Programming study (section 2.2) and Layout study (section 2.3). Similar to our methods section, we hereafter describe the results for each sub-study separately.

3.1 Parameter Study

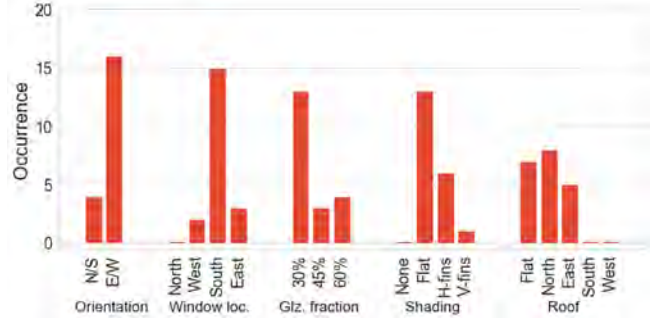


Figure 5. Occurrences of features within the best comfort performing modules from the parameter study.

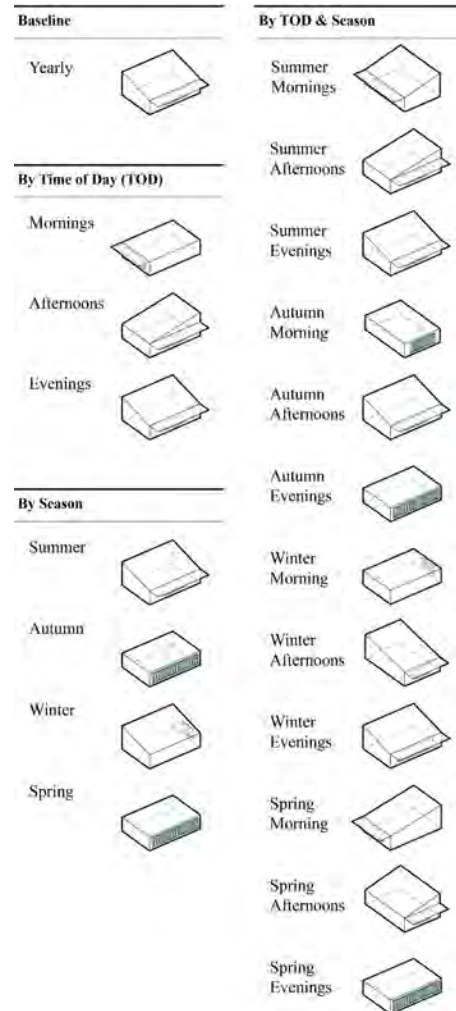


Figure 6. Best comfort performing modules from the parameter study, categorized by various analysis periods.

In the parameter study, we ran year-round environmental analyses for a total of 480 modules. Out of these, we selected 20 of the best performing modules, categorized by various analysis periods in which they excelled. Only these 20 resulting modules were considered in the proceeding studies. The histograms in figure 6 show the occurrences of each feature in the set of winner modules. The dominating variable choices were east-west oriented with south facing windows and low glazing fraction. Each winner module had a shading element. Roof types were selected in similar numbers between flat, north and east facing (figures 5 and 6). Several modules ended up with the same phenotype.

3.2 Programming Study

The goal of the programming study was to explore various combinations of modules on a fictitious school campus in terms of comfort performance. The Overall module in figure 6 was the one that performed best when taking the entire year into account. As a baseline configuration, we simulated a campus consisting only of this module. Figure 7 shows out of 111,690 occupied hours (3285h per year * 34 classrooms), 74,358 were within comfortable range. The other variations were evaluated by comparing their improvement in terms of this hour number.


Case	Programming	Comfortable Hours
Baseline	48x 	74358

Figure 7. Performance of the baseline case.

Figure 8 shows that the “equal amounts” approach resulted in slightly better comfort performances in the TOD case, and substantial improvements in the two other cases. The pie charts indicate how much each module type was utilized throughout the operational hours; here, modules were used in similar ratios. In the last step, we allowed an evolutionary algorithm to optimize the numbers of each available module to use. Figure 9 shows that in each case, this led to a performance increase when compared to using equal numbers of modules (figure 8). Now, all cases faired considerably better than their Equal Amounts counterparts, essentially quadrupling the added comfortable hours in the TOD case while doubling the already large benefits of the other two cases. The winning case by a small margin was TOD+Season. The numbers of modules used turned out to be unintuitively variant, and in some cases excluded the use of module types entirely.

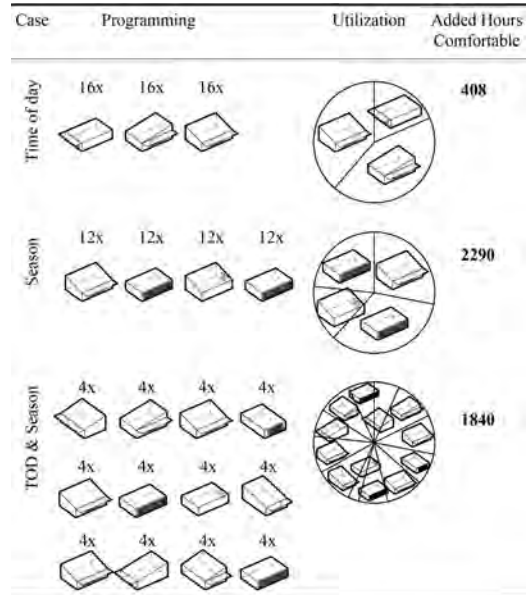


Figure 8. Adaptive occupancy simulation using equal amounts of each module.

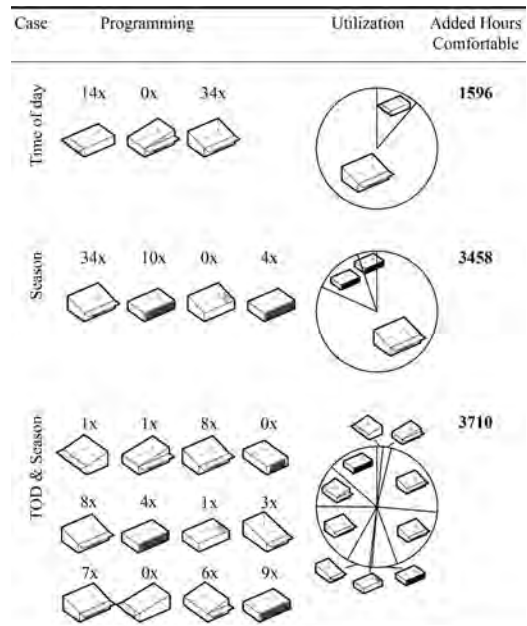


Figure 9. Adaptive occupancy simulation using optimized numbers of each module.

3.3 Layout Study

Contrary to our initial expectation, all simulated layouts resulted in comfort score improvements, and all layouts performed better than their counterparts from the programming study (figure 11). We suspect that the reason for this is that comfort inhibition was mainly due to overheating, and that the overshadowing from neighboring modules generally had a positive influence on reducing this. This is supported by the utilization profiles; especially the Compact baseline layout shows how modules located at the edges were disfavored. For each layout scheme, the comfort

optimized configuration of modules outperformed its baseline counterpart, almost doubling it in each case. The best performance overall was observed for the Compact layout of the comfort optimized case.

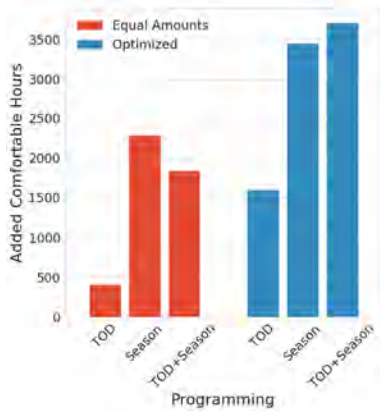


Figure 10. Comfort improvements of each programming case in relation to the baseline case.

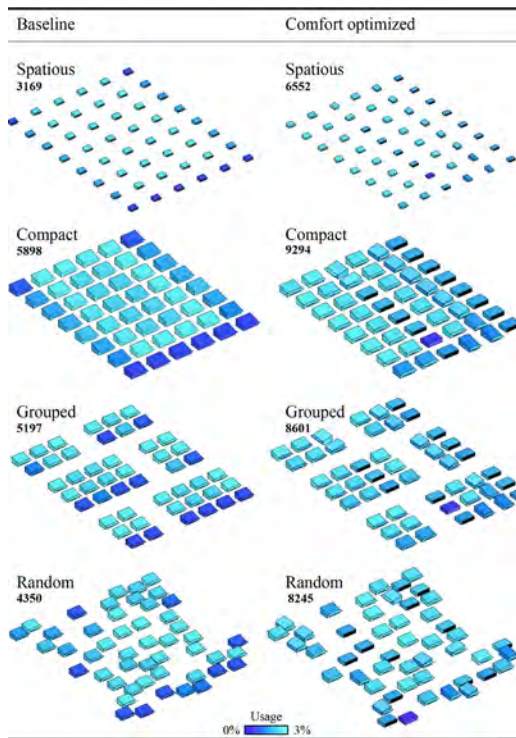


Figure 11. Comfort score for various design layouts, both for the baseline case and the comfort optimized configuration.

4 DISCUSSION

4.1 Building Capacity

Our design study is based on the premise that buildings are usually not occupied to capacity. Therefore, offering a range of microclimates through different building typologies is suggested as a potential method of maximizing the range of hours where comfortable conditions can be met without the use of mechanical systems. To fully investigate the feasibility of this concept requires a more in-depth analysis

of occupancy patterns in schools. One implication of the digital age is a higher demand for customizability. For school operation, this trend may bring with it a future increase in customizable enrolment procedures and individual lesson plans, leading to a decrease in predictability of occupancy patterns. Exploiting the benefits of adaptive occupancy scheduling may on the one hand be achieved by optimizing the operation of existing buildings with redundancies, on the other hand by investing in spatial redundancies in the planning process of new buildings. The benefits of doing so must be carefully balanced against the initial investment. Environmental optimization usually constitutes only one of many criteria that need to be considered in the building design process. While its importance should not be overestimated in comparison to other design factors, this study has illuminated potentials for environmental considerations to diversify and possibly benefit the building functionality and user experience. However, we propose this method not necessarily as a primary driver for design decisions, but rather as a subtle way of increasing comfort and energy efficiency when the opportunity presents itself.

4.2 Implications for Design and Operation

“Blue is the most restful color, but no one would argue for a monochromatic world.” Lisa Heschong [8] used this analogy to question the notion of an ‘optimal’ temperature which modern building technology attempts to maintain uniformly in space and time. Instead, she advocates allowing a range of natural microclimates to occur in order to prevent a phenomenon known as ‘thermal boredom’ [10]. Indeed, thermal comfort research has long demonstrated that allowing occupants a connection to outdoor climates through free-running building concepts increases well-being and the range of conditions that are experienced as comfortable [12]. Heschong advocates for architectural expression as a means of enhancing the human experience of buildings and increasing their environmental awareness. Our study supports this notion by indicating that comfort through natural means can be extended using greater local architectural diversity. This concept requires classrooms to be adaptable for a spectrum of teaching modes and subjects. Flexibility is a property that is already recommended in school architecture recommendations by the Department for Education and Training [14], who predict the traditional classroom setup of desk rows to be superseded in future by a more varied space usage. One suggestion includes installing multi-functional, movable interior elements. Another aspect of current and predicted school evolution is an upswing in digitization. Increasingly, personal electronic devices such as laptops and tablets are integrated into everyday school life. While the opportunities and risks of introducing such technologies into education are part of a contentious debate among parents, politicians, teachers and school directors, we are tempted to interpret it as an indicator of an inevitable development towards a more networked and technology infused school infrastructure. This would facilitate the integration of data-driven operational methods such as the

one we have proposed in this paper, and would solve some considerations that come with it. For example, our method raises the question of how the students would be notified of where their next class is taking place; an issue that could be solved through notifications on personal devices. Similarly, using devices would reduce the need for physical textbooks, thereby facilitating the utilization of a single classroom for multiple subjects, without constantly having to shift learning materials throughout the campus.

4.3 Limitations and Further Research

The current study did not take the dynamic effects into account that would occur in spaces that are intermittently unoccupied, instead considering only the simulation outputs with fully occupied spaces. Furthermore, we simplified the comfort analysis by merely recording the percentage of hours within comfortable range, not the extent to which it deviated. The extent may affect energy expenditure when mechanical systems are used, an evaluation metric to be explored in future. We intend to extend the geometric diversity of the study to include buildings with multiple rooms and floors, since the current study is limited in that each space is a separate building. Finally, this paper raises general questions about space efficiency at schools, which may be addressed by combining the adaptive occupancy method with existing classroom assignment algorithms [e.g. 5].

5 CONCLUSION

Based on the observation that buildings are rarely occupied to full capacity, we have suggested an operation mode that dynamically prescribes occupancy schedules according to microclimate variations measured by sensor networks, in order to adapt the utilization of spaces to maximize comfort and energy efficiency. Since this suggests designing buildings with varying typologies to offer a spectrum of microclimate conditions for different times of day and year, we conducted a design study to determine ideal building configurations for a school campus in the climate of Melbourne, Australia. Our methods included a range of workflows and tools, from algorithmic modelling in architectural software to brute force parameter studies, novel data visualization and evolutionary optimization. Our initial results indicate that, if adaptive occupancy is allowed, a higher degree of local architectural diversity increases comfort and decreases the need for mechanical systems.

REFERENCES

1. Auditor-Gen. VIC. (2008). School Buildings: Planning, Maintenance and Renewal.
2. Chevez, A., Coster, S., McIntosh, C., & Sloman, P. (2016). Rethinking density in contemporary workplace environments. *Corporate Real Estate Journal*, 5.2(Winter), 135–153.
3. Davis, D. (2017). Spatial Analytics: New Ways of Understanding Architecture at WeWork R&D.

Retrieved from <https://www.wework.com/blog/posts/spatial-analytics>

4. De Dear, R. J., & Brager, G. S. (2002). Thermal comfort in naturally ventilated buildings: Revisions to ASHRAE Standard 55. *Energy and Buildings*, 34(6), 549–561.
5. Elloumi, A., Kamoun, H., Jarboui, B., & Dammak, A. (2014). The classroom assignment problem: Complexity, size reduction and heuristics. *Applied Soft Computing Journal*, 14(PART C), 677–686.
6. Fisk, W. J., Seppanen, O., Faulkner, D., Seppänen, O., & Huang, J. (2003). Economizer system cost effectiveness: Accounting for the influence of ventilation rate on sick leave Publication Date. Retrieved from <https://cloudfront.escholarship.org/dist/prd/content/qt2px1f1mw>
7. Gunay, H. B., Beausoleil-Morrison, I., O'Brien, W., & Bursill, J. (2016). Implementation of an adaptive occupancy and building learning temperature setback algorithm. *ASHRAE Transactions*, 122, 179–192.
8. Heschong, L. (1979). *Thermal Delight in Architecture*. Cambridge, MA: The MIT Press.
9. Intergovernmental Panel on Climate Change (Ed.). (2007). *Climate Change 2007: Mitigation of Climate Change*. New York: Cambridge University Press.
10. Kwok, A. G. (2000). Thermal Boredom. *Plea 2000*, 1–2.
11. Lyons, J. B. (2000). *Alternative Use of K-12 School Buildings: Opportunities for Expanded Uses*. U.S. Department of Education, (January).
12. Nicol, J. F., & Humphreys, M. A. (2002). Adaptive thermal comfort and sustainable thermal standards for buildings. *Energy and Buildings*, 34(6), 563–572.
13. Sekki, T., Airaksinen, M., & Saari, A. (2015). Impact of building usage and occupancy on energy consumption in Finnish daycare and school buildings. *Energy and Buildings*, 105, 247–257.
14. State of Victoria. (2018). *Building Quality Standards Handbook*. Retrieved from <https://www.education.vic.gov.au/Documents/>
15. Victoria State Government Department for Education and Training. (2018). *Summary Statistics for Victorian Schools*. Retrieved from www.education.vic.gov.au/about/department/Pages/
16. Wood, T., & Blowers, D. (2018). *Mostly Working: Australia's wholesale electricity market*.
17. Zeytinoglu, I. U., Cooke, G. B., & Mann, S. L. (2009). Flexibility: Whose choice is it anyway? *Industrial Relations*, 64(4), 555–574.



Toward a Multi-Level and Multi-Paradigm Platform for Building Occupant Simulation

Davide Schaumann^{*1}, Seonghyeon Moon^{*1}, Muhammad Usman², Rhys Goldstein³, Simon Breslav³, Azam Khan³, Petros Faloutsos^{2,4} and Mubbasir Kapadia¹

¹Rutgers University
Piscataway, USA
{ds1540; sm2062, mk1353}@cs.rutgers.edu

²York University
Toronto, Canada
{usman; pfal}@cse.yorku.ca

³Autodesk Research
{first.last}@autodesk.com
Toronto, Canada

⁴UHN - Toronto
Rehabilitation Institute
Toronto, Canada

ABSTRACT

In recent years, simulation has been used to investigate building-occupant relations while focusing on pedestrian movement, day-to-day occupancy, and energy use. Most of these efforts employ discrete-time simulation, where building and occupant properties are constantly updated at fixed time steps to reflect building and occupant dynamics. Real-world occupant behavior, however, involves a variety of decision-making patterns that unfold over different time scales and are often triggered by discrete events rather than gradual change. In working toward a platform supporting the full range of human activities in buildings, we embed a discrete-time occupant movement simulator called SteerSuite within a general-purpose discrete-event simulation framework called SyDEVS. With preexisting SteerSuite functions providing low-level steering behavior, and newly implemented SyDEVS nodes providing high-level planning behavior, our prototype represents a multi-level and multi-paradigm approach to occupant simulation for building design applications.

Author Keywords

Multi-Paradigm Simulation; Discrete-Event; Building Occupants; Multi-Level Decision-Making; Discrete-Time.

ACM Classification Keywords

I.6.3 SIMULATION AND MODELING : Applications; I.6.5 SIMULATION AND MODELING : Model Development; I.6.8 SIMULATION AND MODELING : Types of Simulation; J.6 COMPUTER-AIDED ENGINEERING: .

1 INTRODUCTION

Predicting and analyzing the mutual relationship between a building design and the behavior of its occupants is a complex task. In architectural design, architects often use their

knowledge and intuition to foresee how a building will impact the movement and activities of its occupants and vice versa. Complete reliance on intuition, however, can bring about a discrepancy between expected occupant behavior and the behavior that actually occurs when the designed environment is built. In some cases, unanticipated behavior can lead to inefficient layouts, occupant dissatisfaction, and wasted energy.

In recent years, simulation methods have been developed to help designers foresee and analyze building-human interactions during the design phase, and thus identify and address design issues before a building is constructed and inhabited. Occupant behavior models developed for building performance simulations (BPS) try to predict how occupants' presence and actions affect, and are affected by, various building systems including heating, ventilation and air-conditioning [28, 14]. Other approaches—some of which stem from computer graphics research—focus on pedestrian movement in emergency and normal operating scenarios [3, 23], as well as day-to-day activities specific to offices [7], universities [22], and hospitals [21].

In most approaches, time advances at discrete time steps. This method is well-suited to approximate the behavior of continuous variables such as the temperature of a building or the movement of an occupant in a space. However, some occupant actions, such as the decision to open a window or to follow a specific route while navigating a built environment, take place at irregular time intervals. These actions are most naturally modeled with a discrete-event approach. Using a discrete-time approach for event-driven actions has a number of disadvantages: (a) some time precision may be lost, since event times may not align with the prescribed time step; (b) some calculations may be redundant, since decisions may end up being evaluated at every time step rather than when necessary; and (c) the integration of multiple models may become

* These authors contributed equally to the work
SimAUD 2019 April 07-09 Atlanta, Georgia
© 2019 Society for Modeling & Simulation International (SCS)

more difficult, since no one time step is optimal for all solvers [10, 20].

To address these issues, we prototype a multi-level and multi-paradigm approach that couples a discrete-event framework based on the Discrete Event System Specification (DEVS) formalism with a discrete-time simulator. The DEVS framework we use is SyDEVS, an open source C++ library featuring base classes from which modelers can derive nodes representing systems and processes in essentially any domain. To demonstrate the type of model composition we envision for occupant-building simulations, we prototype a set of nodes representing building thermodynamics, human comfort, and high-level occupant decisions. The discrete-time simulator is SteerSuite [23], an established crowd simulator. The objective of combining these libraries is to provide a holistic, modular, and extensible model of building occupancy that covers multiple domains and captures behavioral patterns unfolding at different time scales.

Compared with prior work [9], our approach includes a multi-level representation of occupant behavior which accounts for the following: (a) *higher-level* discrete-event decision-making (e.g. defining an agent’s movement target) that occurs when specific conditions (events) are triggered (e.g. when the agent’s comfort threshold is surpassed); (b) *lower-level* discrete-time representations of phenomena that vary continuously over time, including a building’s physical properties (e.g. temperature) and occupant movement, which is influenced by the built environment as well as the dynamic presence and movement of other agents’ in the same space.

The demonstrated multi-level and multi-paradigm approach holds promise to enable architects and engineers to integrate independent simulation methods into a shared platform to analyze how a building design will affect its future occupants, how the occupants will affect the building, and ultimately how the overall system will impact the natural environment.

The paper is organized as follows. First, we review existing building occupant modeling and simulation approaches. Then, we introduce our multi-paradigm and multi-level prototype. Next, we demonstrate our approach using a case study. Finally, we draw our conclusions and outline the benefits and limitations of our approach.

2 APPROACHES FOR OCCUPANT SIMULATION

One of the most important challenges that architects, engineers, and building owners face when designing a building is to foresee and analyze the mutual relations between a built environment and the movement and activities of its occupants. This is a complicated task, due to the dynamic, stochastic, and context-dependent nature of human behavior, which both affects and is affected by the built environment as well as the presence and behaviors of other occupants.

To address this challenge, a plethora of simulation methods have been developed in recent years to investigate different aspects of building-occupant interactions. These methods can be classified in a number of ways, including by level of abstraction and by modeling paradigm. We observe three commonly used levels of abstraction: *aggregate*, *planning*, and

steering. Aggregate models track the utilization of various spaces, but do not represent individual occupants. Planning models track individual occupants, but only capture the high-level decisions that govern which spaces occupants inhabit, which routes they take, and what actions they perform with some degree of deliberation. Steering models also track individuals, but focus on detailed movement and capture low-level decisions such as where to step and how to avoid collisions. Separate from these three levels are two paradigms: discrete-time simulation and discrete-event simulation. The discrete-time paradigm is the more common of the two, and involves fixed time steps at which the state of the represented system is updated. The discrete-event paradigm involves the repeated advancement of time to the next event, generally resulting in variable time steps [9].

Table 1 is a matrix that intersects the three observed levels with both paradigms. This classification strategy creates six categories, and the table lists the most prominent form of occupant simulation in each of them.

	Discrete-Time Paradigm	Discrete-Event Paradigm
Aggregate Level	Building-Centric Hourly Profiles	Building-Centric Survival Models
Planning Level	Discrete-Time Markov Chains	Discrete-Event Multi-Agent Models
Steering Level	Discrete-Time Crowd Simulation	Discrete-Event Movement Models

Table 1. Classification of occupant simulation methods. Highlighted cells indicate the approaches used in this work.

Among the simplest occupancy models are what we refer to as building-centric hourly profiles. With this method, various spaces in a building are each assigned a profile giving the expected number occupants for each hour of the day. The most prominent examples are the profiles provided by ASHRAE [1] and subsequent versions of Standard 90.1. These models are nearly ubiquitous in energy modeling practice, though tools exist to instead employ more sophisticated survival models and Markov Chains [8].

Survival models are loosely based on those that estimate the lifetime of a specimen or entity. Building-centric survival models can be used to simulate the time until the number of occupants in a space changes. This research area began with observations of single-person offices performed by Wang et al. [27]. The more recent work of Parys et al. [20] is informed by a number of preceding survival models in the building performance simulation field.

Various works on discrete-time Markov Chains begin to introduce the concept of tracking individual occupants into energy modeling research. In these models, occupants’ transitions from one state to another are based on probabilities, which are examined at every time step. The model of Page et al. [19] only recognized each occupant’s presence or absence in a space. Wang et al. [26] use an enhanced version of the method to track occupants from one space to another.

Discrete-event multi-agent models also track individual occupants as they move through a built environment, but each

occupant remains in its current state until the next event occurs. There are no fixed time steps at which all occupants are updated. Instead, occupants are treated asynchronously with respect to simulated time. In an example by Goldstein et al. [7], a gamma distribution is used to randomize the time each occupant spends on each task before transitioning to a new activity in a new location. The mathematics is similar to the survival models described above, except that time durations are calculated for each occupant instead of each space. Zimmermann [30] provides another example of occupants modeled as agents with highly asynchronous behavior.

Discrete-time crowd simulations model the flow of pedestrians through a built environment. A variety of techniques are used to predict the dynamics of human behavior in crowd situations. Some of these techniques capture human movement at a very fine level of abstraction; an example is the work of Kapadia et al. [15], which accounts for individual footsteps. Some works employ coarser approximations of the human form, and strive to support large crowds [12]. The majority of implementations employ fixed time steps, which simplifies mechanisms for avoiding collisions. Crowd simulation is used for design applications in industry [17].

Discrete-event movement models have been explored in a few research efforts. Buss and Sánchez [2] provide a complete description of piecewise linear object movement where events correspond with trajectory changes. Another simple example of discrete-event movement arises when agents move at a constant speed on a grid [5], as a diagonal step should take roughly 40% longer than a step to an adjacent grid cell.

Not all research efforts involving occupant simulation fall cleanly into any single one of the above categories. Schumann et al. [21] investigate narrative-based modeling approaches where workplace procedures involving multiple locations and agents are modeled explicitly. In this work, the choice between discrete time and discrete event is of secondary importance, as the greater challenge is how to specify and recreate the complex collaborative activities that unfold in process-driven facilities like hospitals and factories.

Our interest lies in the pursuit of complex yet scalable occupant models that combine the above mentioned approaches. We focus on the integration of discrete-event multi-agent models for high-level “planning” decisions, with discrete-time crowd simulation models for low-level “steering”. This combination spans multiple abstraction levels and both paradigms. There are various techniques for integrating different types of simulation models [4]. A popular one is co-simulation, where multiple simulation engines are run simultaneously and exchange information over time. A relevant example of co-simulation is the occupant behavior modeling tool by Hong et al. [13], which enables co-simulation with building energy modeling software using a functional mock-up interface (FMI). We adopt a more classic formal modeling approach where models are implemented with a common interface, allowing them to be combined hierarchically and coordinated by a single general-purpose simulator [25]. Importantly, this classic approach does not preclude one from making use of preexisting simulation code. In fact, the

multi-level and multi-paradigm aspects of our prototype are achieved by integrating two independently developed simulation libraries: the SyDEVS discrete-event framework and the SteerSuite discrete-time crowd simulator. SyDEVS provides the coordinating simulation engine and SteerSuite’s capabilities made available by wrapping key parts of the API in a SyDEVS node.

3 A DISCRETE-TIME AND DISCRETE-EVENT PLATFORM FOR BUILDING OCCUPANT SIMULATION

We prototype a multi-level and multi-paradigm platform that couples a discrete-event framework with a discrete-time simulator. High-level occupant decisions (e.g. the next location to visit) are treated using a discrete-event approach, while low-level behaviors (e.g. how to get to the chosen location) are represented using the discrete-time paradigm. Both high-level decisions and low level behaviors impact and are impacted by dynamic environmental conditions, such as the current temperature in the building. For example, occupants’ presence contributes to increased building heat. Excessive heat, however, can cause other occupants to move to a different location. A decrease in the number of agents in a room, in turn, will likely lead to a gradual reduction in air temperature.

3.1 Conceptual framework

Figure 1 provides an overview of our conceptual framework. Building data (e.g. building geometry and material properties) and occupant data (e.g. number of occupants, velocities, and initial targets) are used as input for a simulation phase. In this phase, a dynamic building status (e.g. temperature) and an occupant status (e.g. thermal comfort) are updated over time while accounting for their influence on one another. Both statuses inform an occupant behavior calculation system, which is composed of the following components. A high-level discrete-event decision-making system determines the next action that an occupant should perform (e.g. move to a specific target). These high-level actions occur not at every time step, but when a specific event occurs (e.g. the occupant temperature is above a specific threshold). A low-level discrete-time steering algorithm calculates an optimal path to reach a chosen target while avoiding obstacles and accounting for the movement of other agents. Agent movement thus affects the status of the building and the occupants which, in turn, may trigger additional high-level decisions. The simulation results can be visualized at discrete-time steps or when the simulation is complete.

3.2 SyDEVS: A Discrete-Event simulation platform

The Discrete Event System Specification (DEVS) formalism is a set of conventions for representing essentially any discrete event system [29]. The rationale for using DEVS is to support a modular and hierarchical approach to model development while ensuring all time advancement patterns are accommodated. There are a number of simulation frameworks based on DEVS or one of its variants. The framework we use is an open source C++ library called SyDEVS (<https://autodesk.github.io/sydevs/>).

SyDEVS nodes can be of two types: *function* nodes or *simulation* nodes (Figure 2). *Function* nodes are the basic type of

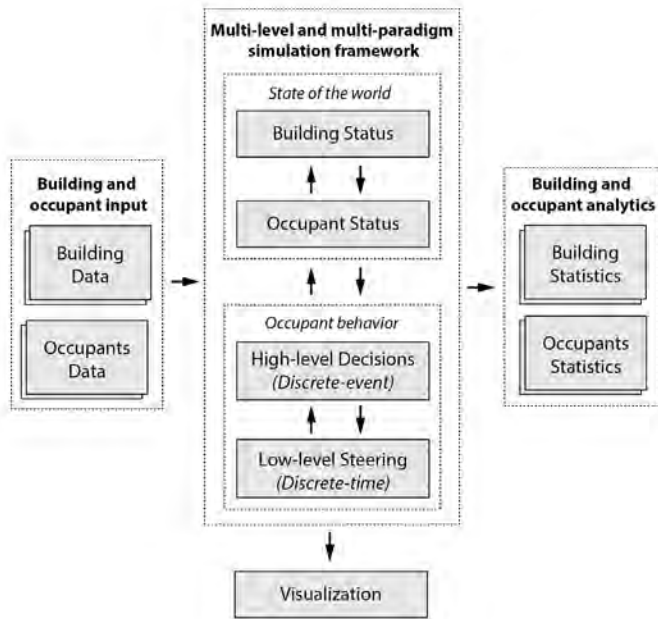


Figure 1. Conceptual framework for a multi-level and multi-paradigm occupant behavior simulation.

dataflow node. They represent a single function that handles one flow event. This function reads a set of input values and calculates a set of output values. *Simulation* nodes represent behavior that unfolds over simulated time. They handle the following types of events: *Initialization Events* are invoked once at the beginning of the simulation; *Unplanned Events* are invoked every time a message is received at unexpected times; *Planned Events* are scheduled by the node; and *Finalization Events* are invoked once at the end of the simulation.

Simulation nodes can be *Atomic*, or can be organized in hierarchical compositions. *Collection* nodes contain any number of instances of an atomic node. *Composite* nodes contain networks (dataflow + DEVS + dataflow) of other nodes, which can themselves be composite nodes, thus forming a hierarchy.

Different types of simulators can be encapsulated within SyDEVS nodes to create modular, hierarchical and extensible data workflows that operate at different time scales. Because the framework employs a multiscale time representation [6], models requiring dramatically different levels of time precision (e.g. seconds, days, femtoseconds) can be linked together and allowed to interact.

3.3 SteerSuite: A Discrete-Time crowd simulator

SteerSuite is an open source C++ framework for crowd simulations (<http://steersuite.eecs.yorku.ca/>). It simulates multi-agent navigation and steering in built environments while responding to the dynamic presence and movement of other agents in space. SteerSuite includes the infrastructure required by typical AI and steering algorithms (i.e. a simulation engine, a spatial database, planning functionality and classes to read and write simulation recordings). It thus facilitates the development of new steering algorithms or the

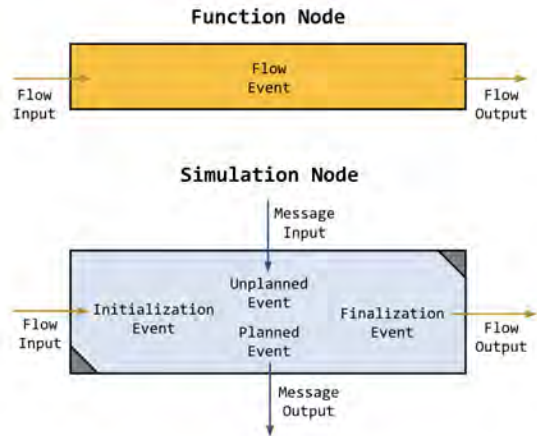


Figure 2. Node types in SyDEVS that can be combined into larger, hierarchical node networks.

use of the following established steering approaches: (a) PPR [23] combines reactions, predictions and planning in one single framework, (b) ORCA [24] uses reciprocal velocity obstacles for goal-directed collision avoidance, and (c) SF [11] uses social forces for resolving collisions between interacting agents in dense crowds. Additionally, SteerSuite visualizes real-time or pre-recorded simulations in 3D environments, and provides built-in modules to analyze the results with respect to a set of customary or user-defined benchmarks.

3.4 Integrated platform

The proposed platform couples the functionality of SyDEVS and SteerSuite to define an integrated framework for multi-level and multi-paradigm occupant-behavior simulation. While SyDEVS supports the modeling of potentially any type of system, in this prototype we have created a specific node composition that demonstrates the multi-level and multi-paradigm nature of the approach. Figure 3 shows an overview of the platform using the SyDEVS notation [16].

The platform consists of a SyDEVS composite node that contains the following data workflow. In an *initialization* phase, a series of function nodes specify building-related and occupant-related parameters including building geometry, external weather conditions, occupants' initial goals, speed, and direction, and a temperature threshold that, if passed, triggers a high-level occupant decision about where to move next.

This data is used as input for a *simulation* phase, where a combination of atomic nodes (connected by means of an event messaging system) represent dynamic interactions between the occupants and the built environment they inhabit. In this prototype, a "weather" node calculates the outdoor temperature and communicates it to a "thermodynamics" node, which calculates the indoor temperature, while accounting for the occupants' latent heat, modeled in the "heat source" node. The indoor temperature is used to calculate occupants' comfort levels in a "comfort" node.

The temperature perceived by each occupant as well as a temperature threshold defined for each occupant are input to a

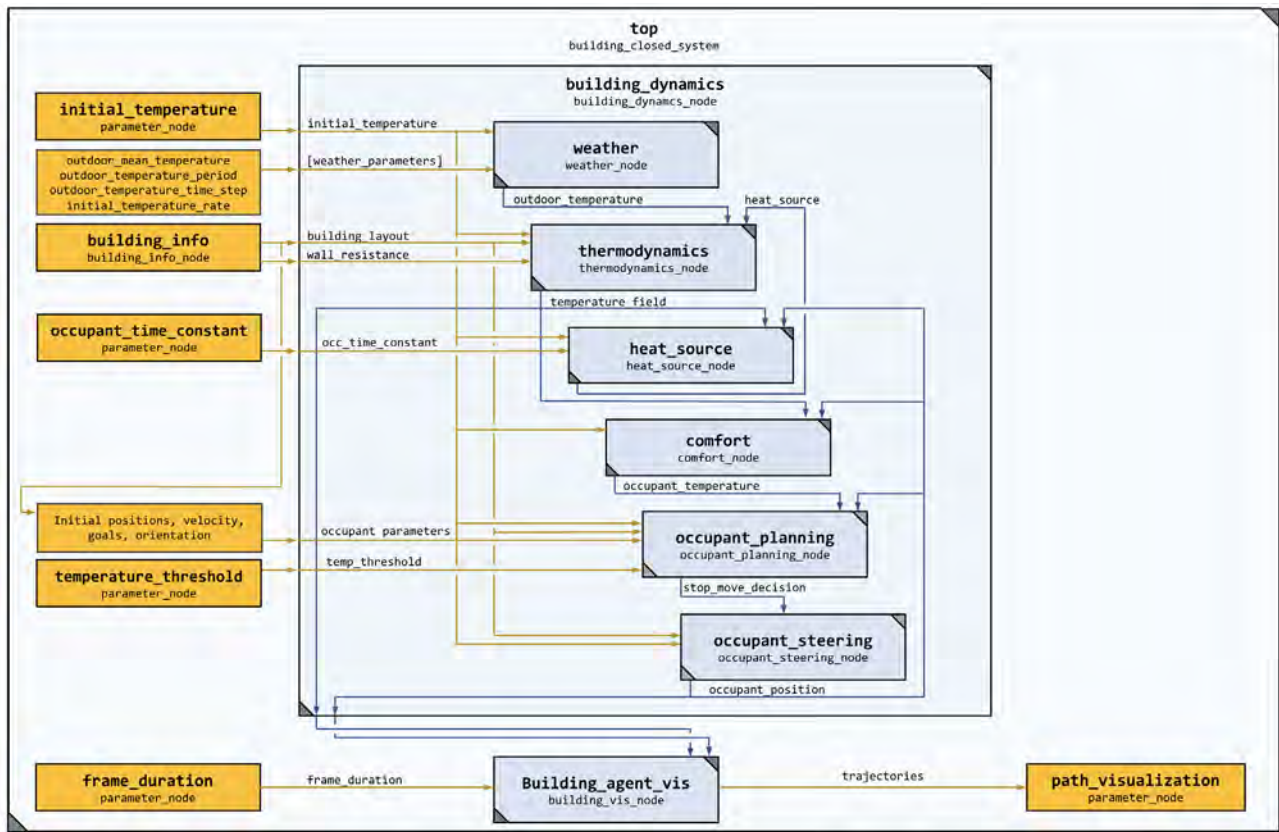


Figure 3. Simulation platform. Multiple SyDEVS nodes are organized into a hierarchical network to represent occupant behavior using a multi-level and multi-paradigm approach.

high-level “occupant planning” node, which compares the occupant temperature with its tolerance threshold. If the threshold is passed, the agent is assigned a movement target randomly selected from a user-defined target list. While this node could be modeled as a collection of individual decision making nodes (one for each occupant), in this prototype we implemented a centralized decision-making node that determines which action each occupant should perform. Even though the first approach would enable each occupant to feature an independent decision node that is agnostic to the decision of other agents, the second approach facilitates high-level behavior coordination between multiple occupants, as demonstrated in other multi-agent approaches [21].

The selected occupant’s movement target is then communicated to an “occupant steering” node, which encapsulates SteerSuite core functionality. This node calculates agents’ movement while accounting for obstacles as well as the presence and movement of other occupants. In this atomic node, a discrete-time approach is used, since agents’ path must be re-calculated at specific time steps to account for the dynamic state of the world. The updated occupants’ positions are fed back to the previous nodes, which can thus update the indoor temperature and comfort levels, and check whether each occupant’s temperature threshold is passed.

A “building agent viz” node collects input from the “thermodynamics” and “occupant steering” nodes to visualize occupant movement and the building temperature over time using SteerSuite functionality. In a *finalization* phase, simulation data is analyzed to represent aggregated occupancy data in the form of movement traces.

4 CASE STUDY

We apply the proposed platform to simulate the behavior of several occupants in an office space. The building is populated by several occupants, each of which can either work at his/her own desk, or participate in a group meeting. While working, or during a meeting, the simulation monitors the occupant temperature, which is calculated as a combination of the external temperature and the occupants’ latent heat. If the occupant’s temperature exceeds his/her own specified threshold of tolerance, the occupant will execute a high-level discrete-event decision to change his/her location. In this prototype, we use a low-level discrete-time social force model to calculate agents’ steering, although other approaches are supported as well (as mentioned in Section 3.3). In this study, we do not account for occupants’ abilities to operate other building systems (e.g. HVAC or windows). However, the proposed framework supports the prototyping of additional nodes that could handle such operations.

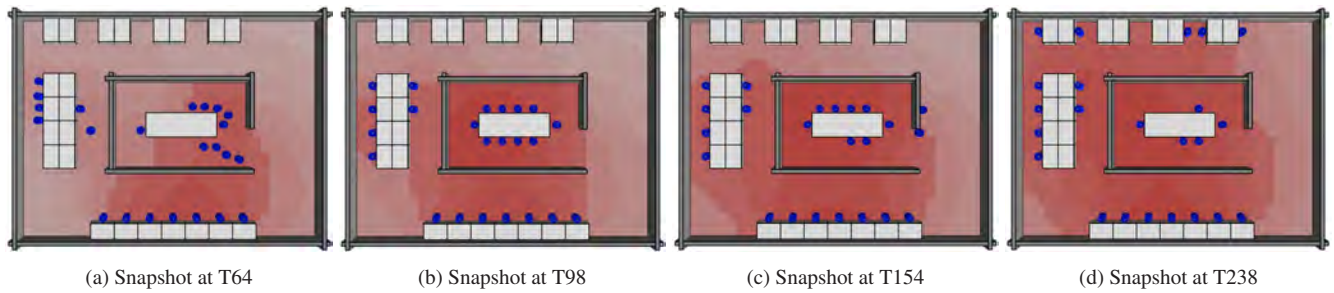


Figure 4. Preliminary study in an abstract office space. A number of occupants are directed either to their desks or to a meeting room (T64). Due to their latent heat, the indoor temperature increases (T98). If the temperature reaches an occupant-defined threshold, the occupant leaves the room (T154). The indoor temperature decreases in the meeting room and it increases in the newly occupied spaces (T238)

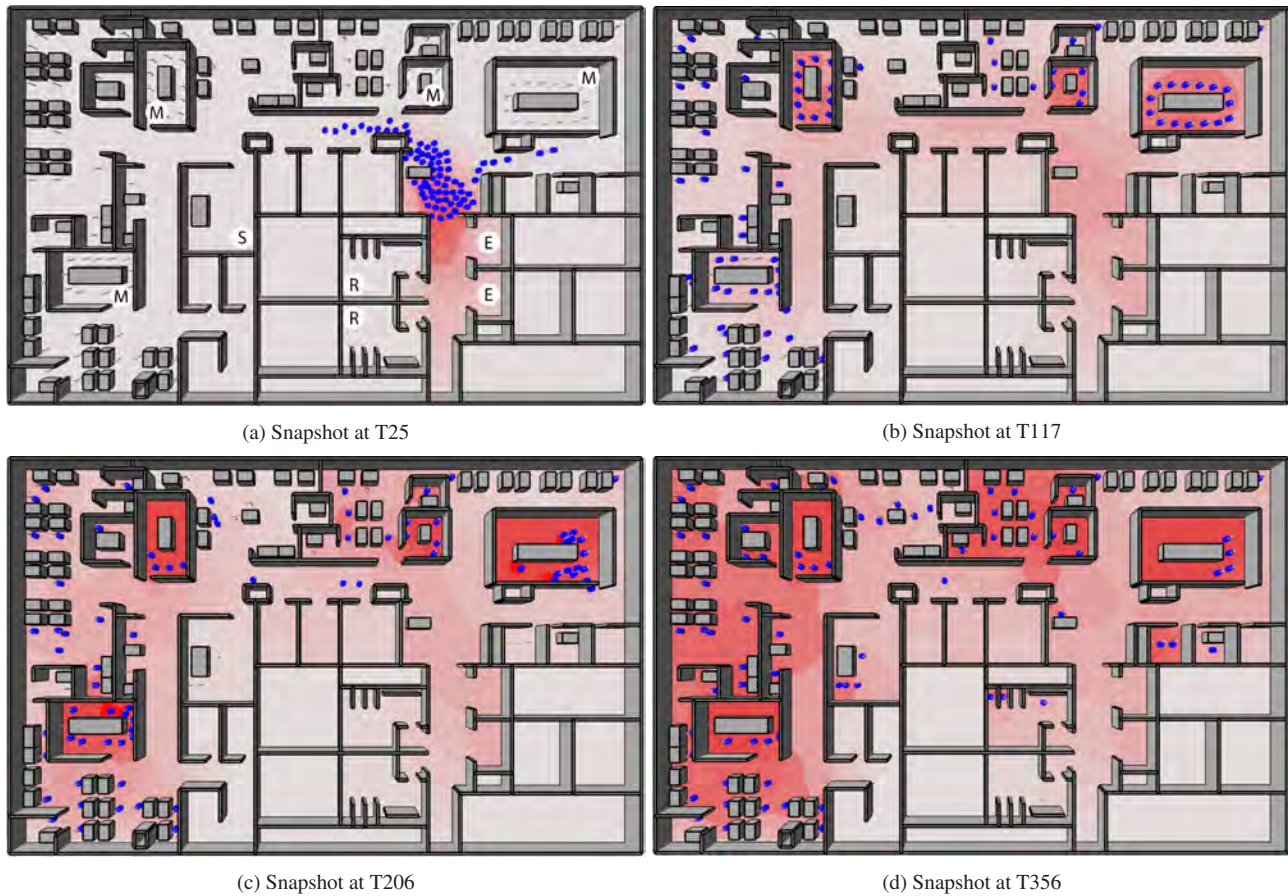


Figure 5. Study in an office building, where (E) are the elevators, (M) are the meeting rooms, (R) are the restrooms, and (S) is a social area. 70 occupants are directed either to their desks or to a series of meeting rooms (T25). The indoor temperature increases due to agents' presence and weather conditions (T117). When the indoor temperature reaches an occupant-defined threshold, the occupant is directed either to his/her desk, a social area, or the restrooms (T206). The indoor temperature changes due to occupants' movement to a different location (T356).

Figure 4 shows a preliminary study in an abstract office space. Building occupants are represented in blue, while the current indoor temperature is displayed using different intensities of red (the higher the temperature, the more intense the red). In Figure 4a, the occupants are moving towards their desk or the

meeting room. In Figure 4b, a temperature heat map reveals increased indoor temperature in the meeting room. In Figure 4c, some of the occupants leave the room since the current indoor temperature is higher than their threshold of tolerance. In Figure 4d, more occupants leave the meeting room causing



Figure 6. Analysis of occupants' trajectories.

decreased temperature in the room and increased temperature in the newly occupied spaces.

Figure 5 shows a simulation study in a larger office building, populated by 70 occupants that behave in a similar fashion compared to the preliminary study. Some of the occupants go to their desks, while others gather in different meeting rooms. When the occupants' temperature threshold is surpassed, the agents are directed either to a randomly selected targets such as their desks, the restroom, or a social space. Figure 6 displays the aggregated occupants' movement trajectories. A simulation video can be found here: (<https://youtu.be/AgTu6iHD-jc>)

Implementation Details. The building model has been generated in Autodesk Revit, an established BIM tool. The building walls and desks have been exported as XML files using a custom-made exporter. Other building information, such as the weather data as well as wall resistance to heat has been encoded directly into SyDEVS. The initial agents' targets, velocities, orientation and initial positions have also been defined using an XML format and imported into SyDEVS. The visualization of agents' movement and path trajectories has been calculated using SteerSuite.

5 CONCLUSION AND DISCUSSION

The paper introduces initial steps toward a multi-level and multi-paradigm platform for occupant behavior simulation. Our goal is to develop a computational framework that benefits from the advantages of discrete-time and discrete-event representations to capture a wide spectrum of building-occupant interactions that ultimately affect the natural environment. Such an integrated approach would be beneficial since, at a macro level, it could describe the discrete-event decision-making of individual occupants in response to specific environmental changes (e.g. when the indoor temperature reaches a certain threshold) as well as various aspects of the building dynamics. At a micro level, instead, it will be possible to simulate more mundane agents interaction such as movement and obstacle avoidance, which must incorporate constant updates at regular time steps to account for the continuous changes of the state of the world (e.g. the varying position of other agents in a space).

More broadly, our platform enables the simulation of the mutual interactions between building systems and occupant decision-making. In the preliminary studies considered in this paper, we have demonstrated an example of such 2-way interaction. The presence of people in a space affects the indoor temperature; in turn, an excessively high temperature may lead some occupants to leave the room; upon leaving, the indoor temperature may lower down due reduced latent heat produced by the occupant. Other factors that may affect the indoor temperature and the decision-making of the occupant have not been considered in this study (e.g. the operation of other building systems, such as the HVAC).

In our platform, we use SyDEVS as discrete-event framework and SteerSuite as discrete-time steering simulator. SyDEVS features the modeling of node graphs, where each node can encapsulate simulations at different time scales. A specific node composition has been developed for this project. The SyDEVS framework, however, can be fully extended to incorporate additional nodes that extend our current thermal simulation and decision-making systems. Future work will involve integrating the platform with additional nodes, and combining it with an energy simulator, such as Energy Plus. Additionally, we aim to extend occupants decision-making abilities to account for schedules and a more advanced way-finding model that operates at two different levels of abstraction. A high-level decision-making will determine which route, while a low-level decision will calculate more fine-grained movement while avoiding obstacles.

Emerging approaches to design, such as the MaRS Discovery District generative design project [18], test new ways to incorporate human experience metrics into built environments' layouts. In the building science community, researchers are actively exploring how multi-agent occupant simulations could potentially impact energy use predictions [13]. We argue that the proposed approach sets a stepping stone towards a platform that can be used across disciplines to study building-human interactions. Such a platform, could potentially be integrated in architectural design workflows to design settings that maximize occupant needs while minimizing the collective impact on the natural environment.

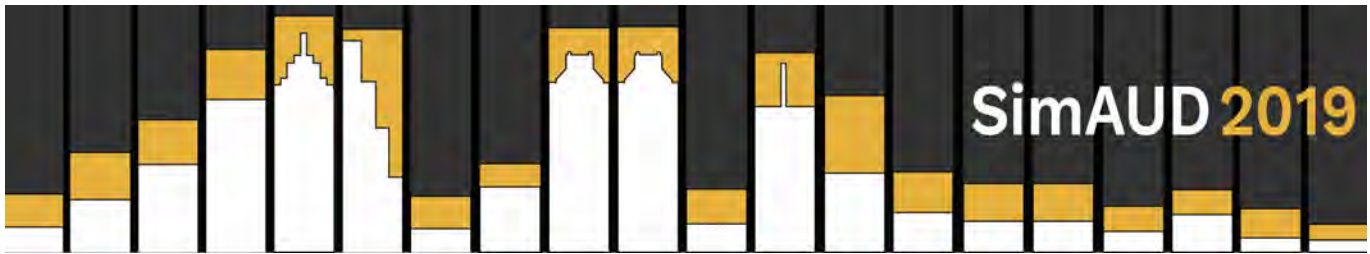
ACKNOWLEDGEMENTS

This research has been partially funded by grants from the NSERC Discovery and Create programs, NSF IIS-1703883, NSF SAS-1723869, DARPA SocialSim-W911NF-17-C-0098, and the Murray Fellowship. We thank Taewon Kim and Nikhil Jiju for their contribution to this project.

REFERENCES

1. ASHRAE. *Standard 90.1, Appendix G*, 2004.
2. Buss, A. H., and Snchez, P. J. Simple movement and detection in discrete event simulation. In *Proceedings of the 37th Conference on Winter Simulation*, Winter Simulation Conference (2005), 992–1000.
3. Chu, M. L., and Law, K. Computational framework incorporating human behaviors for egress simulations. *Journal of Computing in Civil Engineering* 27, 6 (2013), 699–707.

4. Goldstein, R., Breslav, S., and Khan, A. Using general modeling conventions for the shared development of building performance simulation software. In *Proceedings of the International Building Simulation Conference* (2013).
5. Goldstein, R., Breslav, S., and Khan, A. Towards voxel-based algorithms for building performance simulation. In *Proceedings of the IBPSA-Canada eSim Conference* (2014).
6. Goldstein, R., Khan, A., Dalle, O., and Wainer, G. Multiscale representation of simulated time. *Simulation* (2017), 0037549717726868.
7. Goldstein, R., Tessier, A., and Khan, A. Space layout in occupant behavior simulation. In *Conference Proceedings: IBPSA-AIRAH Building Simulation Conference* (2011), 1073–1080.
8. Gunay, B., O'Brien, W., and Beausoleil-Morrison, I. A toolkit for developing data-driven occupant behaviour and presence models. In *Proceedings of the IBPSA-Canada eSim Conference* (2016).
9. Gunay, H. B., O'Brien, W., Beausoleil-Morrison, I., Goldstein, R., Breslav, S., and Khan, A. Coupling stochastic occupant models to building performance simulation using the discrete event system specification formalism. *Journal of Building Performance Simulation* 7, 6 (Nov. 2014), 457–478.
10. Haldi, F., and Robinson, D. Interactions with window openings by office occupants. *Building and Environment* 44, 12 (2009), 2378–2395.
11. Helbing, D., and Molnar, P. Social force model for pedestrian dynamics. *Physical review E* 51, 5 (1995), 4282.
12. Hesham, O., and Wainer, G. A. Context-sensitive personal space for dense crowd simulation. In *Symposium on Simulation for Architecture and Urban Design* (2016).
13. Hong, T., Sun, H., Chen, Y., Taylor-Lange, S. C., and Yan, D. An occupant behavior modeling tool for co-simulation. *Energy and Buildings* 117 (Apr. 2016), 272–281.
14. Hong, T., Taylor-Lange, S. C., D'Oca, S., Yan, D., and Corgnati, S. P. Advances in research and applications of energy-related occupant behavior in buildings. *Energy and Buildings* 116 (2016), 694–702.
15. Kapadia, M., Pelechano, N., Allbeck, J., and Badler, N. Virtual crowds: Steps toward behavioral realism. *Synthesis Lectures on Visual Computing: Computer Graphics, Animation, Computational Photography, and Imaging* 7, 4 (2015), 1–270.
16. Maleki, M., Woodbury, R., Goldstein, R., Breslav, S., and Khan, A. Designing devs visual interfaces for end-user programmers. *Simulation* 91, 8 (2015), 715–734.
17. Morrow, E., Mackenzie, I., Nema, G., and Park, D. Evaluating three dimensional vision fields in pedestrian micro-simulations. *Transportation Research Procedia* 2 (2014), 436 – 441. The Conference on Pedestrian and Evacuation Dynamics 2014 (PED 2014), 22-24 October 2014, Delft, The Netherlands.
18. Nagy, D., Lau, D., Locke, J., Stoddart, J., Villaggi, L., Wang, R., Zhao, D., and Benjamin, D. Project discover: An application of generative design for architectural space planning. In *Symposium on Simulation for Architecture and Urban Design* (2017).
19. Page, J., Robinson, D., Morel, N., and Scartezzini, J. L. A generalised stochastic model for the simulation of occupant presence. *Energy and Buildings* 40, 2 (2008), 83–98.
20. Parys, W., Saelens, D., and Hens, H. Coupling of dynamic building simulation with stochastic modelling of occupant behaviour in offices—a review-based integrated methodology. *Journal of Building Performance Simulation* 4, 4 (2011), 339–358.
21. Schaumann, D., Breslav, S., Goldstein, R., Khan, A., and Kalay, Y. E. Simulating use scenarios in hospitals using multi-agent narratives. *Journal of Building Performance Simulation* 10, 5-6 (2017), 636–652.
22. Shen, W., Zhang, X., Shen, G. Q., and Fernando, T. The user pre-occupancy evaluation method in designer–client communication in early design stage: A case study. *Automation in Construction* 32 (2013), 112–124.
23. Singh, S., Kapadia, M., Hewlett, B., Reinman, G., and Faloutsos, P. A modular framework for adaptive agent-based steering. In *Symposium on Interactive 3D Graphics and Games*, ACM (2011), 141–150.
24. Van Den Berg, J., Guy, S. J., Lin, M., and Manocha, D. Reciprocal n-body collision avoidance. In *Robotics research*. Springer, 2011, 3–19.
25. Vangheluwe, H., De Lara, J., and Mosterman, P. J. An introduction to multi-paradigm modelling and simulation. In *Proceedings of the AIS'2002 conference (AI, Simulation and Planning in High Autonomy Systems)*, Lisboa, Portugal (2002), 9–20.
26. Wang, C., Yan, D., and Jiang, Y. A novel approach for building occupancy simulation. *Building Simulation* 4, 2 (Jun 2011), 149–167.
27. Wang, D., Federspiel, C. C., and Rubinstein, F. Modeling occupancy in single person offices. *Energy and Buildings* 37, 2 (2005), 121–126.
28. Yan, D., O'Brien, W., Hong, T., Feng, X., Gunay, H. B., Tahmasebi, F., and Mahdavi, A. Occupant behavior modeling for building performance simulation: Current state and future challenges. *Energy and Buildings* 107 (2015), 264–278.
29. Zeigler, B. P., Kim, T. G., and Praehofer, H. *Theory of Modeling and Simulation*. Academic Press, Jan. 2000.
30. Zimmermann, G. Agent-based modeling and simulation of individual building occupants. In *Proceedings of SimBuild 2010 conference: IBPSA-USA* (2010), 269–276.



Multi-Constrained Authoring of Occupant Behavior Narratives in Architectural Design

Xun Zhang¹, Davide Schaumann¹, Brandon Haworth², Petros Faloutsos^{2,3}, and Mubbasir Kapadia¹

¹Rutgers University
Piscataway, USA
{xz348, ds1540, mk1353}@cs.rutgers.edu

²York University
Toronto, Canada
{brandon, pfall}@cse.yorku.ca

³UHN - Toronto
Rehabilitation Institute
Toronto, Canada

ABSTRACT

Building-Information Modeling (BIM) tools provide static representations of built environments, disjointed from the expected behaviors of their future inhabitants. Current approaches for simulating buildings in use can be categorized as *building-centric*, where occupancy distributions are specified, *behavior-centric*, where multi-agent behaviors are modeled, or *occupant-centric*, where occupants behave based on their individual motivations. In this paper, we combine these methods into an integrated framework to author narratives that satisfy multi-level time-varying constraints, such as (a) *building-level* occupancy specifications, (b) *zone-level* behavior distributions, and (c) *occupant-level* motivations. Such information is encoded into customizable templates associated with BIM models. A case study highlights the ability of this approach to seamlessly author behavior narratives that can be used for visualizing, analyzing and communicating how buildings may be used by their future inhabitants.

Author Keywords

Building Occupancy Simulation; Human Behavior Narratives; Behavior Authoring; Building Semantics; Multi-Agent Systems; Building Information Modeling.

ACM Classification Keywords

I.6.3 SIMULATION AND MODELING: Applications; I.6.5 SIMULATION AND MODELING Model Development; J6 COMPUTER-AIDED ENGINEERING.

1 INTRODUCTION

Envisioning how buildings will be used by their occupants prior to their construction is a fundamental challenge in architectural design. Current Computer-Aided Design (CAD) and Building Information Modeling (BIM) tools provide static representations of built environments, which fail to account for the prospective building users and their dynamic activities. As result, architects mostly rely on their knowledge

and intuition to foresee and analyze building-human interactions. Full reliance on intuition, however, can lead to a discrepancy between expected behaviors and actual behaviors enacted once the building will be built.

Current approaches to represent buildings in use can be classified in three broad categories. *Building-centric* approaches define occupancy schedules over time [2]. However, they do not represent agent movement and dynamic activities. *Behavior-centric* approaches model context-dependent behaviors involving multiple occupants [7, 16], without specifying building occupancy patterns and agents' motivations to perform specific behaviors. *Occupant-centric* approaches represent the movement and activities of multiple agents in response to individual desires and motivations, while ignoring collaborative day-to-day behaviors and occupancy distributions in semantically-rich spaces [6].

In this work, we propose an integrated narrative modeling framework that integrates building, behavior, and occupant-centric constraints to represent the behavior of heterogeneous occupants engaged in collaborative activities that unfold in semantically rich spaces. The input of the proposed approach consists of (a) a BIM-generated architectural design model, where each zone (discrete portion of space) and equipment is associated with semantic information (e.g. office, meeting room, kitchen, desk) and (b) a set of templates that define *building-level occupancy specifications*, indicating the number of occupants expected in a zone at a given time, *zone-level behavior distributions*, where behaviors are modeled in the form of Events [7, 16], and *occupant-level motivations*, specifying the desire of each agent to participate in specific behaviors at a given time.

An optimization algorithm solves the spatiotemporal allocation of agents to a discrete set of individual and collaborative behaviors while maximizing the convergence with building-level occupancy specifications, zone-level behavior distributions, and occupant-level motivations. We demonstrate this approach by simulating the behavior of a hundred agents involved in a variety of activities in an office lab. Based on the simulation results, we explore different approaches for visu-

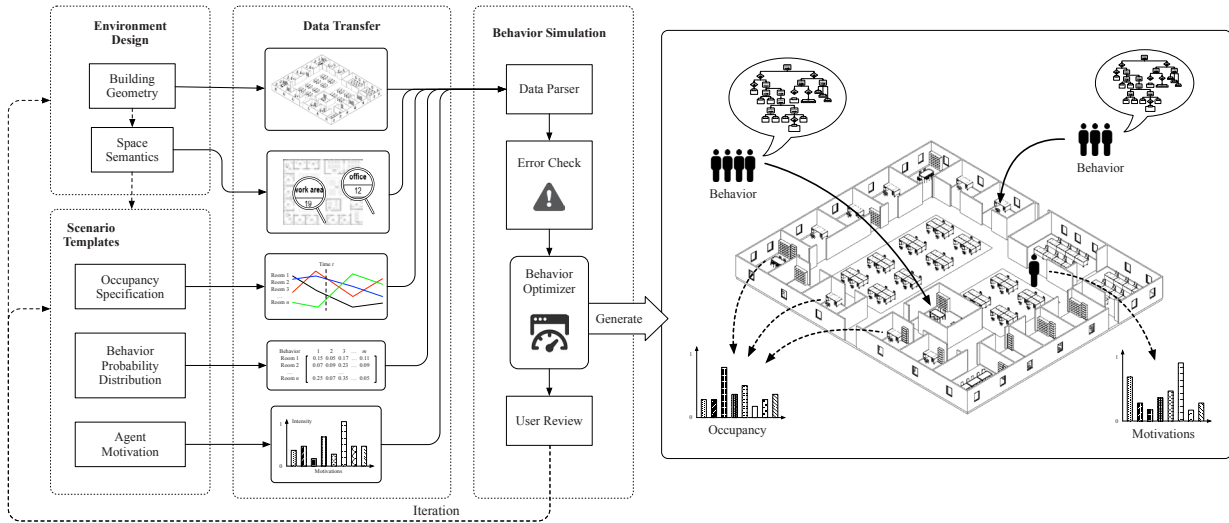


Figure 1. Framework overview. Our approach enables a multi-constrained authoring of occupant behavior narratives that accounts for building-level occupancy specifications, zone-level behavior distributions, and occupant-level motivations.

alizing narratives and extrapolating analytical data that can inform architectural design decisions.

We argue that the proposed approach holds promise to help architects visualize and analyze building-human interactions in not-yet built environments, and facilitate communication with design stakeholders who may benefit for the proposed visualization to better understand the implication of design decisions on how buildings will be used.

2 RELATED WORK

Modeling buildings in use is a rich area of research. We classify existing approaches into three categories, as follows.

Building-centric authoring. Occupant behavior is often modeled using deterministic profiles that leverage collected data to determine hourly information of space usage [9]. Stochastic models use probability theory to represent observed behavioral patterns that include occupants’ presence in a space [22] and actions that have implications for energy consumption [4]. Occupant schedules have been incorporated into occupancy simulation frameworks to represent more accurate occupancy patterns [3, 2]. These models provide a static representation of building occupancy, which potentially misses dynamic aspects of occupant movement and collaborative activities.

Behavior-centric authoring. These approaches use top-down coordination systems to model activity patterns and agent allocation. Schedule-based approaches define fixed temporal sequences of activities to direct agent movements and activities across multiple spaces [17]. Event-based approaches abstract behavior logic from the agents to synthetic directors that control collaborative behavior [19, 7, 16]. Events use parameterized behavior trees that describe hierarchical, modular and reusable behavior patterns [18]. Narrative management systems dynamically trigger events when specific spatial and social conditions are met. Top-down man-

agement systems dynamically allocate agents to events using time-varying priorities, without accounting for spatial occupancy factors and agent motivations [15]. Stochastic behavior distribution approaches use optimization techniques to tune occupant behavior parameters to meet specific behavior constraints [11]. This latter approach, however, pre-computes transitions to satisfy behavior constraints and may not account for collaborative behaviors.

Occupant-centric authoring. Occupant movement under a range of conditions has been represented using agent-centric particle models, such as particle dynamics [14], social forces [5], velocity-based methods [21, 12], continuum models [20, 10], and space-time planning [1]. Influence maps have been used to compute the attraction that a spatial location exerts on an agent (or groups of agents) while accounting for their inner motivations [8]. Belief-Desire-Intention approaches drive agent behavior based on their inner motivations [13]. These methods, however, focus behavior patterns that often ignore the collaboration among agents, spatial occupancy distributions, and the performing of structured sequences of activities that unfold over time across various semantically rich spaces.

Our approach. We combine the aforementioned approaches into an integrated narrative authoring framework that satisfies multiple constraints, such as time-varying building-level occupancy specifications, zone-level behavior distributions, and occupant-level motivations. The main contributions of this approach can be summarized as follows: (a) A narrative authoring framework tailored to BIM that progressively satisfies building-level occupancy specification, zone-level behavior distributions, and occupant-level motivations to simulate collaborative behaviors of heterogeneous agents in semantically rich environments; (b) A flexible and customizable template approach to specify different building use parameters; (c) An optimization strategy that dynamically allo-

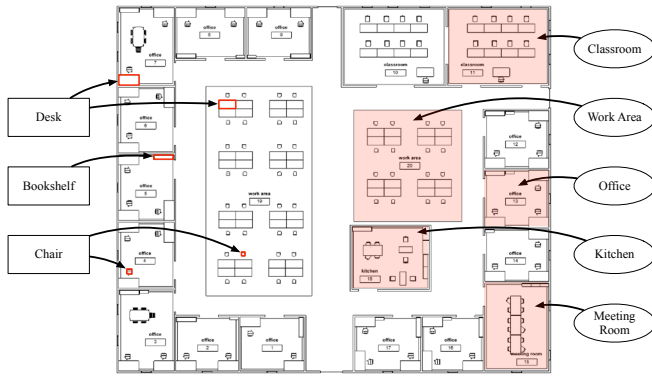


Figure 2. Model of a computer science lab building that includes geometric and semantic information.

cates agents to specific behaviors while satisfying occupancy, behavior, and motivation constraints.

3 PROPOSED FRAMEWORK

The proposed framework is illustrated in Figure 1. It involves the following steps.

3.1 Building Model

A building design is modeled in Autodesk Revit®, an established BIM tool. The model encapsulates physical building components (e.g., walls, doors, desks, and chairs), and non-physical components (e.g., rooms and open-spaces), which are modeled as ‘zones’, discrete portions of space that host different types of behaviors. Both types of components include geometric and semantic properties which indicate how they can be used (e.g. ‘chairs’, ‘desks’, ‘offices’, ‘meeting rooms’, ‘classrooms’, etc.). Figure 2 shows an example of a building model.

3.2 Template-Based Modeling

Three types of templates provide information on how a building can be used, and by whom. We detail these templates in the following paragraphs. Table 1 shows an example for each type of template.

Building-level Occupancy. Occupancy templates indicate the number of agents located in a space at a given time while disregarding the types of behaviors performed in a specific zone and the agents that participate in them. Occupancy is specified at discrete simulation times (e.g. t_1, t_2, t_3). Our system interpolates the expected occupancy between the specified time to guarantee a continuous matching process. Occupancy profiles can be based on expectations for a given environment or can be produced from data collected in existing office settings.

Zone-level Behavior Distribution. For each zone type, we specify a set of behaviors, that require varying numbers of agents. For instance, an “eating” behavior requires only one agent, while a “meeting” behavior requires at least two agents to be allocated. Each behavior is associated with a specific distribution, e.g., in an “office” room, 80% of the occupants

Zone type	T_0	T_1	T_2
Office	0.4	0.3	0.3
Meeting Room	0.1	0.1	0.2
Classroom	0.0	0.4	0.0
Work Area	0.4	0.1	0.5
Kitchen	0.1	0.1	0.0

(a) Building-level occupancy specification.

Zone Type	Work (1)	Eat (1)	Meet (2)	Lecture (4)
Office	0.7	0.1	0.2	0.0
Meeting Room	0.1	0.0	0.9	0.0
Classroom	0.1	0.0	0.1	0.8
Work Area	0.8	0.1	0.1	0.0
Kitchen	0.1	0.7	0.2	0.0

(b) Zone-level behavior distribution. In parenthesis, the number of occupants involved in the behavior.

Agent Type	Work	Eat	Meet	Lecture
Professor	0.4	0.2	0.3	0.1
Grad. Student	0.3	0.1	0.2	0.4
Undergrad. Student	0.3	0.2	0.1	0.4

(c) Agent-level Motivations.

Table 1. Templates that specify different levels of narrative constraints.

are expected to work, while 20% are expected to meet. Furthermore, different zone types have varying distributions. For example, agents in an “office” should have a higher chance of working than in a “kitchen”. These behaviors are modeled in the form of *events*, as detailed in Section 4.2.

Occupant-level Motivation Definition. We define a selected number of occupant profiles with different preferences for the considered behaviors. For example, “professors” can be associated with a higher preference for participating in meetings rather than in lectures, as opposed to “undergraduate students”. These preferences affect the choice of which agent will participate in a given narrative.

In this approach, not all three levels of constraints must be specified. For example, a user can specify only building-level zone occupancy, without specifying zone-level behavior distributions or occupants’ motivations. Our simulation will complete the missing information by considering a generic behavior performed in all the zones by a generic agent. Similarly, a user can specify building occupancy and zone-level behaviors, without specifying occupant motivations. In this way, our framework can be suitable for different stages of the design process where information about how designs are used can be made progressively available as the design unfolds.

3.3 Behavior Simulation

Our approach involves the following steps.

Semantic Fault Identification. A rule-based system checks for errors in the design and template definition phase. For example, it checks if every desk is associated to a chair, and if the sitting spots contained in work-related zones (e.g. a lecture room) are sufficient to perform the collaborative behaviors specified in the templates (e.g. a lecture event, which involves multiple agents). Additionally, it checks if the sum

of the occupancy specifications, behavior distributions, and agent motivations form proper probability distributions.

Scene population. Different from other approaches where the number and types of agents must be manually specified by the user [16], in this approach we automate this step by leveraging semantic data contained in the building model and templates. For example, if we consider the agent types defined in Table 1c, we instantiate 'professor' occupants based on the number of desks located in office rooms, and 'graduate' and 'undergraduate students' based on the number of desks in work areas, so that each occupant is associated with a work station.

Behavior optimization. A hierarchical optimization algorithm (detailed in Section 4) dynamically allocates agents to specific events to progressively satisfy building-level, zone-level, and occupant-level constraints by minimizing the difference between expected and actual occupancy, behavior distributions, and to maximize agent motivations.

User review. The simulation results can be viewed and analyzed using quantitative and qualitative measures. Based on these insights, the user can modify the building design or the templates and run additional simulations.

4 MULTI-CONSTRAINED NARRATIVE SIMULATION

We propose a multi-constrained approach to coordinate occupant behavior narratives that satisfy building-level, zone-level and occupant-level specifications.

4.1 Building-level Occupancy Specification

Given a building with n rooms, we define a normalized space occupancy vector as follows:

$$\mathbf{o}(t) = [o_1(t), o_2(t), \dots, o_n(t)] \quad \text{where} \quad \sum_{i=1}^n o_i(t) = 1.$$

For example, for a building with three rooms, we can specify the initial occupancy (at time zero) as

$$\mathbf{o}(t=0) = (0.28, 0.19, 0.53).$$

4.2 Zone-level Behavior Distribution

After defining an initial occupancy, we now consider the behaviors occurring in each zone. Such behaviors are modeled in the form of Events [7, 16], computational constructs that direct the behavior of multiple agents and equipment objects to perform a structured sequence of activities, modeled as parametric behavior trees[18].

Each behavior b_i contains: (a) a set G of participating occupants; (b) a set $S \supseteq G$ of all smart objects (i.e., the equipment); (c) a set of pre-conditions $\phi_i(b_i, S_i) \in \{0, 1\}$, where S_i is the set of participating occupants and smart objects of the corresponding behavior; (d) a parametric behavior tree controlling the behavior of the agents; (e) a set of post-conditions $\delta_i(b_i, S_i)$.

Parametric behavior trees store a sequence of actions that define an occupant's behavior. For example, a "meet" behavior can be modeled as a sequence of

(MoveTo(agent), Speak()) actions. More complex behavior trees include repeating loops, selector branches and additional logical operator that can affect the performing of the specified actions.

We specify a list of behaviors with a desired occurrence distribution that involve one or more agents and take place in a specific zone. For any room R_i , we use

$$\mathbf{p}_i = [p_1, p_2, \dots, p_m]$$

as a vector representing the desired distribution of the m behaviors

$$\mathbf{b} = [b_1, b_2, \dots, b_m],$$

where

$$p_1, p_2, \dots, p_m \in [0, 1] \quad \text{and} \quad \sum_{i=1}^m p_i = 1.$$

We combine the desired behavior distribution of each zone in a matrix as follows:

$$\mathbf{A}_{des} = [\mathbf{p}_1 \ \mathbf{p}_2 \ \dots \ \mathbf{p}_n]^T.$$

At any time t during simulation, \mathbf{A}_{des} specifies the behavior distribution within a single zone. To consider the behavior distribution in all zones, we define an occupancy vector $\mathbf{o}(t)$ as the conditioned distribution for all zones. Before using the occupancy vector, we define an element-wise multiplication operation, \odot , between a matrix \mathbf{A} and a vector \mathbf{b} that

$$\begin{aligned} \mathbf{A} \odot \mathbf{b} &= [\mathbf{a}_1 \ \mathbf{a}_2 \ \dots \ \mathbf{a}_n]^T \odot [b_1, b_2, \dots, b_n] \\ &= [b_1 \mathbf{a}_1 \ b_2 \mathbf{a}_2 \ \dots \ b_n \mathbf{a}_n]^T \end{aligned}$$

The conditioned distribution matrix is hence

$$\mathbf{A}_{con} = \mathbf{A}_{des} \odot \mathbf{o}.$$

By combining the occupancy with behavior distribution, we obtain a matrix that describes the distribution of all behaviors in all the rooms. For example, an environment containing 4 behaviors and 3 rooms would have a desired distribution matrix as follows

$$\mathbf{A}_{des} = \begin{bmatrix} 0.10 & 0.75 & 0.03 & 0.12 \\ 0.23 & 0.66 & 0.02 & 0.09 \\ 0.54 & 0.05 & 0.33 & 0.08 \end{bmatrix}$$

and an initial occupancy distribution vector.

$$\mathbf{o}(0) = (0.28, 0.19, 0.53),$$

Thus, the conditioned distribution matrix is

$$\mathbf{A}_{con} = \begin{bmatrix} 0.028 & 0.210 & 0.008 & 0.034 \\ 0.044 & 0.125 & 0.004 & 0.017 \\ 0.286 & 0.027 & 0.175 & 0.424 \end{bmatrix}$$

4.3 Occupant-level Motivations

After specifying behavior distributions, we add an additional layer of complexity. We define agents with different motivations that can participate in the specified behaviors. At time

t , the motivations corresponding to the m behaviors of the agent g are represented by the vector

$$\mathbf{v}_g(t) = (v_1, v_2, \dots, v_m).$$

Motivations are specified in the templates and are dynamically updated during the simulation. For example, some motivations systematically increase with time (e.g. motivation for eating). In general, when an agent completes the execution of a behavior, the event that controlled the agent will adjust the corresponding motivation causing the other motivations to adjust relatively, so that the normalized motivations add up to 1.0. Specifically, we decrease motivations by a pre-defined factor α ,

$$v'_{work} = (1 - \alpha)v_{work},$$

4.4 Behavior Optimization

After specifying a desired occupancy, behavior distribution, and occupant motivations, our goal is to assign each occupant to a specific behavior while satisfying the aforementioned constraints. We treat this as an optimization problem where limited amount of resources (i.e. occupants) must be allocated to a discrete amount of tasks (i.e. behaviors) while minimizing the difference between the actual behavior distribution and occupancy and the desired one, while selecting agents with higher motivations. Namely, given the desired distribution matrix \mathbf{A}_{con} , the behavior of the occupants should converge to such values. This is a challenging task since the number of occupants in a building may not suffice to satisfy sparsely distributed occupancy values and behaviors across rooms. For example, in a building with 10 rooms and 5 expected behaviors per room, 50 behavior distributions must be satisfied. However, there may not be enough agents in the building to satisfy such distribution. Additionally, the considered behaviors may require multiple agents to be performed, which makes stochastic optimization methods inefficient.

For any room R_i at some state t , in addition to the desired behavior distribution, the actual behavior distributions can also be represented by a matrix that

$$\mathbf{A}_{act} = [\bar{p}_1 \ \bar{p}_2 \ \dots \ \bar{p}_n],$$

where \bar{p}_i is the observed distribution of behaviors.

Our aim is to instantiate a set of behaviors $B = \{b_1, b_2, \dots, b_l\}$ that minimizes the deviation of the desired distribution and the actual observed distribution, while every occupant and equipment object is allocated to only one behavior at a given time, formally written as

$$B = \arg \min_{\forall b_i \in B, \phi_i(b_i, S_i) \wedge \forall i \neq j, S_i \cap S_j = \emptyset} \|\mathbf{A}_{act} - \mathbf{A}_{des}\|.$$

Furthermore, we consider the agent motivation. Hence, with the set of agents G as the participants and the error rate $E(G)$ of incorrectly allocated motivations of the agents, the optimization over the behaviors B is

$$B = \arg \min_{\forall b_i \in B, \phi_i(b_i, S_i) \wedge \forall i \neq j, S_i \cap S_j = \emptyset} w_1 \|\mathbf{A}_{act} - \mathbf{A}_{des}\| + w_2 E(G).$$

4.5 Optimization Algorithm

We use a heuristic search to allocate the agents to events according to the distribution expectation (\mathbf{A}_{des}), expected occupancy (\mathbf{o}), behaviors (\mathbf{b}), and the set of participating agents (G). The output is the set of behaviors B that minimize the distribution error. Our approach is shown in Algorithm 1. The optimizer will first collect all the agents available and allocate memory to store the matrices used for future calculation. Two factors in the algorithm guarantee a near-optimal solution: (i) minimizing the calculated error of the actual distribution of the behaviors, and (ii) minimizing the agent's motivation error when participating in the behaviors. Also, for large environments, the algorithm uses block matrix operations to speed up the calculation and optimization process.

Algorithm 1 Behavior Optimizer

input : desired distribution matrix, occupancy vector, behaviors, participating agents
output: optimized behaviors

```

1 Calculate the normalized matrix
2 while all agents are not allocated do
3   Create matrix permutation list with size  $m \times n$ 
4   In the list, increase each element in every permutation
   matrix by 1 accordingly
5   for each matrix in the permutation list do
6     Calculate the error with the normalized distribution
     matrix and insert into the error list
7   Sort the error list
8   for each error value in the error list do
9     Select the behavior corresponding to the error
10    Sort the participating agents with regard to the behav-
    ior motivation
11    Select the first agent
12    while the behavior still needs more agents to start do
13      if the motivation is the highest one for the agent
      then
14        Add the agent to the behavior pending list
15      else
16        Move the agent to the end of the agent list
17      if preconditions of the behavior satisfied then
18        Start the behavior
19  if No more agents were allocated then
20    Stop optimizer

```

4.6 Scheduler

A scheduler triggers the optimization algorithm at fixed points in time or when specific conditions are met to ensure a robust narrative generation. Strategies for dynamic re-scheduling could involve identifying the total number of agents that satisfy a set of conditions to be re-optimized, including but not limited to: (a) an agent's availability flag;

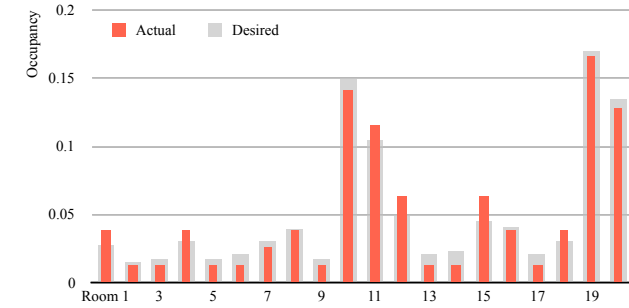
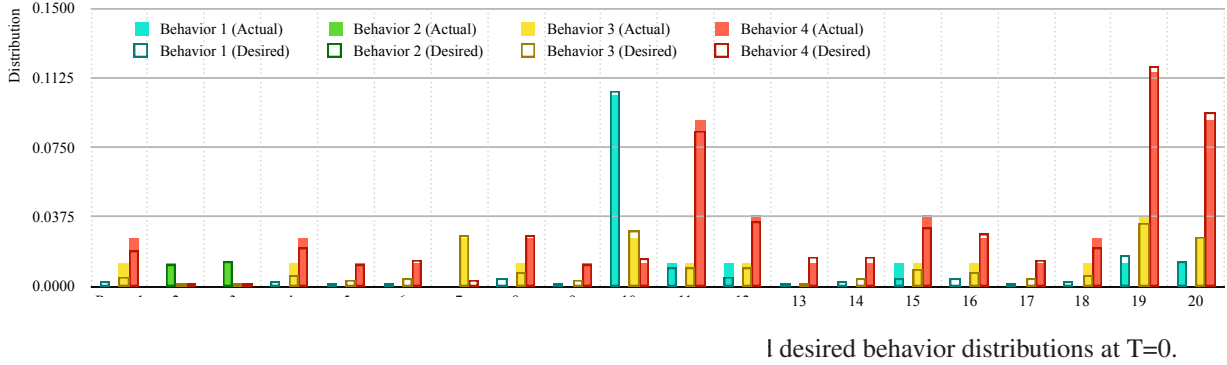


Figure 4. Building-level optimization. Comparison between actual and desired occupancy distributions at T=0.

(b) an interruptibility flag of the agent’s current behavior; (c) other agent-dependent conditions. When the number of such agents exceeds a certain threshold r , the optimizer is invoked and these agents will be re-allocated. The optimizer scheduler algorithm is shown in Algorithm 2.

Algorithm 2 The optimizer scheduler (called in every simulation frame)

input : tolerance threshold, participating agents

```

1 for each agent do
2   | if the agent satisfies all conditions then
3   |   | Add the agent to pending group
4 Calculate the ratio of  $\frac{\text{pending group}}{\text{participating agents}}$ 
5 if the ratio exceeds the tolerance threshold then
6   | Run the behavior optimizer

```

5 CASE STUDY

1

In this study, we demonstrate our proposed multi-constrained narrative-based simulation approach, and we explore different methods to visualize and analyze the simulation results to inform decision-making in architectural design.

5.1 Multi-constrained narrative simulation

We consider the building design of a computer science lab, illustrated in Figure 2. The building is divided into 20 zones that include offices, work areas, meeting rooms, and a kitchen.

The first constraint specified in this approach is the building-level occupancy. Specifically, we consider the occupancy distributions specified in the template illustrated in Table 1a, with minor random perturbations to create variance among zones. Then, we specify a zone-level behavior distribution that depends on the zone semantics. The behaviors considered in this study are “work, “lecture, “eat, “meet, which involve respectively 1, 4, 1, and 2 agents. The behavior distributions considered in this study are encoded in Table 1b. Finally, we specify the agent types and their motivations. We consider: “professors, “undergraduate students, and “graduate students, as illustrated in Table 1c. After performing each behavior, the behavior weight are reduced by an empirical value of 40%. Then, the behavior weights are backward mapped to the motivations to reflect the change.

After verifying that the building design and the templates do not contain semantic errors (as detailed in Section 3.3), our algorithm automatically populates the scene with 104 agents, based on the number of work stations included in the building. Then, an optimization system dynamically allocates the occupants to the different behaviors to satisfy the multiple constraints. In this example, we repeat the optimization process when when 30% agents are available for re-planning (i.e. they either completed a behavior or they are engaged in a behavior that can be interrupted).

Figure 5 shows a simulation snapshot where several occupants are engaged in a variety of behaviors in semantically rich spaces. The figure also illustrates occupancy and behavior distribution data for a selected number of rooms, and it reveals the current motivation of specific individuals. The occupancy and behavior distributions at the consider point in simulated time are detailed in Figure 4 and 3, respectively. Both figures show minimal discrepancy between desired occupancy and behavior distributions and the actual ones.

Despite the optimal agent allocation produced by this approach, minor discrepancies arise due to the following considerations: (a) our algorithm allocates discrete resources (i.e. 104 occupants) to satisfy continuous occupancy distributions (i.e. 0.043 agents in Room 1, 0.017 agents in Room 2, etc.); (b) the algorithm allocates 104 occupants to 80 behavior distributions (4 behaviors for each of the 20 rooms), while half of the considered behaviors require multiple agents; and (c) if several agents are engaged in events that cannot be inter-

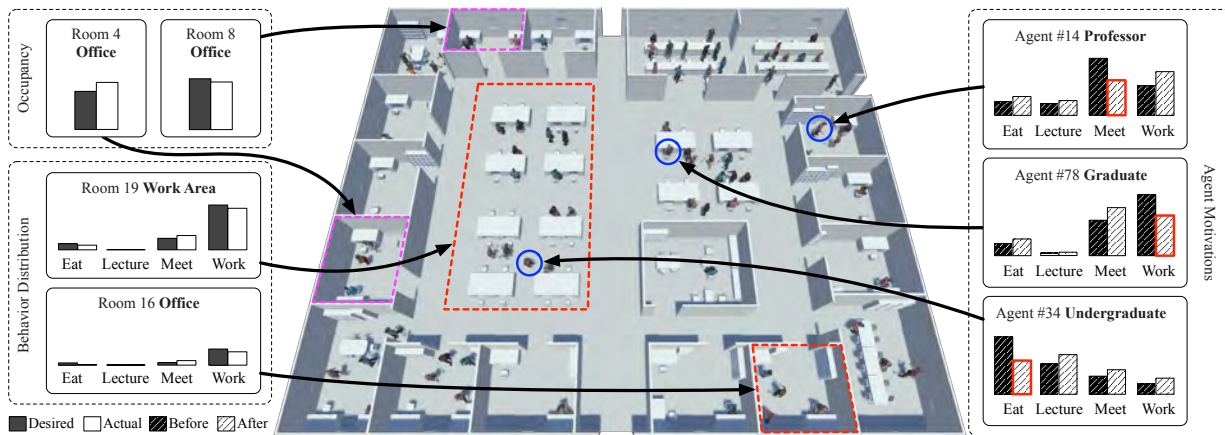


Figure 5. Simulation Snapshot at T=0 with additional information on building-level occupancy, zone-level behaviors and agent-level motivations. We highlight in Red the motivations that have been satisfied by triggering the current occupant’s behavior.

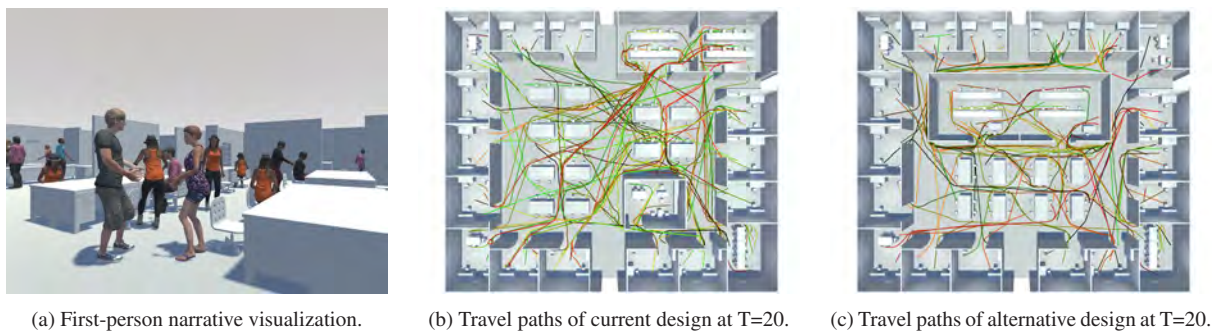


Figure 6. Narrative analysis and visualization to support decision-making in architectural design.

rupted, the scheduler may not be able to re-allocate those agents to satisfy the desired behavior distributions.

Regarding occupants motivations, our results show that for the initial optimization, 82% of the agents have been allocated to events that match their highest motivation. This partially optimal result is due to the fact that our algorithm first satisfies occupancy specifications, then behavior distributions, and finally agents motivations. For example, if the kitchens occupancy is set to be minimal at a given hour, but a high number of agents present high motivations to eat, the optimization algorithm will first satisfy the occupancy constraints, matching the motivations of only a limited number of agents.

5.2 Narrative visualization and analysis

Our framework provides various types of feedback to aid the architectural design process. First, it enables the architects, clients and other stakeholders to visualize a building in use using a third-person view, as shown in Figure 5, or a first-person view, as shown in 6a. Both kinds of visualization could potentially improve designer-client communication by supporting an interactive building walkthrough. Different from [23], the user is able to experience an environment populated with several agents whose behavior dynamically adapts to time-varying occupancy constraints and motivations.

Second, it calculates and visualizes analytical data, such as the walking paths of the different occupants. Figure 6b reveals that spatial bottlenecks could emerge in the central area of the building, in proximity to the students’ working areas. Based on such results, additional scenarios can be tested, where the same input templates are applied to a different building design. Figure 6c reveals a different design for the lab building, where the classrooms are located in the center of the space, rather than at the margins. This layout reduces the possible emergence of spatial bottlenecks in the central area, since it distributes the circulation around the central core. However, it causes increased traffic in the corridors in front of the offices. Based on such analyses, trade-offs between design options could be systematically explored.

6 CONCLUSION AND DISCUSSION

We presented a framework for authoring multi-agent narratives involving multiple occupants that perform individual or collaborative behaviors in semantically rich environments. Different from previous approaches, our system generates narratives that account for building-level occupancy specifications, zone-level behavior distributions, and occupant-level motivations using semantic templates. An optimization algorithm solves a spatiotemporal resource allocation problem by dynamically assigning agents to individual and collaborative behaviors to minimize the deviation from the expected occu-

pancy patterns and behavior distributions while maximizing agent motivations.

Architects could benefit from the proposed approach to better communicate with the different design stakeholders how a building may be used by its future inhabitants. Our system could potentially be adopted at the different stages of the design process, where occupancy and occupants' data can be progressively made available. Such information can be progressively incorporated into the system to produce narratives at an increasing level of detail.

Future work will involve: (a) automating the template generation process to incorporate real-world data; (b) conducting a user study to evaluate the usability of the proposed system; and (c) generating an interactive building walkthrough where users can navigate a space using an avatar and dynamically affect the narrative unfolding.

ACKNOWLEDGEMENTS

This research has been partially funded by grants from the NSERC Discovery and Create programs, and in part by NSF IIS-1703883, NSF SAS-1723869, DARPA SocialSim-W911NF-17-C-0098, and the Murray Fellowship.

REFERENCES

1. Berseth, G., Kapadia, M., and Faloutsos, P. Robust space-time footsteps for agent-based steering. *Computer Animation and Virtual Worlds* (2015).
2. Chen, Y., Luo, X., and Hong, T. An agent-based occupancy simulator for building performance simulation.
3. Goldstein, R., Tessier, A., and Khan, A. Schedule-calibrated occupant behavior simulation. In *Proceedings of the 2010 Spring Simulation Multiconference*, Society for Computer Simulation International (2010), 180.
4. Haldi, F., and Robinson, D. The impact of occupants' behaviour on building energy demand. *Journal of Building Performance Simulation* 4, 4 (Dec. 2011), 323–338.
5. Helbing, D., and Molnar, P. Social force model for pedestrian dynamics. *Physical review E* 51, 5 (1995), 4282.
6. Kapadia, M., Pelechano, N., Allbeck, J., and Badler, N. *Virtual Crowds: Steps Toward Behavioral Realism*, vol. 7. Nov. 2015.
7. Kapadia, M., Shoulson, A., Steimer, C., Oberholzer, S., Sumner, R. W., and Gross, M. An event-centric approach to authoring stories in crowds. In *Proceedings of the 9th International Conference on Motion in Games*, ACM (2016), 15–24.
8. Krontiris, A., Bekris, K. E., and Kapadia, M. ACUMEN: Activity-Centric Crowd Authoring Using Influence Maps. In *Proceedings of the 29th International Conference on Computer Animation and Social Agents, CASA '16*, ACM (New York, NY, USA, 2016), 61–69.
9. Mahdavi, A., and Tahmasebi, F. Predicting people's presence in buildings: An empirically based model performance analysis. *Energy and Buildings* 86 (Jan. 2015), 349–355.
10. Narain, R., Golas, A., Curtis, S., and Lin, M. C. Aggregate dynamics for dense crowd simulation. In *ACM Transactions on Graphics (TOG)*, vol. 28, ACM (2009), 122.
11. Normoyle, A., Likhachev, M., and Safonova, A. Stochastic activity authoring with direct user control. In *Proceedings of the 18th Meeting of the ACM SIGGRAPH Symposium on Interactive 3D Graphics and Games, I3D '14*, ACM (New York, NY, USA, 2014), 31–38.
12. Paris, S., Pettr, J., and Donikian, S. Pedestrian reactive navigation for crowd simulation: a predictive approach. In *Computer Graphics Forum*, vol. 26, Wiley Online Library (2007), 665–674.
13. Rao, A. S., Georgeff, M. P., et al. Bdi agents: from theory to practice. In *ICMAS*, vol. 95 (1995), 312–319.
14. Reynolds, C. W. Steering behaviors for autonomous characters. In *Game developers conference*, vol. 1999, Citeseer (1999), 763–782.
15. Schaumann, D., Breslav, S., Goldstein, R., Khan, A., and Kalay, Y. E. Simulating use scenarios in hospitals using multi-agent narratives. *Journal of Building Performance Simulation* 10, 5-6 (2017), 636–652.
16. Schaumann, D., Date, K., and Kalay, Y. E. An Event Modeling Language (EML) to Simulate Use Patterns in Built Environments. In *Proceedings of the Symposium on Simulation for Architecture & Urban Design* (Toronto, 2017), 189–196.
17. Shen, W., Shen, Q., and Sun, Q. Building Information Modeling-based user activity simulation and evaluation method for improving designeruser communications. *Automation in Construction* 21 (2012), 148–160.
18. Shoulson, A., Garcia, F., Jones, M., Mead, R., and Badler, N. Parameterizing behavior trees. *Motion in Games* (2011), 144–155.
19. Stocker, C., Sun, L., Huang, P., Qin, W., Allbeck, J. M., and Badler, N. I. Smart Events and Primed Agents. In *Intelligent Virtual Agents, IVA 2010, Philadelphia, PA, USA*, (2010), 15–27.
20. Treuille, A., Cooper, S., and Popovi, Z. Continuum crowds. In *ACM Transactions on Graphics (TOG)*, vol. 25, ACM (2006), 1160–1168.
21. Van Den Berg, J., Guy, S. J., Lin, M., and Manocha, D. Reciprocal n-body collision avoidance. In *Robotics research*. Springer, 2011, 3–19.
22. Wang, D., Federspiel, C. C., and Rubinstein, F. Modeling occupancy in single person offices. *Energy and buildings* 37, 2 (2005), 121–126.
23. Yan, W., Culp, C., and Graf, R. Integrating BIM and gaming for real-time interactive architectural visualization. *Automation in Construction* 20, 4 (2011), 446–458.



Including Occupant Behavior in Building Simulation: Comparison of a Deterministic vs. a Stochastic Approach

Max Marschall¹, Farhang Tahmasebi² and Jane Burry³

¹RMIT University
Melbourne, Australia
max.marschall@rmit.edu.au

²University College London
London, United Kingdom
f.tahmasebi@ucl.ac.uk

³Swinburne University
Melbourne, Australia
jburry@swin.edu.au

ABSTRACT

Data capture and analysis are transforming entire industries, enabling novel solutions developed from a numeric evaluation of real-world phenomena. This generally relies on gathering data on physical conditions and users to create accurate, predictive models and provide customized solutions. Increasingly, data-driven approaches are also becoming a part of architectural design, with the goal of creating user-centric and sustainable buildings. However, while simulation software can accurately model deterministic physical effects, it is still difficult to incorporate stochastic effects related to human factors. This paper analyses one aspect of occupant behavior – window operation – to give designers an intuition of the impact of occupant behavior and associated modelling approaches on building performance. To this end, behavioral patterns observed in a previous field study were incorporated into a dynamic energy simulation and compared to a deterministically modelled baseline. While the stochastic models appear to better capture the dynamic and probabilistic nature of occupants' actions, the present study highlights the extent to which the assumption with regard to occupant behavior can influence the simulation-assisted performance based design process. The paper also makes suggestions as to how to interpret such simulation results in a way that quantifies the intrinsic uncertainty in stochastic models. We argue that increased data capture and analysis of building inhabitants could lead to a better understanding of their behavior, thereby affecting the decision-making process in favor of a more sustainable and responsive architecture.

Author Keywords

Occupant behavior; EnergyPlus; window operation model; dynamic; stochastic; Markov chain; logistic regression; thermal comfort.

1 INTRODUCTION

Many industries are now relying on gathering user data to create predictive models and provide tailored products.

There are several indicators of architecture also becoming an increasingly data-driven field: performance based contracts holding designers accountable for whether their buildings perform in the real world as on paper; green building certifications requiring post-occupancy evaluations (POE); smart building concepts of capturing occupant data to auto-adjust building systems in real-time. In fact, it can be argued that there is a rising cultural expectation of customizable and responsive systems, prompting architects to consider incorporating data-driven design approaches into architectural practice.

Computational design has enabled architects to use simulation software to model various performance aspects of proposed building designs, for instance in respect to their thermal characteristics and structural rigidity. While these applications facilitate modelling deterministic physical effects with largely satisfactory accuracy, the predominant metrics for which architects seek to optimize their designs often relate to how the future occupants will use and perceive a space. Anticipating such phenomena is more challenging since they are intrinsically stochastic and multivariate. For example, modelling occupants' interactions with building control devices (such as windows, shades, etc.) generally involves extracting statistical models from data obtained in field studies. These are then analyzed to find a link between environmental parameters and the probability of control devices being operated at any given time. Inclusion of such probabilistic models into performance-based design process yields new opportunities and threats toward creation of occupant-centric buildings, which will require systematic studies in this emerging field of research in the building industry.

2 OBJECTIVE

This paper analyses a single aspect of occupant behavior, namely window opening behavior. Many years of comfort research have demonstrated the advantages of natural ventilation for sustainable building concepts and human comfort [7]. Natural ventilation can have large impacts on the performance of buildings and the comfort of its

inhabitants [8]. However, providing occupants with adaptive environmental controls creates uncertainty of whether they will be used efficiently. Traditionally, energy simulation software is used to model human behavior deterministically, e.g. assuming that windows are opened at a specific predetermined indoor temperature. Such over-simplifications of occupant behavior have often been identified as a cause for the considerable discrepancies frequently observed between building simulation and built reality [4, 9]. Being able to more accurately model human behavior in buildings would therefore not only help architects design more sustainable and user-centric spaces [1], but also make physical simulations more accurate. Several recent field studies have therefore analyzed occupant behavior in terms of adaptive control behavior to inform energy models [3, 5, 9].

In this context, this paper aims to apply a data-driven stochastic model of window operation into early stage building simulations; to give designers an intuition of the effect that occupants can have on the performance of buildings, as well as to describe methods of interpreting the intrinsically uncertain results from predictions of stochastic behavior.

3 METHODS

3.1 Field Data and Statistical Models

The model used for the following simulations was obtained from [11], who conducted a one-year field study in a naturally ventilated office space in Vienna, Austria. The occupants' presence, state of windows and several environmental parameters (including indoor and outdoor air temperature) were monitored on a continuous basis. A logistic regression model was fit to the field data:

$$P = \frac{\exp(\beta_0 + \beta_1\theta_{in} + \beta_2\theta_{out} + \beta_3\theta_{in}\theta_{out})}{1 + \exp(\beta_0 + \beta_1\theta_{in} + \beta_2\theta_{out} + \beta_3\theta_{in}\theta_{out})}$$

in which P is the probability of opening or closing a window, θ_{in} and θ_{out} are indoor and outdoor temperature respectively, and β_0 to β_3 are regression coefficients. These modeling techniques have been widely used in the studies pertaining to occupant behavior modeling [e.g., 3,7,11]. For the current study, the authors used the models developed in [10], which also analyzed inter-occupant diversity by obtaining regression coefficients for each occupant in the field study separately (Table 1). To develop an intuition for the range of possible behavioral patterns and their effects on building performance, we used a best-worst-case approach by running the model for the most 'active' and 'passive' behaviors found in the field study (Figure 1). As for the validity of these models, the aforementioned study demonstrates that the models provide a better representation of occupants' interactions with windows in a free-running office building in Viennese climate [10].

3.2 Model Parameters and Implementation

We used the Rhino/Grasshopper architectural software platform to generate the geometry, set the simulation parameters, trigger the simulation and visualize the results. The simulations were run with EnergyPlus, using the Ladybug/Honeybee plugins for Grasshopper as an interface (figure 2). Dynamically changing window states according to current environmental conditions at each time step required inputting custom EnergyPlus Runtime Language (ERL) code; in each EnergyPlus simulation timestep, sensor objects record the occupancy, θ_{in} , θ_{out} and current window states; the probability of the window opening in the next timestep is then calculated using the logit function with the appropriate coefficients and variables. The next state is determined via Inverse Transform Sampling Method, involving a comparison of the resulting probability P with random numbers. Comfort temperatures θ_{comf} were calculated using Ladybug's implementation of the Adaptive Thermal Comfort model from ASHRAE 55 [2] and compared to the simulated indoor temperatures.

Table 1. Regression coefficients from [11].

Action	Variable	Passive	Aggregate	Active
Opening	Intercept	-10.6882	-22.4190	-10.4233
	θ_{in}	0.2187	0.8031	0.0905
	θ_{in}	0.2100	0.3130	0.2047
	Interaction	-0.0052	-22.4190	-0.0034
Closing	Intercept	23.9665	16.6416	7.9830
	θ_{in}	-1.0969	-0.7013	-0.4323
	θ_{in}	-0.9172	-0.5011	-0.3756
	Interaction	0.0376	0.0186	0.0144

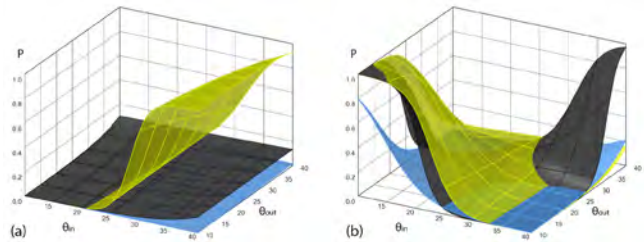


Figure 1. Probability (P) of opening (a) and closing (b) a window based on indoor (θ_{in}) and outdoor (θ_{out}) air temperature, for average (gray), 'active' (yellow) and 'passive' (blue) occupants.

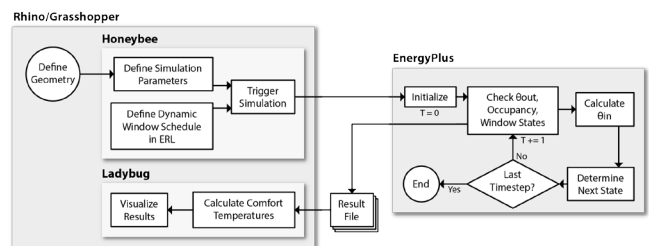


Figure 2. Workflow.

To focus on the implication of occupant behavior models for the early design state simulation based explorations, we did not attempt to remodel the office space from the field study. Instead, a single rectangular naturally ventilated office space with the dimensions 7×10×4m (width×length×height) was chosen for the climate of Vienna, Austria, from which the field study data stems. The north-south oriented room had a 30% glazing portion in the north and south facades. The office space was simulated to be occupied every day between 9am and 5pm. Other schedules and constructions were obtained from the “Closed Office” zone program defaults. Changes of window states were allowed only during office hours; open window states at 5pm therefore led to night ventilation. We adopted a simplified approach in representing the social context in the multi-occupant office, in that cross-ventilation was chosen for the entire simulation. That is, an open window state signifies that both windows were open. θ_{in} values were calculated for an entire year with hourly resolution for 4 window operation models:

1. Deterministic (windows were opened when $\theta_{in} > 24\text{ }^{\circ}\text{C}$);
2. Determined by logit function for aggregated field results;
3. Determined by logit function for ‘active’ user;
4. Determined by logit function for ‘passive’ user.

4 RESULTS

Each simulation was run via Honeybee in a sub-hourly resolution for an entire year (8760 hours). For the cases 2-4, the simulation was conducted for 100 times to obtain the distribution of results. Figure 3 shows an excerpt of the outputs documented in simulation 2 during a summer week. In the visualized timeframe, θ_{in} was continuously higher than θ_{out} . Opening a window therefore had a cooling effect; longer periods of window openings, especially during night ventilation, caused θ_{in} to approach θ_{out} . The heat maps in figures 4-7 visualize window states, as well as the extent to which θ_{in} differed from θ_{comf} (obtained from the adaptive thermal comfort model) for each of the simulations. These allow to visually detect that window openings were much more common in the deterministic model, which reacted immediately to rising temperatures with window operations. The graphs showing the deviation from θ_{comf} illustrate that for the larger part of the year, θ_{in} was below θ_{comf} . Higher θ_{in} values, and therefore increased thermal discomfort, was observed to be shifted towards the afternoon hours. We used three metrics to summarize these effects (Table 2), taking only into account the model results during office hours: the percentage of hours with open windows, the percentage of hours where θ_{in} was higher than θ_{comf} , and the average

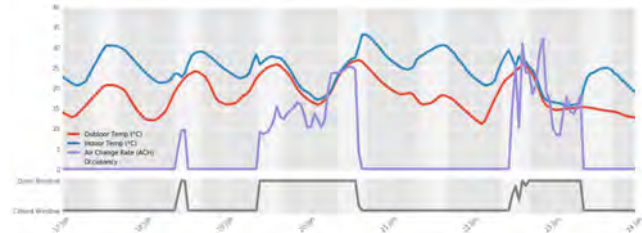


Figure 3. Excerpt from the results of simulation 2.

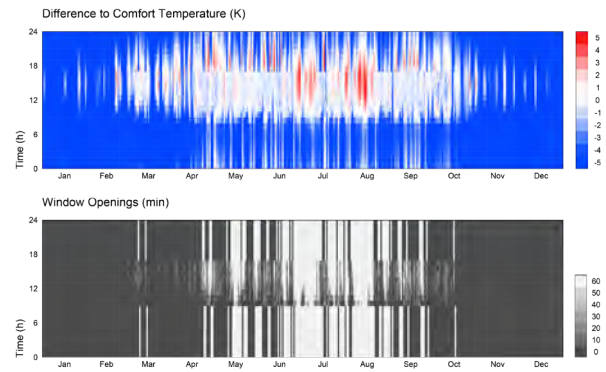


Figure 4. Results from simulation 1 (deterministic model).

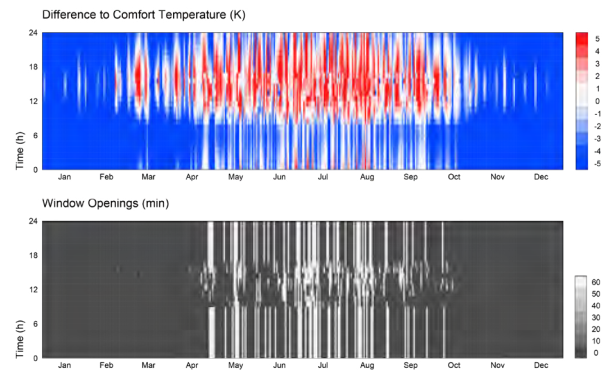


Figure 5. Results from simulation 2 (aggregated occupants).

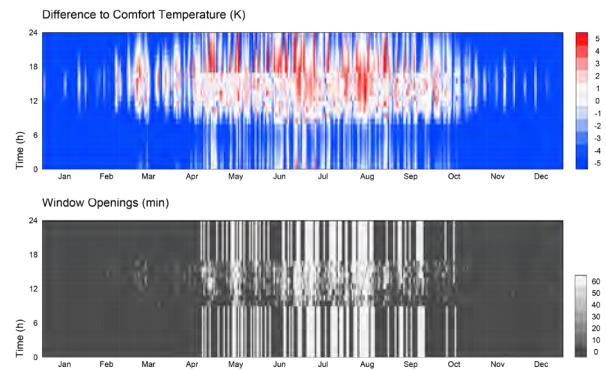


Figure 6. Results from simulation 3 (‘active’ occupant).

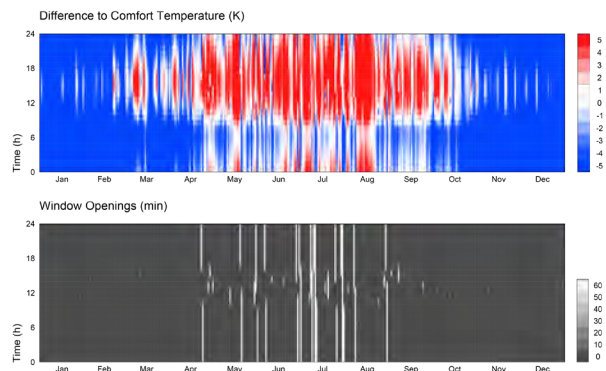


Figure 7. Results from simulation 4 (‘passive’ occupant).

deviation of θ_{in} from θ_{comf} when θ_{in} was higher than θ_{comf} . Simulations with higher proportions of window openings incurred lower occurrences of thermal discomfort due to overheating. The deterministic model over-predicted comfort within the space even as compared with the ‘active’ stochastic model. There were also large inter-occupancy differences when using the logistic regression models; the ‘passive’ model predicted an average 4.55 K above θ_{comf} in comparison to only 1.7 K for the ‘active’ model.

Table 2. Simulation results summarized for office hours.

	Description	% hours with open windows	% hours when $\theta_{in} > \theta_{comf}$	Average $\Delta\theta$ when $\theta_{in} > \theta_{comf}$
1	Deterministic	11%	37%	1.3 [K]
2	Logit (aggregate)	14.25±1.23	43.26 ± 0.44	3.09±0.01
3	Logit (passive)	3.43±0.66	50.04±0.27	4.55±0.01
4	Logit (active)	19.28±0.63	38.26±0.33	1.72±0.0

5 CONCLUSION

The motivation for writing this paper was to address the trend towards data-driven design and the increasing expectations of occupants and clients towards user-centeredness. As an example, we focused on a single aspect of occupant behavior – namely window opening patterns – and how to include this into the design process. We implemented a model derived from field data into a common architectural flexible modelling software.

The results from our case study showed a large deviation between the common way in which architects simulate indoor thermal comfort in early design, and the results from statistical models based on field data. While the stochastic models can in principle better capture the dynamic nature of occupants’ actions, the study showed that a standard model can over-predict comfort. While the current study lacks verification and therefore cannot show which method is more accurate, the observed deviations show that different design solutions may have been driven from the parametric studies. This necessitates further studies toward finding fit-for-purpose occupant behavior models for different simulation-based building design enquiries. In addition, when incorporating field data, we found that inter-occupant behavioral diversity had a large impact on simulation results. Simulations of the kind reported in this paper are proposed to support the choice between free-running, mixed-mode and air-conditioned options for a given design, as well as to determine an appropriate number of operable windows, which can affect the segmentation of the façade as well as the configuration of indoor spaces to make operable windows accessible. Our case study supports the notion that higher volumes of data collection in architecture are useful to foster new insights on occupants and to incorporate human factors into the computational design process. There still exists only limited field study data on occupant behavior,

with observations varying strongly, suggesting that there are many factors influencing behavior. This investigation was limited in that it only attempted to predict window operation, and only did so using temperature as a driving variable. Simulating energy consumption and comfort reliably requires inputting many parameters that are usually not known in early design. Confidence in the results must therefore be managed, and the analysis geared more towards a qualitative understanding of the range of possible outcomes, rather than a primary driver in decision-making.

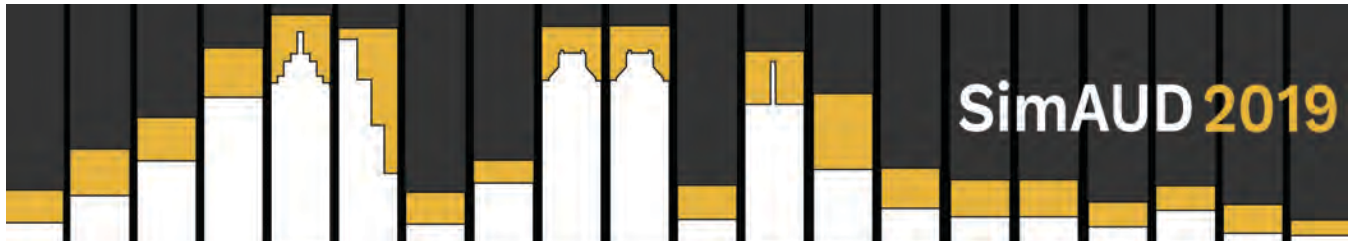
Moreover, as the existing occupant behavior models are mainly derived from limited data sets, they must be subjected to cross-validation studies in different settings [6]. Analyzing results obtained from such models requires caution and skepticism. Rather than expecting model outputs to dictate design materialization, they need to be evaluated critically and in combination with other design considerations.

REFERENCES

- Berry, J., & Park, K. (2017). A Passive System for Quantifying Indoor Space Utilization, 1, 138–145.
- Richard de Dear et al. (1998). Developing an Adaptive Model of Thermal Comfort and Preference.
- Haldi, F., & Robinson, D. (2009). Interactions with window openings by office occupants. *Building and Environment*, 44(12), 2378–2395.
- Hoes, P., Hensen, J. L. M., Loomans, M., de Vries, B., & Bourgeois, D. (2009). User behavior in whole building simulation. *Energy and Bldgs.*, 41(3), 295–302.
- Langevin, J., Wen, J., & Gurian, P. L. (2016). Quantifying the human-building interaction: Considering the active, adaptive occupant in building performance simulation. *Energy and Buildings*, 117, 372–386.
- Tahmasebi, F., Mahdavi, A. (2016). An inquiry into the reliability of window operation models in building performance simulation, *Building & Env.* 105, 343-357.
- Nicol, J. F., & Humphreys, M. A. (2002). Adaptive thermal comfort and sustainable thermal standards for buildings. *Energy and Buildings*, 34(6), 563–572.
- Omrani, S., Garcia-Hansen, V., Capra, B. R., & Drogemuller, R. (2017). Effect of natural ventilation mode on thermal comfort and ventilation performance: Full-scale measurement. *Energy and Bldgs.*, 156, 1–16.
- Rijal, H. B., Tuohy, P., Humphreys, M. A., Nicol, J. F., & Samuel, A. (2011). An algorithm to represent occupant use of windows and fans including situation-specific motivations and constraints. *Building Simulation*, 4(2), 117–134.
- Tahmasebi, F., & Mahdavi, A. (2018). On the utility of occupants’ behavioural diversity information for building performance simulation: An exploratory case study. *Energy & Bldgs.* 176 (2018) 380–389.
- Yan, D., O’Brien, W., Hong, T., Feng, X., Gunay, H. B., Tahmasebi, F., Burak Gunay, H. (2015). Occupant behavior modeling for building performance simulation: Current state and future challenges. *Energy & Bldgs.*, 107, 264–274

Robots that Make

Rotoform - Realization Of Hollow Construction Elements Through Roto-Forming With Hyper-Elastic Membrane Formwork	191
<i>Oliver Tessman and Samim Mehdizadeh</i>	
Environmentally Informed Robotic-Aided Fabrication	199
<i>Carmen Cristiana Matiz, Heather “Brick” McMenomy and Elif Erdine</i>	
Curved-Crease Folding and Robotic Incremental Sheet Forming in Design and Fabrication	207
<i>Elif Erdine, Antiopi Koranaki, Alican Sungur, Angel Fernando Lara Moreira, Alvaro Lopez Rodriguez, George Jeronimidis, Michael Weinstock</i>	



Rotoform - Realization of Hollow Construction Elements Through Roto-Forming with Hyper-Elastic Membrane Formwork

Oliver Tessmann and Samim Mehdizadeh

TU Darmstadt, Digital Design Unit (DDU)

Darmstadt, Germany

{Tessmann, mehdizadeh}@dg.tu-darmstadt.de

ABSTRACT

The paper presents a digital process chain for modeling, simulating and fabricating rotationally molded, individualized hollow concrete components using material-efficient and geometrically flexible formwork systems made from hyperelastic membranes. The hollow concrete components are to be used as prefabricated components for architectural constructions. The inner cavity can be efficient in different ways: To save weight and material, for subsequent filling with other materials (insulating, climate regulating, water heating circulation etc.) or as permanent formwork for solid, reinforced structural components that are poured with concrete. Rotoforming concrete significantly reduces the hydrostatic pressure within a formwork and therefore unlocks completely new possibilities for material-efficient and geometrically flexible formwork systems.

Author Keywords

Complex concrete structures; Casting; Dynamic casting; Membrane formwork; Rotoforming; Minimal surface; Computational design; Simulation; Material behavior; Additive Fabrication.

1 INTRODUCTION

Concrete is one of the most widely used building materials. Mark Wigley conceives of concrete as “*the single biggest form of evidence of our species’ s existence*” on planet earth [16] If the material is everywhere it is inevitable to enhance concrete performance i.e. respond to the socio-economic need for a diverse living environment that consumes less material and energy while adapting to various local contexts. Given the ubiquitous use of concrete even minor improvements have a huge impact.

In the construction industry prefab-concrete elements are still bound to a repetitive and serial logic of production. Customized and site specific building parts on the other hand come with high production costs and material-intensive formwork systems.

Computational design allows the simple creation of geometric differentiation. Digital fabrication offers a series of adequate materialization procedures. Data flows fluently from models of ideation and exploration to data for fabrication. This process chain has been tested and established in the timber industry [17]. If, however, it is transferred to concrete structures, a contradiction arises: The promise of concrete taking every possible shape comes with the price of a formwork that supports the material during the process of curing.

This research seeks to bridge the gap that emerges between the possibilities offered by computational design and robotic fabrication and the geometric constraints of conventional formwork systems. This goal is achieved by developing a process chain from digital modeling, physical formfinding, material and process simulation and robotic fabrication. Through migrating the rotomoulding technology into the process of concreting we could reduce the hydrostatic pressure of liquid concrete significantly which allows for a completely new range of lightweight, hyperelastic, compostable membranes as concrete formwork.

2 RESEARCH CONTEXT

Research in the context of fabric formwork, dynamic formwork systems, rotomolding and robotic fabrication is relevant for this project. Fabric formwork is not new. The technology appears in different eras and contexts of the 20th century. The majority of the work is based on craftsmanship. Since the production process, the textiles and the entire formwork setup have a huge impact on the resulting form designers don’t design through drawing but rather by experimentation with scale models and 1:1 prototypes. Veenendaal et al. propose a taxonomy of different textile formwork systems [15]. Within this taxonomy our hyperelastic membrane falls into the category of bi-axial mechanical prestressed formworks. Computational formfinding - the simulation of external

forces impacting on a material system - is only recently migrated into the realm of fabric formwork. The method is known for finding the geometry of form-active structures. In the context of fabric formwork it becomes a construction method [14]. But more important, tools like Kangaroo allow for simulation within an architectural design environment. Thus simulation allows exploring the design potential of fabric formwork before physically making it. The Block Research Group at the ETH Zurich combines tailored fabric formwork with prestressed cable nets as underlying falsework. Concrete is sprayed onto the formwork in thin layer. The cable net deforms under the weight of the sprayed concrete into the shape that is designed by computational methods developed by the researchers. The research thus developed a computational design process for fabric formwork [13]. As the range of possible forms resulting from the use of fabric formwork is limited to shapes that emerge by fabric being exposed to hydrostatic pressure, other research trajectories explore ways to incrementally improve existing formwork. The increase of material efficiency through the use of recycling and re-shaping formwork material such as wax [8] or water [10] is explored in various research projects. Geometric freedom is furthermore achieved through flexible mechanical-kinetic systems such as dynamically reconfigurable double-curved molding surface shaped by an array of actuators [5]. Another example of a dynamic formwork system is the Smart Dynamic Casting (SDC) project by Gramazio Kohler at the ETH Zurich. SDC is based on the concept of slipforming in which concrete is poured into a continuously moving form. The procedure allows for a continuous and gradual change of the cross section of the cast element by shaping the concrete during curing through the subtle movement of the formwork by a robot [6]. The project exemplifies the importance of merging design intent, digital fabrication processes and material science into one coherent process. The MARS pavilion by Sarafian, Culver and Lewis exemplifies the use of robots in combination with fabric formwork. The system allows fabricating branching concrete structure cast into adjustable fabric formwork. Robots guarantee the exact position of tailored fabric formwork sleeves that are subsequently assembled into a dome-like lattice structure. The aim was to find a cost competitive way to fabricate parametrically designed concrete structures [9]. Martin Bechthold and Jonathan King from Harvard GSD mass customize concrete objects through robotically orienting a mold while the material cures. The project was presented as a workshop at the Robotics in Architecture 2012 Conference in Graz and Vienna.

None of the mentioned projects addresses the reduction of hydrostatic pressure that we regard as a key concept to unlock a completely new range of material efficient formwork materials. This is achieved by migrating the rotomoulding technology into the realm of concrete processing. Roto-forming is a production process in which

a liquid material is poured into a mold. The amount of material is sufficient to adhere to the wall of the slowly rotating formwork, but not enough to fill the entire mold. The manufacturing process is used in the plastics industry for the production of hollow objects such as water tanks, barrels, kayaks, plastic furniture etc. Here massive steel molds are heated to melt the plastic. Al-Dawery et al migrate rotomoulding from the plastic industry into the field of ceramics [1]. Empirical design and prototyping research on the use of hyperelastic membranes as formwork within a DIY rotomoulding process have first been developed by Thomas Vailly and Itay Ohaly for the production of small-scale design objects. The latex membranes allowed the production of different shapes without the need of previous tailoring [12].



Figure 1. A lightweight hollow concrete (UHPC) object rotoformed in a prestressed latex membrane.

3 METHOD

3.1 Material System

Rotoforming is conceived of as a material system in which form, material, structure and its synthesis (materialization, fabrication and assembly) are regarded as integral and closely linked elements.

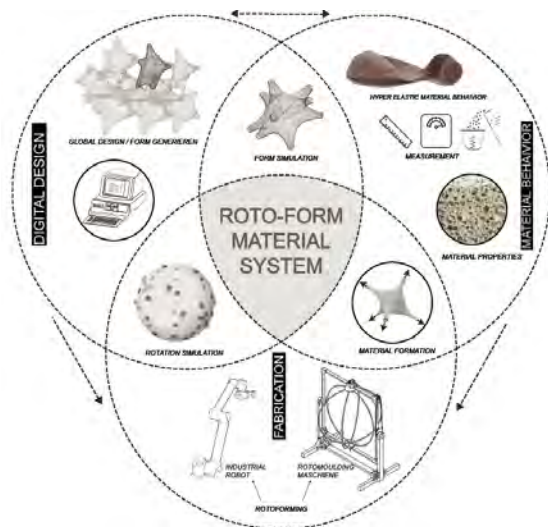


Figure 2. RotoForm Material System

Computational tools and techniques, as part of this system, allow notating and instrumentalizing the intricate interactions between form, material, structure and environment within the architectural design process. Simulating material systems within digital generative models utilizes computation beyond formal and geometrical design schemes. The notion of the model shifts from representation of objects towards the abstraction of a process and the prediction of behavior [3]. The material system approach was used in this project to revisit and challenge conventional formwork systems. Instead of incrementally improving existing formworks we reconsidered the entire process of concreting and identified membranes as formwork material. Besides minimal material consumption these membranes can be tensioned in a wide range of forms without previous tailoring.

We reduced the consumption of both concrete and formwork material and at the same time expanded the design potentials for our built environment. This could be achieved through rotoforming concrete.

3.2 The Simulation-Based Design Tool of RotoForm

Fabric formwork has no significant tradition in the building industry as it is very different from conventional formwork. A rigid formwork is a technological means to transcend geometry envisioned by the architect into matter. Fabric formwork, in contrast, becomes part of the design process as its material performance and boundary conditions have a significant impact on the resulting shape [14]. The forms that emerge when hydrostatic pressure acts on a fabric or a membrane that is prestressed, can hardly be captured by 2D drawings or even 3D models. Hence, physical models, small-scale or 1:1, have been the tools for designers when working with fabric formwork [7]. Making these physical models and prototypes is a craft that requires a different skill set than the production of drawings or digital models. The craft includes experience and tacit knowledge that is not easy to standardize. As Remo Pedreschi describes, the previously separated roles of builder and the designer merge into one:

"The role of the builder or maker of fabric cast concrete involves both the deconstruction of the object into a sequence of steps and the continual re-evaluation and adjustment of the form during the assembly and casting process. The design develops during the making." [2]

As comprehensible as this coalescence may sound, it is however also responsible for the absence of fabric formwork in the construction industry. Designs that only unfold during making cannot be represented in the conventional artifacts that designers produce. Furthermore design decisions are required during the making, which means that the design phase does not stop with the production of representations such as drawings and models. Designers have to be involved into the materialization.

Against this background we sought to develop RotoForm into a material system consisting of digital and physical components (see Figure 1) that are fluently combined, but also clearly sequenced. Designing with rotoformed elements should be possible without the need for physical prototyping but through the use of simulation-based design tools and methods. Design tools incorporate material behavior under the impact of external forces to overcome mere geometric representation. Thus we use Kangaroo in Grasshopper to simulate the prestressing of membranes. These tools are accessible for designers and well integrated into the architectural design environment. The simulation accomplishes both: It is a technical necessity for the subsequent fabrication, but it also contributes to the representation of the design proposal. The formal potential of the material system is visualized. At the same time its geometric limitations and material constraints are displayed. Digital simulation is not meant to replace prototyping and physical modeling but should rather complement these activities.

4 PROCESS

4.1 Design Process

In this research we conceive of rotoformed elements as nodal connections for irregular space-frame structures.

The form of the nodes is a result of a form-finding process in which a particle-spring model is used to find the minimal surface that emerges between all rods intersecting at one point (node) of the space frame. The topology, described by the center-line model, is complemented by a low-polygon solid that approximates the dimensions and orientation of the node (see Figure 3).

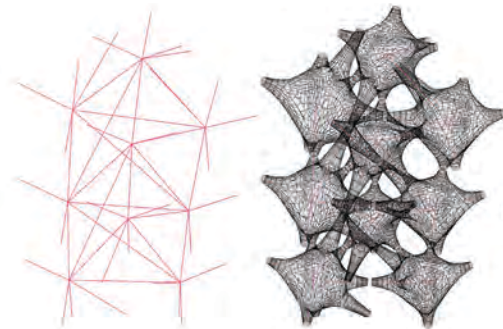


Figure 3. Intersecting centerlines, relaxed mesh of nodal geometry minimal surface.

The mesh resolution is increased for the formfinding simulation using the Grasshopper add-on tool Weaverbird and Meshmachine. Tension forces along the center-lines induce prestressing into the mesh. Mesh edges act as springs and the vertices are exposed to the forces. The particle spring model generates a relaxed mesh approximating the minimal surface that emerges when a hyper-elastic membrane is pre-stressed. Commonly-available software packages, such as Rhinoceros and Grasshopper, Kangaroo are used in order to make the digital process accessible for architects. The same software

packages are also used as a means of direct-communication with a UR 10 Universal Robots and a turning table.

The simulated form of the nodes is subsequently used to calculate its volume and surface area, two important parameters to the rotoforming process. Based on the surface area and the aspired wall thickness of the hollow element, the amount of cast material is calculated.

4.2 Manufacturing Process

To manufacture the digitally designed and simulated nodes the digital geometry is translated into a prestressed latex membrane kept in place by a spherical falsework (see Figure 7). All steps including their methods and tools are described in the following paragraphs.

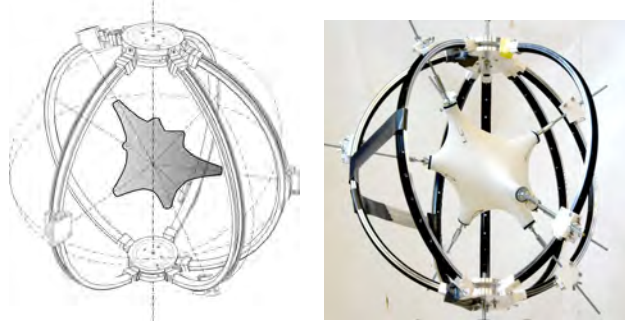


Figure 4. Pretentioned the hyper-elastic membrane formwork in the spherical falsework

The adaptive spherical falsework

The pre-stressed membrane is fixed to a spherical falsework that acts as the boundary resisting the large anchoring forces (see Figure 4). The adaptive falsework is designed to allow for the generation of different membrane shapes by changing the position of the tension anchors.

Two aluminium plates form the poles of the sphere. The poles are tied together by a series of median arcs (between 6 to 10 depending on geometry). The arcs carry clamps that act as anchoring points and take the loads from tensioning the membrane. 3D printed elements connect the rims to the poles. They can slide in a notch to change the location of the meridian arcs. A screw allows tightening or loosening the connector for proper placement. Clamps that slide along the meridian arcs are holding the anchor rods that define the location and direction for tensioning the membrane.

Robotic placement

A robot translates the digital geometry into the physical setup. In this setup, a UR 10 six axis robot and a turning table are used to place a rod in the correct position and orientation in relation to the sphere. The turntable rotation is controlled via a combination of an Arduino single board micro controller and Funken, a serial protocol toolkit for interactive prototyping [11]. The robotically

positioned rod is fixed to the clamps. After all rods are placed, the membrane formwork is placed inside the falsework. The anchor rods penetrate the membrane and connect it to the falsework. Steel and rubber washers

connect the rods to the membrane and transfer the stresses of the subsequent tensioning.

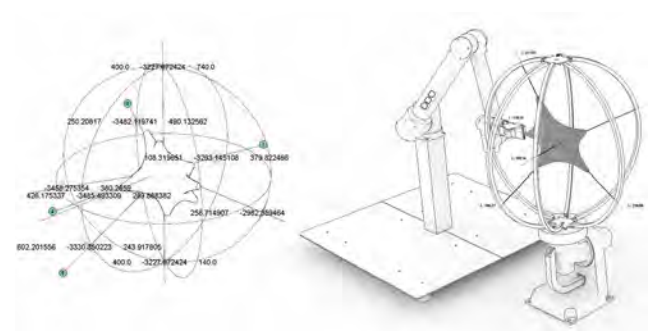


Figure 5. digital data extraction and Robotic Placement

Pre-tensioning membranes

Membranes are flexible, non-rigid structures that transfer loads through tension. They require fixed ends or rigid linear boundaries that withstand the horizontal forces inherent in every form-active system. Their bearing mechanism relies on the material form. Form coincides with the flow of stresses that are equalized or harmonized along the surface. Loads are dispersed in the direction of resultant forces without any shear [4] In this project we used latex membranes as membrane formwork within the rotoforming process. Filled with air, these balloons take a spherical shape due to internal pressure that acts perpendicular to the membrane surface. Filled with liquid concrete the combination of gravity and hydrostatic pressure generates drop-like shapes. Thus these external forces during production would not allow generating any other form. We therefore sought to minimize this effect through the reduction of cast material in the formwork and through prestressing the membrane formwork (see Figure 6). A series of tension-inducing anchor points are connected to the membrane. In order to achieve a harmonized stress distribution and avoid wrinkles in the membrane the anchor points need to be placed in a way that tension creates curvature in all areas of the membrane.

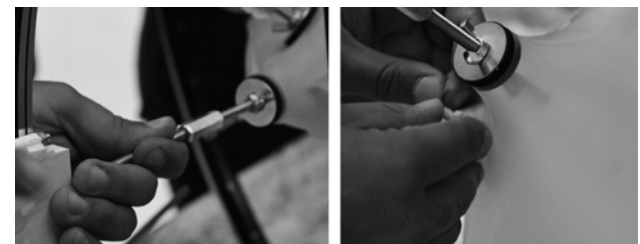


Figure 6. Pre-tensioning membranes

The Rotoforming machine

The rotoforming machine consists of a frame that rotates around a horizontal spindle powered by an electric motor. The frame carries a vertical spindle to which the spherical formwork is connected (see Figure 7). A belt and 90 degree tapered gear wheels transmit the rotational motion.

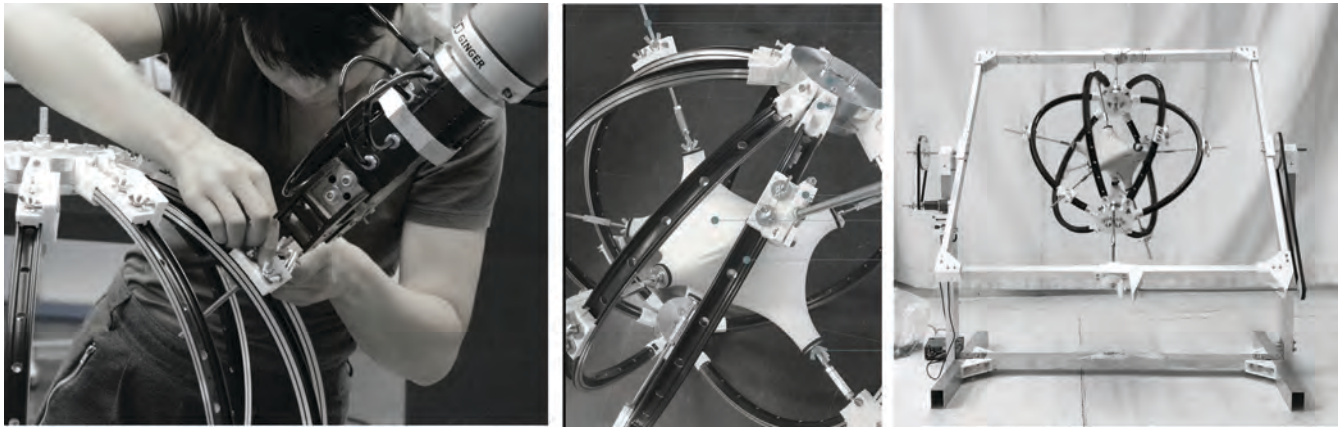


Figure 7: The digital-physical robotic-aided process. From left to right: Robotic placement of rods on spherical scaffold, Prestressed membrane formwork. Rotoforming machine.

The movement of the two spindles needs to be aperiodic to make sure that the formwork is fully rotated and all its regions pass the lowest point as the liquid material flows downwards.

The formwork slowly rotates to disperse the liquid cast material to the membrane. In contrast to spun concrete parts, the material is not allocated through centrifugal forces that tend to stratify the material. The material rather adheres to the membrane surface yielding high quality surfaces.

Cast material

During rotoforming the liquid material is subject to a constant change of shape. The impacting loads are not static. In the early stage of curing the material furthermore deforms according to the geometry of the membrane. For this research, the material needed to be adjusted in such a way that it could absorb the quasi-dynamic load at different phases of rotation in different layer thicknesses without cracking. Component sizes, rotational speeds and production speeds as well as the composition of the formwork material have a decisive influence on the viscosity requirements. Mass inertia, adhesive forces on surfaces and hardening processes must be controlled in combination with layer thickness formation and shrinkage cracking.

Two different materials were tested in the project: An ultra high performance concrete (UHPC) and an acrylic/plaster composite. The composite was used for testing the entire process. Its short curing time allows for a fast production of rotoformed elements. However, the main goal is the production of rotoformed concrete elements. Increased hydrostatic pressure and longer curing periods of concrete pose additional challenges to the process. First concrete prototypes were manufactured in collaboration with the concrete company Gtecz (see Figure 1).

Resulting hollow body component

The materialized object is a lightweight hollow component with approx. 3% of the weight of a solid component in

similar size (180 mm radius and 7 mm shell thickness). The resulting surface is smooth with gradually changing curvature continuously blending all directions of the surface. The cast-in anchor rods serve as connection between two components or between nodes and rods. The cast nodes were subsequently 3d scanned in order to compare the cast object to the empty prestressed membranes in the spherical falsework and to the simulated minimal surface of the particle-spring model. The comparison between object and membrane proof that hydrostatic pressure has no impact on defining the shape of the membrane. The simulated form deviates from the form of the cast object. As the current role of simulation is limited to provide a better formal approximation in the early design stage the current precision is satisfactory.

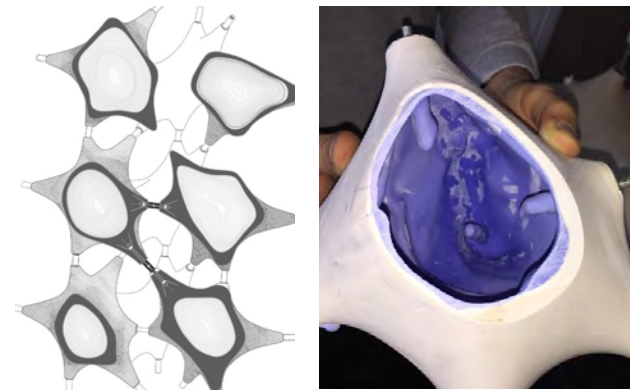


Figure 8. The Section of the resulting demonstrator with hollow body nodal component.

5 CONCLUSION / OUTLOOK

Within our research we could prove through a novel fabrication process and the resulting prototypes that rotoforming concrete in membrane formwork is possible and leads to material-efficient formworks that allow for geometric differentiation without the need of tailoring the formwork. Furthermore, the process yields hollow concrete objects with reduced weight and material consumptions.



Figure 9. The large scale demonstrator of space truss system at AAG Conference 2018 with hollow body concrete nodal component

By adding rotational movement to the process of concreting and thereby reducing hydrostatic pressure we are able to reconsider the established palette of formwork materials towards more lightweight and efficient materials. Besides the important aspect of saving resources these materials also simplify the de-molding of concrete objects and generate high surface qualities. The shape of the minimal surface of the prestressed membrane is perfectly mirrored in the concrete object. The tools and methods developed for the process yield geometric precision of the complex forms. A prototype of a series of six interconnected nodes and a rotoformed base plate demonstrate the validity of the material system (see Figure 8 and 9).

Hydrostatic pressure is no longer the form-defining force in this membrane formwork system. However, the need for an even of harmonic stress distribution in the membrane create novel constraints for the range of possible forms.

One hypothesis of this research was that such a tool and method would allow designers to explore the formal potentials of membrane formwork and make them part of their design. The hypothesis was tested in a series of workshops with students, researchers and professional designers.

We could observe how the teams implemented material performance into their aesthetic approaches: One example is the design of extra tension-spikes for Harmonizing the stress distribution in the membrane requires similar curvature in all regions of the membrane. A lack of tension in the membrane leads to wrinkles and reduced capacity to withstand the liquid material.



Figure 10. The resulting demonstrator with hollow body concrete nodal component.

A constraint that may be in conflict with the location and orientation of space frame rods that tension the membrane.

When testing the system with students in a rotoforming workshop design team added extra tension-spikes that were independent from the space frame rods, in order to generate the necessary pretension in the system. The integration of simulation of the material system into the early stages of the design process in which the shape is of importance for designers generated novel material-appropriate but also aesthetic design solutions.

The roto-formed elements are significantly lighter than massively cast elements and can thus contribute to more lightweight constructions that consume less material. The reduced weight of a rotoformed facade element allows for more lightweight substructures. The effect thus propagates through the entire construction.

Rotoforming comes with challenges that requires future research in the following fields:

The aim of letting a concrete cure while it is being moved is a conceptual contradiction that can only be solved by the careful design of movements coordinates with concrete recipes that allow for the curing under these delicate circumstances. More data needs to be collected and procedures require standardization to be able to reliably reproduce results of similar quality.

Curing generates heat which is currently collected within the closed membrane system. The heat expands the formwork and can lead to a delimitation of the concrete from the formwork and in the worst case to a collapse of the hollow element during rotation. Casting subsequent layers of material is necessary to not deform the delicate

membrane and the first layers of concrete but requires a cumbersome process of filling the material into the formwork without destroying the previous layer of material.

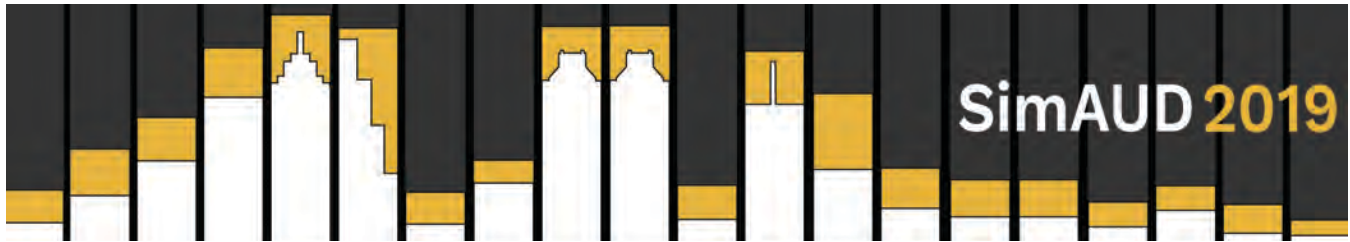
The above mentioned challenges will be addressed in the ongoing research together with questions of enlarging the range of possible forms and Morphologies through variations of the membrane formwork system and its falsework/boundary condition, the integration of reinforcement and mounting elements and the variation of wall thickness through a differentiated and controlled rotational movement.

AKNOWLEDGMENTS

This research greatly benefited from a series of workshops in which participants tested and prototyped. Their feedback and experiences informed our work. Special thanks to the participants of the workshop at the AAG conference 2018 in Chalmers: Johan Dahlberg, Deena ElMahdy, Eftixis Efthimiou, Felix Graf, Fabio Scotto, Franz Theobald, Athanasios Vagias, Yuwei Zhang. First tests with rotoforming concrete have been conducted with the support of G.tecz/Gregor Zimmermann. The Machines has been built with the technical supports of Mirko Feick/PTU, Marecel Bicolay/ VKM, TU Darmstadt, Alexander Stefas, Andrea Rossi and Felix Graf by DDU of TU Darmstadt.

REFERENCES

- Al-Dawery, I., Binner, J., Tari, G., Jackson, P., Murphy, W., & Kearns, M. Rotary moulding of ceramic hollow wares. *Journal of the European Ceramic Society*, 29(5), (2009), 887-891.
- Chandler, A., Pedreschi, R. (edited by). *Fabric Formwork*. London: RIBA Publishing, London UK, 2007
- Hensel, M., Menges, A. (eds.), *Morpho-Ecologies: Towards a Discourse of Heterogeneous Space in Architecture*, AA Publications, London. 2006
- Engel, H. *Structural Systems*, Hatje Cantz Verlag 2007
- Kristensen, Mathias Kraemmergaard; JEPSEN, Christian Raun. Flexible mat for providing a dynamically reconfigurable double-curved moulding surface in a mould. U.S. Patent Nr. 9,168,678, 2015.
- Lloret, E., Shahab, A. R., Linus, M., Flatt, R. J., Gramazio, F., Kohler, M., & Langenberg, S. Complex concrete structures: merging existing casting techniques with digital fabrication. *Computer-Aided Design*, 60, (2015). 40-49.
- MANELIUS, A.-M. *Fabric Formwork. Investigations into Formwork Tectonics and Stereogeneity in Architectural Constructions*. Ph.D. Thesis, Royal Danish Academy of Fine Arts Schools of Architecture, Design and Conservation, School of Architecture, Denmark, 2012.
- Oesterle, S., Vansteenkiste, A., & Mirjan, A. Zero Waste Free-Form Formwork. in *Second International Conference on Flexible Formwork, ICFF. CICM and University of Bath, Dept. of Architecture and Civil Engineering, Bath (2012) 258–267*
- Sarafian, J., Culver, R., Lewis, Trevor S. *Robotic Formwork in the MARS Pavilion: Towards The Creation of Programmable Matter*. In *ACADIA 2017: DISCIPLINES & DISRUPTION [Proceedings of the 37th ACADIA, Cambridge, MA 2-4, (2017) pp. 522- 53*
- Sitnikov, V. *Ice Formwork for High-Performance Concrete: A Model of Lean Production for Prefabricated Concrete Industry*. Structures, Elsevier, 2018
- Stefas, A., Rossi, A. and Tessmann, O. *Funken - Serial Protocol Toolkit for Interactive Prototyping*. In: *Computing for a better tomorrow - Proceedings of the 36th eCAADe Conference - Volume 2*, Lodz University of Technology, Lodz, Poland, 19-21 September (2018), 177-186
- Vailly, T. , Ohaly, I. *The creative Factory* <http://www.vailly.com/projects/the-creative-factory>. As of 15. April 2015
- Van Mele T., Méndez Echenagucia T., Pigram D., Liew A. and Block P. A prototype of a thin, textile-reinforced concrete shell built using a novel, ultra-lightweight, flexible formwork system, *structure*, 1, (2018), 50 - 53
- Veenendaal D. and Block P. *Computational form finding for fabric formworks: an overview and discussion*, *Proceedings of the 2nd international conference on flexible formwork*, Ohr, J. et al. (editors), Bath, UK, (2012), 368-378,
- Veenendaal, D.; Block, P.; West, M. History and overview of fabric formwork: using fabrics for concrete casting. *Structural Concrete* 12, 3 (2011), 164 – 177
- Wigley, M. Foreword, in M. Bell and C. Buckley (eds), *Solid States (Columbia Books on Architecture, Engineering, and Materials)*, Princeton Architectural Press, 2010
- Willmann, J., Knauss, M., Bonwetsch, T., Apolinarska, A. A., Gramazio, F., & Kohler, M. *Robotic timber construction—Expanding additive fabrication to new dimensions*. *Automation in construction*, 61, (2016) 16-23



Environmentally Informed Robotic-Aided Fabrication

Carmen Cristiana Matiz, Heather “Brick” McMenomy and Elif Erdine

Architectural Association
London, United Kingdom

{Matizxcarmen, brick.joshua.mcmenomy}@gmail.com

elif.erdine@aaschool.ac.uk

ABSTRACT

The research presented in this paper addresses the integration of thermal performance with robotic toolpath generation for nomadic settlements. It is part of a larger study that describes the development of a material system and a remote on-site fabrication strategy for African nomadic dwellings using unprocessed locally sourced materials in hot arid environments. Research methods include the employment of computational design and robotic fabrication techniques to facilitate the development of improved housing conditions.

Through the analysis of existing traditional earthen construction strategies, the aim is to develop a novel approach to robotic fabrication of unfired earthen envelopes by incorporating thermal performance simulation in the robotic motion path generation.

The use of robot-aided fabrication eliminates the need for complicated prefabricated moulds, achieving improved environmental performance with reduced material usage. Taking into consideration the material properties and associated drying times, a layer sequencing strategy is introduced to diminish the possible errors and collapse that occur during the fabrication process. Two types of layers are identified in relation to their position within the envelope's structure and are optimized for increasing thermal lag, and respectively, self-shading.

The contribution of the research is a robot-aided fabrication-aware design method for generating complex thermally performant earthen envelopes realized by overlaying continuous layers using simple toolpath geometries.

Author Keywords

Solar Analysis; Locally Sourced Materials; Robotic Fabrication; 3D Printing; Robotic 3d-printing; Earthen construction.

ACM Classification Keywords

D.2.2 DESIGN TOOLS AND TECHNIQUES (Object-oriented design methods); I.2.9 ROBOTICS: (Manipulators); I.3.5 COMPUTATIONAL GEOMETRY AND OBJECT MODELING (Physically based modeling);

1 INTRODUCTION

Robotic fabrication and its capabilities to be used on-site in remote environments is a construction strategy that has been discussed in recent research [13]. As robotic tools are becoming accessible to the general population, they present the capabilities to empower communities by offering autonomy in the construction process. The on-site use of robotic fabrication tools with widely available locally sourced material is a sustainable alternative [5] to current industry solutions and presents itself as a possible construction method for responding to the increasing housing demands. Fabrication tools as Big Delta [3] illustrate a step towards accessible robotic solutions and have successfully enabled 1:1 on-site experiments.

The presented research is part of a wider topic that investigates accessible housing fabrication methods inspired by vernacular building techniques in developing countries, with a focus on nomadic pastoralist in Northern Mali. The proposed restricted context provides an information base that enables problem-solving and innovative solutions that address thermal performance and rapid construction.

The proposed material system is informed by cultural practices and vernacular sustainable construction techniques that lend themselves to the impermanence of the housing type, as the shape of the house changes with the family dynamic. Dwellings in southern Mali and Burkina Faso consist of mud brick structures made of locally sourced sun-dried soil. Housing can take six to eight months to construct and require constant maintenance. Therefore, even primarily earthen structures exist ephemerally, and can be consistently edited by its inhabitants. Rapid construction techniques can be identified in current desert dwelling in northern Mali that include tent structures for nomadic tribes, which can be assembled and deconstructed within three to four hours. While ideal for encampments which last less than one week, tents do not provide the thermal comfort that earthen construction provides, and there is currently no system of dwelling which combine the benefits of tent dwellings with the comfort and security of earthen buildings.

The proposed material system, a modernized wattle and daub system, uses solely local resources for developing dwellings for nomadic pastoralists in Sub Saharan Africa by combining existing tent construction practices with robotically controlled earth extrusion.

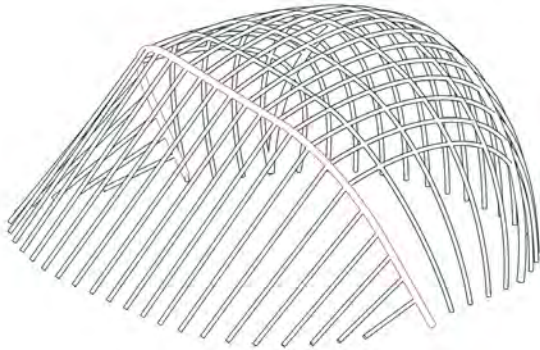


Figure 1. Actively bent grid-shell geometry based on local vernacular construction techniques. Rendille Tent structure [10].

The elastic grid shell was used as a base structure within the material system because of its relation to existing forms of dwellings employed in the Sub-Saharan Region. The types of housing currently used include tensile tent structures and armature tent structures, which consists of actively bent grid shells [10] (Figure 1). An armature system was selected as it would be possible to erect an elastically bent grid shell with a degree of geometric precision that would be difficult to mimic with a fabric formwork in a remote environment.

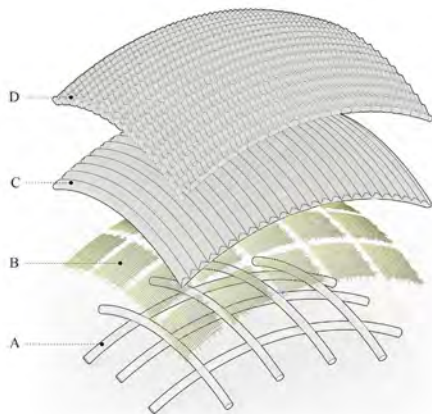


Figure 2. Proposed material system using widely available locally sourced materials (A – Elastic Grid Shell, B -Natural Fiber Mesh, C – Interior Earthen Layers, D - Exterior Earthen Layer)

The armature tent structure acts as a base geometry that informs the fabrication process and is composed of actively bent wooden dowels that form an elastic grid shell (Figure 2-A) It acts as structural support for the extruded earthen layers.

The earthen layers (Figure 2-C, 2-D) have the main role to consolidate the structure while providing thermal comfort.

An intermediate natural fiber layer (Figure 2-B) is interwoven between the dowels acting as formwork for the material deposition. Research in ceramic bricks explores design variations that incorporate environmental performance into the construction process that go beyond thermal resistance calculations. Investigations range from rectangular brick wall assembly that enhances self-shading [7] to additive manufacturing techniques which allow for complex brick geometries [4] that include self-shading and thermal energy geometric control [13]. Robotic fabrication allows efficient material usage due to the possibility of optimizing toolpath geometry. However, as envelope geometries become more complex, the fabrication time and the possibility of collapse during fabrication increase correspondingly. Experiments in two-step robotic fabrication processes that investigate rapid fabrication for thermally responsive envelope design through convection by altering the envelopes surface finish have recently been developed by initially deploying a rough concrete layer and then altering the surface geometry with [2]. This paper proposes a design strategy that investigates time-sensitive methods for incorporating environmental performance as a result of self-shading within the fabrication process and will focus on the design development and fabrication method of the earthen envelope through layer sequencing and extrusion toolpath pattern design.

2 ENVIRONMENTAL PERFORMANCE: OPTIMIZATION STRATEGIES

Computational design workflow allows for validated simulations to be integrated into all phases of the design process [9]. The location of study was chosen in Timbuktu, Mali, a desert arid hot climate, which is characterized by direct solar radiation, little rainfall, and requires special façade considerations to minimize solar heat gain.

2.1 Preliminary Studies

For daylight analysis and physical experimentation, initial base surfaces were created by referencing the physical properties of the actively bent grid shell. First, the degree of curvature at the breaking point of wooden dowels was studied computationally and physically, showing that an acacia wood dowel with a radius of 9 mm, 15 mm, and 20 mm would achieve a maximum curvature equivalent to the following minimum radii of curvature: 415 mm, 679 mm, and 906 mm, respectively.

Daylight simulations have been conducted for the possible curvatures in all relevant orientations. Extreme conditions were identified and considered for further research. These curvatures were applied uniformly to a surface within a 400mm by 500mm rectangular frame, which served to explore the local geometry scale.

The soil composition developed for material experiments was created with consideration of the local earth texture in Timbuktu, Mali and the performance of the material. The dry mix consisted of 20% clay and 80% fine grained sand. Viscosity studies were conducted to achieve the optimum

water-soil ratio for an adequate material behavior calibrated for the nozzle geometry and extrusion. This was realized by incrementally altering each component of the mix starting from a near solid state, using a volumetric unit and visually assessed by sample extrusions. The extrusion process has been tested to ensure constant material flow, layer adherence and ability to maintain geometry under self-weight. The final composition of the material used in the physical experiments is a ratio of 1:4:2 corresponding to the levels of clay, sand and water, respectively.

2.2 Evaluation Methods

Derived from the innate characteristics of the material, two main criteria are considered for the evaluation of the earthen envelope's thermal performance:

Thermal lag

A relevant property of earthen materials when considering thermal performance is thermal mass. In hot arid environments, a consequence of this property is thermal lag, essential for ensuring indoor thermal comfort. Thermal lag is defined as the time delay necessary for thermal energy to reach the interior environment from the exterior environment [11]. The geometric variation of material distribution, within the envelope thickness, can alter this time delay by increasing the energy flow path, enhancing thermal performance.

Self-Shading

For assessing self-shading performance of toolpath geometry, a comparative study has been undertaken, taking into account solar radiation analysis results to minimize the amount of direct solar radiation that reaches the external layer, as well as daylight analysis to maximize the shading percentage, calculated considering the number of hours the analyzed area is shaded during peak solar window on 23 July in Timbuktu, Mali.

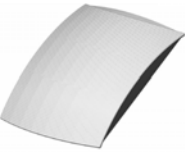
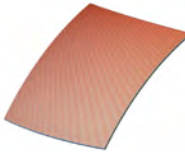
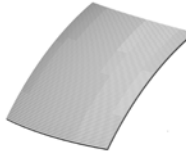
Geometry	Solar Radiation	Self-Shading
		
Material volume: 0,0024 m ³	Total solar radiation: 3,730 kWh/m ²	Shading Percentage: 17,19%

Table 1. Evaluation criteria for thermal performance: Base geometry analysis (Daylight analysis performed for peak solar window on 23 July in Timbuktu, Mali. The surfaces have a southern orientation).

The digital experiments have been done using validated simulation engines available through Ladybug Tools [8], an

environmental design software package for Computer-Aided Design (CAD). A flat continuous layer that follows the base surface is used for comparison (Table 1).

The shading percentage is calculated by subdividing the design output geometry and identifying the surface area units that receive a minimum 1 hour of direct sunlight during the chosen timeline of a specific day through daylight analysis. For each surface unit, a maximum of 12 hours of daylight is established as 0 % self-shading, meaning that during the time period, the surface unit does not receive shading. The total number of hours of received direct sunlight is summed and divided by the total maximum hours of potential direct sunlight to establish the value of self-shading percentage.

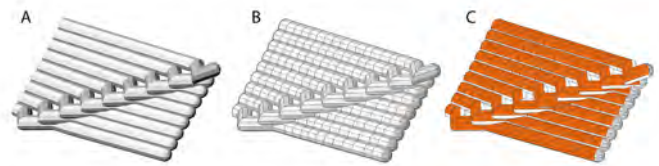


Figure 3. Subdividing and selecting relevant surface units for self-shading analysis.

2.3 Environmentally Informed Fabrication

Integrating environmental parameters directly into the toolpath development strategy allows for the creation of a mono-material thermally efficient envelope by manipulating the designed geometry.

3 INFORMED MATERIAL DEPOSITION

A way of achieving material deposition optimization is by controlling the parameters of the production setup. Investigations focus on the impact of pattern variation and material deposition distribution of the designed grid shell envelope on overall energy performance. The material deposition design process is briefly described as follows.

3.1 Adapting toolpath to existing formwork geometry

An initial parameter considered in the design process was the orientation of the extruder as the design method was strictly developed alongside the fabrication technique. Two possible orientations have been tested:

Orienting the tool head to the normal vector of the base surface (Figure 4-A) did not present conclusive result during experimentation. While extrusion could begin at any point on the surface, adhesion between layers as well as the base surface is not ensured.

A vertical orientation of the tool head (Figure 4-B), on the other hand ensures a continuous material flow. The adjacent layers present a strong bound and the extrusion follows closely the surface curvature. Due to its low failure rate, toolpaths were generated considering a vertical material deposition process.

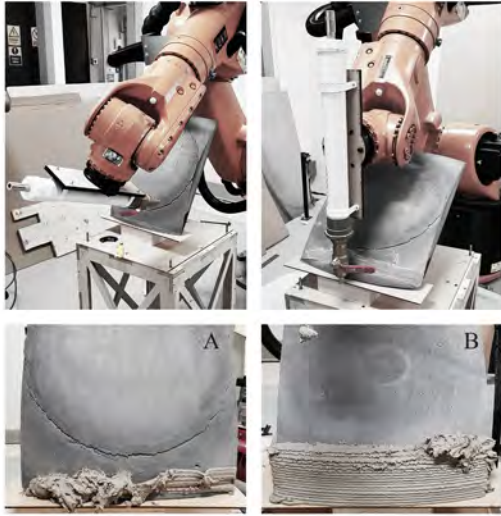


Figure 4. Experiments in effect the orientation of the extruder has on the overall performance of the material (A – Extruder oriented to the normal of the surface, B – Extruder oriented vertical)

Toolpath generation

Consistent soil extrusion requires a continuous and evenly spaced polyline to serve as the robotic-motion path. A subdivision strategy was created and applied to a surface which mimics the shape of actively bent grid shells used in the study. The resulting polyline was then altered, to create different patterns described in latter sections of the study, informed by the nozzle geometry.

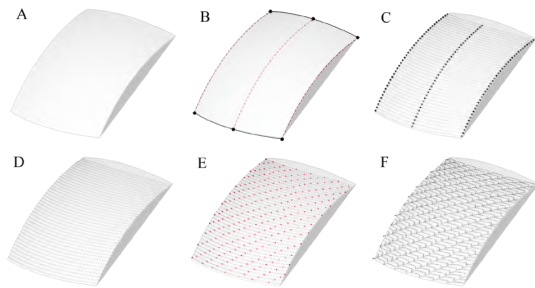


Figure 5. Robot motion path generation: Geometrical sequences of adapting the fabrication process to the existing geometry.

The base surfaces for thermal simulations and material tests (Figure 5-A) were created to have a uniform degree of curvature so that material irregularities would be unaffected by changes in surface curvature and would exhibit the extruded material behavior in relation to a doubly curved surface. Although elastica curves more accurately mimic the geometric properties of actively bent members, circular arcs provide the consistency needed to isolate the effects of toolpath variation and were therefore used in the duration of this study.

Toolpaths for the physical and numerical tests were generated from equally spaced latitudinal bands. To do this, the vertical edges of the surface were extracted and divided by equal lengths (Figure 5-B, C). Then, arcs were drawn

along the surface, connecting the ends of the equal length segments. Each arc was spaced at 64% of the diameter of the extrusion nozzle to ensure layer adherence. When connected, these arcs (Figure 5-D) created a single toolpath adjacent to the surface.

To create thermally efficient patterns on the surface, each arc was divided into equal length segments, and selected endpoints of the divided segments were moved away from the surface (Figure 5-E). A polyline was drawn from the endpoints to reconnect each latitudinal band, and individual bands were connected using the same method as the flat toolpath (Figure 5-F). The protrusions have been generated perpendicular to the extrusion orientation, to ensure layer adhesion and stability.

Proper control of the path overlap, coordinated with the rate of deposition and speed of the robotic arm movement, results in uniform cohesion of the earthen material into a homogenous part. Robots [12], a visual programming software plug-in, was used for simulating machine behavior during fabrication and translating designed toolpath geometry into a movement path program. This resulted in an initial fabrication-aware feedback loop in the design process before the actual implementation of physical experiments.

3.2 Layer geometric variation

Each layer is treated as a continuous surface that acts as an earthen shell across the existing grid shell formwork. By overlaying multiple layer geometries, a thermally performant envelope is achieved.

Pattern variation is realized by the differentiating protrusion values of tool path geometry that affects energy consumption through two factors: thermal mass and self-shading. Depending on its position within the envelope in relation to the formwork, two types of layer geometries are proposed:

Interior layers

Designed to increase thermal lag by geometrical design optimization, the interior layers enhance performance by incorporating air cavities in the envelope geometry. As a result, material usage is considerably decreased and as well as the fabrication time as it allows for a faster drying process due to increased air exposure. Air gaps have the potential to enhance the thermal insulation properties of the envelope as the thermal conduction properties of air are far lower than earthen materials [13].

Studies developed for ceramic bricks investigate optimal air gap geometry for insulation properties and thermal lag. Cavities are proven inefficient if their thickness is larger than 40mm as it allows for thermal convection to form. Taking this into account, a hollow absolute ratio of 51% has the potential to reduce indoor temperature with 7.18°C [1]. The research presented in this paper investigates the potential of vertical continuous and alternating toolpath variations for integrating air gaps in the structure of the envelope, thus increasing thermal lag. Adhesion capabilities and layer

structural stability are studied physically, while thermal properties are studied computationally.

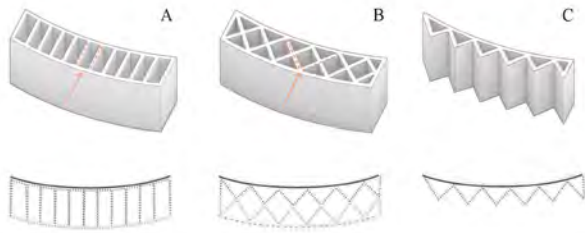


Figure 6. Geometrical variation of overlapped interior layers and resulting air cavities.

Exterior layers

Being in direct contact with solar radiation, the exterior layer geometry is solely optimized for an efficient distribution of radiation across its surface and enhancing self-shading.

Using simple geometric variations, the positions of the tool path protrusion and protrusion length is constricted to the limitations derived from the nozzle size and shape. Pattern variations of robotic motion path with 20mm and 40mm deviation from the base surface have been analyzed. The protrusion values are a result of physical extrusion tests to prevent potential errors and collapse during the fabrication process.

To ensure the geometric simplicity of the toolpath, linear variations are used to generate layer patterns. Vertical, alternating and angled linear protrusion variation have been generated and studied to identify their self-shading properties when distributed on a double curved base surface.

Vertical patterns, while showing mild improvements in self-shading, also significantly increase the total solar radiation amount that reaches the surface. Alternating patterns with 40 mm protrusions improve thermal performance, but the geometric accuracy during fabrication cannot be assured. Angled patterns produced the most desirable computational results, and the possibility of reorienting its tilt in relation to the base geometry increases its performative potential.

Daylighting simulations identify the 30° angled linear pattern with 40 mm protrusion as an optimal design solution considering self-shading and solar radiation exposure, exhibiting a 23,25% shading increase when compared to the base flat layer surface.

3.3 Layer sequencing

Developing each continuous layer as an independent element allows for the creation of complex envelope geometries by using simple continuous toolpath line variations. Overlaying continuous material layers can be sequenced to develop thermally performant earthen enveloped without the need of complex fabrication techniques or prefabricated moulds.

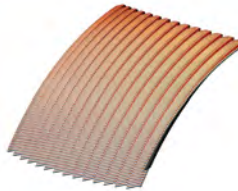
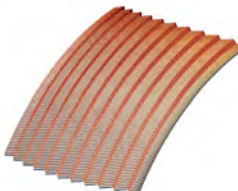


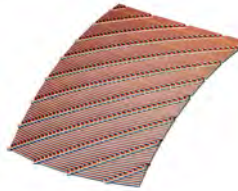

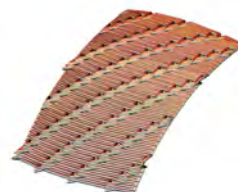
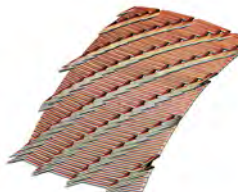
	20 mm Extrusion	40 mm Extrusion
Continuous Vertical Variation	 Total solar radiation: 4,162 kWh/m ² Shading percentage: 25,11%	 Total solar radiation: 3,556 kWh/m ² Shading percentage: 30,32%
Alternating Vertical Variation	 Total solar radiation: 3,86 kWh/m ² Shading percentage: 32,39%	 Total solar radiation: 2,97 kWh/m ² Shading percentage: 36,75%
60° Angled Variation	 Total solar radiation: 4,162 kWh/m ² Shading percentage: 25,11%	 Total solar radiation: 3,44 kWh/m ² Shading percentage: 38,54%
30° Angled Variation	 Total solar radiation: 3,078 kWh/m ² Shading percentage: 30,11%	 Total solar radiation: 2,867 kWh/m ² Shading percentage: 40,45%

Table 2. Thermal performance: comparative analysis of exterior layer geometry variation using solar exposure and daylight simulations (The size of the base surfaces is 400 mm by 500mm).

This method reduces the probability of collapse by allowing the incorporation of necessary material drying time after the deposition of each layer.

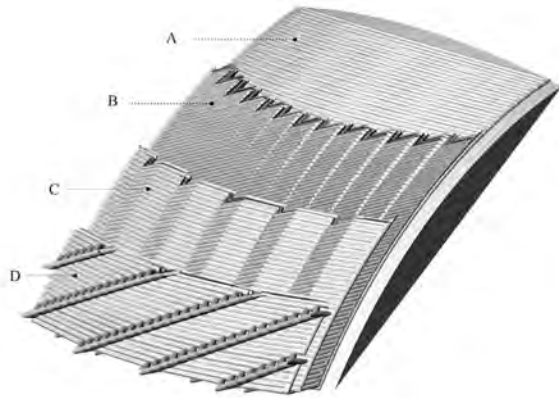


Figure 7. Layering sequence. Complex envelope geometry developed with simple overlaid toolpath geometries

The layer sequencing is described as following: An initial flat layer (Figure 7 -A) is extruded on the base surface to incorporate existing surface tolerances and improve surface adhesion. Subsequent vertical interior layers (Figure 7 – B, C) are overlaid to ensure the necessary thermal lag. The internal structure can be adapted to local environmental performance demands. The last layer is an external layer optimized for self-shading.

Using this technique, larger continuous envelopes can be achieved without the need of rationalization of geometry into bricks, as in hot arid environments the resultant geometry can be air-dried in an efficient manner. Physical experiments have been done to ensure the necessary adhesion between overlaid layers can be achieved.

4 ROBOTIC FABRICATION

The material deposition process during the experimentation phase is facilitated by a custom extrusion system (Figure 8) that is carried out by the robotic arm (KUKA R-60). As a method of material deposition, a pump mechanism powered by air pressure is used.

For material extrusion tests, the previously discussed 400x500 mm base surfaces have been CNC milled using grey foam and fixed to a wooden frame for accuracy.

4.1 Extrusion

The extrusion method employed for experimentation is using a custom in-house end-effector design. The extruder is assembled from off-the-shelf pressure graded supplies and an adapted 3D printed interchangeable nozzle. The extrusion process is powered by an air compressor. Preliminary experiments have been conducted for calibrating the level of air pressure according to the material composition and deposition speed. The extrusion generates an optimal material flow at air pressures that range between 1 to 1,5 bar. A continuous material intake would improve fabrication time.

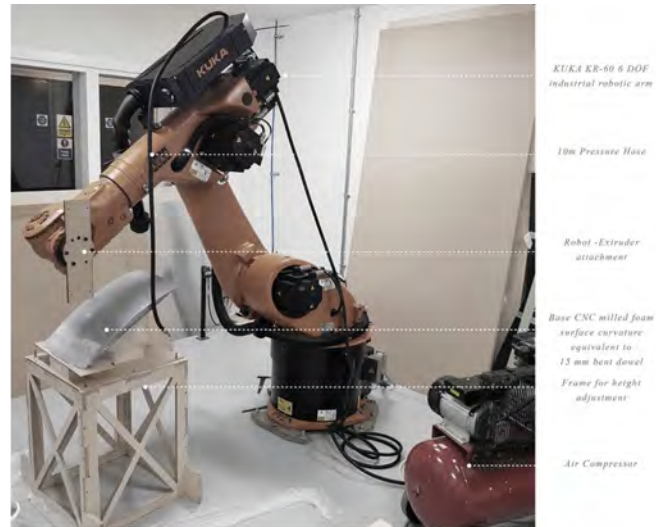


Figure 8. Robotic fabrication setup.

Nozzle geometries

Multiple nozzle geometries have been tested in order to enhance surface adhesion and reduce errors produced by natural material variations.

R= 5 mm	R=10mm	R=10mm	R=10mm
Round	Round	Textured	Textured

Table 3. Nozzle geometry

While textured nozzles presented improved layer adhesion, their precision is affected by the extrusion direction (Figure 9). Because the textured extrusion increases the exposed area, it performed poorly in initial solar analyses. Further experimentation is necessary for extracting conclusive results regarding the textured nozzle geometry.

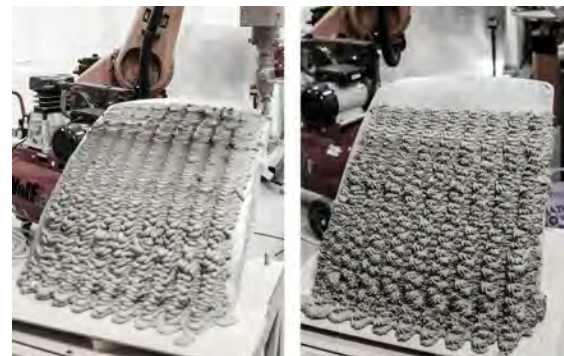


Figure 9. Vertical layer variation fabrication test. Round nozzle and textured nozzle comparison.

A 5mm radius round nozzle was predominantly used during experimentation as it could provide adequate precision while not substantially increasing fabrication time.

4.1 1:1 Prototypes

The robotic fabrication process was tested with the production of 1:1 scale prototypes of retrieved 400x500mm sections of envelope geometry. The physical tests aimed to identify further constraints that the fabrication process imposes on the design method. Initial experiments use a CNC milled foam base that replicates the curvature and geometry of the proposed grid-shell. Later experiments use acacia and fiber formwork to incorporate tolerances involving precision and surface adhesion into the design process.

Interior layer fabrication

Due to natural material inconsistency, small variations in material flow determine protrusions smaller than 20mm not to incorporate enough tolerance for accommodating minor fabrication errors, resulting in irrelevant air gap geometries. Protrusions of 40 mm represent a balanced solution.

Air cavities incorporated in the interior layers also improve drying time significantly. Access to air and increased surface area reduces the time necessary for the material to solidify, but in the same time work against thermal responsiveness if positioned as an exterior layer.

Self-shading patterns

Physical experiments revealed that double curvature surfaces prevent slumping of material, meaning the global geometry reduces the need for surface adhesion concerns. Fabrication precision is essential when considering self-shading patterns as additional sun-exposed surfaces decrease thermal performance. Angled pattern variations over 45° have proven to be more sensible to extrusion errors. Considering thermal performance and fabrication experiment feedback, a 30° angled pattern presents an optimal behaviour. Consistent air pressure and material mixture is necessary for extruding forms in a predictable way.

Base surfaces fabricated from locally sourced materials, acacia and fibre formwork, were tested for robot-aided extrusion and presented an increased surface adhesion output. Minor geometrical inaccuracies of the base surface did not affect substantially the designed toolpath geometry. Testing the sequence of overlaying different layer geometries determined significant observations to be incorporated into the fabrication process.

Improved layer adhesion is seen when the humidity of the initial layer is under 70%. Incorporating sufficient drying time into the fabrication process allows for a better performance of the geometry under the weight of the new layer.

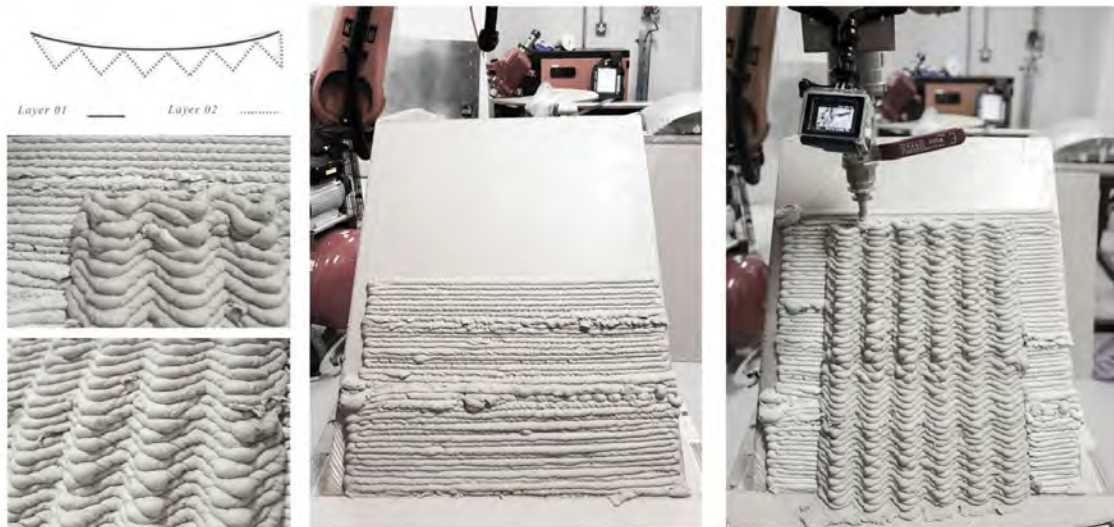


Figure 10. Material deposition layering sequence. Determining layer interaction during fabrication process.

5 CONCLUSION AND DISCUSSION

This paper presents a fabrication-aware earthen envelope design method and robot-aided fabrication strategy driven by thermal performance. The topic has implications for many nomadic pastoralism peoples in desert territories that are undergoing rapid social and climatic change. The strategy to develop a material system for robotic construction from local resources has significant potential for employing earth

structures in developing countries. The incorporation of environmental parameters as design drivers into the fabrication process by using robotically-aided informed material deposition allows the creation of a thermally performant mono-material envelope developed from locally available resources. By geometrically altering the envelope structure and introducing air gaps within the designed geometry, an enhanced environmental performance can be

achieved with significant fabrication time and material reduction. Further explorations of pattern variation in relation to seasonal variation, building orientation and sun angles can be integrated into a feedback loop to create an optimized pattern gradation.

While the physical experimentation and prototyping has been carried out with an industrial robot, the proposed fabrication system does not necessitate industrial robots for the construction scenario. It is important to note that as technology becomes more available to the general public, in recent years more accessible devices and interfaces are constantly being developed in the field of robotics. Examples of the democratization of robotics can be seen on Reprap or Instructables projects.

The physical fabrication experiments conducted with an extruder attached to an industrial robot and powered by an air compressor has revealed some useful insights on the types of equipment that would be necessary to carry out the work on site. Firstly, it is observed that a continuous material supply incorporated into the extrusion process would provide increased time-efficiency during material deposition and would eliminate the probability of errors that occur from pausing and restarting the process. Hence, a material container that is directly connected to the nozzle would be ideal. It has been detected that the 6 DOF the industrial robot provides are not needed in this specific toolpath generation study, and therefore a simplified robotic tool is proposed to induce the types of various movements necessary for robotic earth 3d-printing.

Therefore, this research aims to propose the incorporation of robotic fabrication into the construction process as a scenario that can be easily implemented in remote areas of Africa, providing opportunities for the self-sustainability of nomadic communities. While the proposed context and scenario provided essential insight for the research process, the resulted method has the potential for a wider applicability.

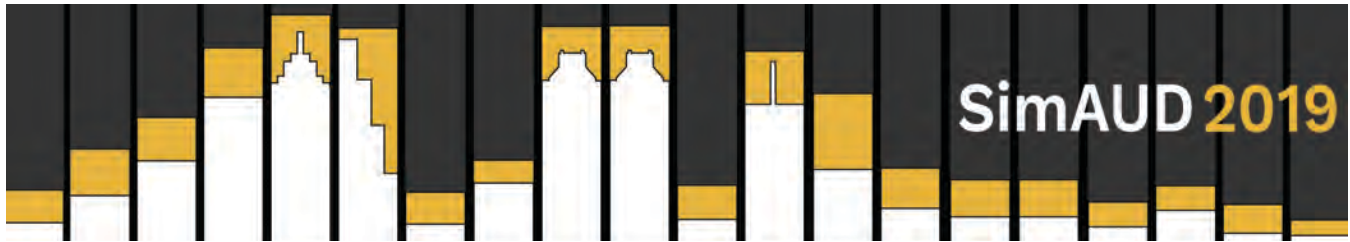
ACKNOWLEDGMENTS

We gratefully thank Dr. Michael Weinstock for his guidance during this process, as well as Angel Lara Moreira and Alvaro Lopez for their support during the fabrication process.

REFERENCES

1. Al-Tamimi, A.S., Al-Osta, M.A., Al-Amoudi, O.S.B. and Ben-Mansour, R., 2017, *Effect of Geometry of Holes on Heat Transfer of Concrete Masonry Bricks Using Numerical Analysis*. Arabian Journal for Science and Engineering, 42(9), pp.3733-3749.

2. Bard, Joshua, et al. *Thermally Informed Robotic Topologies: Profile-3D-Printing for the Robotic Construction of Concrete Panels, Thermally Tuned Through High Resolution Surface Geometry*. Robotic Fabrication in Architecture, Art and Design. Springer, Cham, 2018.
3. Big Delta, <https://www.3dwaspp.com/en/giant-3d-printer-bigdelta-wasp-12mt/>, Accessed 10 January 2019
4. Dubor, A., Cabay, E., & Chronis, A.: *Energy Efficient Design for 3D Printed Earth Architecture*. In Humanizing Digital Reality (pp. 383-393). Springer, Singapore, 2018
5. Dubor, A., IZARD JB., Cabay, E., Sollazzo, A., Markopoulou, A., Rodriguez, M., *On-Site Robotics for Sustainable Construction*. In: Willmann J., Block et al (ed) Robotic Fabrication in Architecture, Art and Design 2018. ROBARCH 2018. Springer, Cham
6. Dunn, K., O'Connor, D.W., Niemelä, M., Ulacco, G.: *Free form clay deposition in custom generated mold*. In: Reinhardt, D., Saunders, R., Burry, J. (eds.) Robotic Fabrication Architecture, Art and Design 2016, pp. 317–326. Springer International Publishing, Switzerland (2016)
7. Khaled T., Abdelmohsen S, Hassan A, El-Dabaa R, and Elghazi Y. "Parametric Investigation of Brick Extrusion Patterns Using Thermal Simulation.", Proceedings of BSO 2018: 4th Building Simulation and Optimization Conference, Cambridge, UK, September 2018
8. Ladybug Tools, <https://www.ladybug.tools>, Accessed 20 January 2019
9. Mostafavi, S., Bier, H., Bodea, S. and Anton, A.M., 2015. *Informed Design to Robotic Production Systems; Developing Robotic 3D Printing System for Informed Material Deposition*, Proceedings of the 33rd eCAADe Conference. Vol. 2., 2015.
10. Prussin, L., *African Nomadic Architecture: Space, Place and Gender*, Smithsonian Books, 1997
11. Rael, R., *Earth Architecture*. New York, New York: Princeton Architectural Press, 2009
12. Robots, <https://github.com/visose/Robots> Accessed 20 January 2019
13. Terraperforma: 3D Printed Performative Wall. <https://iaac.net/research-projects/large-scale-3d-printing/terraperforma> - As of: 01 November 2018
14. Wu, P., Wang, J. and Wang, X., 2016. *A critical review of the use of 3-D printing in the construction industry*, In: Automation in Construction, 68, pp.21-31.



Curved-Crease Folding and Robotic Incremental Sheet Forming in Design and Fabrication

Elif Erdine, Antiopi Koronaki, Alican Sungur, Angel Fernando Lara Moreira, Alvaro Lopez

Rodriguez, George Jeronimidis and Michael Weinstock

Architectural Association (AA) School of Architecture
London, United Kingdom

{elif.erdine, antiopi.koronaki, alican.sungur, lara-moreira, lopez-rodriguez,
mweinstock}@aaschool.ac.uk
g.jeronimidis@reading.ac.uk

ABSTRACT

The research presented in this paper addresses the themes of generative design, material computation, large-scale fabrication and assembly technologies by incorporating two research fields, Curved Folding and Robotically Aided Single Point Incremental Sheet Forming (RA-SPIF) of sheet metal panels. The design and construction of a large-scale prototype made of complex panels of sheet metal serves as the case study for the proposed methodology. Global geometry panelisation is implemented through a multiple-criteria Evolutionary Algorithm to establish an equal subdivision approximation of the initial geometry. The mathematical principles of Curved Folding are applied on the resulting mesh geometry. Iterative FEA of the component assembly defines areas where Incremental Sheet Forming needs to be applied to the curved folded components. Selected panels are formed with RA-SPIF to enhance the structure's performance for wind loading. The primary contribution of the research is the demonstration of a methodology that integrates the precise computation of curved folded geometries and the employment of FEA as a design driver for the application of incremental sheet forming towards the geometrical and material stiffening of sheet material.

Author Keywords

Robotic fabrication; Robotically Aided Single Point Incremental Forming (RA-SPIF); Curved-folding; Linear and Non-linear FEA; Evolutionary Algorithm; Computational form-finding; Fabrication workflow.

ACM Classification Keywords

I.3.5 Computational Geometry and Object Modeling (Physically based modeling); J.2 Physical Sciences and Engineering (Physics); J.5 Arts and Humanities (Architecture); J.6 Computer-aided design; J.6 Computer-aided manufacturing (CAM).

1 INTRODUCTION

The research presented in this paper outlines an innovative strategy that incorporates Curved Folding and Robotically Aided Single Point Incremental Sheet Forming (RA-SPIF) to design and fabricate doubly-curved complex geometries for large-scale architectural artefacts. One of the major considerations of the research is the enhancement of the local stiffness of a sheet panel at the local scale, while improving the overall rigidity of the structure using curved-folding and RA-SPIF within carefully selected panel locations as a result of iterative Finite Element Analysis (FEA) processes.

Curved folding is a highly efficient fabrication method for the manufacturing of curved surfaces from flat sheet material without stretching, tearing, or cutting, demonstrating a novel way of producing lightweight and stiff components. The lack of appropriate computational tools in CAD software and algorithmic packages for the accurate application of curved-folding to a complex geometry presents itself as a design opportunity. The existing methods for describing such geometries includes the definition of curved-folded tessellations as a geometrical approximation [3], scanning of physical models and planar quad-meshing [8], sequential generation of curved-folded surfaces with the method of reflection [9]. These individual methods do not answer the problem of defining precise curved-folded geometries as building blocks on a complex doubly-curved geometry. The possibility to apply curved-folded components on various structural configurations has the potential to yield materially efficient large-scale architectural artefacts. Parameters including the curvature of the curved crease, folding depth, component size, joint detailing, and material specific attributes have the capacity to increase the structural performance of a component as well as an aggregation of components.

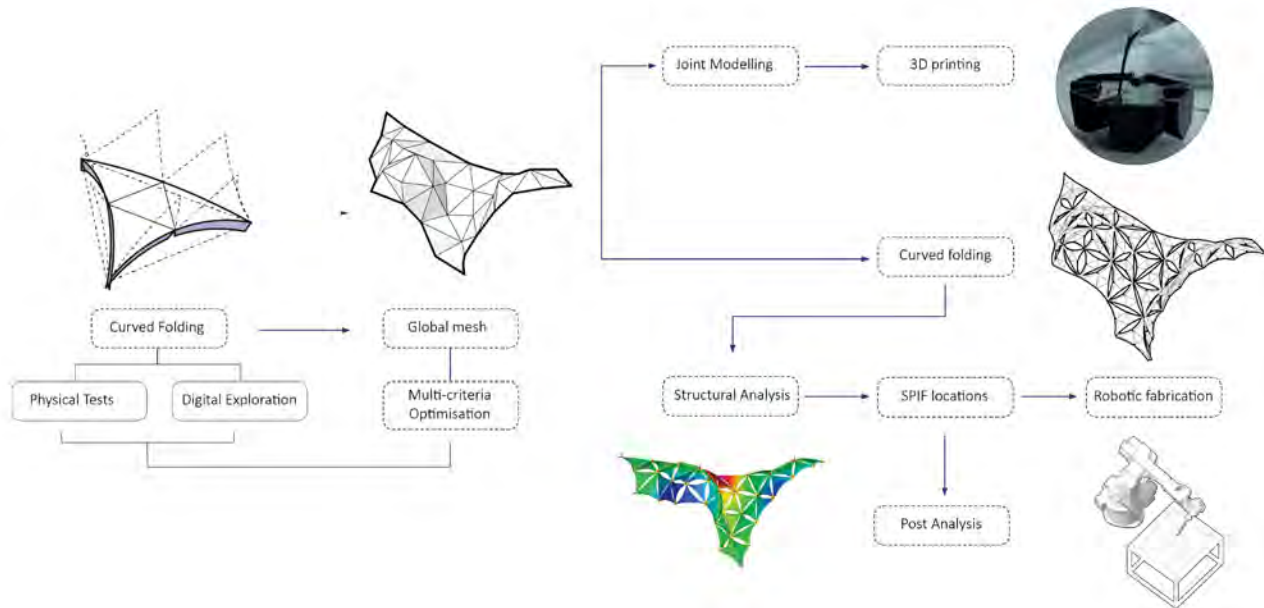


Figure 1. Overall workflow sequence demonstrating the interdependencies between multiple scales.

Traditional sheet forming techniques employ incremental deformations to a sheet until it is formed into its final shape [4], and the forming tool can be attached to a CNC machine or a robotic arm. Robotic incremental sheet forming opens new opportunities in the design and fabrication of component-based aggregations that can be facilitated for cladding purposes or spatial enclosures. The versatility, multi-axis freedom, precision, and adaptable programmability of a generic robotic arm introduces new approaches and techniques to the metal sheet forming process [5]. By the careful correlation of form-finding techniques, multi-criteria optimization, and iterative structural analysis (FEA), curved folding and robotically assisted metal sheet forming can contribute to the structural performance of architectural configurations.

The primary contribution of the research is the demonstration of a methodology that integrates the precise computation of curved folded geometries and the employment of finite element analysis (FEA) as a design driver for the application of incremental sheet forming towards the geometrical and material stiffening of sheet material.

The one-to-one scale prototype presented in this paper is a case study to test the proposed methodology with the design and construction of a complex doubly-curved geometry from sheet metal panels that are curved folded and incrementally formed with the use of an industrial robot. The dimensions of the structure are 2,700 mm. width, 4,330 mm. length, and 2,520 mm. height. The location of the case study is the outdoor area of the Architectural Association (AA) School of Architecture.

2 COMPUTATIONAL METHODOLOGY

2.1 Initial Material Experimentation and Computational Form-finding

The computational methodology developed for the research simultaneously incorporates material and algorithmic experimentation on a panel scale and global geometry scale (Figure 1). Initial studies have focused on the material behavior of aluminum, copper, and zinc sheets subjected to RA-SPIF process. Zinc has been chosen for its combination of stiffness, ductility and corrosion resistance.

The initial decision on material selection has been followed by component scale experimentation on curved folding. A range of curved folding patterns have been generated and applied to zinc sheets via scoring to observe the maximum depth that could be achieved for a panel with the size of 800 mm. width, 800 mm. length, and 0.8 mm. thickness. The geometrical shape of the flat components has varied between triangular and quadrangular forms. These material experiments have revealed three key outcomes. Firstly, as the scoring of the material was carried out with a CNC machine, it was concluded that it would be more efficient and time-saving to score the mountain and valley folds from one side of the material instead of alternating sides. This process saves up almost twice as much time than scoring mountain and valley folds on opposite sides of the sheet material, as it eliminates the necessity to alternate the sides during scoring process. After running several tests on scoring depths, it was observed that 25% material removal would be appropriate for mountain folds to ensure that the sheet did not break, and that 50% material removal would be appropriate for valley folds to make sure that the fold would take the desired form. Secondly, it was detected that the sheet could be bent comfortably to achieve a structural

depth on a range between 40 mm. and 80 mm., and that the sheet itself started to deform for a structural depth higher than 80 mm. Finally, it was discovered that as the shape of the components was varied from regular triangular or quadrangular forms to irregular ones, the folded sheet displayed deformations. Hence, it was determined that a regular flat sheet panel form made of equilateral triangles or squares would be ideal to achieve the desired structural depth.

Simultaneously, computational experimentation on the local sheet scale have been carried out to cross-examine various curved-folding methods with the objective of inferring which method would be most appropriate. Initial experimentation was carried out with Kangaroo, the live physics engine for interactive simulation, optimization and form-finding in Grasshopper [7]. Kangaroo is a powerful tool for simulating physics behavior via mesh discretization; however, the discretization process means that the final curved-folded geometry is an approximation and therefore can lead to tolerance differences during the fabrication and assembly of the sheet elements. For this reason, the mathematical definition of curved-folding via the mirror reflection method has been adopted, as this method allows for the analytical generation of curved-folding as long as the folds are planar [12]. This method posits that a form generated by applying mirror reflection to part of a developable surface is also a developable surface. Hence, the computational workflow applies the plane reflection method on ruled surfaces with planar curves to accurately calculate curved-crease folds (Figure 2). The application of this method comprises the generation of planar arcs with an assigned depth on a triangular surface, the creation of ruled surfaces from these edge curves, the creation of reflection reference surfaces by using the arc planes as mirror planes, the extension of the reflection surfaces to create two flaps per edge, and finally closing the gaps between the two flaps by adding a planar triangular surface. This method enables the generation of a single flap along each edge with G1 continuity, and it can also be used for quadrangular surfaces.

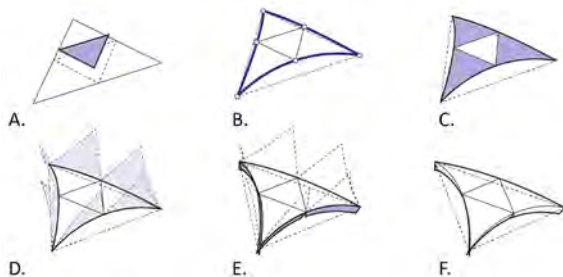


Figure 2. A. Divide each triangular panel into 4 parts and move the central subdivision in normal direction, B. Draw planar arcs, C. Create ruled surfaces from edge curves, D. Create reflection reference surfaces, E. Extend reflection surfaces to create flaps, F. Create closed flaps by adding mid-point triangles.

2.2 Application of Evolutionary Algorithm for Global Mesh Geometry

As one of the key considerations of the research has been the application of curved-folded components on various structural configurations, the objective has been to utilize the curved-crease folding algorithm based on mirror reflection method on doubly-curved complex surfaces.

During the design process of the global doubly-curved surface, attention was kept reducing the loads on the flooring as the construction area is part of a listed building, and two existing posts of 2,350 mm. were utilized to transfer the loads of the structure to the primary structural system without traversing the flooring directly. Hence, the global geometry is defined as a doubly-curved surface that is supported by the existing columns, railings, and meets the flooring on a minimal surface area. This surface has been initially converted into a triangular mesh in Grasshopper. The observations gained from physical experiments on the local component scale have suggested that the global form needs to be formed by an approximation of equilateral triangles (Section 2.1). Hence, a multi-criteria optimization process based on Evolutionary Algorithms (EA) has been developed in Octopus, Grasshopper's add-on for applying evolutionary principles to parametric design [10]. The fitness criteria are:

- Maximum edge length of a triangle edge must be less than 700 mm. This length is selected to ensure that an appropriate distance is kept between the component and the edge of a zinc panel (800 mm.) in order to allow for fabrication-related tolerances such as tool clamping and frame-work to hold the panels in place.
- The edges of each triangle should not be shorter than 500 mm. and longer than 700 mm. This fitness objective is introduced as a distinct one from the first one, as it allows to analyze the consecutive edge lengths of each triangle. It also ensures that the edge lengths do not exceed the prescribed domain of 500 – 700 mm. in order to eliminate the possibility of generating small-sized components.
- The angle between each consecutive edge should not be less than 45 degrees. This objective is selected to diverge from isosceles triangles in the candidate forms.

The Octopus simulation has been run for 1,222 generations, with 200 individuals in each generation. Convergence of results has been achieved after 1,000 generations (Figure 3). The selected global form is made up of an approximation of equilateral triangles, affirming that the curved-crease folding algorithm can be applied on individual triangles.

The information gained from physical experiments (Section 2.1) has demonstrated that for the defined panel size and thickness, a structural depth ranging between 40 mm. – 80 mm. can be achieved for each component. This information has then been employed in the curved-crease folding algorithm, whereby each triangular panel is given the

assigned structural depth through the variation of the curved-folding degree (Figure 4).

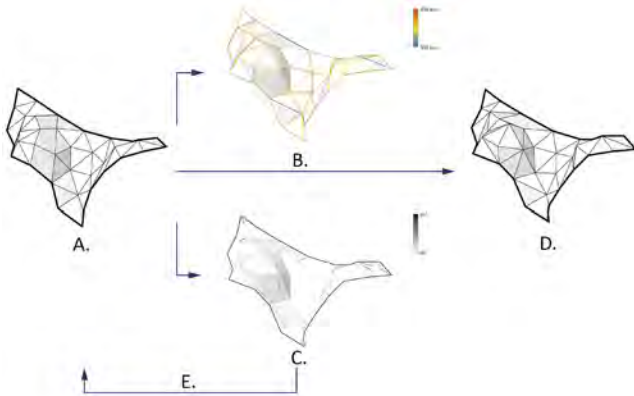


Figure 3. Octopus simulation diagram: A. Design model, B. Panel size evaluation, C. Connection angle analysis, D. Assembly mesh, E. Feedback (multi-criteria optimization)

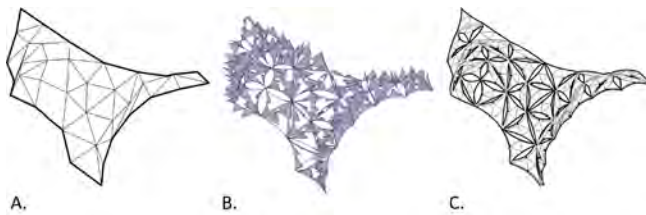


Figure 4. Application of curved folding on the global geometry – A. Global geometry base mesh from EA, B. Curved folding mirror planes, C. Curved folded panels.

2.3 FEA and the Application of SPIF on Selected Panels

FEA analyses have been carried out using Strand 7 software [11]. The structural stiffness of SPIF and NO-SPIF single panels that have been curved folded has been evaluated first. The digital information has been used to create a model where a SPIF and a NO-SPIF panel are compared for stiffness under self-weight and self-weight + wind load. Plate elements have been used for the curved-folded panels. Typical properties of the zinc material are: Young’s modulus between 90 and 110 GPa, density of 7140 kgm⁻³ and yield stress between 75 and 110 MPa [2]. The Strand7 analysis uses a Young’s modulus of 108 GPa and a yield stress of 100 MPa (a soft zinc alloy was chosen given that it can be folded after scoring). In the FEA model (Figure 5) panels are oriented with gravity and global pressure due to wind (135 Pa, equivalent to a wind speed of 15m/s [13]) acting in the negative Z direction. The three corners of the folded, curved triangular panels are in the XY plane. Two boundary conditions have been simulated: corners fixed in all three directions (Fixed) and corners fixed only in the Z direction (Simply-supported, SS). The maximum deflection in the Z direction, in mm., is a measure of the stiffness of the panel (Figure 5). Under the combination of self-weight and global pressure, the NO-SPIF panel deflects by 0.245

mm with Fixed boundary conditions, and by 0.475 mm with SS boundary conditions. The SPIF panel deflects by 0.101 mm (Fixed) and by 0.276mm (SS). This result shows that the SPIF panel is intrinsically significantly stiffer than a NO-SPIF panel and justifies the application of SPIF in the design of the prototype.

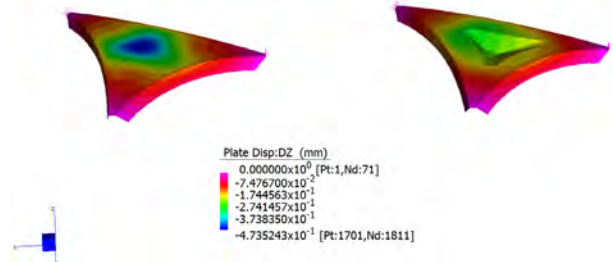


Figure 5. Vertical displacement of SPIF (left) and NO-SPIF (right) panels under self-weight and wind pressure load (Simply-supported boundary conditions)

The effect of scoring the panels for folding, i.e. to assess whether the local thinning of the zinc sheet needed for scoring has a significant effect on the stiffness of the panel, the NO-SPIF single panel model has been modified by introducing a set of thin plates (1.5 mm wide, on average) along the two sides of each folded curved edge. The thickness of these plates has been set at 0.6 mm, simulating score 0.2 mm deep (this is actually a worse case than the real fold which is only about 1mm wide). The result of the FEA analysis shows that the decrease in global stiffness with scoring is of the order of 5% which can be considered negligible.

Modelling each individual joint is time consuming and quite heavy computationally because their complex geometry requires fine meshes using solid tetrahedral elements (Figure 10). In order to verify that the joints can be simulated using rigid links/springs two models have been set up. One of them has a fully modelled joint connecting six panels (Figure 6, right), the six panels being “glued” to the joint. Simply-supported boundary conditions have been applied to the free corners of the panels. In the second model (Figure 6, left), the end of each panel attached to the joint has been closed, to simulate the connection to the real joint, and rigid links (yellow lines) have been used to connect the ends of the units to a point (yellow ball) which simulates the geometrical center of the real joint and carries the mass of real joint. This comparison has been done to simplify the FEA of the whole installation. The load acting on the model is the self-weight of the panels and the mass of the specific joint chosen (0.5kg). The joint is made of thermoplastic polymer, ABS, with typical properties of 1.2 GPa for the elastic modulus and 1100 kg/m³ for the density.

The maximum vertical displacement of the model with the real joint is -0.347 and that of the rigid links simulating the joint is -0.325 mm. The two displacements are very close,

differing only by 7%, and Figure 6 shows that the displacement fields of the two models are virtually identical. This suggests that joints can be simulated using rigid links and point masses equivalent to the mass of the real joints. Using this approach simplifies considerably the FEA of the analysis of the installation.

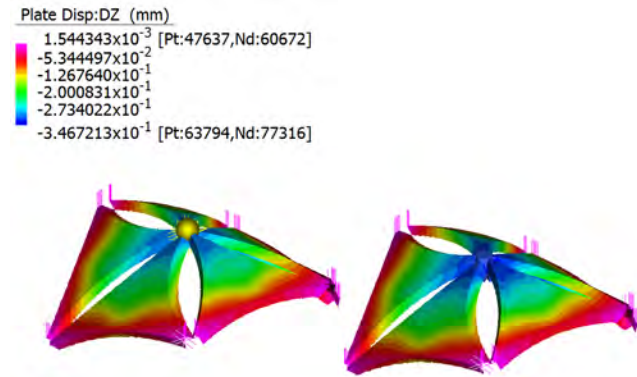


Figure 6. Vertical displacement of NO-SPIF panels with rigid links to simulate the joint (left) and with the real joint (right) under self-weight (Simply-supported boundary conditions)

Therefore, in the FEA model of the global structure the joints have been simulated using rigid links and non-structural point masses (Figure 7). This model combines SPIF and NO-SPIF panels that are all curved folded. From direct measurements carried out, a typical joint weighs an average 0.5 kg and this value was used for each joint. The wind load acting on the plates is simulated as the normal component to the plate surfaces of the global pressure acting in the X direction (inward normal to the plane of Figure 7). This direction was chosen since it represents a worst-case condition. A detailed CFD analysis can provide the actual pressure acting on each curved plate, as opposed to the average value of 135 Pa used here. Figure 7 shows the vertical displacement (global Z axis) under self-weight and rigid links to connect the plates. The maximum predicted displacement is -6.1 mm downwards (blue region). When the wind load is added (Figure 8), the maximum vertical displacement in the blue region increases to -21.9 mm.



Figure 7. Vertical displacement of structure under self-weight.

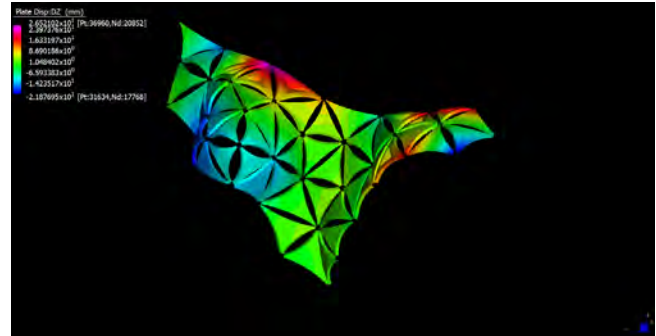


Figure 8. Vertical displacement of structure under self-weight and wind load.

In both cases the displacements are relatively small, suggesting that the structure does develop the necessary structural stiffness to be self-supporting and to resist wind loads. In this analysis above, the curved panels are joined by rigid links and this overestimates the stiffness of the system. It has been shown earlier that the rigid links overestimate the structural stiffness by 7%. This result suggests that predicted maximum deflection under the given load (self-weight + wind pressure) for the structure with ABS joints will increase to around 12mm, an acceptable value.

3 ROBOTIC TOOL PATH AND JOINT DEVELOPMENT

3.1 Robotic Tool Path Development

The proposed methodology requires the material to undergo two distinct treatments, engraving the curved creases, which is applied on all components, and RA-SPIF, applied only on certain components. Moreover, the size of zinc sheets available was 800 mm. by 800 mm., allowing for the fabrication of multiple components on a single sheet. It is therefore evident that defining the fabrication sequence and the equipment setup for each of these processes was an essential part of the fabrication.

The first step of the process included the engraving of the curved creases of all components. The fabrication files were generated by unrolling the global geometry and placing the components on the material sheets. During this process the zinc sheets were fixed along the boundaries on a custom created bed to minimize the spring back effect and maintain the material in place. The following step was the application of the RA-SPIF. The low Young's modulus of the zinc sheets (108 GPa) presented a considerable challenge due to the risk of local sheet deformation, tearing and spring-back. Different tests took place to study the parameters affecting this behavior, such as the sequence of forming, tooling, spring-back, sheet deformation, heat and friction.

To protect the material from tearing along the curved creases during the robotic forming, a temporary frame was placed along them on both sides of the zinc sheet. The geometry of the formed part was taken as an offset of the

component's creases, to make maximum use of its surface area, while its size was dictated by the boundaries of the temporary frame.

Different materials and shapes were tested for the forming tool, as they are directly linked to the manufacturing process and geometrical output. Stainless steel 316 was chosen for the tool-head, due to its higher degree of hardness (2,200 MPa) and stiffness (205 GPa) compared to the zinc sheet material. As the size and shape of the tool likewise influences the speed of manufacture and toolpath generation, a custom-made tool with a rounded nose of approximately 4mm was fashioned from a rod of 12mm, resulting in a very stiff tool with a very low deformation and high resistance to scratches. The tool was then installed in a milling spindle attached to a 6 axis KUKA KR60 robotic arm.

From a hardware perspective, three different tool configurations were tested to determine the ideal forming process: fixed tool, free rotation and controlled spinning. Heat and friction posed a challenge as they led to the tool piercing the metal sheet. A series of tests determined controlled spinning at 2,000 rpms and the addition of a lubricant agent seemed to have a positive effect, as it also decreased the initial bounce action of the material. In addition, a robust mild steel frame of 800 x 800 x 700 mm. was created to hold the sheets in the XY planes while freeing the Z direction during the forming process.

Tool path generation considered the dimensions, spinning speed and strength of the custom-made tool, sheet material thickness, stiffness and the desired output geometry. The selected approach consisted of spiralling the target surface in increments of 3-5mm, adapting the stepdown between lines according to the depth (1 to 3mm) and the tangent angle of the final geometry (Figure 9). The need to use the tool perpendicularly to the sheet material to avoid punctures and have a steady path necessitated the use of Linear (LIN) movement for the robot, its only drawback being the decrease of the working area to avoid collisions due to tool size limitations. In extreme cases where the geometry proved out of reach of the robotic arm due to tooling considerations, the toolpath was further expanded to create a normal vector for tool orientation that was assisted by the robots 7th axis, in this case a rotary table.

Overall, the flexibility and control over the forming method allowed to tender to the different geometries explored in the research in terms of curvature angles, steepness and local position, suggesting that this technique can be applied with other forming tools, metals and different materials thicknesses to generate an optimized toolpath for RA-SPIF.

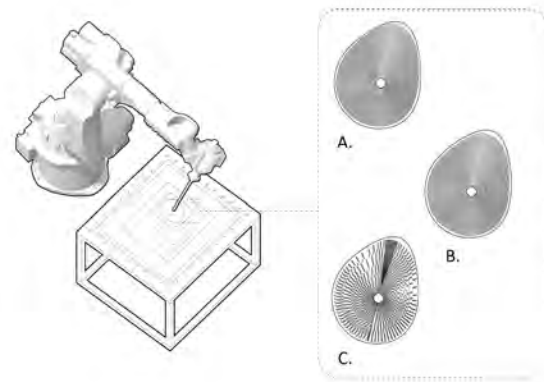


Figure 9. Tool path generation – A. Topographic curves, B. Spiral with constant surface offset, C. Robotic tool path.

3.2 Joint Design & Development

Joints have played a crucial factor in the fabrication and assembly process of the structure. The challenge in their design lied in accommodating the geometrical complexity of the design surface and at the same time ensuring structural integrity and continuity between the different components.

The structure comprises of 37 joints in total, with unique geometrical characteristics. The design of the joints includes a central cylindrical node with protruding legs, whose number and relative position was dictated by the geometrical characteristics of the components connected at the joint. The size of the legs was prescribed by the need to accommodate bolts and screws along their edges for assembly. Given the high degree of variance between the elements, the level of accuracy required and their scale, methods of rapid prototyping were studied for their fabrication, with a focus on 3D printing [14].

Sample joints were printed on a 1:1 scale to evaluate the efficiency of this fabrication method. The high level of accuracy allowed for the joint to represent the geometrical complexity of the design and to accommodate the connecting components. However, the time associated with the production of each joint rendered this approach impractical. A composite joint type was hence developed, which consisted on a 3D printed mold, in which epoxy resin was cast. The efficiency of this joint type lies in the fact that the time-expensive method of 3D printing was applied only at specific areas of the design, which required a high level of geometrical accuracy. On the contrary, the time-efficient method of casting, ensured continuity and structural integrity, thus leading to a drastic decrease of the production time (Figure 10).

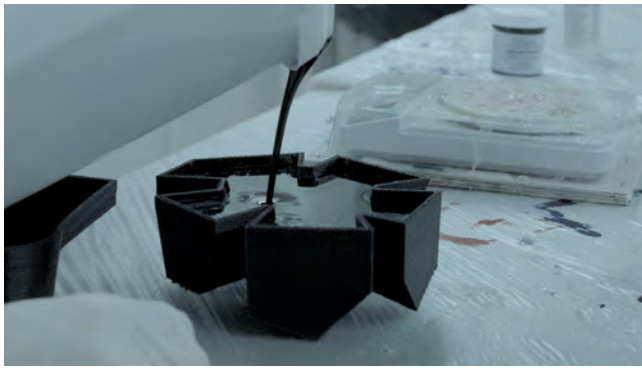


Figure 10. Joint detail: Epoxy resin casting inside 3d-printed mold.

The appropriateness of the joint fabrication process is directly linked to the scale and degree of variance of the specific structure. Despite the advantages of 3D printing regarding accuracy and customization, this fabrication process is currently restricted to the capacity of the 3D printing hardware. Moreover, bespoke certification of the end products' material properties is often required, as their long-term performance is suspect to fatigue and wear [6]. An application of the proposed methodology on a long-term or large-scale project may therefore require a revisiting of the joints' fabrication process.

4 POST ANALYSIS

Post-analysis of the installation was carried out to evaluate the efficiency of the proposed methodology. Using the Autodesk ReCap software [1], a photogrammetric model of the physical model was generated by the collision of a series of pictures of the installation taken. Overlaying the two models (Figure 11) highlighted a small discrepancy between them. This can be attributed to the random loading patterns applied to the structure during the manual assembly process, its self-weight as well as random loading imposed by the environment. More precisely, the critical role of joints in the structure's load-path and its overall structural performance led to their plastic deformation and in effect to the discrepancy between the physical and digital model. The effect of these factors overcame any spring-back effect that occurred at a component level.

Future applications of the proposed fabrication process can address this issue both at the local level of the joints, as well as at a global scale. At a local level, a stiffer joint design could be achieved by increasing the contact area between the components and the joints. At the current design proposal, each component edge is mechanically connected to the joint via bolts at three points. Gluing the components to the joint or creating a closed tube, where the joint could be inserted, would automatically increase the surface area between them and create a stiffer, chemical connection. At the global level, on the other hand, the stability of the structure could be enhanced using temporary scaffolding. Stabilizing the relative position of the components and joints would render the structure resistant

to the uncertain loading patterns associated with a manual assembly process.



Figure 11. Post analysis carried out in Autodesk Recap.

5 DISCUSSION

The driving ambition of this research project was to integrate precise computation of curved folded geometries with finite element analysis (FEA) as a design driver for a fabrication procedure that stiffened sheet material by incrementally deforming it to geometrically defined parameters (Figure 12).

There is a challenge that arises in all complex three-dimensional assemblies of components, and that is the degree of spatial precision that needs to be achieved in physical dimensions. What is perfectly feasible to achieve in a computer is very often not nearly so easy when it comes to physical assemblies. The cause for the difference between computational and physical assemblies is the accumulation of small dimensional errors and tolerances, some of which are due to the buildup of stresses and subsequent deformations that occur as more and more components are linked to each other. Component assemblies tend not to be fully rigid or self-supporting until all the components are in place, and so small dimensional changes are induced as assembly proceeds and accumulate as larger deformations. This limitation will be addressed in future research by investigating methods of achieving a stiffer component to component joinery system by investigating the use of glass-fiber fabrics with a resin matrix for the joint system, which has the potential to achieve higher stiffness, as well as altering the geometry to gain larger contact surface area with the formed metal components. Further experimentation will be made with RA-SPIF on the surfaces of metal panels of varying sizes, and the stiffening effect on clusters and assemblies of

differing orders analyzed for spring-back control and to explore the relationship of local deformation to regional and global deformations.

Zinc has been chosen for its ductility and non-corrosiveness for this research. Further research will address the employment of harder metals. The change of material would have a direct impact on the choice of the robotic forming tool, a reconsideration of the panel framework and additional supports, as well as material specific considerations such as spring-back. Nevertheless, the computational workflow can be applied for panels of varying geometries and different sheet metal types.

Material experimentation and FEA analyses have demonstrated that a panel formed with Curved Folding and RA-SPIF is significantly stiffer than a panel formed with Curved Folding only. Hence, the research demonstrates that curved folding and metal sheet forming can enhance the structural performance of architectural configurations. The employment of material and fabrication parameters coupled with structural behavior as design drivers during the early stages of design has the potential to address multiple performance criteria embedded in the high level of complexity of design processes. This research addresses this objective through the careful correlation of data pertaining to material properties, the integration of curved folding and RA-SPIF, and structural performance as design drivers.



Figure 12. Final assembly photo.

ACKNOWLEDGEMENTS

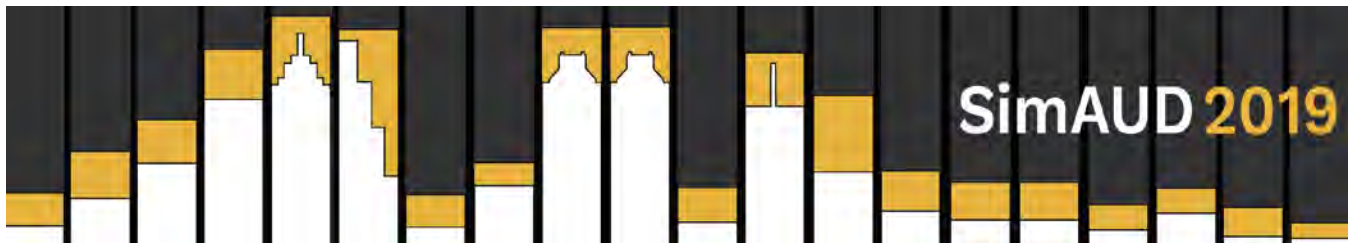
The work presented is part of the research undertaken at Architectural Association (AA) Emergent Technologies & Design (EmTech) Post-Graduate Programme. We would like to thank EmTech 2017-18 cohort, AA Digital Prototyping Lab (DPL) staff, and BuoHappold Engineering team for their great efforts.

REFERENCES

1. Autodesk Recap. <https://www.autodesk.co.uk/products/recap/overview>. Accessed 07 November 2018.
2. Azom. <https://www.azom.com/properties.aspx?ArticleID=749>. Accessed 01 June 2018.
3. Chandra, S., et. al. ‘Computing Curved-Folded Tessellations through Straight-Folding Approximation’, in H. Samuelson, S. Bhooshan, and R. Goldstein (eds.) *SimAUD 2015 Proceedings of the Symposium on Simulation for Architecture & Urban Design 2015*. 152-159.
4. Emmens, W. C., Gerd Sebastiani, and Antonius H. van den Boogaard. ‘The technology of incremental sheet forming—a brief review of the history’, in *Journal of Materials Processing Technology* 210.8 (2010): 981-997.
5. Kalo, A., Newsum, M.J. ‘An Investigation of Robotic Incremental Sheet Metal Forming as a Method for Prototyping Parametric Architectural Skins’, in McGee W., Ponce de Leon M. (Eds.) *Robotic Fabrication in Architecture, Art and Design 2014*. 33-49.
6. Kalpakjian, S. and Schmid, S.R. *Manufacturing Engineering and Technology*. 7a ed. Cambridge, UK: Pearson, (2013).
7. Kangaroo. <https://www.grasshopper3d.com/group/kangaroo>. Accessed 04 April 2018. Piker, Daniel. ‘Kangaroo: Form Finding with Computational Physics’, in *Architectural Design*, 83.2 (2013): 136-137.
8. Kilian, M., et. al. ‘Curved folding’, in *ACM SIGGRAPH 2008 Papers*, (2008), Article No. 75.
9. Mitani, J., Igarashi, T. ‘Interactive design of Planar Curved Folding by Reflection’, in *Pacific Graphics*, (2011).
10. Octopus. <https://www.grasshopper3d.com/group/octopus>. Accessed 10 June 2018. Vierlinger, Robert. ‘Towards AI Drawing Agents’, in *Modelling Behaviour*, Springer, Cham, 2015. 357-369.
11. Strand 7. <http://www.strand7.com/>. Accessed 01 June 2018.
12. Tachi, T., Epps, G. ‘Designing One-DOF Mechanisms for Architecture by Rationalizing Curved Folding’, in *Proceedings of the International Symposium on Algorithmic Design for Architecture and Urban Design, ALGODE TOKYO (2011)*
13. Wind-Loading. https://www.engineeringtoolbox.com/wind-load-d_1775.html. Accessed 03 May 2018.
14. Wu, P., Wang, J., Wang, X. ‘A Critical Review of The Use Of 3-D Printing in The Construction Industry’, in *Automation in Construction*, Elsevier B.V., 68, (2016), pp. 21–31. [doi:10.1016/j.autcon.2016.04.005].

Performative Structures

Structural Performance of Semi-regular Topological Interlocking Assemblies	217
<i>Michael Weizmann, Oded Amir and Yasha Jacob Grobman</i>	
Data-driven Material System of Graded Concrete Structures	225
<i>Elisabeth Riederer and Anuradha Suryavanshi</i>	
Modularizing Tensegrity Systems: An Approach to Controllable Independent Modules	231
<i>Arian Seedfar and Paniz Farrokhsiar</i>	
A Framework for Cost-Optimal Zero-Energy Lightweight Construction	239
<i>Mohamed Amer and Shady Attia</i>	



Structural Performance of Semi-regular Topological Interlocking Assemblies

Michael Weizmann¹, Oded Amir² and Yasha Jacob Grobman³

¹ Faculty of Architecture and Town Planning, Technion Haifa, Israel
wmichael@technion.ac.il

² Faculty of Civil and Environmental Engineering, Technion, Haifa, Israel
odedamir@cv.technion.ac.il

³ Faculty of Architecture and Town Planning, Technion Haifa, Israel
yasha@technion.ac.il

ABSTRACT

The principle of Topological Interlocking (TI) suggests using discrete blocks for assembling self-supporting structures. Several studies showed high quality Finite Element analyses for simple types of interlocking assemblies, composed of either tetrahedral or cubic blocks. Recent research has revealed that there are many more types of blocks suitable for assembling interlocking structures. The presented paper is part of an ongoing research on TI in architecture. The current stage of the research focuses on the correlation between the geometry of TI blocks and the structural performance of the whole assembly. The paper presents the results of a series of numerical analyses of various TI-based structures, revealing interesting relations between geometrical parameters and the force-deformation response of TI assemblies.

Author Keywords

Topological interlocking; structural analysis; masonry; performative geometry.

1 INTRODUCTION

Recent developments in architectural digital design and fabrication imply that in the near future, the possibilities of designing and fabricating complex architectural geometries will be almost unlimited. In a time of departure from the modernist ideas of standard and repetition, it seems both necessary and desirable to examine new approaches to design and fabrication of building structural elements that depart from the orthogonal modernist tradition.

One of such approaches is the principle of topological interlocking (TI) – a special case of masonry in which building elements are arranged in a way that an entire structure is held together by kinematic constraints inflicted through the geometry and through the mutual arrangement of the elements [7]. Topological interlocking systems have several potential advantages in comparison to other structural systems. Fragmented systems that are made from small elements can be easily fabricated and transported to the

building site. From the perspective of efficient construction, the possibility to maximize the number of prefabricated elements and the small size of the single tile can offer a decrease in construction time. Another important attribute of TI systems is their inherent vibration attenuation mechanism that can be advantageous in the design of seismic-resistant structures [18]. Moreover, straightforward disassembly of TI systems makes them also attractive for temporary buildings.

Despite their noticeable potential advantages, topological interlocking-based building systems were mainly developed for shell structures. Only little attention has been given for the potential to develop horizontal surfaces (flat arches/floors). This can be explained by the lack of knowledge on the structural behavior of complex TI assemblies, the lack of design tools that can assist in developing complex TI assemblies and the lack of fabrication methods for TI tiles.

The paper is part of a research project that focuses on the potential of employing TI based structure in buildings. Previous research stages have focused on the following directions:

- A thorough review of the history of TI and of the state of the art research on the concept of TI [15], [16].
- Development of an algorithm and a computational tool for creating new valid TI assemblies [16].
- Discovery of numerous new types of TI block geometries and creation of a catalogue of known TI block assemblies, based on the suggested algorithm [17].
- Defining possible directions for building floor assembly systems that are based on TI tiles [17].

Existing research on TI includes studies in several directions. Studies that deal with architectural applications of TI mainly focus on the aesthetic value of TI assemblies, on developing design, fabrication and assembling methods of geometrically

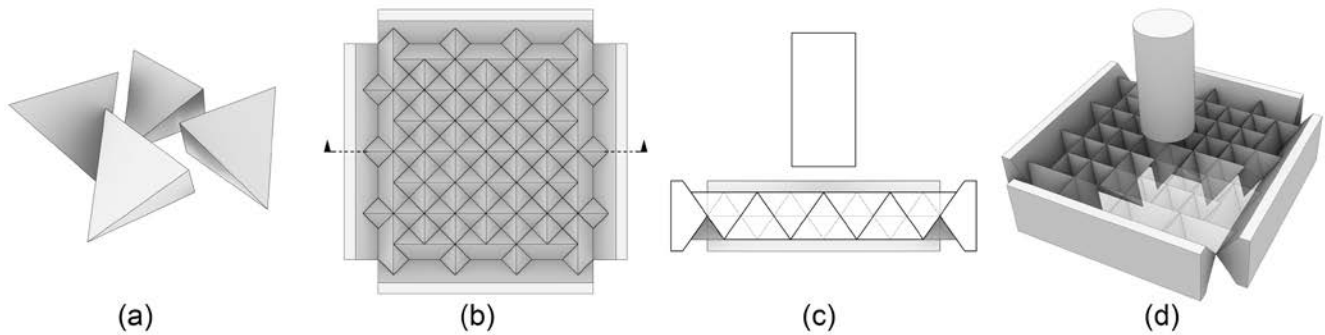


Figure 1. Geometry of the analysis method validation model. (a) sample arrangement of four blocks; (b) top view of the examined structure of 7*7 blocks; (c) model section; (d) perspective view of the analysis model.

complex structures and the potential diversity in tile geometries [1]–[3], [8], [13], [14]. Research on TI-based systems as structural elements mainly deals with the structural performance of specific tile geometries and materials [5], [7], [9], [11], [12]. Additional TI research directions focus on the effect of varying a specific geometric property of a block on the structural behavior of an interlocking assembly. For example, using blocks of the same type but with different dimensions, or alternating the finish of block faces from smooth to rough surfaces, thus increasing the friction between the blocks [4], [6]. However, these lines of research focused on different geometric properties within the same block typology. Therefore, the connection between the tile’s geometry and the structural behavior of the TI assembly is still largely unknown. Especially in relation to the new TI typologies that were discovered in the previous stages of the research [15].

The presented research aims to contribute to the body of knowledge on the correlation between different tile geometries and their structural performance by systematically mapping and comparing various types of topological interlocking assemblies. The structural performance of the TI assemblies is evaluated and compared through numerical simulations. The simulations are performed in Itasca 3DEC, a discrete element modelling software [10]. Since 3DEC was designed especially for analyzing discontinuous elements and discrete blocks, such as rocks or masonry, it was found to be an appropriate software for this type of analysis.

The first part of the paper presents the analysis methodology. The second part presents the results and discusses their significance. The paper ends with a discussion on the future research directions and the challenges in defining the effect of block geometry on the structural performance of TI-based structures.

2 RESEARCH METHODOLOGY

The research methodology consists of three stages. The first stage focuses on the validation of our numerical analysis model, comparing its result with experimental and numerical results from literature. The second stage focuses on a parametric study of the structural behavior of TI assemblies

based on tetrahedral blocks, and the third stage focuses on examining the structural behavior of semi-regular and non-regular TI assemblies.

2.1 Stage 1 – Model Validation

The simulation results were validated by comparing them to the results reported by Feng et al. [9] using an identical structure that was analyzed in 3DEC. The model that was used for the validation was composed of 49 structural blocks arranged in an orthogonal grid of 7x7 cells, four beams, acting as a fixed boundary of the model, and a cylindrical block used as the indenter (Figure 1). All the building blocks were identical regular tetrahedra with the edge length of 25 mm, height of 17.68 mm and face inclination angle of ~35 degrees (between each face and a vertical plane). The free span between the supporting beams was 87.5 mm. The indenter was a cylinder with the radius of 12 mm, positioned at the center of the structure. The material properties of the block, made of ABS, were density of 950 kg/m³, Bulk modulus of 2.03 GPa and Shear modulus of 0.676 GPa (which correspond to Young’s modulus of 1.827 GPa and Poisson ratio of 0.35). The calibrated joint material properties were contact normal stiffness of 2 GPa, contact shear stiffness of 0.028 GPa, and friction angle of 17 degrees (corresponding to the friction coefficient of 0.3). The frame beams and the indenter were defined as rigid blocks made of steel. The displacement of the frame was restricted in all three directions; the X and Y displacement of the cylinder was restricted and a constant velocity of -0.5 units was applied in Z direction. The sum of reaction forces in Z direction of the four boundary beams and the maximum displacement in Z direction of the blocks were calculated at every time step.

Various model parameters – mainly contact coefficients and numerical time steps – that are specific to each analysis software, had to be calibrated based on the force-displacement graph until achieving a satisfactory result. **Figure 2** shows a very good agreement between the experimental response and the simulation, in terms of the force-displacement curve.

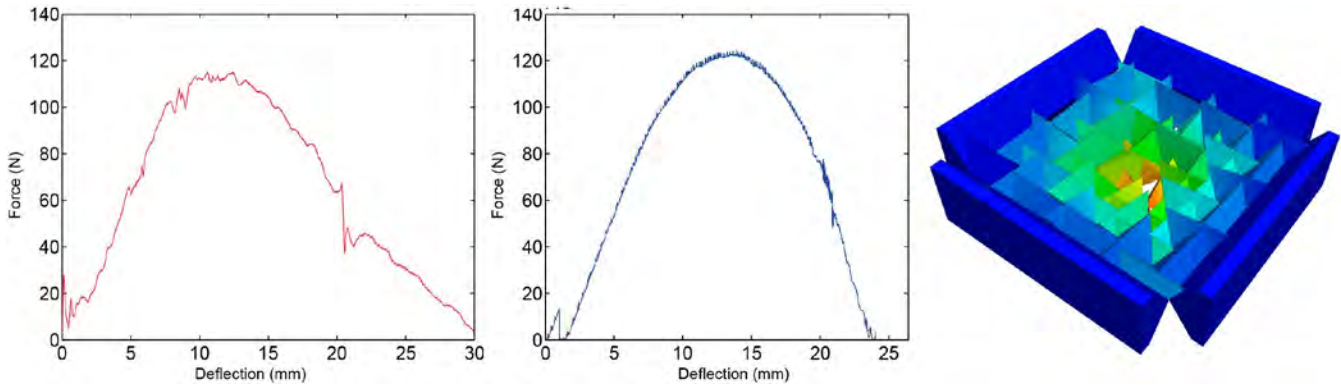


Figure 2. Reaction/displacement curves for a base model of 7x7 tetrahedra. Left-to-right: experimental results presented by Feng et al. [9], numerical prediction obtained in this research, displacement of the model.

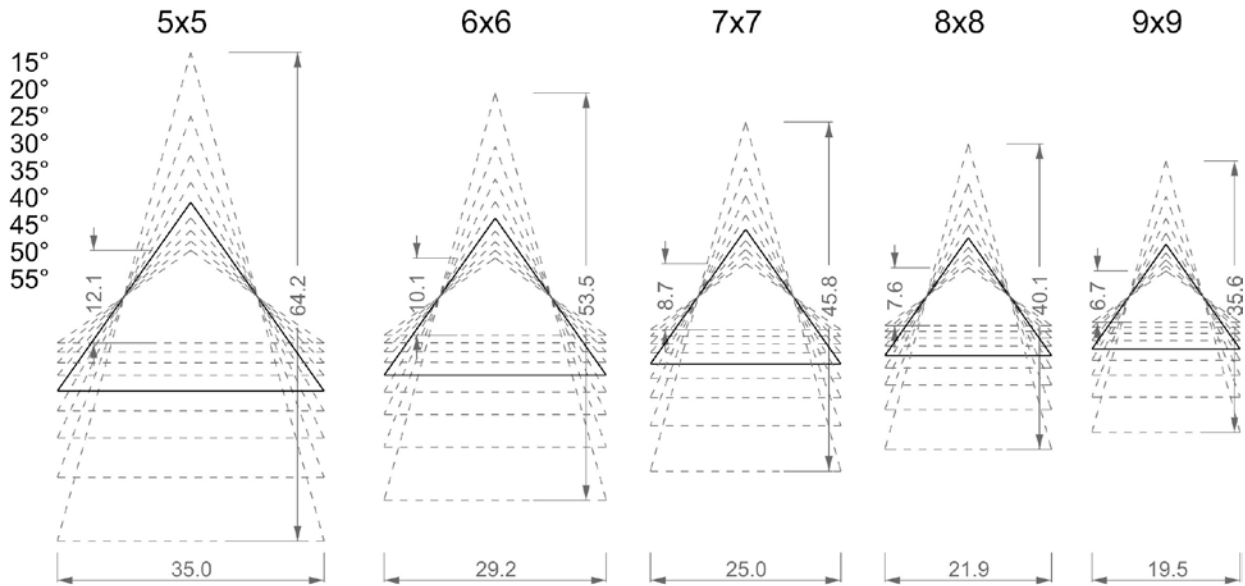


Figure 3. Unit dimensions of the main group of models. Left-to-right: 5x5, 6x6, 7x7, 8x8, and 9x9 unit models

2.2 Stage 2 – Parametric Study of the Tetrahedral Blocks

Three different sets of models were analyzed to examine the effect of basic geometric properties of tetrahedral blocks on the structural performance of the assembly. The two main parameters that varied were the number of blocks in the assembly and the face angle of the blocks. Both parameters are supposed to affect the performance of the structure: using larger blocks is expected to make the assembly more rigid due to the lower number of blocks and, therefore, less contact area for block sliding; the inclination angle of the block's faces is assumed to affect the friction between the blocks and their ability to slide along each other. The number of blocks varied from 5x5 to 9x9 blocks in each assembly. Face inclination angles ranged between 15 to 55 degrees in 5-degree steps. In the first group, consisting of 45 models, assembly thickness and total material volume changed according to the changes of these two parameters (Figure 3). The second group consisted of 23 structures that resembled the models from the first group but were trimmed to the same thickness

of 17.68 mm of the base model (7x7 units with 35-degree face angle). The third group of models used identical structural blocks but implied a different geometry of the boundary frame – instead of using four smooth beams, the boundary was composed of the same blocks as the structure itself. A similar study that focused on 5x5 meter stone structure was conducted by Brocato and Mondarini [4]. While their work used a similar strategy, analyzing assemblies with varying number of blocks and face angle, the study focused on defining whether a flat interlocking assembly of tetrahedral blocks behaves more like a bending truss or more like a catenary structure. The focus of the research presented in this paper is the effect of geometry on the maximum load bearing capacity of a structure. The results section also presents how the geometry of the supporting beams affects the performance of the structures.

2.3 Stage 3 – Topological Interlocking of Semi-Regular and Non-Regular Assemblies

The second stage of the research examined a set of TI-based assemblies composed of semi- and non-regular

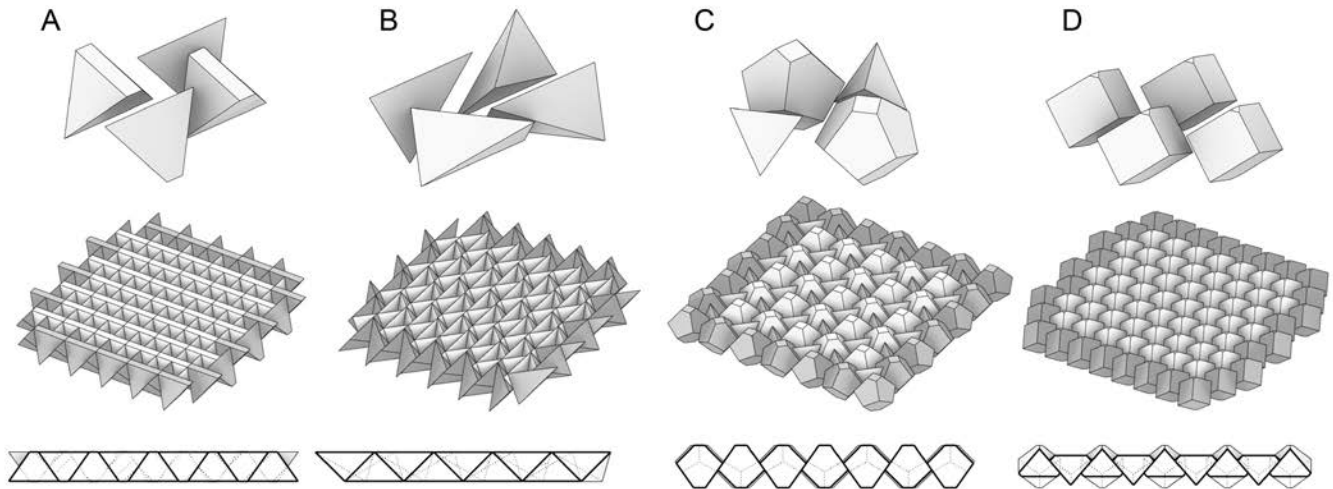


Figure 4. A sample arrangement of four blocks, a perspective view, and a section of each of the additional four models studied in stage three. A – grid of 7x10 trimmed tetrahedra; B – grid of 7x10 skewed tetrahedra; C – a model composed of two different polyhedra, based on horizontal grid of 5x5 octagons and 6x6 squares; D – assembly of 7x7 cubes, based on 2d grid of non-regular hexagons.

solids. For comparison, several parameters were kept similar for all the structures – the overall dimensions of the structure; the face angle of 35 degrees; and all blocks that exceeded the thickness of 17.68 mm (the thickness of the base tetrahedra model) were trimmed to that value. Figure 4 presents four models that were analyzed at this stage.

3 RESULTS

3.1 Stage 2 Results

The performance of the models was compared based on the reaction force per unit volume. Figure 5 summarizes the relation between the vertical reaction force per unit volume and the face inclination of the first group of 44 structures. The performance of the two other groups of structures, composed of 23 models each, is presented in Figure 6. The results of the first three groups of structures showed similar trends related to the examined parameters.

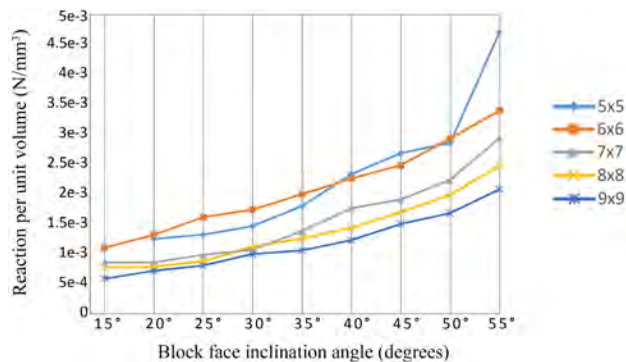


Figure 5. Vertical reaction force (N) per unit volume (mm^3) of the first group of tetrahedra-based structures.

The results show a clear relation between the number of blocks and the strength of the structure – assemblies with fewer blocks sustain higher loads. In these analyses, the deformation of the structure is dominated by sliding of the blocks caused by the indenter and not by fracture of the

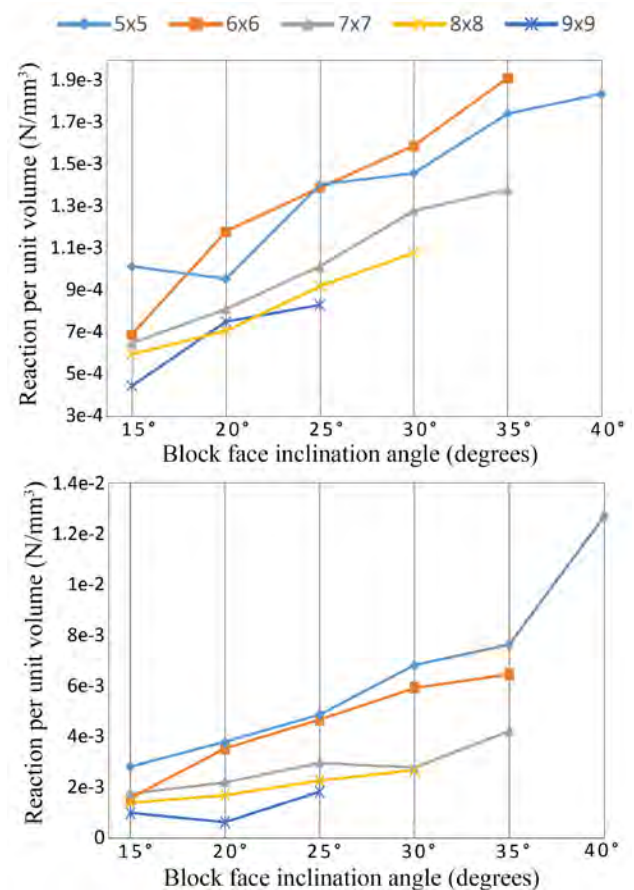


Figure 6. Vertical reaction force (N) per unit volume (mm^3) of tetrahedra-based models trimmed to the same thickness. 23 structure variations supported with smooth beams (top) and 23 variations supported with tetrahedra-shaped beams (bottom).

blocks. Hence, models with more blocks have more sliding interfaces and the blocks themselves are smaller.

Therefore, these models are more flexible and the opening that a unit can fall through can be smaller.

An additional observation is that the sustained load increases with the increase in the face inclination angle. This behavior is reasonable because as the inclination angle increases, larger forces are transmitted by normal contact on the block's face, and smaller forces are transmitted by tangential friction. This provides an increase in the overall load-bearing capacity.

The results of the third group show that the use of more complex boundary geometry instead of smooth beams significantly increases the strength of the structure. The assemblies in the third group performed 15%-40% better than their equivalents from the second group. While in the first two groups the units are restrained by the beams in only one horizontal direction – perpendicular to the beam, in the third group both perpendicular and parallel movement to the beam is blocked in the horizontal plane, leading to an increase in the magnitude of the sustained load.

3.2 Stage 3 Results

Stage 3 examined the structural behavior of semi-regular and non-regular TI assemblies, see Figure 4 for the examined geometries. The maximum reaction magnitude per unit volume obtained for the models 'A', 'B', 'C' and 'D' was 2.94×10^{-3} , 1.05×10^{-3} , 6.77×10^{-3} and 1.49×10^{-2} N respectively (see also Figure 7). Figure 8 presents the deflection of the four models by the end of the analysis. Model 'A' had a reasonably reduced performance, compared to the base assembly of 7×7 tetrahedra since it uses a larger number of blocks. Case 'B' presumably performs worse than case 'A', even having the same number of units, due to the lack of symmetry – the horizontal forces acting on each block do not stabilize each other, but rather cause rotation of the blocks and earlier horizontal expansion of the structure.

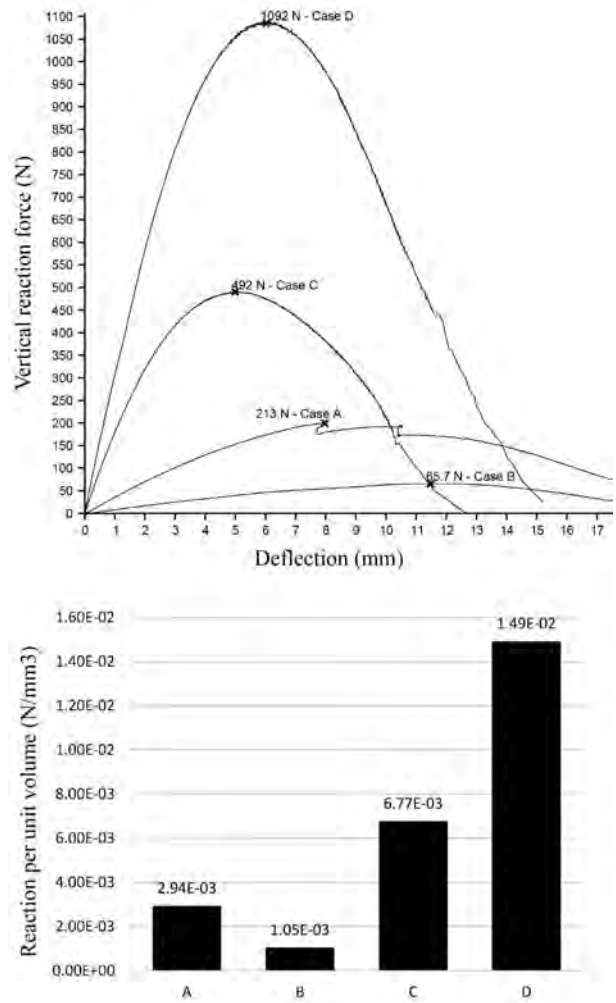


Figure 7. Stage 3 results summary. Force/deflection curves of the four models (top) and max reaction per unit volume (bottom).

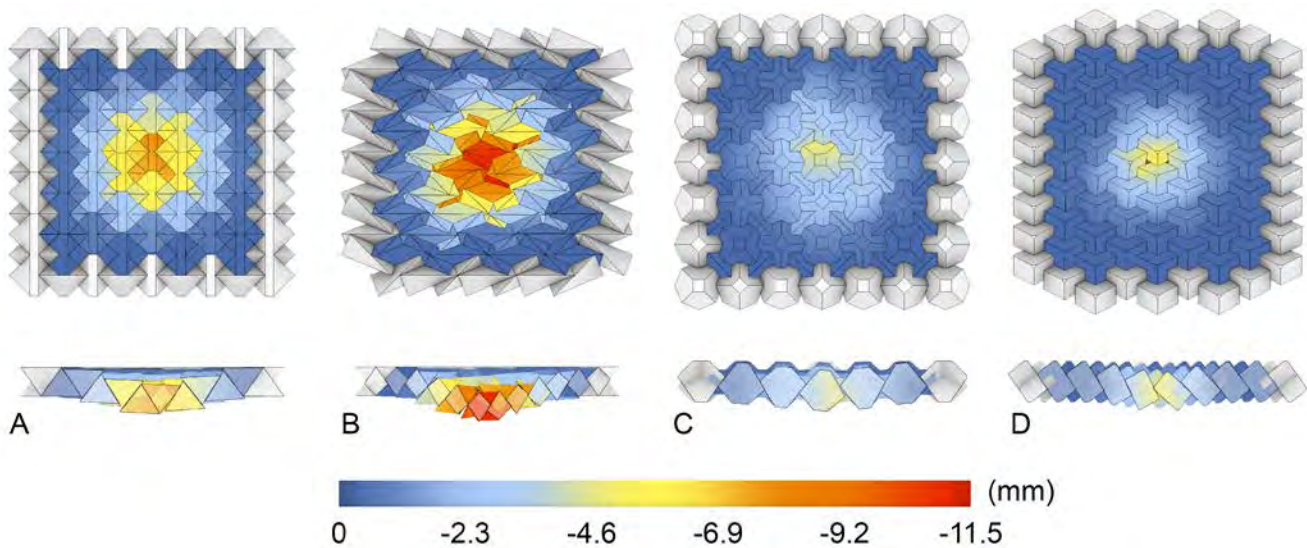


Figure 8. Vertical displacement top and section views of the four structures tested in stage 3 at max reaction moment.

However, confirming this idea requires further investigation of non-regular blocks. While model ‘C’ was composed of 61 blocks, its performance per unit volume was similar to the assembly of 6x6 tetrahedra, and just slightly lower than that of 5x5 blocks. In this case the increased performance is caused by the fact that model ‘C’ is composed of a main grid of 5x5 large blocks and a secondary grid of small tetrahedral blocks. The additional tetrahedral blocks may compromise the performance of the structure, but at the same time they also reduce the relative volume significantly, making better use of the material.

In case ‘D’ the structure was composed of 51 slightly distorted cubes and, surprisingly, it performed much better than any of the previously described models. In terms of the geometry, there were two main differences between this assembly and the others. First, on two opposite sides of the fixed boundary beams, three faces were supporting each block of the structure and not just two faces as in other cases. Second, the distribution of the loads seemed to be more effective in a hexagonal grid of blocks, and, therefore, the whole structure performed better than other cases, that were based on orthogonal grids.

4 CONCLUSIONS AND FUTURE RESEARCH

This paper presents the results of an ongoing research that focuses on the potential to employ TI-based tiles for building floor elements. The current stage of the research addresses the relation between the geometry and dimensions of TI blocks and the structural performance of the assembly.

The systematic analysis of 90 tetrahedra-based structures points out a direct relationship between the number of units in an assembly and the face angle of individual tetrahedral, and the structure’s effectiveness per unit volume. The results show that a higher number of tiles, and also using blocks with lower face inclination angle reduce the structure’s strength.

It is important to note that although our simulations were validated based on the results of previous research, it is important to validate and calibrate the simulations with physical experiments that we plan to perform in the next stage of the research.

Additional research is needed to broaden the investigation on the dependence of the structural performance of TI assemblies on the block geometry. Future work will focus on analyzing the various new TI block geometries that were discovered at earlier stages of this research.

Examining possible ways to support the boundaries of TI block assemblies seems to be another research direction worth pursuing - analyzing two different types of boundary beams revealed that the design of the beams has a significant effect on the strength of the whole structure.

REFERENCES

1. I. Ariza, T. S. Sutherland, J. B. Durham, C. T. Mueller, W. Mcgee, and B. Clifford, “ROBOTIC FABRICATION OF STONE ASSEMBLY DETAILS,” in *Fabricate 2017*, A. Menges, B. Sheil, R. Glynn, and M. Skavara, Eds. UCL Press, 2017, pp. 106–113.
2. P. Block *et al.*, “Armadillo Vault - An extreme discrete stone shell,” *DETAIL*, vol. 10, pp. 940–942, Oct. 2016.
3. A. and K. Borhani, “APART but TOGETHER - The Interplay of Geometric Relationships in Aggregated Interlocking Systems,” in *Fioravanti, A, Cursi, S, Elahmar, S, Gargaro, S, Loffreda, G, Novembri, G, Trento, A (eds.), ShoCK! - Sharing Computational Knowledge! - Proceedings of the 35th eCAADe Conference - Volume 1, Sapienza University of Rome, Rome, Italy, 20-22 September 2017*, pp. 639-648, 2017.
4. M. Brocato and L. Mondardini, “Parametric analysis of structures from flat vaults to reciprocal grids,” *Int. J. Solids Struct.*, vol. 54, pp. 50–65, 2015.
5. L. Djumas, A. Molotnikov, G. P. Simon, and Y. Estrin, “Enhanced Mechanical Performance of Bio-Inspired Hybrid Structures Utilising Topological Interlocking Geometry,” *Sci. Rep.*, vol. 6, p. 26706, May 2016.
6. L. Djumas, G. P. Simon, Y. Estrin, and A. Molotnikov, “Deformation mechanics of non-planar topologically interlocked assemblies with structural hierarchy and varying geometry,” *Sci. Rep.*, vol. 7, no. 1, p. 11844, Sep. 2017.
7. Y. Estrin, A. V. Dyskin, and E. Pasternak, “Topological interlocking as a material design concept,” *Mater. Sci. Eng. C*, vol. 31, no. 6, pp. 1189–1194, 2011.
8. G. Fallacara and V. Mienna, *Stereotomic Design*. Edizioni Gioffreda, 2014.
9. Y. Feng, T. Siegmund, E. Habtour, and J. Riddick, “Impact mechanics of topologically interlocked material assemblies,” *Int. J. Impact Eng.*, vol. 75, pp. 140–149, Jan. 2015.
10. Itasca Consulting Group, “3DEC Version 4.1 User’s Guide.” 2007.
11. M. Mirkhalaf, J. Tanguay, and F. Barthelat, “Carving 3D architectures within glass: Exploring new strategies to transform the mechanics and performance of materials,” *Extreme Mech. Lett.*, vol. 7, pp. 104–113, Jun. 2016.
12. A. Rezaee Javan, H. Seifi, S. XU, and Y. M. Xie, “Design of a new type of interlocking brick and evaluation of its dynamic performance,” in *Spatial Structures in the 21st Century*, Tokyo, Japan, 2016.
13. O. Tessmann and M. Becker, “Extremely Heavy and Incredibly Light – Performative Assemblies in Dynamic Environments,” in *Open Systems: Proceedings of the 18th International Conference on*

- Computer-Aided Architectural Design Research in Asia*, Singapore, 2013, pp. 469–478.
14. I. M. and K. Vella, “Geometric Versatility of Abeille Vault - A Stereotomic Topological Interlocking Assembly,” in *Herneoja, Aulikki; Toni Österlund and Piia Markkanen (eds.), Complexity & Simplicity - Proceedings of the 34th eCAADe Conference - Volume 2, University of Oulu, Oulu, Finland, 22-26 August 2016*, pp. 391-397, 2016.
 15. M. Weizmann, O. Amir, and Y. J. Grobman, “Topological Interlocking in Architectural Design,” in *Emerging Experience in Past, Present and Future of Digital Architecture*, Daegu, Republic of Korea, 2015, pp. 107–116.
 16. M. Weizmann, O. Amir, and Y. J. Grobman, “Topological interlocking in architecture: A new design method and computational tool for designing building floors,” *Int. J. Archit. Comput.*, vol. 15, no. 2, pp. 107–118, Jun. 2017.
 17. M. Weizmann, O. Amir, and Y. J. Grobman, “Topological interlocking in buildings: A case for the design and construction of floors,” *Autom. Constr.*, vol. 72, Part 1, pp. 18–25, Dec. 2016.
 18. H. T. D. Yong, “Utilisation of topologically-interlocking osteomorphic blocks for multi-purpose civil construction.,” PhD, University of Western Australia, 2011.



Data-Driven Material System of Graded Concrete Structures

Elisabeth Riederer¹ and Anuradha Suryavanshi²

¹Architectural Association (AA)
London, United Kingdom
Riederer@aalumni.org

² Architectural Association (AA)
London, United Kingdom
anuradha.suryavansi@gmail.com

ABSTRACT

This paper describes the development and results of strategies for improving the environmental and economic aspects of concrete structures. As (marine) sand suitable for concrete construction is becoming increasingly scarce, concrete construction is becoming consequently increasingly expensive. Thus, the need for an alternative building material arises.

The inclusion of PET as a replacement for sand and making use of 3D printing as a fabrication method is examined, and the effect on structural performance will be examined further by using a gradient of plastic content. Research methods include the employment of computational design and 3D-printing fabrication tools that incorporate geometric and material constraints tested one-to-one on physical samples.

Due to the fact that the material composite functions best in compression, a shell is chosen as a specimen for computational analysis. Based on the global shell's structural limitations of concrete the effect of local variation in material composition is analysed and evaluated.

The goal of the present research is to illustrate a design approach for similar material systems with the aim of improving material properties for use in more environmentally tolerable, efficient and economical building, while testing geometric and material constraints as well as using low cost fabrication methods.

Author Keywords

Material-system; 3D Printing concrete; functional gradient; PET in concrete; environmental and economic sustainability.

1 INTRODUCTION

The age of mass industrialization has resulted in emergence of strategies for material optimization as an outcome of post-rationalization of the component's morphological characteristics. In the architectural paradigm, this approach

has been translated as 'Material follows form'. With the advent of the digital era 'material informs structure informs form' is the new design paradigm. Architecture up to the neo-modernist era has witnessed component assemblies wherein the structural properties remain constant even as the geometric parameters of the global form vary. In nature, however most materials are engineered with anisotropic structuring to adapt to external constraints introduced upon them during growth [1].

This paper describes the outcomes of research conducted as a part of a master's thesis during the Emergent Technologies and Design Program (2018) at the Architectural Association, London. The aim was to develop a novel strategy for the construction of low-cost concrete structures by additive manufacturing of a cement-based composite using recycled PET bottles as replacement for sand. Research methods take into consideration the material limitations and geometry optimization to employ computational analysis in fabrication techniques. Research objectives focus on the re-interpretation of a traditional material system - plain cement concrete, towards its advancement within the domain of additive manufacturing and advanced computational techniques.

Material exploration along with advanced computational design can aid in optimizing architectural solutions for achieving higher structural and environmental performance. By identifying the range of material properties through series of experiments, a range of possible architectural outcomes can be predicted. To widen the response of architectural assemblies to external parameters a gradient of material properties is thus tested and evaluated. A shell typology is deemed ideal for implementing and analysing the performance of a functional gradient as the fabrication methodology. This is due to the fact that domes function best in compression as well as due to uniform curvature along both directions.

Sand is a major component (2/3) of concrete. As (marine) sand suitable for concrete construction is becoming

increasingly scarce [2], concrete construction is becoming consequently increasingly expensive. Thus, the need for an alternative building material arises.

Most affected are economically weak areas that are dependent on concrete as a construction material. One such example is Mumbai.

In previous research, polyethylene terephthalate (PET) as a replacement for sand has been found to be a more environmentally tolerable and economic component of concrete, although the low bonding nature of PET and the material matrix of PET resulted in lower compressive and tensile strength [3]. Recent studies at MIT have shown that the treatment of PET with gamma irradiation changes PET's properties such that the PET-concrete mixture was 15% stronger than conventional concrete [4]. This research shows one method of improving the materials performance while making it more environmentally tolerable by reducing the amount of cement in concrete. This is an attempt to extend the application of PET in concrete outside the research domain into novel architectural systems.

The goal of the present research is to develop a design approach for similar material systems with the aim of improving material properties for use in a more economic means of building that is environmentally tolerable and efficient and at the same time to testing geometric and material constraints, as well as the use of low cost fabrication methods.

2 RESEARCH DEVELOPMENT

This section describes the analytical procedures that permit critical reflections on the investigation of the material, the development of the material system and the design proposal allowing for a sustainable usage of the material system.

2.1 Material Adaptation to Extrusion Standards

In the use of plastic in concrete, casting is the only fabrication method presently employed. However, it is known that bonding in concrete is increased by extrusion. This effect would appear to be a logical tool for improving the weak bonding between PET and cement.

Extrusion of PET in concrete shows the need for a drastic decrease in water content. With respect to the water/cement ratio on the one hand, water reduces the material strength, so that its content is kept as low as possible. On the other hand, adequate water content is essential for encasing the aggregate. This assures a higher bonding surface area, which is one of the criteria defining material strength [5].

Therefore the addition of plasticizer is needed. In addition, fly ash was added to make the material composition more pasty. Another result following from the transition from casting to extrusion was the need to reduce PET flake size from 4 to 3 mm, while in casting it was found that the maximum flake size is most efficient in terms of material strength [3].



Figure 1. Samples for structural tests of Concrete and of PET in Concrete as a gradient

Material	C.01 (%)	C.02 (%)	C.03 (%)	C.04 (%)
Aggregate (Sand+PET)	A.60 (S.100)	A.60 (S.80+P.20)	A.60 (S.50+P.50)	A.60 (S.77+P.23)
Cement	30	30	30	30
Water	10	4.4	1	5,1
Plasticiser	-	3	5	2,7
Fly ash	-	2.6	4	2.2

Table 1. Comparisons of Extrusion Composition of plain concrete (C.01), 20% PET in concrete (C.02), 50% PET in concrete (C.03), and a functional gradient from plain concrete to 20% PET in concrete to 50% PET in Concrete (C.04)

In the following compositions and parameters of the inclusion of 0% (C.01), 20% (C.02) and 50% PET (C.03) in concrete are described. (see table 1)

Variable parameters: Water/cement ratio, percentage of PET replacing sand. Fixed parameters: PET flake size (3 mm), cement/aggregate ratio (1:2). It is known that water absorption of plastic is low so that there is a higher amount of free water when PET is included in the composite. Increasing the amount of PET in concrete therefore required reduction of the water/cement ratio. An extremely low content of water was concluded as it prevents the separation of water from the material matrix (free water). Under these conditions the bonding of PET to the material matrix appeared to be low. The addition of a plasticiser was therefore held to be necessary to achieve the right balance of fluidity.

Variable parameters: Plasticiser, percentage of PET replacing sand. Fixed parameters: PET flake size (3 mm), cement/aggregate ratio (1:2), water/cement ratio adapted to amount of PET in concrete. Plasticisers are added to concrete to reduce the necessary amount of water. Increasing the amount of PET therefor increases the necessary amount of plasticiser.

Variable parameters: Fly ash, percentage of PET replacing sand. Fixed parameters: PET flake size (3 mm), cement/aggregate ratio (1:2), water/cement ratio adapted to amount of PET in concrete. Fly ash is used to make the material composition more pasty, which is a required property for the extrusion of concrete [6]. The water content

is reduced while the amount of PET, plasticiser and fly ash is increased.

A constant factor for both fabrication methods is the maximum percentage of PET flakes (50%). The best buildability was achieved by a rectangular nozzle cross-section with an area of 600 mm². The explored material composition adapted to achieve extrudability also corresponds to a reasonable workability of about 45 min.

2.2 Examination of the Extrusion Method

All mechanisms were first tested with plain concrete and, if successful, tests were made successively with 20% and 50% PET in concrete. The first tests were conducted by making use of a gear mechanism. Generally, this method is employed when using concrete, while a constraint is the maximum particle size of 1 mm. Both The size of PET particles and the clay-based nature of the cement used might be the reason for the failure of the mechanism. A pump mechanism allowed plain concrete to be extruded successfully. On the other hand, addition of PET reduced the extrudability to nearly zero. Air pressure is a fabrication method that is generally used for the extrusion of clay. Test results were unsuccessful. The material emission could not be controlled as the lighter material (PET) splashed out or did not extrude. The reason for the lack of control over the material when extruding could be the presence of sand. The necessity for a more equal application of pressure is implied. A manual pump mechanism achieved successful extrudability. However, a man-made process could not achieve equal distribution. This could be a result of the applied force not being constant. A lever mechanism was then employed and resulted in equal distribution and therefore leads to well-controllable extrusion of PET in concrete (see figure 2).

2.3 Evaluation of Material Performance

The criteria for material performance are the elastic modulus and the flexural and compressive strength. Tests conducted should provide an understanding of the material properties. Tests are applied on the three different material compositions of plain concrete, 20 % PET in concrete, 50% PET in concrete and the functional gradient composition (From Plain concrete, to 20% PET in concrete, and to 50% PET in concrete). Since the availability of tools was limited, physical tests are carried out on a smaller scale than generally required and thus leading to a more abstract representation in the increasing forces.

Bending test: The 3-point bending test evaluates the tensile strength and elastic modulus of the material. A sample of 2 x 2 cm (width x height) and a length of 10 cm was tested. A concentrated load is applied to the centre while the two ends rest on supports. Tests values are evaluated on the slope and angular coefficient of the stress deflection curve. As a source of force a bucket of water is used and is centrally installed on the sample. This allows incremental increases of force by adding water.

Compression test: In this test, the force applied to the sample is increased until the material reaches its compression limit and cracks. The material sample, in the form of a cylinder with a diameter of 2 cm and a height of 2 cm, is placed on a flat surface and loads of 1 kg are applied. Increasing the force uniformly and continuously was not possible due to the restricted tools available. This method is thus an approximation for load application and therefore the measures of compressive strength are not precise.

A comparison with other construction materials is made to position the extruded PET in concrete in the context of building materials. For the selection of the materials, lightweight concrete and materials with high compressive strength are compared with PET in concrete [7]. The improved strength is hoped to stimulate the usage of plastic in concrete in architecture. By using extrusion as a fabrication method material performance of PET in concrete increased. Although the values still show substantial differences in material performance of concrete, especially with regard to compressive strength (see table 2.).

Material	Compressiv MPa	Flexural MPa	Elastic m. GPa
Granit	130	4.8	52
Concrete	53	5	38
Gradient 50%PET to Concrete	45	4.7	31
Concrete 20% PET	28	4.5	24
Concrete 50% PET	17	4.2	13
Common brickwork	7	0.35	9.6
Optical fibre	50	7	27

Table 2. Comparison of results for compressive strength, flexural strength and elastic modulus between different plastic in concrete compositions and other building materials



Figure 2. from left to right: Gear, Pump, Air pressure, Lever mechanism

2.4 The Gradient Subjected to its Morphology

With the aim of proposing an alternative to concrete as a building material, a functional gradient is suggested as a means of further improving material performance. By the functional use of different material compositions, ranging from 50% PET in concrete to plain concrete we hope to achieve similar material performance, while including the maximum amount of PET in concrete. We propose a material system with a functional gradient between strength and ductility responding to the stresses in a shell. The functional gradient consists of three different compositions: Plain concrete, 20% PET in concrete and 50% PET in concrete (see table 1). The functional implementation of the different material compositions is applied to the thickness and varies layer-wise. The logic of the functional material gradient is inspired by the anatomical principle of the human skull. In other words, in a shell, more ductile material forms the inner part, whereas the stronger material must be distributed on the surfaces (outermost layers = concrete; following layers = 20% PET in concrete; innermost layers = 50% PET in concrete) (see figure 1). The structural performance of a functional gradient applied to the thickness is tested. The layer-wise change of the different compositions from plain concrete to sand replacement by 20% PET in concrete to sand replacement by 50% PET in concrete showed no effect on the bonding of the layers. Using the same test set-up as described above, material performance of the functional gradient shows values that are approximately the same as those of plain concrete (see table 2).

2.5 Global Form Finding

To understand the spatial boundaries of structures fabricated with a gradient in thickness from 50% PET in concrete to plain concrete, a digital model of a shell was constructed on the basis of the material properties. The starting point for the model was a simplified model of the Pantheon, the dome which has the largest span of unreinforced concrete [8]. The construction parameters were then optimised until the applied membrane forces were in equilibrium. The maximum span-to-thickness ratio for constructing hemispherical shells using a gradient from 50% PET in concrete to plain concrete was 40:1. Geometry and amount of curvature influence the structural stability of shells [9]. It was observed that under self-weight, a gradient from 50% PET in concrete to plain concrete can withstand loads for up to a span-to-height ratio of 1.11. (see Figure 3). For further lower span-to-height ratios, the compressive stresses exceeded the yield point (45 MPa) (see figure 3).

2.6 Geometric Constraints

In order to evaluate effects of the proposed material system, physical and computational examinations are conducted on the proposed material system and plain concrete. To explore geometrical constraints, both a maximum mesh span and the maximum achievable curvature were tested physically. The data should be further examined in digital

experiments to define limits of global dimensions and mesh dimensions.

Mesh span: The mesh span experiments were conducted on a double-curved formwork. Positive results in the application of the material gradient on complex surfaces were seen (Gaussian curvature from +5 to -5). The maximum mesh size achieved by the material system is 8 cm, while plain concrete could span a maximum mesh size of 12cm. (see figure 4)

Curvature: To explore the extrusion on high slopes and high curvatures, extrusion is implemented on a sphere. Extrusion of the functional gradient material composite could be conducted up to a slope of 72°, whereas for extrusion of plain concrete the maximum slope was 69° (see figure 4).

This data is further examined in digital experiments to define the specimen's limits of global dimensions and mesh dimensions. As a computational specimen a shell is chosen. A concrete shell and a shell consisting of the functional gradient from 50% PET in concrete to concrete are compared to examine the effect of the reduction of sand in the latter one, while taking into account the capability of concrete to withstand higher stresses. The two shells have the same global dimensions (radius 2.0) while one shell is given the maximum mesh dimensions and material constraints of the material system and the other one is given maximum mesh dimensions and material constraints of concrete. Topology optimization was used in order to evaluate the effect of the proposed material while taking into account the capability of concrete to withstanding higher stresses.

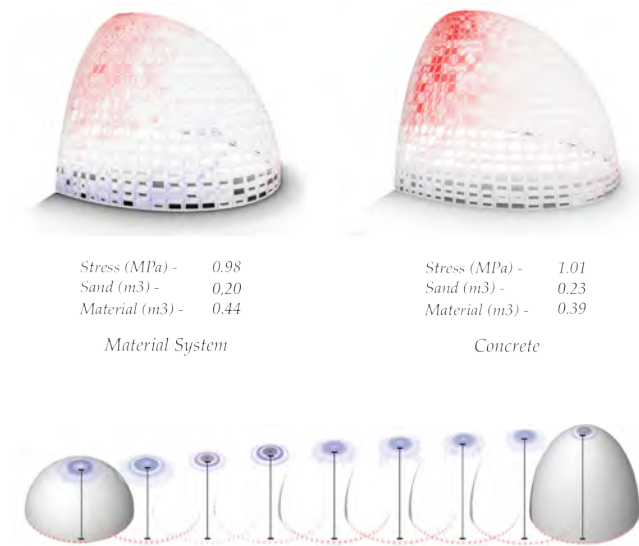


Figure 3. top: computational specimen of a shell of the proposed material system and concrete. Bottom: Range of possible span-to-height ratios for hemispherical shells proposed with plastic in concrete

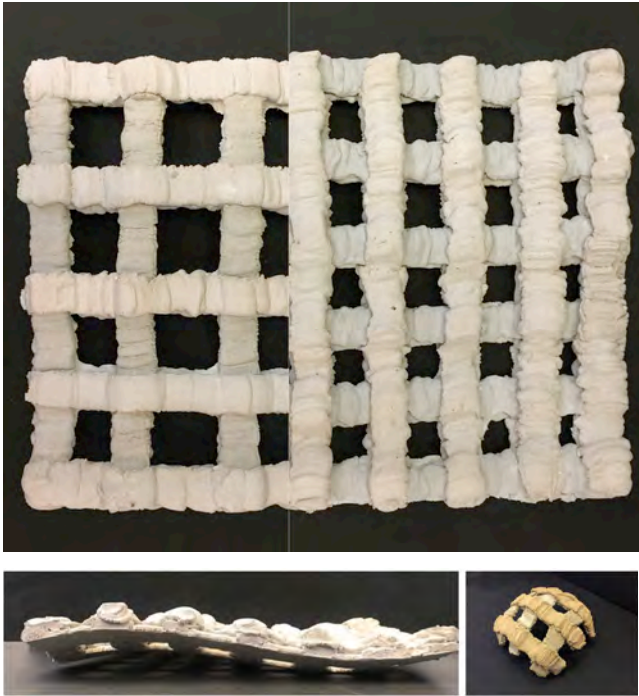


Figure 4. top: max mesh spans achieved by concrete (left) and the proposed material system (right). Bottom: Tests on double curvature and on a dome in order to explore material constraints

The outcome of typology optimization results in the minimum amount of material capable of withstanding the stresses acting on the specimen. In addition, the produced stresses are examined here. The amount of material defines the amount of sand being used and therefore the effect of reducing sand in concrete by means of the proposed material system. The computational model shows that the proposed material system requires 13.1% less sand than the plain concrete shell (see figure 3).

In conclusion the initial reduction of 23% of the amount of sand compared to conventional concrete was decreased to 13.1% due to material and geometrical constraints.

DISCUSSION

The use of PET as a replacement for sand in concrete should trigger more research in exploring other replacement materials for sand. With respect to this, rubber might be considered for testing as a replacement for sand. The selection of the replacement can be site-specific and respond to both environmental and spatial needs.

One of the key aims of this research is to illustrate a design approach for similar material systems using a functional gradient to improve material properties and to offer a more efficient, environmentally tolerable and economic way of building. The presented strategy for the material gradient (strength to ductility) is specific to its morphology (hemispherical shells) and its architectural application. The gradient is therefore subject to analysis of its global shape. Making use of the forces acting on the material during extrusion can also provide information for further

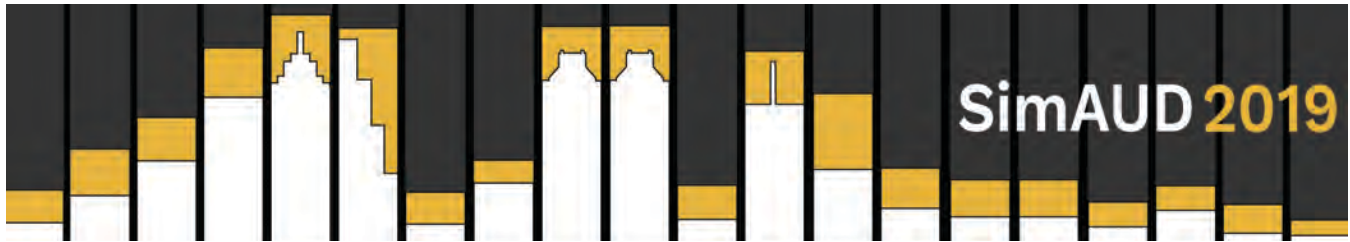
improvement of other material systems. This requires firstly examination and analysis of potential material adaptation to extrusion standards (such as adaptation to millimetre scale, to viscosity grade) and, where applicable, the effects of compressive forces in the extrusion process. Further, a computational analysis examines and evaluates the material system on an architectural scale. In order to take the differences of the compared composites in their capability to withstand forces into account, typology optimisation is found to be an adequate tool for comparing the material systems.

ACKNOWLEDGMENTS

We would like to thank Michael Weinstock and Elif Erdine for their advice and support during the research. We also express gratitude to Mohammed Makki, Antiopi Koronaki, Alican Sungur, Lidia Badarnah and George Jeronimidis for their help and sincere interest in the development of this research. The research paper contains transcripts from the MSc dissertation “Gradients in recycled composite materials”, developed by the authors at the Emergent Technologies and Design Program at the Architectural Association School of Architecture in London, UK, 2018.

REFERENCES

1. Oxman, Neri, et al. (2008): ‘Structuring Materiality’, http://neri.media.mit.edu/assets/pdf/Publications_SM.pdf
2. Peduzzi, Pascal (United Nations Environment Programme) (2014): ‘Sand, rarer than one thinks’, https://na.unep.net/geas/getUNEP-PageWithArticleIDScript.php?article_id=110
3. Akcaözoglu, Semiha, et al. (2010): ‘An investigation on the use of shredded waste PET bottles as aggregate in lightweight concrete’, *Waste Management*, 30: 285-290.
4. Chu, Jennifer (2017): ‘MIT students fortify concrete by adding recycled plastic’, <http://news.mit.edu/2017/fortify-concrete-adding-recycled-plastic-1025>
5. Torres, Kind-Barkauskas, Friedbert (2002): Concrete in architecture, in: Kind-Barkauskas, Friedbert et al. (Eds.). *Concrete Construction Manual*. Munich: Birkhäuser – Publishers for Architecture, pp. 8-45.
6. Hardjito, Djwantoro, et al. (2004): ‘On the Development of Fly Ash-Based Geopolymer Concrete’, *ACI Materials Journal*, 101: 467-472.
7. Ilangovana, R. et al. (2008): ‘Strength and Durability Properties of Concrete Containing Quarry Rock Dust as Fine Aggregate’, *Journal of Engineering and Applied Sciences*, 3: 20-26.
8. Dewidar, Khaled M. (2016): ‘The Pantheon’, https://www.researchgate.net/publication/310597898_The_Pantheon
9. Ney, Laurent, and Adriaenssens, Sigrid (2014): Shaping forces, in: Adriaenssens et al. (Eds.). *Shell Structures for Architecture. Form Finding and Optimization*. New York: Routledge, pp. 15-20



Modularizing Tensegrity Systems: An Approach to Controllable Independent Modules

Arian Saeedfar¹ and Paniz Farrokhsiar²

¹Autodesk
University Park, PA, USA
arian.saeedfar@autodesk.com

²Penn State University
University Park, PA, USA
puf69@psu.edu

ABSTRACT

Tensegrity structures are among the most efficient types of structures. Since the introduction of tensegrity structures by Richard Buckminster Fuller, there has been a lot of interest from architects and engineers to further study tensegrity structures and expand their use cases and application. Roadblocks such as complexity of simulation and unpredictability of their behavior, as well as their nonlinear reaction to side forces, have made it difficult to use them routinely in the realms of architecture and engineering. Many research projects have studied the dynamics of tensegrity structures and possibilities for expanding them beyond a single module. While most of the previous research contributes to the control systems for interdependent tensegrity modules, limited research has been performed on simple ways to expand the tensegrity systems using independent modules or blocks. The objective of this paper is to introduce a new method for easy expansion of tensegrity structures using independent modules. Leveraging experimental methods, a new component called “node” is introduced to the tensegrity module to provide the possibility for the interaction of two adjacent modules. Simple grids of the new expandable modules are simulated to verify the stability of newly designed systems and identify the key variables for controlling interdependent modules. Factors such as tension, displacement, and utilization are also analyzed in the simulations.

Author Keywords

Tensegrity; Lightweight Structures; Parametric Simulation; Modularization; Performance Analysis.

1 INTRODUCTION

There are a lot of forces, internal or external, acting on each building. Some of these forces, called compressive, push the building elements, while the other ones, called tensile, pull them. Until the recent decades, the only available materials for building the structures were only able to resist compressive forces. The advancements in the development of durable tensile materials in the past few decades have

provided the opportunity to use these materials more conveniently in the structure of the buildings [11].

Richard Buckminster Fuller found the gap between the complicated structures in nature and the man-made structures heavily focused on resisting compressive forces. Buckminster Fuller was interested in finding a way to add the neglected tensile part to the man-made structures. Therefore, he came up with the word “Tensegrity” which is derived from the phrase “tensional integrity”. Tensegrity structures have received a lot of attention in the recent decades by architects and engineers mainly because of their efficient structure and geometry [11].

Based on the definition by Anthony Pugh [11], a Tensegrity system is “a set of discontinuous compressive components interacting with a set of continuous tensile components to define a stable volume in space”. The simultaneous use of compressive and tensile components in tensegrity structures has made them lightweight. Therefore, they provide high structural stability as a result of their pre-stressed shape [6] and mass efficiency [13]. Another advantage of using tensegrity structures is their responsiveness to external forces and events like earthquakes and winds which makes tensegrity a great structure to be used in responsive architecture [13].

A significant amount of research has been performed on deployable tensegrity structures and tensegrity form-finding. Sultan et al. [14] have developed control strategies for tensegrity structures. Other research has focused on the form analysis and the stability of the tensegrity structures to overcome the static problems. Pellegrino [10] has focused on the form-finding of tensegrity structures to build a class of tensegrity domes. The other research papers on tensegrity form-finding include the work of Vasart and Motro [16] and Motro [7].

Despite the wide range of research on the tensegrity structures mainly focused on optimization and form-finding, limited research has been performed on the use cases of these structures in civil engineering such as buildings, bridges, etc.

External loads make the tensegrity structures react in a nonlinear way. Considering that tensegrity structures are often lightweight and flexible, small amounts of external force might have big impacts on the stability and formation of the critical components [12]. Therefore, one of the challenges in working with tensegrity structures have been the complexity of predicting their behavior and determining their state when applying forces [12]. There have been studies to predict the behavior of tensegrity structures using nonlinear techniques [9]. Barnes [1] introduces a technique called dynamic relaxation, Vasart and Motro [16] offer the force density technique, and Paul et al [8] offer the stochastic search method. A review of most of these methods and other form-finding methods can also be found in the work of Tibert and Pellegrino [15], as well as Juan and Tur [3]. Nonlinear methods are also developed in this area by Kebiche et al [4]. Most research studies have focused on the optimization of tensegrity structures to be used as lightweight structures that are controllable by changing the tensional and compressive variables and components [5].

2 DEVELOPING TENSEGRITY MODULES

Pugh [11] offers a variety of elementary tensegrity modules based on polygonal forms. The simplest method for defining tensegrity is using two-dimensional polygons in which the compressive components (struts) are the diagonals of the polygon and the tendons are the edges of the polygon. Figure 1 represents two samples of two-dimensional modules.

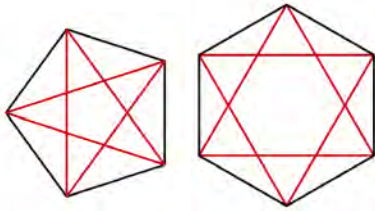


Figure 1. Samples of two-dimensional modules. Red lines represent compressive components and black lines represent tensile components.

Three-dimensional modules are developed by adding elements to the two-dimensional modules. The simplest three-dimensional modules introduced by Pugh [11] are created by forming platonic polyhedrons like cube or octahedron, in which the struts pass through their center and form the edges of the polyhedron and the tendons for their diagonals.

After providing a few samples of simple tensegrity modules, Pugh [11] introduces more complex modules that can be created by the diamond pattern or the circuit pattern. Pugh has used these patterns to explain the processes of expanding the basic two-dimensional figures to four-layer patterns. He uses the geodesic polyhedrons studied by Buckminster Fuller [2] and the circuit pattern to explain the creation of tensegrity modules based on geodesic polyhedrons. Pugh [11] argues that geodesic polyhedrons can be used to develop large complicated circuit-pattern tensegrity systems.

3 PROBLEM STATEMENT

Despite all studies on the optimization of tensegrity structures, limited methods are offered for simple modularization of tensegrity structures. Most methods studied in the literature review involve complicated calculations or are not compatible with the common definition of tensegrity structures which relies on “discontinuous” compressive components and “continuous” tensile components [11]. There are a few methods offered in the literature review including methods by Pugh [11] to create a modular system for tensegrity structures. However, a method for modularizing tensegrity structures using independent tensegrity blocks could not be found. The objective of this research is to design tensegrity modules that can independently work together to form a tensegrity surface or grid. Pugh [11] suggests that two effective methods for evolving new tensegrity systems are to find a “new relationship” between compressive and tensile components, as well as “extending an existing idea or figure”. Considering these two methods and manipulating existing modules, this study offers a novel technique for expanding tensegrity systems using independent tensegrity modules or blocks. Simulations have been performed on the designed blocks and grid to analyze the forces acting on the structures and identify the variables impacting the stability and form of the outcome tensegrity grid.

4 METHODOLOGY

4.1 Experiments with Existing Modules

In this research, the common existing polyhedron-based tensegrity modules developed by Buckminster Fuller [2] are chosen for the experimental design of a new tensegrity system. Various physical models of the existing tensegrity systems were created to understand the possibility of manipulating the modules to create a new system for expanding tensegrity structures. The models based on platonic polyhedrons were used in these experiments.

In the experiments, the feasibility of combining different modules by placing them adjacent to one another was also studied. The outcome of combining the modules without any manipulation usually results in crossing compressive components or discontinuity in the tensile components which will violate the definition presented by Pugh [11].

4.2 Manipulating the Existing Modules

In the next step of the experiments, the possibility of manipulating the existing modules was studied. Based on the experiments, manipulating the compressive components violated the definitions of tensegrity or did not create new opportunities for further expansion and developments of the tensegrity systems.

In a separate set of experiments, the possibility of manipulating tensile components was studied. Considering the tensile components as tensile surfaces, manipulating the tensile components is feasible if the net forces of the new pattern equal the net forces of the existing tensile surface. Therefore, in tensile surfaces of each component, the edges

of the surface can be replaced with tensile components that meet at the centroid of the surface and have the same net forces. As represented in Figure 2, in a triangle, the two vectors can be replaced by their resultant vector and the concept can be expanded to the existing tensegrity patterns. The top row shows the triangular pattern of the tensile surfaces for different existing tensegrity shapes. The bottom row shows the proposed components to be replaced with the original components while maintaining the same net forces. The method could be applied to all elementary modules introduced by Pugh [11] (Figure 3). In the experiments of this study, the possibility of manipulating the tensile components in icosahedron module was studied. In the icosahedron module, which has triangular tensile surfaces, in each triangle, if the edges are replaced with components that meet at the centroid of the triangle, the net forces of the tensile components would remain the same. However, it will create a new component at the centroid which does not exist in the old module.

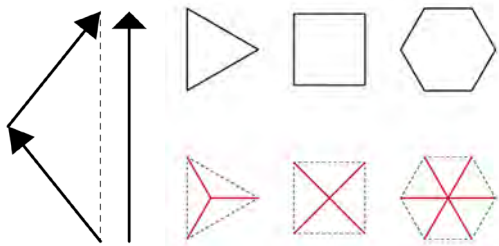


Figure 2. Manipulation of tensile surfaces while maintaining the same net forces.

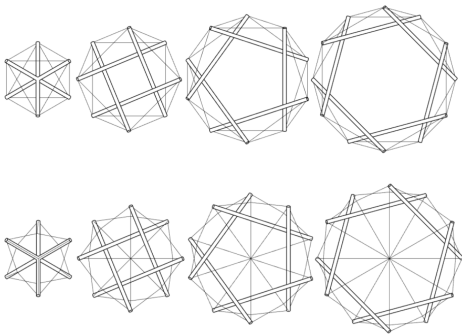


Figure 3. Replacing the edges with components meeting at the centroid in elementary tensegrity modules.

4.3 Newly Added Component

The new centroid component which will be called a “node” in this study, keeps the stability of the module with keeping the net forces constant while providing the opportunity to engage the tensile surface with the compressive components of the adjacent module. Replacing the eight triangular tensile surfaces of the old module, with the new pattern results in the same number of tensile components plus eight nodes. Figure 4 shows these nodes in the evolved icosahedron module.

Further experiments were performed to study the expandability of the new icosahedron module by placing the

modules adjacent to one another. As Figures 5 and 6 represent, the newly added “node” component helps to connect the compressive components of one module to the nodes of an adjacent module. Although it cannot produce a free-form tensegrity surface or grid, it creates an expandable system using independent tensegrity blocks or modules. While most of the research performed on the expansion of tensegrity structures, including the studies by Pugh [11] focus on the expansion of one module or finding new patterns using complicated calculations, the expansion patterns in those studies create interdependent modules, meaning that the structure would not be stable until all compressive and tensile components are placed. The method offered in this study using nodes will eliminate the need for dependent modules. Each module can be constructed separately and be combined with the adjacent modules for further expansion using the appropriate joints and construction details. This characteristic helps to overcome one of the most common problems of tensegrity structures which is the complexity of expanded system design. Using the proposed method, the modules can be prefabricated and then combined at the location.

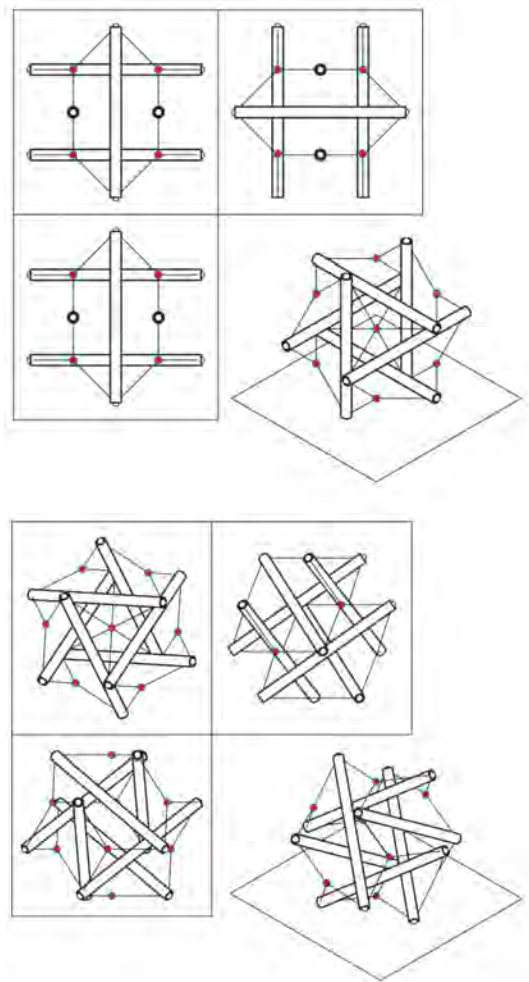


Figure 4. The newly added “node” component (highlighted in red) in the icosahedron module from different views.

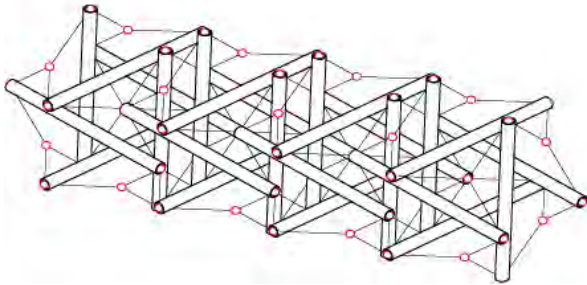
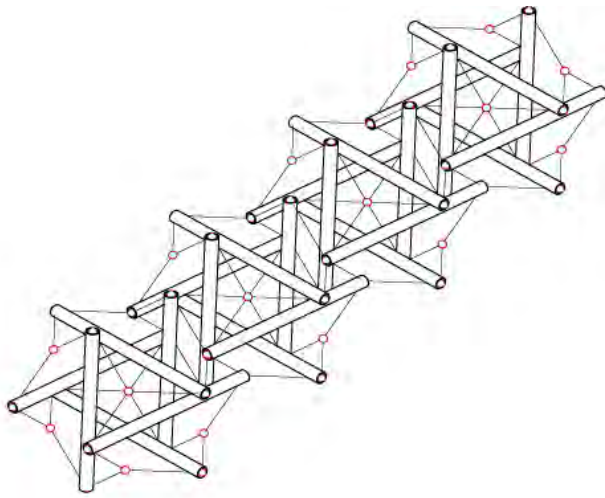


Figure 5. The expanded icosahedron module. The nodes of each module are connected to the struts of the adjacent module.

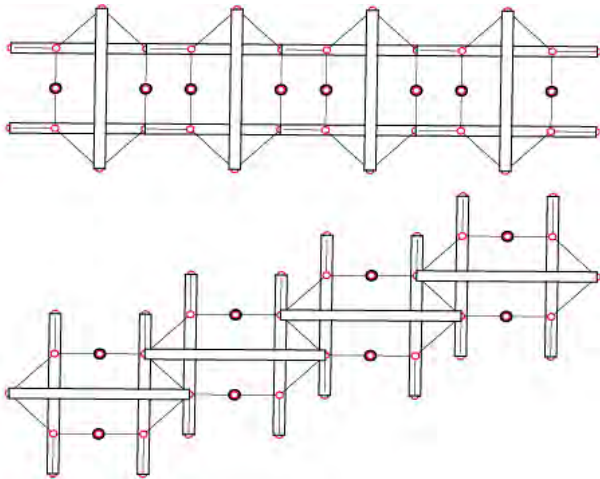


Figure 6. Linear expansion of the icosahedron module, a) front view. b) plan view.

The same changes are applicable to other circuit-pattern modules introduced by Pugh [11]. If the old tensegrity components are replaced with the new ones plus the node, the modules could be expanded. Figure 7 represents the changes in some circuit-pattern modules. The evolved modules can possibly be expanded to linear forms or grids with the addition of the nodes (Figures 8 and 9).

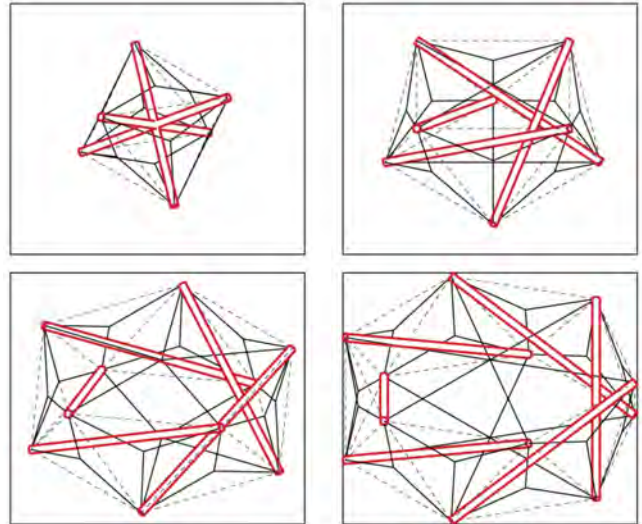


Figure 7. Evolving circuit-pattern modules with the addition of nodes.

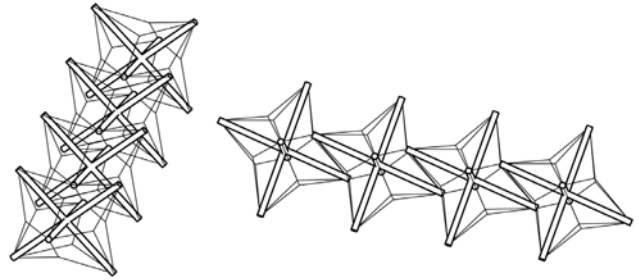


Figure 8. Linear expansion of a simple evolved module.

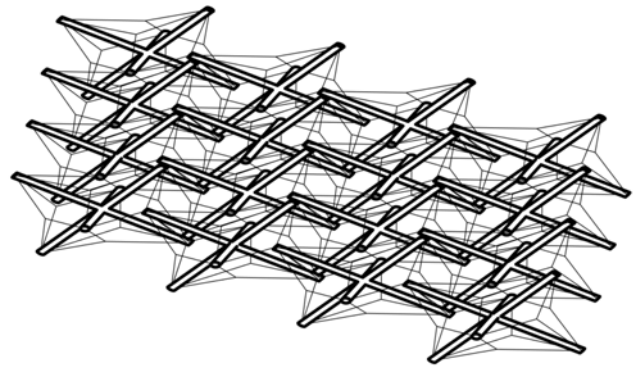


Figure 9. Expansion of a simple evolved module to a tensegrity grid with the addition of nodes.

5 SIMULATING THE PERFORMANCE

5.1 Analyzing Tension

After the experiments to design a new system for expanding tensegrity modules with adding new “node” components, the new system is simulated to verify the stability and to identify the variables impacting the form and design of the new grids. Tensegrity structures are geometrically nonlinear. Therefore, when the structure is reached to a stable configuration,

identifying the length of compressive components and the tension in the tensile components allow controlling the stress level of the structure [15]. Kangaroo physics engine was used as the tool for simulating the tensions and formation of the evolved grid. Kangaroo is an interactive simulation engine used for form-finding, optimization, and solving constraints. In the expansion methods studied in the literature review, the stability of the entire system is dependent on every single compressive and tensile element. Therefore, the tensegrity system would not be stable until all components are in place. The objective of simulations performed in this study aims at finding out whether independent self-stable modules can also form a stable grid. A grid of evolved icosahedron modules was modeled to be tested in terms of stability and formation. Three sets of simulations were defined, and various pretension indexes were applied to each set of experiment. In the first two sets, the grid is considered as a covering structure similar to a roof, and in the third set, the grid is considered as a dividing structure such as a wall.

In the first set of experiments, the grid was set to be hanging from four supports on the corners of the grid. Simulations were performed with tension indexes ranging from 0.0 to 1.0. Figure 10 represents the form of the grid relative to each index.

In the next set of experiments, the same grid was defined and tested with the pretension indexes ranging from 0.0 to 1.0. This time, the supports were increased to all compressive components on the edges of the grid. Figure 11 shows the form of the grid after applying each pretension index.

In the last set of simulations, the same grid was placed vertically on the ground, with all compressive components touching the ground acting as supports. Similar to previous experiments, pretension indexes of 0.0 to 1.0 were applied to the grid (Figure 12). The observations in this set of simulations conclude that when the supports are placed on the ground, the pretension variable does not have significant impacts on the form of the evolved grid.

5.2 Utilization and Displacement Analysis

In order to understand how independent modules react in the grid in terms of loads and stress, simulations have been performed using Karamba 3D. Karamba 3D is a structural analysis tool that analyzes the spatial frames and trusses. The same grid used as a dividing structure was also used in this simulation. The grid was analyzed in terms of displacement and utilization to identify whether the independent modules can tolerate the loads and stress of the adjacent modules. Figure 13 represents the displacement values of the vertical grid. Displacement shows how much the components are moved under loads. The utilization factor is shown in Figure 14. Utilization represents the stress of the elements under the loading. Based on the observations, the grid of independent modules tested in this experiment shows large values of displacement while it does not show risky values of utilization, making the independent modules form a stable grid.

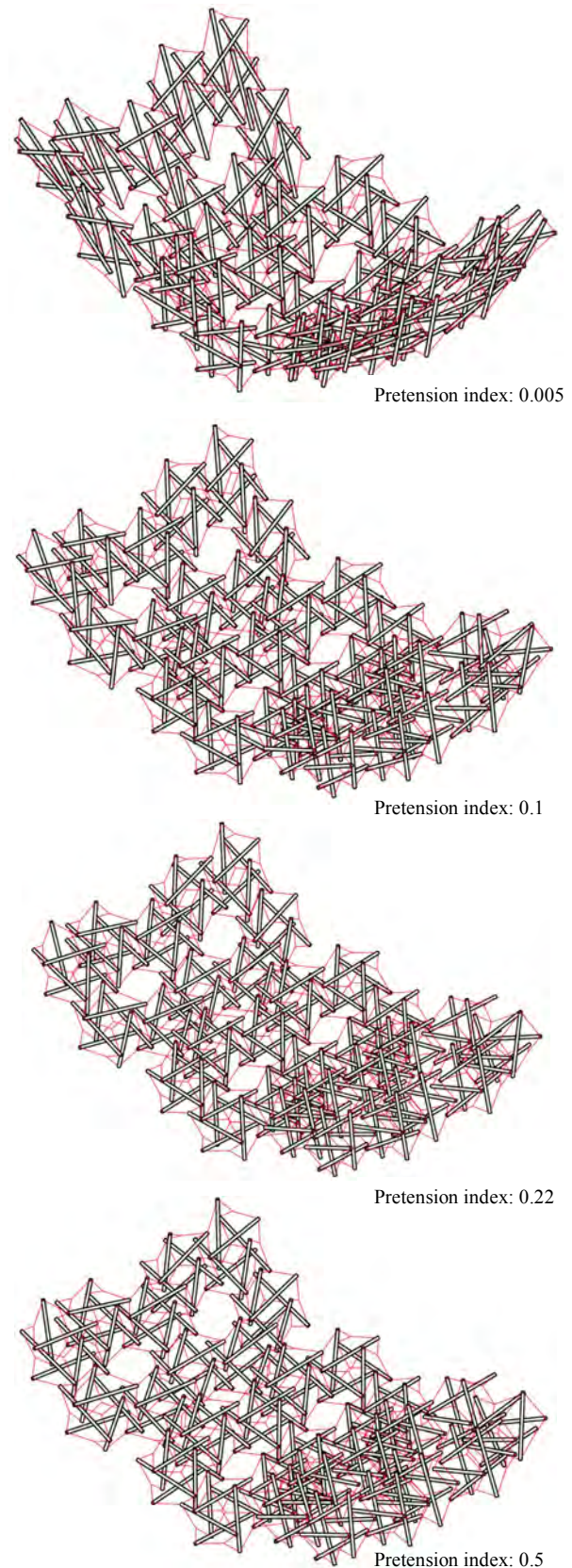


Figure 10. Analyzing tension with the grid hanging from four supports.

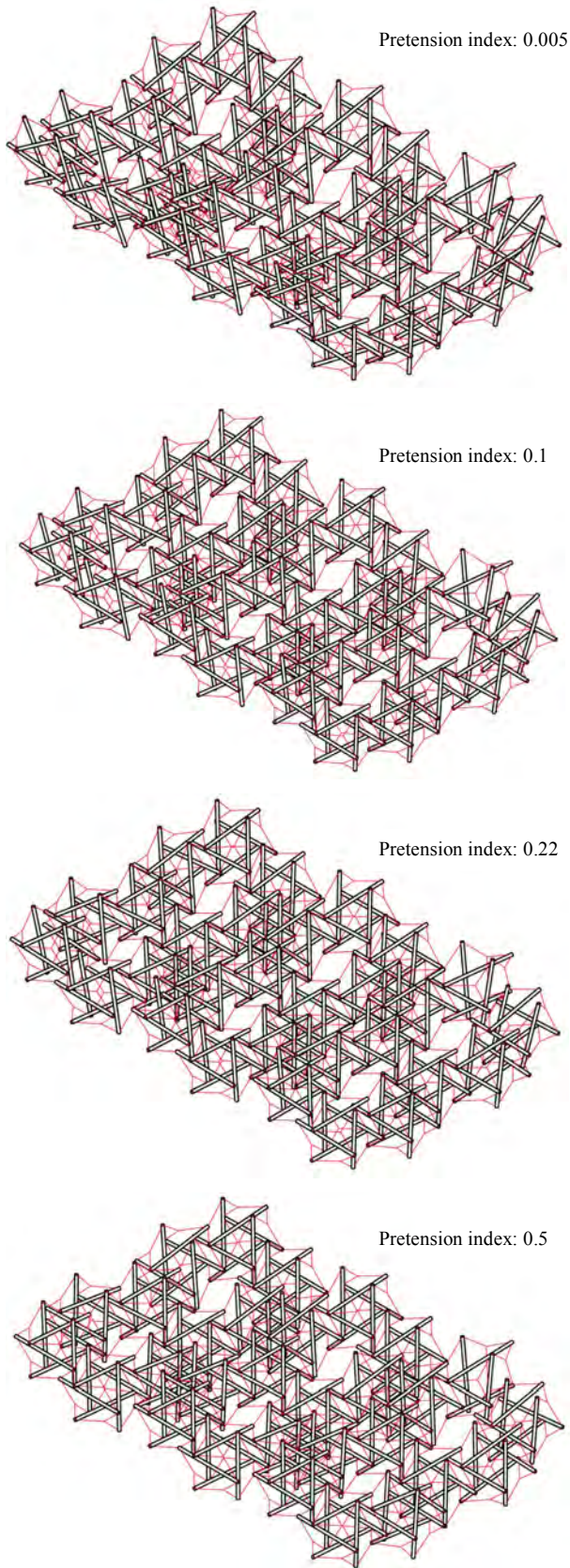


Figure 11. Analyzing tension with the grid hanging from supports across the edges of the grid.

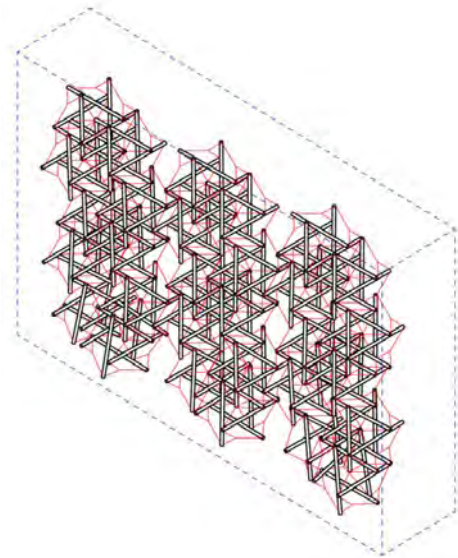


Figure 12. Analyzing the tension of the vertical grid with ground supports.

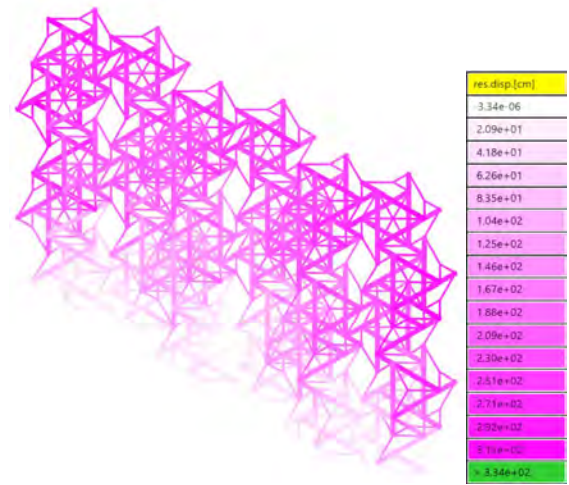


Figure 13. Displacement analysis of the vertical grid.

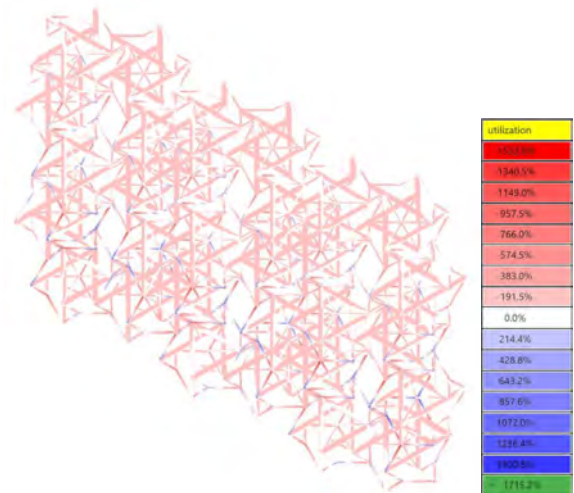


Figure 14. Utilization analysis of the vertical grid.

6 DISCUSSION AND CONCLUSION

Tensegrity structures have been around for decades. However, the use of tensegrity structures is not common, especially in architecture and civil engineering. While there have been many studies on the optimization of tensegrity structures, limited research has been performed on their modularization. Unlike common methods of expanding tensegrity structures which involves every single component, the method proposed in this research consists of independent modules expanded using a new component called "node". Adding a node at the centroid of the tensile surfaces in tensegrity modules provides the opportunity to combine adjacent independent modules while maintaining compliance with the common definition of tensegrity structures. To verify the stability of structures in the proposed method, simulations have been performed to analyze the tension, displacement, and utilization of the modules. The variables involved in the formation of the grids are the pretension index in the tensile components and number of supports. With adjusting the number of supports and the pretension index of the tensile components, the form of the grid can be controlled. Displacement analysis shows large displacements values, specifically for the modules that are located further from the supports, which demonstrates the need for more control of the displaced independent modules when they are located far from the supports. Utilization analysis represents that the simulated grid, does not show risky stress values.

7 FUTURE WORK

Further research is needed to analyze the behavior of the modules when the variables such as tension and support are controlled independently for each individual module. With designing a more advanced simulation system in which the modules are simulated independently, a new method of form-finding could be established for the expanded grids. With controlling the variables involved in the formation of the grid, different forms of desired surfaces might be developed (Figure 15). This would help to enhance the use cases of tensegrity structures in architecture and civil engineering. Additionally, a more inclusive study is needed to analyze grids created from other types of tensegrity modules. The simulations in the current study are limited to the icosahedron module.

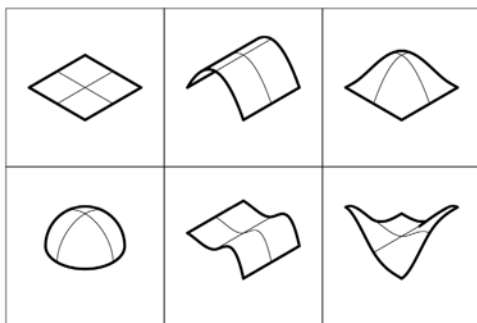


Figure 15. Possible forms of tensegrity grids by controlling the structural variables

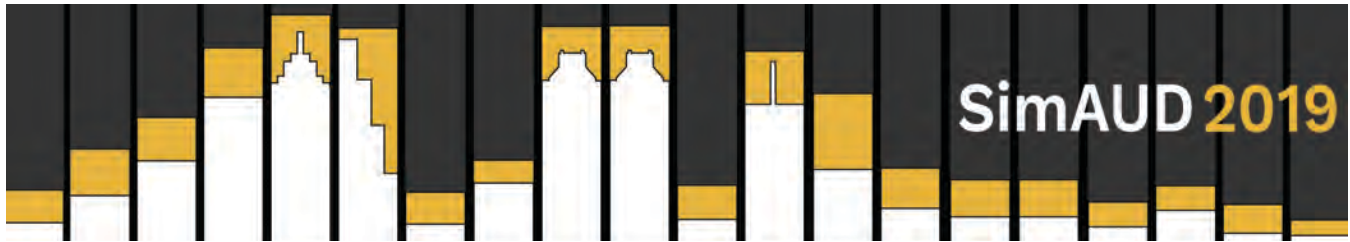
ACKNOWLEDGMENTS

The Authors wish to express their gratitude to Hadi Teimouri, Hooman Amin, Hossein Falahati, and Niloofar Hosseini for their contributions in the initial phases of this research. The authors also sincerely thank Dr. Mahdi Saedvandi, Assistant Professor of Architecture at the Art University of Isfahan, for his support in this project.

REFERENCES

1. Barnes, Michael R. "Form Finding and Analysis of Tension Structures by Dynamic Relaxation." *International Journal of Space Structures* 14, no. 2 (1999): 89-104. doi:10.1260/0266351991494722.
2. Fuller, Richard Buckminster. *Synergetics: Explorations in the Geometry of Thinking*. New York: Macmillan, 1982.
3. Juan, Sergi Hernández, and Josep M. Mirats Tur. "Tensegrity Frameworks: Static Analysis Review." *Mechanism and Machine Theory* 43, no. 7 (2008): 859-81. doi:10.1016/j.mechmachtheory.2007.06.010.
4. Kebiche, K., M.n. Kazi-Aoual, and R. Motro. "Geometrical Non-linear Analysis of Tensegrity Systems." *Engineering Structures* 21, no. 9 (1999): 864-76. doi:10.1016/s0141-0296(98)00014-5.
5. Masic, Milenko, Robert E. Skelton, and Philip E. Gill. "Optimization of Tensegrity Structures." *International Journal of Solids and Structures* 43, no. 16 (2006): 4687-703. doi:10.1016/j.ijsolstr.2005.07.046.
6. Mirhosseini, Homeira, and Shane Ida Smith. "Socio-environmental Framework for Integration of Lightweight Tensile Structure Windcatchers in Contemporary Hot-arid Urban Context of Tehran." In *World Sustainable Built Environment Conference 2017 Hong Kong*, 1445-451. Proceedings. Hong Kong: Construction Industry Council, 2017.
7. Motro, R. "Tensegrity Systems: The State of the Art." *International Journal of Space Structures* 7, no. 2 (1992): 75-83. doi:10.1177/026635119200700201.
8. Paul, Chandana, Hod Lipson, and Francisco J. Valero Cuevas. "Evolutionary Form-finding of Tensegrity Structures." *Proceedings of the 2005 Conference on Genetic and Evolutionary Computation - GECCO 05*, 2005. doi:10.1145/1068009.1068011.
9. Pellegrino, S. *Mechanics of Kinematically Indeterminate Structures*. University of Cambridge, 1986.
10. Pellegrino, Sergio. "A class of tensegrity domes." *International Journal of Space Structures* 7, no. 2 (1992): 127-142.
11. Pugh, Anthony. *An Introduction to Tensegrity*. Berkeley, CA: University of California Press, 1976.
12. Rhode-Barbarigos, Landolf, Nizar Bel Hadj Ali, René Motro, and Ian F.c. Smith. "Designing Tensegrity Modules for Pedestrian Bridges." *Engineering*

- Structures* 32, no. 4 (2010): 1158-167.
doi:10.1016/j.engstruct.2009.12.042.
13. Skelton, Robert E., and Mauricio C. De. Oliveira.
Tensegrity Systems. Dordrecht: Springer, 2009.
14. Sultan, Cornel, Martin Corless, and Robert E. Skelton.
"Symmetrical reconfiguration of tensegrity structures."
International Journal of Solids and Structures 39, no. 8
(2002): 2215-2234.
15. Tibert, A.g., and S. Pellegrino. "Review of Form-
Finding Methods for Tensegrity Structures."
International Journal of Space Structures 26, no. 3
(2011): 241-55. doi:10.1260/0266-3511.26.3.241.
16. Vassart, N., and R. Motro. "Multiparametered
Formfinding Method: Application to Tensegrity
Systems." *International Journal of Space Structures* 14,
no. 2 (1999): 147-54. doi:10.1260/0266351991494768.



A Framework for Cost-Optimal Zero-Energy Lightweight Construction

Mohamed Amer and Shady Attia

SBD Lab, Faculty of Applied Sciences, Université de Liège
Liège, Belgium
{mohamed.amer, shady.attia}@uliege.be

ABSTRACT

During the last decade, several roof extensions took place in the European cities with the purpose to increase the height of existing buildings using timber as a lightweight material. However, building regulations and green codes do not usually guarantee the achievement of multi-objective and highly performance roof extensions. Accordingly, this research aims to develop a state of the art framework to achieve cost-optimal zero-energy for timber construction, specifically when building on rooftops. Through a simulated and calibrated passive house model, the boundary conditions of the study have been identified and further parametric simulation and optimization have been carried out.

This research aims at linking scientific research with practice. The framework provides a fast track measurement that provides a solutions space for building engineers who are in charge of decision making on the design and construction process. Best practices of roof construction could be achieved in terms of cost and energy, giving a vast potential for a complete and deep renovation, and, therefore, reducing the overall ecological footprint on the city level.

Author Keywords

Multi-criteria optimization; parametric simulation; roof stacking; urban densification; methodology.

ACM Classification Keywords

I.6.3 Applications; I.6.8 Types of Simulation;

1 INTRODUCTION

As stated by the European Commission, construction sector is responsible for more than 40% of the total energy consumption and 36% of the CO₂ emissions in Europe. Thus, building's energy performance has been put forward as a key element to achieve the European Union's (EU) targets for 2020 to reduce each of the Green House Gas (GHG) and primary energy savings by 20%. A safe way towards fighting climate change could be achieved through providing cost-effective and highly energy efficient buildings [8]. Achieving zero-energy buildings requires

using thick walls and insulations, which is accompanied in most cases with additional weight in construction [3]. For a conventional stick building, this does not represent a problem. However, when building on the rooftops of existing buildings, the weight of the construction is considered a main issue, especially when using prefabricated components (off-site construction) methods, which are needed to be transported and lifted over the rooftop. Moreover, cost-optimal measure has been a big concern in the last decade. On 2010, the European Commission has produced the Energy Performance of Building Directive EPBD-recast, which made it possible to make informed choices that aim to help saving energy while increasing cost-effectiveness. Since then, several tools and methods have been proposed scientifically and practically to achieve zero-energy levels while maintaining cost-optimal targets. For instance, Georges et al. [6] examined a single-family houses in Belgium by investigating a combination of heating systems and building designs. Marszal and Heiselberg [9] aimed to find optimum life cycle cost measure for net-zero energy residential house in Denmark by examining three energy demand and supply systems. Hamdy et al. [7] carried out a multi-stage, multi-objective optimization that aims to achieve cost-optimal and nearly zero energy building solutions through optimizing building envelop, active system and onsite renewable energy resources respectively, followed by a sensitivity analysis for the escalation rates of energy prices and their effect on the overall optimization results.

However, none of those methods or tools has been dedicated to include additional parameters concerned with using lightweight materials in construction. Accordingly, in this study, we propose a framework that aim to achieve cost-optimal lightweight construction for roof stacking. By bringing building performance simulation and parametric design tools, optimizing building's energy and cost performance could be achieved, while providing a space of solutions for lightweight building envelope sections, which is more likely to be preferred by the designers generally and architects specifically.

2 METHODOLOGY

The methodology consists of four stages as shown in Figure 1. First, reference model has been selected. Second, boundary conditions are identified. Third, the reference model is simulated, calibrated and adjusted to represent a typical roof-stacking model in Brussels Capital Region in Belgium. In the last stage, a multi-criteria optimization is conducted and a space of nearly optimal solutions for building envelope measures are identified taking in consideration the identification of the specification and area of renewable energies to reach zero energy levels.

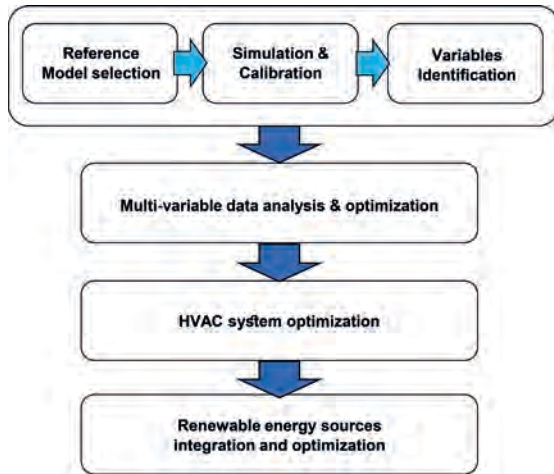


Figure 1. Framework for cost-optimal lightweight construction

2.1 Reference Model Selection

Given the shortage in the information available on roof stacking, a reference model for a full passive house has been used in this research. Several constrains have been set up for the selection of the reference model to ensure a maximum compatibility with the required roof stacking model. First, the selection of a passive house reference model has been set up as a prerequisite. The reason behind choosing a passive house reference model returns back to the requirement of the local regulations of Brussels Capital Region, which state that as of 2015, all new construction should comply the passive house standard requirements. Second, the usage of lightweight materials represents one of the main objectives of this study. Given that timber is considered a promising building material that satisfies the lightweight aspect, a reference model built in timber has been set for the selection criteria. Third, the reference model has to lie within the same climatic region of the case study, which is 5b climate zone according to ASHRAE classification.

A passive house reference model has been selected to meet the aforementioned constrains of selection. The specifications and measurements of the passive house reference model has been found in a cluster of 22 passive house built in Hannover-Kronsberg in Germany which is published by the Passivhaus institute [5]. The layout of the passive house reference model has been adjusted to match the layout and dimensions of the roof stacking case study in Brussels according to earlier studies [1,2,4].

2.2 Modeling, Simulation and Calibration

The modelling process has been carried out using Grasshopper parametric tool integrated in Rhinoceros 3D software. As for the simulation, Ladybug and Honeybee plugins have been used [10]. Ladybug tools have been used to load weather files and generate primary climate analysis, which is integrated with Honeybee tools that works as an interface for OpenStudio simulation software and EnergyPlus simulation engine. Honeybee is responsible of generating thermal zones and energy simulations. Lastly, Colibri plugin has been used to parametrically run the simulations and exporting results to Excel files.

The calibration process has been carried out in accordance with the monthly average monitored heating loads. Two indices are used to assess the *goodness-of-fit* of the building energy model: the Mean Bias Error (MBE) as shown in equation (1), and the Coefficient of Variation of the Root Mean Square Error (CV (RMSE)) as shown in equation (2).

$$MBE = \frac{\sum_{i=1}^{Np} (m_i - s_i)}{\sum_{i=1}^{Np} m_i} \quad [\%] \quad (1)$$

$$CV (RMSE) = \sqrt{\frac{\sum_{i=1}^{Np} (m_i - s_i)^2}{Np}} \quad [\%] \quad (2)$$

where m_i : ($i = 1, 2, \dots, Np$) represents measured data points, and s_i : ($i = 1, 2, \dots, Np$) represents simulated data points. According to ASHRAE guidelines 14-2002 and 2014, a maximum value of 5% is required for MBE when monthly data points are calibrated and a maximum value of 10% when hourly data points are calibrated. Whereas for CV (RMSE), the maximum value of 15% is required when monthly data points are calibrated and maximum value of 30% when hourly data points are calibrated. In this study, the values of each of MBE and CV (RMSE) have met 2.1% and 7.3% respectively. The MBE is a non-dimensional measure of the overall bias error between the measured and simulated data in a known time resolution, and it is usually expressed as a percentage. Whereas RMSD represents the sample standard deviation of the differences between predicted values and observed ones. The RMSD serves to aggregate the magnitudes of the errors in predictions for various times into a single measure of predictive power.

Occupancy and operational schedules of windows have been hypothetically estimated based on the best practice, and then set as a variable to meet the calibration thresholds on one hand. On the other hand, indoor temperatures have been considered in the calibration process. According to the monitored indoor temperature of the passive house reference model, an average temperature of 20.9°C has been found even during the coldest days. Thus, during calibration, the same average indoor temperature has been maintained while ensuring the required ratio of goodness-of-fit values.

2.3 Boundary Conditions

Boundary conditions have been identified under four categories. The first category identifies fixed parameters represented by the weather file, layout, occupancy and operation schedules. The second, third and fourth categories identifies each of the variable measures of the building envelope, HVAC and renewable energy system respectively.

First, the weather file of Brussels city has been used. The layout of the case study has been identified according to the middle-class housing typology, which represents more than 75% of the housing typologies in Brussels. The layout is exposed to the North-South orientation, whereas the East-West facades are directly attached to neighboring houses (non-exposed surfaces). Occupancy and operational schedules are left the same to those have been used in the calibration process of the passive house reference model.

On the building envelope level, 6 items are given several variables. Starting with a construction type, two different timber construction types are examined: Timber framing and Cross Laminated Timber (CLT). A layer of insulation is added to the timber, in which four different types are examined: EPS, Cellulose, Mineral Wool and Wood Fiber. The thickness of the insulation ranges between 20cm and 40cm with 4cm uniform step. The variations of the insulation type and thickness had a maximum U-value of $0.15 \text{ W/m}^2\cdot\text{K}$, to comply with passive house standards, and minimum U-value of $0.095 \text{ W/m}^2\cdot\text{K}$. The U-value of the floor slab has been set to $0.125 \text{ W/m}^2\cdot\text{K}$ and not been considered in the parametric simulation. The air tightness of the building has been keep the same of the reference building in order to comply with Passive House standard level, which requires a value of 0.6 air changes per hour for 50 Pascal pressure. The window has a U-value of $0.6 \text{ W/m}^2\cdot\text{K}$ (which complies passive house standard requirement of a maximum U-value $0.8 \text{ W/m}^2\cdot\text{K}$ and g-value 50% for glazing surfaces). However, Window to Wall Ratio (WWR) varies between 10% up to 90%. Two different shading types are examined: interior venetian blinds and exterior shading rollers.

On the HVAC level, a heat pump has been used for heating and cooling purposes, in addition to a ventilation system with heat recovery. The variations have been given to the heat recovery effectiveness, which ranges from 70% to 90%, and the Coefficient of Performance (COP) of the heat pump, which ranges from 2 to 5. Finally, on the renewable energy level, each of a multi-crystalline silicon Photovoltaic (PV) panels and solar thermal system are examined. PV panels' area ranges from $0 - 50 \text{ m}^2$, while solar heater system's area ranges from $0 - 20 \text{ m}^2$, with an efficiency of 20% for the PV panel and 70% for the solar heater.

2.4 Multi-Objective Optimization

This study proposes a bi-objective optimization approach that addresses energy savings and cost-optimality. The bi-objective optimization comprises the results of different weight of construction. In order to achieve results, the optimization process took place on three stages. On the first

stage, the 6 items of the building envelope are optimized, followed by the HVAC system, and finally renewable energy resources are added to ensure reaching zero energy targets while maintaining cost-optimality. Simulation and optimization have been conducted using Grasshopper with Honeybee plugin. Buildings materials' specifications have been obtained from the European timber materials database "Dataholz", whereas the equivalent prices for each building material, HVAC and renewable energy systems are provided by the Belgian database of construction works "Bordereau des Prix Unitaires".

3 RESULTS

In this paper, the primary results of the optimization process are presented. Parametric simulation has been conducted to generate over 600 attributions for the building envelope as shown in Figure 2.

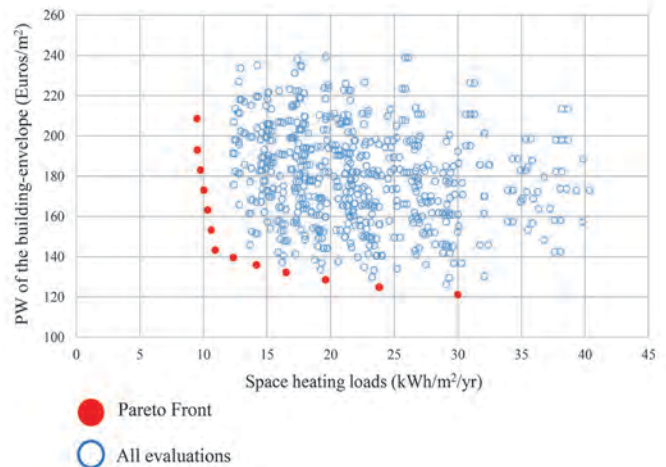


Figure 2. Multi-objective optimization for building envelope

In order to identify optimum results out of the generated attributions, MATLAB software has been used to generate Pareto Frontier (the attribution in red color). Pareto optimality frontier is the mathematical method that is used to identify optimum results giving two different objectives. Figure 3 shows a further step for bi-objective optimization. In this stage, the differences in Life Cycle Cost (LCC) have been considered instead of just initial cost. LCC takes in consideration initial, replacement, maintenance, and operational costs. Furthermore, the total energy consumption in terms of heating, cooling and fans (for heat pump and ventilation system) has been calculated. The results in Figure 3 are grouped into clusters according to their weight of construction. We found that the more weight added to the construction (that reaches up to 300 Kg/m^2), the better performance it achieves in terms of saving heating loads, and the less savings in terms of LCC. In contrary, the less weight of construction (less than 200 Kg/m^2) the more energy is consumed for heating and cooling. Hence, we found that by applying Pareto Front, we are able to choose optimum results, which represents a compromise between heavy and lightweight construction selections as shown in Figure 3.

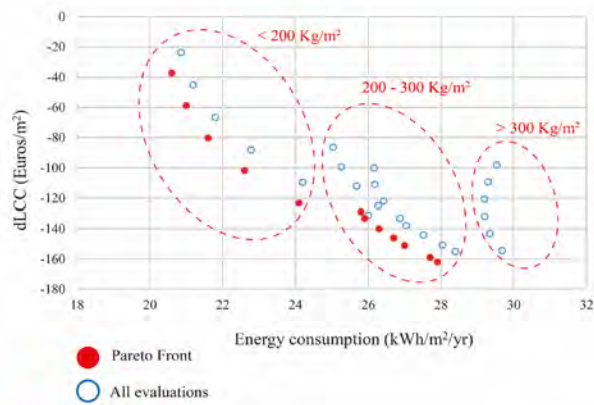


Figure 3. Cost-optimal measures for different sets of lightweight construction

CONCLUSION

This paper presents a framework that aims to achieve cost-optimal zero-energy lightweight construction. This paper is a part of research work that puts forward solutions to effectively increase the density of European cities through building on the rooftops of existing buildings.

We found that the more weight added to wall sections, the more energy efficient. However, within the space of solutions of the Pareto Front, energy efficient measures could be achieved with lightweight construction trading off with LCC values. While, construction that weights more than 300 kg/m² was not found to be selected in the optimization curve. The majority of the selected solutions were found in the intermediate zone, with construction that weights between 200 and 300 Kg/m², which is self-evident within the selection method of optimized results.

The results of this paper will be followed with optimizations for the heat pump and ventilation system. Moreover, electricity from photovoltaic panels and hot water from solar heaters will be integrated in the optimized solutions. The overall weight of the panels on the rooftop will be added and possible savings in the operational costs will be calculated within the whole Life Cycle Cost of the building.

ACKNOWLEDGMENTS

This research was funded by a welcome grant provided by Liège University, which is gratefully acknowledged. We would like to acknowledge the Sustainable Building Design (SBD) Lab for the access to dataset and the use of monitoring equipment in this research and the valuable support during the experiments and the analysis of data.

REFERENCES

1. Amer, M., Mustafa, A., Teller, J., Attia, S., and Reiter, S. A methodology to determine the potential of urban densification through roof stacking. *Sustainable Cities and Society*, 35, Supplement C (2017), 677–691.
2. Amer, M., Reiter, S., and Attia, S. Urban Densification through Roof Stacking: Case Study. In *European Network for Housing Research (ENHR) Annual Conference 2018*. Uppsala University, Uppsala, Sweden, 2018.
3. Attia, S. *Net Zero Energy Buildings (NZEB): Concepts, Frameworks and Roadmap for Project Analysis and Implementation*. Elsevier, 2018.
4. Dessouroux, C., Bensliman, R., Bernard, N., et al. *Note de synthèse BSI. Le logement à Bruxelles: diagnostic et enjeux*. Brussels Studies Institute, 2016.
5. Feist, W., Peper, S., and Von Oesen, M. *Klimaneutrale Passivhaus- Reihenhausiedlung Hannover-Kronsberg*. Passivhaus Institut, Hannover, Germany, 2001.
6. Georges, L., Massart, C., Van Moeseke, G., and De Herde, A. Environmental and economic performance of heating systems for energy-efficient dwellings: Case of passive and low-energy single-family houses. *Energy Policy*, 40, (2012), 452–464.
7. Hamdy, M., Hasan, A., and Siren, K. A multi-stage optimization method for cost-optimal and nearly-zero-energy building solutions in line with the EPBD-recast 2010. *Energy and Buildings*, 56, Supplement C (2013), 189–203.
8. Knoop, K. and Lechtenböhmer, S. The potential for energy efficiency in the EU Member States – A comparison of studies. *Renewable and Sustainable Energy Reviews*, 68, (2017), 1097–1105.
9. Marszal, A.J. and Heiselberg, P. Life cycle cost analysis of a multi-storey residential Net Zero Energy Building in Denmark. *Energy*, 36, 9 (2011), 5600–5609.
10. Sadeghipour Roudsari, M. and Pak, M. Ladybug: A Parametric Environmental Plugin for Grasshopper to Help Designers Create an Environmentally-Conscious Design. In *Proceedings of BS2013: 13th Conference of International Building Performance Simulation Association, Chambéry, France, August 26-28*. Chambéry, France, 2013.

Design Decision Models

An Automated Framework Creating Parametric BIM from GIS Data to Support
Design Decisions 245

Chengde Wu, Saied Zarrinmehr, Mohammad Rahmani Asl and Mark J. Clayton

Digital Energy Performance Signature Extensible Markup Language (DEPSxml):
Towards a New Characterization Framework for Sharing Simulation and Measured
Data on Building Design and Energy Performance 253

Justin McCarty and Adam Rysanek

From Optimization to Performance-Informed Design 261

Thomas Wortmann and Thomas Schroepfer

Linear and Classification Learner Models for Building Energy Predictions and
Predicting Saving Estimations 269

Kevin Eaton, Nabil Nassif, Pyria Rai and Alexander Rodrigues



An Automated Framework Creating Parametric BIM from GIS Data to Support Design Decisions

Chengde Wu¹, Saied Zarrinmehr², Mohammad Rahmani Asl³ and Mark J. Clayton²

¹UNC Charlotte
Charlotte, USA
chdwu22@gmail.com

²Dassault Systems
Denver, USA
szarinmehr@gmail.com

³Autodesk
San Francisco, USA
mrahmaniasl@gmail.com

⁴Texas A&M Univ.
College Station, USA
mark-clayton@tamu.edu

ABSTRACT

GIS has been primarily used for urban scale projects. On the other hand, BIM has been mainly used for building scale projects. Understanding surrounding site context is essential in building design. Thus, architects often utilize GIS data to build 3D digital and physical models of the surrounding urban/natural context to help them make better design decisions. The primary challenge of building 3D models from GIS data is that the modeling process requires tremendous load of manual work due to the fact that the data scheme used in GIS is not directly compatible with the data scheme used in BIM. In this research, we analyzed the difference between GIS and BIM data schemes, formulated a data mapping protocol, devised algorithms to correctly convert 2D GIS data to 3D geometries in BIM, programed a software prototype that can automatically convert a model from GIS to BIM, and conducted pilot tests of two different cities to verify the validity of the overall framework. This automated system greatly reduced the modeling time, manual workload, and potential manmade errors. It is expected to facilitate architects in rapidly creating 3D models and study the surrounding urban/natural context.

Author Keywords

BIM; GIS; Interoperability; Parametric BIM; Semantic Mapping.

ACM Classification Keywords

Spatial-temporal systems; Interoperability;

1 INTRODUCTION

Urban planners and architects both use advanced information technologies for documentation and analysis. However, the two disciplines use very different technologies. Urban planners often use Geographic Information System (GIS) while architects increasingly use Building Information Modeling (BIM). Although GIS holds information that is important for architects and urban designers, it is not an ideal tool for architects in modeling aspect. Since BIM authorization tools are more suited for architectural design,

there is a demand for the exchange of data between GIS and BIM.

Mapping GIS to BIM requires understanding the similarities and differences between the two data schemes. Both GIS and BIM have evolved from Computer Aided Design (CAD) system which was originally a drafting technology. CAD files primarily consist of vectors, associated line types, and layer identifications. The early development in CAD systems associated blocks of data and text to the CAD files. The advent of 3D modeling turned the focus from drawings and 3D images to the data itself [7]. GIS and BIM went through different processes in their transition from drafting technology to information modeling tools.

BIM is an object-based data scheme and each of its object classes is a representation of one type of building component [16]. BIM defines relations among objects, so that when one object is modified, its dependent objects will automatically change. BIM allows the designers to add their domain-specific data to the single shared model, reducing or eliminating inconsistencies among input files to various analytic and simulation tools [4]. According to other definitions, spatial modeling with quantity takeoff, construction scheduling and cost estimating are also the features of BIM. In short, BIM can be defined as shared digital repositories, rich 3D geometric and non-geometric models, design platforms, simulation environment, and collaborative and performance-based design processes.

GIS employs two different data schemes which are either object-based or relational (i.e. layer-based). As a relational database, GIS overlays various layers of data using a common spatial coordinate system. Relational GIS includes mechanisms for (1) inputting data from maps, aerial photos, satellites, surveys, and other sources; (2) storing, retrieving, and querying data; (3) translating, analyzing, and modeling data [9]. GIS data can include geographic and environmental regions, such as those relating to ecology, Municipality jurisdiction boundaries, drainage, and other natural and man-made structures. Layer-based GIS includes a relational

database in which CAD drawings are associated with the tabular information.

Unlike layer-based GIS, object-based GIS uses 3D objects to represent the built environment. City Geographic Markup Language (CityGML) is an example of object-based GIS that uses XML to encode the representation, storage, and exchange of virtual 3D city and landscape models [5]. Similar to BIM, CityGML suggests an object-based data scheme to describe the geometry, topology, and semantics of 3D objects [15]. Object-based GIS uses a hierarchical structure for nesting 3D objects into each other. Each object at this hierarchical data structure represents a Level of Detail (LOD). The concept of LOD is central to object-based GIS and is employed for efficient visualization, data integration, application requirements, and data capturing methods [10]. While the significance of LODs for 3D city modeling is widely acknowledged, there is not a generally accepted definition among practitioners, standards, and institutions. Biljecki et al. [3] have discussed the need for a formalized definition for LODs and suggested ten different levels of details for city models. 3D objects in CityGML are defined at five different LODs [14].

CityGML is focused on creating a data repository when different levels of details are available. At building and urban design phases, the high LODs are not available and the focus is at the generation of data (i.e. design process). QUASY (Quartierdaten-Managementsystem) offers object model of buildings that can be changed easily. This building model parametrically stores the non-geometrical attributes of buildings. The building model of QUASY aggregates different variants, each of them containing a complete geometrical and semantical model of the building part. Variants, which are an essential part of QUASY, are very similar to LODs in CityGML. According to the focus of QUASY to design, variants in QUASY describe different planning states of temporal situations of the buildings [2].

At early stages of the planning, layer-based GIS data is often a major source to access important geometric and non-geometric building information, from site topography, block and parcel information, building footprints, land use, and zoning codes, etc. Many of the design decisions can be based on the information that is available in GIS. The design process includes making several decisions to generate solutions and possibly changing them to find the best alternatives. Neither object-based GIS nor layer-based GIS is specialized for design process at building scale.

In this research, we analyzed the difference between GIS and BIM data schemes, formulated a data mapping protocol, devised algorithms to correctly convert 2D GIS data to 3D geometries in BIM, programmed a software prototype that can automatically convert a model from GIS to BIM, and conducted pilot tests of two different cities to verify the validity of the overall framework. This automated system greatly reduced the modeling time, manual workload, and

potential manmade errors. It is expected to facilitate architects in rapidly building 3D models and study the surrounding urban/natural context.

2 INTEROPERABILITY BETWEEN GIS AND BIM

Data interoperability is widely accepted to be one of the main challenges for system integration. In an integrated system, the data generated by any party must be properly interpreted by all other parties with consistent protocols and languages [19]. The BIM implementation has the advantages of 3D representing building geometries, preserving spatial hierarchy and rich semantics of BIM, evolving and updating the geospatial models based on interventions on the current states of BIM, query of indoor geometry, and clear space subdivisions. BIM also includes hosting relationships between building objects and has different classes to represent the object types compared to GIS [11,12].

To create an interoperable framework between GIS and BIM two main challenges should be addressed: geometric translation and semantics mapping. 3D building objects can be represented using Constructive Solid Geometry (CSG) or Boundary Representation (BRep). CSG method utilizes Boolean operation of simpler objects to create a complex geometry. On the other hand, the BRep method presents shapes using limits (boundaries). Semantic of an object type is a complex concept that refers to the types of building objects. It encapsulates information about the geometry type, behaviors and parametric relationships of instances of that building object. While there are different flexible methods to geometrically represent an object, the semantics of an object determines its functionality. An interoperable system between BIM and GIS should inherently include a mechanism for semantic mapping and geometric translation. Nagel et al. have discussed that the reconstruction of BIM from uninterpreted 3D models sets the bar very high for an automated interpretation process because it demands exploring numerous possibilities that may exist [18]. Their study shows that to reconstruct IFC or CityGML from 3D models, the semantic mapping is easier when there are non-geometric concepts attached to the pure geometric objects. CityGML was the preferred GIS model because its object-based data scheme closely resembles BIM. At early stages of the design phase, when the design process starts, object-based GIS data does not exist. Even when the object-based GIS data is available, in building renovation scenarios building objects will be replaced. If object-based GIS data is going to be used without the building scale details, the LOD of the data would be as low as layer-based GIS data.

3 TRANSLATION FRAMEWORK

3.1 Data Schemes and Mapping

ArcGIS (a GIS application developed by ESRI) shapefiles use feature classes to represent homogeneous collections of spatial data. Each feature class has a common set of attribute columns to which new fields of information (i.e. columns) can be added. Geometric objects are associated with a series of information in one row of the attribute table.

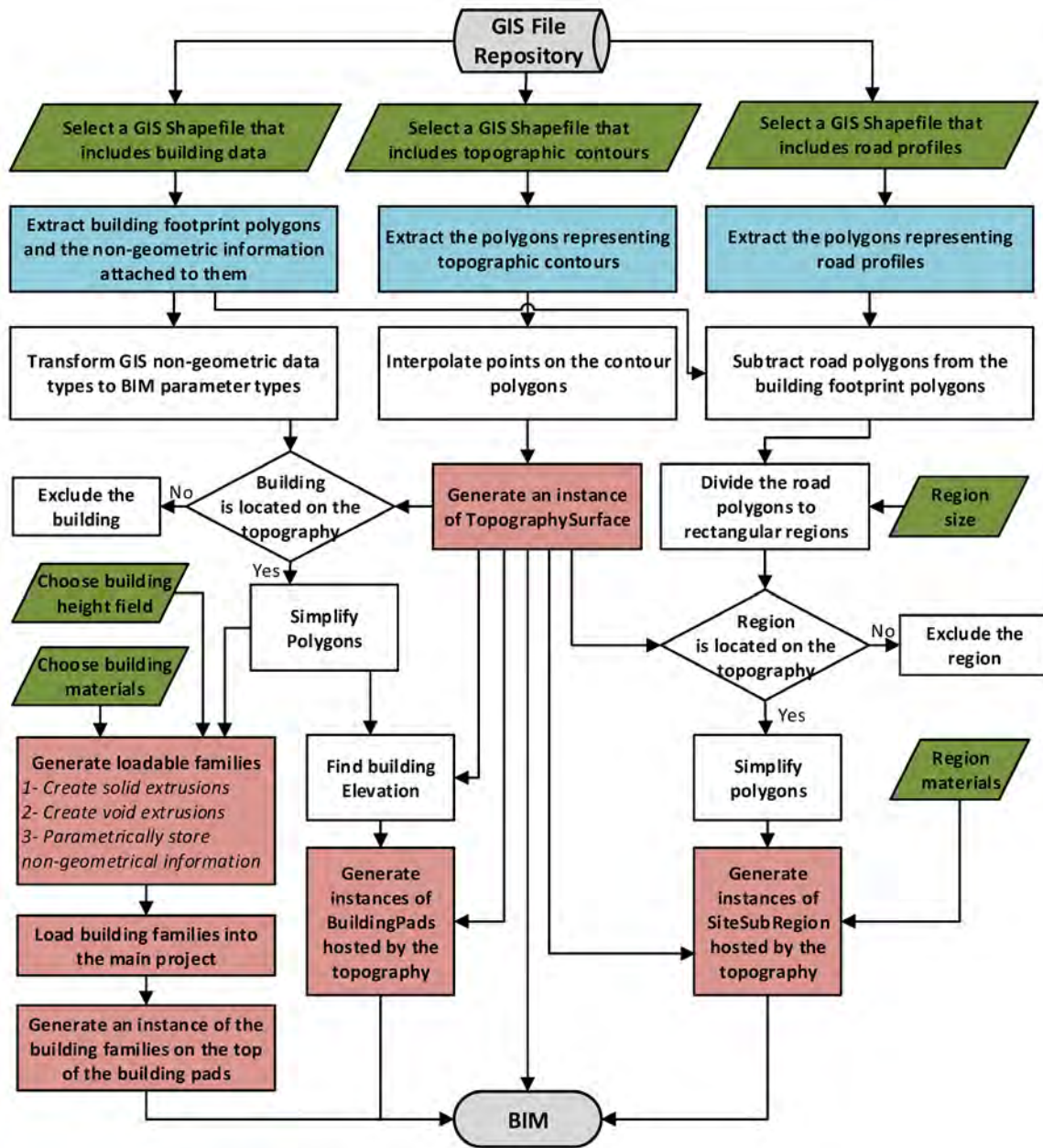


Figure 1. The process of translating GIS data to a BIM. The phases for inputting data are dark green. The tasks that use ArcGIS API libraries are blue and those that use Revit API libraries are red.

ArcGIS supports seven different feature classes including Points, Lines, Polygons, Annotation, Dimension, Multipoints, and Multipatches [8]. A building component type or family in Autodesk Revit is a group of elements with shared parameters and a related graphical representation [1]. Families are classes of building objects from which several instances can be created. Revit includes three types of families: system families, loadable families, and in-place families. System families define basic building element types such as walls, roofs, floors, and ducts. Loadable families are more complex types of building objects that are usually purchased, delivered and installed such as windows, doors, casework, fixtures, furniture. In-place families are used to

create unique building components. Families also have different categories, according to their industrial classification and behavior.

The use of GIS data in this paper is limited to polygon feature classes. Each polygon is a list of points that can be closed or open. In urban context polygons are often used to represent roads, topographic contours, parcels, blocks, and building footprints. In this study, GIS polygonal data will be translated to topography, roads and buildings in BIM. In Autodesk Revit roads and topography are represented with SiteSubRegion and TopographySurface classes which are system families. The geometry of SiteSubRegion and

TopographySurface objects are of mesh type. SiteSubRegion is hosted by the TopographySurface. Mass family is loadable and represents the volume of the buildings. BuildingPad class, which is a system family and hosted by the TopographySurface, creates a flat surface on the topography to locate mass instances. Geometrically, mass families can include CSG and BRep elements, BuildingPad family only include CSG elements, and SiteSubRegion and TopographySurface families only use BRep.

Figure 1 shows the translating process from GIS data to BIM. Various tasks in this process will be discussed in the following section. In this process, the user input tasks are colored in green. For example, choosing a GIS Shapefile of building information is the task assigned to the user. This process uses the Application Programming Interface (API) libraries of ArcGIS in Python language to extract information from the GIS files. The blue tasks of the process use the ArcGIS API library. The tasks with no color assigned process the extracted GIS information with a set of geometric algorithms to make it ready for BIM object creation. Finally, the processed information will be fed to the functions available in Revit API libraries to create BIM objects.

3.2 Non-Geometric Data Type Conversion

The non-geometric data types in polygon feature classes of ArcGIS shapefiles are different from the parameter types in Revit. In our suggested framework GIS data types are first converted to .NET data types and then translated to Revit parameter types. The diagram in figure 2 shows the data type mapping. The data types in this diagram do not cover all data types in GIS and Revit. For example, GIS does not include the information needed to create BIM materials which are complex non-geometric data types.

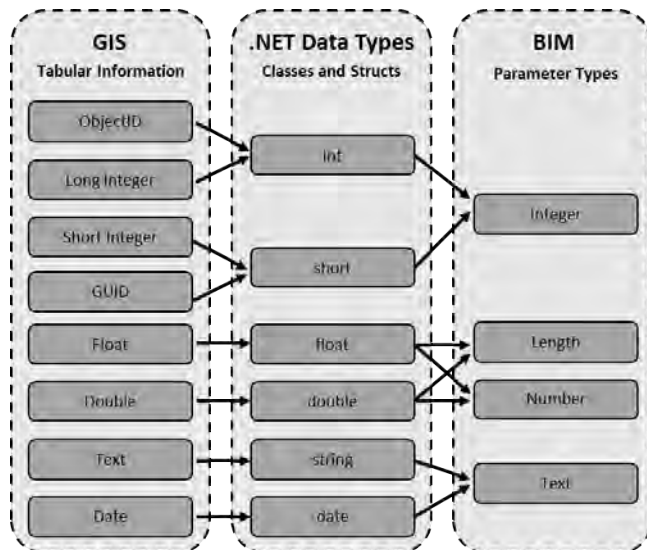


Figure 2. Mapping the non-geometric data types between ArcGIS shapefiles and Autodesk Revit.

3.3 Geometry Processing

Topography. GIS uses topographic contours for representing terrain features whereas Revit uses a Delaunay

triangulated mesh. Figure 3 shows that by interpolating the points on the GIS contours, a list of points can be created. The resulted points are stored in a .NET dictionary to filter out the duplicates with the time complexity order of 1 [17]. Finally, a topographic mesh can be created by feeding the point collection to a function in Revit API library.

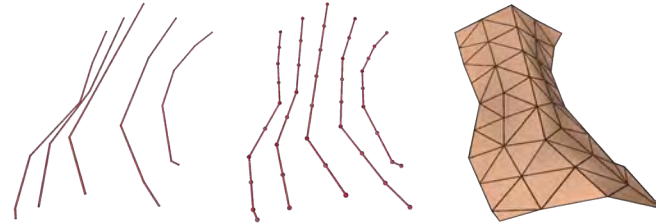


Figure 3. Triangulating the vertices of the topographic polygons which are directly extracted from GIS (Left) often fail to produce an instance of topography object in Revit. Generate topography mesh in Revit (right) using interpolated points (middle) can solve this problem.

Roads. Revit uses SiteSubRegion class to represent parts of the topography with different functionalities such as roads. SiteSubRegion objects should be hosted by the topography in Revit to prevent the intersections between the two. **Due to the inaccuracies in GIS data, intersections between the two types of objects are very common.** Therefore, geometric operations are needed between roads and building footprints.

The second challenge is that currently available polygonal Boolean solutions, including the “Clipper” library [13] which we used for our software solution, do not guarantee unifying polygons with common edges while offering unification solutions for polygons with overlapping areas. We used “shrinking and expanding” algorithm to remove the common polygon edges (figure 4).

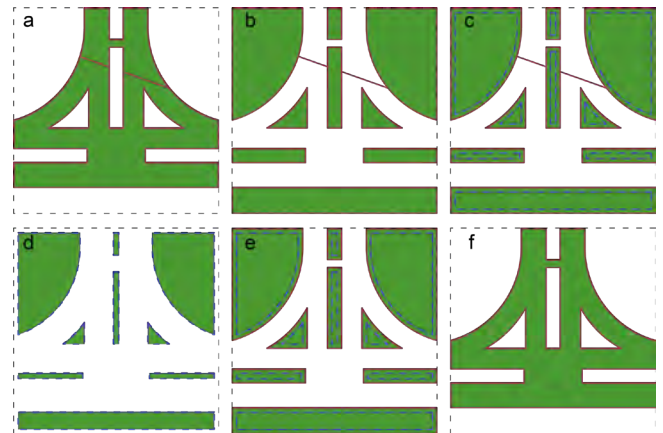


Figure 4. A series of Boolean operations to remove the common edges of some polygons. a) subtracting the regions from the cell. b) inverting the region. c) shrinking the region. d) removing the common edges. e) expanding the region. f) final road polygons.

The third challenge of using GIS data for creating BIM objects arises from the complexity of the shapes of GIS polygons. Revit prohibits the profiles (i.e. footprints) of SiteSubRegion, BuildingPads, and Mass families from

containing collinear line segments, consecutive edges with slight angle change, and edges that are smaller than 0.00256 inch. A shape simplification process which was inspired by Ramer-Douglas-Peucker algorithm [6] was developed to simplify GIS polygons. In this algorithm, the polygon points are stored in a binary heap which is sorted based on two criteria. First, the points that are closer than Revit's tolerance will be pushed to the top of the heap. The second criterion of sorting pushes the points according to the angles that they make with their neighbor(s) in a polygon. The algorithm will keep removing the first point at the top of the heap until the top point's distance and angle both gain significance. Since this mechanism uses a binary heap, the order of time complexity of shape simplification would be $n * \log_2(n)$. Figures 5-b to 5-d show how the complex shape shown in figure 5-a is simplified using this idea while preserving the original shape features.

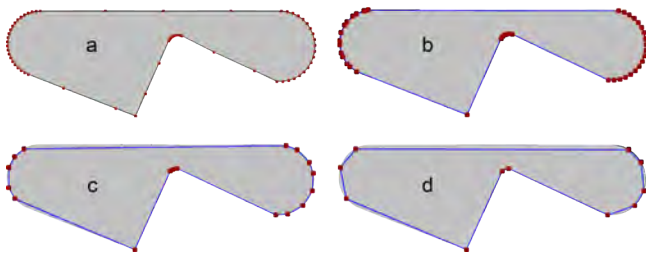


Figure 5. Shape angular simplification includes recursively finding the point with lowest angular significance, removing it and updating the polygon until it passes the angle tolerance.

Buildings. Loadable mass families are used to represent the volume of buildings. In Revit building pad objects are hosted by the topography and prepare flat surfaces for placing the building masses. Apart from a building footprint profile, a building pad also needs an elevation value to determine the vertical location of a building. *GIS data does not explicitly provide the elevation of the buildings.* The elevation of the buildings can be calculated by projecting the building footprints on to the topography. With the calculated building elevation and the building height information in the ArcGIS table, BuildingPads and building masses can be generated based on the projected building footprint polygons. If the “height” field is missing from the GIS table, a default value that is proportional to the footprint area is used to generate building masses. The height of the buildings then can be adjusted parametrically in Revit interface.

3.4 Software Prototype Implementation

A software prototype was developed based on the proposed translation framework. Figure 6 shows the user interface (UI) of the prototype. The user inputs are determined based on the translation framework presented in figure 1. It also shows that different fields of information, including building height, can be chosen from the attribute table of the building footprint Shapefile to be passed to the BIM. The UI also asks for additional information including the interpolation distance of the contours, the proximity tolerance of points on the contours, the desired cellular dimension of the sub-

regions, as well as other settings. Data mapping includes selecting ArcGIS Shapefiles and “height” field in the building table.

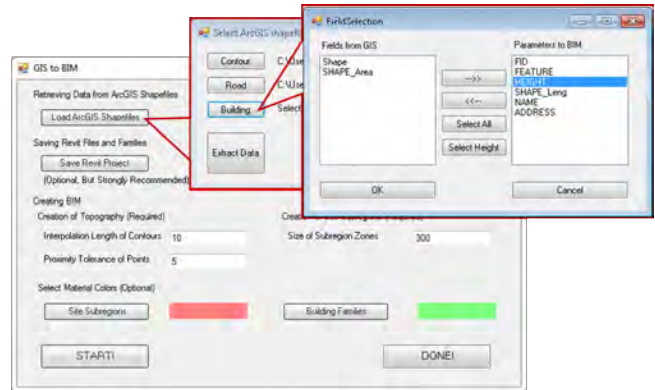


Figure 6. The interface of the translation framework in a software solution. The user of the framework should map data to BIM objects.

3.5 Test Cases

The proposed translation framework and the software prototype have been tested in two test cases. Post-tornado rebuild urban plan for West Liberty in Kentucky was tested to create a parametric BIM (figure 7). In addition, a model for Texas A&M University main campus was created as shown in figure 8. Figure 9 and 10 shows that a building family instance parametrically inherits the information fields and values from a GIS shapefile. The highlighted parts of figures 9 and 10 also show that the non-geometric information of the BIM has inherited from GIS parametrically. Examples of these parameters include “NAME” and “ADDRESS” of the buildings.



Figure 7. The BIM model of post-tornado rebuild urban plan for West Liberty, Kentucky.

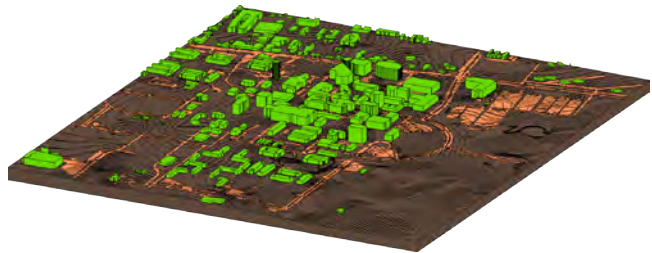


Figure 8. The BIM model of Texas A&M University campus created from GIS data.

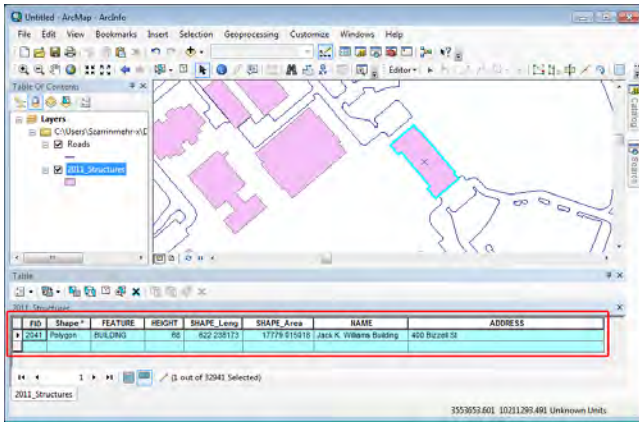


Figure 9. The attribute table of the GIS Shapetable and the values that it contains for the selected building footprint.

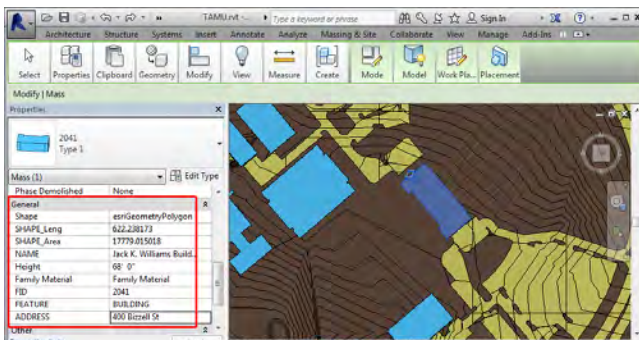


Figure 10. The model in Revit which was created using the proposed translation framework. It shows that the corresponding building family instance parametrically inherits the information from the GIS attribute table.

The BIM model that is generated based on the GIS data can be used in various ways to support design decision making. BIM models can be used for simulations [20, 21], design evaluations, digital fabrications, etc. Figure 11 shows automated facades generation based on the mass model. Figure 12 shows the exploration of the urban environment in a virtual reality setting. Figure 13 shows the physical model of Texas A&M (12.5' x 8.75') fabricated with CNC machines and later cutters. Figure 14 shows that the energy simulation of a building within the context of surrounding buildings produce more accurate simulation results.



Figure 11. The non-geometric information which the BIM objects inherit from GIS can be used for automated façade design.

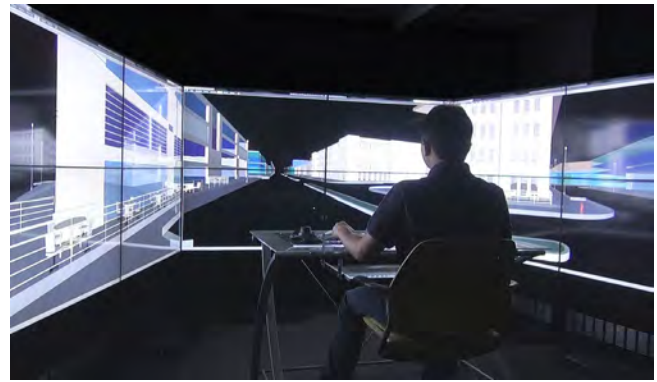


Figure 12. A designer evaluating design schemes by interacting with the façade generation in a virtual reality environment.



Figure 13. Fabricated physical model of Texas A&M University campus from the BIM which is inherited from GIS data.

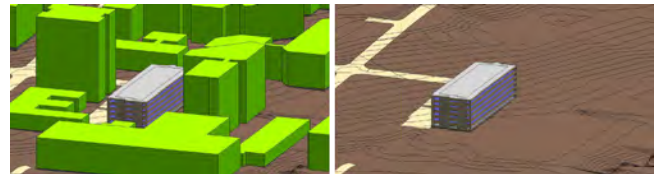


Figure 14. The total annual cost of the energy is decreased from \$135,828 to \$127,690 and the Energy Use Intensity (EUI) is decreased from 49.3 to 46.2 (kBtu/ft²/year) for the highlighted building when the impact of the surrounding buildings is considered.

4 CONCLUSION

Layer-based GIS and BIM have innate structural differences which impede GIS to BIM conversion. This research presented a framework that automatically generate BIM models from GIS data to support design decisions. This process is accomplished at two major steps. An automated translation framework was introduced for extracting the geometric and non-geometric data from GIS, process the extracted data with custom algorithms and generate parametric BIM model. This translation addressed significant challenges in converting GIS data types into BIM objects. A software prototype is then developed and tested to validate the translation algorithms. The software prototype was able to greatly reduce the time to construct a BIM model from GIS data with minimum manual work involved. This is expected to help architects to make better design decisions.

REFERENCES

1. Autodesk (2015). "About Families." Autodesk Revit 2016 Help, <<http://help.autodesk.com/view/RVT/2016/ENU/?guid=GUID-6DDC1D52-E847-4835-8F9A-466531E5FD29>>.
2. Benner, J., Geiger, A., and Leinemann, K. (2005). "Flexible generation of semantic 3D building models." Proc., Workshop on Next Generation 3D City Models, 17-22.
3. Biljecki, F., Ledoux, H., Stoter, J., and Zhao, J. (2014). "Formalisation of the level of detail in 3D city modelling." Computers, Environment and Urban Systems, 48, 1-15.
4. buildingSMART. (2014). "About BIM." <<http://www.buildingsmart.org/openbim/bim/2/1/about-bim>>.
5. Consortium, O. G. (2012). "OGC City Geography Markup Language (CityGML) Encoding Standard." <<http://www.opengeospatial.org/standards/citygml>>.
6. Douglas, D. H., and Peucker, T. K. (2011). "Algorithms for the Reduction of the Number of Points Required to Represent a Digitized Line or its Caricature." Classics in Cartography, John Wiley & Sons, Ltd, 15-28.
7. Eastman, C. M. (2008). BIM Handbook: A Guide to Building Information Modeling for Owners, Managers, Designers, Engineers and Contractors, Wiley, Hoboken, N.J.
8. ESRI (2014). "ArcGIS Help 10.1: Data types in the DBMS."
9. Foote, K. E., and Lynch, M. (1995). "Geographic Information Systems as an integrating technology: context, concepts, and definitions."
10. Gröger, G., and Plümer, L. (2012). "CityGML – Interoperable semantic 3D city models." ISPRS Journal of Photogrammetry and Remote Sensing, 71, 12-33.
11. Isikdag, U., and Zlatanova, S. (2009). "A SWOT analysis on the implementation of Building Information Models within the Geospatial Environment." Urban and Regional Data Management, CRC Press, The Netherlands, 15-30.
12. Isikdag, U., and Zlatanova, S. (2009). "Towards Defining a Framework for Automatic Generation of Buildings in CityGML Using Building Information Models." 3D Geo-Information Sciences, J. Lee, and S. Zlatanova, eds., Springer Berlin Heidelberg, 79-96.
13. Johnson, A. (2014). Clipper: Polygon and line clipping and offsetting library, version 6.1.3<<http://sourceforge.net/>>.
14. Kolbe, T. (2009). "Representing and Exchanging 3D City Models with CityGML." 3D Geo-Information Sciences, J. Lee, and S. Zlatanova, eds., Springer Berlin Heidelberg, 15-31.
15. Kolbe, T. H. (2012). "Virtual City Models: What is CityGML?"
16. Lee, G., Sacks, R., and Eastman, C. M. (2006). "Specifying parametric building object behavior (BOB) for a building information modeling system." Automation in Construction, 15, 758-776.
17. msdn. (2014). "Dictionary<TKey, TValue>.ContainsKey Method." <<http://msdn.microsoft.com/en-us/library/kw5aaca4.aspx>>.
18. Nagel, C., Stadler, A., and Kolbe, T. H. (2009). "Conceptual requirements for the automatic reconstruction of building information models from uninterpreted 3D models." Proc., International Archives of Photogrammetry, Remote Sensing and Spatial Information Sciences.
19. Shen, W., Hao, Q., Mak, H., Neelamkavil, J., Xie, H., Dickinson, J., Thomas, R., Pardasani, A., and Xue, H. (2010). "Systems integration and collaboration in architecture, engineering, construction, and facilities management: A review." Advanced Engineering Informatics, 24, 196-207.
20. Wu, C., Clayton, M. (2013). "BIM-based acoustic simulation Framework". 30th CIB W78 International Conference. 99-108
21. Wu, C., Zarrinmehr, S., Rahmani, M., Clayton, M. (2015). "Facilitating fire and smoke simulation using Building Information Modeling". International Conference on Computer-Aided Architectural Design Futures. 366-382



Digital Energy Performance Signature Extensible Markup Language (DEPSxml): Towards a New Characterization Framework for Sharing Simulation and Measured Data on Building Design and Energy Performance

Justin McCarty and Adam Rysanek

School of Architecture and Landscape Architecture,
University of British Columbia
Vancouver, Canada
{Jmccarty, arysanek}@sala.ubc.ca

ABSTRACT

This paper introduces a new filetype that has the potential to improve data analytics in the building sector. The aim of the paper is to explore the general logic and hierarchy of the file type, explore the mechanism in which it would transmit data, and define initial user groups and the process by which they would use the file and server system.

The filetype utilizes a popular green building filetype (gbXML) as a base schema. The manner in which the base schema is expanded upon is explored in the paper to clarify how a live link to a building's automation system and utility network may be established in an Extensible Markup Language (XML) file format.

The last section of the paper contributes several potential uses for the new filetype that will be put into place during the beta phase.

Author Keywords

building performance data; standardized file formats; building audits; gbXML.

ACM Classification Keywords

E.5 Data (e.g. FILES) I.6.0 Simulation and Modeling (e.g. General)

1 INTRODUCTION

The global buildings sector faces long-standing and well-studied drivers and barriers to investments in building energy-efficiency retrofits [28]. This is especially pertinent given the importance of the buildings sector to climate change mitigation policy. Energy use within existing buildings accounts for over 30% of global, annual anthropogenic greenhouse gas emissions and, in absolute terms, is continuing to rise at a rate of 1.5% annually [23]. The Organisation for Economic Co-operation and

Development (OECD) region specifically contributes to roughly half of global building-attributed greenhouse gas (GHG) emissions and is unlikely to see significant construction of new buildings over the coming century [19]. While the real estate market of British Columbia's major cities has generated a unique condition, where new building construction and property replacement rates well exceed the North American average, the Provincial Government still views decarbonisation of its existing building stock as a vital contribution to its climate change mitigation and adaptation strategy.

In 2017, the Pembina Institute, a Canadian non-profit think tank, released a broad-based study on the viability and costs of 'deeply' retrofitting buildings in British Columbia (BC) in order to achieve the province's GHG emissions targets [11]. The conclusions of the report, which identified prevailing drivers and barriers to deep retrofits in the province, broadly aligned with prior global studies of drivers and barriers to decarbonization of the building stocks, such as that of Ürge-Vorsatz et al. [28]. The report recommended nine strategies to be adopted across government, industry and academic institutions in the province in order to address its carbon reduction commitments in the building stock. These included:

1. adopt and enforce minimum energy performance standards for all buildings performing any degree of renovations;
2. create a public financing authority, or 'green bank' to support capital expenditures on green building retrofits across the province;
3. adopt mandatory energy labelling and benchmarking for all residential and non-residential buildings;

4. expand data collection of and assessment of BC building conditions for facilitation of retrofit analysis; and
5. improve training and certification of building retrofit assessors and related practitioners in the BC buildings industry.

Overall, the Pembina report portrayed many of the challenges facing widespread uptake of building retrofits to be complex and interdependent. However, what emerged particularly clearly from the report, just as seen in the work of Ürge-Vorsatz et al. is that “insufficient knowledge” remains one of the most prevailing barriers affecting delivery of energy-efficient buildings in the province [26]. This research paper seeks to address the nature of knowledge transfer within the building industry, specifically how building design information, inclusive of building performance data, is collected, stored, shared, and ultimately implemented. It seeks to propose a new Extended Markup Language (XML) schema, that is based on the established ‘gbXML’ file format but conveys both simulation-derived building design information and measured building performance.

1.1 Relevant Prior Work

The buildings sector utilizes a network of professional trades, consultants, and review boards to generate the information required for the construction of each project. Each of these groups utilizes one or several data file formats to communicate this information. The focus of this paper is particularly on the types of data files, and file formats, used to communicate information regarding the predictive and measured performance of a building. It calls on a review of two interrelated topics: 1) the current use of standard files for conveying building performance simulation information, and 2) the current approach by major governmental organizations to collect and communicate building performance data and metadata.

1.1.1 Development of Green Building Extended Markup Language (gbXML)

The Extensible Markup Language (XML) is a widely used and simple text-based language used for transferring structured information between programs [30]. The Green Building Extensible Markup Language (gbXML) was developed by Green Building Studio in 2000, becoming a single entity in 2009. gbXML has become, alongside Industry Foundation Class (IFC), an industry standard for data and model exchange. It can be used for a multitude of building performance simulation platforms such as OpenStudio and Rhino/Grasshopper Ladybug and has been developed with extensibility in mind [9]. gbXML files have been implemented in a range of research areas including the authoring of gbXML files from point clouds or mapping existing thermal properties to a file for analysis [12] [13]. gbXML files encode information on geometry as well as thermal attributes. gbXML is ideal for transferring thermal information given the geometry and necessary data are stored

in the same succinct file that is merely pulled from an existing Building Information Model (BIM). Complex geometries such as curving walls are not always translated appropriately and often tools for correcting the file need to be employed [15].

This information can then be transferred from authoring tools such as Autodesk’s Revit to energy analysis programs such as Ladybug LLC’s Honeybee or Autodesk’s Ecotect and then onto EnergyPlus for simulation [25]. Once utilized for simulation, the gbXML file is discarded for either a new iteration of the design following the simulation results, or the building will move on to construction.

The concept for a new XML filetype proposed here is to extend the base gbXML schema to create a file type that becomes useful after the design is completed and links the constructed building to a database of building energy data. The majority of the base gbXML schema will remain intact, such as elements for surfaces, zones, and openings.

The extension is the addition of a storage capability for the elements of gbXML that change with time. For instance, the thermal resistance of a wall or roof does not improve or become worse every half hour of the day, but a room occupancy sensor may detect changes in area occupancy every half an hour. These detected changes are then fed into a system of feedbacks that adjust the comfort levels of the building to suit the set requirements. The extensions will expand these dynamic building elements by adding location information and a call number that will allow the new file to store and associate collected performance and occupancy data on a central server. Through this extension the gbXML file will be transformed into a live-building database, a performance-centric digital clone of the building.

1.1.2 Energy Performance Data Collection and Benchmarking at the Building Stock Scale

Municipalities, nations, and international bodies have attempted to provide extensive datasets on measured building performance, several of which are currently available for use by researchers. Programs such as the United States Department of Energy Building Performance Database (BPD) and the Royal Institute of British Architects (RIBA) Chartered Institution of Building Services Engineers (CIBSE) Platform (CarbonBuzz) are two such datasets [5] [27].

As of November 2018, there are currently over 1,000,000 U.S. buildings uploaded to the BPD system. Individual dwelling units or entire buildings are organized by occupancy type and persons count, in addition to several coarse attributes for the year in which the data has been input by users, such as Electric Energy Use Intensity (EUI). It has been used by researchers to develop retrofit tools and perform retrofit analysis but has been criticized for being

	IFC LEVELS OF DEVELOPMENT	CITYGML ELVELS OF DETAIL	DEPS ENERGY LEVELS OF DETAIL
LOD 0	N/A	A 2D representation of the urban geospatial information. Typically, a footprint or roof area polygon.	Thermal information is held in table form, assigned to a longitude and latitude or parcel address.
LOD 1	Model elements are not represented by model geometry, but their existence and information are embed in other model elements.	Model elements are represented by non-specific volumes with no regard to roof type or detail on the exterior.	Thermal data non-spatial and generalized across floor area. Location, year of construction, and monthly energy usage available.
LOD 2	Model elements are represented by some sort of volumetric geometry but are still generic.	Roof structures and prominent details like balconies are present	Thermal information is assigned to boundary surfaces such as wall, floor, and roof.
LOD 3	Model elements are geometrically specified in the model without the need of accessory information, such as a door schedule.	Model elements are simple architectural models with detailed roof and wall surfaces that show overhangs and fenestration.	Boundary surfaces are assigned openings. Building models are separated into thermal zones.
LOD 3.5	Model elements are connected and can be understood using solely the model, such as structural ties.	N/A	N/A
LOD 4	Model elements are detailed and accurate to be fabricated using nothing but the geometry.	Model elements are completed with interior rooms and details such as furniture. These elements may also be visualized using a texture map.	Individual elements such as lights, sensors, and assembly layers are represented geometrically and semantically.

Table 1. The existing Levels of Detail used in the industry (IFC and cityGML) and the proposed Energy Levels of Detail (eLOD).

potentially under-representative of the U.S. building stock [16] [29].

CarbonBuzz, a project from the RIBA CIBSE, is a portal for benchmarking and tracking the predicted and actual energy use as well as carbon emissions of individual projects.

Through a login-secured portal, project owners or designers can input project data such as occupancy type, predicted energy use and methodology, measured energy use, etc. The program behind CarbonBuzz will then compare predicted energy information to measured and deliver the user with comparative charts. The CarbonBuzz program is largely based on the Display Energy Certificate (DEC). The DEC is the United Kingdom’s energy label program, which is mandated for most public buildings and voluntary for others. It requires measured energy use for certification. While innovative in its conception, CarbonBuzz is a small dataset (just over 400 shared projects) and erroneous entries are common.

The European Union’s Energy Performance Credit (EPC) system was in part designed as an assessment program with data harvesting capabilities. For any assessed building the auditing process behind this energy labeling program generates a snapshot of either predicted or measured energy performance, most often the former. The label assigned to a building is a grade based on a calculation using performance

data that is then rated compared to a benchmark building that is similar. While the EU’s Energy Performance of Buildings Directive (EPBD) is an inspiring legislation, the various EPC programs that fulfill a portion of the Directive have not entirely delivered on the ambition to enable retrofits and tie energy performance directly to the housing market [5]. In a review of country specific EPC programs, it was found that at the cause of the EPCs’ shortcomings were a lack of engagement between the building owner and the label after its initial creation [2] [4] [6] [22].

1.1.3 Similar Interoperability Standards and Filetypes

Development of Industry Foundation Class, an XML project, has been primarily focused on interoperability between actors involved in the design and fabrication of a single built object, often a building. It allows for simple file exchange by various consultants, design firms, and construction specialists throughout design and construction. While IFC has been utilized for energy and thermal comfort studies, gbXML has become the energy simulation and analysis industry standard [3] [8].

CityGML is a part of the Geography Markup Language, an XML grammar system intended for exchanging geographic information. CityGML has become a success in file interchange and is being adopted by some urban energy simulation researchers for its ability to encapsulate energy performance data at a variety of Levels of Detail (LOD).

Recently, an extension, the Energy Application Domain Extension (ADE) was introduced to help expand energy analysis efforts at an urban simulation scale [1]. This ADE is viewed as complimentary file type for urban scale modeling to a new XML schema based on gbXML, known as the Digital Energy Performance Signature (DEPS or DEPSxml).

Two of the more direct antecedents to DEPSxml files may be the BuildingSync® XML schema and Building Energy Data Exchange Specification (BEDES). BuildingSync is a standardized format for communicating the results of building audits, including post-occupancy assessments [10]. BEDES provides a standardized dictionary of terms and nomenclature for communicating building design information and data amongst stakeholders in the built environment [20].

2 DESCRIPTION OF DIGITAL ENERGY PERFORMANCE SIGNATURE (DEPS) FRAMEWORK

Presented here is a conceptual framework for the storage of a building's energy performance and occupancy data, the storage and access mechanisms, and several potential applications. This framework has been envisioned as a new XML-based file type that is essentially a highly detailed digital clone of a building. The file would act as a link to the analysis of the building's energy performance from the design stage, construction, and through the operative life of the building.

2.1 Introduction of the Digital Energy Performance Signature Extended Markup Language (DEPSxml)

DEPSxml will utilize a similar base schema as gbXML but will allow for the live connection and analysis of building energy information through Application Program Interfaces (APIs). These APIs will provide an interconnection between a central server housing all DEPSxml files, known as the DEPS server, and building sensors and meters that will populate the file periodically. The aim is to continuously embed measured building performance in a DEPSxml.

Hierarchy of Data Stored in DEPSxml

The primary logic for what will be called Digital Energy Performance Signatures (DEPS) is seated in an LOD system, similar to hierarchical data structures found in IFC and the cityGML [8]. This Energy Levels of Detail (eLOD) will ensure a smoother interoperability across scales, while the XML format will ensure a simple translation of elements and attributes between end-user file types. Table 1 compares the three LOD logics.

The logic of the eLOD is that the energy information stored in DEPS can be spread across disciplines and scales, where very fine levels of detail (high LOD) are not necessary or always available. All DEPS files will hold not only the high eLOD developed and tracked, but the logic will allow for lower levels to be pulled without the interference of high-level data.

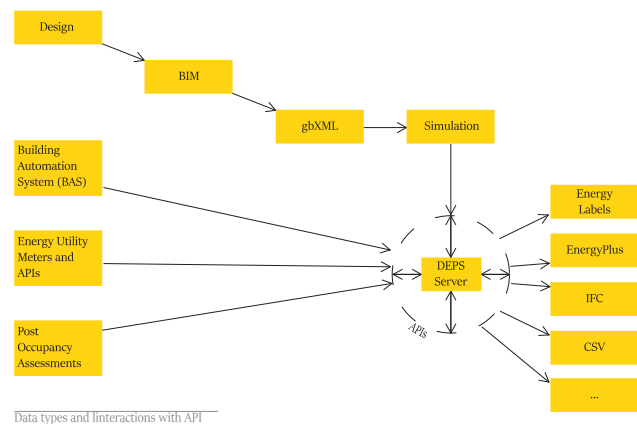


Figure 1. The variety of data that will be used to build a DEPSxml file and the various interactions of APIs.

Type data stored in the DEPSxml file

The process begins with the design of the space or building. As the model is developed, following a defined protocol, not unlike the guides created by professional organizations like the American Institute of Architects or CIBSE the designer would create a model for energy analysis, as is typical in the industry. A gbXML file, would then be used for a predicted performance benchmark. The results of this benchmark would then be stored on a central database and assigned a unique identifying code. The code would be submitted as metadata of the gbXML file and BIM file. This is a permanent link that allows for simple interaction with the database API for that unique project. This is the building's DEPS (Figure 1).

An ongoing contribution to the performance gap are changes made after design. These site-decisions or budget related alterations can create inconsistencies between the predicted and actual performance [7]. Construction updates to the design will need to be updated in the digital model space and updates to the benchmark DEPSxml uploaded. A longer objective of the DEPS project will be the development of a lifecycle manual for maintenance of a DEPSxml.

Measured Energy Performance Data

A great deal of the performance gap is due to the difficulties of modeling occupant behavior. As updates are made to the building, the model will need to be updated accordingly. The building's sensor network, which was modeled initially and is stored in DEPS will need to be connected to the server's API in order to record usage statistics.

Post-Occupancy Evaluations

Post-occupancy evaluations (POE) are assessments of the building once construction has been completed and activities have been ongoing for some time. These assessments are key to understanding the performance gap and can lead to better operational systems and retrofits of a building after construction. DEPSxml will track these evaluations in order to provide a central location to compare assessments throughout the building's lifecycle.

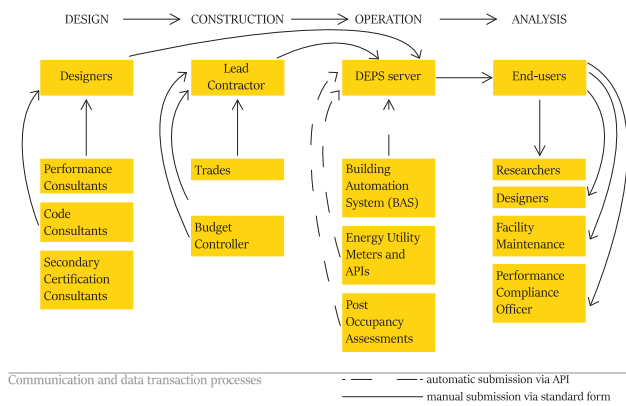


Figure 2. The flow of data through input users and end users in the DEPS environment.

Data Collection and Management Process via Central DEPS Servers

DEPSxml files will store building performance data and POE information in a database format linked to a central server. Throughout the design and construction phase data will be contributed to the DEPSxml file by either the designers, consultants, or contractors (Figure 2). Through automated submission the building's DEPSxml will be populated with consumption and performance data. Any manual data entry will be submitted through standardized forms. Files being uploaded to the server will go through a validation process standard to many XML filetypes to ensure schema compliance.

Creation of Central DEPS Repository with Application Program Interface (APIs)

The DEPS Server will act as a repository for individual text files and is the major driver of their use. Through application program interface (API) technology the server will allow for upload and download in a secure manner and without the need for programming knowledge.

Submission of building design information by consultants and designers

Consultants and designers will be the first to interact with the DEPS Server as they will be submitting initial performance simulation information and geometry. This will largely be manual work using either conversion scripts for file specific information such as gbXML or standardized forms for non-file specific information such as general building profile information. It is envisioned that in larger projects either the design firm or a single consultant will handle this environment to ensure a rigorous process. However, the entire process is being developed with small-to-midsize projects in mind knowing that only a handful of individuals may be available to input data.

Submission of Metered Energy Consumption by Energy Providers and Building Automation Systems (BAS)

The primary driver of DEPSxml is building real-time energy consumption data and occupant activity data, obtained primarily through an extensive set of sensors. Through energy provider APIs and a direct link with the building

automation system (BAS) the DEPSxml will be continuously fed with performance data. This data will be stored chronologically by meter or sensor in the DEPSxml file.

Submission of Post-Occupancy Evaluation Information

POE is vital to closing the performance gap [21]. If available POE data will be submitted using standardized forms that will allow for comparative profiles to be created. This will require a flexible submission interface that can meet the needs of the various POE methodologies. There are a multitude of POE frameworks in practice today. Li et al. explored these in a comprehensive review finding that the POE process has yet to be completely developed worldwide [17].

3 POTENTIAL APPLICATIONS OF THE DEPSXML FILETYPE AND ENVIRONMENT

While DEPS is under development it will be used for several initial research projects using a university campus building dataset and complementary energy consumption meter network. The initial applications are the development of an energy label and retrofit recommendation platform, the scaling and converting of building scale data to urban simulation scales and linking individual models with an augmented reality interface to enhance operational efficiency and facility maintenance.

3.1 Energy Labeling and Performance Requirements

The framework and DEPS protocol is being developed for initial testing at the scale of a large public university. In order to develop and fine tune the file structure it will be created with the input of dozens of existing institutional and residential buildings for which sensor systems are in place, and BIM models exist in a variety of LODs. The initial test of the DEPS usefulness will be an energy label protocol for the campus. It is intended however for this label to depart from the existing paradigm of labeling which is static.

Instead the label created will primarily be a tool for continuous performance improvement. Once the initial performance assessment is made, a grade will be assigned to the building, similarly to the current EPC process. However, in the digital labeling environment a projection will be created as a baseline of performance throughout the day, based on predicted occupancy. This projection will track along actual performance throughout the building's lifetime allowing a monitor or monitoring program to recognize when different operation patterns are necessary.

Furthermore, continuous tracking would be used to inform recommended retrofits, proposing not only energy efficiency but also financially efficient and comfort centric recommendations. The logic with the latter being that a building that is occupant managed would be managed from a comfort centric mindset, not necessarily purely energy or financial efficiency. Therefore, the building's management system could, over time, understand the comfort needs of occupants based on programming and activity in thermal zones.

3.2 Energy Modeling at Multiple Scales

As municipalities focus more on retrofit and replace scenarios to decarbonize building stocks, the field of urban building energy modeling has expanded [24]. This is a bottom up modeling approach in which parcels and often the buildings assigned to the parcels are modeled in a 3D environment. Performance information is then assigned to the building via profiles or templates and simulations are conducted. Several specialized tools have been developed over the years to streamline this workflow and integrate it with other urban aspects such as changing energy supplies or network analysis. The development of the DEPS server will help with the often-primary barrier to thorough modeling, a lack of comprehensive and detailed datasets for large building stocks.

This field primarily employs Geospatial Information Systems (GIS) tools and has increasingly relied on cityGML and its LOD logic for spatial modeling and analysis. With the introduction of the Energy ADE and with the aid of eLODs, it will become simpler to convert building scale performance models to the urban scale. A conversion path built in Safe Software's FME is being explored to bring gbXML semantics in line with those found in cityGML and the Energy ADE. Once established large retrofit scenario models can be utilized to explore potential retrofit scenarios on the campus building stock.

3.3 Enhancing Building Operation and Maintenance Through Machine Learning and Augmented Reality

While software and machine learning have, in many ways, made the operation of buildings simpler and more automated there still exists a gap for day-to-day maintenance – that is in person building maintenance. Researchers concerned with the maintenance and operation of buildings optimizing of building energy use during its lifetime have looked to enhancing day-to-day maintenance through augmented and virtual reality interfaces [26]. Through the DEPS sensor link live building data could be explored in person during maintenance walkthroughs or in emergency situations. Anomalies could be accessed in a much more intuitive manner or Indoor Environmental Quality (IEQ) issues, such as CO₂ concentration, could be spatialized. This immediate link to the building's unseen activity could greatly enhance maintenance efficiency and safety.

4 DEMONSTRATION OF SCHEMA

An example DEPSxml file is. Further information can be found at: <http://blogs.ubc.ca/etalab/depsxml>.

5 CONCLUSIONS

Despite the efforts of governments and NGOs carbon emissions in the built environment have yet to reach rates on track with a 1.5°C or even 2°C future [18]. This is to say that existing policy and implementation are inadequate for preventing a future in which climate change is devastating. While global efforts have been slow, there has been an increased focus on physical simulation tools for building energy performance and thermal comfort analysis. This

focus on simulation has led to an increased focus on data analytics and availability within the industry. The result of this when mixed with intelligent low carbon policy has been more efficient HVAC systems, tighter and thermally proficient building envelopes, and more consideration of passive design principles throughout the design process. However, the overall availability of high-resolution performance data is lacking, as evidenced by the recognition of the performance gap. Creating an environment in which comprehensive performance-centric datasets for buildings are stored, updated, and made available for research is absolutely necessary to increase the likelihood of achieving ambitious carbon reduction goals.

In this paper the framework for a new energy performance data collection and management environment has been introduced. In this framework a new file type (DEPSxml) and interoperable logic (eLOD) is situated. The intention of this new framework is to enhance operational and research efforts for carbon reduction and overall building performance. It is key for the DEPS project to focus on enhancing the building's overall value not only from a performance standpoint, but also as an architectural element. The data produced by this system will link *measurable* building performance directly to building design information and real occupant activity, allowing researchers and practitioners to understand more directly the phenomenon of comfort as it relates to building energy consumption. The DEPS system situates itself beside comparable schemas such as BuildingSync or gbXML and does not intend to replace their use in the buildings domain. Instead, one may consider the DEPSxml to be an XML of XMLs, whereby its core purpose is to provide stakeholders with standardized access to wide range of building data via a common API.

The shortage of widely available finely detailed building performance data has brought about an environment in which designers' efforts to predict energy performance are considerably criticized [14]. A framework and repository for energy simulation datasets could enable extensive and coordinated modeling efforts, useful post-occupancy analysis, spur a wave of deep retrofits, inform urban design policy, and make the operation and maintenance of buildings more efficient and confidently predictable.

ACKNOWLEDGMENTS

The authors wish to acknowledge the support provided by the Pacific Institute for Climate Solutions for this project.

REFERENCES

1. Agugiaro, Giorgio, Joachim Benner, Piergiorgio Cipriano, and Romain Nouvel. "The Energy Application Domain Extension for CityGML: Enhancing Interoperability for Urban Energy Simulations." *Open Geospatial Data, Software and Standards*, 2018. 3(2): p. 1-30

2. Amecke, Hermann. "The Impact of Energy Performance Certificates: A Survey of German Home Owners." *Energy Policy*, 2012. 46 (July): p. 4–14.
3. Andriamamonjy, Ando, Dirk Saelens, and Ralf Klein. "An Automated IFC-Based Workflow for Building Energy Performance Simulation with Modelica." *Automation in Construction*, 2018. 91 (July): p.166–181.
4. Backhaus, Julia, Casper Tigchelaar, and Marjolein de Best-Waldhober. "Key Findings & Policy Recommendations to Improve Effectiveness of Energy Performance Certificates & the Energy Performance of Buildings Directive," *Ideal EPBD*, 2011. <https://www.ecn.nl/docs/library/report/2011/o11083.pdf>
5. "CarbonBuzz : RIBA CIBSE Platform." Accessed 24 November 2018. <https://www.carbonbuzz.org/about.jsp>.
6. Christensen, Toke Haunstrup, Kirsten Gram-Hanssen, Marjolein de Best-Waldhober, and Afi Adjei. "Energy Retrofits of Danish Homes: Is the Energy Performance Certificate Useful?" *Building Research & Information*, 2014. 42 (4): p. 489–500.
7. de Wilde, Pieter. "The Gap between Predicted and Measured Energy Performance of Buildings: A Framework for Investigation." *Automation in Construction*, 2014. 41 (May): p. 40–49.
8. Do, Huyen, and Kristen S. Cetin. "Residential Building Energy Consumption: A Review of Energy Data Availability, Characteristics, and Energy Performance Prediction Methods." *Current Sustainable/Renewable Energy Reports*, 2018. 5(1): p. 76-85.
9. Dong, B, K P Lam, and Y C Huang. "A Comparative Study of the IFC and GbXML Informational Infrastructures for Data Exchange in Computational Design Support Environments." *IBPSA Building Simulation*, 2017. P. 1530-1537. http://www.ibpsa.org/proceedings/BS2007/p363_final.pdf
10. Eley, C. "Standardizing Energy Modeling Output." *Proceedings of SimBuild*, 2016. 6(1): p. 365-361. <http://ibpsa-usa.org/index.php/ibpusa/article/view/380/366>
11. Frappé-Sénéclauze, Tom-Pierre, Dylan Heerema, and Karen Tam Wu. "Deep Emissions Reduction in the Existing Building Stock: Key Elements of a Retrofit Strategy for B.C. Results from the November 2016 Thought Ledger Forum," April 2017. *Pembina Institute for Appropriate Development*. <http://www.pembina.org/reports/retrofit-strategy-bc-summary-2017.pdf>
12. Garwood, Tom Lloyd, Ben Richard Hughes, Dominic O'Connor, John K. Calautit, Michael R. Oates, and Thomas Hodgson. "A Framework for Producing GbXML Building Geometry from Point Clouds for Accurate and Efficient Building Energy Modelling." *Applied Energy*, 2018. 224 (August): p. 527–537.
13. Ham, Youngjib, and Mani Golparvar-Fard. "Mapping Actual Thermal Properties to Building Elements in GbXML-Based BIM for Reliable Building Energy Performance Modeling." *Automation in Construction*, 30th ISARC Special Issue, 2015. 49 (January): p. 214–224.
14. Imam, Salah, David A Coley, and Ian Walker. "The Building Performance Gap: Are Modellers Literate?" *Building Services Engineering Research and Technology*, 2017. 38 (3): p. 351–375.
15. Kamel, Ehsan, and Ali M. Memari. "Automated Building Energy Modeling and Assessment Tool (ABEMAT)." *Energy*, 2018. 147 (March): p. 15–24.
16. Lee, Sang Hoon, Tianzhen Hong, Mary Ann Piette, Geof Sawaya, Yixing Chen, and Sarah C. Taylor-Lange. "Accelerating the Energy Retrofit of Commercial Buildings Using a Database of Energy Efficiency Performance." *Energy*, 2015. 90 (pt. 1 October): p. 738–747.
17. Li, Peixian, Thomas M. Froese, and Gail Brager. "Post-Occupancy Evaluation: State-of-the-Art Analysis and State-of-the-Practice Review." *Building and Environment*, 2018. 133 (April): p. 187–202.
18. Lucon O., D. Üрге-Vorsatz, A. Zain Ahmed, H. Akbari, P. Bertoldi, L. F. Cabeza, N. Eyre, A. Gadgil, L. D. D. Harvey, Y. Jiang, E. Liphoto, S. Mirasgedis, S. Murakami, J. Parikh, C. Pyke, and M.V. Vilariño, 2014: Buildings. In: *Climate Change 2014: Mitigation of Climate Change. Contribution of Working Group III to the Fifth Assessment Report of the Intergovernmental Panel on Climate Change [Edenhofer, O., R. Pichs-Madruga, Y. Sokona, E. Farahani, S. Kadner, K. Seyboth, A. Adler, I. Baum, S. Brunner, P. Eickemeier, B. Kriemann, J. Savolainen, S. Schlömer, C. von Stechow, T. Zwickel and J.C. Minx (eds.)]*. Cambridge University Press, Cambridge, United Kingdom and New York, NY, USA.
19. Ma, Zhenjun, Paul Cooper, Daniel Daly, and Laia Ledo. "Existing Building Retrofits: Methodology and State-of-the-Art." *Energy and Buildings*, Cool Roofs, Cool Pavements, Cool Cities, and Cool World, 2012. 55 (December): p. 889–902. doi:10.1016/j.enbuild.2012.08.018.
20. Mathew, P. A., Dunn, L. N., Sohn, M. D., Mercado, A., Custudio, C., & Walter, T. "Big-data for building energy performance: Lessons from assembling a very large national database of building energy use." *Applied Energy*, 2015. 140: p. 85-93.
21. Menezes, Anna Carolina, Andrew Cripps, Dino Bouchlaghem, and Richard Buswell. "Predicted vs. Actual Energy Performance of Non-Domestic Buildings: Using Post-Occupancy Evaluation Data to Reduce the Performance Gap." *Applied Energy, Energy Solutions for a Sustainable World - Proceedings of the Third International Conference on Applied Energy in 2011*, 2012. 97 (September): p. 355–364.

22. Murphy, Lorraine. "The Influence of the Energy Performance Certificate: The Dutch Case." *Energy Policy*, 2014. 67 (April): p. 664–672.
23. Pérez-Lombard, Luis, José Ortiz, and Christine Pout. "A Review on Buildings Energy Consumption Information." *Energy and Buildings*, 2008. 40 (3): p. 394–398.
24. Reinhart, Christoph F., and Carlos Cerezo Davila. "Urban Building Energy Modeling – A Review of a Nascent Field." *Building and Environment*, 2016. 97 (February): p. 196–202. doi:10.1016/j.buildenv.2015.12.001.
25. Roudsari, Mostpaha Sadehipour, Michelle Pak, and Adrian Smith + Gordon Gill Architecture. "Ladybug: A parametric environmental plugin for grasshopper to help designers create an environmentally-conscious design." *IBPSA BS2013*, 2013. p. 3128–3135.
26. Rysanek, Adam, Clayton Miller, and Arno Schlueter. 2017. "A Workflow for Managing Building Information and Performance Data Using Virtual Reality: An Alternative to BIM for Existing Buildings?," *IBPSA BS2017*, 2017. p. 2767–2774.
27. United States of America, Department of Energy: Building Performance Database. Accessed 24 November 2018. <https://bpd.lbl.gov/#explore>
28. Ürgе-Vorsatz, Diana, and Bert Metz. "Energy Efficiency: How Far Does It Get Us in Controlling Climate Change?" *Energy Efficiency*, 2009. 2 (2): p. 87–94.
29. Walter, Travis, and Michael D. Sohn. "A Regression-Based Approach to Estimating Retrofit Savings Using the Building Performance Database." *Applied Energy*, 2016. 179 (October): p. 996–1005.
30. "XML Essentials - W3C." 2018. Accessed 24 November 2018. <https://www.w3.org/standards/xml/core>.



From Optimization to Performance-Informed Design

Thomas Wortmann¹ and Thomas Schroepfer²

¹Xi'an Jiaotong Liverpool University
Suzhou, Jiangsu, China
thomas.wortmann@xjtlu.edu.cn

¹Singapore University of Technology and Design
Singapore
thomasschroepfer@sutd.edu.sg

ABSTRACT

This paper introduces performance-informed design space exploration (DSE) to question the relationship between explicit, quantitative optimization problems and “wicked”, co-evolving architectural design problems and to support the reframing of architectural design optimization as a medium for reflection. The paper proposes selection, refinement, and understanding as key aspects of performance-informed DSE and surveys current approaches to performance-informed DSE: (1) Clustering and Pareto-based optimization support selection by reducing large numbers of parametric design candidates into smaller and more meaningful sets of choices. (2) Surrogate modelling supports refinement by approximating time-intensive simulations in real-time, which is important for interactivity. (3) Multi-variate visualizations and statistical analyses support understanding by providing insights into characteristics of design spaces and fitness landscapes. Finally, the paper discusses a novel tool for visual and interactive, performance-informed DSE, Performance Explorer. Performance Explorer combines the real-time feedback afforded by surrogate models with a multi-variate visualization of fitness landscapes. A user test of Performance Explorer uncovered several performance-informed DSE strategies followed by the participants. Consisting of different combinations of selection, refinement, and understanding, these strategies illustrate and—to some extent—validate the proposed framework for performance-informed DSE.

AUTHOR KEYWORDS

Simulation-based Design Tools and Methods; Architectural Design Optimization; Visualization of Optimization Results.

ACM CLASSIFICATION KEYWORDS

I.6.6: Simulation Output Analysis

1 INTRODUCTION

This paper introduces *performance-informed* design space exploration (DSE), a novel concept that links parametric designs with their (simulated) performances and recalibrates the integration of optimization into architectural design processes. Performance, in the context of this paper, refers to

quantifiable aspects of the built environment, such as resource and/or energy consumption. Architectural Design Optimization (ADO) is the automated search for high-performing design candidates in parametric design spaces, for example with the popular genetic algorithms [29].

Developing high-performing designs that reduce resource and energy consumption is crucial for meeting global challenges such as climate change. But, in contrast to other concepts, performance-informed design recognizes that architectural design is a *wicked* problem that cannot be reduced to one or more quantifiable performance objectives [19]. Rather, performance-informed design aims to inform designers about the quantifiable impacts of their decisions while maintaining their freedom to explore other, qualitative aspects, such as spatial experience or aesthetic delight.

This paper reframes optimization as a medium for reflection and contrasts performance-informed design with related concepts such as *performance-driven* or *performance-based* design. The latter concepts amount to automatically searching for single high-performing design candidates, most prominently through optimization methods. The paper presents selection, refinement, and understanding as three key aspects of performance-informed design and surveys existing approaches, methods, and tools. Finally, the paper introduces Performance Explorer, a novel, visual and interactive tool that—by supporting selection, refinement, and understanding—affords a variety of performance-informed design strategies.

2 THE NEED FOR PERFORMANCE-INFORMED DESIGN SPACE EXPLORATION

This section identifies a need for computational methods and tools that better support exploratory divergent thinking and introduces performance-informed DSE as a framework for the development of such methods and tools.

2.1 Optimization as a Medium for Reflection

Next to automatically finding high-performing design candidates, optimization methods provide a medium for reflection and conceptual development of architectural designs. Schaffranek argues that architects should not accept optimized solutions prepared by “computer scientists and

mathematicians,” and instead learn to use optimization themselves [21]: “Those algorithms might not generate an optimal solution but they help to understand the possible outcomes of the rules defined through the algorithm ...”

The framing of optimization as not only a source of “good enough” solutions, but as a generator for insights is supported by Bradner et. al [2]: “One key finding is that professionals use design optimization to gain understanding about the design space, not simply to generate the highest performing solution. Professionals reported that the computed optimum was often used as the starting point for design exploration, not the end product.”

Stouffs and Rafiq propose a similar conception of optimization [24]: “... the aim is less on optimization per se and more on exploration: the results from optimization are about changing one’s way of thinking more than choosing a single design and then realizing it.”

The above authors emphasize that, for ADO, understanding optimization problems, i.e., fitness landscapes, is more important than finding optimal solutions. Fitness landscapes are multi-dimensional spaces that relate design parameters to one or more performance objectives. Johnson concludes that ADO “workflows present powerful ways of executing the convergent portion of the divergent–convergent design cycle,” but that “stronger support for exploratory divergent thinking” is needed [13].

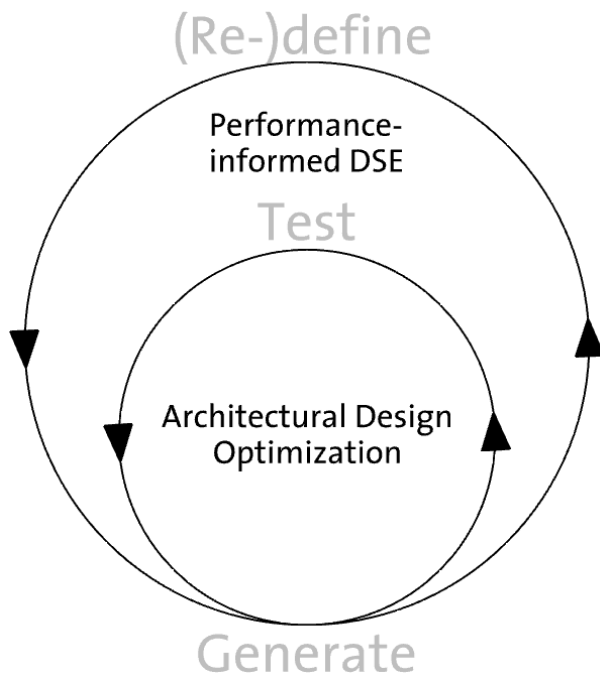


Figure 1. Nested Architectural Design Cycles. (1) (Re-)define problem, (2) generate design candidates, (3) test design candidates, with (3) leading back to (1). ADO automates the (smaller) Generate-and-Test cycle, while Performance-Informed Design aims to support the larger cycle of problem-solution co-evolution.

In summary, using ADO to automate the search for high-performing design candidates is not enough, because optimized design candidates do not represent solutions to architectural design problems. Instead, they serve to reframe the original problem by enhancing a designer’s understanding in an iterative process of co-evolving problems and solutions [9]. Performance-Informed DSE aims to support better support this co-evolution (Figure 1).

2.2 Towards Performance-Informed DSE

The wickedness of architectural design problems makes their solution with ADO problematic, especially for full building designs. Nevertheless, optimization is useful for a wide range of subproblems from, for example sustainable and structural design, and has found a small number of (published) real applications in architectural practice [29]. To further integrate optimization methods into architectural design processes, their potential as a medium for reflection should be harnessed more fully.

This paper proposes the concept of performance-informed DSE to enhance understanding and to support both exploratory divergent thinking and exploitive convergent thinking. Performance-informed DSE should support (1) selection, i.e., present designers with a meaningful choice from (groups of) design candidates and their performance instead of only a single solution, (2) refinement, i.e., allow direct parameter changes and indicate directions for potential improvement, and (3) understanding, i.e., represent the relationships between design parameters, appearance, and performance.

Refinement can serve two distinct purposes: (1) adjusting a well-performing design candidate found by an automated process (e.g., an optimization method) according to preferences not formulated as part of the automation (e.g., aesthetics or other qualitative criteria) and (2) adjusting a design candidate preferred by a designer to improve its quantitative performance. Arguably, refinement in the former sense also fulfills a psychological need to retain ownership of automated processes by customizing their results.

As such, performance-informed DSE contrasts with other computational design concepts, such as *performance-driven* design [22], *performative* or *performance-based* design [17], *post-parametric automation* [1], and *generative* design [16], which emphasize mostly automated DSE, i.e., optimization.

3 SELECTION

This section considers two approaches that support selection: Clustering and Pareto-based optimization.

3.1 Clustering

A popular approach to progress from optimization to selection and understanding is K-means clustering [15]. K-means clustering is an unsupervised machine learning method that works for arbitrary numbers of parameters and sorts data into a pre-defined number of groups, based on similar parameter values. Approaches that support selection

often employ a clustering method to group large numbers of parametric design candidates—resulting, for example, from optimization—into clusters of similar candidates. A single design candidate from each cluster can then represent the corresponding “type” of designs, which makes it easier to select a design candidate for further development.

Stasiuk et al. cluster over 2,000 evaluated candidates of a bending-active structure—found by a genetic algorithm—according to 18 characteristics [23]. Their analysis yields 80 clusters, i.e., 80 archetypal design candidates (Figure 2). However, due to this considerable number, a human designer might struggle to select a design for further development or to understand the characteristics of these 80 candidates in relationship to their performance.

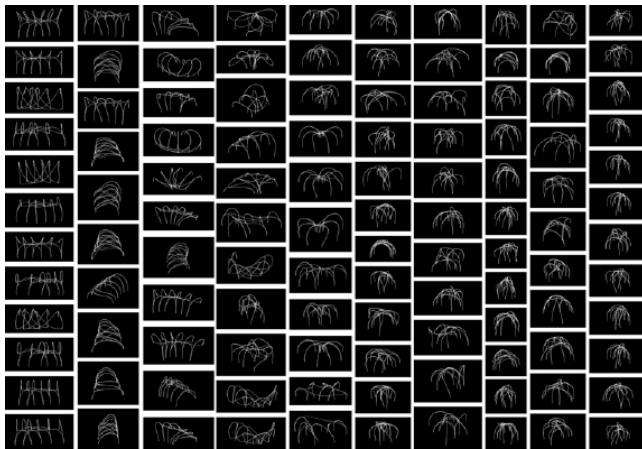


Figure 2. Each of the ten columns presents design candidates from one of 80 clusters. Illustration: (Stasiuk et al. 2014)

Chen et al. define a twelve-dimensional parametric model of an abstract building geometry, resulting in a space of 752,640 design candidates [4]. They search this space with a multi-objective, Pareto-based GA that aims to minimize the building envelope’s thermal transfer and cost and to maximize the available daylight, yielding 5,000 evaluated candidates. They then use K-means clustering to identify relationships between design parameters and performance, though with only partial success.

Nevertheless, that one must provide the number of clusters *a priori* is a principal disadvantage. A promising approach to overcome this disadvantage is bipartite modularity, which requires only the specification of what constitutes a meaningful difference of parameter values [6].

3.2 Pareto-based Optimization

Pareto-based optimization (i.e., optimization with multiple performance objectives) has long been understood to support selection by allowing designers to select from a limited set of *non-dominated* design candidates and to understand tradeoffs between different performance objectives [e.g., 18]. Non-dominated design candidates are “equally good” in the sense that improvements in one objective imply losses in others. In other words, Pareto fronts represents trade-offs

between multiple performance objectives and allow designers to select design candidates based on these trade-offs. But, in the context of performance-informed DSE, Pareto-based optimization has several disadvantages:

Compared to single-objective optimization, Pareto-based optimization is exponentially more difficult. While proponents of Pareto-based optimization have been arguing that advances in computational power will overcome this difficulty, the complexity of simulations has kept pace with such advances. As such, the trade-offs represented by Pareto-fronts can be misleading [27].

Each additional optimization objective exponentially increases this computational difficulty. In addition, when more than two performance objectives are optimized, the results of Pareto-based optimization can be hard to visualize and interpret. For example, Nagy et al. optimize an office layout in terms of six performance objectives [16]. Similarly to [4], they cluster and visualize a set of 10,000 design candidates, but have difficulty with identifying meaningful trends (Figure 3).

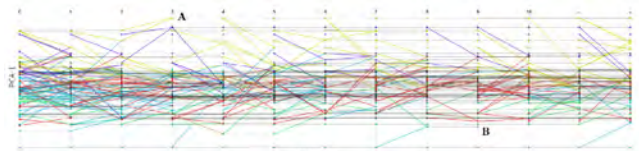


Figure 3. Visualization of the history of design candidates over several optimization iterations (i.e., generation). The colors indicate designs from different clusters.

Pareto-based optimization does not represent design spaces, but trade-off spaces. As such, it does not support designers’ freedom to explore dominated solutions, i.e., solutions that do not lie on the Pareto front. In addition, Pareto fronts cannot visualize relationships between performance objectives and design parameters, i.e., design spaces. These relationships are critical for understanding why certain kinds of designs perform better than others.

4 REFINEMENT

Compared to selection, supporting refinement is relatively straightforward. Allowing the intuitive adjustment of individual design parameters is a basic feature of visual programming platforms such as Grasshopper [20]. A more indirect approach to refinement is interactive optimization, which—to some extent—allows designer to direct automated search processes [7].

4.1 Surrogate Modelling and Model-based Optimization

Surrogate models (which, after a learning phase, approximate time-intensive simulations in real-time) provide designers with real-time performance feedback to design parameter adjustments. Such models (also known as meta-models) approximate time-intensive simulations with machine-learning-related or statistical techniques. The rapid performance estimates provided by surrogate models are crucial for supporting performance-informed design in terms

of refinement and understanding. Surrogate modeling “not only provides an estimate of the optimal point, but also facilitates the development of intuition and understanding about what is going on in the model” [14].

For example, Tseranidis et al. construct surrogate models for the structural and energy performance of a parametrically-defined airport terminal with six parameters [25]. They use 1,000 samples, i.e., 1,000 simulated design candidates that they chose quasi-randomly, to construct several types of surrogate models with varying accuracy.

But note that, for finding high-performing design candidates, quasi-random sampling is far less efficient than optimization [30], and that the accuracy of surrogate models is necessarily constrained by the quality of the found solutions. By contrast, model-based optimization algorithms create and iteratively refine surrogate models during optimization [27]. In other words, model-based optimization is a form of adaptive sampling that, for well-performing design candidates, achieves good accuracy with relatively small numbers of samples.

5 UNDERSTANDING

Although understanding relationships between design parameters and performance is an end goal of performance-oriented design, it is hard to achieve and measure directly. The proposed paper discusses three approaches to supporting understanding: (1) multi-variate visualization, (2) real-time feedback, and (3) statistical analysis.

5.1 Multi-variate Visualizations

Multi-variate (i.e., high-dimensional) visualizations visually represent the multiple dimensions (i.e., design parameters) of parametric design spaces [28]. Many approaches to performance-informed DSE include visualizations, with parallel coordinates being the most common (Figure 4a).

Multivariate visualizations harness humans' perceptual abilities to “look for structure, features, patterns, trends, anomalies, and relationships in data” [12] and “are now being used both to convey results of [data] mining algorithms in a manner more understandable to end users and to help them understand how an algorithm works” [8]. This paper

proposes that performance-informed DSE can likewise benefit from multivariate visualization, by, instead of presenting only one or a small selection of design candidates, providing designers with an overview of entire design spaces and/or fitness landscapes. Combining different visualizations, i.e., providing multiple representations, can enhance creativity [31].

Harding proposes *Self-Organizing Maps* to visualize high-dimensional fitness landscapes in ADO [11]. Self-organizing Maps are neural networks that arrange high-dimensional data in two-dimensional grids based on similarity. Such maps are well-suited to organizing design candidates but make it difficult to understand relationships between design parameters and performance, because this mapping is nondeterministic and different for each parameter. In other words, self-organizing Maps “distort” design spaces.

Parallel Coordinates introduce a set of parallel—usually vertical—axes equal to the number of parameters of the data. To display a datum, one marks the value of each parameter on the corresponding axis and connects the resulting points with a polyline (Figure 4a). A variation of this method uses radial axes, which allow the representation of data as closed polylines (Figure 4b). Although such visualizations are easy to construct and understand, they become hard to read when representing many data, since the polylines tend to overlap (e.g., Figure 5). Naturally, such visualization methods also become harder to understand as the number of parameters, i.e. coordinate axes, increases.

Design Explorer [32], an online visualization tool developed by structural engineering consultants Thornton Tomasetti, uses parallel coordinates to represent design candidates (Figure 5). Confusingly, the tool’s representation does not distinguish between design parameters and performance objectives and plots them on the same set of axes. Nevertheless, Design Explorer represents an approach that, through multiple representations, supports both selection and understanding. Similarly, Fuchkina et al. present an online “design space exploration framework” that combines K-means clustering, self-organizing maps, and parallel coordinates [10].

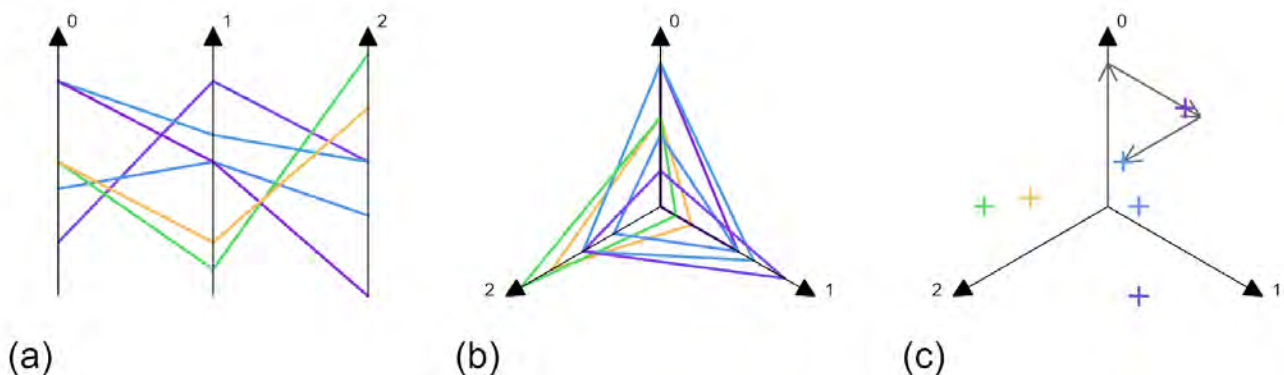


Figure 4. Three methods to visualize a set of 3-dimensional points in two dimensions: Parallel Coordinates (a), Radial Coordinates (b), and Star Coordinates (c).

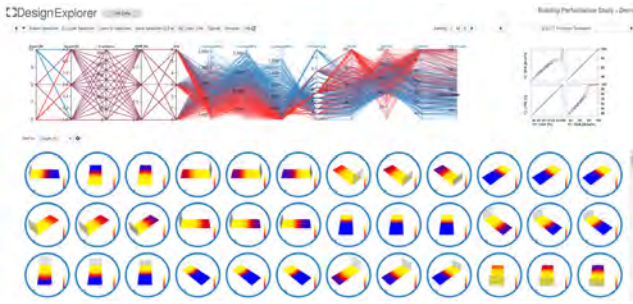


Figure 5. Screenshot of Design Explorer (<http://t-acm.github.io/DesignExplorer/>, accessed 24.10.2017)

Star Coordinates also uses one coordinate axis per parameter, with the axes typically arranged radially (Figure 4c). In contrast to parallel coordinates, star coordinates display a datum not as a closed polyline but as a single point. As a point-based representation, star coordinates can represent many more data than parallel coordinates, and even display a continuous field to represent the space of the data, although at the price of making individual parameters less readable.

An important advantage of parallel and radial visualizations is that their coordinate axes allow the estimation of numerical parameters. This advantage contrasts with other methods such as clustering and self-organizing maps, which cannot directly represent numerical relationships.

5.2 Performance Maps

Wortmann presents Performance Maps [28], a multivariate visualization for fitness landscapes. Performance Maps project multi-variate design candidates (i.e., design candidates with multiple design parameters) onto two dimensions with star coordinates, interpolate the underlying fitness landscape through a triangulation of the projected design candidates and with barycentric coordinates (Figure 6a), and evaluate the performance of the interpolated design candidates through direct interpolations, explicit simulations, or with a surrogate model (Figure 6b). The surrogate model hastens the evaluation of interpolated design candidates in the performance map and thus improves its interactivity.

Performance Maps employ a *surjective* mapping, where every design candidate corresponds to a point on a Performance Map, but several design candidates can correspond to the same point. But in practice, the employed interpolation provides a one-to-one mapping between high-dimensional fitness landscapes and their two-dimensional representations as Performance Maps, albeit with some losses.

5.3 Statistical Analysis

Statistical methods aim to predict and quantify the impact of individual design parameters on performance, which is the most direct way of understanding a design space in terms of a performance objective.

Conti and Kaijima use probabilistic graphical models to approximate relationships between design parameters and performance [5]. Using statistical inferences, these probabilistic models not only approximate the performance of design candidates (like surrogate models), but also predict the most likely ranges of design parameter values for a desired performance value. Probabilistic models present designer with a range of possibilities to achieve a desired outcome, instead of with one or more high-performing design candidates. Like other statistical approaches, probabilistic models require many samples to make accurate predictions. (The rapid performance estimates provided by surrogate models can help to overcome this disadvantage.) An example structural design problem with six variables required 4,000 pseudo-random samples, i.e., simulations, to achieve a root-mean-square prediction error below 10% [5]. But since no optimization was performed, it is likely that the best performing designs were not included in the test set.

Brown and Mueller [3] present a case study of a parametric design for an airport terminal. They analyze the significance of design variables and combine them into a single variable via *Principal Components Analysis* and *Canonical Correlation Analysis*. This new variable is more “meaningful” since it more directly controls a trade-off between structural and daylight performance.

But designers should be careful when performing such simplifications: For a building energy problem with thirteen parameters, only two seemed significant, according to a sensitivity analysis of total effects with 15,000 SOBOL samples [30]. But when performing optimization on the same problem, all optimization algorithms almost immediately found design candidates that performed better than any of the 15,000 samples.

This result implies that, at least in terms of finding the highest-performing design candidates, only the non-significant variables were relevant, because the optimization algorithms immediately chose good values for the significant ones. In other words, even when statistical analyses use very large numbers of quasi-random samples, they can be misleading for at least some types of fitness landscapes. As such, designers should verify and contextualize statistical insights with ADO, because the differences between well-performing and highest-performing design candidates can be informative by themselves.

6 PERFORMANCE-INFORMED DSE STRATEGIES WITH PERFORMANCE EXPLORER

Wortmann introduces Performance Explorer, a novel tool for visual and interactive, performance-informed DSE [26]. He further describes several performance-informed DSE strategies followed by participants in a user test of Performance Explorer. Consisting of different combinations of selection, refinement, and understanding, these strategies illustrate and—to some extent—validate the proposed framework for performance-informed DSE.

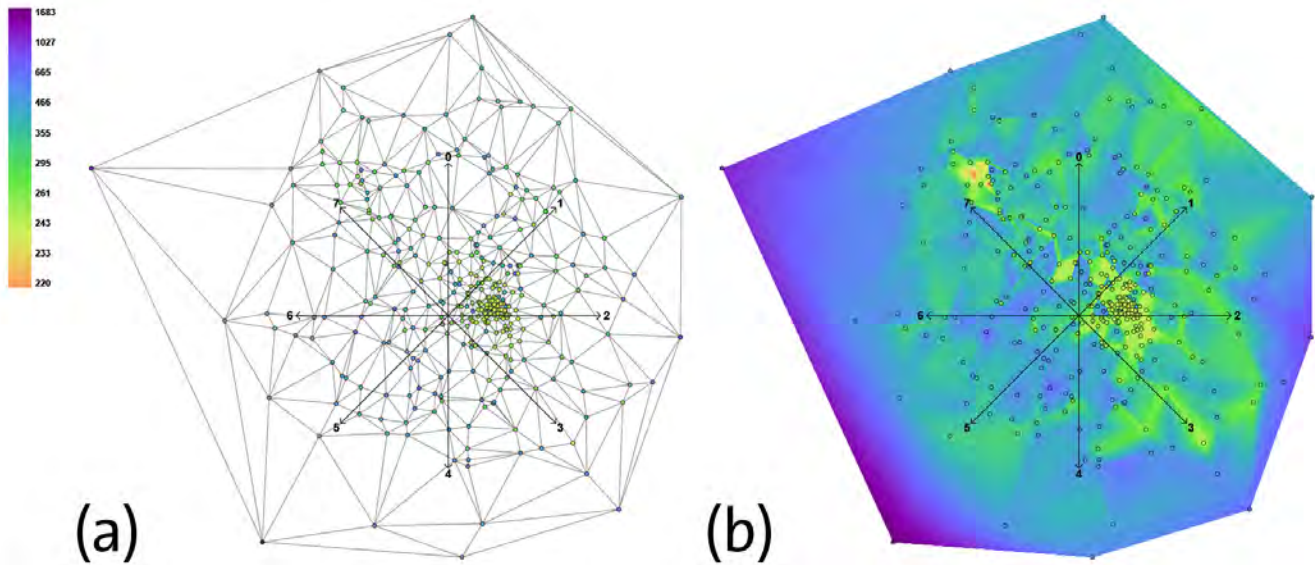


Figure 6. Performance Map of a structural design problem with eight parameters. (a) displays the triangulation of simulated design candidates, and (b) the interpolated performance map resulting from the triangulation.

6.1 Performance Explorer Features and User Test

After an optimization phase with a model-based algorithm, Performance Explorer displays an interactive Performance Map, based on the surrogate model resulting from optimization. Performance Explorer is integrated with Grasshopper, a 3D modelling and simulation platform. This integration allows bi-directional, real-time feedback between Grasshopper and Performance Explorer: The Performance Map reflects parameter changes in Grasshopper, and Grasshopper follows parameter changes on the Performance Map. In this way, Performance Explorer presents designers with (1) a design candidate's appearance in Grasshopper, (2) its design parameters, represented as a radial plot, (3) its (approximated) performance, and (4) its location in the fitness landscape relative to other candidates (Figure 7).

In addition to these multiple representations, Performance Explorer allows users to verify the approximated performance of promising design candidates through simulations, and to refresh the Performance Map and underlying surrogate model based on the simulation results. In this way, users interactively enhance the surrogate model's accuracy by adding additional samples based on their preferences.

A user test with thirty participants found that, compared to manual DSE (i.e., manipulating design parameters by hand) and automated DSE (i.e., optimization), Performance Explorer was more enjoyable to use and provided more support for the test's performance-informed design task [26]. The design task asked participants to find, for a given parametric model of a small pavilion, a structurally well-performing design candidate that was a promising starting point for further development from an architectural point of view.

6.2 Performance-informed DSE Strategies

This section presents performance-informed DSE strategies that resulted from a survey conducted during the user test, which asked participants why and how they selected their final design candidates. As such, the categorization of the participants' answers into strategies is somewhat subjective.

None of the participants accepted the best optimization result as the preferred design candidate. This non-acceptance indicates that Performance Explorer encourages selection and/or exploration.

Two participants randomly adjusted design parameters. Compared to manual and automated DSE, this strategy is easier to implement with Performance Explorer, since, instead of adjusting individual parameter values, one can drag across the performance map: "Navigating through the design space (quite randomly) and trying to find a solution that looks good according to my concept." Three participants adjusted parameters according to a plan: "A constraint of a smaller span was first set, with a greater variation in the three heights." This (random or strategic) manipulation of design parameters is an example of refinement.

One participant tried to understand relationships between parameters and performance by manipulating parameters by hand: "I tried to understand the relationship between design results regarding the displacement value."

Nine participants selected design candidates from optimization results. In contrast to automated DSE, selective strategies can include an extra step with Performance Explorer: Verifying the performance of design candidates that are predicted to perform well by the surrogate model through a simulation: "I chose points in the [well-performing] sections of the graph and tested out which one

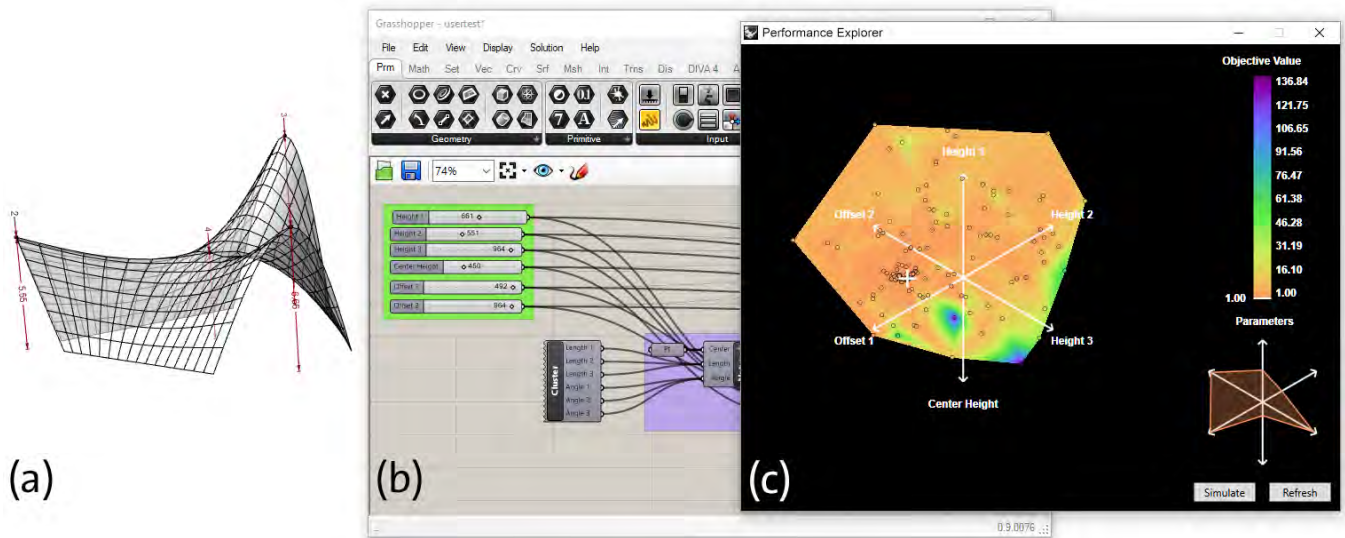


Figure 7. Performance Explorer in Grasshopper. From left to right: (a) Morphology (i.e., appearance) of the current design candidate, (b) definition of the parametric model in Grasshopper (note the green box with the number sliders representing the design parameters and their current values), and (c) the Performance Explorer window.

simulates to give the best maximum displacement values and design.”

Four participants selected a well-performing design candidate and adjusted it: “I was clicking through the [design candidates] to see the overall range of results and fixed on the one that I felt was more sculpturally looking and began to tweak it with the sliders.” Six participants selected an appealing design candidate and used the performance map to refine it in terms of structural performance: “Find the region that closely [approximates] the final massing that I want by using the mapping, change the sliders manually to see how the objective changes (whether it is moving to a ‘bad value; region or not.”

Five participants enhanced the visualization of the fitness landscape in terms of scope and/or accuracy and selected an appealing design candidate with satisfactory performance: “I explored the solution space extensively. First, I generated extra points to understand areas that also score highly, but not as high as the optimal zone. Then, I went around the solution space, [simulating] as I went, to explore everything. I settled for an area with a good (but not the best) score that resulted in a shape that I liked.”

In summary, Performance Explorer supports (1) selection by representing individual design candidates relative to the positions of other design candidates in the fitness landscape, (2) refinement by providing real-time feedback to parameter changes and by visualizing what kinds of parameter adjustments might lead to better performance, and (3) understanding by visualizing the entire fitness landscape, which allows the identification of problem characteristics and promising areas for further exploration, and through multiple representations. This support is discernable from the fact that the largest group of participants applied selection,

and comparatively large groups strategies with selection and refinement and/or understanding. These results clarify that selection, refinement, and understanding are not exclusive categories, but rather approaches that should be mixed-and-matched based on individual design strategies.

7 CONCLUSION

Performance-oriented DSE is a novel framework for the analysis and further development of approaches that bridge the gap between explicit problem formulations and “wicked” design problems. Such approaches aim to better support designers in their computational searches for high-performing parametric design candidates than optimization alone. The paper identifies selection, refinement, and understanding as three key aspects of performance-informed design and surveys existing approaches in terms of these aspects. The survey finds clustering, real-time feedback via surrogate models, multivariate visualizations, and statistical analyses as important methods and discusses their advantages and disadvantages. It describes Performance Explorer, a novel tool for performance-informed design that employs multiple representations and allows designers to mix-and-match selection, refinement, and understanding.

Future directions include further refining and validating the proposed framework, adapting some of these methods to multiple performance objectives, to explore and/or develop other types of visualizations, and to make more of these methods available as easy-to-use tools that work in conjunction with each other. Integrating the model-based optimization algorithm with Performance Explorer would allow alternating between optimization and exploration of the Performance Map and—by re-running optimization with ranges of parameters limited according to insights gained from this exploration—interactive optimization or “automated refinement.”

ACKNOWLEDGMENTS

This paper is based on two chapters from the first author's PhD thesis [26]. Performance Explorer was developed at SUTD's Advanced Architecture Lab and supported by the SUTD-MIT International Design Centre under grant numbers IDG215001100 and IDG2170010.

REFERENCES

1. Andia, A. and Spiegelhalter, T. *Post-parametric Automation in Design and Construction*. Artech House, 2015.
2. Bradner, E., Iorio, F. and Davis, M. Parameters tell the design story: ideation and abstraction in design optimization. *SimAUD 2014*, SCS (2014).
3. Brown, N.C. and Mueller, C.T. 2018. Design variable analysis and generation for performance-based parametric modeling in architecture. *IJAC* (2018).
4. Chen, K.W., Janssen, P. and Schlüter, A. Analysing Populations of Design Variants Using Clustering and Archetypal Analysis. *eCAADe 2015*, 251–260.
5. Conti, Z.X. and Kajijima, S. A Knowledge-oriented Approach to Performance-driven design Using Probabilistic Graphical Models. *IASS 2017*.
6. Costa, A., Proverbio, M. and Smith, I.F.C. Cyber Civil Infrastructure and IoT for Cities. *IEEE SSCI 2017*.
7. Danhaive, R.A. and Mueller, C.T. 2015. Combining parametric modeling and interactive optimization for high performance and creative structural design. *IASS 2015*.
8. De Oliveira, M.C.F. and Levkowitz, H. From visual data exploration to visual data mining: a survey. *TVCG* 9, 3 (2003), 378–394.
9. Dorst, K. and Cross, N. Creativity in the design process: co-evolution of problem–solution. *Design Studies* 22, 5 (2001), 425–437.
10. Fuchkina, E., Schneider, S., Bertel, S. and Osintseva, I. Design Space Exploration Framework. *eCAADe 2018*, 367–376.
11. Harding, J. Dimensionality Reduction for Parametric Design Exploration. *AAG 2016*, 274–287.
12. Hoffman, P. and Grinstein, G. Introduction to Data Visualization. *Information Visualization in Data Mining and Knowledge Discovery*. U. Fayyad, G.G. Grinstein, and A. Wierse, eds. Academic Press, 2002, 21–45.
13. Johnson, B.R. *Design computing: an overview of an emergent field*. Routledge, 2017.
14. Jones, D.R., Schonlau, M. and Welch, W.J. Efficient global optimization of expensive black-box functions. *J Glob Optim* 13, 4 (1998), 455–492.
15. MacQueen, J. Some methods for classification and analysis of multivariate observations. *Fifth Berkeley Symposium on Mathematical Statistics and Probability*, (1967), 1:281–297.
16. Nagy, D., Lau, D., Locke, J., Stoddart, J., Villaggi, L., Wang, R., Zhao, D. and Benjamin, D. Project Discover: An application of generative design for architectural space planning. *SimAUD 2017*, SCS (2017), 59–66.
17. Oxman, R. Performance-based design: current practices and research issues. *IJAC* 6, 1 (2008), 1–17.
18. Radford, A.D. and Gero, J.S. On Optimization in Computer Aided Architectural Design. *Build Environ* 15 (1980), 73–80.
19. Rittel, H.W. and Webber, M.M. Dilemmas in a general theory of planning. *Policy Sciences* 4, 2 (1973), 155–169.
20. Grasshopper®. Robert McNeel and Associates, 2010.
21. Schaffranek, R. Just Good Enough, is Good Enough for Architecture: Optimizing - a Task for the Architect. *Productive Limits: Architects Gone Exploratory*. Sonderzahl, 2012. 89–99.
22. Shea, K., Aish, R. and Gourtovaia, M. Towards integrated performance-driven generative design tools. *Automat Constr* 14, 2 (2005), 253–264.
23. Stasiuk, D., Thomsen, M.R. and Thompson, E.M. Learning to be a Vault. *eCAADe 2014*, 381–390.
24. Stouffs, R. and Rafiq, Y. Generative and evolutionary design exploration. *AIEDAM* 29, 4 (2015), 329–331.
25. Tseranidis, S., Brown, N.C. and Mueller, C.T. Data-driven approximation algorithms for rapid performance evaluation and optimization of civil structures. *Automat Constr* 72 (2016), 279–293.
26. Wortmann, T. *Efficient, Visual, and Interactive Architectural Design Optimization with Model-based Methods*. Singapore University of Technology and Design, 2018.
27. Wortmann, T. Model-based Optimization for Architectural Design: Optimizing Daylight and Glare in Grasshopper. *TAD* 1, 2 (2017), 176–185.
28. Wortmann, T. Surveying design spaces with performance maps. *IJAC* 15, 1 (2017), 38–53.
29. Wortmann, T. and Nannicini, G. Introduction to Architectural Design Optimization. *City Networks - Planning for Health and Sustainability*. A. Karakitsiou, A. Migdalas, P.M. Pardalos, and S. Rassaia, eds. Springer International Publishing, 2017, 259–278.
30. Wortmann, T., Waibel, C., Nannicini, G., Evins, R., Schroepfer, T. and Carmeliet, J. Are Genetic Algorithms really the best choice for Building Energy Optimization? *SimAUD 2017*, SCS (2017), 51–58.
31. Yamamoto, Y. and Nakakoji, K. Interaction design of tools for fostering creativity in the early stages of information design. *Int J Hum Comput Stud* 63, 4–5 (2005), 513–535.
32. Design Explorer. Thornton Tomasetti. 2015.



Linear and Classification Learner Models for Building Energy Predictions and Predicting Saving Estimations

Kevin Eaton, Nabil Nassif, Pyrian Rai and Alexander Rodrigues

University of Cincinnati

Cincinnati, United States

{eatonko, nassifnl, raipy, rodrigax}@mail.uc.edu

ABSTRACT

The need for creating building systems with smart systems is growing. Saving energy in buildings is both important in aiding the environment and saving money for the companies and organizations who run those buildings. Most buildings are now equipped with technology to produce accurate electrical outputs that can be used for improving the accuracy of energy models. This paper discusses typical data-based building energy models and proposes new improvements by utilizing a classification learner. Estimating sub-hourly and hourly electric energy consumptions are discussed using four different data-based models. The first model is a linear fit model using one regressor, the second is a linear change point fit using one regressor, and the third model is a two regressor model using a linear fit. The fourth model is a proposed Classification Learning model using three regressors. Two different types of data were collected: simulation and actual data. There are four buildings total: two with simulation and two with actual data. The results show that the proposed Classification Fine KNN model can provide accurate predictions for the data as compared to traditional linear modeling techniques. These models are then utilized to calculate saving percentage, which is then compared to the actual percentage.

1 INTRODUCTION

As energy concerns continue to grow, the need for creating more efficient building systems has increased. This requires us to use modeling techniques to save energy more accurately and efficiently. Most modern buildings include electric power meters that can read out the energy data at specific time intervals. This data is extremely useful, and, in most buildings, it is underutilized. This data paired with the temperature and what day of the week is useful for predicting how much energy a building will consume. There is a need to investigate how modern computing techniques can benefit these buildings. The single or multivariate regression model is widely employed as a means of identifying energy efficiency measures,

monitoring energy consumptions, and measurement and verification projects [1][3]. These models, however, may not be as accurate as using advanced techniques. The hope is to have intelligent applications in the building system to find efficiency, optimization, energy assessment, and fault detection [1][3][4][5]. Applying these advanced prediction techniques can aid in many areas. The model being proposed in this paper is the Fine KNN model. A KNN model is an algorithm that interprets the data based on the inputs given and what the output should be and creates a fit based on the data. A Nearest Neighbor model was chosen to be a proposed model because it evolves based on the data and surrounding points. This makes it excellent for training and testing on evolving data, such as building energy consumption. These predictions will aid in being able to calculate savings. The saving can be calculated after simulating optimizations to the air conditioning systems. Saving can then be calculated and estimated to determine which model creates the best estimation for saving calculation.

2 DATA COLLECTION

The data is collected from the entire energy consumption of the buildings. Building 1 and 2 are collected from a simulation data using the energy simulation program eQUEST [2]. Building 1 is a simulated building with specific dimensions in New York and building 2 is the same building in Greensboro, North Carolina. Buildings 3 and 4 are both real buildings using their actual data in North Carolina. Both buildings have different dimensions and attributes. Figure 1 shows the whole building electric consumptions for the four buildings used as functions of dry bulb temperature.

Building 1 and 2, as seen in Figure 1, have similar looking data. The data differs at the higher dry bulb temperatures due to location. Building 2 is located in North Carolina which has a higher temperature more often. This affects the energy consumption and creates many higher energy output data points around higher temperatures when the air conditioning has to be turned on. For the real data of building 3 and 4, They also have much different looking shapes. This is because they are two different buildings with different energy consumption needs. Building 4 consumes much less energy which may be because of the way the building is laid out or the amount of people in the building, etc.

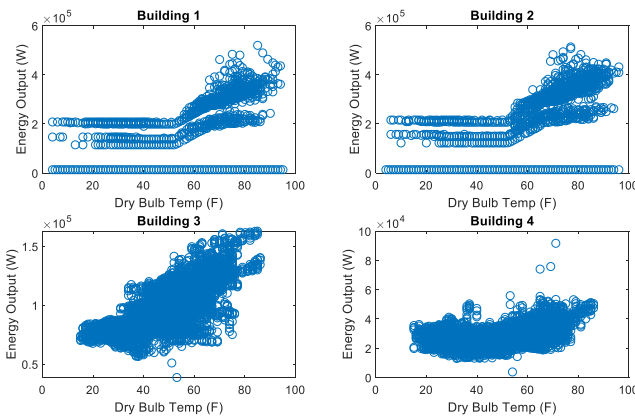


Figure 1. Whole building electric consumptions of buildings being investigated as functions of outside dry air temperature.

3 BUILDING ESTIMATION MODELS

There are two main ways for energy consumption to be approached in modeling, a forward method and an inverse method. The forward method is to use the detailed parts of the existing system to predict how the system will act in the building [3]. The inverse method is using the actual data of an existing system and making models based on the data acquired by the system. This paper will investigate the inverse method. The inverse method can use multiple regressors or just one. There is no single model that is appropriate for all buildings and system. This paper investigates new techniques to estimate the energy consumption on a sub-hourly or hourly basis for each building as well as the type of day and dry bulb temperature. The four different models listed in Table 1 are discussed. The first two are linear models used by systems today. The third is a two regressor model using temperature and dew point. The fourth model is a proposed Classification Learner model.

Note	Models	Regressor (t_a, t_{dp})	Parameter (a, b, c)	Equations
Model 1	Single Variant	1	2	$Y = a + b.t_a$
Model 2	Single Variant Change-Point t_l	1	2	$Y = a + b.(t_a - t_l)$
Model 3	Double-Variant	2	3	$Y = a + b.t_a + c.t_{dp}$
Model 4	Classification Learner	3	-	-

Table 1. Models 1 - 4 and detailed description of each model.

The Single-Variant Model (Model 1) is a simple linear model. This model is based on only one regressor, the dry bulb temperature t_a . The a and b values are based on the best fit method. The single-variant change-point model (Model 2) uses the dry bulb temperature t_a as the only regressor variable but only at 55°F will the model be more than just the “ a ” value for the plot. The “+” indicates that the interior of the parenthesis will become zero if outside temperature t_a is less than t_l . Model 3 uses two different regressors, dry bulb temperature, t_a , and dew point, t_{dp} . Model 3 then uses a simple one degree poly fit to estimate what the energy consumption would be. These models (Model 1, 2, and 3) are used widely across commercial and residential areas. These models are easily applied and have data that is easily accessible. Data for these models can be obtained easily from electricity bills and simple output algorithms within the building. These models do not consider the day of the week or hours of each day when the air conditioning is on or not. These factors are considered in Model 4. Model 4 is a Fine KNN. KNN stands for K Nearest Neighbor which is a classification learning technique. The nearest neighbor determines several samples that can be classified as a certain group (Yong, 2013). Usually, this technique is used with binary data sets where there are few classifications it can be described to, such as a “+” or “-“. For the energy consumption data, the KNN model predicts the data into small pockets of many possible outcomes. This is the reason a “Fine” method is used. The “Fine” version of the KNN only places data into a category if the data is very close and fits well. Since there are many outcomes to be trained for, the algorithm must be certain that the predicted value is correct. “Fine” describes how far away the neighbors are that the data is trained off. The “Fine” version of the KNN uses close data around it to train and trusts them to be accurate. The fine setting was chosen because the data is reliable enough that using nearest neighbors with a fine detail and create an accurate

model. The learner takes multiple inputs, as shown by Figure 2.

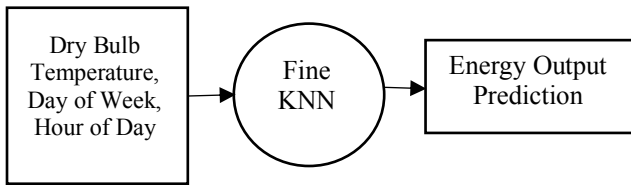


Figure 2. Inputs and outputs that define the Classification Learner

4 RESULTS

The one-year data collected are divided between training data that is for the first nine months of the data and testing data covering three months. All models are developed by taking the training data and placing the model against the testing data. An example of the training and testing is shown below in Figure 3.

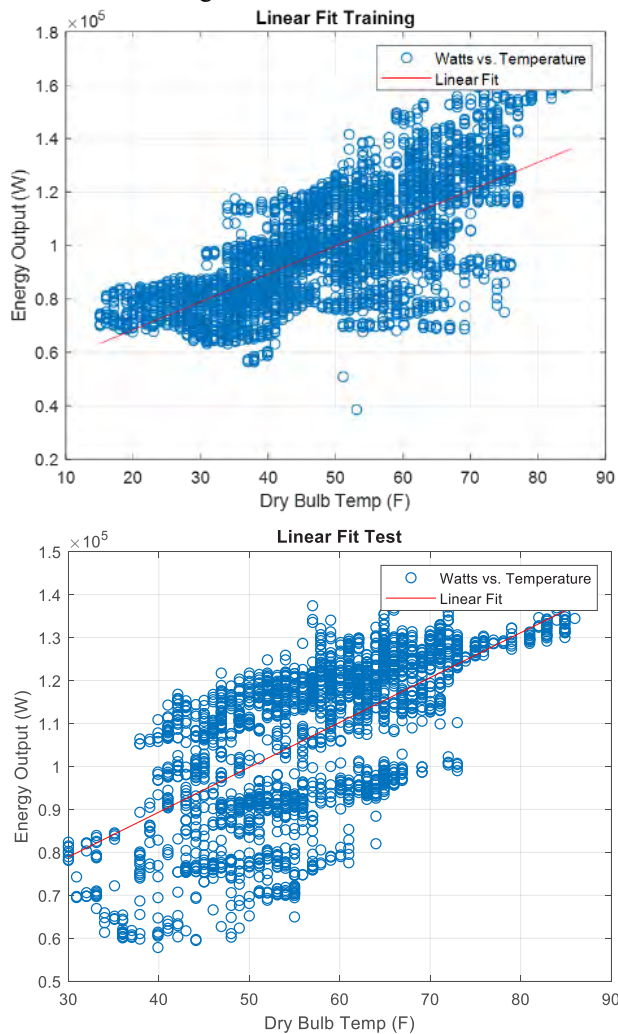


Figure 3. Training and Testing data with a linear fit line for Building 3.

To discuss these results, the performance of each model will be analyzed for all buildings. In a general sense, the Linear models (Models 1, Model 2, and Model 3) have a lower training and testing R-Squared value as compared to the Classification Learner.

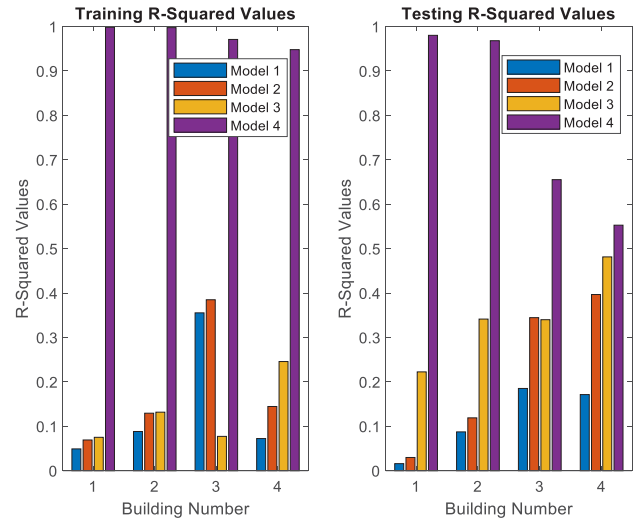


Figure 4. R-Squared Values for each building and model.

Looking at Model 1, we see that the test values fall below 0.2 for all buildings. This demonstrates how the single linear model does not fit the data very well. This can also be seen in the Figure 5 with the poor fit onto both buildings. The data is spread widely for all the dry bulb points and having a single linear line to fit to the data does not predict the data well. The two times where the R-Squared was high for model 1, buildings 3 and 4, the data collected had much noise on it due to the acquired data being from a real building with fluctuations in the amount of total energy consumed.

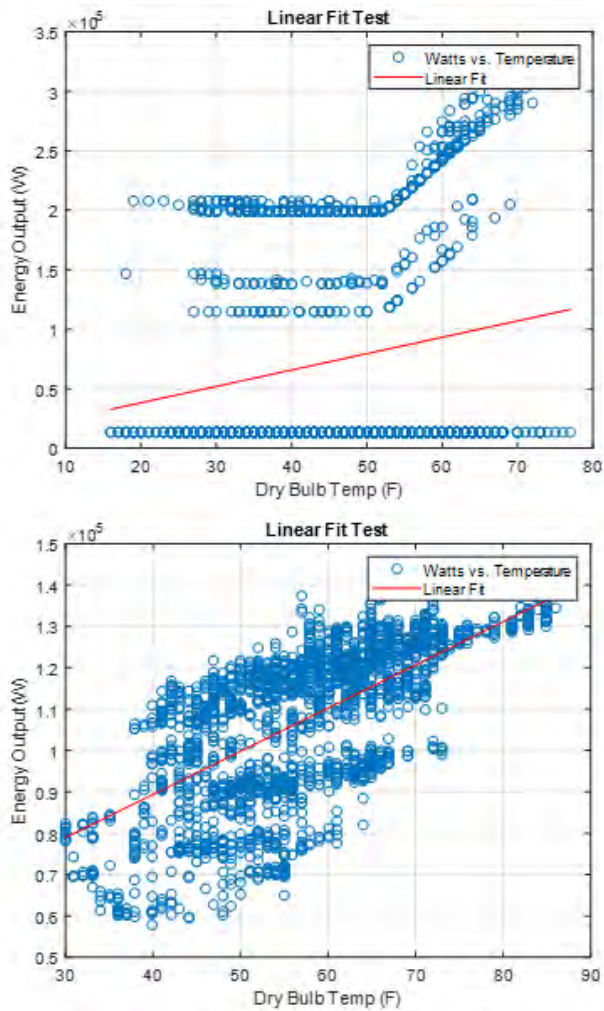


Figure 5. Results of Model 1 on Building 1 and Building 3

Model 2 creates a better fit than Model 1. In every building the testing results of Model 2 is an increase on Model 1 R-Squared result. This improvement comes from the change point considering how the air conditioning system works. The air conditioning systems come on at around 55 degrees Fahrenheit which increases energy consumption. Figure 6 shows how the testing fit on the real and simulated buildings is more accurate than in Figure 5 but still not as accurate as possible. In the simulated data, the change point fit only is accurate for a small fraction of the data. Figure 4 illustrates this point as well because the R-Squared for the testing data for Model 1 is less than Model 2 for both Building 2 and 4.

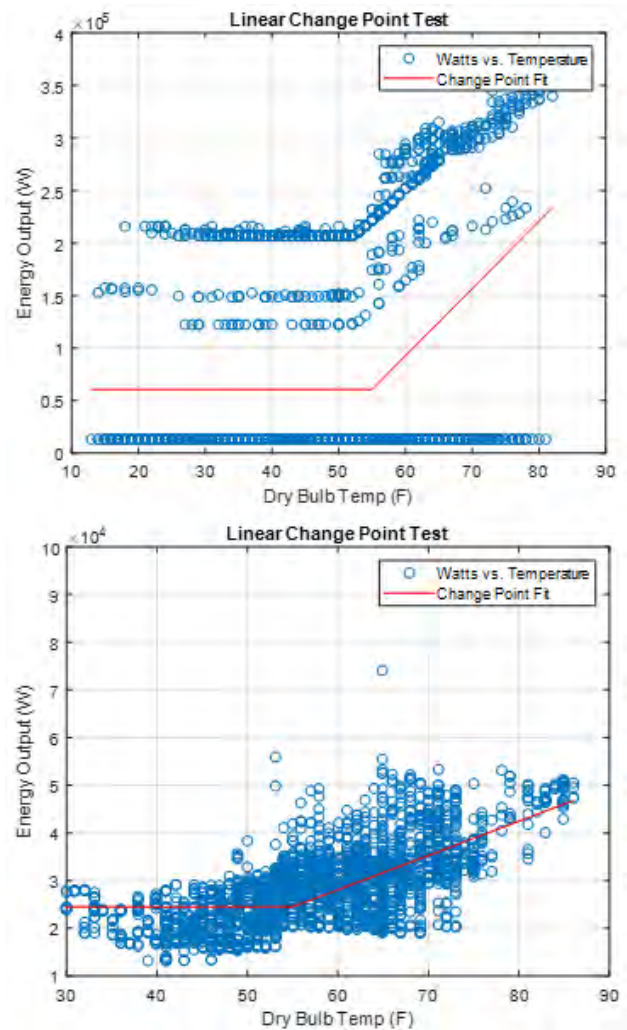


Figure 6. Results of Model 2 on Building 2 and Building 4

Model 3 creates a better fit than Model 1 and 2 in all buildings except Building 3. This may be due to how R-Squared is calculated. Since it falls within the middle of the data and R-Squared calculations take the difference from each data point, the R-Squared value may be giving a misleading number when calculated. When looking at figure 7, it appears that the second graph is only linear. It is not linear though because it does slightly spread in the middle. The data does not spread as much in the real data because the data points are closer in relation to each other without much jumping as in the simulation data.

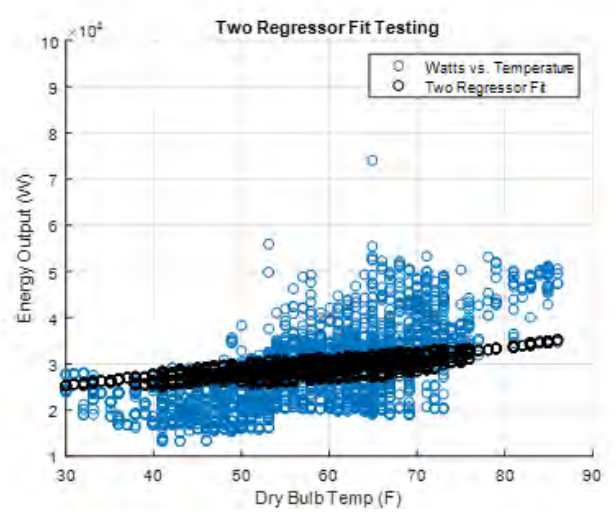
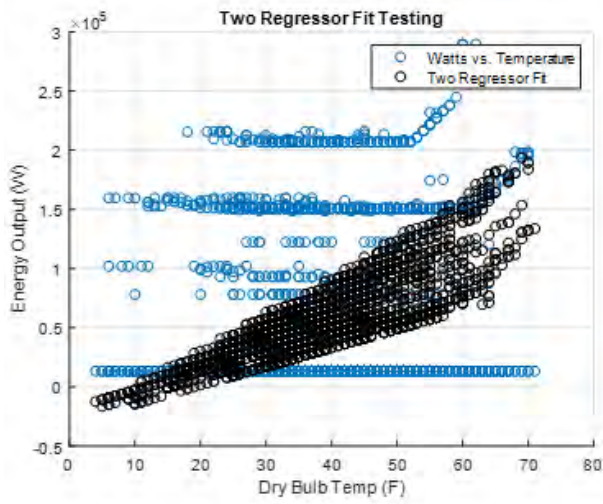


Figure 7. Building 2 and 4 with Model 3 fit onto the data.

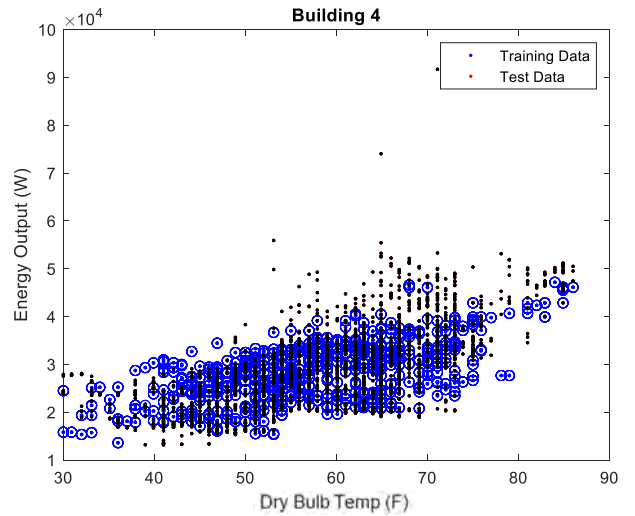
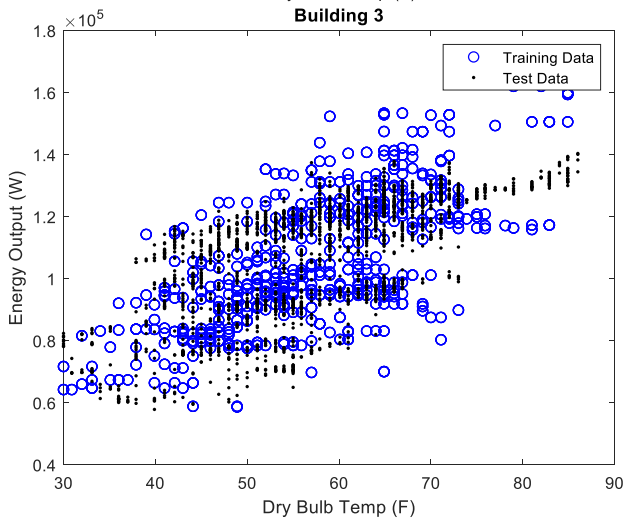
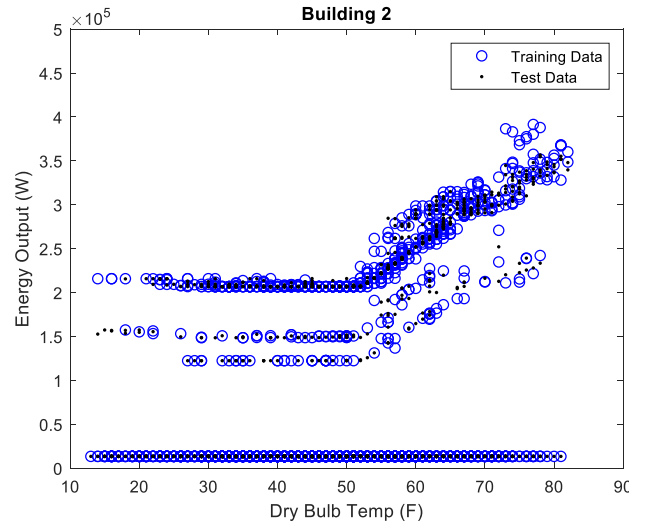
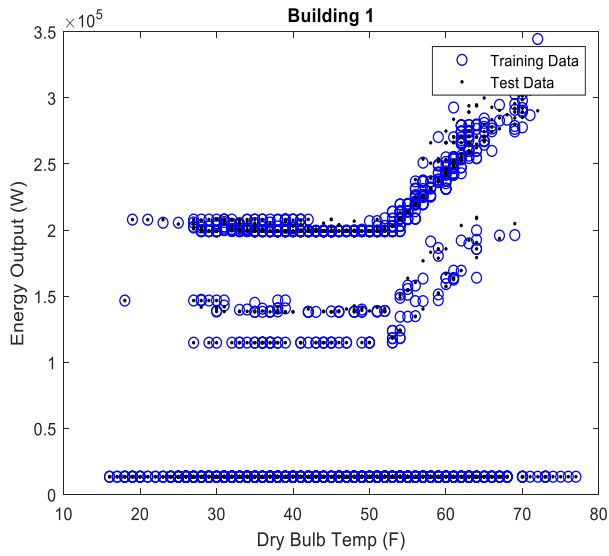


Figure 8. All proposed model results on Buildings 1-4.

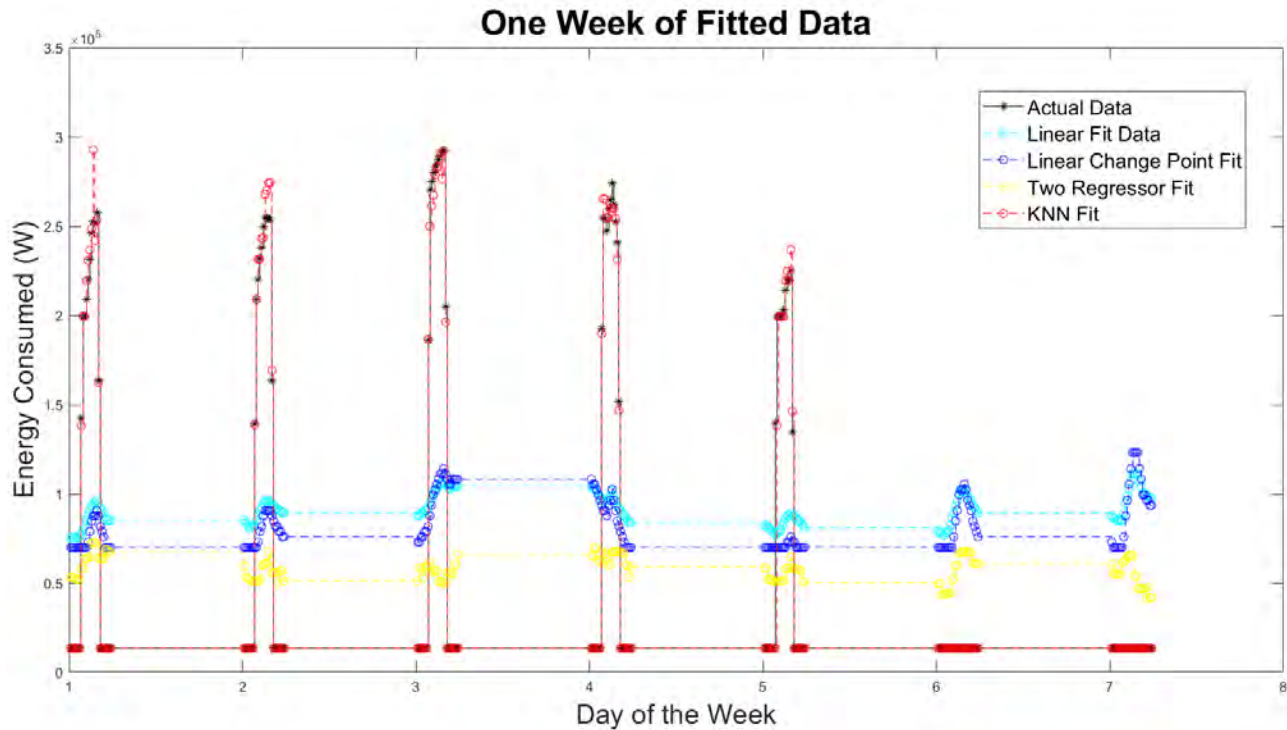


Figure 9. One week of testing data for Building 1

Overall, Model 4 does the best when compared to the other three models. By training the Classification Learner with more than one regressor as well as using neural network to train create the model, the R-Squared values were greater than the linear model. Figure 7 shows how the testing fit onto the data matches the fit and more accurately represents the data. The data points predicted to fit onto the data set are visibly closer than a single line of fit. The data also backs this up by showing that all R-Squared values are greater in the Classification Model as compared to the linear fit models, as seen in Figure 4.

Figure 9 shows how the models fit as compared to the actual data per one week of data. On the x-axis, one being Monday and seven being Sunday. The proposed model, model 4, fits very closely to the actual data unlike model 1, 2, and 3. This demonstrates how unwell these models fit the actual data as compared to Model 4. This can also be seen in Figure 4 with Model 4 being much closer of a fit with the R-Squared values

Annual saving calculations were done on the simulation buildings. The eQuest simulation program was used to simulate optimized energy consumption. The optimized factors were a light change from 1.2 to 0.8 watts per square foot, a Fan Premium, and Optimal Supply Air Temperature. The estimated data was created by training the all the models from Table 1 with the optimized data using nine months of training and three months of testing. As seen in Table 3, the saving percentage is all positive. That is because the actual data used more energy than the optimized data, so the saving percent is positive. The estimated data in Table 3 is within two percent of the actual data, showing that using the classification learner is a good fit of estimating actual savings for the simulation data. Model 1 outperforms Model 4 in Building #2 but this may come because of circumstance of the data due to Model 1 being much less accurate for Building 1. Model 4 also is the most consistent with its errors as compared to the other three models because it is close by similar percentages, a little less than two percent, unlike the variations of the other two models.

5 SAVING CALCULATIONS

	Actual	Model 1	Model 2	Model 3	Model 4
Building #1	27.82%	23.54%	33.43%	39.98%	26.93%
Building #2	35.51%	36.81%	44.21%	52.36%	33.30%

Table 2. Estimated Saving Percent for each model.

6 CONCLUSION

Four different data-based models or estimating energy consumptions were tested on four buildings. The models are two single regressor models, a two regressor model, and one classification learning model. The data was collected from a simulation and from real building data. The models were evaluated using these data sets. The

testing results indicated that the regression model with the proposed classification learning could improve the models' accuracy. In Building 1, Model 1 had an R-Squared value of 0.06, Model 2 had a value of 0.09, Model 3 had a value of 0.33. These values are low and do not fit the data well, unlike the classification learner which had an R-Squared testing value of 0.97. In Building 4, this pattern is seen again with Model 1, 2, and 3 having R-Squared values of 0.17, 0.35, and 0.46. Model 4 was only slightly greater at 0.55. This result comes from issues with how noisy the data is in the actual buildings and affects the r-squared value. Overall, the proposed model performed better than any of the other three models. While in building 4 the r-squared value of model 3 gets close to model 4, model 4 shows its benefit by being more consistent with its results always above 0.5 r-squared value. By using a Nearest Neighbor model to predict how the energy consumption of the building, it is effective in predicting models. The Fine KNN model is also effective because of the short training period it takes. If used for saving calculation, it can be effective for all businesses to implement this prediction model and predict and optimize their building for saving 0.39 for test values, respectively. Model 4 has an R-Squared value of 0.53, higher than the other models. Overall, using the classification learner compared to the linear models is more accurate and reliable at predicting the behavior of the data in real and simulated data. This can be applied to real buildings in order to optimize and save energy within buildings. Table 3 demonstrates that predicting the saving with the Classification Learner is

close, within 2%, of the actual predicted savings when used with optimization data within Buildings 1 and 2.

7 ACKNOWLEDGMENTS

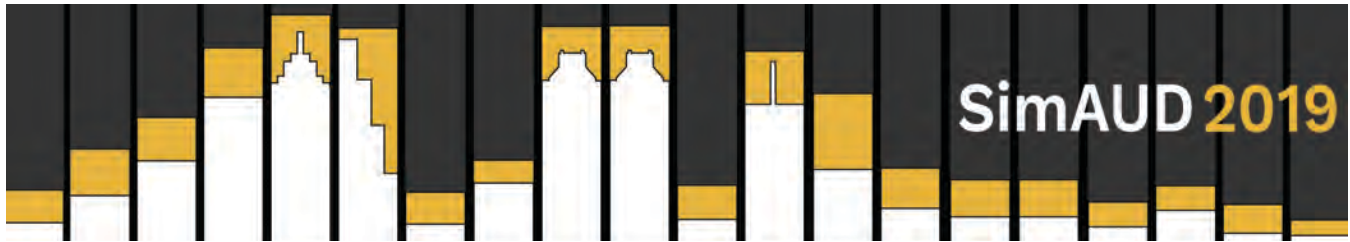
The authors would like to thank all the volunteers, and all publications support and staff, who wrote and provided helpful comments on previous versions of this document.

8 REFERENCES

1. ASHRAE. 2015. ASHRAE Handbook-Applications. Chapter 41. Atlanta: American Society of Heating Refrigeration and Air Conditioning Engineers, Inc.
2. eQuest. **QU**ick **E**nergy **S**imulation **T**ool, eQUEST Version 3.65. <http://www.doe2.com/equest/>
3. Nassif, N. (2018). Regression and Artificial Neural Network Models with Data Classifications for Building Energy Predictions, ASHRAE Transactions 124 (2).
4. Seem, J.E. (2007). Using intelligent data analysis to detect abnormal energy consumption in buildings. *Energy and Buildings* 39: 52–58.
5. Wang, S.W., Q. Zhou, and F. Xiao. 2010. A System-level Fault Detection and Diagnosis Strategy for HVAC Systems Involving Sensor Faults. *Energy and Buildings*, 42: 477-490.
6. Yong Xu, Qi Zhu, Zizhu Fan, Minna Qiu, Yan Chen, and Hong Liu. 2013. Coarse to fine K nearest neighbor classifier. *Pattern Recognition Letters*, 34: 980-986.

Geometric Explorations

From Drawing Shapes to Scripting Shapes: Architectural Theory Mediated by Shape Machine	279
<i>Heather Ligler and Athanassios Economou</i>	
Interpreting Non-Flat Surfaces for Walkability Analysis	287
<i>Mathew Schwartz and Subhajit Das</i>	
Generating Acoustic Diffuser Arrays with Shape Grammars	295
<i>Jonathan Dessi-Olive and Timothy Hsu</i>	
A Unified Framework for Optimizing the Performance of a Kinetic Façade.	303
<i>Ok-Kyun Im, Kyoung-Hee Kim, Armin Amirazar and Churlu Lim</i>	



From Drawing Shapes to Scripting Shapes: Architectural Theory Mediated by Shape Machine

Heather Ligler and Athanassios Economou

Georgia Institute of Technology
Atlanta, USA
{h.ligler, economou}@gatech.edu

ABSTRACT

The shape grammar formalism has offered a visual, rule-based framework for interpreting architectural languages for over forty years. However, the ability to implement grammars within a technology that allows for direct engagement with shape rules and productions so that they can be dynamically simulated, shared, understood, modified, and brought into a more active theoretical dialogue is only partially achieved. The work here asks how a new technology that allows shape rules to be implemented by drawing shapes to specify scripts instead of writing code can reinvigorate shape computation to advance formal analysis and synthesis in architectural research. More precisely, a case study to implement an analog grammar on John Portman's domestic language with a new shape grammar interpreter, the Shape Machine, is presented to take on this question. The results are illustrated as a visual catalog of sample designs generated in the software. The results suggest further insights on Portman's language of the house prompted by the machine-based specification.

Author Keywords

Shape Grammars; Shape Grammar Interpreter; Shape Computation; Formal Composition; Rule-Based Design.

ACM Classification Keywords

D.1.7 VISUAL PROGRAMMING; I.2.1 ARTIFICIAL INTELLIGENCE; I.6.1 SIMULATION AND MODELING; J.5. ARTS AND HUMANITIES – Architecture

1 INTRODUCTION

Questions on the role of the computer in architectural research cover a variety of concerns to date, but in the late twentieth century a significant body of work in formal, visual computations to understand architectural composition was advanced. This specific trend was formalized in the 70s with research in shape grammars and continued prominently into the 90s. However, the initial value proposition of visual calculating remains incompletely realized in available software implementations to date. What happened? Do we need formal theories in architectural design? Does

computing them add any value? Can a technology help to support and communicate the implications of a theoretical proposition? Was this trend merely a fad? Was it too abstract or too complicated to engage broader participation? Was it ahead of its time? And by extension, has it been simply misunderstood in the context of available technologies?

This study adopts a hypothesis that a new technology can help revitalize possibilities for shape computation in architectural research by providing a medium for engaging shape rules and productions. To follow this aim, the research experiments with an interpreter that allows a shape grammar to be represented by drawing shapes in visual rules to specify formal relationships and automating a production process to generate designs without requiring users to interface directly with the background script. The only programming required of the grammar designer is authored in a visual language by drawing shapes. Notably, the implementation is based on an existing analog grammar computed by hand to speculate on John Portman's architectural principles as characterized by his 1964 house, Entelechy I [1]. By translating from a hand-authored grammar to a machine-based specification, the research questions how the technology can inform the theory on Portman's architectural language. The visual calculations are accomplished in the Shape Machine, a shape grammar interpreter implemented as a plug-in for Rhino. In all, the research aims to experiment with this prototype environment for shape computation to critically engage in formal analysis and synthesis with the machine.

2 BACKGROUND

The notion of visual algorithms for the description, interpretation, and evaluation of creative artifacts emerged in the 70s with the invention of the shape grammar formalism. Shape grammars were introduced by Stiny and Gips to define generative specifications for painting and sculpture [2], a project that grew to consider how computer models could more broadly inform criticism and design across the arts in a theory of algorithmic aesthetics [3]. An initial expansion of the project to address architecture focused on the language of Andrea Palladio, resulting in Stiny and Mitchell's

Palladian grammar. Essentially, the grammar is a computational theory for generating Palladian villa plans constructively with shape rules. Designs produced in the grammar include both actual designs from Palladio's corpus and new interpretations that conjecture artificial design solutions that Palladio never realized himself. Their novelty is in how they precisely comply with the theory on his architectural language as described by the rules [4]. This algorithmic approach to architectural theory inspired another project in the 90s to author a custom software so that possible Palladian villas could be generated in plans and elevations. The project was inspired by the theory of shape grammars and especially the Palladian grammar, but in the end offered another interpretation on Palladio that departed from the grammar in much of its theoretical import. The details are articulated by the authors, but what is more interesting to consider here is how the research motivated Hersey and Freedman to propose an argument for a new type of theory for architectural history, where possible and actual villas would be studied together to foreground the architectural style, symmetry, and geometry of a language of designs [5].

These initial strands of computational studies on Palladio share an ambition to interpret a formal speculation with a robust technology to rethink and enliven architectural theory. By privileging a visual mode of representation and a mechanical mode of interaction, they aim to offer an understanding of rule-based geometric productions where the computer model can be considered a partner [6]. The project here revisits this aim in the context of recent developments in shape computation. The research addresses the current state of the art on shape grammars in terms of theoretical foundations and refinements [7-9] as well as on the implementation front to address the issue of an appropriate technology for formal inquiry. Notably, research progress in the last decade has delivered an increased ability to experiment with more robust shape grammar interpreters and implementations. Nonetheless, recent assessments on the current landscape of the technology identify that the available solutions still leave much to be desired in relation to key concepts of shape grammar theory. The notion of simple means to engage the user on the frontend that can support emergence throughout a generative process is especially unresolved [10].

The specific methods here test the impact of a new interpreter in addressing John Portman's domestic language. The starting point is an initial shape grammar on the house that was computed by drafting in an analog mode [1]. The new interpreter, the Shape Machine, provides an unprecedented medium for implementing this research to explore visual calculating in Portman's language of the house. The Shape Machine is authored in Python and structured on the maximal representation defined in the shape grammar discourse to specify a minimum draftsman's representation for any shape [7, 11]. The backend recognition algorithms of the machine are characterized by this maximal representation [12, 13]. The current prototype provides this support for a

vocabulary of shapes that can be specified on the frontend in an intuitive way by drawing arrangements of straight lines and arcs in two-dimensional space. Interaction with the engine occurs exclusively in the standard Rhino workspace so that no hard-coded scripting is required of the user. Recognition algorithms allow the machine to search for any part embedded as a subshape of a given shape or an overall design in progress as specified by a drawing. To complete the plug-in, shape modification algorithms facilitate productions in the engine, which are currently available for all Euclidean transformations [13].

3 METHOD

The process of automating a shape grammar in the Shape Machine is straightforward in the sense that the entire activity occurs within the Rhino design environment. The current version of the Shape Machine plug-in is operated with five major components on the frontend: (a) the viewport workspace for graphical definitions, preview displays of candidate matches for rule application, and the generation of a design; (b) the standard toolbar for drawing shapes composed of lines and arcs to serve as inputs for the engine; (c) a custom toolbar that calls the functions of the engine as encoded for the transformations under which shape recognition and shape modification apply; (d) the layers panel for assigning attributes to shapes; and (e) the standard command line to communicate feedback from the engine and prompt user action or selection as required.

Programming by drawing shapes is achieved with a rule template and an initial shape that can be defined anywhere within the viewport workspace. The Shape Machine rule template provides a format for specifying a left-hand side (LHS) defining the search space for a rule to query in a design and a right-hand side (RHS) defining the transformation to change the shape as drawn in the rule. These sides are separated by an arrow pointing from the LHS to the RHS and stabilized with cross-shaped registration marks in the lower left part of each side of the rule to precisely coordinate the geometric transformation (see Figures 2-6). Rhino layers are assigned in the plug-in as labeling devices for attributes that distinguish the template and shapes by default. Layers can be further customized to encode additional descriptions to aid in the specificity of rule application following common computer-aided design conventions. Following this setup, calculations in the grammar are in the direct product algebras $U_n \times V_n$ to specify a design space of straight lines, arcs, and labelled lines in two-dimensions [8]. Assuming a shape rule is composed with respect to this vocabulary and within the space of the shape rule template, it is ready for application.

Rule application is initiated by selecting the transformation under which the rule applies from the Shape Machine toolbar. For the purposes of this study, only the isometry and similarity transformations were used for applying rules. Once the transformation is specified, the Shape Machine asks the user to select a shape rule. This selection must

include the rule template which is essential to the precise encoding of the geometric data. Subsequently, the Shape Machine requests the input of a design where the rule should be applied, which prompts the designer to select an initial shape or design already instantiated in the workspace. Then, the command line provides the information for how many matches are found based on these inputs and the graphical display highlights a single match of the LHS in one color with a preview of the application of the RHS highlighted in a second color. At this point, if there is more than one match for the shape rule, the user can cycle through a preview of each match to understand the complete implications of the rule with respect to the design under consideration. The user can then choose whether to apply the rule, try another one, or exit the production. Rule application can be selected in two modes so that a rule can either be applied directly for one match or in parallel for all matches under a command in the software called “apply all.” When a rule is applied, the entire design selection is redrafted in its maximal representation.

4 CASE STUDY

The implementation focuses on the automation of the Entelechy grammar. To distinguish this project from previous work, the shape-machined grammar is more precisely called the Portm-Ino grammar. The name is given to postulate how the house in Portman’s conception is a systematic, residential configuration along the lines of Le Corbusier’s Dom-Ino framework. Readers interested in more background information on the formal analysis of the original house design and the resulting analog grammar are referred to [1]. The key detail to include briefly is that the

house is composed systematically as a nested framework of major and minor spaces. The major spaces define the underlying field of square $n \times m$ cells so that Entelechy I is characterized by a 3×5 major grid resulting in fifteen major spaces layered with a minor grid of twenty-four circular minor spaces centered at the corner intersections of major cells in the grid. In the original Entelechy I design, major spaces are divided to demarcate one side of the house for public entertaining use with double-height living spaces (denoted by an X in the plans) and the other side for private family use with bedrooms and adjacent casual living spaces. Within the housing system, the minor spaces are articulated with hollow or exploded curvilinear columns utilized as support spaces for atmospheric and accessory uses including lightwells, stair wells, closets, studies, libraries, half-bathrooms, and micro-galleries.

Figure 1 is useful for a visual overview of the generation of a design in the Shape Machine. The detailed derivation for a 3×3 major grid as automated in the software is shown in a boustrophedon manner to briefly outline the character of each of the stages and to introduce the system of the house language. Two plans execute the shape rules of stage 1 to define a framework as a tartan grid (Figures 1a-1b); the next six steps in the production illustrate the development in stage 2 to clarify a configuration in the language (Figures 1c-1h); and the remaining process illustrates the application of the shape rules of stage 3 until the last plan, which is produced with a combination of the final shape rules of stage 3 and the termination process to end the automation (Figures 1i-1o).

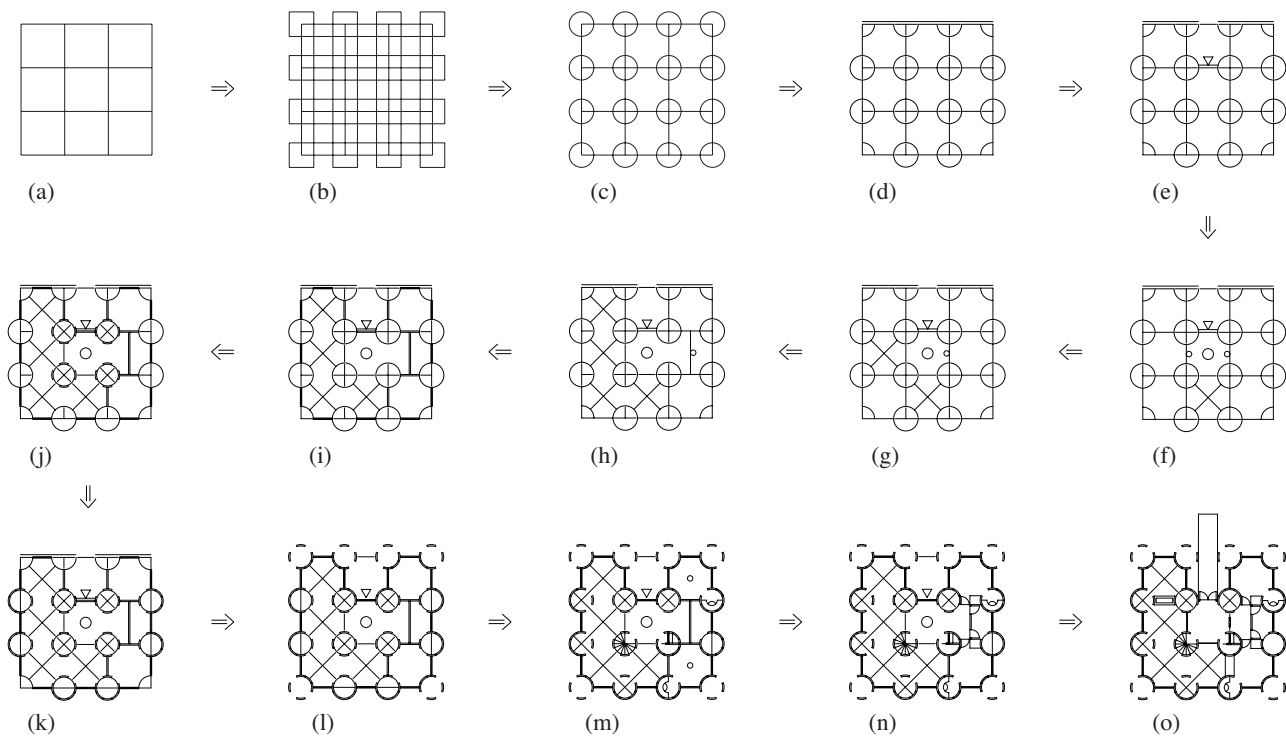


Figure 1. A sample derivation for a 3×3 design as produced by Portm-Ino grammar implemented in the Shape Machine.

These stages follow the logic of the Entelechy grammar for ease of comparison. Readers familiar with the analog grammar will notice a simplified output so that shape rules and productions are focused on a single plan. Given its function as a piano nobile defining the entry of the house, the upper level is privileged. It follows that the ground level and roof can be derived from the logic of the intermediate floor that mediates above and below. Parallel productions are left for future work when the interface can more readily support these computations without manual intervention. A visual illustration demonstrating the application of the subset of shape rules used in the production of Figure 1 is available at <http://www.shape.gatech.edu/Machine/>.

Additional detail on the implemented grammar is presented in two parts. First, a selection of rules (Figures 2-6) will be discussed in terms of their visual and verbal specification. In order to illustrate rule application, each rule is also paired with a subsequent matching illustration that shows each non-equivalent LHS match for that rule found in the Shape Machine (Figures 7-11). This set of illustrations all refer to the design production of Figure 1 to give a more comprehensive picture of interacting with the shape rules and productions of the grammar in the software. Following this snapshot, a sample catalog of complete designs generated in the machine-based specification is presented and discussed to illustrate some results from the implementation.

The power of programming with shape rules is in their ability to encode precise relationships that interpret a design intention with a visual representation. Figures 2-6 illustrate rules from stages 2 and 3 of the grammar chosen to give examples of how shape rules can describe the specification of an entry, walls, elements of structure and exterior skin, bedrooms, and a fireplace. Each rule is articulated with the Shape Machine rule template to specify the transformation from LHS to RHS. The rules are exported directly from the software and depict the visual specification needed to apply the rule in a shape computation.

Figure 2 gives an example of how a rule can be programmed to specify a primary entry for a configuration in stage 2 of the grammar. On the LHS, the emergent eight-sided shape of lines and arcs reflects the resultant major space produced when the minor grid of circles is added to a design (Figure 1c). The double line on top of the figure designates the front orientation (Figure 1d). On the RHS, the double line is translated to reflect the recessed entry and the exterior-oriented side of the eight-sided shape is trimmed so that the space will no longer be recognized as a closed interior shape. A triangle shape label is also added on the RHS to further articulate the entry. The rule is applied under similarity in the Shape Machine to the design of Figure 1d to produce the design of Figure 1e. Figure 7 shows how the machine finds three non-equivalent matches of the LHS of the rule, each reflecting an instance of the embedded shape that can potentially become the main entry of a design. The entry choice relates to both exterior conditions as influenced by the

site context and interior conditions as the entry implies the possibilities for the symmetric or asymmetric arrangement of the interior space. The match of Figure 7b was applied in the implementation of the 3 x 3 design to reflect a bilaterally symmetric organization as shown in Figure 1.

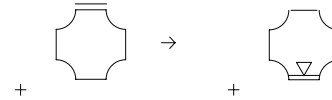


Figure 2. A shape rule to locate the primary recessed entry.

The next four rules are from stage 3 to define the detailed architectonics of a design. This stage had significant development in the Portm-Ino grammar as the implementation raised the bar in terms of the desirable level of detail, with a goal to achieve the articulation expected in an architectural floor plan. Figure 3 depicts a rule for generating wall locations after the development of a configuration has carved out the spaces and volumes of a design, leaving the lines of the resulting enclosed spaces intact as shown in Figure 1h. The LHS of this rule essentially looks for the remaining lines of the major grid that demarcate a division of space as measured between the circular minor spaces. The RHS develops the representation from a single line to a double line to effectively produce a wall. Figure 8 shows the seventeen non-equivalent LHS matches of this rule when applied under similarity in the Shape Machine to the design of Figure 1h. These are all applied in parallel to generate the thickened walls of a design.



Figure 3. A shape rule to designate generic thickened walls.

Proceeding to the architectonic development of minor spaces, Figure 4 illustrates a shape rule for specifying the curvilinear wall segments that form the enclosure for an exterior hollow column along the side and back orientation of the perimeter. The LHS looks for the circular minor spaces with the T-shape inside that designates these locations as shown in Figure 1j. The RHS adds the elements, which include the four structural components of the column oriented to the cardinal directions and two exterior partitions that continue the enclosure system when it meets these particular hollow columns at the perimeter. The resulting enclosed minor space is also labelled with a line to denote an unassigned space in the plan that can be developed in the rules that follow for a particular use or feature of a design. Figure 9 shows the six matches of the LHS of this rule found in the Shape Machine. All of these matches are applied in parallel in the production of the Figure 1 design.

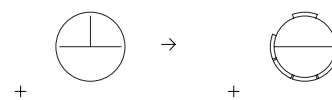


Figure 4. A shape rule to add curvilinear wall elements.

Moving on to the particularities of the interior spatial arrangement, the relationship defining bedroom locations is specified in Figure 5. Bedrooms in the language of the house are always in direct connection with one minor space that is enclosed as a private bedroom study or closet. Additionally, bedrooms always have exposure to at least one operable window wall for an immediate connection to natural light, view, and ventilation. The LHS designates this relationship by defining a search space that includes: (a) an unassigned minor space denoted by the circle with a line centered across its diameter; and (b) a major space enclosed by three walls, one of which must be located on the exterior. The RHS develops the bedroom to articulate the assignment of the single minor space, the curvilinear enclosure elements that close off the space from the other three adjacent minor spaces, and the labeling of the bedroom as denoted by the circular label. Figure 10 shows the three non-equivalent matches of the LHS of the rule found when applied to Figure 11. The matches of Figure 10a and c were instantiated in two applications of the rule in the Figure 1 design.

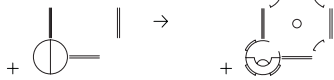


Figure 5. A shape rule to locate bedrooms.

To complete the description of select specific rules and their applications, Figure 6 is offered to illustrate a rule for placing the fireplace. The LHS specifies a query for a space characterized by two adjacent double-height major spaces. The RHS adds the double-height fireplace centered within this volume and oriented to provide potential access from both sides. The fireplace is tailored to fit between two hollow columns. Figure 11 depicts the three non-equivalent matches for this rule when applied in the Shape Machine under similarity. The match of Figure 11a was applied to produce the final 3 x 3 design as shown in Figure 10.

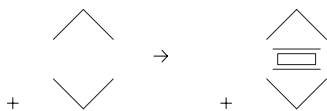


Figure 6. A shape rule to locate a fireplace.

This account of select shape rules and their production demonstrates how abstract rules can represent architectural reasoning in a compressed visual medium. These rules depend entirely on their context, so that a change in the range of inquiry equally shifts the possibilities of the description [14]. To gain a more comprehensive view of the grammar, Figure 12 illustrates thirty plans produced in the software with the complete set of shape rules. The resulting catalog includes sample designs in the language for a series of $n \times m$ grids. The pair of 3 x 5 designs includes the plan of the original Entelechy I as produced in the machine (Figure 12n). Read as five columns, the contrast between pairs of variations captures the flexibility of the language as the $n \times m$ canvas increases from XS to S to M to L to XL. The

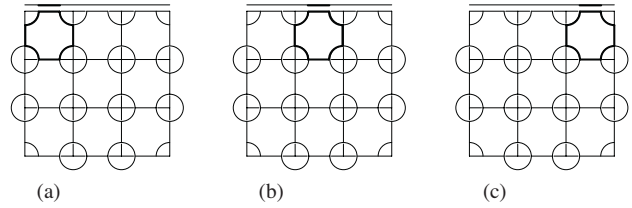


Figure 7. Three non-equivalent matches of the LHS of the shape rule to locate the entry (Figure 2).

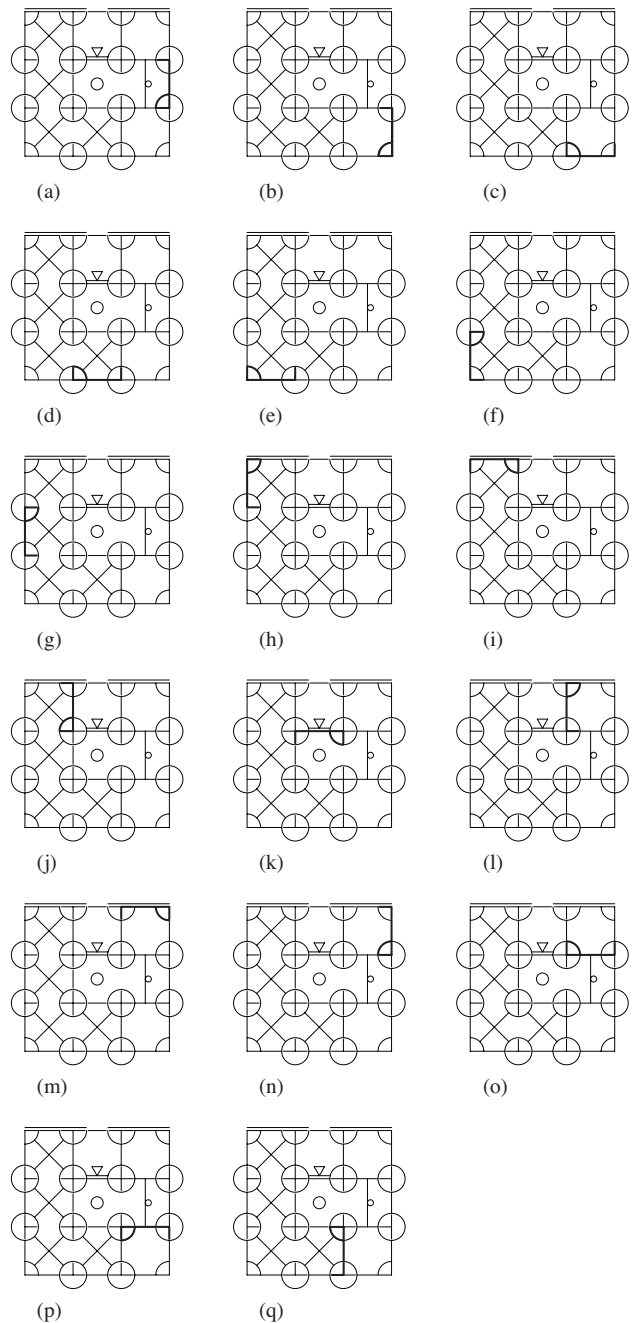


Figure 8. Seventeen non-equivalent matches of the LHS of the shape rule to locate walls (Figure 3).

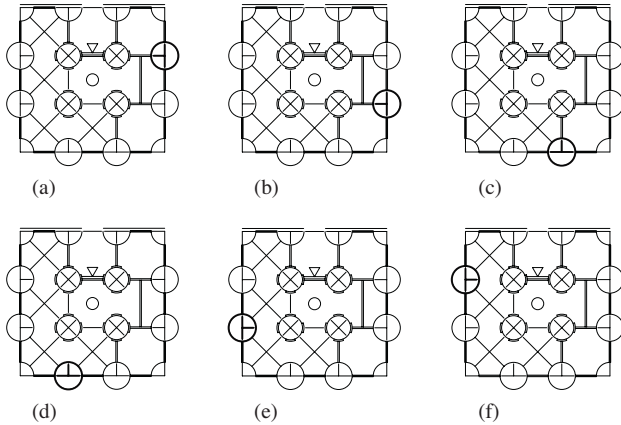


Figure 9. Six non-equivalent matches of the LHS of the shape rule to add curvilinear wall elements to non-corner perimeter hollow columns at the side and back orientations (Figure 4).

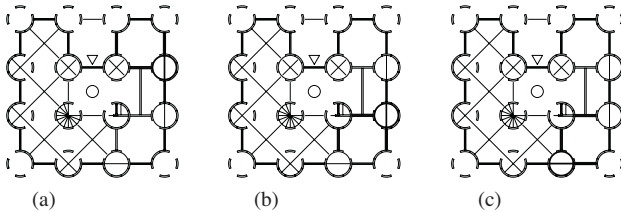


Figure 10. Three non-equivalent matches of the LHS of the shape rule to locate bedrooms (Figure 5).

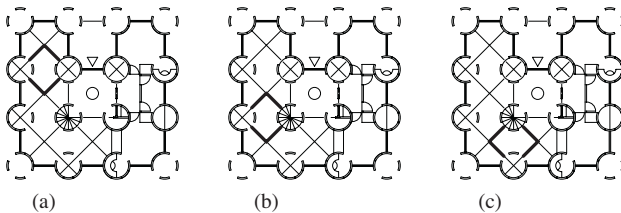


Figure 11. Three non-equivalent matches of the LHS of the shape rule to locate a double-height fireplace (Figure 6).

designs can additionally be read as six rows characterized by the depth of their major grid structure as a 2-series in the top pair of rows, a 3-series in the middle pair, and a 4-series in the bottom pair of rows.

These results verify a sample of possible designs in the house language though more candidates can be generated with the grammar. A first grouping of designs distinguishes a subset characterized by the axial division of public and private zones observed in the design of Entelechy I to include Figure 12a, c, f, g, j, k, m, n, p, q, and z. While these designs certainly convey the systematic expressiveness of the house language, the question brought forward by implementing the grammar in the Shape Machine focused on how this system could address not just potential Entelechy variations that look nearly alike, but what other designs the system could generate through possible variations of the house language Portman never considered. The more precise inquiry focused on how to release the constraints of the axial division of

public and private space to explore alternative potentials in the new medium. This pursuit extends the investigation to understand how the distribution of major volumes in a design expressed vertically to connect levels as well as horizontally to define circulation halls can be more expressive. The hypothesis developed in shape rules to test its possibilities in the productions suggests that the organization depends on the relationship between the entry and the planar circulation of the upper level as mitigated by the modular structure of the major grid. This relationship is arranged in terms of an entry sequence that connects to the embedded network of figural minor spaces for another layer of connection. This multivalent coordination foreshadows Portman's elaborate use of circulation in his designs for commercial hotels and urban habitats that are primed for further expansion.

Considering the columns of XS, S, M, L, and XL designs, each shows a different range of possible locations for the entry to initiate this understanding as assigned in the shape rule of Figure 2. We can elaborate possibilities by discussing the 2, 3, and 4-series of designs in sequence. To start, Figure 12 a-j all represent designs in the 2-series. These designs all have the same entry sequence from the entry bridge to the foyer, which meets the perimeter offering a view out to the surrounding site. Circulation halls and double-height volumes in these programs define rectangular and L-shaped spaces, with the exception of a U-shaped hall in Figure 12d. In terms of larger open volumes provided by major spaces to vertically connect levels, designs range from having zero openings (Figure 12a) to up to three openings (Figure 12e, j). These reflect further possibilities in room arrangement from open loft designs to three-bedroom programs.

Increasing capacity for variation with an enlarged canvas, all designs in the 3-series have the characteristic entry sequence to match the original Entelechy I (Figure 12k-t). Additional figures of circulation halls and continuous double-height volumes include a +-shape (Figure 12m) and T-shapes (Figure 12n, o, s, t). Designs in the 3-series range in their major double-height openings from one opening (Figure 12k, m, p) all the way to an expansive six openings (Figure 12o).

Lastly, the 4-series builds on this logic with the same entry sequence from the entry bridge to a foyer to a double-height space that meets the perimeter (Figure 12u-dd). The designs of the 4-series are unique in their foyers and central halls that are doubled in depth so that the planar space emerges as an expanded single-height volume with additional expressive possibilities. For example, the design in Figure 12w shows a rotational symmetry at the interior hall so that three corner bedrooms each have their own bathroom and adjacent major double-height volume, suggesting a context where desirable views are offered on all sides. To contrast this, Figure 12bb illustrates a long double-height hall along the back of the house terminated by a corner bedroom, offering a significant volumetric and visual connection to the exterior site. In this series, open double-height volumes at the major scale increase to consider up to seven openings (Figure 12y).

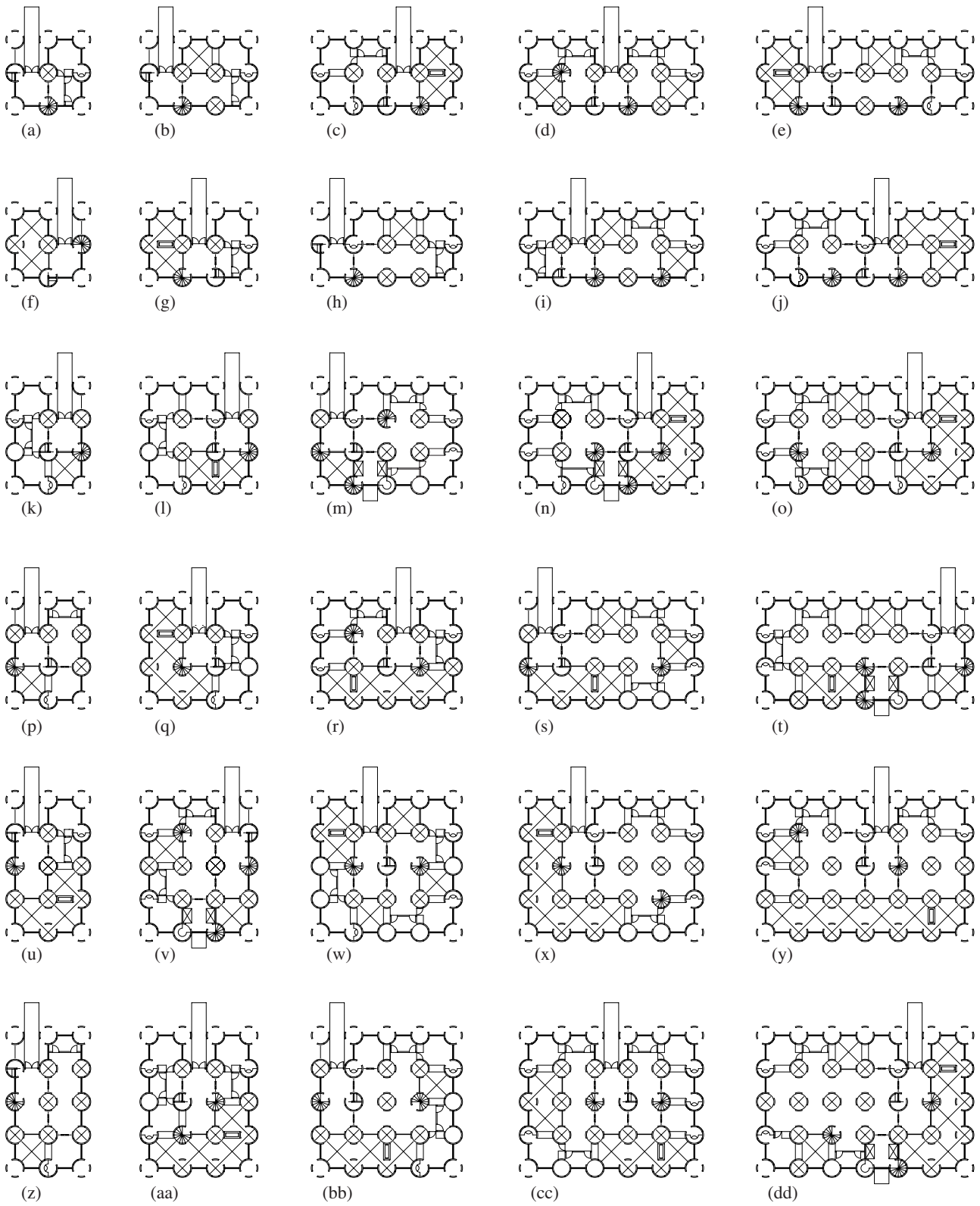


Figure 12. A visual sample of mechanically produced design variations in the Entelechy language for a series of $n \times m$ grids. The 3 x 5 plan labeled n is the original 1964 design of Entelechy I as produced by Portm-Iino grammar implemented in the Shape Machine.

5 CONCLUSION

The Shape Machine provides a generous medium for elaborating the formal theory on Portman's language of the house in an active way. Like working in any new medium, opportunities were found in the process that confirmed the novelty of this environment and provided new insights on the architectural theory too. Specifically, three theoretical concepts to differentiate Portman's language of the house came forward. First, a logic of networked circulation preconditioned for expansion is seen in the house as a system initiated at the entry. This circulation in the house is horizontally built into the logic of major spaces and vertically built into the minor spaces to suggest a network ready for change to address new concerns. Second, a modular measure for parameters that scale is inscribed in the house to pragmatically allow for adaptations mitigated by the module. This modularity is intentionally plural to provide multiple interrelated measures based on increments that allow for playful symmetries, asymmetries, and proportions to be explored within a design in the language. Finally, the language of the house illustrates a structural character that tests the expressiveness of simple geometries. This simplicity is seen in the fact that the geometric vocabulary is essentially defined by a circle and a square. Future work will aim to address how the language can be restructured in the Shape Machine for arguments beyond the domestic scale.

More generally, the shape-machined implementation promotes a rule-based visual approach that can be readily picked up and continued. This productive format is conducive to our paradigms of knowledge sharing today – via machine-readable files, scripts, searches, hashtags, and more. The advantages of this prototype environment cannot be overemphasized in terms of the simplicity and accessibility of the user interface, the time-savings afforded by being able to encode a custom function by programming with shapes, and the alleviation of fatigue from repetitive tasks that can be easily automated. The current prototype of the Shape Machine computes with shapes composed of straight lines and arcs in two-dimensional space. Rules are applicable under all Euclidean transformations. Shape computation as a comprehensive program suggests an expansion of the engine to include shapes in two and three-dimensional space as well as further transformations, parametric definitions, parallel productions, and interfaces for recording or predictively suggesting rules.

The Shape Machine provides researchers with a technology that allows them to try shape rules out, test the hypotheses they put forward, and generate productions that synthesize the overall expressiveness and impact of their interpretation. More specifically, the methods presented here provide a way to precisely define a formal theory in architectural research. Automating the process in the Shape Machine confirmed analytical intuitions, challenged them productively, and also demonstrated how a shape rule can be recast just like a design

– for many different decompositions according to purposes that evolve [14]. As a medium, the Shape Machine provides a way to critically foreground a variety of architectural issues in a dynamic interaction to suggest that a computational architectural theory is within reach.

ACKNOWLEDGMENTS

This work relies on the generous collaboration of the Shape Computation Lab (SCL). Shape Machine is a project of the SCL at the School of Architecture, College of Design, Georgia Institute of Technology. The research and implementation of the interpreter is led by Tzu-Chieh Kurt Hong.

REFERENCES

1. Ligler, H. and Economou, A. Entelechy revisited: On the generative specification of John Portman's architectural language. *Environment and Planning B: Urban Analytics and City Science*, 45(4), 623–648, 2018.
2. Stiny, G. and Gips, J. Shape Grammars and the Generative Specification of Painting and Sculpture. In C.V. Frieman (Ed.) *Information Processing* 71, 1972.
3. Stiny, G. and Gips, J. *Algorithmic Aesthetics: Computer Models for Criticism and Design in the Arts*. University of California Press, Cambridge, MA, USA, 1978.
4. Stiny, G. and Mitchell, W.J. The Palladian Grammar. *Environment and Planning B: Planning and Design* 5: 1978, 5-18.
5. Hersey, G. and Freedman, R. *Possible Palladian Villas*. MIT Press, Cambridge, MA, USA, 1992.
6. Knight, T. and Stiny, G. Classical and non-classical computation. *ARQ: Architectural Research Quarterly* 5: 2001, 355-372.
7. Stiny, G. Introduction to shape and shape grammars. *Environment and Planning B: Planning and Design* 7: 1980, 343-351.
8. Stiny, G. *Shape: Talking about Seeing and Doing*. MIT Press, Cambridge, MA, USA, 2006.
9. Knight, T. *Transformations in design: A formal approach to innovation in the visual arts*. Cambridge University Press, Cambridge, UK, 1994.
10. Eloy, S., Pauwels, P., and Economou, A. AI EDAM special issue: Advances in implemented shape grammars: Solutions and applications. *Artificial Intelligence for Engineering Design, Analysis and Manufacturing*, 32(2), 131-137, 2018.
11. Stiny, G. A new line on drafting systems. *Design Computing*. 1: 1986, 5-19.
12. Krishnamurti, R. The construction of shapes. *Environment and Planning B: Planning and Design* 8: 1981, 5-40.
13. Hong, T. K. and Economou, A. Shape Machine. Forthcoming.
14. Earl, C. Shape boundaries. *Environment and Planning B: Planning and Design* 24: 1997, 669-687.



Interpreting non-flat surfaces for walkability analysis

Mathew Schwartz¹ and Subhajit Das²

¹New Jersey Institute of Technology
Newark, USA
cadop@umich.edu

²Georgia Institute of Technology
Atlanta, USA
das@gatech.edu

ABSTRACT

Through laser scanning, GIS data, new manufacturing methods, and complex designs, analysis of terrain in relation to human mobility is becoming ever more necessary. While standards for wheelchair ramps exist, they rarely show the entire picture, nor do they account for surface variation beyond a single axis. Although graph creation techniques in CAD exist for flat terrain, directional edge weights accounting for this variation are lacking. In this paper, a summary of research from both biomechanics and architecture in relation to surface walkability is presented, followed by a review of creation methods for a searchable graph representing an environment in CAD. A novel graph creation method that can respond to variations in surface height for walkability analysis is presented, where the edge weights of the graph are based on surface condition of parent-child height variations.

Author Keywords

human factors; walkability; computation; graph, analysis; architecture; space syntax; evaluation, urban design

ACM Classification Keywords

I.6 SIMULATION AND MODELING : [General]; J.5 ARTS AND HUMANITIES: [Architecture]; D.2.2 SOFTWARE ENGINEERING: Design Tools and Techniques—*Human Factors*; I.3.6 COMPUTER GRAPHICS: Methodology and Techniques—*Ergonomics*

1 INTRODUCTION

While acoustics, lighting, and thermal comforts are commonplace in building analysis, more individualized human factors are often left out. Two main challenges to integrating these individual factors are: the simulation and specific analysis from a human perspective, and the interpretation of a building or environment to run these metrics on. The latter issue is the focus of this paper, as the former is often the focus of biomechanics research through human subject studies and can be used as reference data.

To calculate walking distance and visibility in space, various academic approaches to the problem have been developed,

largely revolving around line of sight and overall shortest path movement from different rooms. However, the manufacturing and traditional construction methods of the past kept the ground floor of a building flat. With newer technology and a look at the urban scale, this flat ground is not guaranteed. It is the goal of this paper to introduce an algorithmic approach to interpreting an unknown terrain or building environment in CAD as a searchable and directional graph whose nodes exist only in user-defined accessible terms. While the term walkability is used in various contexts, this paper focuses on the generation of the graph in which additional analysis can be generated.

1.1 Human Factors Based Evaluation

There is often a misunderstanding from the design perspective of the role of localized human factor analysis in buildings. While a building can be considered a structural frame or blank template that allow an occupant to freely move within, the layout, shape, and small details such as carpet type can have a profoundly larger impact than many realize. Furthermore, the lack of tools and analysis methods makes it nearly impossible for a designer to have the background knowledge and mental computation to make choices related to the human. Therefore, various building codes and standards have been developed to aid in the process, and bring some minimum standardization to the built environment.

In the case of accessibility, building codes such as the American Disabilities Act (ADA), while a good step towards securing a minimum standard, have also left many architects and designers assuming this standard is satisfactory. On the other hand, the ADA is often viewed as a hindrance to a building design, especially if the architect is unaware of the methodology behind a particular regulation. While at first this attitude toward the ADA may seem insensitive, this view is not entirely unwarranted, as the ADA is based on a prescriptive code. In fact, just three years after the ADA was enacted, researchers in architecture had developed computer-aided tools for interpreting the environment based on people, specifically pointing out the lack of quantitative methods for assessing a design in relation to the goals of the ADA [11]. Examples of standards lacking justification through research are too common for designers to blindly follow. In the case of stair width,

it had been defined as 44 inches for 2 files of people; however, no evidence had been used for arriving at this number. Likewise, assumptions have been made, such as an increment of 6 inches is too small to impact flow, that turn out to be incorrect [20].

In a comparison of perception of design elements between designers and medical staff, designers were more likely to focus on psychological elements such as views of nature or color, while the medical staff focused on physical health such as handrails and safety bars [10]. Part of this discrepancy may be due to the approaches and interactions each discipline has with the built environment, as designers may view the built environment on a macro scale, while the medical staff are inside, with localized interactions. The straightforward solution to this is through simulation and analysis; Design tools can alert and inform about these localized interactions, just as lighting and thermal analysis tools do now.

Notably, the increased use of machine learning in nearly every discipline has inevitably found its way into the design of the built environment. While the implementation details and results are out of scope for this paper, the approach taken and key observations are important. Specifically, in order to generate metrics to be optimized, [29] reviewed numerous papers and strategies of design in relation to the human, pointing out interior design metrics such as "a television should maintain a certain distance from the normal viewing area...The width of a pathway should depend on the habitant's body width..." [29]. While these may seem more or less obvious to a designer, the access to these metrics in CAD tools is still missing.

This paper focuses on the physical attributes to traversing a space through human mobility. In considering the walkability of a non-flat surface, the types of surfaces for human traversal can be characterized as:

- Flat (leveled floor)
- Ramp (slope along the progression axis)
- Cross-slope (slope perpendicular to the progression axis)
- Staggered (stairs)
- Uneven (variations in curvature, natural topography)
- Uneven staggered (faceted surfaces, bricks in walkway)

The items in this list, with even minor variations between them, have a profoundly different impact on people. Each of these items can be studied and referenced in the biomechanical literature. Furthermore the impact of these surface conditions are not always obvious. In the case of a staggered surface (most commonly presented as stairs), recent stair-climbing studies on the relationship between the rise and run of a step and the probability of a fall [19] have had an impact on architecture by leading to a 2015 change in building code for stairs [24]. Of importance for simulation and evaluation, the building code value of stair tread is not an absolute cut-off to fall probability and should still be evaluated on a case-by-case basis.

In non-flat ground condition studies through an instrumented treadmill, 62% increase in hip work was found, with an over-

all increase of 28% in net metabolic energy expenditure [27]. In the case of cross-slope walking, the asymmetrical movement required may lead to falls [6]. On an even more specific ground condition, small variations in brick height of walk-ways, often caused by weather over time, were found to cause a person to lower their center of mass for additional stability, while also increasing flexion in some joints, likely leading to a higher energy expenditure [5].

Walk-ability on various ground conditions at a large scale, such as within an urban environment, provide an improved metric to assess the space. In [28], the authors look at urban analysis in various ways, including comfort and mobility, with implications towards new zoning rules and regulations. Metrics such as mobility are directly impacted, as seen in the literature, by the ground condition, and likewise, so is comfort. In [16], various design metrics are outlined as having opportunity to be calculated with modern tools, including *Adjacency preference* and *Buzz*. Likewise, the accuracy of these metrics would be impacted by varying ground conditions, making it harder to reach a certain location, or causing changes in circulation speed at various locations.

An indoor walkability index (IWI) was defined as "a measure on which a path has good performance for pedestrians in the building" [13]. In particular, [13] describes three factors that make up the assessment: *Distance*, *Accessibility*, and *Pedestrian-friendliness* for evaluating indoor walkability. However, surface quality, which through biomechanics research (stated above) has the largest impact on walkability, is not accounted for.

1.2 Graph Generation

The generation of a graph that can be used to evaluate metrics of a building has been approached in multiple ways within architecture research, largely revolving around the specific metrics in focus. Early work in this area revolved around the concept of an isovist, or visible points in space [1]. Following this intention, the graph constructed in the building was based on, and held information to, the visibility within the space [25]. Likewise, analysis of circulation throughout an entire building has been demonstrated by [12], referred to as the Universal Circulation Network (UCN). Rather than a dense graph of adjacent nodes, the UCN leverages the data structures within BIM to build a graph based on visible paths and shortest distances.

The visibility graph defined in [25] uses a combination of even grid projections and vertex intersections. The authors note the intention and possible use for considering the vertices as potentially occupiable spaces. While the idea of a permeability graph, in which a visibility graph is constructed at floor level, could be used for obstacle detection and accessibility, it is not demonstrated or explicit. A problem in using the visibility graph in [25] for accessibility is the distribution of an even grid in plan at eye-level. In particular, the need to connect staircases to separate graphs on each floor illustrates the single dimensionality of the approach. Given a ramp or slope ground condition, the visibility graph plane would intersect, not completing the series of connections described.

Implementing 3D Isovists, [21] projects rays spherically at what is referred to as an *observation point*, although the authors do not detail how these points are decided. The use of these spherical projections is to essentially map visible depths throughout a space, similar to Lidar on an autonomous robot, and classify the space based on feature extractions. The isovist in this case, while analogous to vision through the possible lines of sight dictated by the rays, is not employing a method of human factor analysis, but rather a tool for parsing and understanding the environment. In the case of binocular vision, [9] analyzes the human view from nodes placed through possible sitting locations. The nodes in the graph are populated along a curve using user input parameters.

A common technique in generating a building graph is the distribution of a rectangular and equally spaced graph across a floorplan. This may be done either through a generation of points, or a method employing ray tracing. This method, similar to [25], comes with important drawbacks. First, for cases in which the floor plan is shaped as an L or U, a large number of unused points are generated and need to be dealt with through wasted computation. Second, the planar aspect limits the ability to interpret uneven surfaces. Finally, edge connections may be generated in inaccessible locations within the environment. A method for reducing the node/edge connections is culling, as demonstrated in [17], where the intersection between an object and the line connected from two nodes invalidates the edge. Alternative strategies have followed the implementation of the UCN, with navigational boundaries dictated by the convex points of objects projected onto the plane [7]. In [8], a voxel based approach in which the entire environment is discretized, with each voxel containing additional properties for use in a large variety of evaluations.

Graph search for navigation

Graph search for spatial navigation is a well-established technique in path finding problems in the domains of automation and planning, robotics and game development. An early work in this area by Botea et al. showed a hierarchical path finding method to find optimal paths on grid based maps. Following a clustered map approach, they showed the hierarchy could be extended to more than two levels [2]. In the context of Architectural planning and human behavior simulation, the work of Chu et al. shows a way to sense the vicinity of the physical obstacles within a visible space to simulate the influence of social behavior on evacuation. They discretized the continuous 2D space into square cells forming a 2D grid, which is further connected via edges linking visible navigation points [3]. Turner et al. showed their technique can improve human behavioral response using artificial evolution of existing navigation rules. Their technique proves that human's guidance mechanism does not depend on the spatial properties acting on their direct perception [26].

Path-finding in sloped-terrains

A smoothest path through a sloped surface or terrain is a topic of research within gaming and robotics which overlaps with the goals presented here. Roles et al. showed a novel technique to compute the smoothest path through a sloped terrain [22]. Based on Dijkstras algorithm, their technique optimized distance and slope to retrieve the least rigorous path between

two queried points A and B on sloped terrain. These points were chosen from a set of points V which are retrieved from the input mesh geometry. They hypothesized that a minimally sloped path would be most desirable over terrain or sloped land surface for various reasons, i.e., in hospital, etc. Their algorithm is based on a node, edge graph system, where a starting point A appends all the adjacent vertices or nodes nearest to A by a threshold distance. Then they compute a set m where vertices of least weights to each explored nodes in the graph are added. This is repeated till the ending vertex or point B is reached. Finally, the smoothest path is retrieved starting from the ending point B to starting point A . The weights of each node are computed using traditional shortest path method, i.e., the sum of between two nodes and the distance already traveled.

Liu et al. studied and implemented slope constraint for terrain surfaces. Further, their method involved intelligent surface simplifications in searching for shortest paths using the input slope constraint efficiently. They described the technique of surface simplification to reduce the complexity of finding the shortest path [14]. One intuitive benefit of surface simplification is gain in speed to compute the shortest path (i.e., less number of nodes, thus fewer computations). However, one key challenge is the slope of the simplified surface might not satisfy the slope constraints of the original surface. Even if the slope constraints are satisfied, it might be longer than the shortest smooth path discovered on the original surface. To address the second challenge, the authors introduced a distance requirement in addition to the slope requirement while searching for the shortest path. Our technique however differs by deploying a novel technique of graph creation on an input 3D geometry representing any architectural or urban space.

Agents on terrain

While human behavior analysis in terms of architectural spaces often benefits from character path detection for evacuation, shortest paths for nurses to patient beds, etc., these techniques help in simulating critical scenarios like natural disasters. Beyond the large scope of agent based simulation, the control methods for an agent on a surface are relevant to this work.

One common method is to use physics-based environment controls so that a character (e.g., occupant or agent) remains on the ground due to physics-based constraints or the character automatically knows how to orient oneself to stabilize its posture naturally given the dynamically changing neighboring terrain and environmental condition. Further, navigational paths and accessibility within the environment are then decided on-the-fly based on the characters interaction, position, and orientation (e.g., [15]). As this works on a single and relative location, it is not a suitable technique for complete building analysis.

In general, the following assumption can be made based on prior literature: a dense graph containing nodes only in human accessible locations can be used for a large span of evaluative metrics. Albeit through an IWI, a buzz metric, or visibility maps, resolution of the graph with directional edges is advantageous. The drawback to the dense graph approach is

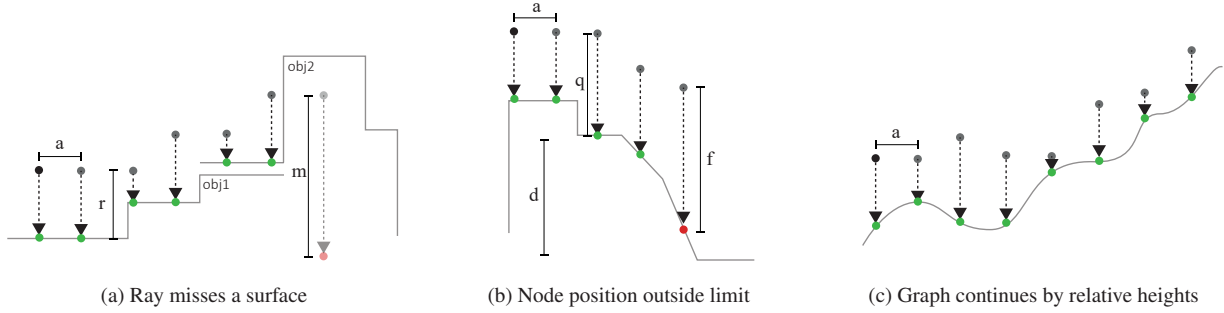


Figure 1: Illustration of three common occurrences in graph creation of non-flat surfaces. Green circles represent a valid node and red circle as invalid based on the parameters given as variables.

computational time in generating and searching through. In some cases, the computational time is reduced through the selective node/edge pair generation. In the case of search times, various methods in computer science have addressed the issue through a variety of datastructure reduction techniques, suggesting a dense graph could take the form of a superset composed of multiple optimized subsets for a particular metric. Importantly, the sparsity of the graph cannot be so that variations in ground conditions that would impact mobility are missed.

2 METHODOLOGY

In this section we define an accessibility graph, where all nodes are possible locations of an occupant in an environment, given user-specified parameters (e.g., a 12:1 slope). The graph itself is directed, and nodes consist of a parent-child relationship. The algorithm for generating the graph, and the method for implementing the system in the Grasshopper environment of Rhino3D are shown.

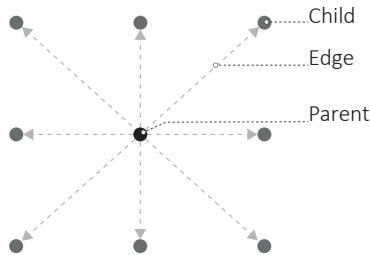


Figure 2: The parent-child relationship in the (xy) plane.

2.1 Graph Creation

Given a known possible occupant location in the environment, possibly the sidewalk of an urban space or lobby in a building, the other possible locations of an occupant can be found by using ray casting and a queue, such as in [23]. There are two main components to the directed graph $G = \{N, E\}$ with N nodes and E edges. In concrete terms, the set N represents the accessible locations of an environment for a person given a specific starting location, while E is the set of costs between these locations. As the graph is directed, a cost value $e_{i,j}$, where $e \in E$, corresponds to an ordered pair

(n_i, n_j) where $n \in N$. The ordered pair of nodes (n_i, n_j) is referred to in this paper as the parent-child relation (Fig. 2), where n_i is the parent and n_j is the child, with the corresponding cost $e_{i,j}$ applied from the parent to the child. The cost can be calculated both at the time the node pair is created or after the construction of N is complete, as described later in this section.

The algorithm to build the graph using recursion can be seen in Algorithm 1 (can be implemented with a loop as well). The given start location initializes the first parent node p . The parent set P is derived from the first node n_i in the parent-child relation (n_i, n_j) contained in $P = \{n_i | \forall (n_i, n_j) \in N\}$. During each iteration of the algorithm, the given parent node is checked for valid children. If a child is valid, a parent-child relation is created and an edge cost is assigned to that ordered pair. The cost value is defined in $\text{setEdgeCost}(p, c)$, where a typical definition of the edge cost for the ordered pair may be Euclidean distance. However, weighted parameters for various surface conditions can be used as well (see Sec. Edges). Finally, the children that are not in the parent set are then added to the queue Q and passed to the $\text{buildGraph}(G, Q)$ function until all possible parents and children have been evaluated, and $Q = \emptyset$.

Algorithm 1: Build directed graph of nodes and edges

```

 $N, E \leftarrow \emptyset, \emptyset$ 
 $G \leftarrow \{N, E\}$ 
 $Q[0] \leftarrow \text{start location}$ 
Function  $\text{buildGraph}(G, Q)$  :
   $p \leftarrow Q.\text{pop}()$ 
   $C \leftarrow \text{getNode}(p)$ 
  for  $c \in C$  do
     $e_{p,c} \leftarrow \text{setEdgeCost}(p, c)$ 
     $N \ni (p, c)$ 
     $E \ni e_{p,c}$ 
    if  $c \notin P$  then
       $Q \ni c$ 
  return  $\text{buildGraph}(G, Q)$ 

```

Nodes

While N defines the edges used in search algorithms, N itself is useful as well. In particular, the set N can be tessellated to

generate a valid walkable surface, and used in ways similar to that detailed in Section Introduction. Furthermore, this set can be used in data structures to define additional parameters and qualities of specific locations throughout the environment; albeit acoustic, lighting, and view-ability, reach, or fall probability (e.g., [23]) in which a building graph for circulation (e.g., [12]) alone does not provide the resolution for.

An important contribution of this paper is the extension of the node creation protocol from [23] to include height variations when generating the graph. Similarly, the number of nodes in the set N increases as each valid node location is used to check for additional valid nodes in immediate proximity (i.e., finding the child nodes). While the initial configuration of the parent-child relation is the same in the (xy) plane (Fig. 2), modifications to the inclusion of a child node were made to extend the graph creation to non-flat surfaces. To illustrate how the graph creation accounts for non-flat surfaces when generating nodes, Figure 1 shows the node evaluation in the (xz) plane where the ray cast direction is $-\hat{z}$, and as the graph is in relation to physical space, $-\hat{z}$ corresponds to the direction of gravity. The surfaces illustrated provide examples of a step, faceted surface, and natural topography (e.g., a hill or mountain). Each sub-figure uses the same parameters but illustrates various situations in which a node can be valid or invalid. The variables used in this figure are also used in the equations and algorithms. In Figure 1a a is the parent-child offset in the (xy) plane, r is the set height increment in \hat{z} from parent to child, $m = \infty$, such that a ray that does not hit a surface. In Figure 1b d is the allowable height variation from a parent in $-\hat{z}$ such that $q \leq d$ and $f > d$, resulting in an invalid node (red). When a possible node is invalid, it is not added to the possible parents queue Q , and in the simple example within the figure, the graph completes. To further illustrate the relative positioning of parent-child nodes, the vertical increase shown in Figure 1c demonstrates how the height offset r is relative to the previous node (when viewing left to right). Likewise, for each valid (green) node, the node to the left would be the parent.

The explicit definition of the valid nodes is given in Eq. 1.

$$N = \{n_i | n_i \in (n_i, n_j) | (n_i, n_j) \in E\} \quad (1)$$

After defining a starting location, Algorithm 1 tests the start as the initial parent node by calling the function `getNodes(p)` to check for possible children. This function is shown Algorithm 2.

The parent node p passed to `getNodes(p)` is checked for possible children by initializing locations in the (xy) plane in eight directions of a bounding square with a length of $2a$ (visualized in Fig. 2). The z component of the parent node is then added with the height threshold r . The possible child is then passed to a function `getChild(c)` that checks a ray for intersection with the nearest surface or geometry using the start location c and direction $-\hat{z}$. If the intersection is outside the defined criteria for a valid node (i.e., intersection distance is $> d$), or there is no intersection found, the function returns

Algorithm 2: Check for valid child nodes

```

Function getNodes( $p$ ):
    // Check parent  $p$  for valid children  $c$ 

    for  $i \leftarrow -1$  to  $1$  do
        for  $j \leftarrow -1$  to  $1$  do
             $c \leftarrow (p.x + (i \times a), p.y + (j \times a), p.z + r)$ 
             $c \leftarrow \text{getChild}(c)$ 
            if  $c \neq \text{false}$  then
                 $c \in C$ 
    return  $C$ 

```

false. If the intersection matches the criteria for a valid node, the intersection location is returned.

After checking for valid child nodes, `getNodes(p)` returns the child set C , where $c | c_i \in C$. Given at least one valid child in `buildGraph(G, Q)` of Algorithm 1, such that $C \neq \emptyset$, the parent is added to the graph with a directional edge to its child node(s). The child is then added to the queue if it is not already a parent in the graph.

As established in [23], the use of ray tracing to build the graph has a specific advantage when it comes to unknown geometry. Illustrated in 1a, the ray intersection allows the graph to be indifferent to the construction of object geometry. Given two objects *obj1* and *obj2*, the geometry of the two can overlap. Albeit from incorrect modeling or through issues with automated surfacing. More common may be the alignment of two different polygons or surfaces at the edge. While mesh planarization and algorithms used in various fields for understanding slopes in Cartesian space exist, the recognition of where one object ends and another begins can be ambiguous and only important in relation to the accessibility of the space. Simple additions in any CAD program, such as objects contained on different layers, can provide additional refinement to the building graph creation.

Edges

The final graph is composed of ordered pairs of nodes that correspond to an edge with a cost value. A parent-child relation for nodes n_i and n_j is valid given in Eq. 2. We define the vector \vec{V}_i as parent and \vec{V}_j child x, y, z positions, where $\vec{V}_{i_{xy}} = \langle n_{i_x}, n_{i_y}, 0 \rangle$ and $\vec{V}_{j_{xy}} = \langle n_{j_x}, n_{j_y}, 0 \rangle$.

$$E = \{(n_i, n_j) = \gamma | (\delta = a \vee \delta = \sqrt{2a}) \wedge ((0 < \beta \leq r) \vee (0 > \beta \leq d) | \beta = (n_{i_z} - n_{j_z}))\} \quad (2)$$

Where δ is $\|\vec{V}_{i_{xy}} - \vec{V}_{j_{xy}}\|$, γ is the calculated edge cost, a is the spacing factor between nodes in (xy) , r is the threshold value for \hat{z} , and d is the threshold for $-\hat{z}$, corresponding to Fig. 1.

The cost for moving from a parent to child node is defined by the edge value. While this value is ambiguously defined in this paper through `setEdgeCost(p, c)` in Algorithm 1 for each child c at a time, it can be modified at any point after

the graph is generated. In the simplest implementation, the cost e of a parent-child pair is the euclidean distance. This can often be a safe metric to use within the scope of the built environment, especially when the set of nodes has already accounted for accessibility. However, as the node relationships are stored and locations are known, the cost function can include the slope from parent to child, a similar technique used in [22, 14], making upward and downward transitions weighted differently. As multiple directions are considered in the set of children for a given parent node, cross-slope information can also be used in the cost function. Furthermore, using the relation between all children to a given parent, scoring methods for a node can be applied, such as chemical diffusion rates for agent modeling shown in [18]. It is this fine-grained graph that affords integrating the human based metrics described in 1.1. At the urban scale, the inclusion of varying ground conditions to walkability analysis that can better predict comfort and fatigue can also be realized.

2.2 Data and Implementation

The algorithms described above were implemented in the Grasshopper environment of Rhino 3D software. For user control, the offsets and various parameters were implemented with the UI elements, while the majority of code was written in python using the *GhPython* component and interfacing with the Rhino Python API. The red nodes and green line for visualization rely on the drawing elements of Grasshopper in Rhino.

The graph is stored in a Python dictionary consisting of parent-child relationships. The average lookup time complexity of $\mathcal{O}(1)$ for the dictionary provides an efficient method for interacting with the dense and high-fidelity graph. The algorithm was initially and conceptually recursive, however default limits in python made implementation with a *while* loop more robust.

While there have been projects for expanding the Rhino ironpython scope [30, 4], they have specialized scripts and installations not included in the standard python library. Due to the simplicity, a Socket based communication was implemented to communicate with a machine-local python instance with the SciPy library. Using the *scipy.sparse.csgraph.shortest_path* method, any search algorithm type available can be used and applied to the graph. In the examples within this paper, Dijkstras search algorithm was used.

3 RESULTS AND DISCUSSION

3.1 Uneven

As a demonstration of the graph's ability to include only accessible spaces, we first look at Fig 3a, in which an entire topology is included in the graph. This case may be prevalent when using GIS data and/or Lidar scans of a topology for a site-specific study. Important to note, this is not from a planar grid above, but rather from the start point A . In the search, A to B is clearly defined as the shortest path outlined in green. The reason the resulting graph is complete across the surface is that there is no threshold that limits the height variation between a parent and child, meaning all nodes are connected.

However, in the case that this topology represents a mountain or urban environment, it is unlikely a user would be able to follow this path as the height variation between a parent-child node relation is excessive for a reasonable person to be able to access.

Beyond accessibility standards or guidelines, the continually changing terrain makes the shortest path by distance an unlikely representation of a path a user would follow. If all locations of the topology are considered accessible, the notion of the shortest path can be modified to account for energy requirements of the terrain. For example, a cost function of the slope can be associated to an edge, whereby the shortest path would be not based on distance alone. However, if certain limits are placed on the ability to traverse a terrain, or within some guideline, parameters of the graph creation can be set to include only those spaces.

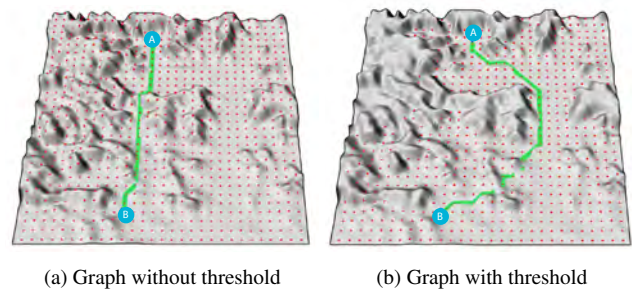


Figure 3: A topology with nodes generated from A , parsing the entire surface. The green line is the search algorithm finding the shortest path from A to B . In 3a, the threshold for parent-child height variation is larger than the terrain while in 3b the lower threshold changes the graph

Fig 3b demonstrates the user-centric graph in which a height variation limiter can be used. The resulting graph is the accessibility graph for that user parameter, and the same points A and B are used for the search algorithm, which now follows a more level and easy terrain. Combined with the options to modify the cost described previously, this graph search can be used for city or urban planning to find the least costly, or most efficient, method of terrain removal for human comfort and accessibility.

3.2 Staggered

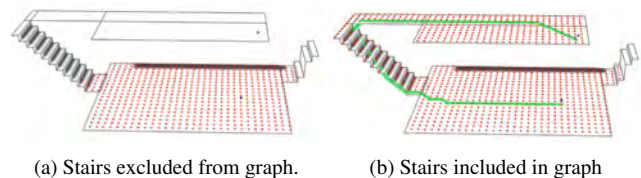


Figure 4: Nodes of the graph visualized in red, with the calculated path shown in green. (4a) A limiting height variable preventing the graph from including stairs. (4b) A limiting height variable that allows the inclusion of short steps on the left, but not the taller steps on the right.

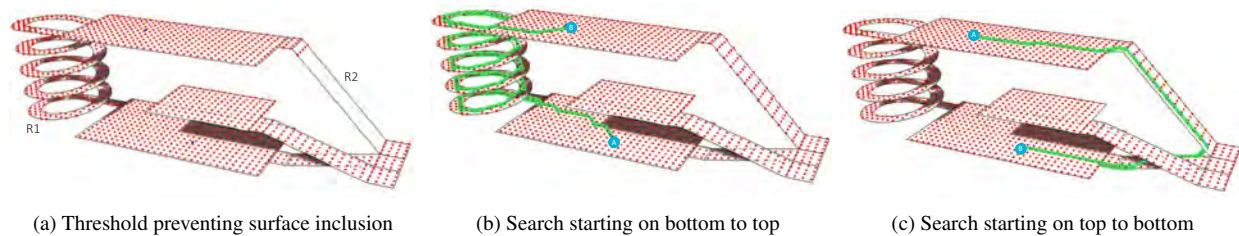


Figure 5: Nodes of the graph visualized in red, with the calculated path shown in green. The two main ramps are labeled as *R1* and *R2* (5a) Equal thresholds prevent the graph from including nodes on *R2*. (5b) Nodes are on all surfaces, while the shortest distance from *A* to *B* uses *R1* rather than *R2* due to the directional graph. (5c) The shortest path is taken from the top surface to the bottom surface, utilizing *R2*.

In the case of stairs, an important value is in the elimination of steps from a building graph, just as much as it is important to be able to include them. In particular, a building occupant in a wheelchair would not be able to traverse steps. In this case Fig 4a demonstrates a second floor surface that is not included in the building graph.

Conversely, Fig 4b demonstrates a modification in the height variable such that the graph automatically can traverse the steps and include the second floor. This traversal is relative, as described in the methodology, and can be seen by the still too large right sided steps. While these steps are in the world co-ordinate system, lower than the steps and second floor plane, they are not included based on the height offset.

3.3 Ramp and Cross-slope

As a final complex demonstration, Figure 5 shows three applicable cases to the height variation and directional graph. In the first example, the graph is built with a height offset setting equal when moving up and down. Within this threshold, all but the ramp *R2* is covered in nodes. As the ramp *R1* is set at a smaller incline, the top surface can be included in the graph.

Next is a case in which nodes cover all surfaces. However, node locations alone do not provide enough information about the environment. In this case, the tolerance for an edge to be created with the child node being higher than the parent is smaller than the tolerance for an edge to be created with the child node being lower than the parent. This distinction can be seen by the shortest path algorithm applied to the nodes *A* and *B*, where *A* is on the bottom plane. The shortest path uses the *R1* ramp, while physical distance between nodes is shorter with the *R2* ramp. This relationship can be further understood by using the same graph but inverting the location of *A* and *B*. When starting from the top surface the shortest path uses the *R2* ramp.

While both up and downhill walking create additional load on the human body, there are many instances in which one direction can still accommodate for a comfortable and safe path. For example, going downhill may pose additional risks for falling or balance compared to moving uphill. In this example, multiple ramps at various slopes are used for simplicity and clarity of the overall system. However, the linear ramps (*R2*) could easily be replaced by stairs, such as in Fig. 4, and then demonstrate that it is not accessible by an occupant with a wheelchair (e.g., in Fig. 5a).

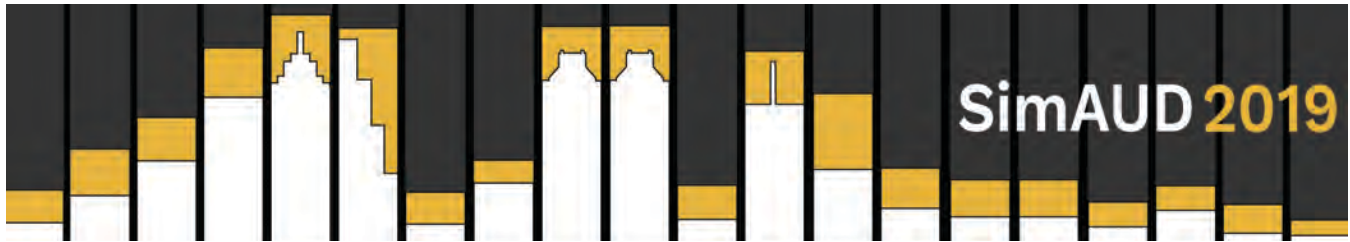
3.4 Discussion

In this paper, we present a method for building a directional graph that can interpret non-flat ground conditions. The literature and approach are focused on the physical act of mobility without regard for social or economic factors. However, the resulting graph contains nodes that, when associated with locations of interest, additional metrics can be incorporated. Through thresholds in the algorithm, variations in the ground condition can prevent the graph from including certain spaces, allowing the designer to see which parts are too extreme or inaccessible for a given occupant. Additionally, this method allows for the graph creation to account for staircases without explicit reference, staying true to the ability to interpret unknown geometries in CAD. The algorithm presented and the method for creation provides a platform for layering complex and human-based analysis methods at both the building and urban scale with high-fidelity and dense node creation.

REFERENCES

1. Benedikt, M. L. To take hold of space: isovists and isovist fields. *Environment and Planning B: Planning and design* 6, 1 (1979), 47–65.
2. Botea, A., Miller, M., and Schaeffer, J. Near optimal hierarchical path-finding. *Journal of Game Development* 1 (2004), 7–28.
3. Chu, M. L., Parigi, P., Law, K., and Latombe, J.-C. Safegress: a flexible platform to study the effect of human and social behaviors on egress performance. In *Proceedings of the Symposium on Simulation for Architecture & Urban Design*, Society for Computer Simulation International (2014), 4.
4. Digital-Structures. Regular python from ironpython in rhino/grasshopper. <https://github.com/Digital-Structures/ghpythonremote>, 2017. [Online; accessed 26-Nov-2018].
5. Dixon, P. C., Jacobs, J. V., Dennerlein, J. T., and Schiffman, J. M. Late-cueing of gait tasks on an uneven brick surface impacts coordination and center of mass control in older adults. *Gait & posture* 65 (2018), 143–148.

6. Dixon, P. C., and Pearsall, D. J. Gait dynamics on a cross-slope walking surface. *Journal of Applied Biomechanics* 26, 1 (2010), 17–25.
7. Doherty, B., Rumery, D., Barnes, B., and Zhou, B. A spatial query & analysis tool for architects. In *Proceedings of the 2012 Symposium on Simulation for Architecture and Urban Design*, Society for Computer Simulation International (2012), 4.
8. Goldstein, R., Breslav, S., and Khan, A. Towards voxel-based algorithms for building performance simulation. In *Proceedings of the IBPSA-Canada eSim Conference* (2014).
9. Hudson, R., and Westlake, M. Simulating human visual experience in stadiums. In *Proceedings of the Symposium on Simulation for Architecture & Urban Design*, Society for Computer Simulation International (2015), 164–171.
10. Kim, D., Lee, J. H., and Ha, M. Exploring perceptions of designers and medical staff in south korea about design elements for the elder-friendly hospital. *Journal of Interior Design* 39, 4 (2014), 15–32.
11. Lantrip, D. B. Environmental constraint of human movement: A new computer-aided approach. In *Proceedings of the Human Factors and Ergonomics Society Annual Meeting*, vol. 37, SAGE Publications Sage CA: Los Angeles, CA (1993), 1043–1043.
12. Lee, J.-k., Eastman, C. M., Lee, J., Kannala, M., and Jeong, Y.-s. Computing walking distances within buildings using the universal circulation network. *Environment and Planning B: Planning and Design* 37, 4 (2010), 628–645.
13. Lee, J.-K., Shin, J., and Lee, Y. Circulation analysis of design alternatives for elderly housing unit allocation using building information modelling-enabled indoor walkability index. *Indoor and Built Environment* (2018), 1420326X18763892.
14. Liu, L., and Wong, R. C.-W. Finding shortest path on land surface. In *Proceedings of the 2011 ACM SIGMOD International Conference on Management of Data*, SIGMOD '11, ACM (New York, NY, USA, 2011), 433–444.
15. Liu, L., Yin, K., van de Panne, M., and Guo, B. Terrain runner: control, parameterization, composition, and planning for highly dynamic motions. *ACM Transactions on Graphics (TOG)* 31, 6 (2012), 154.
16. Nagy, D., Lau, D., Locke, J., Stoddart, J., Villaggi, L., Wang, R., Zhao, D., and Benjamin, D. Project discover: An application of generative design for architectural space planning. In *SimAUD 2017 Conference proceedings: Symposium on Simulation for Architecture and Urban Design* (2017).
17. Nagy, D., Villaggi, L., Stoddart, J., and Benjamin, D. The buzz metric: A graph-based method for quantifying productive congestion in generative space planning for architecture. *Technology—Architecture+ Design* 1, 2 (2017), 186–195.
18. Narahara, T. *Self-organizing Computation A Framework for Generative Approaches to Architectural Design*. Harvard University, 2010.
19. Novak, A. C., Reid, S. M., Costigan, P. A., and Brouwer, B. Stair negotiation alters stability in older adults. *Lower Extremity Review* 2, 10 (2010), 47–51.
20. Pauls, J. L., Fruin, J. J., and Zupan, J. M. Minimum stair width for evacuation, overtaking movement and counterflow technical bases and suggestions for the past, present and future. In *Pedestrian and evacuation dynamics 2005*. Springer, 2007, 57–69.
21. Peng, W., Zhang, F., and Nagakura, T. Machines perception of space: Employing 3d isovist methods and a convolutional neural network in architectural space classification.
22. Roles, J. A., and ElAarag, H. A smoothest path algorithm and its visualization tool. In *2013 Proceedings of IEEE Southeastcon* (April 2013), 1–6.
23. Schwartz, M., Azeez, A., and Patel, K. Human task and disability based automated evaluation of space and design in cad. In *Proceedings of the Symposium on Simulation for Architecture and Urban Design*, SIMAUD '18, Society for Computer Simulation International (San Diego, CA, USA, 2018), 18:1–18:8.
24. Senn, M. *TORONTO REHAB RESEARCHERS HELP CHANGE BUILDING CODE FOR STAIRS*, 2015 (accessed November 25, 2018). https://www.uhn.ca/corporate/News/Pages/toronto_rehab_researchers_help_change_building_code.aspx.
25. Turner, A., Doxa, M., O'sullivan, D., and Penn, A. From isovists to visibility graphs: a methodology for the analysis of architectural space. *Environment and Planning B: Planning and Design* 28, 1 (2001), 103–121.
26. Turner, A., and Penn, A. Evolving direct perception models of human behavior in building systems. In *Pedestrian and Evacuation Dynamics 2005*. Springer, 2007, 411–422.
27. Voloshina, A. S., Kuo, A. D., Daley, M. A., and Ferris, D. P. Biomechanics and energetics of walking on uneven terrain. *Journal of Experimental Biology* (2013), jeb-081711.
28. Wilson, L., Danforth, J., Harvey, D., and LiCalzi, N. Quantifying the urban experience: Establishing criteria for performance based zoning. In *Proceedings of the Symposium on Simulation for Architecture and Urban Design (simAUD 2018)*, simAUD (2018).
29. Yu, L. F., Yeung, S. K., Tang, C. K., Terzopoulos, D., Chan, T. F., and Osher, S. J. Make it home: automatic optimization of furniture arrangement.
30. Zurich, B. R. G. E. Compas. <https://compas-dev.github.io/main/tutorial/xfuncs.html/>. [Online; accessed 26-Nov-2018].



Generating Acoustic Diffuser Arrays with Shape Grammars

Jonathan Dessi-Olive¹ and Timothy Hsu²

¹ School of Architecture,
Georgia Institute of Technology
Atlanta, Georgia, USA
jdo@design.gatech.edu

² Department of Music and Arts Technology
Indiana University-Purdue University
Indianapolis, Indiana, USA
hsut@iu.edu

ABSTRACT

This paper presents research on a rule-based approach to designing creative acoustic diffuser arrays. A shape grammar-influenced design method is specified that uses shape rules to recursively design arrays of quadratic residue diffusers (QRD) in ways that are neither mechanical nor deterministic.

Author Keywords

Architectural acoustics; diffusion; Schroeder diffuser arrays; shape grammars; design computation

1 INTRODUCTION

The shapes of surfaces have a significant impact on the acoustic quality of spaces, yet design processes for architectural acoustics are often highly conventional. With the exception of notable examples [8], acoustical designers have preferred to use knowledge from historical examples, elementary acoustic shape concepts from known equations, and templates from standard principles of performative success. This is particularly true for surface treatments using diffuser products. Acoustic diffusers [4] are surfaces that are not flat and exhibit geometries on the surface that cause reflections to disperse not only in reflected directions, but also in phase and temporal distribution. These non-flat geometries have taken various common forms such as hemispheres, pyramids, arcs, fractals, and number theory generated shapes such as Schroeder diffusers. Surface treatments for diffusion typically use prefabricated products aggregated in ways that perform sufficiently but are visually predictable and monolithic. *This paper addresses the critical issue of design homogeneity in architectural acoustics by proposing a shape grammar approach to designing acoustic diffuser arrays.* This paper will first review principles of diffusion and diffusers and give an overview of previous work with applied shape grammars, propose and demonstrate the diffuser grammar, and discuss how this visual computing method suggests further possibilities of creative and

intentional designs of diffuser arrays that consider performative and aesthetic criteria.

2 ACOUSTIC DIFFUSION AND DIFFUSERS

Acoustic diffusers are geometric surfaces that are designed to break up sound waves and create reflections in different directions [4]. Practically, diffusers are deployed in rooms to mitigate acoustic artifacts such as strong specular reflections or flutter echoes [10]. To alter these reflections, rough surfaces are needed to reflect the initial sound wave back at different angles and phases. Diffuser designers have used geometry, number theory, and performance optimization to design diffusers for desired time and spatial responses [4]. In this section, a background of diffusers and quadratic residue diffuser (QRD) design will be presented.

2.1 Background to Diffusion

When a plane wave strikes a perfectly reflective flat/smooth surface, the resultant wave reflects at the same amplitude as the initial wave and reflects back at an angle equivalent to the incident wave [12]. Diffusion is a frequency dependent phenomenon; thus, the size and depth of the surface geometries affect the effective frequencies of the diffusion. Deeper geometries allow for lower frequency diffusion and shallow geometries diffuse higher frequencies. The depth of the geometry is therefore related to the wavelength of the design frequency of the diffuser. A specific example of this relationship is given below for the quadratic residue diffuser depth. With purposeful acoustic design, these reflections can reinforce the desired sounds and increase factors such as speech intelligibility [10]. Specular reflections can also cause acoustic defects such as flutter echo or acoustic focusing [10]. Waves that strike rough surfaces are diffused: the initial wave is reflected into several new waves that propagate at lower amplitude, at various angles, and at different phases. Previous studies have demonstrated the time and directivity difference of pure reflection, absorption, and diffusion (Figure 1). Careful use of diffusers can suppress flutter echoes and acoustic fluttering, can promote spaciousness in a room, and can help control early reflections in large spaces

[10]. Due to the temporal distribution of the reflected wave, the frequency response of the reflected wave is also be altered by the diffuser [4]. Users suggest that the effect of too much diffusion can create spaces where source localization is difficult and desired sounds are not being reinforced; however, more rigorous studies are required in this area [3]. For example, Cox and D'Antonio suggest that the apparent size of the reflected image is broadened with a diffuser [4]. Optimizing the placement, amount, type, and spatial/temporal properties of diffusers is critical to the acoustical success of a space.

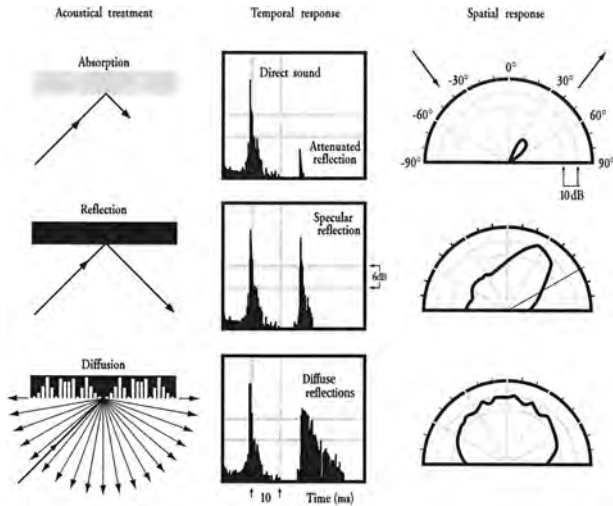


Figure 1. Characteristics in temporal and polar response of absorption, reflection and diffusion of an incident sound wave. [4]

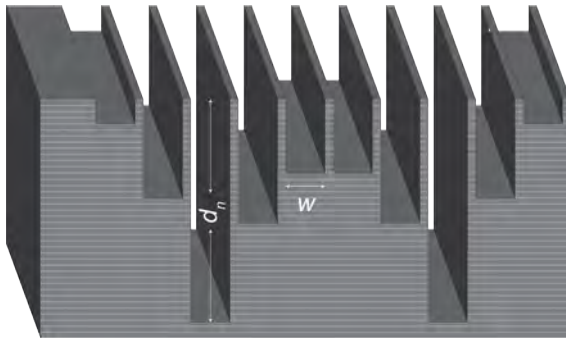


Figure 2. Example of an N11 QRD, showing relationships between the well width, well depth and wall thickness.

2.2 Quadratic Residue Diffusers

Manfred Schroeder invented the phase grating diffuser [14], consisting of a series of wells of different depths separated by thin fins. When a wave strikes a Schroeder diffuser, the waves reflect from the bottom of each well. Due to the differences of depth, the reflected waves have a different phase associated with the depth of each respective well. This phase difference causes a diffuse spatial distribution of reflected sounds. Thus, the well design is the primary parameter that dictates spatial and temporal properties of acoustic diffusion. The simplest diffusers are one-dimensional, corresponding to wave diffusion in only one

plane, perpendicular to the fins of the diffuser [4]. Two-dimensional diffusers can be designed with perpendicular and parallel fins to diffuse sound waves into both planes. Due to the physical dimensions of the wells, diffusers are frequency-dependent [4]. Figure 2 shows a schematic diagram of a Schroeder diffuser. The well depth is derived:

$$w = \frac{\lambda_{min}}{2}$$

where

$$\lambda_{min} = \frac{c}{f_{max}}$$

In this equation, w is the well width, λ_{min} is the minimum wavelength before cross modes emerge, c is the speed of sound, and f_{max} is the maximum frequency of diffusion. Practically, well widths are at least 2.5 cm and are commonly 5 cm [4]. Narrow well widths can cause unintended absorption from the viscous boundary layer, and wide well widths limit the frequency range of effective diffusion. The depth of the n^{th} well is governed by the following equation:

$$d_n = \frac{s_n \lambda_0}{2N}$$

where s_n is the sequence number, λ_0 is the design wavelength, and N is a prime number that corresponds to the number of total wells in the diffuser. For a design frequency, f_d , the desired wavelength can be calculated from:

$$\lambda_0 = \frac{c}{f_d}$$

It can be seen through these calculations that a high design frequency, f_d , results in shallower depths, and lower design frequencies will lead to deeper wells. This relationship of well depth to frequency is also shown in Figure 3. For Schroeder diffusers, a mathematical sequence is the basis for the well depth derivation. The sequence number, s_n , can be generated using maximum length sequences, primitive root sequences, Legendre sequences, amongst a variety of possibilities. The quadratic residue sequence (QRD) continues to be one of the popular choices, derived from the following equation:

$$s_n = n^2 \bmod N.$$

In the case where $N=11$, $s_n = \{0, 1, 4, 9, 5, 3, 3, 5, 9, 4, 1\}$.

Combining the process from above, it can be shown that for a design frequency of 1000 Hz and speed of sound of 343 m/s, the well depths, for an $N=11$ QRD diffuser is

$$d_n = \{0, 16, 62, 140, 78, 47, 47, 78, 140, 62, 16\} \text{ mm.}$$

2.3 Evolution of Diffusers

Within these phase grating designs, there have been several standard designs that are commonly used in the industry, with few variations since their invention. One such variation consisted of an "L-shaped" well to essentially make a 2-dimensional QRD diffuser [6], but this has not seen wide

implementation in the market. Other variations also include thin panel designs, sloped wells, and even an embedded QRD inside a well of a larger QRD. While there has been large scale deployment of diffusers in spaces like concert halls, the computational approach for simulation of these large-scale deployments has been more limited. There are studies that show detailed directivity and temporal responses to individual diffusers or small arrays of diffusers [4]; but for these larger room simulation models, simpler diffusion and scattering coefficients are utilized. Developing better computational approaches to quantify large surfaces of diffusion that can better inform computer simulation methods is an area of future study.

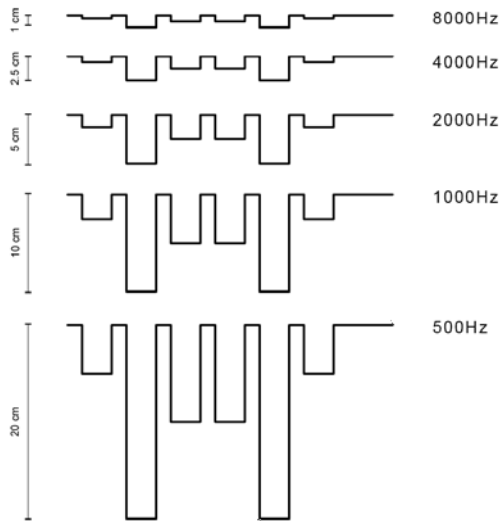


Figure 3. Schroeder diffuser sections for a N=7 design with different design frequencies, from 500Hz to 8000Hz.

3 SHAPE GRAMMARS

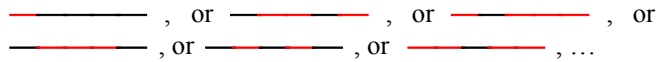
Shape grammars are a computational design methodology that use the notion of *recursion and embedding* for computing with shapes, as an extension of Turing’s “recursion and identity” for computing with symbols [11]. Shape grammars have been used to define *languages* of design in nearly all areas, but little has been done to combine them with acoustics. This section will review the origins of shape grammars, their basic formalism, and the range of previous applications in design fields.

3.1 Fundamental Principle: Embedding

Shape grammars are distinguished from other theories of computation through their use of *embedding*, which grounds them as primarily a *visual* enterprise. Symbols (like points), are 0-dimensional objects, which means they can only be identified as themselves. Shape descriptions of things can operate under the notion of identity, but also under the notion of embedding which privileges the infinite possibilities of what one can see. This can be illustrated by looking at a line:



Lines can be identified as themselves. However, one could also visually identify any number of other lines embedded in that line (shown in red):



This is true for any shape made of lines, faces or solids (1, 2, or 3-dimensional shapes). Shape grammar theory and its applications have demonstrated how shape-based generative systems are more expansive than symbol-based systems because they benefit from the notion of embedding. Working with shape descriptions lets designers work visually, yet rigorously through rule-based shape transformations. Shape grammars rely on a basic formalism, described below.

3.2 Basic Shape Grammar Formalism

The shape grammar formalism has evolved significantly since it was first introduced. Initially Stiny and Gips [18] relied heavily on linguistic analogies that formulated a rigorous mathematical apparatus [16]. Shape grammars have since been simplified to sets of shape rules, labels and weights, and schemas, which classify rules.

3.2.1. Shape Rules

A *shape rule* is written in the form $A \rightarrow B$, where A is a labeled shape that is transformed into a labeled shape B [16]. An example of a shape rule that aggregates \square might be:

$$\square \rightarrow \square \square$$

Each time the rule is applied, a new \square is copied and pasted:

$$\square \Rightarrow \square \square \Rightarrow \square \square \square \Rightarrow \dots \Rightarrow \square \square \square \square \square$$

Shapes can be transformed through spatial transformations (translation, rotation, reflection, scaling), Boolean operations (union, intersection, subtraction), and combinations of the two. When applied recursively, shape rules can generate new and surprising shapes in a rigorous yet and intuitive manner.

3.2.2. Labels and Weights

Shape rules can be augmented by *labels and weights*, which restrict rules or specify how they are applied. *Labels* are 0-dimensional symbols, treated as points rather than shapes:

$$\square \rightarrow \square^{\circ}$$

Weights can specify line type and thickness. Planes can have additional graphic properties, such as texture, color, or tone:

$$\square \rightarrow \square$$

$$\square \rightarrow \blacksquare$$

$$\square \rightarrow \blacksquare$$

Practically, *weights* can serve as a means of associating shape descriptions with physical properties of the designs they represent [17]. Such properties could include structural

or other performative criteria, material specifications, or methods of construction and fabrication.

3.2.3. Schemas

Parametric shape grammars, more commonly known as *schemas*, extend shape grammars by generalizing shape rules into schemata written in the form, $x \rightarrow y$, where x and y are variable terms that can be assigned any parametric shape. The shape rule $\square \rightarrow \square$ can be generalized: $x \rightarrow x+t(x)$, where x can include any parametric variation of \square according to well defined dimensioning and proportion rules. The “copy and move” transformation is generalized as an additive schema $x+t(x)$, where an identity schema $x \rightarrow x$ keeps the original shape in place and a translation of that shape $t(x)$, is added. Schemas are important for design because they serve as universal rules of formation that reveal how shape rules are related, and new ways to use them.

3.3 Review of Shape Grammar Applications

A significant portion of shape grammar scholarship has been dedicated to developing computational mechanisms that demonstrate expanded possibilities of architectural designs in particular styles. Shape rules and schemas have seen broad success in studying historical bodies of architecture such as the plans of villas by Renaissance architect Andrea Palladio [19], houses by Frank Lloyd Wright [7], and the houses of Alvaro Siza at Malagueira [5]. The shape grammar systems defined by these architectural studies shed light on the generative possibilities of their respective architectural languages. While successful in defining generative systems, their production does not extend beyond shape descriptions. A specialized sub-set of shape grammars were introduced that could handle physical and performative properties of the designs they described. In 1991, William Mitchell introduced *functional grammars* [13] for generating designs of shed structures. This important work inspired shape grammar formalisms in other fields such as electro-mechanical engineering [2] and product design [1]. In structural engineering, shape grammars have been used for designing truss structures [15]. More recently, a trans-typology structural grammar was developed that combined shape grammars and graphic statics [9].

Despite numerous applications of shape grammars across virtually all areas of design, very little has been done with acoustics. A recent paper [20] proposes a shape grammar that generates absorber panels, however, performance criteria are not rigorously integrated into how the panel shapes are generated to make an array. Furthermore, only one design is proposed, which seems counter-intuitive to using shape grammars in the first place. The grammar proposed here aims to directly integrate the form-performance relationship of Schroeder diffusers.

4 A LANGUAGE OF DIFFUSION

One advantage of using QRDs for diffuser surface treatments in architectural acoustics is they have a reliable form-performance relationship. Wall treatments with QRDs, typically consist of prefabricated panels that meet desired

performance criteria; aggregated with little or no variation over an entire wall surface (Figure 4). While these arrays may perform sufficiently and predictably, they are visually uninteresting and monolithic. *Why are the rules of aggregation for diffuser panels so unchanging?*

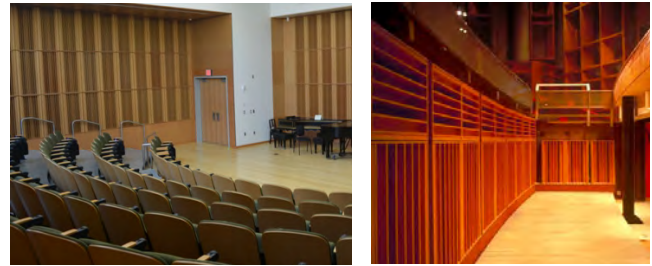


Figure 4. Examples of how Schroeder diffuser products are typically deployed in diffuser wall treatments [21, 22].

This paper addresses the critical issue of design homogeneity in architectural acoustics by proposing a shape grammar methodology for designing quadratic residue diffuser arrays. The diffuser grammar is a two-dimensional parametric shape grammar that uses labeled generative shape descriptions of quadratic residue diffusers as their basic element. QRDs are simple enough that a two-dimensional shape description is sufficient for computing these types of arrays. A coupled form-performance relation is described with labeling systems and weights to associate shape descriptions of QRDs with their physical and performative properties. Weights will indicate a design frequency and the number of wells of a panel. Labels will indicate the orientation of the panel, and direction of their well sequence. The 5-steps of computing (Figure 5) are specified in this section. Computing begins with an initial labeled shape; shape rules are applied recursively. Grid rules aggregate initial shapes into arrays, grid-configuration rules make compound transformations, and form/frequency rules associate shape descriptions with material and performative properties. Computing ends either when no more rules can be applied or when the designer chooses to stop because they like what they see.

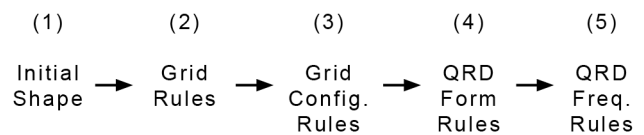


Figure 5. Computing Steps for QRD Shape Grammar

4.1 Initial Labeled Shape

Diffusion arrays in this grammar stem from a square panel. The grammar starts with an initial shape: a labeled square that represents a 60cm x 60cm diffuser panel. An *initial shape rule* (Figure 6) places a labeled square somewhere in the diffusion area. At this stage, the panel does not specify diffuser form or performance properties. The labels on the square serve to indicate the center of the panel with a dot, and to orient the panel in space with an arrow. The arrow-dot label indicates a one-dimensional QRD panel. Later, the initial labels will be replaced with weights and other label

systems to specify the number of wells, the direction of the well sequence, and the design frequency of the panel.

4.2 Grid Rules

Grid rules aggregate the initial shape and manipulate the labels in those initial shape configurations (Figure 7). Rules (G1) and (G2) are aggregation rules that copy and paste the initial shape according to the schema $x \rightarrow x+t(x)$. Together, they can generate rectangular arrays, but also irregular or asymmetrical configurations of squares. Rule (G4) changes the initial shape for a one-dimensional QRD, to an initial shape for a two-dimensional QRD panel. The rule removes the red circle, and adds and rotates a second arrow that connects to the first. Rule (G3) changes the orientation of an initial shape, which equates to rotating a one-dimensional QRD panel from a vertical to horizontal orientation, as shown in the image on the right of Figure 3. Rule (G5) rotates the initial shapes for two-dimensional diffuser panels. Both rotation rules operate according to the schema, $x \rightarrow t(x)$.

4.3 Grid-Configuration Rules

Grid rules are a powerful means of introducing variation and change to arrays of diffuser panels by graphically distinguishing between one and two-dimensional diffusers and introducing the ability to rotate their labeled shape descriptions in a design. These transformations can be tedious however, because they apply to one panel at a time. *Grid-configuration* rules are an emergent class of compound diffuser rules that use *embedding*. These rules let a designer invent new rules as they work. Groupings of labeled shapes can be picked out to apply multiple grid transformation rules simultaneously. The rules (Figure 8) change pairs of labeled squares from one to two-dimensional diffuser descriptions and also pick out square, T-shaped, L-shaped grid figures to perform compound rotations. Though simple, these rules illustrate how expansive the design possibilities can be when new compound rules such as these are written.

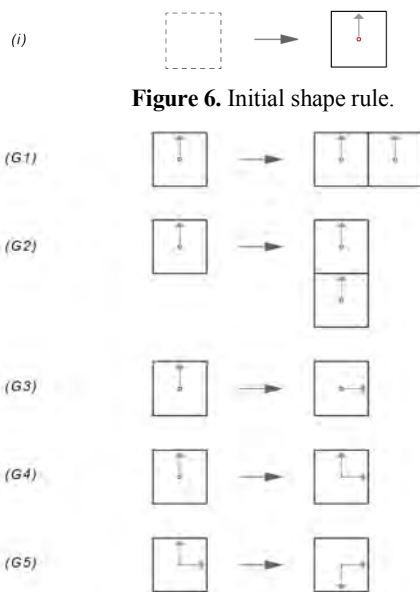


Figure 6. Initial shape rule.

Figure 7. Grid Rules

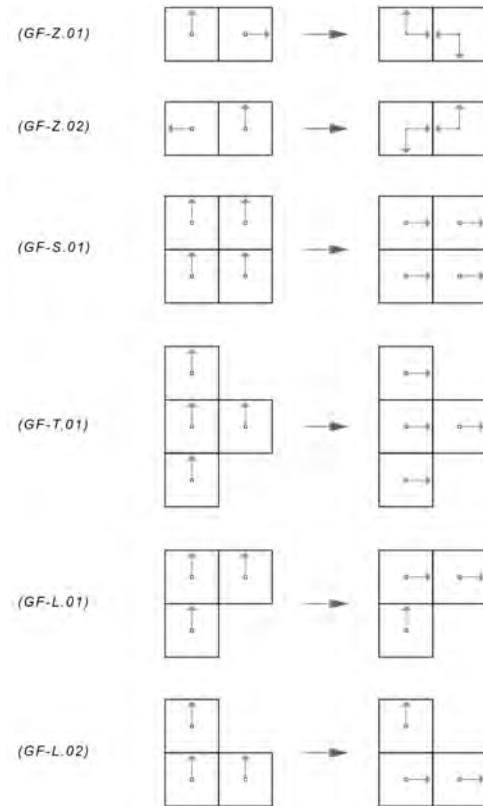


Figure 8. Grid-Configuration Rules.

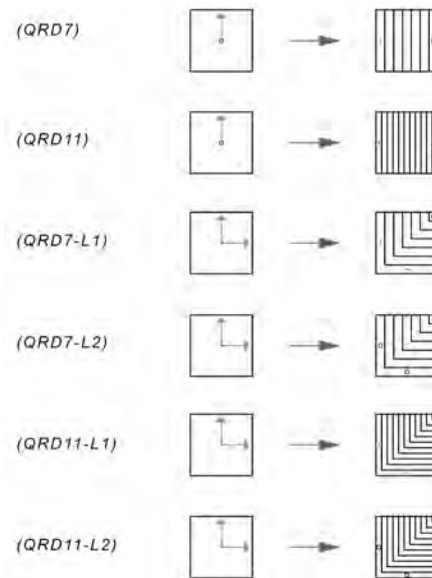


Figure 9. QRD assignment rules specify types of QRD panels.

4.4 QRD Form Assignment Rules

A *form-performance relation* of Schroeder diffusers in the grammar is specified with labeling and weight systems. QRD form and performance rules associate physical and performative properties of diffusers with their shape

descriptions. *QRD form assignment rules* (Figure 9) specify the number of wells the diffuser panel will have. A label system indicates the direction of the well-depth sequence, which includes a value of zero (see sample sequence in section 2.2). The circle indicates the location of the zero-depth well. Rules (*QRD7*) and (*QRD11*) removes the arrow-dot labels from initial shapes and draws the fins of one-dimensional QRD panels. A 60 x 60 cm panel could have as few as seven wells and as many as eleven. Two-dimensional diffuser panels with L-shaped fins [7] are specified in the grammar as well. QRD form assignment rules can be applied at any time during a computation, however they terminate grid manipulations. To change the orientation or type of QRD panel in a design, the grid-figure rules have to be applied in reverse to return the panel back to an initial shape with an arrow-based label.

4.5 QRD Frequency Assignment Rules

QRD frequency assignment rules specify the design performance of panels in a design. These rules apply a tone to the QRD shape descriptions. Common design frequencies for diffusion surface treatments were selected and assigned tones. The rules look for the well-depth sequence labels applied in the previous step and apply different tones across the array. Figure 10 specifies five design frequency rules that use the one-dimensional well-depth sequence labels. Figure 11 specifies frequency rules that include the use the other two well-depth sequence labels for two-dimensional diffusers, with the same range of frequency-indicating tones. Applying different tones in a single array presents opportunities to generate multi-band diffuser treatments. Once the two-step form-performance assignments have been made, a designer can make material and fabrication specifications for a design based on the visual descriptions generated by the grammar.

5 EXAMPLE COMPUTATIONS

Shape grammars have the ability to not only generate known designs, but also other surprising and unexpected designs in the language. Figure 12 shows simple step-by-step computations using rules (*G1*) and (*G2*) to make 2x2 panel arrays. Rule (*G3*) rotates panels to make patterns that are recognizable, and include the designs in [Figure 3]. More complex arrays can also be generated by applying rules differently – and to larger numbers of panels. Figure 13 shows examples of 4x4 panel arrays generated from grid-configuration rules and 1D QRD panels oriented either vertically or horizontally. Figure 14 shows two other example computations that use parametric variations of the L-shaped grid-configuration rules. Figure 15 gives examples of larger QRD arrays that produce visually evocative, surprising, and irregular patterns.

6 DISCUSSION AND FUTURE WORK

The grammar demonstrates how designing diffuser arrays can be open-ended and creative. By challenging the manner in which QRD panels are typically deployed, this paper addresses *how to design with acoustic diffusers* in architectural acoustics.

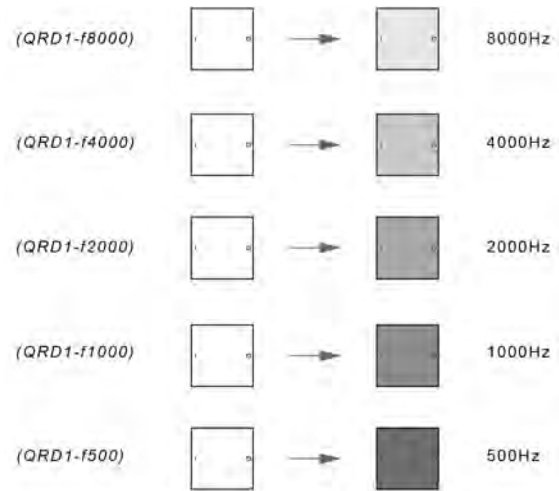


Figure 10. Sample 1D QRD assignment rules to specify frequency.

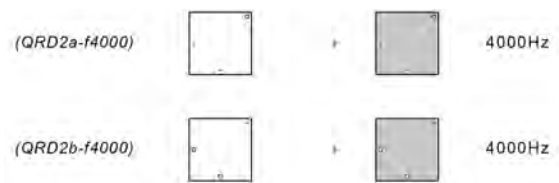


Figure 11. Sample 2D QRD assignment rules to specify frequency

Though already quite expansive, the grammar should be expanded further:

Initial shapes – the rules in this diffuser grammar currently is based on grids of a common 60cm x 60cm square QRD panel design. Although rules have only been written for one and two-dimensional diffusers with either seven or eleven wells, one could easily specify rules for QRD versions that have eight, nine, or ten wells on the same size panel. The physical dimensions of a physical QRD panel are ultimately dependent on the number of wells, the design frequency and also fabrication limitations, so other initial shapes could be specified for panels of other sizes/well counts.

Grid and grid-configuration rules – configuration rules have the most expansive potential to produce new and unexpected designs of diffuser arrays in this grammar because they capitalize on the notion of embedding. By continuing to find shapes embedded in the panel grids, new configurations of panel types, well-counts, or even frequency could be specified. For instance, one could imagine several more grid-figures rules that use parametric variations of L's, T's, rectangles. In addition to making compound rotations, grid-configuration figure rules could be extended to specify compound additions of panels, that would generate even more surprising possibilities of diffuser arrays. They could also begin erasing grid lines in order to describe new panels whose new shape comes from fusing visual descriptions of panels together in a computation. The labeling systems in the

grid rules are currently quite restrictive. They assure that any array produced by the grammar is made up of known QRD panels, which severely limit the possibility for the recombination of panels. Future work on diffuser grammars should strive to loosen the labeling rules and permit for unexpected scaling and overlapping to occur. Future developments should also be focused on better incorporating and further capitalizing on embedding to design panels. Figure 16 shows how embedding can be used to generate the L-shaped QRD [6].

Diffuser form-performance assignment rules – the assignment rules are limited to known panel types because they have a reliable form-performance relation. In addition to Schroeder diffusers, there are several other known and more complex types of diffusers that could be given shape

descriptions and specified in the is diffuser grammar. However, different panels used in the grammar should also perform reliably based on its particular form (form-performance relation). As the grammar expands to produce new panels and configurations ways described above, a means of validating performance will be needed. Future work should include ways to quantitatively characterize the acoustic performance of large-scale panels by investigating the appropriateness of typical metrics such as diffusion and scattering coefficients for surfaces generate by shape grammars, as well as developing computer simulations that describe the diffuse reflections. A workflow between panel/array generation and acoustic simulation should lead to new form-performance rules that can be specified by current label and weight systems to continue broadening the possibilities of this computational design method.



Figure 12. Simple computations showing aggregation and rotation rules for one-dimensional QRD panels.

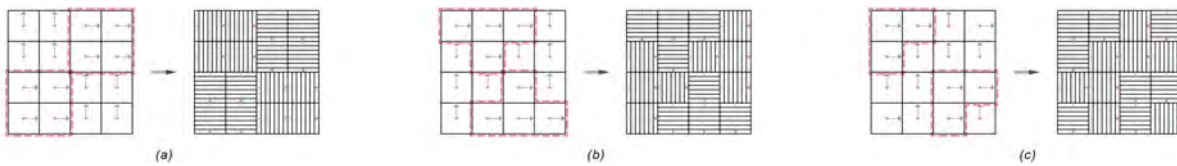


Figure 13. Examples of other small arrays of one-dimensional panels using grid-configuration rules.

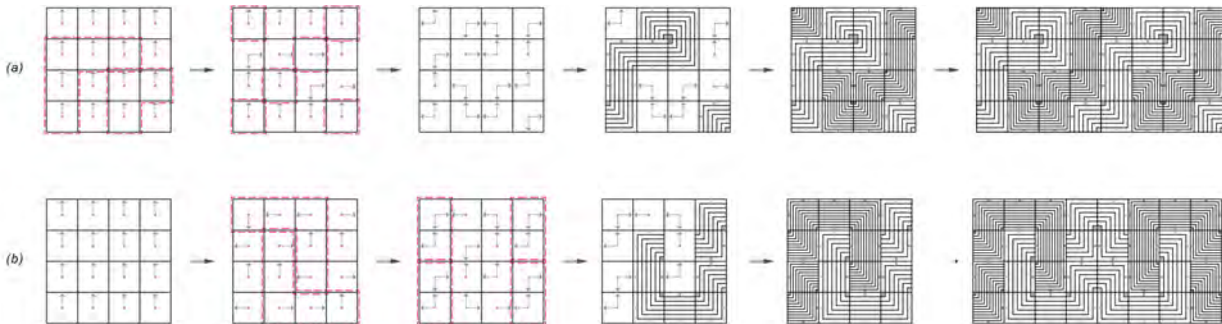


Figure 14. Computations of 4x4 arrays using one and two-dimensional panels, and varying well-counts.

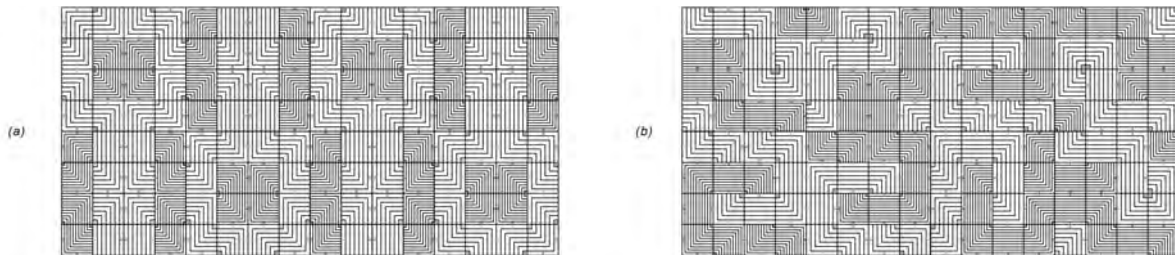


Figure 15. Two possible designs for large QRD arrays in the same language.

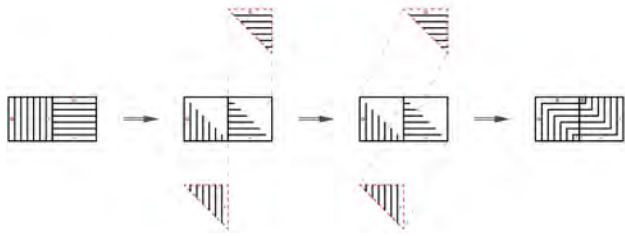


Figure 16. Example of how embedding notion can be applied to generate designs of known panel types.

7 CONCLUSION

The shape grammar proposed here uses form-performance coupled shape-rule schemata to generate aggregations of known Schroeder diffuser shapes to demonstrate how old habits in diffuser deploying techniques can be broken. Most diffuser design is limited to considering single panels using known equations that give known forms. Individual Schroeder diffusers are designed parametrically based on the number of wells and the design frequency, that produce the characteristic stepped section. These variables, which define form-performance relations of Schroeder diffusers, are specified in the grammar according to a system of weights and labels to associate designs of diffusers with their shape representation in the grammar. Generating QRD arrays with this methodology is neither mechanical nor deterministic, and can produce new and visually surprising diffusion arrays that perform reliably according to the equation that generated the individual panels.

ACKNOWLEDGMENTS

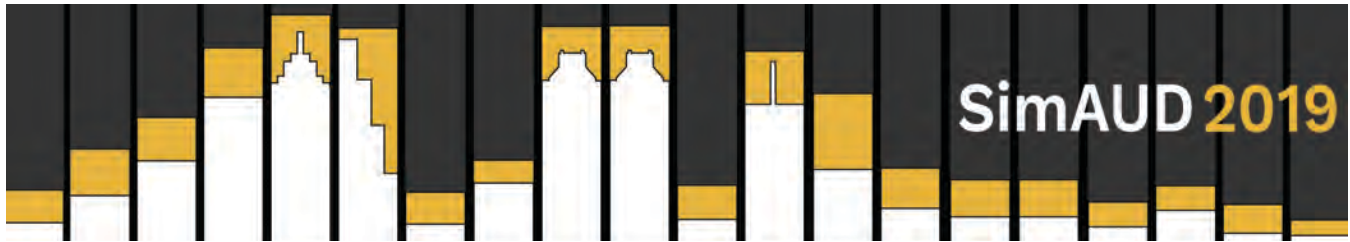
The authors would like to acknowledge support from the Georgia Institute of Technology and Indiana University Purdue University – Indianapolis. The first author would like to acknowledge support from the Ventulett NEXT Generation Visting Fellowship.

REFERENCES

1. Agarwal, M. and Cagan, J. A blend of different tastes: the language of coffeemakers. *Environment and Planning B*, 25, 1998, 205-226.
2. Agarwal, M., Cagan, J. and Stiny, G. A micro language: generating MEMS resonators by using a coupled form-function shape grammar. *Environment and Planning B*, 27, 2000, 615-626.
3. Cox, T. J. Acoustic Diffusers: The Good the Bad and the Ugly. *Proc. to the Inst. of Acoustics*. 2006.
4. Cox, T. J. and D'Antonio, P. *Acoustic absorbers and diffusers: theory, design and application*, Third Edition. CRC Press, 2017.
5. Duarte, J.P. Toward mass customization of housing: the grammar of Siza's houses at Malagueira. *Environment and Planning B*, 32, 2005, 347-380.
6. Järvinen, A., Melkas, K., and Savioja, L. Numerical Simulations of the Modified Schroeder Diffuser Structure. *Proc. to the 16th Int. Congress on Acoustics*, Seattle, USA, 1998.
7. Koning, H. and Eizenberg, J. The Language of the Prairie: Frank Lloyd Wright's Prairie Houses. *Environment and Planning B*, 8, 1981, 295-323.
8. Koren, B.S and Müller, T. Digital Fabrication of Non-Standard Sound Diffusing Panels in the Large Hall of the Elbphilharmonie. *Fabricate*. Eds. Menges, A. et al. UCL Press, 2017, 122-129.
9. Lee, J., Fivet, C. and Mueller, C. Modelling with Forces: Grammar-based graphic statics for diverse architectural designs. *Modeling Behavior*, Springer Publishing, 2015, 49-504
10. Long, M. *Architectural Acoustics*, 2nd Edition. Academic Press, 2014.
11. March, L. Forty Years of Shape and Shape Grammars, 1971-2011. *Nexus Network Journal*, 13, 1, 2011, 5-13.
12. Mehta, M., Johnson, J. and Rocafort, J. *Architectural Acoustics: Principles and Design*, 1st Edition. Prentice Hall, 1998.
13. Mitchell, W. J. Functional grammars: An introduction. *Computer Aided Design in Architecture '91: Reality and Virtual Reality*, Eds. G. Goldman, G. and M. Zdepski, ACADIA, Troy, NY, USA, 1991, 167-176.
14. Schroeder, M.R. Diffuse sound reflection by maximum-length sequences. *Journal of the Acoustical Society of America*, 57 (1975), 149-150.
15. Shea, K., Cagan, J. The design of novel roof trusses with shape annealing: assessing the ability of a computational method in aiding structural designers with varying design intent. *Design Studies*, 20, 1999, 3-23.
16. Stiny, G. Introduction to shape and shape grammars. *Environment and Planning B*, 7, 1980, 343-351.
17. Stiny, G. *Shape: Talking about seeing and doing*. The MIT Press, Cambridge, MA, USA, 2006.
18. Stiny, G. and Gips, J. Shape Grammars and the Generative Specification of Painting and Sculpture. *Information Processing 71*, 1972, 1460-1465.
19. Stiny, G. and Mitchell, W.J. The Palladian Grammar. *Environment and Planning B*, 5, 1978, 5-18.
20. Yavuz, E. , Çolakoğlu, B., and Aktaş, B. From pattern making to acoustic panel making using shape grammars. *Proc. to eCAADe*, 36, 2018, 477-486.

IMAGE CREDITS

21. Real Acoustix project at Reed College
<<http://www.realacoustixllc.com/reed-college>>
22. RPG Acoustics <<https://rpgacoustic.com/qrd-734>>



A Unified Framework for Optimizing the Performance of a Kinetic Façade

Ok-Kyun Im, Kyoung-Hee Kim, Armin Amirazar and Churlzu Lim

UNC Charlotte
Charlotte, NC
oim@uncc.edu

ABSTRACT

A noble kinetic façade system, Oculi Kinetic Façade System (OKFS) was developed to balance solar heat gain, daylighting, and user satisfaction. The study focused on a dynamic control scheme that incorporates simulation data to determine optimal angles of the OKFS for given hours. This research considered daylighting and solar irradiance as the performance metrics. In order to reflect two metrics, we employed a min-max normalization method with a weighting factor in the proposed scheme. The weighting factor is determined by the performance of OKFS at the given time. The implementation of the control scheme is demonstrated via a case study, where simulation data was generated through the Grasshopper Diva 4.0. The result indicated that the optimal control of the rotational angle of OKFS can improve the daylight performance up to around 10%. It is expected that the findings from this study can contribute to developing a systematic optimization model of a kinetic façade system as well as an evaluation scheme for the performance of kinetic façade system.

Author Keywords

Kinetic façade; Daylight; Solar irradiance; Optimization; Normalization; Integration

1 INTRODUCTION

Building envelopes play an important role in controlling and/or admitting the various elements of external environments. Designing a well-daylit space requires a proper balance between daylight provision and control. A wise use of daylight is preferred by building occupants in working spaces as it is proven that it does not only increase the workers' satisfaction and productivity [2] as well as improve occupants' visual comfort, but also enhance occupant's health and well-being [1] within the built environment. However, an excessive amount of natural light coming through the window can cause visual discomfort in the form of glare and rise of internal loads. Therefore, the goal of advanced shading technologies is to keep the balance

between the advantages and disadvantages of sunlight penetration.

In 1970s, William Zuk and Roger H. Clark [11] introduced the term Kinetic architecture. Data from several studies suggest that employing kinetic façade considerably reduces the need for external energy consumption by decreasing unwanted solar heat gain or loss and by increasing the use of natural lighting. Through the variability of the system, the façade will adapt itself to the best situation for the given environmental condition and thus increase its potential impact. Kinetic façade systems can help mitigate environmental problems, by decreasing the need for mechanical systems such as HVAC systems and artificial lighting while offering the occupants' comfort. These kinetic systems are not intended to replace mechanical systems, but they could decrease the energy demands of a building significantly. However, few studies investigated the impact of kinetic façades on indoor day lighting and energy usage. Unlike the traditional shading device, the oculi kinetic façade system (OKFS) proposed in this research responds to the external solar position in order to reduce the energy usage and increase the user comfort at the same time. It can be distinguished from the traditional shading system in terms of dynamically finding optimal conditions considering the thermal performance and visual comfort. The responsive feature of OKFS makes it possible to find an optimal balance between solar irradiance and daylighting at a given time.

While Useful Daylight Illuminance (UDI) and Daylight Autonomy (DA) are ranked as the most favorable indices to evaluate the indoor daylight condition on yearly basis, it is difficult to assess the daylight variation of the indoor space according to the dynamic motion of a kinetic façade system with the existing method. Therefore, a new method for daylight evaluation that can consider a time frame responding to the characteristics of a kinetic system is required. The hourly spatial daylight autonomy was adopted as an evaluation criterion in order to analyze dynamic daylighting performance [4]. Another daylighting study evaluated the hourly illuminance distribution of indoor space

according to the deformation of the hexagonal kinetic façade by using the LEED V4's 300-3000lux daylighting requirement [7].

In addition, most kinetic façade systems share a common problem evaluating the thermal performance due to its complex or small-scale geometries. The complex geometry of a kinetic façade system has a limitation in applying to Energy Plus, a validated whole building energy simulation program. Most typical buildings or simple shading devices are recognized by Energy Plus, but a complex form of a kinetic façade system cannot be applied into Energy Plus. For a time efficient evaluation process, the complex kinetic façade was converted into a simple geometry having the same opening ratio [6]. Additionally, other analysis utilized an integrated calculation method that combines solar irradiance, hourly shading coefficient, and hourly transparency schedule for energy performance evaluation of perforated solar facades [3]. Following those works, it is necessary to employ a new method such as hourly daylight evaluation or thermal performance evaluation of a kinetic façade system using complex geometries in analyzing the performance of the kinetic system. This paper aims to provide an integrated methodology for OKFS in order to identify an optimal rotation angle considering daylight and solar irradiance. With this methodology, it is possible to evaluate and decide the optimum rotation angle of a kinetic façade system that provides maximum daylight availability in the indoor space while finding an appropriate level of solar irradiance.

2 METHODOLOGY

The proposed methodology is divided into three main phases and it is shown in Figure 1. In the first phase, we designed the Oculus Kinetic Unit which can rotate in a clockwise or counterclockwise direction to control the daylight. Then the group of Oculus Kinetic Units applied into the south-facing window of a simulation model.

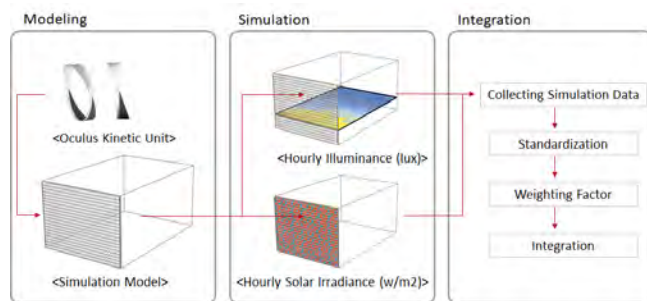


Figure 1. Framework of integrated optimal performance of OKFS

In the second phase, two different simulations were carried out to evaluate the OKFS performance. The first is to investigate the daylight condition of different rotation angle of OKFS by calculating the percentage of the floor area satisfying the daylight criteria. Then, the average amount of solar irradiation for each of six from six different angle of OKFS is calculated. In the third phase, the collected data of

daylit and solar irradiance is applied into the normalization method, where the weighting factor considering the performance of OKFS at each time is multiplied to the normalized value. Each normalized value multiplied by the weighting factor is unified into one integrated metric. The value of the integrated metric is used to determine an optimal rotation angle considering the daylight condition and the solar irradiance.

2.1 Case Study

Sidelit open-office space with the fully glazed window at south-facing façade located in Charlotte, NC is modeled to evaluate the optimal OKFS configuration. An office space is modeled using 3-D modeling software Rhinoceros [9] in which room geometry and orientation are assigned to the model. Once the 3-D model is built, it is imported into Grasshopper [5], a visual programming language for a parametric design, where the OKFS is applied into the south-facing window and the radiance materials are assigned to all surfaces through the open-source plugin DIVA 4.0 [10]. The 3-D model including a detailed schematic design of an office building is presented in Figure 1. The model properties are presented in Table 1 and Radiance simulation parameters are presented in Table 2. It is important to note that the model is analyzed without the presence of electric lighting and only considers daylight as the only source of lighting.

Property		Value	
Climate		Charlotte, NC	
Oculus Kinetic Unit	Height	14 cm	
	Depth	5 cm	
Simulation Model	Height	3m	
	Width	4m	
	Depth	6m	
Analysis Surface	Illuminance (lux)	Height	0.76 m above the floor
		Grid Spacing	0.5 m
	Solar Irradiance (w/m ²)	Height	Coplanar with Window surface
		Grid Spacing	0.05 m
Reflectance	Interior Ceiling		0.8
	Interior Wall		0.5
	Interior Floor		0.2
	Oculus Kinetic Unit		0.7

Table 1. Model properties

aa = 0.1	ab = 4	ad = 1024	ar = 256
----------	--------	-----------	----------

dr = 2	ds = 0.2	Ir = 6	Lw = 0.004
dj = 0	sj = 0.15	st = 0.15	

Table 2. Model radiance parameters

2.2 Oculi kinetic façade system (OKFS)

In this study, a kinetic façade unit which has the form of an oculus is developed as a dynamic shading device (see Figure 2). A key enhancement compared to other kinetic façades is that the OKFS is able to control the amount of incoming daylight to improve the indoor visual comfort and also reduce the energy consumption at the same time. Moreover, a clear area of the south-facing window for the external view can be maintained consistently while the OKFS is rotating. As can be seen in Figure 3, the total of six cases is created through a combination between the rotational motion of the oculi kinetic unit from 0 to 300 degree with an increment of 60 degrees in order to respond to a variability of sun position.

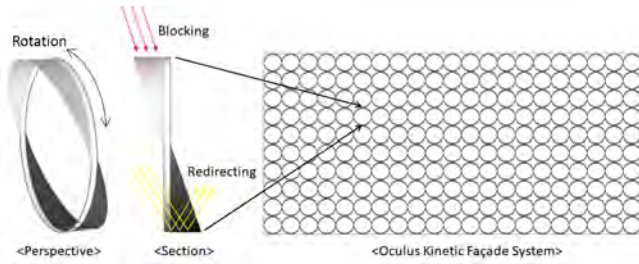


Figure 2. Prototype of the oculi kinetic unit

OKFS 0°	OKFS 60°	OKFS 120°	OKFS 180°	OKFS 240°	OKFS 300°

Table 3. Rotational motion of OKFS

2.3 Daylighting simulation

The aim of this phase is to analyze the daylighting performance of OKFS by changing the rotation angle at four days of the year; March 21st, June 21st, September 21st, and December 21st. These days were selected as they represent four extreme solar positions considering altitude and azimuth throughout the year. Annual daylight simulation using DIVA 4.0 was carried out to get the hourly illuminance values for all sensors distributed throughout the indoor space. 96 sensors are placed throughout a horizontal measurement grid with 0.5 m spacing 0.76 cm above the floor to measure the horizontal illuminance (see Table 3). The illuminance value

of each sensor is sorted by the LEED criteria and the number of sensors satisfying the target illuminance range is calculated. In order to compare the number of satisfied sensors depending on the rotation angle, a total of seven simulations including no oculi (base case) condition are carried out. Then, the optimal rotation angle is decided as one of seven rotation cases providing the largest satisfied sensor number which has the same meaning with the maximized daylit area.

In the daylighting simulation, LEED v4 is used as the performance criteria to evaluate the daylight performance of OKFS based on three illumination levels for the floor area: “daylit”, “partially daylit”, and “overlit” areas. The illuminance range between 300 and 3000 lux is defined as “daylit” which is an appropriate illuminance distribution in the office areas recommended by the ASHRAE and IES standards(ref). “overlit” indicates the illuminance range over 3000 lux causing the glare, and the “partially daylit” achieves the illuminance levels below 300 lux which is required to have an artificial lighting for satisfying the office illuminance level.

2.4 Solar Irradiance Simulation

The level of influence of solar irradiance on thermal comfort and energy consumption can be controlled by the shading device. In this phase, the optimal rotation angle of OKFS is determined by comparing the results of solar irradiance calculated from different rotation angle. Unlike the daylight simulation, the optimal criteria of the solar irradiance is altered in response to the changing seasons. The maximized solar irradiance value during summer increases the indoor cooling load, whereas the maximized solar irradiance decreases the heating load during the winter time. For deciding an optimal rotation angle of OKFS, it is required to understand that the effect of solar irradiance to the thermal comfort is different depending on the season.

Therefore, the rotational angle of OKFS providing the minimized solar irradiance is considered as the optimal condition during the summer season. In contrast, the rotational angle of OKFS accepting the maximized solar irradiance is defined as the optimal condition during the winter season.

In order to produce the hourly solar irradiance data, this research utilized the Daysim within Diva 4.0. The simulation plane was placed on the coplanar with the south-facing window located behind the OKFS and the grid spacing was set to 10cm considering the oculi kinetic unit size. By this setting, a total of 1,200 sensors installed on the simulation plane to collect the hourly solar irradiance value. Similar to daylighting simulation, a total of seven simulations with different rotation angles are performed to compare each of the average solar irradiance value.

2.5 Integration

The goal of this stage is to integrate the results of two simulations which have different units and scales. To achieve this, the min-max normalization method [8] is utilized to convert the original simulation data into the normalized value range from 0 to 1. By applying this method, two different simulation results can be comparable on the same scale. Figure 3 shows the whole procedure of integrating two different simulation results using the normalization method and the weighting factor.

2.5.1 Normalization method

The min-max normalization method [8] to scale the original data between the 0 and 1 can be described as follow. The original simulation values are converted by the following equation:

$$\overline{Si} = (Si - Min S) / (Max S - Min S) \quad (1)$$

\overline{Si} represents the normalized value from the equation (1) and Si represents the original simulation value. $Min S$ represents the minimum value of the original data, and $Max S$ represents the maximum value of the original data.

In the case of daylight simulation, for example, the meaning of the normalized value '1' means that it has the maximized daylit area among the compared cases. In contrast, the normalized value '0' indicates the lowest performance which has the least daylit area.

In the case of the solar irradiance, the meaning of the normalized value is changed according to the season. In table 3, the normalized solar irradiance value '0' means the best condition for June 21st, which provides the minimized solar irradiance. This is because the minimized solar irradiance can help reduce the cooling load. In order to make the minimized normalized value best, '-1' is multiplied to the normalized solar irradiance value on June 21st. In other words, the maximized solar irradiance indicates the lowest performance. In Dec 21st, on the other hand, the normalized value '1' means the best condition which has the maximized solar irradiance and the normalized value '0' indicates the minimized solar irradiance. The table 4 below shows the criteria of the normalized value by the season.

		Worst		Best
June 21st	Solar Irradiance	-1	~	0
	daylit	0	~	1
	Value Range	-1 ~ 1		
Dec 21st	Solar Irradiance	0	~	1
	daylit	0	~	1
	Value Range	0 ~ 2		

Table 4. Seasonal normalization range

2.5.2 Weighting factor

If there is only small difference between the minimum and the maximum values of a simulation result at the given time, the small difference is enlarged in the normalization stage. Since the normalized value has a significant influence on the final integration result, we used the weighting factor to find an optimal condition considering the performance at that time. In particular, we used the following equation to find a suitable value of the weighting factor considering the simulation performance:

$$\alpha * (Max.D - Min.D) = \beta * (Max.SI - Min.SI), \quad (2)$$

where

α = the weighting factor of Solar irradiance

β = the weighting factor of Daylight

In this equation, $Max.D$ and $Min.D$ represent the maximum and the minimum results of Daylight simulation. Similarly, $Max.SI$ and $Min.SI$ represent the maximum and the minimum values of Solar Irradiance simulation at the given time. The sum of α and β is 1. After applying the min-max value of each simulation at the given time, α and β can be obtained by the equation (2). Then the value of α and β , which make the equation (2) equal, become the weighting factor of the opposite simulation. We assumed that if a simulation result is more influenced by the OKFS, it has a large weighting factor than another. For example, if there is daylight simulation result has a large difference between the maximum and the minimum, a large value is assigned to the daylight weighting factor, i.e., β .

3 RESULTS OF CASE STUDY

3.1 Daylight performance

The results of daylight simulation show the indoor daylight condition satisfying the daylit criteria with different rotation angles. Since there are many factors such as the curved units of OKFS and the material properties that affect the daylight results, it is difficult to find a consistent correlation between the optimal rotational angle and the time.

	No OKFS	OKFS 0°	OKFS 60°	OKFS 120°	OKFS 180°	OKFS 240°	OKFS 300°
9 A M							
PD	49.0	56.3	58.3	57.3	56.3	56.3	57.3
D	51.0	43.8	41.7	42.7	43.8	43.8	42.7
OL	0.0	0.0	0.0	0.0	0.0	0.0	0.0
12 P M							
PD	34.4	40.6	39.6	42.7	38.5	40.6	38.5

D	52.1	59.4	60.4	57.3	61.5	58.3	60.4
OL	13.5	0.0	0.0	0.0	0.0	1.0	1.0
15 P M							
PD	36.5	47.9	45.8	46.9	44.8	44.8	44.8
D	62.5	52.1	54.2	53.1	55.2	55.2	55.2
OL	1.0	0.0	0.0	0.0	0.0	0.0	0.0

PD: Partially Daylit / D: Daylit / OL: Overlit

Table 5. Daylight simulation result at June 21st

Let No_OKFS denotes the simulation without OKFS. At 12 PM on June 21st, the daylight result shows that the OKFS increases the daylit area around 5 to 10% than the one without OKFS, but the daylit area (%) of 9AM and 15PM was decreased than the one without OKFS. This result is significantly affected by the overlit condition. There is no overlit condition which has over 3000 lux value at 9AM and 15 PM. Under this condition, the illuminance value of the indoor space was reduced by the OKFS because the opaque external shading device blocks the incoming daylight.

On the contrary, in case of 12 PM, there is 13.5 % overlit area causing glare. In order to improve occupants' visual comfort, the overlit area needs to be reduced. By the OKFS, the overlit area was turned into the daylit condition, so the indoor daylight condition is improved. According to the rotation angle of OKFS, it shows slight difference of the daylit condition, and 180 degree provided the maximized daylit area at 12 o'clock.

3.2 Solar irradiance performance

Since there is a performance difference in blocking solar irradiance depending on the rotation angle, the result of the solar irradiance (Table 6) indicates that the solar irradiance is reduced about 20-40% by the OKFS. Also, the reduced amount of the solar irradiance changed by the season. In June 21st, the OKFS reduces up to 40% of the solar irradiance compared to the one without OKFS. But, in Dec 21st, the OKFS reduces around 20% of the solar irradiance compared to the one without OKFS. The difference between the seasons can be explained by the relation between the form of the Oculus unit and the solar position. During the summer season, when the altitude of the sun is high, a large amount of solar radiation is blocked by the OKFS. However, the blocked solar irradiance by the OKFS decreases in winter.

Table 6 displays also reports the irradiance value for different angles of OKFS. For example, at 12 PM on June 21st, the optimal rotation angle is 180° which produced the minimum solar irradiance value (Table 7). This result is somewhat expected because when considering the solar position at noon, 180° is the most effective angle to block the solar radiation since the OKFS with angle 180° has a similar arrangement of a horizontal shading system. In winter, on the

other hand, the optimal condition is the angle that can receive the maximum solar irradiance to reduce the heating load. From this point of view, at 12 PM on Dec 21st, the optimal rotation angle is 120° which can receive the most solar irradiance among those rotation angles tested.

	No_OKFS	0°	60°	120°	180°	240°	300°
March 21st (Min): 60°(9AM)/0°(12PM)/300°(15PM)							
9AM	169.25	117.96	100.78	112.81	125.01	104.83	111.87
12PM	640.61	472.74	492.26	522.86	477.51	491.49	526.53
15PM	569.98	411.41	459.30	415.20	412.78	444.60	390.40
June 21st (Min): 300°(9AM)/180°(12PM)/0°(15PM)							
9AM	73.38	69.26	66.82	67.13	68.34	66.28	65.85
12PM	237.64	137.29	137.88	146.74	132.98	147.08	150.38
15PM	199.82	105.89	118.79	107.64	109.59	120.32	114.06
Sept 21st (Min): 60°(9AM)/0°(12PM)/300°(15PM)							
9AM	286.86	192.92	147.15	177.57	211.96	157.38	172.53
12PM	598.59	441.77	459.60	487.26	446.38	459.07	490.45
15PM	424.22	306.09	336.26	307.19	308.41	327.32	291.24
Dec 21st (Max): 180°(9AM)/120°(12PM)/240°(15PM)							
9AM	91.65	71.73	66.76	69.85	72.58	67.87	70.86
12PM	288.67	231.40	232.31	237.09	233.21	232.84	236.73
15PM	95.74	70.38	71.57	70.76	71.62	71.75	70.09

Table 6. Solar irradiance simulation result of 4 days

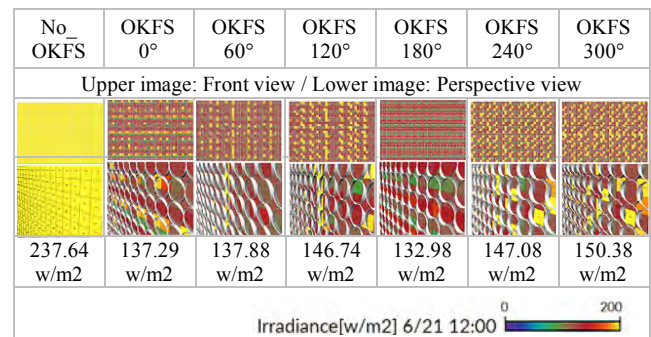


Table 7. Solar irradiance result images at 12 PM on June 21st

3.3 Integrated performance

In this phase, two simulation results were unified to make a decision on the optimal rotation angle. Figure 3 shows how two different simulation values are unified into one integrated result. The simulation results of a rotation angle are normalized into the value range between 0 to 1. Then the normalized value multiplied with the weighting factor considering the simulation performance at the given time.

Therefore, a value of weighting factor is changed by the time. In the integration process, the weighted normalized value of each simulation is added to return one integrated result. This integration process is repeated by changing the rotation angle of OKFS.

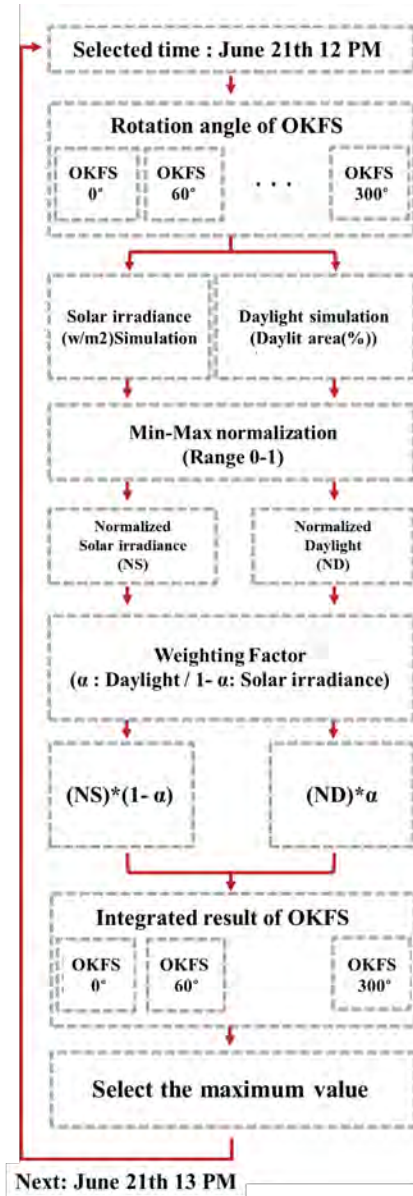


Figure 3. Integration process diagram

		Daylit area	Solar irradiance
OKFS 0°	Simulation	59.4(%)	137.29(w/m2)
	Normalization	0.5	-0.25
	Weighting	0.19	0.81
	Integration	(0.5*0.19) + (-0.25*0.81)	
	Result	-0.11	
		Daylit area	Solar irradiance

OKFS 60°	Simulation	60.4(%)	137.88(w/m2)
	Normalization	0.74	-0.28
	Weighting	0.19	0.81
	Integration	(0.74*0.19) + (-0.28*0.81)	
	Result	-0.09	
		Daylit area	Solar irradiance
OKFS 120°	Simulation	59.4(%)	146.74(w/m2)
	Normalization	0	-0.79
	Weighting	0.19	0.81
	Integration	(0*0.19) + (-0.79*0.81)	
	Result	-0.64	
		Daylit area	Solar irradiance
OKFS 180°	Simulation	61.5(%)	132.98(w/m2)
	Normalization	1.0	0
	Weighting	0.19	0.81
	Integration	(1.0*0.19) + (0*0.81)	
	Result	0.19	
		Daylit area	Solar irradiance
OKFS 240°	Simulation	58.3(%)	147.08(w/m2)
	Normalization	1.0	-0.81
	Weighting	0.19	0.81
	Integration	(1.0*0.19) + (-0.81*0.81)	
	Result	-0.47	
		Daylit area	Solar irradiance
OKFS 300°	Simulation	60.4(%)	150.38(w/m2)
	Normalization	0.75	-1.0
	Weighting	0.19	0.81
	Integration	(0.75*0.19) + (-1.0*0.81)	
	Result	-0.67	

Table 8. Integrated results of OKFS at June 21st

At 12 PM on June 21st, the weighting factor of daylighting and solar irradiance have 0.19 and 0.81, respectively, and the weighting factor means that the rotational motion of OKFS at this time is determined based more on the solar irradiance performance than controlling daylight condition (Table 8).

Since the corresponding simulation condition is summer, the normalized value of the solar irradiance is distributed between -1 and 0 according to the rule set in 2.5.1 normalization method. By this criterion, 180° is considered as the most effective rotational angle at 12 PM on June 21st. On the other hand, daylight condition has a normalized value between 0 and 1 regardless of the season. Therefore 240° angle can be considered as the best condition at the given time.

Time		Daylit (%)	Solar Irradiance (w/m2)	Integrated result
9 AM	Mar 21st	120°	60°	60°
	June 21st	0°/180°/240°	300°	240°
	Sept 21st	300°	60°	60°
	Dec 21st	300°	180°	180°
12 PM	Mar 21st	0°	0°	0°
	June 21st	240°	180°	180°
	Sept 21st	180°	0°	0°
	Dec 21st	0°	120°	120°
15 PM	Mar 21st	180°	300°	300°
	June 21st	180°	0°	0°
	Sept 21st	0/180°	300°	300°
	Dec 21st	300°	240°	300°

Table 9. Optimal rotational angle at the given time

The last column of Table 9 shows the optimal integrated angles for 12 cases. Each integrated optimal result was created through the integration process. Also, table 9 shows the optimal rotation angle of daylit and solar irradiance. There are two observations between the optimal angle of each simulation result and the integrated result. First, the integrated result does not provide a new angle as the optimal condition considering different two objectives, the integrated result has the same angle condition with one of two simulation results.

For example, at 15 PM on June 21st, the optimal angle of daylit simulation is 180° and the solar irradiance optimal condition is 0°. The integrated result is 0° which is the same angle with the solar irradiance result, not the different rotation angle like 60° or 120° which is located between 0° and 180°. This is because the weighting factor for daylit has a significant effect on deciding the integrated result.

Since there is no absolute standard for deciding the weighting factor, and the weighting factor can be decided by the user, if a user set a different value, a different rotation angle can be selected as the integrated result.

Second, it is possible to infer that which performance is more influenced by the OKFS at the given time by comparing the angle information. For example, at 9 AM on March 21st, it can be considered that the OKFS is more effective in controlling the solar irradiance because the integrated result has same rotation angle with the optimal angle of solar irradiance. Similarly, at 9 AM on June 21st, we can consider that the OKFS shows a better performance for daylighting condition than controlling solar irradiance.

4 DISCUSSION & CONCLUSION

As a way to improve building energy performance, a kinetic façade system is attracting considerable interest. Therefore, a new method for evaluating the performance of a kinetic façade system is required to provide information to designers in the early design stage. This research has investigated the integration process using the normalization method in order

to find an optimal rotational angle of oculi at the given time. In addition, the weighting factors were applied to the normalized values considering the simulation results. Through the integration method suggested in this study, we found that the rotational motion of OKFS has an important effect on the daylight and solar irradiance condition. The results of this study provide insight for designers to evaluate the performance of kinetic systems and establish criteria for kinetic design. In the case of using an optimized rotation angle in summer, the indoor daylit area was increased by about 15% compared with the area without OKFS condition. Furthermore, the overlit area causing the glare discomfort was significantly mitigated by the OKFS. At the same time, solar irradiance was reduced about 44% by the optimal rotation angle. In winter condition, the daylit area was increased up to 15% and the overlit area causing glare discomfort was reduced by 50% compared with the one without OKFS condition. As for the solar irradiance in winter, the rotation angle which offsets the solar irradiance to the minimum is considered as the optimal condition. With this criterion, the optimal rotation angle of OKFS overall reduces 18% solar irradiation compared to the same space without OKFS.

Based on these results, this research found that the solar irradiance performance of OKFS was closely related to the season. In the case of summer, dynamic OKFS with optimum rotational angles reduced 44% of solar transmission compared to the façade without OKFS. In addition, static OKFS blocked 36% of solar irradiance compared to the one without OKFS. These analysis results indicate that the rotational motion of OKFS makes a difference about 8% in summer compared to the static OKFS. On the other hand, there was a difference about 2% between dynamic OKFS and static OKFS in winter. As far as the daylight performance is concerned, this research found that about 10% of daylit area is changed by the rotational motion regardless of the season. In the future work, we will design different geometries of an oculus to understand how different oculus forms and the optimal rotation angle have an effect on solar response, and analyze the relationship between the oculus geometry and the oculus optimal angle.

ACKNOWLEDGEMENTS

The authors would like to thank INES and School of Architecture at UNCC for supporting the project.

REFERENCES

1. Amirazar, A., et al. *Assessing the circadian potential of an office building in the southeastern US.* in *Proceedings of the Symposium on Simulation for Architecture and Urban Design.* 2018. Society for Computer Simulation International.
2. Amirazar, A., et al., *Questionnaire Survey on Factors Influencing Occupants' Overall Satisfaction on Different Office Layout in a Mixed-Humid Climate.* 2017.

3. Chi, D.A., D. Moreno, and J. Navarro, *Design optimisation of perforated solar façades in order to balance daylighting with thermal performance*. Building and Environment, 2017. **125**: p. 383-400.
4. Elghazi, Y., A. Wagdy, and S. Abdalwahab. *Simulation driven design for kinetic system; optimize kaledocycle facade configuration for daylighting adequacy in hot arid climates*. in *Conference of International Building Performance Simulation Association*. 2015.
5. Grasshopper Algorithmic Modeling Program for Rhino. <http://www.grasshopper3d.com/>.
6. Kim, H., M.R. Asl, and W. Yan. *Parametric BIM-based energy simulation for buildings with complex kinetic façades*. in *Proceedings of the 33rd eCAADe Conference*. 2015.
7. Mahmoud, A.H.A. and Y. Elghazi, *Parametric-based designs for kinetic facades to optimize daylight performance: Comparing rotation and translation kinetic motion for hexagonal facade patterns*. Solar Energy, 2016. **126**: p. 111-127.
8. Patro, S. and K.K. Sahu, *Normalization: A preprocessing stage*. arXiv preprint arXiv:1503.06462, 2015.
9. Rhinoceros 3-D Modeling Program. <http://www.en.na.mcneel.com/contact.htm>.
10. Solemma, DIVA for Rhino. <http://diva4rhino.com>.
11. Zuk, W. and R.H. Clark, *Kinetic architecture*. 1970: Van Nostrand Reinhold.

Author Index

A

Abbasabadi, Narjes 71
 Aijazi, Arfa N.. 37
 Amer, Mohamed239
 Amir, Oded217
 Amirazar, Armin. 147, 303
 Arens, Edward135
 Ashrafi, Roshanak.147
 Asl, Mohammad Rahmani . . .245
 Attia, Shady239
 Azarbayjani, Mona147

B

Bartosh, Amber 65
 Bayomi, Norhan. 45
 Breslav, Simon169
 Burry, Jane 161, 185

C

Campanile, Claudio105
 Chamilothori, Kynthia 57
 Chen, Kian Wee.143
 Clayton, Mark J.245
 Cox, Robert.147

D

Danforth, Jason113
 Danzo, Eric 11
 Das, Subhajit.287

Davila, Carlos Cerezo113
 De Luca, Francesco 3
 de Regt, Elizabeth 19
 Deak, Tomothy 19
 Dessi-Olive, Jonathan295

E

Eaton, Kevin269
 Economou, Athanassios279
 Erdine, Elif 199, 207

F

Faloutsos, Petros177
 Farrokhsiar, Paniz.231
 Fernandez, John 45
 Futrell, Benjamin147

G

Girling, Cynthia129
 Glass, Joseph.147
 Glicksman, Leon 37
 Goldstein, Rhys.169
 Grobman, Yasha Jacob217
 Gu, Rongzhu 65

H

Harvey, Dee.113
 Hashem, Farzad 95
 Haworth, Brandon.177

Hsu, Timothy295

I

Im, Ok-Kyun303

J

Jenning, Petra121
 Jeronimidis, George207

K

Kamari, Aliakbar 29
 Kapadia, Mubbasir . . . 169, 177
 Khan, Azam169
 Kim, Kyoung-Hee303
 Kirkegaard, Poul Henning . . . 29
 Konig, Reinhard 79
 Kontar, Rawad El 87
 Koranaki, Antiopi207
 Krietemeyer, Bess. 87

L

Lharchi, Ayoub 51
 Li, Xiaofeg155
 Ligler, Heather279
 Lim, Churlu.303

M

Malekpour, Diba 95
 Malm, Henrik.121

Marschall, Max	161, 185	Rakha, Tarek	45	Tessman, Oliver	191
Martino, Nicholas	129	Reinhart, Christoph	45	Thomsen, MetteRamsgaard . . .	51
Matiz, Carmen Cristiana	199	Richardson, Henry David . . .	135	Tono, Alberto	135
McCarty, Justin	253	Riederer, Elisabeth	225	Trigueiro, Edja	129
McMenomy, Heather “Brick” .	199	Rodrigues, Alexander	269		
Meggers, Forrest	143	Rodriguez, Alvaro Lopez . . .	207	U	
Mehdizadeh, Samim	191	Rysanek, Adam	143, 253	Usman, Muhammad	169
Moon, Seonghyeon	169				
Moreira, Angel Fernando Lara	207	S		W	
Morschek, Julius	79	Sawyer, Azadeh	57	Weinstock, Michael	207
		Schaumann, Davide	169, 177	Weizmann, Michael	217
N		Schiavon, Stefano	135	Wilson, Luc	113
Naboni, Emanuele	11	Schneider, Sven	79	Wortmann, Thomas	261
Nagpal, Shreshth	45	Schroepfer, Thomas	261	Wu, Chengde	245
Nassif, Nabil	269	Schultz, Carl Peter Leslie . . .	29	Wuu, Shih Hsin	105
		Schwartz, Mathew	287		
O		Seedfar, Arian	231	Z	
Ofria, Luca	11	Shi, Yuchen	155	Zani, Andrea	135
		Sungur, Alican	207	Zarrabi, Amir	147
P		Suryavanshi, Anuradha	225	Zarrinmehr, Saied	245
Pantelic, Jovan	143			Zhang, Xun	177
Passe, Ulrike	95	T			
		Tabard-Fortecoef, Vinciane . . .	95		
R		Tahmasebi, Farhang	185		
Rai, Pyria	269	Tamke, Martin	51		
		Teitelbaum, Eric	143		

Presenting Authors



Narjes Abbasabadi

Narjes Abbasabadi an Adjunct Professor in the College of Architecture at Illinois Institute of Technology (IIT) and she is currently a Ph.D. Candidate in Architecture (Technologies of the Built Environment track) at IIT with an expected degree in May 2019. Her doctoral dissertation develops and tests an integrated framework for urban energy use modeling (UEUM) that captures urban building and transport energy use through a bottom-up data-driven methodology. She has also received several research grants and design awards. Being part of a graduate team from IIT, her team was awarded the 'Second Prize' recognition in the 2018 U.S. Department of Energy (DOE)'s Race to Zero Design Competition. Prior to her PhD, she received several research grants from the Iranian government to develop codes and prototypes for low energy buildings in Iran. Currently, she has been working as the editor for to-be-published Journal of the the IIT PhD program in Architecture, Prometheus: Architecture, Culture, & Technology. Professionally and along with her PhD studies, she has worked as a full-time architect at Adrian Smith + Gordon Gill (AS+GG), an architecture firm in Chicago engaged in the design and development of energy-efficient and sustainable architecture.



Arfa Aijazi

Arfa Aijazi is currently a PhD student in Building Science in Architecture at the University of California, Berkeley, and also works as a graduate student researcher at the Center for the Built Environment. She received a Masters in Building Technology (2017) and Bachelors in Materials Science and Engineering (2013) from the Massachusetts Institute of Technology. Her doctoral research evaluates how climate change impacts building performance by using future weather files in existing simulation tools in order to design more climate resilient buildings.



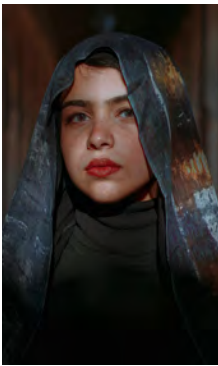
Mohamed Amer

Mohamed Amer is currently a PhD researcher at the Sustainable Building Design (SBD) Lab, at the Faculty of Applied Sciences at the University of Liege, Belgium. His research expertise is in climate responsive, zero-energy and cost-optimal designs. Currently, Amer's research focuses on multi-criteria optimization for roof extensions, promoting for sustainable urban densification in Europe. Prior to his current position, Amer has been awarded a fellowship at Transsolar in Stuttgart, one of the leading companies in the field of climate engineering. There he had hands-on experience in environmental design, energy modelling, and daylighting simulations. He has worked on several projects worldwide and on different scales. Amer previously got his Master's double degree in Integrated Urbanism and Sustainable Design (IUSD) from the University of Stuttgart in Germany and University of Ain-Shams in Egypt, where he focused his research on retrofitting existing building through parametric simulation and optimization for energy consumption and daylighting.



Roshanak Ashrafi

Roshanak Ashrafi is a PhD student in the University of North Carolina at Charlotte. She is currently studying in the interdisciplinary program of Infrastructures and Environmental Systems (INES). She is working as a teaching assistant and a research assistant at the Daylight and Energy Performance Lab in the Architecture department at UNCC. She has a B.S. in Civil engineering and M.S in Architectural engineering with her master’s thesis in the field of participatory design. She has done research about building energy systems, building integration systems and human comfort in indoor space. She has also participated in projects about lighting calculations and indoor lighting configuration. Her current research is about integrating building components for a human-centered design by the application of IOT and Complex adaptive systems. She is also studying the use of Machine learning algorithms to create an integrated user centric controlling system for the perimeter zone of the building.



Norhan Magdy Mohamed Bayomi

Norhan is a PhD students in the Building Technology program at MIT and a research assistant in the Urban Metabolism group. She received her BSc. In Architecture from Cairo University and MSc in Building Technology from MIT. Norhan’s research is focused on Climate change science and possible impacts in developing regions and what role can the built environment play in this dilemma. Her research is focusing on exploring potential human health risks associated with increased temperature in cities and how using aerial technology can assist in better understanding building and urban design while defining suitable adaptation strategies. Norhan has recently developed a web platform dedicated to climate change challenges in the MENA Region (MENA-CC). The tool seeks to contribute to the enrichment of climate change mitigation and adaptation in the region. The platform also has an interactive archive on global heatwave from 1800s to 2018, documenting impacts of rising temperature on human health risks. Norhan is also a founding member of a startup company “AirWorks” that was formed in MIT in 2017. AirWorks focuses on using Aerial technology for real-time urban data analysis and construction intelligence through machine learning.



Amber Bartosh

Amber Bartosh is a LEED-accredited architect and interior designer who has designed and managed award-winning projects in the United States, China, Kuwait, and the U.A.E. She received her B.A. in Art and Architecture from Rice University and her M.Arch from the Southern California Institute of Architecture (SCI-Arc). Amber is currently an Assistant Professor at Syracuse University School of Architecture, a Syracuse Center of Excellence Faculty Fellow, and co-director of the Interactive Design and Visualization Lab (IDVL). Her work focuses on the architectural application of emergent materials through physical prototyping and advanced visualization technologies including hybrid reality simulations.



Claudio Campanile

Claudio is a qualified Architect with MSc in Emergent Technologies and Design from the AA School of Architecture and holds a MEng in Architectural Engineering. He works as a R&D computational engineer at Bryden Wood's Creative Technologies team, with a special focus on data analytics and numerical optimization methods for design related to geo-spatial data and civil engineering. By applying his technical expertise at a multiscale level, from collection, manipulation and visualisation of alternate data sources, Claudio focuses on developing various tools to exploit data to extract useful layers of information. Therefore, research and delivery are mixed to produce evidence-based decision making and design tools in tandem with clients and stakeholders. Moreover, Claudio is a course tutor at the AA Landscape Urbanism graduate programme, where his research explores the potential of data analytics for the civil, territorial and spatial practice.



Jason Danforth

Jason Danforth is a computational designer and member of the KPFF team. Working at the intersection of architecture, urbanism, and technology, Jason's recent work includes a computational urban design methodology for large-scale master planning, machine learning workflows for managing large design spaces, and leading the development of a cloud-based platform for distributing simulations across virtual machines on AWS. Jason earned his Master of Architecture from Columbia University's Graduate School of Architecture, Planning and Preservation, receiving the Henry Adams Medal, the GSAPP Visualization Award, and a William Kinne Fellows Traveling Prize. Jason is also an Adjunct Assistant Professor at Columbia University's GSAPP, and a Guest Lecturer at the Syracuse University School of Architecture.



Jonathan Dessi-Olive

Jonathan Dessi-Olive is the inaugural Ventulett NEXT visiting Fellow (2017-2019) at the Georgia Tech School of Architecture. His work takes a critical approach to technology while integrating history and theory of architecture, contemporary construction, and computational design. Prior to joining Georgia Tech, he completed a Master of Science in Design and Computation at MIT, and a Master of Architecture at PennDesign. His recent contributions have been to develop new methodologies for designing and building high-performance, sustainable building technologies in the United States, Europe, and East Africa. As a designer, builder and academic, Jonathan's motivation is to help designers and builders to learn to design more intuitively, systematically, and visually. His work seeks to combine issues of contemporary design tools and methodologies, and our necessity to make breakthroughs in sustainable building technologies. He has led research and construction efforts that test material strategies for concrete and masonry vault structures. Recently his work has also looked at developing new strategies for lightweight and deployable structures, and computational design methods for acoustical surface treatments. His design and construction work has been exhibited in several public venues such as the Venice Architecture Biennale and TEDxPenn.



Francesco De Luca

Francesco De Luca (Architect, PhD) is Research Scientist at the Department of Civil Engineering and Architecture of Tallinn University of Technology (TalTech) in the field of daylight, solar design and urban microclimate. His research is situated at the intersection of performance-driven design and computational design for architecture and planning. He has been appointed Research Assistant and Lecturer at the Faculty of Architecture of the University Sapienza of Rome (2001-2006) and Visiting Associate Professor of Architecture at the Faculty of Landscape Architecture of Tallinn University of Technology (2010-2014). He lectured and tutored workshops at Aalto University, Oslo School of Architecture, Cornell University and TU Delft among others. He is author of books and papers published in scientific journals such as Analysis of the Insolation Criteria for nearly-Zero Energy Buildings in Estonia (Science and Technology for the Built Environment – Taylor & Francis). His work has been selected for presentation and published in the proceedings of various conferences among which SimAUD, CAAD Futures, eCAADe and ACADIA.



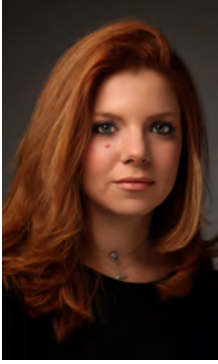
Elizabeth de Regt

Elizabeth de Regt, AIA, LEED AP ND, is a Seattle-based architect and urban designer at ZGF Architects. Her passion lies at the intersection of these two fields, with a focus on master plans that enhance sustainability at an urban scale and facilitate living in the city. Elizabeth’s design ethos encompasses placemaking, increasing access to daylight, and addressing the implications of density and other issues impacting urban living. Her passion for sustainable design and livability shines through in the variety of projects she has worked on, from commercial office buildings and mixed-use residential developments, to Seattle’s Mandatory Housing Affordability program and numerous LEED Neighborhood Development master plans. She is also active in various American Institute of Architects (AIA) policy communities, chairing AIA WA’s Climate Committee and serving on AIA Seattle’s Public Policy Board. Elizabeth received a Bachelor of Science in architectural design from the Massachusetts Institute of Technology and a Master of Architecture from the University of Texas at Austin.



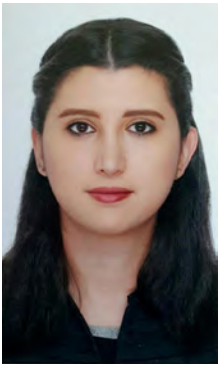
Kevin Eaton

Kevin Eaton is a second-year computer science student at the University of Cincinnati. He was selected to participate in research during the fall semester of 2018 led by Dr. Nabil Nassif. He worked daily under Dr. Nassif’s supervision to create models and research papers as well as assist with research for other PhD and graduate students. He currently is working part time under Dr. Nassif to assist with other research papers. Outside of research, Kevin is a member of Cyber@UC, a cyber security club focused on teaching and educating students about cyber security. He is also an active member in music ensembles across the University. He is a member of the Bearcat Marching Band where he plays Mellophone. This ensemble plays at football and basketball games in the fall and spring as well as various events on campus. He is also active in the Bearcat Concert Band and Bearcat Jazz band.



Elif Erdine

Elif Erdine is an architect, designer, and researcher. Currently, she is the Studio Master at Emergent Technologies and Design Graduate Programme, at the Architectural Association (AA) School of Architecture. During 2010-2015, she conducted her PhD at the Architectural Association PhD in Design Programme, titled ‘Generative Processes in Tower Design: Algorithms for the Integration of Tower Subsystems’. Since 2010 she has been directing various AA Visiting School programmes (AA Istanbul VS, AA Summer DLAB), exploring generative design techniques, integration of algorithmic design methods with large-scale digital fabrication tools. Her research interests include the role of the individual building within complex urban systems, the exploration of urban data as design drivers, biomimicry, and robotic design and fabrication. She has presented her research in Design Studies, eCAADe, CAAD Futures, SimAUD, and ACADIA, among others. She has worked for Zaha Hadid Architects during 2006 - 2010. She received her B.Arch. degree from Istanbul Technical University in 2003 (High Honors), and M.Arch. degree from the AA Design Research Lab (AA DRL) in 2006 (Project Distinction).



Paniz Farrokhsiar

Paniz Farrokhsiar is an architect, computational designer, and researcher. She is studying Master of Science in Architecture (Design Computing) at Pennsylvania State University. She got her Bachelor of Architectural Engineering from University of Tehran, Iran in 2015. After graduation, she has collaborated in many educational courses, including Digi-Made workshop series, Delta-Z in collaboration with IAAC school of Architecture, Code-Structured-Skin, Hedracrete workshops and Caai School of Architecture as researcher, tutor and assistant tutor. Her research interests are structural design, digital fabrication, robotic architecture, also designing prefabricated, low-cost, low-space and self-sufficient buildings. She is a founder and member of ADAPt group. The first project of the group is a free-form compression-only thin-tile vault built in Isfahan, Iran, called “FaBRICKate” which has been awarded the Architizer A+ Awards Jury and Popular Choice under Brick category in 2017, and one of the finalists in 2A Asia Architecture Award 2017.



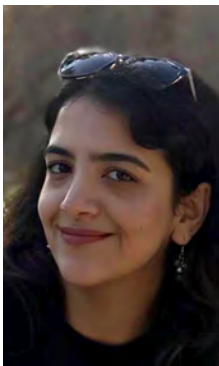
Ok-Kyun Im

Ok-Kyun Im is a Ph.D. candidate in the infrastructure and environmental system (INES) program, where he is conducting various researches for the development and performance evaluation of a kinetic facade system. He has a Master of Science degree in architecture and has been awarded two patents related to the building kinetic facade system. He is interested in studying the influence of kinetic facade systems on indoor daylight condition and building energy consumption. He is also interested in optimizing the kinetic system using regression analysis. Ok-Kyun Im plans to continue his research on kinetic facade system and optimization of kinetic movement considering multiple objectives related to energy use, user comfort, etc.



Aliakbar Kamari

Aliakbar Kamari, b. 1987, finished B.E. Architectural Engineering in 2009 and M.E. Civil Engineering in Construction & Management in 2012. He spent the triennium of his Ph.D. studies for a fully funded double degree Ph.D. program in Department of Engineering, Aarhus University, DENMARK, and Department of Architecture, University of Palermo, ITALY, carrying out an INTERDISCIPLINARY research study related to Renovation/Retrofitting of the Existing Buildings. He is presently performing a postdoc period within Value Creation by Energy Renovation and Transformation of the Built Environment associated with the ReVALUE project, in the Department of Engineering, Aarhus University, DENMARK. Aliakbar is vastly interested to perform further research related to the Integrated Building Design Methodology, Systems Thinking & Theory, BIM methodology, and BIM-based Decision Support Systems. The main mission of his research is to explore, adapt, and develop new problem-oriented approaches to building design, and the methods and tools that support them. That leads to increase and enhance the integration related to people, process, and technologies in the earlier stages of the building design process for development of more holistic sustainable design solutions, aiming at bridging architecture topics into the engineering and vice versa.



Diba Malekpour Koupaei

Diba Malekpour Koupaei is a first-year Ph.D. student and graduate research assistant in the department of Civil, Construction and Environmental Engineering at Iowa State University. She holds a master’s degree in Sustainable Environments from Iowa State University and received her bachelor’s degree from Art University of Isfahan in Architectural Engineering. As part of the final creative component of her graduate studies, she investigated the interplay between built form and tradition in a historic residential neighborhood and proposed a theoretical framework for revitalization of such neighborhoods. Over the course of past few years, her main research activities have all been concerned with energy efficiency in the built environment, specifically residential buildings in the urban landscape. Currently, as a member of the Sustainable Cities multidisciplinary research group at Iowa State University, she follows her passion for integrating the human dimension of energy consumption into the efficiency equation for mitigating and adoption to climate change.



Bess Krietemeyer

Bess Krietemeyer is an architectural designer, educator, and researcher whose expertise lies at the intersection of advanced building technologies, interactive visualization tools, and human and energy feedback systems in the design of sustainable built environments. Prior to joining the faculty as Assistant Professor at the Syracuse University School of Architecture, she received her Ph.D. in Architectural Sciences from the Rensselaer Polytechnic Institute Center for Architecture Science and Ecology. Dr. Krietemeyer is a Faculty Research Fellow at the Syracuse Center of Excellence, where she leads the Interactive Design and Visualization Lab (IDVL). Her interdisciplinary research focuses on developing simulation software that merges contemporary techniques for energy modeling with new visualization and interactive methods in order to facilitate the integration of user input and energy feedback systems in the design process. Her research has been sponsored through numerous grants, including a recent National Science Foundation grant through the Smart and Connected Communities program. Her work has been published in journals including Architectural Design (AD), Technology | Architecture + Design (TAD), and in the books Architecture in Formation, Inside Smartgeometry: Expanding the Architectural Possibilities of Computational Design, and in Architecture and Interaction: Human-Computer-Interaction in Space and Place.



Ayoub Lharchi

Ayoub Lharchi is a research associate and doctoral candidate at CITA (Center for Information Technology and Architecture) at the Royal Danish Academy of Fine Arts, School of Architecture. He is a registered Architect at the Moroccan National Architects Board with a keen interest in computational design, complex geometries and digital fabrication. After his graduation from the National School of Architecture Rabat with honors, he joined the University of Stuttgart where he earned his Master's of Science degree (M.Sc. ITECH). Previously, Ayoub worked and taught workshops in multiple countries (Germany, United States of America, Belgium, Switzerland and others). At the moment, Ayoub is a Marie-Curie fellow and is part of large European Training Network, InnoChain, where he is conducting research that involves the development of computational methods for the analysis, communication and planning of assembly in complex timber structures. The research is carried out in collaboration with two industrial partners; Design to Production and Blumer Lehmann.



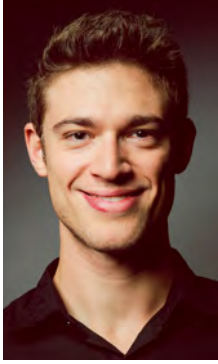
Heather Ligler

Heather Ligler is a PhD Candidate in the Design Computation concentration in the School of Architecture, College of Design at Georgia Institute of Technology. Within the School, she is also a research assistant in the Shape Computation Lab and a lecturer for the Architectonics in Greece + Italy Program. Her ongoing research investigates the evolution of John Portman's architectural language from his 1964 Atlanta residence, Entelechy I, to his emblematic mega-projects for atrium hotels and mixed-use urban developments all over the world. Her larger research interests focus on how shape computation provides another lens to explore geometric logic in architectural theory and design. Heather is a registered architect in the State of Georgia and a member of the American Institute of Architects. Her background includes professional experience with John Portman & Associates (2007-2013), Gensler (2007), and Cooper Carry (2005-2006). Heather holds a MS Arch from Georgia Tech and dual Bachelor of Architecture and Bachelor of Interior Architecture degrees from Auburn University.



Henrik Malm

Henrik Malm is an Architect and Computational Design Specialist at FOJAB in Sweden. He has an MSc in Computer Engineering and a PhD in Applied Mathematics, with a thesis focused on Computer Vision. He was a researcher in Biomimetic Computer Vision at the Zoology Department at Lund University for a few years, where he developed night vision systems based on nocturnal animals' eyes, before getting his MArch from Lund School of Architecture. Before joining FOJAB, Henrik was an Associate and a member of the Applied Research and Development Team at Foster+Partners in London where he worked on the computational design of a number of high profile projects, incl. Mexico City Airport, the UAE Expo Pavillion 2015 and the Prado Museum Extension in Madrid. He has also been a teacher and a critic at e.g. the Bartlett School of Architecture and at Lund School of Architecture and led numerous workshops. In his current position, as Head of Development at FOJABcode, FOJAB's computational design department, he develops both simulation and analysis software for planning and architectural design, as well as works integratively with computational design and complex geometry in the office's architectural projects.



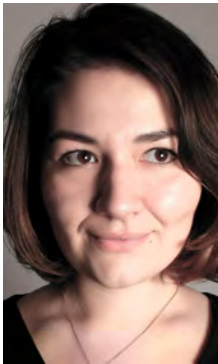
Max Marschall

Max Marschall, born in Berlin, Germany, is currently a PhD candidate at the Spatial Information Architecture Laboratory (SIAL) within the school of Architecture & Urban Design at RMIT University in Melbourne, Australia. He completed his architectural degree at the Berlin University of the Arts and has worked as an architect and computational designer for various architecture and engineering companies in Germany and Australia, including gmp Architects, HENN Architects, Paul Morgan Architects and Bollinger+Grohmann Ingenieure. His PhD research is focused on human-centric, sustainable building design and investigates novel methods of monitoring and modelling microclimates, occupant behaviour and thermal comfort within building simulation. This is achieved through algorithmic modelling, multi-physics simulation and data-driven design approaches. The research has involved developing custom sensing devices to monitor numerous environmental factors of indoor climates. These methods are incorporated into the design of digital tools that enable architects to analyse microclimate performance in the early design stages.



Nicholas Martino

Master's candidate of Architecture and Urban Planning at the Federal University of Rio Grande do Norte and visiting international research student at the elementslab in the University of British Columbia.



Carmen Cristiana Matiz

Carmen Matiz is an architectural assistant, computational designer and researcher based in London. She graduated from UAUIM Bucharest where she became a trained architect. Romanian born, she worked in Krakow and Barcelona before pursuing a Masters in Emergent Technologies and Design at the Architectural Association in London to further develop her research and computational skills. Having a key role in the Emtech Design and Build 2018 Pavilion, she was in charge of designing, developing and producing custom 3D printed joints. She is familiar with the latest digital fabrication technologies in the industry and is proficient at applying them to the needs of each project, analysing the complex relationship between design and making. Currently she is focusing on developing custom tool sets for performance driven design and robotic fabrication to explore adaptive integrated computational design workflows that are informed by fabrication.



Justin McCarty

Justin McCarty attends the School of Architecture and Landscape Architecture at the University of British Columbia (UBC) in Vancouver, BC. He is studying in a three-year professional Master of Architecture program. Justin's research interests stem from an undergraduate education in climate change solutions relating to renewable energy deployment, efficiency programs, and the design of the built environment as it relates to climate change. Justin conducts research within two labs at UBC, the elementslab led by Cynthia Girling and Ronald Kellett and The Energy, Technology, and Architecture (ETA) Lab, or η Lab led by Dr. Adam Rysanek. Within this dual-environment Justin looks for ways to bridge the gap in scale between the urban (elementslab) and the building (η Lab). His research is currently concerned with the development of a project focused on creating a digital signature for buildings that could serve the purposes of researchers, policy makers, operators, and maintenance personnel.



Heather “Brick” McMenemy

Brick is a computational designer specializing in the use of robotic fabrication and emergent technologies to develop architectural forms. Beginning their career at the University of California, Berkeley, Brick received their Bachelor's in Architecture, with minor concentrations in Sustainable Design and Urbanism of Developing Nations. They received the juror's prize for their design work in 2010 and 2011, and was featured in Wurster Hall galleries for the majority of their attendance. Following their degree, Brick worked as a residential designer, specializing in mid-density housing developments in the San Francisco Bay Area. Following this, they pursued their Master's Degree in Emergent Technologies and Design from the Architectural Association School of Architecture. There, their thesis work combined evolutionary algorithms and robotic fabrication to achieve democratic access to contemporary building technology. Brick is committed to the integration of computational design, accessibility, and sustainability.



Samim Mehdizadeh

Samim Mehdizadeh is an architect and a research fellow at the Digital Design Unit (DDU) in Darmstadt. He graduated at the Technische Universität Darmstadt, Digital Design Unit in 2017. His research-in-design thesis explored the Roto-moulding technique for concrete components and the novel design potentials of the material system in architecture. In 2016 and 2017 Samim has been working with Achim Menges (ICD Stuttgart-Menges-Scheffler Architekten BDA) on the stage envelopment Project on Pier 17 building in Manhattan, New York. Prior experiences in practice include the engineering office o-s-d in Frankfurt and a collaboration with the artist Thomas Bayrle. Samim is currently seeking an application Methods of Material Systems in urban scale installations and architecture discipline in practice. Samim Mehdizadeh received the Heinz-Stillger-Award for research in architectural design in 2017 and Award of best Project in poster presentation category at Rilem 1st international digital concrete conference for exploring roto-moulding technique, light casting and dynamic formworks in an architectural context.



Julius Morschek

Julius Morschek is a junior researcher at the Center for Energy at the Smart and Resilient Cities competence unit at the Austrian Institute of Technology (AIT) in Vienna. His current research interests are optimization methods to enforce spatial resilience within the planning process, parametric modeling techniques and computer assisted urban design. Julius studied architecture at the Bauhaus-University in Weimar between 2012 and 2018. In 2014 he spent six months at Eidgenössische Technische Hochschule Zürich (ETHZ) as a guest student. He worked in architecture offices in Munich, Berlin and Zurich. During his master studies, he focused on integrating flooding resilience methods into the planning process (master thesis: „The Spatial Resilience Toolbox Flooding - Development and operation of an integrated urban planning and simulation framework to enforce spatial resilience towards flooding hazards“). He finished his studies with a master's degree in November 2018 and continued his research work at the Austrian Institute of Technology.



Emanuele Naboni

Dr Emanuele Naboni is Associate Professor at the Institute of Architectural Design and Technology of the Royal Danish Academy in Copenhagen, School of Architecture (KADK). He teaches, researches and practices in the field of Sustainable Environmental Design at different scales: Urban, Buildings and Components with a focus on linking Ecosystems and Humans via Digital Design. Emanuele is invited Professor at ETH Future Cities Lab in Singapore, he was an invited Professor at EPFL Lausanne, UC Berkeley, Architectural Association. He was a doctoral and postdoctoral researcher at the Lawrence Berkeley National Laboratory (LBNL). Emanuele was a specialist at the “Performance Design Studio” of Skidmore, Owings and Merrill LLP in San Francisco for a number of years. He consulted foremost international architectural offices including BIG, William McDonough and Mario Cucinella Architects in the development of sustainable strategies. He is currently contracted with Taylor and Francis, for the book “Tools for Environmental Design”, expected to be distributed in 2020.



Elisabeth Riederer

Elisabeth is an architect and researcher. She holds a M.Sc. degree from the Architectural Association school of Architecture, London in the Emergent Technologies and Design program and a B.Arts degree from the Applied University of Science in Munich. Her Master’s dissertation ‘Gradients’ (at AA EmTech), proposed a structure situated in a landfill which is transformed from on-site plastic reducing waste formation. It functions as a recycling hub to improve conditions and logistics while optimizing living conditions. Her interest lies within the domain of advanced technologies and computational design with a mission to make a positive impact on the future global challenges. She aims to create innovative design solutions focusing on influencing climate change scenarios. Seeking to design inhabitable organisms that are capable of developing functions and integrating the processes of the natural world her research engages in a coexistence of architecture and nature. Her research interests include material research, biomimetic, complex geometries and robotic design and fabrication. She was also a contributing in the pavilion collaborative student project MetaFold 2018, which was nominated by Rob|Arch. 2018.



Arian Saeedfar

Arian Saeedfar is an architect and BIM specialist. He graduated with a Master of Science in Construction Management degree from the University of Houston in 2016 and a Bachelor of Architectural Engineering degree from Art University of Isfahan, Iran in 2014. He currently works as part of the Preconstruction team at Autodesk and helps in developing a unified BIM platform for the AEC industry. Arian has previously worked as a designer at Logical Process in Architectural Design (LP Office) in Isfahan, Iran. His research interests include interoperability of design and construction, modular design, off-site construction, project delivery systems, and digital fabrication. His work and research are geared toward developing a data-centric BIM platform for wonders, designers, contractors, and manufacturers. In his previous research as a student, Arian has focused on using digital tools and simulation on interactive construction site planning in order to improve and monitor safety and efficiency on the jobsite.



Azadeh Omidfar Sawyer

Azadeh Omidfar Sawyer is a PhD candidate in the Building Technology program and Rackham Predoctoral Fellow at the University of Michigan. She has a Master of Science in Architecture from the University of Michigan, Master of Design Studies from Harvard University Graduate School of Design, and the 2011 recipient of the Harvard Daniel L. Schodek Award for Technology and Sustainability. Her research focuses on building skin design, performance and evaluation through simulation and immersive virtual reality. She received a Bachelor of Architecture from California College of the Arts in San Francisco with distinction in 2008, where she received the Technology Book award. Azadeh has been a LEED accredited professional since 2008.



Davide Schaumann

Dr. Schaumann is a Postdoctoral Associate in the Department of Computer Science at Rutgers University. He completed his PhD in the Faculty of Architecture and Town Planning at the Technion – Israel Institute of Technology, under the supervision of Professor Yehuda Kalay. He holds B.A. and MSc degrees in Architecture from the Politecnico di Milano, Italy, and has worked for emerging architectural firms in Italy, Spain, Canada, and Israel. Davide’s research lies at the intersection of Architectural Design, Computer Science, and Human Behavior Science with a mission to apply digital technologies for analyzing the dynamic interactions between people, the spaces they inhabit, and the activities they engage in. Specifically, he is interested in developing computer-aided design tools to simulate and analyze human spatial behavior in complex settings. Such tools are aimed to help architects design settings that better support users’ needs. Additionally, Davide is also passionate about studying human behavior in IT-Enhanced environments, which dynamically respond to users’ presence and activities. Davide won several prizes and was recently awarded the Murray Fellowship to support his Postdoctoral position.



Mathew Schwartz

Mathew Schwartz has a BFA and a MSc. in Architecture with a focus on digital technology from the University of Michigan. He worked as a research scientist at the Advanced Institutes of Convergence Technology, Seoul National University, in South Korea, focusing on human factors. From January 2017 he has been an Assistant Professor at NJIT in the College of Architecture and Design. His work, which bridges science and engineering with art and design, makes use of cutting-edge robotics, simulation, and motion capture technology to mimic human characteristics which he then incorporates into commercial applications, architecture, and models used in scientific research. Overall his research focuses on automation in design and the built environment, from integrating autonomous vehicles in buildings to evaluating design based on human factors.



Yuchen Shi

Master Degree Student, Department of Building Science, School of Architecture, Tsinghua University, Beijing, China. Major in air infiltration in buildings and indoor air quality. Has published 4 SCI theses, made 5 oral reports in international conferences and applied for 2 national patents.



Chen Kian Wee

Dr Chen Kian Wee’s research interests lie in the development and use of computational tools for design exploration in the early design stages. His PhD research with Future Cities Laboratory, Department of Architecture, ETH Zurich, focuses on creating an integrated design workflow for the evaluation/optimisation of energy-related design exploration. He joined Singapore MIT Alliance of Research and Technology (SMART) in 2015 as a Postdoctoral Associate looking at the use of optimisation algorithm in the urban design process. He is currently continuing his works at the Princeton University, Andlinger Center for Energy and the Environment as a Distinguished Postdoctoral Fellow.



Michael Weizmann

Michael Weizmann is an architect with a keen interest in the field of computer-aided architectural design and manufacturing, and he is a PhD candidate at the Faculty of Architecture and Town Planning, Technion, Israel. In his PhD research Michael is studying the fascinating properties of geometry that can combine complexity and simplicity in a single object. The research deals with the Topological Interlocking (TI) principle – a special case of masonry that enables assembling simple blocks into large structural elements without using mortar or any other joint types. Michael is developing new design and evaluation methods for new interlocking block types, focusing on the correlation between the geometry of the blocks and the structural performance of the whole assembly. Combined with structural data, the algorithms for parametric design of blocks developed within the research will help maximizing the performance of structural elements just by using the appropriate geometry. The potential outcome of the study is developing TI-based floor systems that will include all the structural benefits of masonry, such as strength and durability, but will benefit from enhanced assembling precision and the lack of mortar that is usually the weakest point of masonry.



Thomas Wortmann

Dr. Thomas Wortmann is a lecturer (assistant professor) at Xi’an Jiaotong Liverpool University. His research and teaching interest is the integration of computation into architectural design processes, focussing on performance-informed design. He has published on parametric design, architectural design optimization, interactive visualization, and parametric shape grammar implementation. Thomas leads the development of Opossum, an award-winning, machine-learning-related optimization tool freely available from food4rhino.com. Currently, he is preparing the release of multi-objective, as well as visual and interactive, versions of Opossum. Thomas holds a PhD in Architecture and Sustainable Design from Singapore University of Technology and Design (SUTD), a Master of Science in Design and Computation from MIT, and a Master of Architecture from the University of Kassel, Germany. He has received SUTD’s Best Dissertation, Design Practice, and Graduate Student Teaching Excellence Awards. Thomas is a registered architect and experienced computational designer, having used computer programming for his own projects, the pioneering digital architecture practice of NOX / Lars Spuybroek, and Web Structures, a multi-disciplinary engineering practice. In 2015, he led the Advanced Architecture Laboratory’s design team for the Future of Us pavilion, a forty-meter span gridshell with around 10.000 individually-sized and -perforated cladding panels in Singapore’s Gardens by the Bay.



Chengde Wu

Chengde Wu is a lecturer at the University of North Carolina at Charlotte. Prior to joining UNC Charlotte, he taught at Texas A&M University for four years and Kaywon University of art and design in Korea for five years. He had also engaged in professional design at Beijing, China and Seoul, Korea for seven years. His design work is primarily focused on high-rise apartment complexes and office buildings. He has received Ph.D. degree in architecture and master's degree in computer science from Texas A&M University. His areas of interest are building simulation, advanced parametric modeling, Building Information Modeling, digital fabrication, machine learning, and virtual reality. His research work is primarily focused on employing digital technologies to facilitate architectural design process.



Shih-Hsin Wu

Shih-Hsin Wu graduated from a five-year undergraduate programme in Cheng Kung University, Taiwan and further studied the master programme in Emergent Technologies and Design in AA School of Architecture. Shih-Hsin's academic background offered her a rigorous, yet innovative mind, and in the meantime shaped her in-depth knowledge of architecture and constant pursuit of architectural novelty. During the study in AA, she specialised in cutting edge computational design research ranging from biomimetic, data-oriented design, to design methodologies assisted via computational models. Consequently, Shih-Hsin become specialised to deal with design complexity through computational methodologies, whilst having developed a mind-set of employing new technologies with a focus on performance-oriented design. Shih-Hsin currently is a computational bridge designer at Knight architects as a bridge designer and exerts on the integration of new technology to deal with structural and design complexity.



Andrea Zani

Andrea Zani is a Facade Project Engineer at Eckersley O'Callaghan in San Francisco where he works with architects and manufacturers throughout the entire design process to deliver high-performance facade systems. Prior to EOC, he worked at Heintges and Arup as Building Science Specialist. Andrea graduated in building engineering from Politecnico di Milano in 2013 where he taught as a teaching assistant in several bachelor and master courses about facade innovation. During his PhD at Politecnico di Milano and University of California Berkeley, he researched new composite materials and performance-based form-finding to optimize daylight and energy performance of solar shading system. In addition to his PhD research, Andrea had the opportunity to collaborate with LBNL Window Group and CBE Berkeley on several research papers. In the last years, Andrea was able to develop a multidisciplinary approach to facade design combining his expertise in facade engineering, building physics, and sustainable design. Currently, he is an active member of IBPSA USA and San Francisco Computational Design User Group.

Organizing Committee



Siobhan Rockcastle [General Chair]

Dr. Siobhan Rockcastle is an Assistant Professor of Architecture at the University of Oregon, Director of the Baker Lighting Lab, and co-founder of OCULIGHT dynamics, a company offering specialized daylight design support to promote healthy indoor occupation. She received her PhD in 2017 from the LIPID lab in the Doctoral Program in Architecture and Sciences of the City (EDAR) at the Swiss Federal Polytechnic in Lausanne, Switzerland (EPFL). Siobhan earned her professional BArch from Cornell University in 2008 and her SMArchS degree in Building Technology from MIT in 2011. Her past work experience includes positions at KVA matX, Snøhetta NY, MSR design, Epiphyte lab, and Gensler NY. Siobhan is on the SimAUD Board, General Chair of SimAUD 2019 and was a Scientific Chair for SimAUD 2018.



Tarek Rakha [Program Chair]

Dr. Tarek Rakha is an architect, building scientist and educator. He is an Assistant Professor of Architecture at Georgia Tech, and Faculty at the High Performance Building (HPB) Lab. His research aims to influence architecture, urban design and planning practices through three areas of expertise: sustainable urban mobility and outdoor thermal comfort; daylighting and energy efficiency in buildings, and building envelope diagnostics using drones. Prior to joining Tech, Dr. Rakha taught at Syracuse University (SU), Rhode Island School of Design (RISD) and MIT. He completed his Ph.D. in building technology at MIT, where he was part of the Sustainable Design Lab as a member of the developing team for *umi*, the urban modeling and simulation platform. As an academic in the United States and a registered architect in Egypt, Dr. Rakha seeks to combine multifaceted research approaches to issues of sustainability in design. He leads efforts in the acquisition and implementation of scholarly collaborations with government, industry and academic partners. Dr. Rakha is on the SimAUD Board and served as the SimAUD 2018 General Chair.



Dimitris Papanikolaou [Scientific Chair]

Dr. Dimitris Papanikolaou is an Assistant Professor at the University of North Carolina at Charlotte (UNCC), jointly between the School of Architecture and the Department of Software Information Systems, and he is the director of the Urban Synergetics Lab (USL). His research integrates areas of big data, complex systems modeling and simulation, and interactive computing, for design and analysis of intelligent urban, building, and mobility systems. Prior UNCC, he worked at Microsoft Research and he taught at New York University (NYU). Dimitris, a licensed architect in Europe, holds a Doctor of Design (DDes) from Harvard University, an MSc from MIT Media Lab, a SMArchS in Design Computation from MIT School of Architecture and Planning, and a Diploma in Architectural Engineering from the National Technical University of Athens in Greece.



Carlos Cerezo Davila [Scientific Chair]

Dr. Carlos Cerezo is a building science researcher and the Environmental Design Director for KPF New York. His work focuses on the development of workflows and tools to incorporate building performance simulation in design at all scales. His research before joining KPF, working as a Research Scientist with the Sustainable Design Lab at MIT, centers on the application of energy simulation and uncertainty analysis at an urban scale, in collaboration with municipalities such as Boston, Chicago, Lisbon, and Kuwait. As an instructor in the Building Technology program at MIT, Carlos has taught environmental modeling to architects and urban planners. Carlos is a licensed architect by the University of Seville (Spain, 2010), having practiced in Spain, Japan and the US, and he holds a Master from Harvard University (2013) and a PhD from MIT (2017).



Tea Žakula [Scientific Chair]

Dr. Tea Žakula is an Assistant Professor and the Head of the Laboratory for Energy Efficiency at the University of Zagreb, Croatia. She collaborates with numerous research institutions and industry on the topics of advanced building control, building participation in smart grids, energy modeling, and optimization. She holds a MS (2010) and PhD (2013) degrees obtained from the MIT (USA). During her postgraduate studies in the USA she was an intern at Harvard University, a lecturer at Northeastern University and a member of the Engineers without Borders. Currently she is a visiting researcher at the Lawrence Berkeley National Laboratory (USA). Furthermore, she is a reviewer for renowned international scientific journals and a member of the Technical Committee for Smart Grids, Technical Committee for Control Theory and Application and Technical Committee for Optimization of ASHRAE. She has also served as a special adviser to the minister in the Croatian Ministry of Environmental Protection and Energy. She has received numerous awards for her work, including the *Best reviewers for IEEE TSG 2017* and *Best reviewers for IEEE TSG 2018* awarded by IEEE Power & Energy Society to the best reviewers of scientific papers and *Croatian Women of Influence 2018* award that recognizes leadership, innovation and community impact.

International Scientific Committee

Hasim Altan <i>University of Sharjah</i>	Daniel Davis <i>WeWork</i>	Ryan Luke Johns <i>GREYSHED</i>
Spyridon Ampanavos <i>Harvard GSD</i>	Catherine De Wolf <i>EPFL</i>	Nathaniel Jones <i>Arup</i>
Alpha Yacob Arsano <i>MIT</i>	Max Doelling <i>Buro Happold Berlin</i>	Alexandros Kallegias <i>Architectural Association/Zaha Hadid</i>
Gideon Aschwanden <i>University of Melbourne</i>	Timur Dogan <i>Cornell University</i>	Alireza Karduni <i>UNCC</i>
Arianna Astolfi <i>Politecnico di Torino</i>	Bing Dong <i>University of Texas at San Antonio</i>	Azam Khan <i>Autodesk</i>
Amber Bartosh <i>Syracuse University</i>	Elif Erdine <i>Architectural Association</i>	Reinhard Koenig <i>Bauhaus-Universität Weimar</i>
Martin Bechtold <i>Harvard GSD</i>	Tomohiro Fukuda <i>Osaka University</i>	Odysseas Kontovourkis <i>University of Cyprus</i>
Geoff Boeing <i>Northeastern University</i>	Jose Luis Garcia Del Castillo <i>Harvard GSD</i>	Anica Landreneau <i>HOK</i>
Johannes Braumann <i>SUTD</i>	Ana Garcia Puyol <i>IrisVR</i>	Anas Lila <i>Cardiff University</i>
Michael Budig <i>Singapore-MIT Alliance for Research and Technology (SMART)</i>	Jeff Geisinger <i>RISD</i>	Thorsten Loemker <i>Zayed University</i>
Bruno Bueno <i>Fraunhofer Institute</i>	David Gerber <i>USC & ARUP</i>	Daniel Macumber <i>NREL</i>
Kynthia Chamilothoni <i>EPFL</i>	Amirhosein Ghaffarianhoseini <i>AUT University</i>	Nathan Melenbrink <i>University of Stuttgart</i>
Giorgia Chinazzo <i>EPFL</i>	Betti Giovanni <i>HENN</i>	Alejandra Menchaca-Brandan <i>Thornton Tomasetti</i>
Joon-Ho Choi <i>USC</i>	Apoorv Goyal <i>HOK</i>	Clayton Miller <i>NUS</i>
Joseph Choma <i>Clemson University</i>	Kenny Gruchalla <i>NREL</i>	Shreshth Nagpal <i>MIT</i>
Sasha Cisar <i>ETH Zurich</i>	Mohammad Heidarinejad <i>IIT</i>	Taro Narahara <i>NJIT</i>
Drury Crawley <i>Bentley</i>	Mary Katherine Heinrich <i>CITA Royal Danish Academy</i>	Emilie Nault <i>EPFL</i>
Jason Danforth <i>KPF</i>	Andrew Heumann <i>WeWork</i>	Liam O'Brian <i>Carlton University</i>

Erik Olsen
Transsolar

Konstantinos-Alketas Oungrinis
TUC

Krista Palen
Transsolar

Luisa Pastore
EPFL

Giuseppe Peronato
EPFL

Stephen Ray
North Park University

Dagmar Reinhardt
The University of Sydney

Paul Ruysssevelt
UCL

Azadeh Sawyer
University of Michigan

Davide Schaumann
Rutgers University

Sven Schneider
Bauhaus-Universitaet Weimar

Stefano Shiavon
UC Berkeley

Rudi Stouffs
NUS

John Sullivan
BuroHappold Engineering

Martin Tamke
Royal Danish Academy of Fine Arts

Martin Tenpierik
TU Delft

Irmak Turan
MIT

Thanos Tzempelikos
Purdue University

Michael Wetter
LBNL

Jan Wienold
EPFL

Eric Wilson
NREL

Luc Wilson
KPF

Gabriel Wurzer
Vienna University of Technology

Arta Yazdanseta
Parsons School of Design

Andrzej Zarzycki
NJIT

Wangda Zuo
University of Colorado Boulder

Georgia Tech Student Volunteers

Alya Hashim

Yun Joon Jung

Di Lu

Tyler Pilet

Mayuri Rajput

High Performance Building PhD students

Sponsors

Platinum



Platinum *(continued)*



Gold

KPF

wemarathon

Silver

O

UNIVERSITY OF
OREGON

College of Design

EDSL Tas

Bronze



In Collaboration With



SimAUD 2019

Symposium on Simulation for
Architecture & Urban Design

CONFERENCE PROCEEDINGS

Simulation Series: Volume 50 #7

